The Chemistry of Blended Cements and Backfills Intended for Use in Radioactive Waste Disposal

R&D Technical Report P98

The Chemistry of Blended Cements and Backfills Intended for Use in Radioactive Waste Disposal

R&D Technical Report P98

F P Glasser, M Tyrer, K Quillin, D Ross, J Pedersen, K Goldthorpe, D Bennett and M Atkins

Research Contractors:

University of Aberdeen
WS Atkins
Building Research Establishment

Further copies of this report are available from:
Environment Agency R&D Dissemination Centre, c/o
WRc, Frankland Road, Swindon, Wilts SN5 8YF

tel: 01793-865000 fax: 01793-514562 e-mail: publications@wrcplc.co.uk

Publishing Organisation:
Environment Agency
Rio House
Waterside Drive
Aztec West
Almondsbury
Bristol BS32 4UD

Tel: 01454 624400 Fax: 01454 624409

ISBN 1 1857 05 157 2

Dissemination status:
Internal: Released to Regions
External: Released to Public Domain

Statement of use:
This report presents the results of a large collaborative research programme to investigate the chemistry of potential backfill materials for a repository for disposal of solid radioactive waste. The information in this document may be used by Agency staff involved in assessing proposals and/or authorisations for disposal of solid radioactive waste.

Research contractor:
This document was produced under R&D Project CPR2/41/1/3 (P3-014) by:
Professor F P Glasser
Department of Chemistry
Meston Walk
University of Aberdeen
Aberdeen, Scotland AB9 2UF
tel: 01224 272906 fax: 01224 272908

Environment Agency's Project Manager:
The Environment Agency's Project Manager for contract P3-014 was:
Dr Susan L Duerden

R&D Technical Report P98

CONTENTS **Page No.**

LIST OF TABLES

LIST OF FIGURES

Figure A13. 60 pfa: 40 OPC in deionised water, 85°C, 20 months showing coarse, sub-prismatic C-A-S-H grain with gel-like surrounding material. Magnification x 28,000.

Figure A14. 60 pfa: 40 OPC in deionised water, 85°C, 20 months showing typical mixture of needles and hexagonal plates. Magnification x 100,000.

Figure A15. 60 pfa: 40 OPC in deionised water, 85°C, 20 months showing aluminosilicate grains. Magnification x 10,000.

Figure A16. 60 pfa: 40 OPC in groundwater A, 85°C, 20 months showing CSH plates and curled-up sheets with some prismatic zeolite. Magnification x 60,000. Electron-dense equant iron oxide grains, possibly coated with gel occur along with CSH plates and curled sheets. A single prismatic zeolite crystal is visible. Magnification x 36,000.

Figure A17 60 pfa: 40 OPC groundwater water, A 85°C, 20 months. Electron-dense equant iron oxide grains possibly coated with gel, along with CSH plates and curled up sheets and a single prismatic zeolite. Magnification x 100,000.

Figure A18. 60 pfa: 40 OPC in groundwater A, 85°C, 20 months, showing coarse rectangular plates of unknown composition. Magnification x 22,000.

Figure A19. 60 pfa: 40 OPC in groundwater A, 85°C, 20 months, showing unusual cluster of gel with a fine grained acicular phase (possibly a zeolite). Note the dark specks in the gel (these may be finely disseminated halite, NaCℓ). Magnification x 22,000.

Figure A20. 60 pfa: 40 OPC in groundwater A, 85°C, 20 months, showing relatively coarse zeolite prisms amongst CSH sheets (whose curled up edges appear as electron-dense spikes). Magnification x 36,000.

Figure A21. 60 pfa: 40 OPC in groundwater A, 85°C, 20 months, showing a few coarse zeolite prisms amongst CSH sheets (whose curled up edges appear as electron-dense spikes), some finer grained prismatic zeolites and a few tiny patches of gel. Magnification x 28,000.

Figure A22. 60 pfa: 40 OPC in groundwater water A, 85°C, 20 months, showing an enlargement of Figure A21 with prismatic zeolites amongst CSH sheets (whose curled up edges appear as electron-dense spikes) and a few tiny patches of gel. Magnification x 80,000.

Figure A23. Backfill in groundwater A, 85°C, 20 months. The large electron-dense region to the lower right is a calcite grain. The large hexagonal plate (and the dark elongated shapes, which may be plates edge-on) are Fe rich. The smaller hexagonal plates forming on these plates are unknown composition but may be portlandite or AFm. Magnification x 60,000.

ACKNOWLEDGEMENT

The editor wishes to thank Mr. S. Black for assistance with graphics.

EXECUTIVE SUMMARY

BACKGROUND

This project was initiated by Her Majesty's Inspectorate of Pollution (HMIP)[1] at the time when UK NIREX had announced its intention to develop a repository for low and intermediate level nuclear waste in the vicinity of Sellafield. In this repository setting, two main barriers existed to the return of radio-isotopes to the biosphere: the natural, or geologic and hydrogeologic barriers, and the man-made barriers. These latter comprise relatively short-lived containers as well as an engineered backfill. The backfill was designed to condition a high pH in the repository, thereby lowering the solubility of many long-lived radionuclides yet not confine gases, which might be generated from chemical and radioactive waste within the repository vault.

The Environment Agency for England and Wales[1] had already taken independent steps to examine the suitability of alkaline backfills, based on Portland cement, limestone flour and $Ca(OH)_2$, for the man-made barriers. Preliminary data on post-closure repository performance assessment at Sellafield suggested the importance of two additional factors which had not hitherto been considered in assessments.

- *temperature*: inclusion of heat generating waste could drive temperatures up to ~80°C in the post closure phase.
- *salinity of deep groundwater*. Much previous work has been done in initially-pure water but borehole analyses indicated high salinity at depth. Other potential deep repositories could also be saline.

These impacts were likely to occur together throughout much of the post-closure phase: backfills were likely to be in prolonged contact with hot, saline groundwater.

Previous studies demonstrated that cements achieve their performance by a sacrificial action. It is however essential that the cementitious materials should not dissolve too rapidly if prolonged backfill performance lifetimes are to be achieved. By dissolving, cement backfills condition permeating water to a high pH and thereby lower the solubilities of many radionuclides. While this conditioning action had been demonstrated to occur for initially-pure water at ~25°C, it had not been demonstrated for hot, saline solutions.

Thus the performance of cements had to be addressed in hot, saline conditions, and a range of elevated temperatures, but the question was how? Many centuries, perhaps millennia, had to be compressed into a relatively brief period of laboratory assessment. It is well known that accelerated testing of materials has many pitfalls and "performance" may not be independent of the test criteria, particularly in accelerated

[1] The contract was commissioned by, Her Majesty's Inspectorate of Pollution (HMIP) for England and Wales. On 01 April, 1996, the contract passed to the Environment Agency for England and Wales (the Agency).

tests. The programme was designed to provide accelerated data but also to take into account previous relevant experience.

PROGRAMME OF RESEARCH : AIMS

i) To undertake a coordinated research programme to determine the influence of saline and environments and elevated temperatures on cementitious material and backfill.

ii) To extend the capabilities of existing thermodynamic models of backfills and blended cements to encompass the range of environmental conditions likely to be experienced at proposed repository sites.

RESULTS AND CONCLUSIONS

The systems studied are complex. Cements contain four principal components: CaO, Al_2O_3, SiO_2 and H_2O. Backfill, with its content of $CaCO_3$, adds a fifth. Very few five-component aqueous systems have been studied completely because the complexity of a system tends to increase factorially with the number of components i.e., for four components, its complexity is 4!, or 24 whereas a fifth component, in this instance $CaCO_3$, increases the complexity to 5!, or 120. Adding two more groundwater components, NaCl and $MgSO_4$, helps explain why many tables and figures are necessary to depict the results. It is found that:

1. NaCl is not of itself detrimental to the ability of cement and backfill to condition a high pH. Both calculation and experiment demonstrate this. The solubility of the calcium component decreases with rising temperature but increases with increasing NaCl concentration. Because NaCl and temperature have opposite effects, the solubility of $Ca(OH)_2$ in 1.5M NaCl at 85°C is not significantly different than in initially pure water at 25°C. Therefore dissolution rates of $Ca(OH)_2$ are not much enhanced, even in worst-case conditions.

2. The presence of $MgSO_4$ is particularly harmful to cement performance. Three reactions occur: (i) Mg replaces Ca, (ii) sulfate replaces hydroxide in the cement solids and (iii) the solubility of the resulting Ca-containing solids increase. For example the solid reaction products of $Ca(OH)_2$ in $MgSO_4$ are $Mg(OH)_2$ and gypsum, $CaSO_4.2H_2O$. These products are not capable of conditioning aqueous pH's to >10, a limit which is frequently taken to mark the end of the performance lifetime for high pH conditioning.

   Similar reactions occur with C-S-H, the gel phase of cements. The magnesium - containing reaction products are mixtures of $Mg(OH)_2$ and sepiolite, or possibly talc. These additional phases do not significantly affect the conclusions about the impact of $MgSO_4$ on pH buffering because the products of complete reaction, although less soluble than $CaSO_4$, condition the aqueous pH to much less than 10. Thus the $MgSO_4$ component of groundwater rapidly reduces the pH buffering capacity of cement barriers.

3. In mixed brines containing NaCl and $MgSO_4$, reaction is accelerated relative to pure water or either salt separately. As Mg replaces Ca, a separate reaction between Ca and SO_4 forms gypsum, $CaSO_4.2H_2O$ (or at high ionic strengths, $CaSO_4$, or mixtures of the two). Sodium chloride significantly enhances the solubility of both $Mg(OH)_2$ and $CaSO_4$ (all forms). It is not possible to give a single acceleration factor but, comparing mixed $MgSO_4$-NaCl brine with distilled water at either 25°C or 85°C, acceleration factors are in the range 10-20. That is, if a cementitious barrier had a given performance lifetime in initially pure water, but a mixed brine were substituted into the same hydrogeologic regime, its performance lifetime would be shortened by a factor typically between 10 and 20.

4. $CaCO_3$ does not react significantly with $Ca(OH)_2$ or the calcium silicate gel phase at temperatures below 140°C, approximately. Above ~ 140°C, scawtite, a calcium silicocarbonate, becomes stable. Its potential for conditioning high pH's is negligible, as is that of $CaCO_3$.

5. The gel phase, CSH, which comprises > 50 % of a Portland cement shows signs of progressive crystallisation. In compositions low in alkali (Na, K) the products are mainly jennite, tobermorite and afwillite. These condition a somewhat lower pH than the equivalent non-crystalline composition. Jennite and afwillite probably have sufficient pH conditioning (≥10.5) to maintain an acceptably high pH; tobermorite is marginal. In experiments made using cement blended with siliceous materials, e.g., fly ash, zeolite crystallisation was observed. Both gismondine and phillipsite were observed to form in prolonged high temperature cure of blended cements. Unfortunately virtually nothing is known about the stability of zeolites in the environments studied, so it is not known whether zeolite formation is ephemeral or if it could be expected to increase with time and, if so, which zeolites were stable. The consequences of zeolite formation to repository performance are unknown.

6. The gel phase, like $Ca(OH)_2$, also reacts strongly with both Mg and sulfate. Thus the backfill buffering capacity is likely to be terminated upon completion of reaction with $MgSO_4$.

7. The phase balances described here are not affected by how the experiment is performed. But even if comparison is restricted to a single chemistry and one isotherm, the *amounts* of product are affected by how the experiment is performed (for example, by the ratio of solid mass to aqueous volume, the schedule of leachant renewal, etc.). These complications are inevitable in complex systems characterised by incongruent dissolution of its constituent solids. Therefore we state those conclusions which are, in general, independent of the way in which the experiments were done.

8. The experiments were not directly laid out to determine reaction kinetics. Nevertheless, the reactions observed always moved in the direction which calculations disclosed to be the equilibrium direction. The design of experiments was such that laboratory trials required respiking, i.e. addition of more reactant, particularly of $MgSO_4$, if target brine concentrations were to be maintained.

9. This respiking procedure was not envisaged in the contract and the decision to effectively titrate the cement samples with brine meant that the anticipated duration of the experiments had to be extended. BRE did not, however, agree to these changes with the result that in their experiments, the $MgSO_4$ reactant was quickly depleted. Therefore, the final state attained in the BRE experiments corresponds most closely to the Aberdeen experiments made with one, or at most, a few respikings. If the correlations between experiments is thus limited, good agreement is obtained. It is considered that respiking reproduces well but in incremental stages, processes which will be achieved slowly and more continuously in a repository environment.

10. An additional advantage of the respiking is that it gives a qualitative insight into reaction kinetics. It was very noticeable that the time taken for a new equilibrium to be established following spikes increased progressively with each spike. Moreover, the pH often decreased even when X-ray diffraction indicated that reactants ordinarily capable of conditioning high aqueous pH's had not been consumed. These considerations, taken together, suggest that chemically-active portions of backfill capable of conditioning high pH can become effectively isolated from aqueous solution, even when the contact period is on the order of a few months.

    Hence extensive disequilibrium may obtain between solids and aqueous phases. In experiments made using suspensions, it was not possible to determine the presence of layers of reaction products but on the cement paste blocks, progressive mineralogical zonation developed as reaction proceeded. The mineralogical zonation followed the sequence observed from suspension experiments which was identical to that predicted from modelling studies.

11. Development of a computational capability is an extremely useful, perhaps essential, in the analysis of these very complex aqueous systems. There are problems concerning the computations: the data base is barely adequate, especially at elevated temperatures, major problems occur in modelling solid solutions, e.g. C-S-H gel, and in making activity corrections at high ionic strength. In order to progress calculation and experiment, it was sometimes necessary to use provisional thermodynamic values when calculations were made in support of experimental work. These ephemeral calculations have not been revised to reflect the final dataset. However, calculations reported in chapters 5 and 6, which may be used in performance assessment, use a self-consistent database.

    In general, many of the experimental findings have been supported by modelling studies which, in turn, are an invaluable aid to correlation, extrapolation and interpolation between experimental data points, and also to bridge potential gaps between data arising from laboratory studies and those obtained on real materials. Perhaps the main weakness, of both experiment and modelling, is the difficulty of assessing reaction kinetics and transport, and of the accompanying changes in molar volume of the residual solids and of the resulting changes in porosity-permeability relations.

12. The period of effective cementitious barrier action, measured by its ability to condition percolating water to pH ≥ 10, is a function of groundwater flow rate, since the main mechanisms responsible for the degradation of cement barriers are sensitive to mass transport. At slow flow rates, characteristic of the hydrologic conditions at an ideal disposal site, cement backfills would work best in a regime dominated by dissolution: precipitation is less desirable because it tends to physically isolate unconsumed backfill.

13. Dissolution reactions are not much influenced by the presence (or absence) of calcium carbonate as a component of the backfill, or by the presence of NaCl up to 1.5M in the temperature range 25°-85°C, but combinations of NaCl and $MgSO_4$ are believed to reduce performance lifetimes perhaps by a factor of 10-20. This reduction occurs by two mechanisms: conversion of solids capable of conditioning a high pH to those with much weaker pH conditioning ability, and by enhanced solubility of the solids, resulting in enhanced mass wastage relative to initially pure water. The results suggest that one criterion for site selection, assuming cement conditioning forms an integral part of the safety case, should be a ground water regime which allows cement-based backfills to perform by slow dissolution, as described above.

14. Advances in modelling calculations and improvements in the associated data base made in the course of this project are believed to enhance confidence in the performance of cement in a range of environments. The results on single phases and calculations are backed up and supported by experiments on actual cements, formulated with commercially available materials. A methodology has also been developed, based on physiochemical functions, which could be used to assess cement barrier performance in a range of hydrogeological regimes, ranging from shallow to deep burial.

KEY WORDS

Backfill, Cement, Cement-Sulphate, Chemical-Physical Degradation, Database, Hydrology, Mathematical Models, Nuclide Migration, pH, Radioactive Wastes, Repository, Salinity.

GLOSSARY

Standard cement nomenclature is used throughout, with the exception of SO_3 and CO_2; see below for symbols used.

C = CaO	M = MgO	A = Al_2O_3	H = H_2O
S = SiO_2	$\overline{C}$, c = CO_2	$\overline{S}$, s = SO_3	F = Fe_2O_3

so that MH is $MgO{\cdot}H_2O$, Cc is $CaO{\cdot}CO_2$ ($CaCO_3$) and so on. Other abbreviations used, for cement types and cement phases are given below.

AFm*	Calcium hydroxyaluminate ($4CaO{\cdot}Al_2O_3{\cdot}xH_2O$, where x is normally 13 or 19)
AFm-Cl	Calcium monochloroaluminate, or Friedel's salt ($3CaO{\cdot}Al_2O_3{\cdot}CaCl_2{\cdot}10H_2O$)
AFm-CO_3	Calcium monocarboaluminate ($3CaO{\cdot}Al_2O_3{\cdot}CaCO_3{\cdot}10H_2O$)
AFm-0.5CO_3	Calcium hemicarboaluminate ($3CaO{\cdot}Al_2O_3{\cdot}0.5CaCO_3{\cdot}0.5Ca(OH)_2{\cdot}10{,}5H_2O$)
AFm-SO_4	Calcium monosulfoaluminate ($3CaO{\cdot}Al_2O_3{\cdot}CaSO_4{\cdot}12H_2O$)
AFm-Cl-SO_4	Calcium chlorosulfoaluminate or Kuzel's salt ($3CaO{\cdot}Al_2O_3{\cdot}0.5CaSO_4{\cdot}0.5CaCl_2{\cdot}12H_2O$)
GH	Gehlenite hydrate or Strätlingite ($2CaO{\cdot}Al_2O_3{\cdot}SiO_2{\cdot}8H_2O$) ($C_2ASH_8$)
C-S-H	Calcium Silicate Hydrogel ($xCaO{\cdot}ySiO_2{\cdot}zH_2O$, where Ca/Si ratio is between 0.8 and ~2.0)
Tob	Tobermorite ($5CaO{\cdot}6SiO_2{\cdot}5H_2O$)
Jen	Jennite ($9CaO{\cdot}6SiO_2{\cdot}11H_2O$)
Afw	Afwillite ($3CaO{\cdot}2SiO_2{\cdot}3H_2O$)
AFt*	Ettringite, or Trisulfoaluminate ($3CaO{\cdot}Al_2O_3{\cdot}3CaSO_4{\cdot}32H_2O$)

* The terms AFm and AFt have been used in this report to depict phases of specific composition. In the literature both terms are often used in a more general sense to describe phase 'families', with a common structure, i.e. including solid solutions and 'end members'. Thus Al_2O_3 (symbol A) may be partially substituted by Fe_2O_3 (symbol F).

AFt-CO_3-SO_4	Thaumasite ($3CaO{\cdot}SiO_2{\cdot}SO_4{\cdot}CO_3{\cdot}12H_2O$)
HG	Hydrogarnet ($3CaO{\cdot}Al_2O_3{\cdot}6H_2O$)
Si-HG	Siliceous Hydrogarnet ($3CaO{\cdot}Al_2O_3{\cdot}xSiO_2{\cdot}6\text{-}2xH_2O$)
Anh	Anhydrite ($CaSO_4$)
Gyp	Gypsum ($CaSO_4{\cdot}2H_2O$)
HT	Hydrotalcite ($4MgO{\cdot}Al_2O_3{\cdot}10H_2O$) ($M_4\ AH_{10}$)
Tho	Thomsonite ($NaCa_2Al_5Si_5O_{20}{\cdot}6H_2O$)
Phi	Phillipsite ($KCa(Si_5Al_3)O_{16}{\cdot}6H_2O$)
Sep	Sepiolite ($Mg_9Si_{12}O{\cdot}\ 10H_2O$)
Gis	Gismondine ($CaAl_2Si_2O_8{\cdot}4H_2O$)
Boe	Boehmite ($AlO(OH){\cdot}xH_2O$)

Some solid solution is accepted without special note, but when it is important to indicate that the structure is not chemically pure, the subscript "ss" is used. For example, an ettringite or AFt phase containing some thaumasite component could be abbreviated AFt_{ss}. Synthetic hydrotalcite appears to have a higher Mg/Al ratio than the naturally - occurring mineral and may contain SO_4, CO_3 and Cl^- partially replacing OH^-. Other abbreviations:

det	determination
DET	Discrete Extraction Test
BH	Borehole
SI	Saturation Index
BFS or ggbs	Granulated blast furnace slag
FA or pfa	Pulverised fuel ash
DD, DDW	Double - distilled water
OPC	Ordinary Portland cement
TGA	Thermogravimetric analysis

Key to Tables

OPC	Ordinary Portland cement
ggbs	ground granulated blastfurnace slag
pfa	Pulverised fuel ash
Groundwater A	Borehole 3 Determination 7
Groundwater B	Borehole 2 Determination 8

Wh	Sample hydrated weight
Wu	Weight of sample before hydration
AFt	Ettringite, $C_6As_3H_{32}$
CH	Calcium hydroxide (portlandite)
CSH	C-S-H gel
Afw	Afwillite
Tob	Tobermorite-like phase
Cc	Calcium carbonate (calcite)
Si-HG	Siliceous hydrogarnet (composition approximately C_3ASH_4)
Afm	Calcium aluminium hydroxide, C_4AH_{13} or a phase with similar XRD pattern
AFm-CO_2	Calcium monocarboaluminate, C_4AcH_{11}, or a phase with similar XRD pattern
AFm-½CO_2	Calcium monocarboaluminate, $C_4A½cH_{12}$, or a phase with similar XRD pattern
AFm-SO_4	Monosulphate, C_4ASH_x
AFm-Cl	Calcium chloride-containing AFm phase similar to Friedel's salt ($C_4AC\ell_2H_{11}$)
Anh	Anhydrous calcium sulphate, $CaSO_4$
Tho	Thomsonite ($NaCa_2Al_5Si_5O_{20}6H_2O$)
Phi	Phillipsite ($KCa(Si_5Al_3)O_{16}6H_2O$)
HT	Hydrotalcite (M_4AH_{10})
GH	Gehlenite hydrate, C_2ASH_8

1 INTRODUCTION

1.1 Background

Current proposals for the disposal of low and intermediate level radioactive waste in the UK involve the construction of a deep, cement conditioned repository. It is possible that the groundwaters at the site will be saline.

The repository is likely to comprise multiple natural and artificial barriers. The first barrier is the waste form itself, perhaps encapsulated in either BFS/OPC or FA/OPC and stored in steel canisters which, until destroyed by corrosion, act as a physical second barrier. The third barrier is the backfill material used to fill the excavated repository. The last natural barrier might vary: it may be a low permeability host rock or in shallow repositories, unconsolidated material. Figure 1.1 illustrates a deep repository concept.

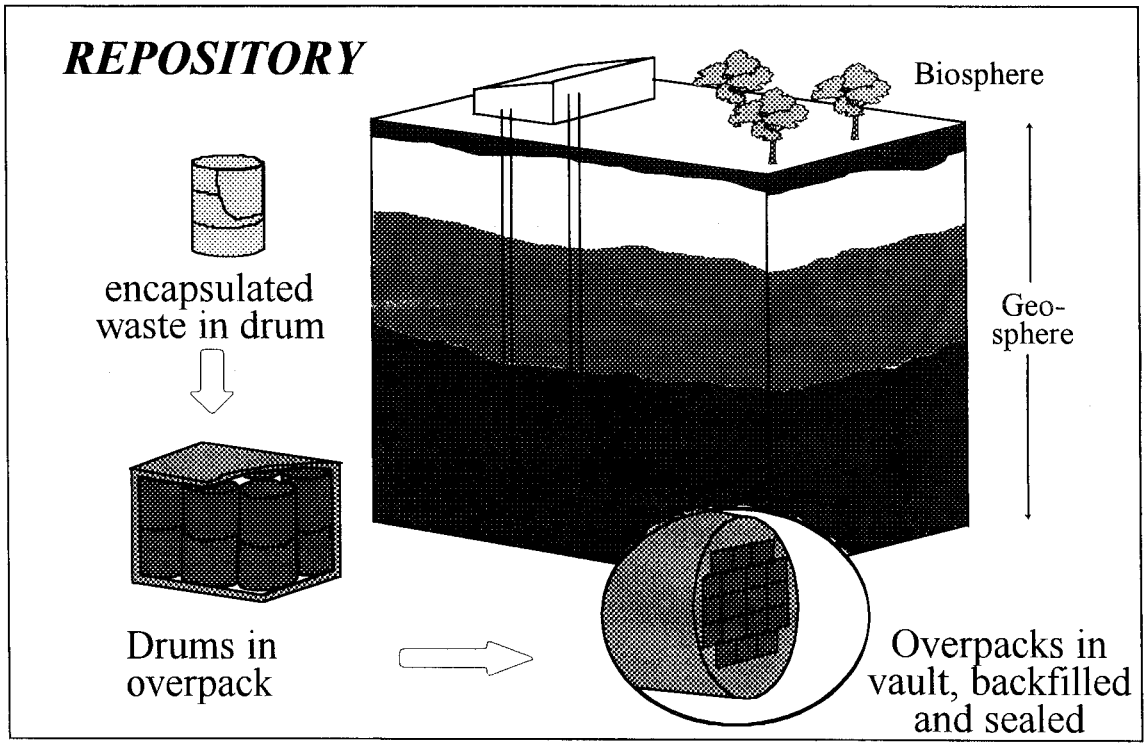

Figure 1.1. Conceptual sketch of a deep cementitious repository after [1]

Scenarios for repository performance rely heavily on (i) geological containment and (ii) the conditioning action of cementitious barriers which, should continue to be effective for approximately 10 half-lives.

The backfill may comprise another engineered barrier. It may be of a high permeability to diffuse gas (generated for example by corrosion of metallic components, degradation of organics and radiolysis): a nearly impermeable barrier might lead to pressure build-up and severe cracking, thereby forming a path for radionuclide release. Other scenario envisage physically-dense barriers. Eventually, the physical barrier will be breached and the radioactive

inventory exposed to groundwater. This is the dominant pathway by which radionuclides can return to the biosphere [2]. The backfill and cementitious materials present are designed to act as chemical barriers due to the high pH of the porewater, thereby limiting the solubility of radionuclides.

Repository temperatures may be substantially above ambient in the post closure phase, depending on design. We use a scenario which has a pulse temperature of ~ 80°C for the first 100 years or so, followed by a slow decay back to ~ 25°C [3]. One of the principal pH buffers in cements is the gel-like $CaO\text{-}SiO_2\text{-}H_2O$ phase which is predicted to persist in the long term ($\sim 10^5$ years) at temperatures near ambient, on the basis of geological and historical evidence [4, 5]. However, Atkins et al. [6, 7] found by experiment that C-S-H will undergo partial crystallisation, to semi-crystalline tobermorite, afwillite, jennite and C-S-H I at 55° and 85°C after 1-2 years curing. Equilibrium pH's in this system are lowered by one or two pH units as a result of crystallisation.

Another complication in understanding the behaviour of cement systems at long ages is the impact of saline groundwater. Data currently available are insufficient to predict the effects of these conditions on repository performance.

Many potential repository sites are in or near coastal regions, or are overlain by salt, with the result that groundwaters are saline. There is an extensive literature on the effect of salt solutions on cement durability at 10° - 30°C. A literature review on seawater discloses:

- Most of the degradation 'power' of seawater is due to its $MgSO_4$ component.
- A 'skin' of brucite, $Mg(OH)_2$, is formed on the surface of concrete, which may itself become coated with $CaCO_3$. These layers can act as an effective barrier to slow further chemical reaction, but at the expense of isolating the cement from contact with the aqueous phase.
- The protective skin may spall, thus exposing fresh cement to attack. Spalling arises because physical expansion occurs due to precipitation in the sub-surface zones.
- The action of seawater is usually less deleterious than $MgSO_4$ alone. This has been attributed to salts in the $CaO\text{-}Al_2O_3\text{-}SO_3\text{-}H_2O$ system being more soluble in NaCl solutions. These salts are then more likely to be dissolved, thereby relieving expansive stresses arising from precipitation reactions.
- Cement degradation in sulphate solutions generally decreases with increasing temperature over the range 25- 85°C. This is probably related to the known increase in solubility of AFm-SO_4 and especially of AFt with increasing temperature.
- Expansion and degradation can also occur in the absence of calcium aluminates because calcium silicates also react with $MgSO_4$. An approximate equation is:

  C-S-H + $3MgSO_4.+5H_2O \rightarrow CaSO_4.2H_2O + 3Mg(OH)_2 + 2SiO_2$ (amorphous) + Ca^{2+} (aqueous).

  The final, least soluble, degradation product is ~ $2MgO.3SiO_2.3H_2O$.

1.2 Research Aims and Objectives

This work is concerned principally with the influence of elevated temperatures and saline waters on cement materials and backfill and to determine the influence relative to radioactive waste disposal. As background:

- A thermodynamic model for blended cements was developed for the 25°C isotherm [6],
- Thermodynamic data applicable to the current modelling work were obtained and thermodynamic modelling of blended cements at elevated temperatures (50-90°C) was reported [7].

The report presents results of an integrated program of work on the effect of elevated temperatures and saline waters on the physical and chemical properties of backfills and blended cements. The work has been carried out by research partners at W.S. Atkins (part of this work was subcontracted to Imperial College of Science, Technology and Medicine) the Building Research Establishment and the University of Aberdeen. W.S. Atkins and Imperial College have concentrated on developing and implementing thermodynamic models (i) suitable for simulating the interaction between cement/backfill pore fluids and saline groundwaters and (ii) a model simulating the interaction between repository and host rock interaction over the temperature range 25°C to 85°C. They have also developed an enhanced solubility model for C-S-H gels in saline waters, assessed the volume changes of blended cements as a result of phase transformations and finally focused on the specifications for an enhanced near field model for use in EA assessment studies.

Work at BRE, centred on the effect of prolonged groundwater attack upon representative cement/backfill formulations proposed for the Sellafield repository. The various blends that have been studied mainly at 25° and 85°C are .

- **OPC** (intended as a control)
- **75% BFS:25%OPC** (a principle encapsulant)
- **60% FA:40%OPC** (mostly used as a 'capping' in steel canisters, sometimes as an encapsulant)
- **Backfill**, (a mixture of $CaCO_3$, $Ca(OH)_2$ and OPC).

The formulations have been cured in two synthetic simulant saline groundwaters and, as a control, in degassed, deionised water.

The University of Aberdeen has concentrated on the synthesis of single cement substances and on reactions of these with NaCl solutions and mixed $MgSO_4$ and NaCl brines. Solubility measurements were used to supplement the thermodynamic database and thermodynamic calculations were performed in support of experiment and vice versa. A comprehensive scheme is developed for assessing the course of reaction between cement backfills and warm, saline groundwaters. This, in turn, will enable performance lifetimes to be evaluated.

The same cement formulations, groundwater compositions and temperatures were used by the three groups. Regular meetings were held to ensure integration of the experimental results and in coordinating modelling with experiment.

REFERENCES

1. P.A.H Saunders. (Sep.1988) 'Research and Safety Assessment'. Nirex Report No. NSS/G100.

2. F.P. Glasser and M.Atkins. (1994) 'Cements in Radioactive Waste Disposal'. MRS Bulletin/December. pp.33-38.

3. C. R. Wilding. (1992) 'The Performance of Cement Based Systems'. Proc. e-MRS Symp. Chemistry of Cements for Nuclear Applications, Strasbourg, Nov. 1991. pp. 299-310.

4. A. Atkinson and J.A. Hearn. (1989) 'The Hydrothermal Chemistry of Portland Cement and its Relevance to Radioactive Waste Disposal'. NIREX Report no. NSS/R 187, UK.

5. H.F.W. Taylor. (1998) 'Chemistry of Cement and Concrete'. Thomas Telford, London.

6. M. Atkins. F.P. Glasser, L.P. Moroni and J.J. Jack. (1993) 'Thermodynamic Modelling of Blended Cements at Elevated Temperature (50-90°C)'. UK DoE Report no. DoE/HMIP/RR/94/011, Aberdeen University, Scotland.

7. M. Atkins et al. (1991) 'A Thermodynamic Model for Blended Cements'. UK DoE Report no. DoE/HMIP/RR/92/005, Aberdeen University, Scotland.

2. THE PRE-PROJECT DATABASE

2.1 Background

The most flexible approach for predicting solution compositions in cement systems over the long term is achieved by thermodynamic modelling, which involves the use of computer speciation programs to calculate solution compositions and elemental speciation in complex chemical systems. These speciation programs are based on the law of mass action and require a database containing relevant thermodynamic quantities, for example, solubility products, enthalpies and heat capacities [1-4]. Most thermodynamic databases have been developed in association with specific geochemical codes but do not contain data relevant to the alkaline environment found in cement pore solutions.

The pre-project thermodynamic databases for aqueous species are given in tables 2.1 and 2.3, and for solid phases, in tables 2.2 and 2.4. These 'in-house' databases are specifically tailored to the requirements of cementitious systems.

The program 'MINEQL/AU' was used in two previous reports [1,5], as has a similar programme called 'PHREEQE'. The two programmes are similar and data given in (1,5) have been transferred into the PHREEQE database.

For the more saline environments, a PHREEQE-related programme called PHRQPITZ has been used. This programme is used for specialist application where the environment is highly saline (ionic strengths, I, in the range 0.5-5.0). It uses Pitzer's relation for calculation of species activities. Like PHREEQE, PHRQPITZ can calculate pH, redox potential, and mass transfer as a function of the extent of reaction. The limitation is that its database lacks information both for some of the parameters required to solve Pitzer's relation and also for the aqueous and solid phases. These are given in tables 2.2 - 2.4.

2.2 The Databases

The chemistry of cement and the composition of the synthetic groundwater requires a thermodynamic database including the following components: Na, Ca, Mg, Al, Si, (all as oxides) SO_4, CO_2, Cl and H_2O. Only aqueous complexes and sparingly soluble salts within this group have been included in tables 2.1 to 2.4 (and CO_2 gas). Potassium forms solid phases but, as these are very soluble and we are concerned about the ability of persistent solid phases to influence aqueous chemistry, they are not deemed to be important in the present context.

The effect of temperature on equilibrium constants is calculated in two different ways:

1. From the simplified Van't Hoff equation, for which PHREEQE/PHRQPITZ assumes that enthalpy is constant and thereby, $\Delta H = 0$. This approximation is only appropriate over relatively short temperature ranges, *ca* $\Delta T \sim 10\text{-}20^{\circ}C$.

2. A polynomial expression, for which the values of the coefficients are specified in the thermodynamic database for each reaction of interest:

$$\log K = a_1 + a_2T + a_3/T + a_4T^2 + a_5/T^2$$

The dataset in table 2.1 shows that practically all ΔH values required for elevated temperature modelling of aqueous complexes are potentially available. There are, however, still gaps for the coefficients of analytical expression for the temperature dependence of log K. This is a common problem in many datasets; the data are simply not available. Data for some of the cement hydrates at elevated temperature are in (5). However, there are still gaps in PHRQPITZ database for many of the important cement hydrates which limit its value in simulating reactions in highly saline systems (table 2.4). Its major limitation is that its database lacks numerical values for most of the parameters used in the Pitzer's relation (γ, π, τ, λ, ζ, B2, C0, B1and B0).

A major part of the programme has been to obtain a database for high temperature and saline-environments. This task has been carried out by W.S. Atkins and Imperial College with assistance from Aberdeen. However, as this was not completed until the end of the programme, the earlier version of PHRQPITZ has been used at Aberdeen for trial calculations. Examples of the integration of experiment and calculation will be presented in subsequent sections.

Table 2.1. Pre-project thermodynamic database for aqueous species in PHREEQE.

Species	charge	Formation reaction	log Ksp	source	ΔHr (kcal/mol)	source	Coefficients of analytical expression for temp-temperature dependence log K a1,a2,a3,a4,a5	source
$CaCO_3$	0	$Ca^{2+} + CO_3^{2-}$	3.15	[4] Hatches	3.547	[4] Hatches	a_1 =-1228.732, a_2 = -0.29944, a_3 = 35512.75, a_4 = 485.818	[4] Hatches
$CaHCO_3$	+	$Ca^{2+} + CO_3^{2-} + H^+$	11.35	[4] Hatches	-0.869	[4] Hatches	a_1 = 1317.0071,a_2 = 0.34546894, a_3 = -39916.84,a_4 = -517.70761,a_5 = 563713.9	[4] Hatches
$CaSO_4$	0	$Ca^{2+} + SO_4^{2-}$	2.31	[4] Hatches	1.47	[4] Hatches	-	-
CaOH	+	$Ca^{2+} + H_2O - H^+$	-12.60	[4] Hatches	14.53	[4] Hatches	-	-
$MgCO_3$	0	$Mg^{2+} + CO_3^{2-}$	2.98	[4] Hatches	2.535	[4] Hatches	a_1=-32.172,a_2= 0.0,a_3=1093.486,a_4=12.72433	[4] Hatches
$MgHCO_3$	+	$Mg^{2+} + H^+ + CO_3^{2-}$	11.40	[4] Hatches	-2.775	[4] Hatches	a_1 = 48.6721, a_2 = 0.03252849, a_3= -2614.335, a_4 = -18.00263,a_5 = 563713.9	[4] Hatches
$MgSO_4$	0	$Mg^{2+} + SO_4^{2-}$	2.25	[4] Hatches	1.4	[4] Hatches	-	-
MgOH	+	$Mg^{2+} + H_2O - H^+$	-11.79	[4] Hatches	15.419	[4] Hatches	-	-
$AlSO_4$	+	$Al^{3+} + SO_4^{2-}$	3.02	[4] Hatches	2.15	[4] Hatches	-	-
$Al(SO_4)_2$	-	Al^{3+} $2SO_4^{2-}$	4.92	[4,16]	2.84	[4] Hatches	-	-
AlOH	2+	$Al^{3+} + H_2O - H^+$	-4.99	[4,16]	11.9	[4] Hatches	-	-
$AlOH_2$	+	$Al^{3+} + 2H_2O - 2H^+$	-10.1	[4,16]	0.0	[4] Hatches	-	-
$AlOH_3$	0	$Al^{3+} + 3H_2O - 3H^+$	-16.0	[4,16]	0.0	[4] Hatches	-	-
$AlOH_4$	-	$Al^{3+} + 4H_2O - 4H^+$	-22.7	[9] USGS	44.06	[4] Hatches	-	-
HCO_3	-	$CO_3^{2-} + H^+$	10.33	[4] Hatches	-3.561	[4] Hatches	a_1 = 107.8871, a_2 = 0.03252849, a_3 = -5151.79,a_4 = -38.92561, a_5 = 563713.9	[4] Hatches
H_2CO_3	0	$CO_3^{2-} + 2H^+ - H_2O$	16.68	[4] Hatches	-5.738	[4] Hatches	a_1 = 464.1965,a_2 = 0.093444813, a_3=-26986.16, a_4 =-165.75951,a_5 = 2248628.9	[4] Hatches
HSO_4	-	$SO_4^{2-} + H^+$	1.99	[4] Hatches	4.91	[4] Hatches	a_1 = -5.3505, a_2 = 0.0183412,a_3 = 557.2461	[4] Hatches
H_2SiO_4	2-	$H_4SiO_4 - 2H^+$	-21.70		29.717	[4] Hatches	a_1 = 39.478,a_2 = -0.065927,a_3 = -12355.1	[4] Hatches
H_3SiO_4	-	$H_4SiO_4 - H^+$	-9.85		8.936	[4] Hatches	a_1= 6.368,a_2 = -0.016346, a_3 = -3405.9	[4] Hatches
$NaCO_3$	-	$Na^+ + CO_3^{2-}$	1.27	[4] Hatches	8.911	[4] Hatches	-	-
$NaHCO_3$	0	$Na^+ + H^+ + CO_3^{2-}$	10.08	[4] Hatches	-3.604	[4] Hatches	-	-
$NaSO_4$	-	$Na^+ + SO_4^{2-}$	0.70	[4] Hatches	1.12	[4] Hatches	-	-
CO_2	0	H_2CO_3	-1.468		-4.776		a_1 = 108.3865, a_2 = 0.01985076, a_3 = -6919.53, a_4 = -40.45154,a_5 = 669365.0	[4] Hatches
OH	-	$H_2O - H^+$	-14.0	[4] Hatches	13.345	[4] Hatches	-	-

Table 2.2 Pre-project thermodynamic database in PHREEQE for solid phases.

Phase	Formation reaction	Log Kdiss	Source	ΔHr (kcal/mol)	Source
Tobermorite	Ca^{2+} (5)H_4SiO_4 (6)H_2O(-2)H^+ (-10)	64.35	[2] AU (64.94)	-187.0	
Jennite	Ca^{2+} (9)H_4 SiO_4 (6)H_2O(8)H^+ (-18)	147.1	[5] 94.001	-187.0	
Afwillite	Ca^{2+} (3)H_4SiO_4 (2)H_2O(2)H^+ (-6)	46.9	[5] 94.001	0.0	
CSH(0.8)	Ca^{2+} (0.8)H_4SiO_4 (1)H_2O(1)H^+ (-1.6)	11.08		0.0	
CSH(1.1)	Ca^{2+} (1.1)H_4 SiO_4 (1)H_2O(3)H^+ (-2.2)	16.72	[18] D.Damidot & FPG	0.0	
CSH(1.8)	Ca^{2+} (1.8)H_4SiO_4 (1)H_2O(5)H^+ (-3.6)	32.60		0.0	
Portlandite	Ca^{2+} (1)H^+ (-2)H_2 O(2)	22.815	[5]94.001[2]AU	0.0	
C_3AH_6	Ca^{2+} (3)Al^{3+} (2)H_2O(12)H^+ (-12)	78.66	[12]Wells et al/[2]AU	-137.0	
C_3AH_6/AU	Ca^{2+} (3)Al^{3+} (2)H_2O(12)H^+ (-12)	80.35	[5] 94.001	0.0	
$C_3AS_{0.5}$	Ca^{2+} (3)Al^{3+} (2)H_2 O(10)H^+ (-12)H_4SiO_4 (0.5)	74.12	[5] 94.011	0.0	
C_3ASH_4	Ca^{2+} (3)Al^{3+} (2)H_2O(8)H^+ (-12)H_4SiO_4 (1)	69.37	[5] 94.011	0.0	
C_2ASH_8	Ca^{2+} (2)Al^{3+} (2)H_4 SiO_4 (1)H_2O(11)H^+ (-10)	49.67	[18] , [2] AU	0.0	
GH/AU	Ca^{2+} (2)Al^{3+} (2)H_4SiO_4 (1)H_2O(11)H^+ (-10)	49.38	[5] 94.011	0.0	
C_2 AH_8	Ca^{2+} (2)Al^{3+} (2)H_2O(13)H^+ (-10)	59.51	[12] Wells, [10]Taylor/[2]AU	-102.5	
SiO_2am	H_4SiO_4 (1)H_2O(-2)	-2.85	[11]Taylor/[2]AU	6.22	
Halloyite	Al^{3+} (2)H_4SiO_4 (2)H_2O(1)H^+ (-6)	13.03	[16] Helm	0.0	
Kaolinite	Al^{3+}(2)H_4 SiO_4(2)H_2O(1)H^+(-6)	5.71	[17] May et al.	0.0	
Chabazite	Ca^{2+}(1)Al^{3+}(2)H_4SiO_4	13.65	[3]	0.0	
Gypsum	Ca^{2+} (1)SO_4^{2-} (1)H_2O(2)	-4.60	[9] Parkhurst/[4]Harwell	-0.28	[9] Parkhurst(-0.028)
Anhydrite	Ca^{2+} (1)SO_4^{2-} (1)	-4.27	[3]	-4.3	[9] Parkhurst
Ettringite	Ca^{2+} (6)Al^{3+} (2)SO+4+$^{2-}$ (3)H_2O(32)H^+ (-12)	55.223	[2] AU, [13] Zang	-80.32	
Monosulfate	Ca^{2+} (4)Al^{3+} (2)SO_4^{2-} (1)H_2O(18)H^+ (-12)	71.36	[2] AU	-120.0	

Table 2.2 Pre-project thermodynamic database in PHREEQE for solid phases.

Phase	Formation reaction	Log Kdiss	Source	ΔHr (kcal/mol)	Source
Calcite	$CO_3^{2-}(1)Ca^{2+}$ (1)	-8.41	[14]Plummer	-2.689	
C_4AH_{13}	Ca^{2+} (4)Al^{3+} (2)$H_2O(20)H^+$ (-14)	103.6	[11,12] [2,11]	-151.2	
Monocarbonate	$Ca^{2+}(4)Al^{3+}(2)CO_2(1)H_2O(17)H^+(-12)$	69.86	[12]Zhang,Zhou/ [2]AU	0.0	
Hemicarbonate	$Ca^{2+}(4)Al^{3+}(2)CO_2(0.5)H_2O(18)H^+(-13)$	86.33	[19]	0.0	
Tricarbonate	$Ca^{2+}(6)Al^{3+}(2)CO_2(3)H_2O(36)H^+(-12)$	51.6	[19]	0.0	
Monochloride	$Ca^{2+}(4)Al^{3+}(2)Cl^-(2)H_2O(16)H^+(-12)$	72.04	[2] AU/[10] Schippa	0.0	
Hemichloride	$Ca^{2+}(4)Al^{3+}(2)Cl^-(1)H_2O(18)H^+(-13)$	87.82	[20]	0.0	
Trichloride	$Ca^{2+}(6)Al^{3+}(2)Cl^-(6)H_2O(36)H^+(-12)$	56.84	[20]	0.0	
3.1.15Cl	$Ca^{2+}(4)Cl^-(2)H_2O(18)H^+(-6)$	68.7	[8] Milikan	0.0	
Oxychloride	$Ca^{2+}(4)Cl^-(2)H_2O(19)H^+(-6)$	68.75	[8]	0.0	
Dolomite	$Ca^{2+}(1)Mg^{2+}(1)CO_3^{2-}(2)$	-17.02	[4]Harwell/Hatches	-8.29	Harwell/Hatches
Magnesite	$Mg^2+(1)CO_3^{2-}(1)$	-7.46	[4]	0.0	Harwell/Hatches
Brucite	$Mg^{2+}(1)H^+(-2)H_2O(1)$	17.11	[4]	0.0	
Grossularite	$Ca^{2+}(3)Al^{3+}(2)H_4SiO_4(3)H^+(-12)$	52.61	[3] (52.134) EQ3/6	0.0	
Talc	$Mg^{2+}(3)H_4SiO_4(4)$	22.41	[15] Bricker	69.02	
Hydrotalcite	$Mg^{2+}(4)Al^{3+}(2)H^+(-14)H_2O(17)$	75.44	[5] 94.011	0.0	
Sepiolite	$Mg^{2+}(4)H_4SiO_4(6)H_2O(1)H^+(-8)$	34.	[7] Kent and Kastner	0.0	
Gibbsite	$Al^{3+}(1)H_2O(3)H^+(-3)$	7.228	[6] Jones/[2] AU	-22.8	Parkhurst
CaP	$Ca^{2+}(1)Al^{3+}(2)H_4SiO_4(2.6)H_2O(2)H^+(-8)$	20.2	[5] 94.011	0.0	
NaP	$Na^+(2)Al^{3+}(2)H_4SiO_4(2.6)H_2O(2)H^+(-8)$	26.4	[5] 94.011	0.0	
Glauberite	$Ca^{2+}(1)SO_4^{2-}(2)Na^+(2)$	-4.6	[4]	0.0	
Gaylusite	$Ca^{2+}(1)Na^+(2)CO_2(2)H_2O(5)$	-9.62	[3] (-9.45) EQ3/6	0.0	

Table 2.3 Pre-project database for aqueous species in saline environments, PHRQPITZ.

Species	charge	Formation reaction	log Ksp	source	ΔHr (kcal/mol)	source	Coefficients of analytical expression for temperature dependance of log K a_1,a_2,a_3,a_4,a_5	source
$CaCO_3$	0	$Ca^{2+} + CO_3^{2-}$	3.15	[4] Hatches	3.547	[4] Hatches	a_1 =-1228.732, a_2 = -0.29944, a_3 = 35512.75, a_4 = 485.818	[4] Hatches
$CaHCO_3$	+	$Ca^{2+} + CO_3^{2-} + H^+$	-	-	-		-	-
$CaSO_4$	0	$Ca^{2+} + SO_4^{2-}$	-	-	-		-	-
CaOH	+	$Ca^{2+} + H_2O - H^+$	-	-	-		-	-
$MgCO_3$	0	$Mg^{2+} + CO_3^{2-}$	2.928		2.535	[4] Hatches	a_1 =-32.172,a_2= 0.0,a_3=1093.486,a_4=12.72433	[4] Hatches
$MgHCO_3$	+	$Mg^{2+} + H^+ + CO_3^{2-}$	-	-	-		-	-
$MgSO_4$	0	$Mg^{2+} + SO_4^{2-}$	-	-	-		-	-
MgOH	+	$Mg^{2+} + H_2O - H^+$	-11.79	[4] Hatches	15.419	[4] Hatches	-	-
$AlSO_4$	+	$Al^{3+} + SO_4^{2-}$	-	-	-	-	-	-
$Al(SO_4)_2$	-	$Al^{3+} + 2SO_4^{2-}$	-	-	-	-	-	-
AlOH	2+	$Al^{3+} + H_2O - H^+$	-	-	-	-	-	-
$AlOH_2$	+	$Al^{3+} + 2H_2O - 2H^+$	-	-	-	-	-	-
$A\ell(OH)_3$	0	$Al^{3+} + 3H_2O - 3H^+$	-	-	-	-	-	-
$A\ell(OH)_4$	-	$Al^{3-} + 4H_2O - 4H^+$	-22.7	[3] USGS	44.06	[4] Hatches	-	-
HCO_3	-	$CO_3^{2-} + H^+$	10.33	[4] Hatches	-3.561	[4] Hatches	a_1 = 107.8871, a_2 = 0.03252849, a_3 = -5151.79, a_4 = -38.92561, a_5 = 563713.9	[4] Hatches
H_2CO_3	0	$CO_3^{2-} + 2H^+ - H_2O$	16.68	[4] Hatches	-5.738	[4] Hatches	a_1 = 464.1965,a_2 = 0.093444813, a_3=-26986.16, a_4 =-165.75951,a_5 = 2248628.9	[4] Hatches
HSO_4	-	$SO_4^{2-} + H^+$	1.99	[4] Hatches	4.91	[4] Hatches	a_1 = -5.3505, a_2 = 0.0183412,a_3 = 557.2461	[4] Hatches
H_2SiO_4	2-	$H_4SiO_4 - 2H^+$	-21.70		29.717	[4] Hatches	a_1 = 39.478, a_2 = -0.065927,a_3 = -12355.1	[4] Hatches
H_3SiO_4	-	$H_4SiO_4 - H^+$	-9.85		8.936	[4] Hatches	a_1= 6.368, a_2 = -0.016346, a_3 = -3405.9	[4] Hatches
$NaCO_3$	-	$Na^+ + CO_3^{2-}$	-	-	-	-	-	-
$NaHCO_3$	0	$Na^+ + H^+ + CO_3^{2-}$	-	-	-	-	-	-
$NaSO_4$	-	$Na^+ + SO_4^{2-}$	-	-	-	-	-	-
CO_2		H_2CO_3	-1.468		-4.776		-	-
OH	-	$H_2O - H^+$	-14.0	[4] Hatches	13.345	[4] Hatches	-	-

Table 2.4 Pre-project thermodynamic database in PHRQPITZ for solid phases.

Phase	Formation reaction	Log Kdiss	Source	ΔHr (kcal/mol)	Source
Tobermorite	$Ca^{2+}(5)H_4SiO_4(6)H_2O(-2)H^+(-10)$	64.35	[2] AU (64.94)	-187.0	
Jennite	$Ca^{2+}(9)H_4SiO_4(6)H_2O(8)H^+(-18)$	150.81		-187.0	
Afwillite	$Ca2+(3)H_4SiO_4(2)H_2O(2)H^+(-6)$	46.9		0.0	
CSH(0.8)	$Ca^{2+}(0.8)H_4SiO_4(1)H_2O(1)H^+(-1.6)$	11.07		0.0	
CSH(1.1)	$Ca^{2+}(1.1)H_4SiO_4(1)H_2O(3)H^+(-2.2)$	16.71	[18] Damidot	0.0	
CSH(1.8)	$Ca^{2+}(1.8)H_4SiO_4(1)H_2O(5)H^+(-3.6)$	32.54		0.0	
Portlandite	$Ca^{2+}(1)H^+(-2)H_2O(2)$	22.94		0.0	
C_3AH_6	$Ca^{2+}(3)Al^{3+}(2)H_2O(12)H^+(-12)$	78.79		-137.0	
C3AH6/AU	$Ca^{2+}(3)Al^{3+}(2)H_2O(12)H^+(-12)$	81.75		0.0	
$C_3ASH_{0.5}$	$Ca^{2+}(3)Al^{3+}(2)H_2O(10)H^+(-12)H_4SiO_4(0.5)$	74.12	[5] 94.011	0.0	
C_3ASH_4	$Ca^{2+}(3)Al^{3+}(2)H_2O(8)H^+(-12)H_4SiO_4(1)$	69.35	[5] 94.011	0.0	
C_2ASH_8	$Ca^{2+}(2)Al^{3+}(2)H_4SiO_4(1)H_2O(11)H^+(-10)$	49.68	[5] , [2] AU	0.0	
GH/AU	$Ca^{2+}(2)Al^{3+}(2)H_4SiO_4(1)H_2O(11)H^+(-10)$	49.38	[5] 94.011	0.0	
C_2AH_8	$Ca^{2+}(2)Al^{3+}(2)H_2O(13)H^+(-10)$	59.67		-102.5	
SiO_2am	$H_4SiO_4(1)H_2O(-2)$	-2.85	[11] Taylor/[2]AU	6.22	
Halloysite	$Al^{3+}(2)H_4SiO_4(2)H_2O(1)H+(-6)$	15.1		0.0	
Kaolinite	$Al^{3+}(2)H_4SiO_4(2)H_2O(1)H^+(-6)$	6.7		0.0	
Chabazite	$Ca^{2+}(1)Al^{3+}(2)H_4SiO_4(4)H_2O(2)H^+(-8)$	13.		0.0	
Gypsum	$Ca^{2+}(1)SO_4^{2-}(1)H_2O(2)$	-4.58		-0.28	[9] Parkhurst(-0.028)
Anhydrite	$Ca^{2+}(1)SO_4^{2-}(1)$	-		-4.3	[9] Parkhurst
Ettringite	$Ca^{2+}(6)Al^{3+}(2)SO_4^{2-}(3)H_2O(32)H^+(-12)$	55.35		-80.32	
Monosulfate	$Ca^{2+}(4)Al^{3+}(2)SO_4^{2-}(1)H_2O(18)H^+(-12)$	71.49		-120.0	
Calcite	$CO_3^{2-}(1)Ca^{2+}(1)$	-8.41	[14]Plummer	-2.689	
C_4AH_{13}	$Ca^{2+}(4)Al^{3+}(2)H_2O(20)H^+(-14)$	104		-151.2	

Table 2.4 Pre-project thermodynamic database in PHRQPITZ for solid phases, continued.

Phase	Formation reaction	Log Kdiss	Source	ΔHr (kcal/mol)	Source
Monocarbonate	$Ca^{2+}(4)Al^{3+}(2)CO_2(1)H_2O(17)H^+(-12)$	69.99		0.0	
Hemicarbonate	$Ca^{2+}(4)Al^{3+}(2)CO_2(0.5)H_2O(18)H^+(-13)$	85.738		0.0	
Tricarbonate	$Ca^{2+}(6)Al^{3+}(2)CO_2(3)H_2O(36)H^+(-12)$	54.595		0.0	
Monochloride	$Ca^{2+}(4)Al^{3+}(2)Cl^-(2)H_2O(16)H^+(-12)$	72.52		0.0	
Hemichloride	$Ca^{2+}(4)Al^{3+}(2)Cl^-(1)H_2O(18)H^+(-13)$	-		0.0	
Trichloride	$Ca^{2+}(6)Al^{3+}(2)Cl^-(6)H_2O(36)H^+(-12)$	-		0.0	
$CaCl_2.6H$	$Ca^{2+}(1)Cl^-(2)H_2O(6)$	2.56		0.0	
1.1.2Cl	$Ca^{2+}(2)Cl^-(2)H_2O(3)H^+(-2)$	25.25		0.0	
3.1.15Cl	$Ca^{2+}(4)Cl^-(2)H_2O(18)H^+(-6)$	68.92		0.0	
Oxychloride	$Ca^{2+}(4)Cl^-(2)H_2O(19)H^+(-6)$	-		0.0	
Dolomite	$Ca^{2+}(1)Mg^{2+}(1)CO_3^{2-}(2)$	-17.08		-8.29	Harwell/Hatches
Magnesite	$Mg^2+(1)CO_3^{2-}(1)$	-7.834	[4]Harwell/Hatches	0.0	Harwell/Hatches
Brucite	$Mg^{2+}(1)H^+(-2)H_2O(1)$	17.11		0.0	
Grossularite	$Ca^{2+}(3)Al^{3+}(2)H_4SiO_4(3)H^+(-12)$	-		0.0	
Talc	$Mg^{2+}(3)H_4SiO_4(4)$	-	[15] Bricker	69.02	
Hydrotalcite	$Mg^{2+}(4)Al^{3+}(2)H^+(-14)H_2O(17)$	83.22		0.0	
Sepiolite	$Mg^{2+}(4)H_4SiO_4(6)H_2O(1)H^+(-8)$	-		0.0	
Gibbsite	$Al^{3+}(1)H_2O(3)H^+(-3)$	7.228	[6] Jones/[2] AU	-22.8	Parkhurst
CaP	$Ca^{2+}(1)Al^{3+}(2)H_4SiO_4(2.6)H_2O(2)H^+(-8)$	20.4		0.0	
NaP	$Na^+(2)Al^{3+}(2)H_4SiO_4(2.6)H_2O(2)H^+(-8)$	26.4	[5] 94.011	0.0	
Glauberite	$Ca^{2+}(1)SO_4^{2-}(2)Na^+(2)$	-5.245		0.0	
Gaylusite	$Ca^{2+}(1)Na^+(2)CO_2(2)H_2O(5)$	-9.421		0.0	
Na_2SO_4	$Na^+(2)SO_4^{2-}(1)$	-0.2875		0.0	

References

1 M.Atkins, F.P. Glasser A. Kindness and D.E. Macphee (1991). 'Solubility Data For Cement Hydrate Phases (25°C)' DoE Report No DoE/HMIP/RR/91/032.

2 D. Damidot and M. Atkins. (1992) AU Unpublished Report. 'Cement Modelling Using MINEQL and PHREEQE Programs'.

3 W.E. Falck, (1992). 'CHEMVAL Project. Critical Evaluation of the CHEMVAL Thermodynamic Database with Respect to its Contents and Relevance to Radioactive Waste Disposal at Sellafield and Dounreay'. W.S. Atkins Report No.M1516.080.

4 J.E. Cross, F.T. Ewart and C.J. Tweed. (1987, Revised 1991) 'Thermodynamic Modelling with Application to Nuclear Waste Processing and Disposal'. *HATCHES* (*HA*rwell/Nirex *T*hermodynamic Database for *CH*emical *E*quilibrium *S*tudies)

5 M. Atkins, F.P.Glasser, L.P. Moroni and J.J. Jack. (1993) 'Thermodynamic Modelling of Blended Cements at Elevated Temperature (50-90°C).DoE Report No DoE/HMIP/RR/94.011

6 F.E. Jones. (1944) 'The Quaternary System CaO-Al_2O_3-$CaSO_4$-H_2O at 25°C. Equilibria with Crystalline $Al_2O_3 \cdot 3H_2O$, Alumina Gel and Solid Solution'. Journal Phys. Chem. **48**(6), 311-356.

7 D.B. Kent and M. Kastner. (1985) 'Mg^{2+} Removal in the System Mg^{2+}- Amorphous SiO_2-H_2O by Adsorption and Mg-hydroxysilicate Precipitation'. Geochimica et Cosmochimica Acta **49**, 1123-1136.

8 J. Milikan. (1917) Zeit. Physik.Chemie, **92**, 496-510.

9 D.L. Parkhurst, D.C. Thorstenson and L.N. Plummer. (1980, Revised 1985) 'PHREEQE-A Computer Program for Geochemical Calculations'. US Geological Survey, Water Resources Investigations Report 80-96.

10 G. Schippa, R. Turriziani. (1955) 'Contribution to the Knowledge of the Hydrated Chloroaluminates of Calcium (In Ital.) La Ricerca Scientitica, **25**, 3102-3106.

11 H.F.W. Taylor, F.G. Buttler and A. Percival. (1960) 'The Precipitation of $CaO \cdot Al_2O_3 \cdot 10H_2O$ from Supersaturated Calcium Aluminate Solutions at 21°C'. Chemistry of Cement. Proceedings of the Fourth International Symposium. National Bureau of Standards Monograph 43-Vol.I, Paper III-S5. pp. 277-283.Washington D.C.

12 L.S. Wells, F. Clarke and H.F. McMurdie. (1943) 'Study of the System CaO-Al_2O_3-H_2O at Temperatures of 21° and 90°C'. Journal of Research of the National Bureau of Standards, **30**, Research Paper 1539

13 F. Zang, Z. Zhou and Z. Lou. (1980) 'Solubility Product and Stability of Ettringite'. Proc. 7th. Int. Symp. Chem. Cem. Vol. II, pp. 88-93, Paris.

14 L.N. Plummer and E. Busenberg. (1982) Geochem. et Cosmochimica Acta, **46**, 1011-1140.

15 O.P. Bricker, H.W. Nesbitt, and W.D. Gunter. (1973) 'The Stability of Talc'. American Mineralogist, **58**, 64-72

16 J.D. Helm. (1973) 'Chemistry of Aluminium in Natural Water'. U.S. Geological Survey: Water Supply Paper 1827-E. Washington, D.C.

17 H.M. May, D.G. Kinniburgh, P.A. Helmke and M.L. Jackson. (1986)' Aqueous Dissolution, Solubilities and Thermodynamic Stabilities of Common Aluminosilicate Clay Minerals: Kaolinite and Smectites'. Geochimica et Cosmochimica Acta, **50**, 1667-1677.

18 D.Damidot and F.P. Glasser. (1995) 'Investigation of the $CaO-Al_2O_3-SiO_2-H_2O$ System at 25°C by Thermodynamic Calculations'. Cement and Concrete Research, **25**(1), 22-28.

19 D. Damidot, S. Stronach, A. Kindness, M. Atkins and F. P. Glasser. (1995) 'Thermodynamic Investigation of the $CaO-Al_2O_3-CaCO_3-H_2O$ System at 25°C and the Influence of Na_2O'. Advances in Cement Res., No.27, 129-134 (1995).

20 D. Damidot and F.P. Glasser. (1997) 'Thermodynamic Investigation of the $CaO-Al_2O_3-CaSO_4-CaC\ell_2-H_2O$ System at 25°C and The Influence of Na_2O'. Proceedings of the 10th International Congress on the Chemistry of Cement, Gothenburg, Sweden. Congrex AB, Gothenburg. Volume 4, paper 4iv 066.

3. EXPERIMENTAL METHODS

3.1. Introduction

The systems chosen for investigation are listed in tables 3.1 and 3.2. tables 3.3, 3.4, 3.5 and figures 3.1 and 3.2 depict phase relations.

Table 3.1 Pure hydrate systems reacted with NaCl: numbers in italics refer to curing time in days.

Temperature	25°C				55°C			85°C		
Target [NaCl] in M	0	0.5	1.0	1.5	0	0.5	1.5	0	0.5	1.5
C-S-H 0.85	*131*	*131*	*131*	*131*	*190*	*190*	*190*	*145*	*145*	*145*
C-S-H 1.1	*131*	*131*	*131*	*131*	*190*	*190*	*190*	*145*	*145*	*145*
C-S-H 1.4	*273*	*273*	*273*	*273*	*190*	*190*	*190*	*145*	*145*	*145*
C-S-H 1.8	*273*	*273*	*273*	*273*	*190*	*190*	*190*	*145*	*145*	*145*
CH	*131*	*131*	*131*	*131*	*190*	*190*	*190*	*145*	*145*	*145*
C_3AH_6	*173*	-	*173*	*173*	*186*	*186*	*186*	*173*	*173*	*173*
AFm-SO_4	*134*	*134*	*134*	*134*	*186*	*186*	*186*	*165*	*165*	*165*
AFt	*151*	*151*	*151*	*151*	*186*	*186*	*186*	*182*	*182*	*182*

In table 3.2, fractional numbers indicate that the sample has been partially respiked by adding solid $MgSO_4$. For example, C-S-H 1.1 in 0.05 M $MgSO_4$, needed to be respiked to increase the calculated concentration by an incremental 0.025M $MgSO_4$. This was carried out to prevent 'overspiking' as a full respike would take the concentration above the target whereas no respiking would leave the solution more dilute than the target.

Table 3.2 Pure hydrate systems reacted with $MgSO_4$: numbers in italics refer to the number of respikes carried out prior to final analysis (see section 3.4). Total time taken for the respikes varied between 9 and 15 months.

Temperature	25°C			55°C			85°C		
Target [$MgSO_4$] in M	0.005	0.01	0.05	0.005	0.01	0.05	0.005	0.01	0.05
C-S-H 0.85	*3*	*3*	*3*	*3.5*	*3.5*	*3.5*	*3.5*	*3.5*	*3.5*
C-S-H 1.1	*3.5*	*3.5*	*3.5*	*4.5*	*4.5*	*4.5*	*4.5*	*4.5*	*4.5*
C-S-H 1.4	*4*	*4*	*4*	*5.5*	*5.5*	*5.5*	*5.5*	*5.5*	*5.5*
C-S-H 1.8	*4*	*5*	*8*	*7*	*7*	*7*	*7*	*7*	*7*
CH	*5*	*6*	*9*	*9*	*9*	*9*	*8*	*8*	*10*
C_3AH_6	*8*	*8*	*8*	*6*	*6*	*6*	*8*	*8*	*8*
AFm-SO_4	*1*	*1*	*1*	*3*	*3*	*3*	*1*	*1*	*1*
AFt	*1*	*1*	*1*	*1*	*1*	*1*	*1*	*1*	*1*

Table 3.3 **CASH and CScH phase formation experiments. The compositions are given in figures 3.1 and 3.2 and in wt% in tables 3.4 and 3.5. The numbers in the double distilled decarbonated column are the curing time in days and the numbers in the brine columns refer to the number of respikes carried out prior to final analysis (See section 3.4). Total time taken for the respikes varied from 8 to 12 months.**

Phase formation	Double distilled decarbonated water		0.5 M NaCl + 0.6 0.02 M $MgSO_4$		3.0 M NaCl + 3.1 0.02 M $MgSO_4$	
Temperature	25°C	85°C	25°C	85°C	25°C	85°C
CASH 1	363	214	*17*	*19*	*17*	*19*
CASH 2	363	214	*2*	*2*	*2*	*2*
CASH 3	363	214	*9*	*11*	*9*	*11*
CASH 4	363	214	*4*	*6*	*4*	*4*
CASH 5	363	214	*4*	*4*	*4*	*4*
CASH 6	363	214	*8*	*10*	*8*	*10*
CScH 1	300	230	*8*	*8*	*8*	*8*
CScH 2	300	230	*10*	*10*	*10*	*10*
CScH 3	300	230	*12*	*12*	*10*	*12*
CScH 4	300	230	*3.5*	*5.5*	*3.5*	*3.5*
CScH 5	300	230	*1*	*1*	*1*	*1*

Tables 3.4 and 3.5 gives the compositions of CASH and CScH in weight %.

Table 3.4 **Weight % for the starting compositions for the CASH system at 25° and 85°C. The weight percent silica is as silica fume, which is *ca* 98-99% SiO_2; the AlO(OH) had 72.37 wt% Al_2O_3 by thermogravimetric analysis.**

Phase formation	wt% CaO	wt% AlO(OH)	wt% SiO_2
CASH 1	75.7	5.5	18.8
CASH 2	19.6	39.2	41.1
CASH 3	47.4	11.9	40.7
CASH 4	27.6	23.1	49.3
CASH 5	27.1	34.1	38.8
CASH 6	41.3	31.1	27.5

Table 3.5 **Weight % for the starting compositions for the CScH system at 25° and 85°C. The weight percent silica is as silica fume, which is *ca* 98-99% SiO_2.**

Phase formation	wt% CaO	wt% SiO_2	wt% $CaCO_3$
CScH 1	42.3	45.3	12.4
CScH 2	43.0	30.8	26.2
CScH 3	41.1	10.2	48.7
CScH 4	16.1	17.1	66.7
CScH 5	8.3	35.8	55.9

Figures 3.1 and 3.2 show the compositions prepared and those of relevant solids.

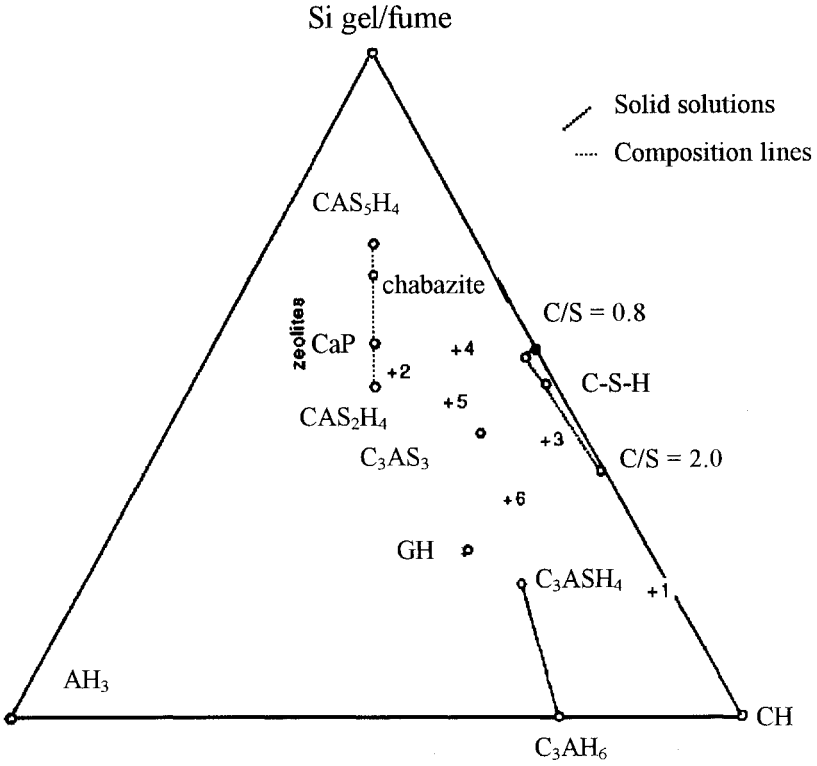

Figure 3.1 Ternary diagram of the CASH (CaO-Al_2O_3-SiO_2-H_2O) system: The compositions of crystalline hydrates known to occur at 50-90°C are shown by mineral or synthetic designations. Sample compositions prepared in the present study are shown by (+). The extent and direction of solid solutions are indicated by dashed lines. The dotted line is a line of constant Ca/Al ratio: several of the silica rich phases, e.g. chabazite, plot on this line.

During preparation, dry solids were weighed out in air without special precautions but all other stages were performed under nitrogen to minimise carbonation. The samples were dispersed in solutions made up with double distilled, degassed water (DDW); sodium chloride and magnesium sulfate solutions were made from 'AnalaR' reagents. The 25°C samples were stored in low density polyethylene (LDPE, wide-mouth bottle, 125ml, No.2103-0004) bottles, supplied by Nalgene Labware and the 55°C samples were stored in high density polyethylene (HDPE, SQ. bottle 100ml. Code 460200) supplied by Kartell[1]. The 85°C samples were stored in Teflon (PTFE, 100 ml, No. BWN 124) bottles. During the programme, better quality leak-proof bottles were obtained from Azlon Products Ltd.

[1] These bottles were not as durable as expected. The Teflon bottles from Azlon, used at 85 °C, had a failure rate < 1%.

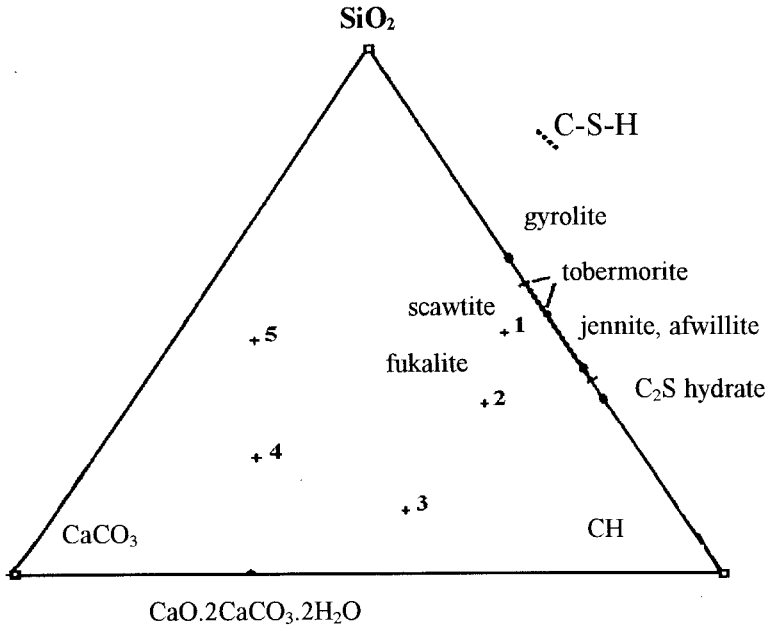

Figure 3.2 **Ternary diagram of the CScH ($CaO-SiO_2-CaCO_3-H_2O$) system: The compositions of crystalline hydrates known to occur at 50-90°C are shown by mineral or synthetic designations. Sample compositions are shown by (+). The cross hatched line shows the range of C-S-H line solid solutions, projected onto which are the compositions of several crystalline calcium silicate hydrates.**

Samples were allowed to equilibrate with intermittent agitation prior to analysis. None of the samples were redispersed. Where redispersed samples are used a fine balance exists to establish the optimal number of redispersions. On the one hand, redispersions help wash out impurities. For solids which dissolve congruently it is best therefore to redisperse a few times, so that the measured solubility relates to a single phase. On the other hand, if the solid dissolves incongruently each dispersion leaches the solid in a non-stoichiometric way, so that other phases will form, even if not initially present, and subsequent solubility measurements will relate to a phase mixture.

After equilibration the slurries were coarse filtered through Whatman grade 52 filter paper using a Buchner funnel with a vacuum pump. The separation was done warm, so that errors arising from temperature-dependent solubility changes were reduced. If the aqueous phase is allowed to cool, precipitation may occur but this can be avoided by immediately diluting the warm solution by a known factor. The solid and aqueous phases thus separated were dealt with as described in 3.3. Characterisation methods are described subsequently.

The systems chosen for investigation are given in table 3.1 for the cement hydrate series cured in NaCl, in table 3.2 for the cement hydrate series cured in $MgSO_4$ and in tables 3.4 and 3.5 for the phase formation series. As preparations cured in $MgSO_4$ underwent rapid Mg depletion, the systems had to be respiked (see section 3.4) to maintain the target

concentration. Because the need for respiking had not been foreseen at the outset, it greatly extended the complexity of the programme.

The pure hydrate cement phases at 55°C were respiked (table 3.2) but because of programme constraints they were not analysed in this project. Data are given in a thesis which was completed after the end of the project [1].

3.2 Cement Hydrate Phases: Synthesis

Cement hydrate phases were prepared as follows:

Calcium Silicate Hydrogel (C-S-H) and Calcium Hydroxide (CH)
C-S-H was prepared by the 'direct reaction' method: 1.0 grams of reactive SiO_2 (Aerosil 300) was mixed with appropriate amounts of CaO (obtained by firing 'AnalaR' $CaCO_3$ at 1000°C). Two grams of CaO were converted to $Ca(OH)_2$ by reaction with water and mixed with reactive SiO_2 to give molar Ca/Si ratios of 0.85, 1.1, 1.4 and 1.8. A constant 80 mls of DDW was added.

Because C-S-H is known to be strongly incongruent in its dissolution behaviour, whole samples were not redispersed. Instead, aliquots (~ 20 mls) of the slurry were taken. Thus the initial Ca/Si mole ratio of the solid was maintained.

Hydrogarnet (C_3AH_6)
C_3A was prepared by mixing stoichiometric amounts of 'AnalaR' $CaCO_3$ and Al_2O_3, fired consecutively at 800°C for one hour, 1000°C for 4 hours, and finally ignited at 1350°C. The product was checked for purity by XRD analysis, reground and ignited. This was repeated until phase pure C_3A was obtained. C_3AH_6 was synthesised by adding a portion of the C_3A to water (w/s ratio ~ 10) in a Teflon autoclave maintained at saturated steam pressure, 150°C, for 14 days. XRD analysis indicated that the product was pure C_3AH_6.

Ettringite (AFt)
AFt was synthesised by making a slurry of CaO at 5°C (w/s ratio = 10). To this was added a solution containing 'AnalaR' $Al_2(SO_4)_3 \cdot H_2O$, to give a $Ca:SO_4$ mole ratio of 2.0. This was stirred continuously for 24 hours, followed by ageing at 25°C. XRD analysis after 2 weeks showed phase pure AFt. Various preparations described in the literature use sugar to enhance Ca solubilities, but these preparations were deemed to be inappropriate for the present study as sugar cannot be completely removed.

Calcium Monosulfoaluminate (AFm-SO_4)
AFm-SO_4 was prepared from a portion of the AFt slurry, after vigorous agitation. The dry weight of AFt in an aliquot was estimated and a calculated amount of C_3A added sufficient to give pure AFm-SO_4:

$$C_3A\overline{S}_3H_{32} + 2C_3A \rightarrow 3C_4A\overline{S}H_{12}$$

The slurry was shaken continuously for 48 hours, followed thereafter by periodic shaking. After 2 weeks of ageing at 5°C, the product was phase-pure AFm-SO_4 was phase pure by XRD.

3.2.1. Phase Relations: Synthesis

CaO-Al_2O_3-SiO_2-H_2O System.
Slurry mixtures were prepared in DDW from CaO, reactive SiO_2 (Aerosil 300), and CERASOL boehmite, $AlO(OH)\cdot xH_2O$ (72.37 wt% Al_2O_3 by TGA). The compositions studied were designed to yield maximum information on phase development and relations in the CaO-Al_2O_3- SiO_2-H_2O system: figure 3.1 and table 3.4.

CaO-SiO_2-$CaCO_3$-H_2O System.
Slurry mixtures were prepared from CaO, reactive SiO_2 (Aerosil 300), $CaCO_3$ and DDW. Compositions studied were designed to determine whether (i) the known calcium silicate carbonate hydrates - scawtite, $(Ca_7(Si_6O_{18})(CO_3)\cdot 2H_2O)$ and fukalite, $Ca_4Si_2O_6(CO_3)(OH)_2$ - might form in saline solutions, and (ii) which phases might develop in the compositional zone of the reference backfill formulation. The compositional relationships are shown in figure 3.2 and table 3.5.

3.3. Analytical Techniques and Instrumentation

Solid Phases
Many of the cement phases are highly hydrated and alkaline in nature and are therefore prone to structural changes if dried too vigorously or exposed to atmospheric CO_2. Controlled drying conditions were employed to minimise these effects: solid phases were dried under nitrogen atmosphere, at a relative humidity of ~ 30%, maintained by equilibration with a saturated $CaCl_2$ solution. After drying, characterisation was carried out by one or more of the following methods.

X-ray diffraction (XRD)

Instrument: Philips Hägg-Guinier camera.
With this method crystalline material can be detected but nearly amorphous material is difficult to detect giving broad diffractions rather than reflections characteristic of crystalline material. Copper K alpha radiation was used throughout, with photographic recording of the spectra.

Symbols used to indicate the visual intensities of the reflections are as follows:

t	=	trace (barely visible)
W	=	weak
M	=	medium
S	=	strong
VS	=	very strong

Analytical Electron Microscopy (AEM)

Instrument: JEOL2000 EX Temscan microscope with a Link AN10000 analytical system. The analytical system is of the energy-dispersive type. With this method both crystalline and amorphous materials were chemically characterised in terms of ratios of elements with atomic numbers >10.

Thermal Analysis

Instrument: Stanton Redcroft STA 780 Thermal analyser. The analyser records simultaneously differential thermal, thermogravimetric and differential thermogravimetric traces. Thermal methods were used to determine the amount of calcium hydroxide and boehmite in the samples.

Nuclear Magnetic Resonance (NMR with MAS) for ^{29}Si and ^{27}Al

Samples were sent to the SERC facility at Durham Industrial Research Laboratory for analysis. The technique affords information on the co-ordination environments of Si and Al.

Aqueous Phase

Aqueous aliquots were passed through a 0.45 micron membrane filter (Millipore) to remove particulates and collected into sealed polythene tubes for analysis of dissolved components. All subsequent analyses were completed at room temperature within a 5 day period to minimise carbonation and precipitation effects.

Aqueous Ca and Mg were determined by atomic absorption spectroscopy with air/acetylene and nitrous oxide/acetylene flames respectively (Varian Spectra AA-10Plus). Na was analysed by flame emission spectroscopy (Corning 400 flame photometer). Si was determined using the molybdenum blue spectrophotometric method of Ramachandran and Gupta (2). Al was determined using the catechol violet spectrophotometric method of Dougan and Wilson (3). SO_4 and Cl were determined by anion chromatography using a Dionex 2010i.

pH:

pH was measured at 25°C with a Mettler Toledo pH combination electrode. K_w, the ion product of water, is markedly temperature dependent. Thus at 55°C its value (conventionally taken as 10^{-14} at 24°C) decreases to about $10^{-13.1}$. That is, at 55°C, the neutral point of water is close to pH 6.5. The equilibria between water and its dissociation products, H^+ and OH^-, is rapid and non-quenchable. Hence pH measured at ~24°C is not the same as that which would be measured at elevated temperatures.

In principle, pH can be measured directly at elevated temperature: glass electrodes have been widely used to determine the effect of temperature and pressure on the self-ionisation of water. But the electrode is not durable at high pH and elevated temperatures, so the reported pH values are obtained at 25°C without taking account of changing K_W with temperature. Values for charge balance and calculated pH were calculated using the following equation for charge balance: OH^- in mmol/l = 2[Ca] + 3[Al] + 4[Si] + [Na] + 2[Mg] -[Cl] -2[SO_4]. If this charge imbalance was too large the values were reviewed and in some cases the analysis was carried out again to check the results. The higher the total charge in solution, the higher

the charge imbalance is likely to be. For example, in highly saline environments a small percentage error can have a big influence on the imbalance: e.g. 3% of 3000 mmol/l = 90 mmol/l error. Since some of the other constituents are present at levels much less than 90 mmol/l, the charge balance is dominated by the high concentrations of Na and Cl. For pH, the calculated pH = 14 - (log[OH]), where [OH] is in molarity. It is suggested that charge balances are most useful as an indication of analytical precision in solutions of low ionic strength. As the ionic strength increases, small errors in measurement of other species present at high concentrations have a disproportionate effect on calculated [OH^-]. Moreover, the extent of bonding of OH^- to other species, e.g., Al is not known at elevated temperatures. However, since the calculations were done as a matter of routine, they are recorded.

Confidence limits
These are described in Appendix 1.

3.4 Kinetics and Respiking of $MgSO_4$ Systems

One aim of this project has been to determine the solubility and stability of selected pure cement hydrate phases and mixtures at selected concentrations of $MgSO_4$. The rationale for this approach is two-fold. Firstly, incoming groundwater will have an essentially fixed composition and it must be presumed that there is a semi - infinite mass of groundwater relative to backfill. Secondly, it is established methodology to restrain the composition of one or more components in the aqueous phase in order to study a complex system. As will be shown, the use of compositional restraints complicates the experiments but to a lesser extent also complicates the interpretation of results. However, due to rapid depletion of the aqueous concentration of both Mg and SO_4 ions, not necessarily at the same rate, it was necessary to reassess the experimental programme. The experiments could have continued at a *fixed total number of moles* of Mg but, given the openness of the most groundwater systems, it was decided instead to maintain the Mg *concentration.* This necessitated respiking the systems with $MgSO_4$. It was concluded that the best procedure for respiking was to add solid $MgSO_4$ (as AnalaR magnesium sulfate heptahydrate) while maintaining a nitrogen atmosphere, even though that meant that the SO_4 concentration might exceed the target concentration. To save time and limit the risk of 'overspiking', and to determine the appropriate respiking interval, a knowledge of how fast the aqueous phase would deplete in Mg was desirable. Besides, it provides background information on what might happen in a repository scenario when, for example, Mg-containing groundwater migrates/diffuses through a permeable backfill or cracks in dense concrete.

3.4.1 Kinetics

The kinetic experiments were carried out at 25°C on freshly prepared samples. In order to establish which systems would provide the most valuable information, computer calculations were carried out to determine the threshold concentration of magnesium required for selected reactions to occur; see the relevant sections in section 4. Furthermore, mass balance calculations serve to highlight those systems which would be expected to deplete most in magnesium; see Appendix 3.

The experiments were constructed from these scoping exercises. After a known curing time the systems were analysed for magnesium and the remaining aqueous volumes estimated to

calculate the respike. The estimations of the remaining volumes are the most significant source of error because the estimation has to be carried out after each analysis and errors tend to be cumulative. The systems were then respiked to the target concentration, shaken vigorously for a period of ~ 2 minutes and cured for a definite time with occasional agitation. The process of respiking, shaking, curing and analysis was repeated until the magnesium concentration no longer diminished significantly from the target value; figure 3.3 illustrates schematically the concentration changes.

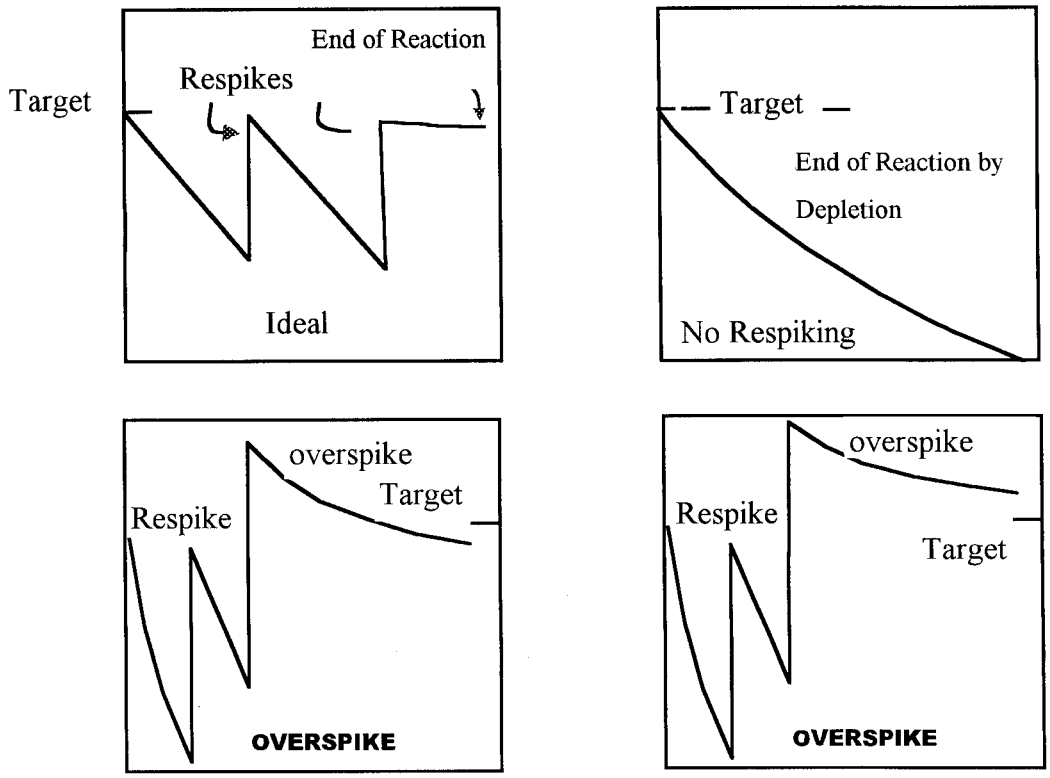

Figure 3.3: Illustration of the respiking procedure, showing (top left) the ideal respiking situation, the situation without spiking (top right) and the overspiking situation, where the target concentration is slightly underachieved or slightly exceeded (lower left and right, respectively). The y axis is time.

3.4.2 Respiking

The actual systems were respiked the numbers of times the kinetic experiments indicated to be necessary and the aqueous phase analysed for all relevant elements. The solids were characterised by XRD and, where necessary, by AEM.

The calculated number of respikes required did not always take the reaction to completion. Three criteria were defined any one of which, if satisfied, was deemed to justify termination of an experiment:

- the magnesium concentration had reached the target concentration, or
- the solid reactant had been completely consumed (non-detectable by XRD), or
- the pH of the solution (leachant) had decreased to 9 or less.

References

1. K. Goldthorpe. (1998) 'Stability of Cementitious Materials in Saline Environments'. PhD Thesis, University of Aberdeen.

2. R. Ramachandran and P.K. Gupta. (1985) 'An Improved Spectrophotometric Determination of Silicate in Water Based on Molybdenum Blue'. Anal. Chim. Acta **172**, pp. 307-311.

3. W.K. Dougan and A.L. Wilson. (1974) ' The Absorptiometric Determination of Al in Water. A Comparison of some Chromogenic Reagents and the Development of an Improved Method'. Analyst **99**, 413.

4. RESULTS AND DISCUSSION

4.1 Cement Hydrate Phases: Solubility Determinations and Stabilities

4.1.1 C-S-H and Calcium Hydroxide

4.1.1.1 Introduction and Background

Calcium Silicate Hydrogel (C-S-H), together with calcium hydroxide, are the most important pH buffers in the near field; models of pH evolution by Atkinson [1], Berner [2], Glasser [3] and Neall (4) predict maintenance of pH >11 to persist in the long term, principally through C-S-H dissolution at 25°C. In this context "long term" is after $Ca(OH)_2$ dissolution occurs.

C-S-H has low crystallinity. There is debate about its degree of crystallinity, which is difficult to characterise: NMR shows the extent of silicate polymerisation to increase with decreasing Ca/Si ratio, as might be expected from the chemistry, but there are also suggestions that at a fixed Ca/Si ratio, the polymerisation state of silica increases with ageing. Formation of short chain silicate species linked to $Ca(OH)_2$ sheets, suggested as a structural model, supports the supposed close structural relationships between C-S-H gel and crystalline calcium silicate hydrates, tobermorite (Ca/Si ratio ~ 0.9) and jennite (Ca/Si ratio ~ 1.5).

There are also disagreements about the variation in C-S-H properties with composition. Most modellers have treated C-S-H as a regular solid solution, i.e. its properties vary smoothly with composition. However, recent NMR studies [5] claim that a discontinuity in properties occurs at Ca/Si ratio = 1.0; also that the composition of the aqueous phase exhibits a change in slope at this ratio.

C-S-H gel, although known to be very persistent in nature at 10 - 20°C, is metastable with respect to crystalline phases such as tobermorite, jennite and afwillite, see figure 4.1.

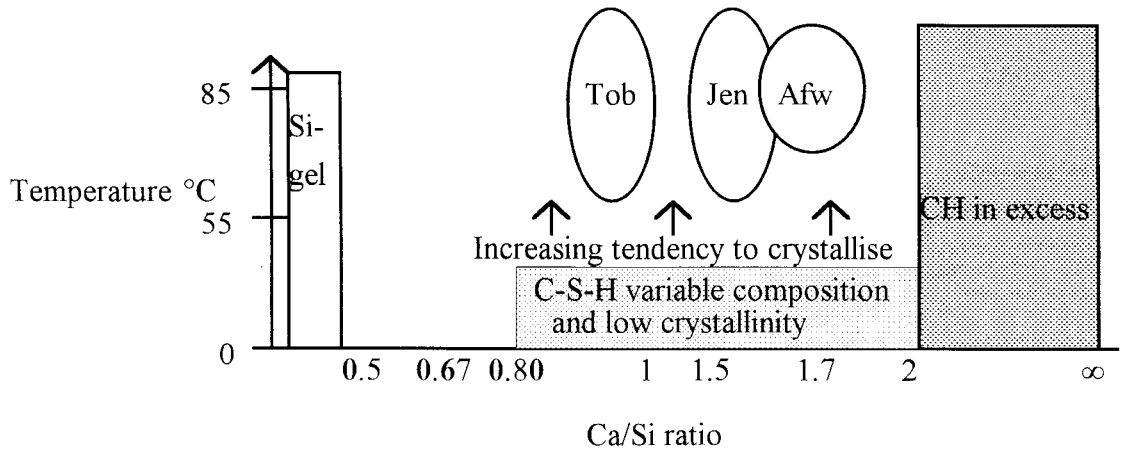

Figure 4.1 Illustration of calcium silicate hydrates formed at temperatures 100°C during prolonged warm cure. Once formed, crystalline hydrates will persist even though the temperature decreases.

C-S-H rich assemblages occur in historic analogues, as at Hadrian's wall [6] and in natural analogues, as at Scawt Hill in Northern Ireland [7]. Another interesting natural analogue occurs at Maqarin, in northern Jordan, [8] where both tobermorite and C-S-H are being precipitated directly from warm aqueous solutions.

Since a repository containing heat-producing wastes will experience a thermal pulse, in one scenario giving temperatures up to ~ 80°C for approximately the first 100 years followed by a slow decay back to ~ 25°C [9], the assumption of C-S-H persistence strongly comes into question. Possible salinity [10] introduces additional uncertainty. Previous work [11] at elevated temperatures (50-90°C) showed that C-S-H underwent partial crystallisation to semi-crystalline tobermorite, afwillite and C-S-H I, the nature of the product depending on the C/S ratio of the precursor gel. At a fixed composition, equilibrium pH in these systems is lowered by at least 0.5-1.0 pH unit as a consequence of crystallisation.

There are no quaternary phases known to exist within the $CaO\text{-}SiO_2\text{-}CaX\text{-}H_2O$ system at temperatures <100°C; X is sulfate, carbonate or chloride. The implication of this is that any attack by the anions listed would have a minimal effect on the phase composition of the system (but not necessarily on solubilities or crystallisation kinetics) until a threshold is attained above which the C-S-H phases are no longer stable [12,13].

In this section we report on the:

- interaction of two selected salts, NaCl and $MgSO_4$, with C-S-H and CH.
- effect on solubility and ability to buffer pH of C-S-H and CH in saline environments at three isotherms (25°, 55°, 85°C).
- uptake of the ions, especially of Na, into C-S-H and other solids.

4.1.1.2 Solubility Data, pH and Solid Phase Compositions for NaCl Systems

25°C Isotherm

Solubility data for C-S-H and CH in double distilled, degassed water (DDW), 0.5, 1.0 and 1.5 M NaCl at 25°C are given in table 4.1: figures 4.2.a and 4.2.b show the solubility equilibria for the gels and CH aged in these solutions. The notionally chloride - free samples do, on analysis, appear to contain some chloride, the source of which is not known.

The data indicate that in NaCl solutions, C-S-H gels and CH display similar solubility trends to those in water: Ca solubility increases and Si decreases with increasing solid Ca/Si ratios. However, absolute Ca and Si concentrations differ: calcium solubility is enhanced in NaCl by the increased electrolyte concentration. Thus for a given Ca/Si ratio, as the NaCl content increases Ca solubility is enhanced. This enhancement is greatest at low Ca/Si ratios: for example, at Ca/Si = 0.85, from 1.25 mmol/l in DDW to 16.09 mmol/l at [NaCl] ~ 1.5 mol/l. The enhancement is roughly proportional to the NaCl concentration: see figure 4.2.a. Silica solubility (table 4.1 and figure 4.2.b), on the other hand, is depressed slightly.

Table 4.1 **C-S-H samples cured at 25°C in DDW and NaCl solutions. C-S-H 0.85, C-S-H 1.1 and CH were analysed after 4.5 months and C-S-H, ratio 1.4 and 1.8, after 9 months.**

Target C/S ratio	Initial [NaCl] mol/l	pH	Aqueous Characterisation, mmol/l				charge imbalance OH, mmol/l	% Na apparent uptake	%Cl apparent uptake
			Na	Cl	Ca	Si			
0.85	0	11.65	<0.09	0.08	1.25	0.28	3.6	-	-
	0.52	11.20	489	453	11.58	0.16	60	1.4	3.0
	1.05	11.14	799	784	12.62	0.19	41	11.2	11.9
	1.46	11.02	1330	1359	16.09	0.17	3.9	5.8	4.5
1.1	0	12.20	0.74	0.75	5.49	0.03	11.09	-	-
	0.52	12.11	435	348	14.80	0.03	117	3.2	6.8
	1.05	12.14	921	880	17.71	0.03	77	11.1	6.7
	1.46	12.12	1283	1373	19.79	0.04	-50	13.8	3.4
1.40	0	12.52	0.61	0.71	12.09	0.04	24	-	-
	0.52	12.41	435	464	14.47	0.04	0.1	3.0	1.9
	1.05	12.41	870	882	19.48	0.02	27	6.2	5.8
	1.46	12.32	1381	1381	21.28	0.02	43	2.7	2.7
1.80	0	12.54	9.48	10.15	16.33	0.01	32	-	-
	0.52	12.50	460	467	22.77	0.02	39	1.8	1.6
	1.05	12.50	890	921	25.17	0.01	19	4.8	3.9
	1.46	12.40	1440	1401	25.84	0.02	91	0.6	1.8
CH	0	12.50	2.27	2.00	20.11	-	40	-	-
	0.52	-	495	489	27.70	-	61	1.0	1.3
	1.05	-	995	924	26.40	-	124	2.2	5.0
	1.46	12.41	1402	1352	26.60	-	103	2.3	4.3

The trends of both Ca and Si solubilities in NaCl are opposite those of C-S-H in NaOH (13) where, with increasing NaOH concentrations, Ca solubility is depressed while Si solubility is enhanced.

The effects on pH are shown in table 4.1 and figure 4.2.c. This shows that pH values are slightly reduced, relative to water, by ~ 0.4 pH units for Ca/Si ratio 0.85 and by ~ 0.2 pH units at higher Ca/Si ratios.

Figure 4.2.a Calcium solubility in C-S-H cured at 25°C, as a function of Ca/Si ratio and initial NaCl concentration.

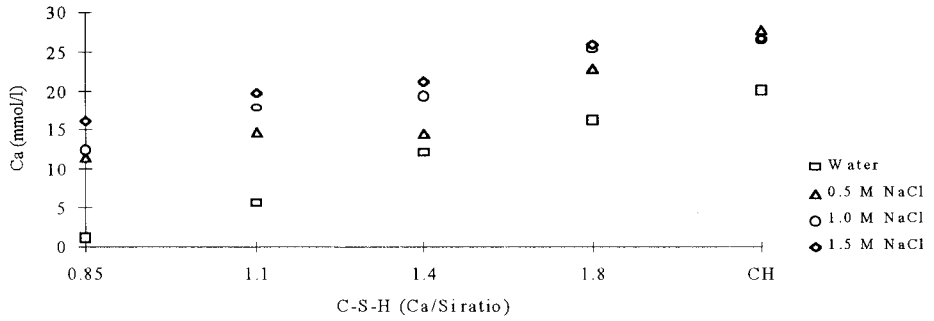

Figure 4.2.b Silica solubility in C-S-H cured at 25°C, as a function of Ca/Si ratio and initial NaCl concentration.

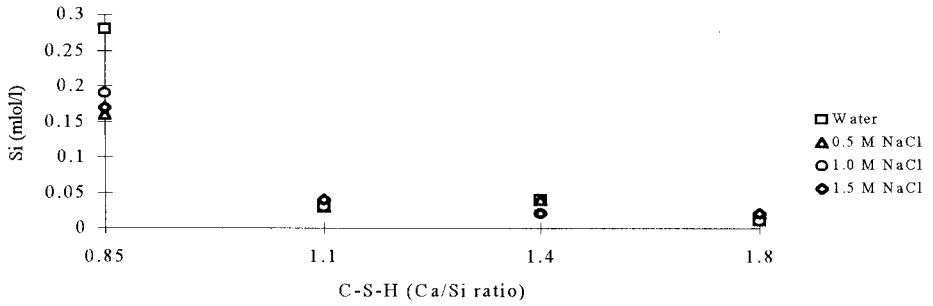

Figure 4.2.c pH of C-S-H cured at 25°C, as a function of Ca/Si ratio and initial NaCl concentration.

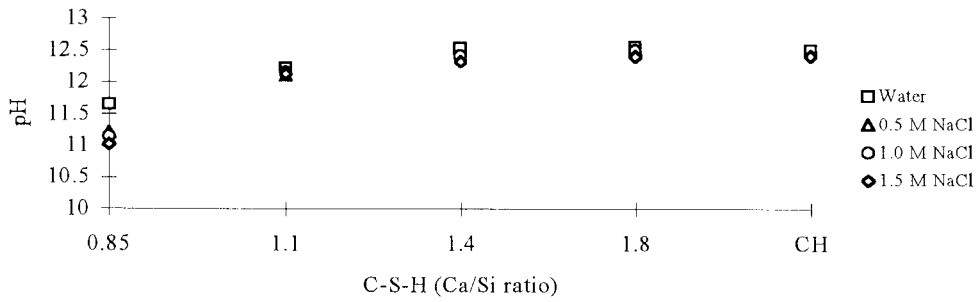

This reduction is insignificant and furthermore may not be real since the glass electrodes used to measure pH are also somewhat sensitive to sodium. Thus measurements of $[H^+]$ and, in turn, of pH are less reliable at high ionic strengths and particularly, high $[Na^+]$. Newton and Sykes [14] found that adding NaCl to a saturated $Ca(OH)_2$ solution did not significantly alter the pH, measured with a selective electrode. Our measurements on the CH systems also show no major alteration of pH. From Newton and Sykes' calibration curve, it is apparent that conventional glass electrodes begin to be non-linear at pH $\geq$12, approximately. Since most of our pH measurements lie in the range above pH 12, the lowered pH in NaCl solutions may not be significant, especially as the changes are within the error-bars of the measurements.

The calculated data in table 4.1 indicate that the extent of sodium uptake by the solid phase is low. The calculated amount is termed "apparent uptake" as the calculation assumes the mass of sorbent to remain constant (see calculations in Appendix 2). But in practice the solid dissolves to some extent. Since the solid contains water (among other constituents), the dissolution process slightly dilutes the aqueous solution. The calculation shows this as an apparent uptake but the real uptake must be less. It is difficult to determine exactly the correction factor but it is believed to be slight. The apparent uptake of sodium does, however, exceed the limits of measurement error.

Direct analysis of the gel for Na and Cl is not helpful. When analysed by AEM, gels contain small crystals of NaCl which indicate that much (or all) of the sodium and chloride measured are physically occluded in the C-S-H gel. In other studies [13] Na uptake is reported to increase with decreasing Ca/Si ratio, but this trend is for solids in contact with NaOH and may not be applicable to NaCl.

Kurdowski and Duszak [15] immersed C-S-H cubes with Ca/Si ratio, initially 1.0, in concentrated chloride solutions at 20°C. The solution composition (in g/l) was: NaCl, 195; $MgCl_2$, 77; KCl, 98; $MgSO_4$, 3; KBr, 8. They found that the C-S-H phase was unaltered by chloride. In dilute solutions, however, chloride was adsorbed in the C-S-H phase. They found that the outer layer of C-S-H was depleted in Ca and its Ca/Si ratio decreased to ~ 0.5. They did not observe either uptake of Na into the C-S-H gel or the formation of crystalline basic calcium chlorides.

X-ray analysis of the gels and of CH cured in 0.5, 1.0 and 1.5 M NaCl at Aberdeen University showed very similar results to those obtained by curing C-S-H and CH in pure water (table 4.2), i.e. the products were 'C-S-H (I)' [16] and CH . At Ca/Si ratio 1.8, $CaCO_3$ was observed as a contaminant.

The data for NaCl show that no phase changes occur even in 1.5M NaCl; C-S-H is persistent. However, for C-S-H 1.4 in 0.5 M and 1.0 M NaCl, two unassigned X-ray d-spacings were identified, at 2.73Å and 3.55Å. Analysis in AEM could not distinguish a phase responsible for these reflections. It was found that the composition of the C-S-H 1.4 gel cured in 1.0M NaCl decreased to C-S-H 1.1. This corresponds to the analysis of the aqueous phase which indicates incongruent dissolution.

After 4.5 months curing of C-S-H 0.85 in 1.5 M NaCl, its solid Ca/Si ratio was ~ 0.84 and its morphology showed crumpled foils typical of C-S-H(I). The diffraction pattern agrees well with Taylor's X-ray powder data for C-S-H (I) [16, p.372]. Its d-spacings were: 5.55, 5.43, 5.03, 3.15, 2.82 and 1.9 Å. Thus C-S-H has partially crystallised.

To investigate the Na and Cl uptake further, more of the samples were analysed by AEM. The sample were collected under nitrogen, initially as a mixture of liquid and solid. Attempts to analyse the solids without washing were not successful as the NaCl crystals interfered with analysis, so samples were washed twice in DDW. The samples were centrifuged between washings and, after washing, quenched in isopropanol.

Table 4.2 Solid characterisation of C-S-H and CH cured in water and NaCl solutions for 4-5 months at 25°C.

Target Ca/Si	Initial NaCl mol/l	CH	C-S-H(I)	Cc	NaCl	Other
0.85	0		M			
	0.52		M		S	
	1.05		M		S	
	1.46		M		S	
1.1	0		S			
	0.52		S		S	
	1.05		M		S	
	1.46		M		S	
1.40	0		S			
	0.52	M	S		S	3.55 Å
	1.05		M		S	3.55 Å
	1.46	W	M		S	
1.80	0	S	M	S		
	0.52	M	M		S	
	1.05	M	S			
	1.46	M	M	S	S	
CH	0	S				
	0.52	S			S	
	1.05	S			S	
	1.46	S			M	

The Na and Cl levels in the analysed solid were very small, typically < 1.5%. The Na/Cl ratio is approximately 1.0. The conclusion is that no significant Na or Cl uptake by the C-S-H gel occurs but that some solid NaCl is precipitated during specimen drying.

SUMMARY OF THE 25°C RESULTS:

- Ca solubility increases with increasing Ca/Si ratio, while Si solubility decreases
- Solubility at Ca/Si ratios > 1.4 is dominated by Ca dissolution
- Ca solubility increases with increasing NaCl concentration, markedly so at low Ca/Si ratios.
- Si solubility, shown in figure 4.2b, is depressed slightly with increasing NaCl concentrations up to 1.5 M.
- Dissolution is incongruent, most especially at high Ca/Si ratios where aqueous Ca>>Si,
- Na and Cl uptakes by solid C-S-H are negligible.
- pH is lowered by approximately 0.4 units at low Ca/Si ratio and 0.2 for higher Ca/Si ratios, but the apparent decrease may be due to the electrode being sensitive to sodium as well as to hydrogen ions.

- No phase changes occur at any NaCl concentrations up to 1.5 M.
- Low-ratio C-S-H gel partially crystallises, to C-S-H I, in NaCl.

55°C Isotherm

Solubility data for C-S-H and CH in initially double distilled, degassed water (DDW), in 0.42 and 1.35 M NaCl are given in table 4.3.

Table 4.3 CSH samples cured at 55°C in DDW and NaCl solutions. Curing time, 190 days.

Target Ca/Si ratio	Initial [NaCl] mol/l	pH	Aqueous Characterisation mmol/l				charge balance OH, mmol/l	calc. pH	% Na apparent uptake	% Cl apparent uptake
			Na	Cl	Ca	Si				
0.85	0	11.46	0.04	0.03	1.02	0.2	2.9	11.45	-	-
	0.42	10.86	430	449	9.56	0.29	1.3	11.11	-1.43	-1.29
	1.35	10.81	1363	1455	14.55	0.23	-62	-	-0.58	-4.68
1.1	0	12.02	5.74	5.64	2.72	0.08	5.9	11.77	-	-
	0.42	11.96	419	434	11.88	0.05	9	11.95	0.04	-0.55
	1.35	11.73	1299	1373	16.39	0.04	-41	-	2.01	-0.91
1.4	0	12.3	1.72	1.54	9.96	0.01	20	12.3	-	-
	0.42	12.25	435	462	14.67	0.02	2.4	11.38	-0.52	-1.45
	1.35	12.02	1285	1267	16.44	0.02	51	-	2.25	2.88
1.8	0	12.56	0.37	0.26	13.67	0.01	27	12.44	-	-
	0.42	12.41	430	413	17.67	0.01	52	12.72	-0.3	0.21
	1.35	12.21	1267	1339	17.69	0.01	-37	-	2.48	0.33
CH	0	12.5	4.18	4.14	14.42	-	29	12.46	-	-
	0.42	12.41	447	475	21.86	-	16	12.2	-1.08	-2.2
	1.35	12.41	1206	1269	23.6	-	-39	-	5.76	3.24

Figures 4.3.a and 4.3.b show the solubility equilibria for the gels and CH aged for 190d. The corresponding aqueous phases pH values are shown in table 4.3 and figure 4.3.c.

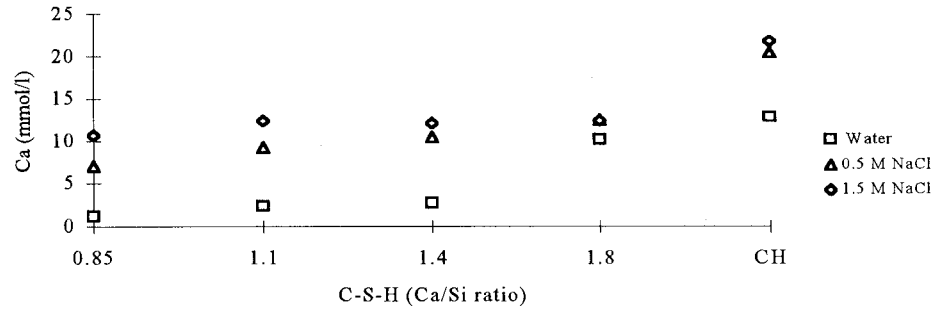

Figure 4.3.a Calcium solubility in C-S-H cured at 55°C as a function of Ca/Si ratio and initial NaCl concentration.

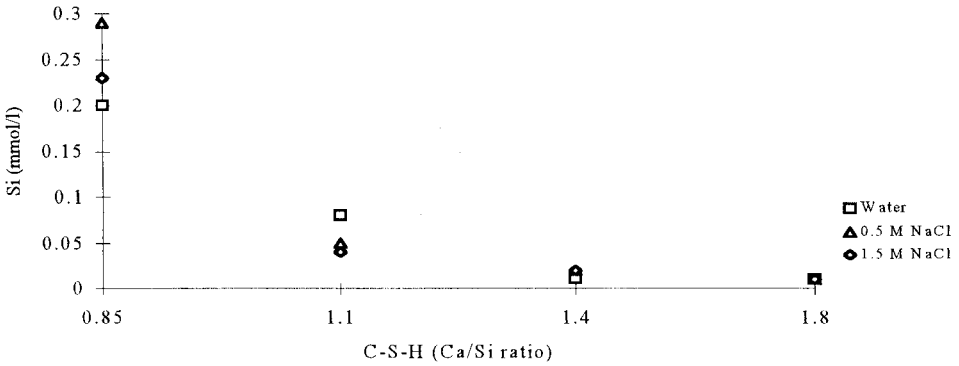

Figure 4.3.b Silicate solubility in C-S-H cured at 55°C, as a function of Ca/Si ratio and initial NaCl concentration.

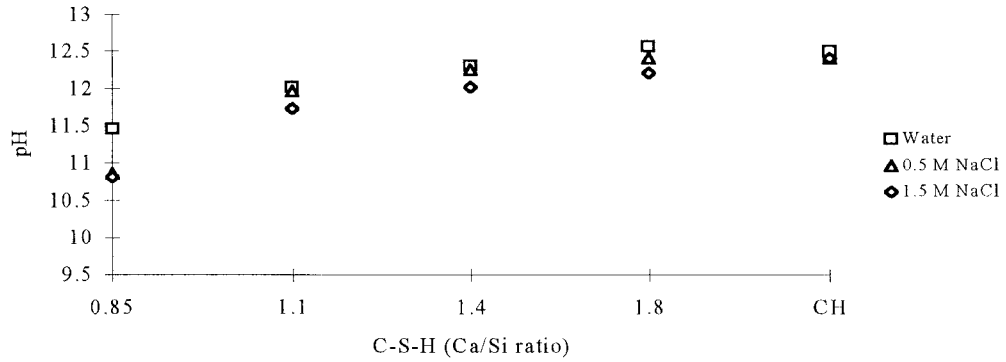

Figure 4.3.c pH in C-S-H cured at 55°C, as a function of Ca/Si ratio and initial NaCl concentration. pH is measured at 25°C.

Solution properties are normally reported in terms of two functions: measured species concentrations and pH. The numerical values recorded from samples equilibrated at elevated temperatures require comment. Solution compositions were determined following separation by filtration of aqueous phases from the coexisting solids. The separation was done warm to eliminate errors arising from temperature-dependent solubility changes.

If the aqueous phase is allowed to cool, precipitation may occur. Errors arising from precipitation can be avoided by spiking the solution with a known aliquot of acid while warm or simply by diluting the solution by a known factor, introduction of which enables the original solution composition to be unequivocally determined.

The pH function is however less straightforward, as described in Appendix 1. Table 4.3 and figure 4.3.c show that pH apparently decreases, but only slightly, with increasing NaCl concentrations, e.g. for C-S-H 1.8, 12.56 decreasing to 12.21. For low Ca/Si ratios, the decrease is typically ~0.6 pH unit. As discussed previously these changes are not necessarily significant and the principal conclusion which emerges is that despite high NaCl concentrations, sacrificial dissolution of C-S-H conditions the solutions to a high pH. Partial crystallisation does not significantly alter pH; high pH is maintained by the presence of the residual unaltered, amorphous material. Complete crystallisation is, however, expected to lead to lower pH's, perhaps by 1 unit [11].

The agreement between measured pH and calculated pH in water and at low NaCl concentrations is good. The values diverge as NaCl concentrations increase because at higher concentrations [OH^-] is small compared with [NaCl]: small experimental errors in either or both Na or Cl concentrations have a profound affect on the calculated [OH^-]: %Na and %Cl uptakes are also given in table 4.3. These were calculated to determine the decrease in the aqueous NaCl concentration, to ensure that batch compositions had not departed appreciably from the target molarity.

Table 4.4 shows the results of the solid analysis. The NaCl, detected in the solid phase by XRD and AEM, is attributed to crystallisation upon drying. Prolonged 55°C cure in water results in partial crystallisation: C-S-H 0.85 gives tobermorite while C-S-H 1.1 gives jennite. No crystallisation was observed at higher C-S-H ratios. Ca solubility for Ca/Si ratio > 1.8 is dominated by $Ca(OH)_2$ dissolution. Crystallisation of tobermorite and jennite is inhibited in NaCl-cured samples. Although any one C-S-H may change its composition as a consequence of partial incongruent dissolution, the final composition of at least one sample should be appropriate for crystallisation of tobermorite or jennite. That crystallisation did not occur indicates inhibition, perhaps as a result of forming semi-crystalline C-S-H I.

Table 4.4 Solid characterisation of C-S-H and CH cured in water and NaCl solutions at 55°C: ✓ = present.

Target Ca/Si ratio	Initial [NaCl] mol/l	CH	C-S-H(I)	Tobermorite	Jennite	NaCl	$CcCO_3$
0.85	0		✓	W/M			
	0.42		✓			W	
	1.35		✓			M	
1.1	0		✓		M		
	0.42		✓			W/M	
	1.35		✓			M	
1.40	0		✓				
	0.42		✓			W	
	1.35		✓			M	
1.80	0	W/M	✓				
	0.42	W	✓			W	
	1.35	W	✓			M	
CH	0	VS					trace
	0.42	S					
	1.35	S					

SUMMARY OF THE 55°C RESULTS:

Trends occurring at 25°C are also observed at 55°C. These are:

- Ca solubility increases with Ca/Si ratio, while Si solubility decreases,
- Solubilities at Ca/Si ratios > 1.4 are dominated by Ca dissolution,
- Ca solubilities increase with increasing NaCl concentrations, most markedly at low Ca/Si ratios.
- Si solubilities are slightly reduced at increased NaCl concentration.
- Dissolution is incongruent, especially at high Ca/Si ratios where aqueous Ca>>Si,
- pH is lowered by approximately 0.6 at low Ca/Si ratios and by ~0.3 for higher Ca/Si ratios but the apparent decrease may be due to the electrode response, which is affected by increasing $[Na^+]$.
- C-S-H 0.85 gives tobermorite and C-S-H 1.1 gives jennite in H_2O. No crystallisation was observed at higher Ca/Si ratios.

85°C Isotherm

Solubility trends similar to those at 25°C and 55°C were observed for samples cured at 85°C: see Table 4.5 and figures 4.4.a and 4.4.b.

Table 4.5 C-S-H cured at 85°C in DDW and NaCl solutions. Curing time 145 days.

Target Ca/Si ratio	Initial [NaCl] mol/l	pH*	Aqueous Characterisation, mmol/l				charge imbalance OH,mmol/l	% Na apparent uptake	%Cl apparent uptake
			Na	Cl	Ca	Si			
0.85	0	11.66	1.59	1.69	1.16	0.08	2.5	-	-
	0.52	11.28	442	486	7.06	0.13	-29	3.48	1.51
	1.46	10.09	1457	1507	10.62	0.19	-28	0.13	-2.1
1.1	0	11.91	1.13	1.12	2.36	0.08	5.1	-	-
	0.52	11.92	435	475	9.21	0.09	-21	3.36	1.78
	1.46	11.85	1327	1451	12.33	0.06	-99	5.25	0.36
1.40	0	12.08	1.15	1.15	2.72	0.07	5.7	-	-
	0.52	12.30	442	484	10.38	0.03	-21	2.71	1.25
	1.46	12.21	1392	1507	12.08	0.03	-91	2.36	-1.63
1.80	0	12.42	0.27	0.21	10.13	0.02	20	-	-
	0.52	12.42	401	436	12.43	0.03	-10	3.55	2.51
	1.46	12.26	1348	1451	12.38	0.02	-78	3.34	0.27
CH	0	-	0.16	0.10	12.77	-	26	-	-
	0.52	12.54	489	524	20.36	-	5.7	1.24	-0.16
	1.46	12.42	1435	1535	21.71	-	-57	1.00	-3.00

*Measured at 25 °C

Figure 4.4.a Calcium solubility in C-S-H cured at 85°C, but measured at 25 °C as a function of Ca/Si ratio and initial NaCl concentration.

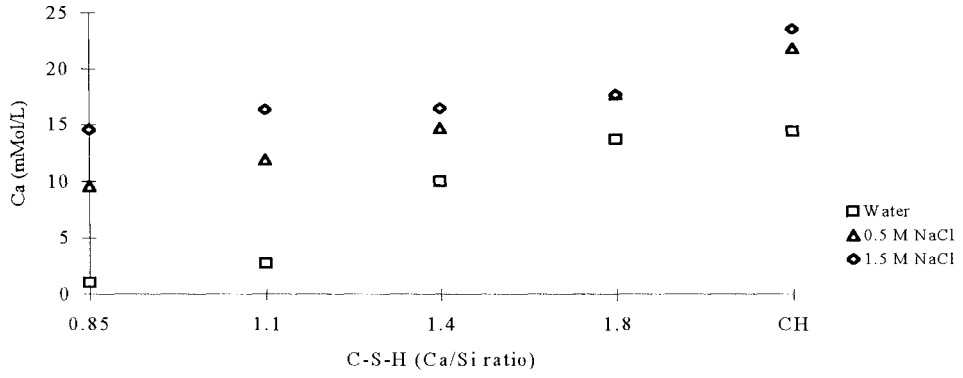

Calcium solubilities increased with increasing NaCl concentrations, while Si solubilities are not much affected except at low Ca/Si ratio where silicon solubility increases from 0.08 mmol/l in DDW to 0.19 mmol/l in 1.5 M NaCl.

The measured pH's are shown in table 4.5 and figure 4.4.c: pH remains nearly constant with increasing NaCl concentration, changing from 12.42 to 12.26 at C-S-H 1.8 and by ~ 0.6 pH at Ca/Si ratio 0.85.

Figure 4.4.b Silica solubility in C-S-H cured at 85°C, but measured at 25 °C, as a function of Ca/Si ratio and initial NaCl concentration.

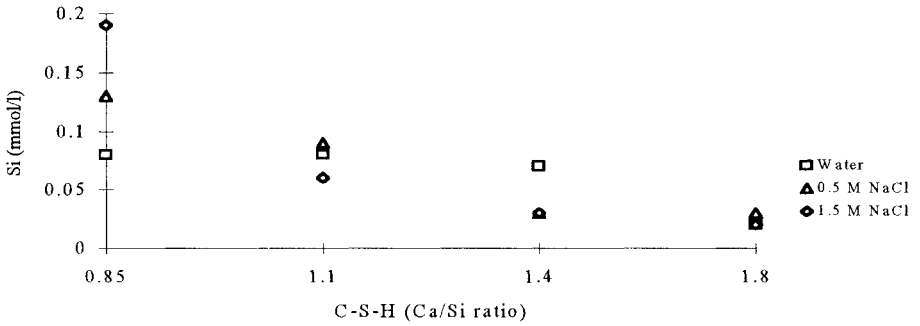

Figure 4.4.c pH of aqueous solution coexisting with C-S-H cured at 85°C, but measured at 25°C.

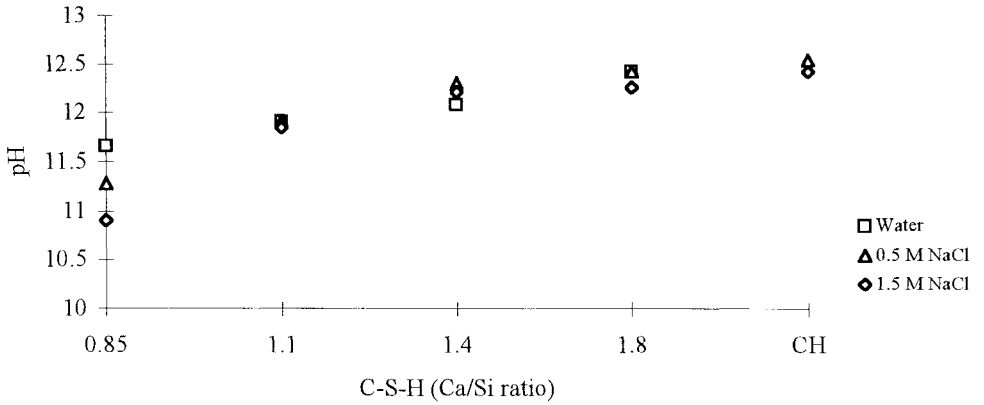

Table 4.6 Solid characterisation of C-S-H and CH cured in water and NaCl solutions at 85°C.

Target Ca/Si ratio	Initial [NaCl] mol/l	CH	C-S-H(I)	Tobermorit	Jennite	Afwillite	NaCl
0.85	0		S	S			
	0.52		S	S			S
	1.46		M	S			S
1.1	0		M		W		
	0.52		M				S
	1.46		S				S
1.40	0	W			S		
	0.52		M		M		S
	1.46		S				S
1.80	0	S	M			M	
	0.52	S	M				S
	1.46		M				S
CH	0	S					
	0.52	S					
	1.46	S					S

Table 4.6 shows the results of the solid analysis. NaCl is attributed to crystallisation on drying.

Partial crystallisation of C-S-H occurs but decreases in extent with increasing Ca/Si ratio. The nature of the crystalline product depends on Ca/Si ratio: at 0.85 it is tobermorite but at higher ratios, jennite or afwillite occur. For example, jennite occurs for C-S-H 1.1 in water and C-S-H 1.4 in both water and 0.5 M NaCl. Afwillite crystallises at Ca/Si ratio 1.8 cured in water. The remaining gel somewhat improves in crystallinity and C-S-H (I) is observed throughout.

Most samples show a tendency to crystallise more slowly in NaCl than in H_2O: note, for example, C-S-H 1.4, where jennite is prominent after curing in water, less so in 0.5M NaCl and apparently absent in 1.5M NaCl.

SUMMARY OF THE 85°C RESULTS:

- Ca solubility increases with Ca/Si ratio, while Si solubility decreases
- Solubility for Ca/Si ratios > 1.4 is dominated by Ca dissolution
- Ca solubility increases with increasing NaCl concentration, markedly so at low Ca/Si ratios
- Si solubility is not much affected by the NaCl concentration except at low Ca/Si ratio where its solubility increases with increasing [NaCl]
- dissolution is incongruent, especially at high Ca/Si ratios where aqueous Ca>>Si
- pH is lowered by approximately 0.6 for low Ca/Si ratio and 0.2 for higher Ca/Si ratios but the apparent decrease may be due to electrode selectivity
- C-S-H 0.85 crystallises yielding tobermorite, while C-S-H 1.1 and 1.4 give jennite and C-S-H 1.8 gives afwillite.
- Crystallisation is inhibited by increasing aqueous NaCl concentrations.

Overall Summary of Solubility Data and Solid Phase Compositions for NaCl Systems.

It was found that the solubility of Ca in C-S-H and CH increases with increasing NaCl concentration, most markedly at low Ca/Si ratios. Si solubilities are not much affected by changing NaCl concentrations. NaCl inhibits crystallisation of tobermorite, jennite and afwillite at and above 55°C.

The following five figures illustrate the trends for the solubility data and the solid phase compositions for C-S-H and CH cured in NaCl at the three selected temperatures for 145d.

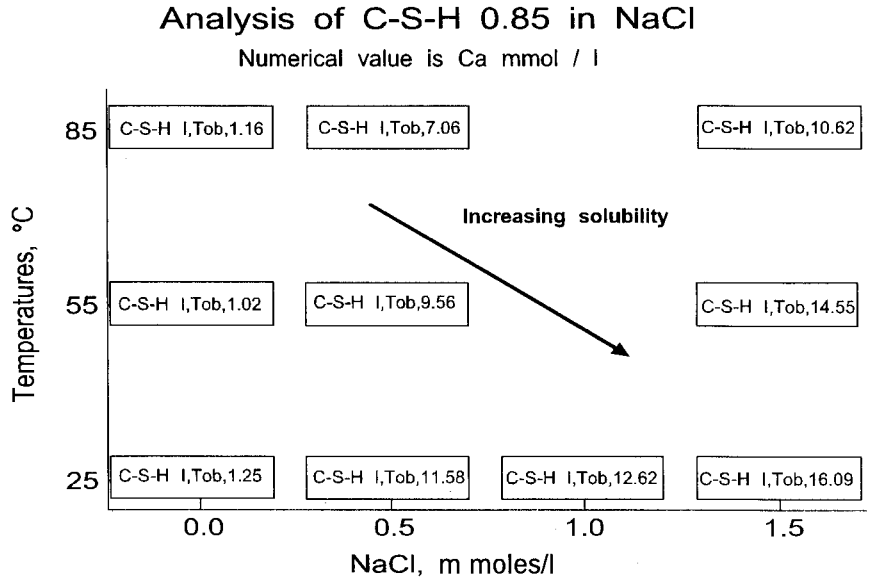

Figure 4.5.a Summary of solid and aqueous analyses of C-S-H 0.85 in NaCl at 25°, 55° and 85°C.

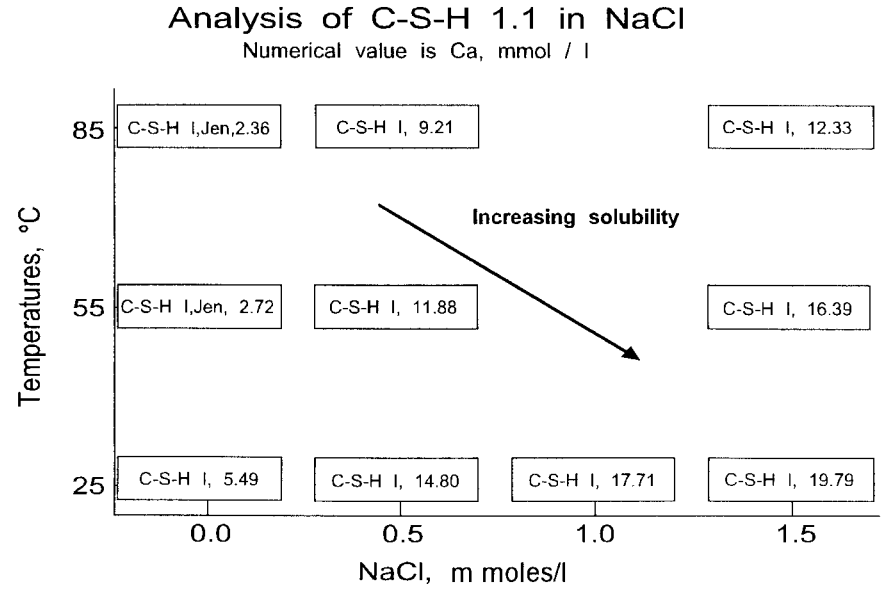

Figure 4.5.b Summary of solid and aqueous analyses of C-S-H 1.1 in NaCl at 25°, 55°and 85°C.

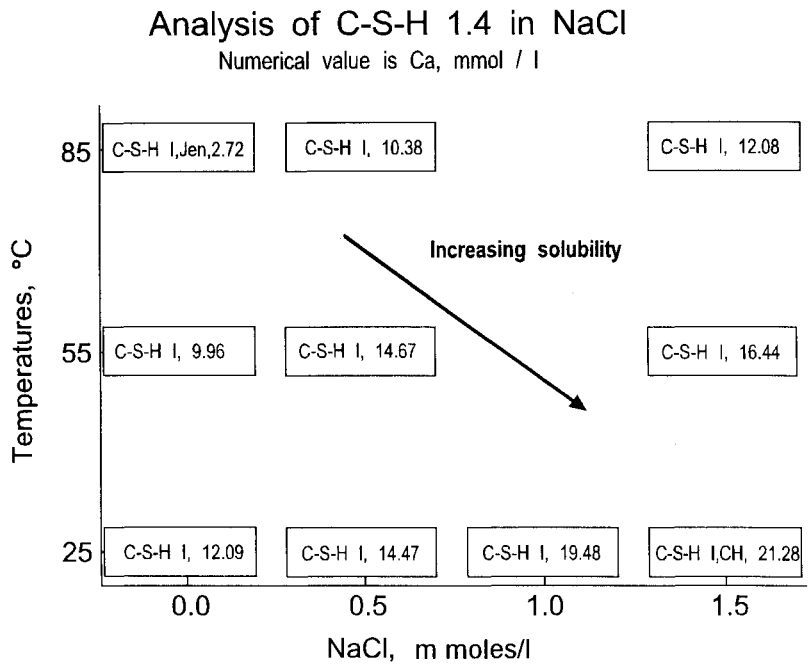

Figure 4.5.c Summary of solid and aqueous analyses of C-S-H 1.4 in NaCl at 25°, 55° and 85°C.

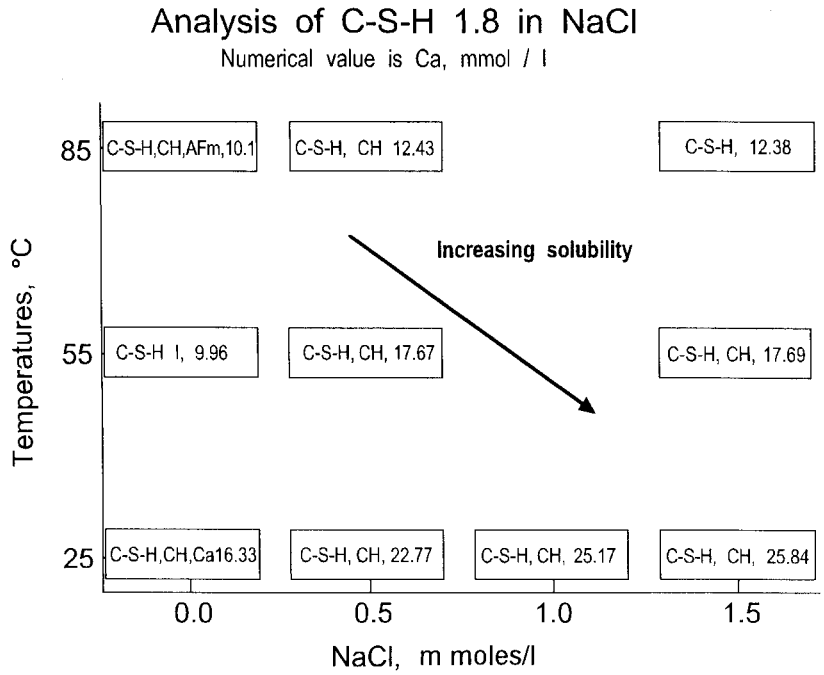

Figure 4.5.d Summary of solid and aqueous analyses of C-S-H 1.8 in NaCl at 25°, 55° and 85°C.

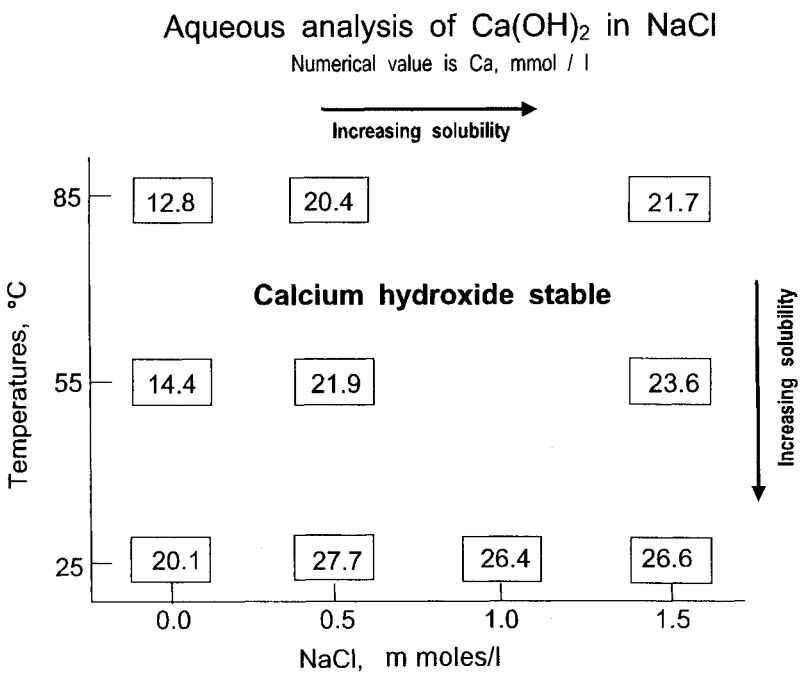

Figure 4.5.e Summary of solid and aqueous analyses of $Ca(OH)_2$ in NaCl at 25°, 55° and 85°C.

4.1.1.3 The Combined Effect of Temperature and Salinity on pH in NaCl Systems

A previous report [11] describes the affect of elevated temperature on C-S-H: equilibrium pHs are lowered by 0.5-1.0 pH units as a consequence of crystallisation. The pH's in these experiments were measured at 25°C, but then back-calculated to obtain the pHs at the temperature of the experiment, using MINEQL/AU, i.e. taking account of speciation and changes in pK_w with temperature. This recalculation has not been carried out in the present study and comparison will be restricted to the "25°C equivalent pH". The comparison discloses that the ability of both CH and C-S-H to buffer pH in NaCl solutions, relative to water, does not change significantly. The pH values of C-S-H are slightly reduced, by ~ 0.6 pH units, especially in the low Ca/Si range as a result of the saline cure. The apparent decrease is believed to be real but its magnitude, approximately 0.6 units pH units, is partly influenced by electrode selectivity and is believed to be less than 0.6 units.

Figures 4.6.a-e present the effect of temperature and salinity on pH for C-S-H and CH at 25°, 55° and 85°C.

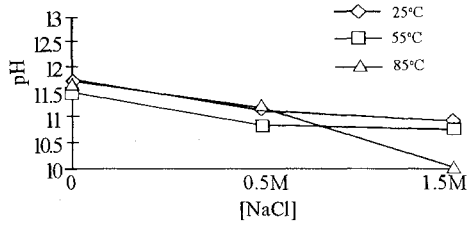

Figure 4.6.a pH as a function of temperature and salinity for C-S-H 0.85.

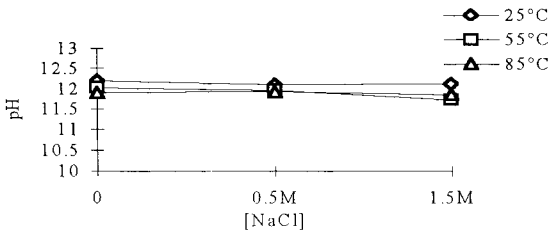

Figure 4.6.b pH as a function of temperature and salinity for C-S-H 1.1.

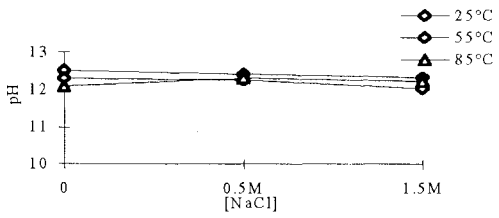

Figure 4.6.c pH as a function of temperature and salinity for C-S-H 1.4.

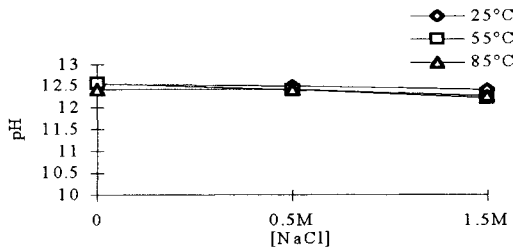

Figure 4.6.d pH as a function of temperature and salinity for C-S-H 1.8.

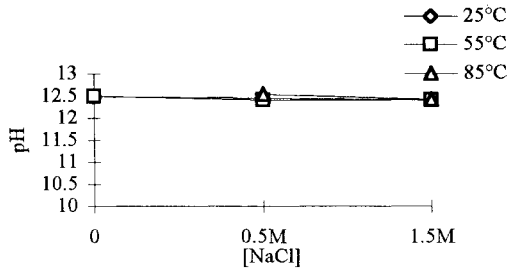

Figure 4.6.e pH as a function of temperature and salinity for calcium hydroxide.

These figures show that increasing salinity and temperature affect pH most strongly for C-S-H gel of low Ca/Si ratio. The lowest pH observed is for C-S-H 0.85, cured at 85°C in the highest NaCl concentration (1.5M) where the pH has decreased to ~10.

4.1.1.4 Kinetics and Respikes for $MgSO_4$ Systems

The kinetic experiments on Mg for Ca replacement were carried out with three reactants: C-S-H with Ca:Si ratios 1.1 and 1.8 and calcium hydroxide. The initial calculations using PHREEQE V2.0 at 25°C indicated that a very low threshold of magnesium concentration was sufficient to form either brucite (at high Ca/Si ratios) or sepiolite (at lower Ca/Si ratios). With CSH(1.8) and CH as reactants, brucite is predicted to precipitate at Mg exceeding ~ $1.3 \cdot 10^{-7}$ mol/kg and for CSH(0.8) sepiolite will precipitate at Mg exceeding ~ $5.6\ 10^{-8}$ mol/kg: see table 4.7 and figure 4.7.

Table 4.7 Calculated solution compositions for the points used to construct the C-S-M-H closed system at 25°C. Concentrations are given in molality (mol/kg).

Solids in equilibrium	[Mg] mol/kg	[Ca] mol/kg	[Si] mol/kg
CH + MH	$1.15\ 10^{-7}$	$2.19\ 10^{-2}$	0
CH + C-S-H(1.8) + MH	$1.15\ 10^{-7}$	$2.19\ 10^{-2}$	$1.85\ 10^{-5}$
C-S-H(1.8) + C-S-H(1.1) + MH	$1.30\ 10^{-7}$	$1.93\ 10^{-2}$	$2.45\ 10^{-5}$
C-S-H(1.1) + Sepiolite	$8.44\ 10^{-8}$	$1.23\ 10^{-3}$	$1.12\ 10^{-3}$
C-S-H(0.8) + C-S-H(1.1) + Sepiolite	$5.93\ 10^{-8}$	$1.25\ 10^{-3}$	$1.47\ 10^{-3}$
C-S-H(0.8) + Sepiolite	$5.64\ 10^{-8}$	$1.24\ 10^{-3}$	$1.55\ 10^{-3}$

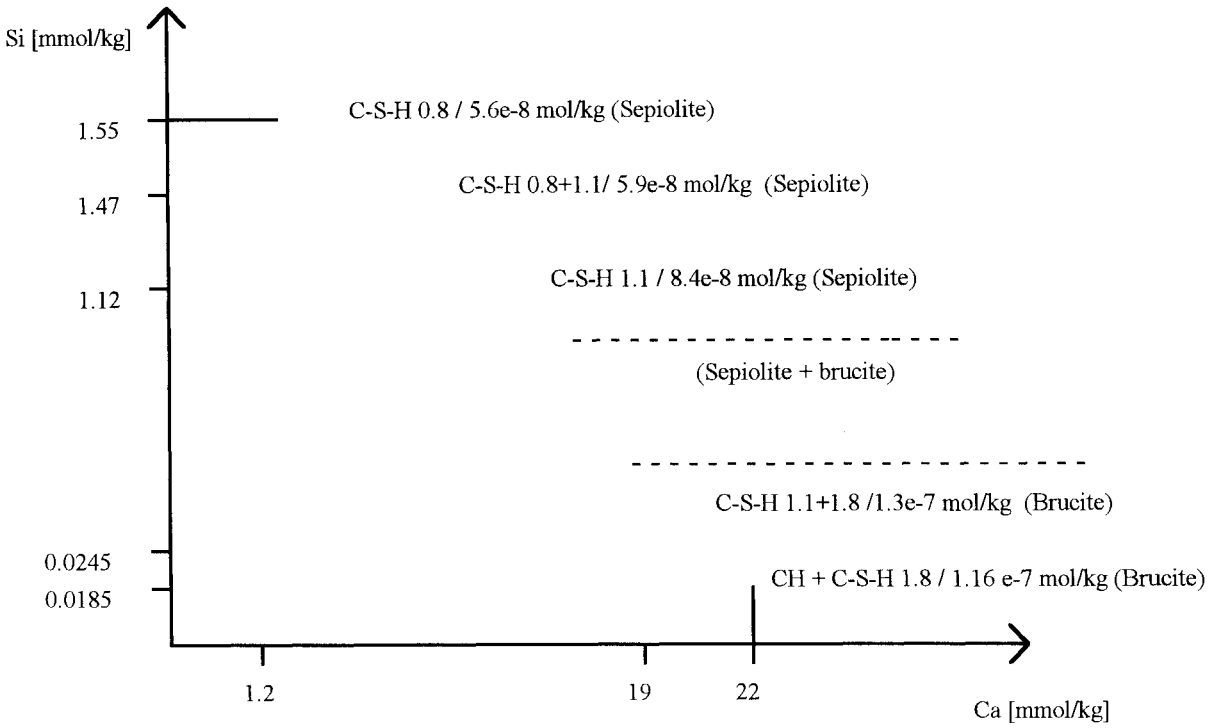

Figure 4.7 Calculated threshold magnesium concentrations for reaction with CaO-SiO_2-H_2O phases at 25°C. Lettering/numbers on the diagram give, in sequence, the Ca/Si ratio, the aqueous Mg concentration and the nature of the magnesium-containing solid. Dashed lines indicate approximate stability boundaries of the Mg-containing phases. See also figure 4.8.

The calculations show that the product formed depends on the original Ca/Si ratio, so that for a low Ca/Si ratio sepiolite (an Mg-hydroxysilicate phase) will precipitate whereas at higher Ca/Si ratios, CH and brucite are the stable products. Figure 4.7 assists in defining at least approximately a solution invariant point at which an aqueous phase coexists with CH, C-S-H, brucite and sepiolite. Other solubility points have a degree of freedom and therefore reflect univariant solubility equilibria. A ternary diagram has been constructed, figure 4.8, illustrating the stable pattern of mineral coexistence.

In chemically complex brines the anion (sulfate in this instance) cannot be neglected. Therefore it is expected that calcium will be partly replaced by magnesium but will also react with sulfate, giving gypsum or anhydrite. The calcium sulfate phase obtained depends on salinity and temperature. The molar Ca/Si ratio is the same in gypsum as in anhydrite, so mass balances (except for water, assumed to be abundant) are unaffected by the nature of the $CaSO_4$ phase.

To calculate the maximum numbers of respikes, mass balances were carried out for each of the pure hydrates. For example, for C-S-H 1.1 the original mass of the Ca in solid = 18 mmol/l, so to achieve a final 0.05 mole/l $MgSO_4$, 4 mmol of $MgSO_4$ have to be added (80mls in total of 0.05 M $MgSO_4$). Thus for total Ca replacement the system will require 4.5 respikings. Results of specimen calculations are shown in table 4.8.

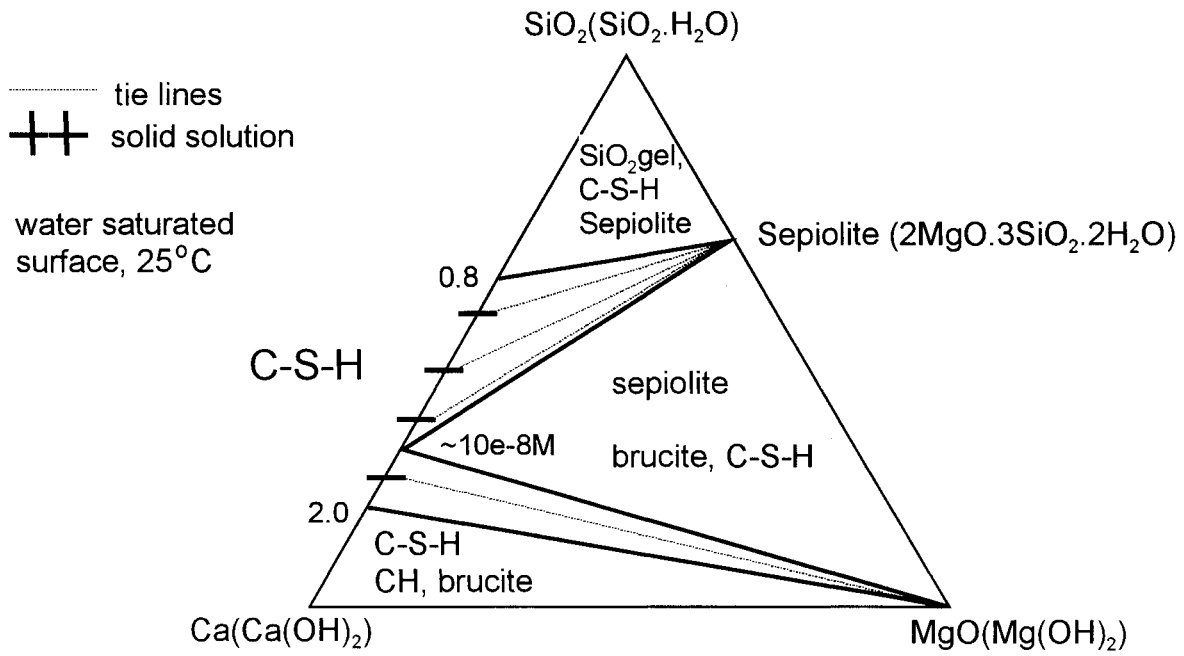

Figure 4.8 **Ternary diagram of the $CaO-MgO-SiO_2-H_2O$ system at 25°C. Solid solution of Mg in C-S-H is assumed to be negligible: 10e-8 M is the equilibrium Mg concentration above which sepiolite and brucite are stable**

Table 4.8 **Calculated respikes for C-S-H 1.1, 1.8 and CH. The calculation is based on the original amount of Ca in the solid.**

Hydrate	Calculated respikes
C-S-H 1.1	4.5
C-S-H 1.8	7.5
CH	9.0

Kinetic results

Experiments carried out at 25°C and at 0.05 M $MgSO_4$ using C-S-H, ratio 1.1, are shown in table 4.9.

Table 4.9 **Kinetic results from C-S-H 1.1 at 25°C and target [$MgSO_4$] = 50mM. The observed [SO_4] was 25.07 mmol/l 48 hours after the 3rd respike and 42.71 mmol/l 48 hours after the 4th respike.**

Magnesium concentration in mmol/l						
Hydrate	Respike N°	24 hrs	48 hrs	144 hrs	168 hrs	4 months
C-S-H 1.1	1	7.6	2.1	0.06		
	2				6.79	
	3		19.74			
	4		39.08			0.02

The results show that uptake of Mg is initially very rapid but thereafter decreases. After 4 respikes [$MgSO_4$] approaches its target concentration. The number of calculated respikes, using a simplistic model of total Mg removal, was 4.5; the experimental results show that the target value for [Mg] is approximately achieved after respiking 4 times.

Results for C-S-H 1.8, 0.05 M $MgSO_4$, 25°C, are given in table 4.10.

Table 4.10 **Kinetic results from C-S-H 1.8 at 25°C and target [$MgSO_4$] = 0.05 M. The [SO_4] = 20.57 mmol/l 72 hrs after the 4th the respike and 46.25 mmol/l 48 hrs after the 5th respike.**

Magnesium concentration in mmol/l						
Hydrate	Respike N°	24 hrs	48 hrs	72 hrs	168 hrs	4 months
C-S-H 1.8	1	0.08				
	2		<0.01			
	3				0.26	
	4			14.40		
	5		46.28			
	6			70.96		0.01

C-S-H 1.8 also shows an initial rapid uptake of Mg but reaction thereafter slows. As predicted, C-S-H 1.8 needs more respikes than C-S-H 1.1. The calculated number was 7.5 and experiment shows that the number of respikes approaches this. However the reaction rate slows down considerably after the 6th respike and, to limit the number of analyses, the first analysis was done after the number of respikes shown in table 4.10.

The results for calcium hydroxide are shown in table 4.11

Table 4.11 Kinetic results from CH at 25°C and target [$MgSO_4$] = 0.05 M. The [SO_4] was 6.44 mmol/l 72 hrs after the 4th respike and 15.63 mmol/l 48 hrs after the 5th respike.

Magnesium concentration in mmol/l						
Hydrate	Respike N°	24 hrs	48 hrs	72 hrs	168 hrs	4 months
CH	1	<0.01				
	2		<0.01			
	3				<0.01	
	4			<0.01		
	5		10.37			
	6			44.22		<0.01

Respikes

From the kinetic experiments and calculations the following numbers of respikes has been found to be appropriate: table 4.12 shows a specimen calculations.

Table 4.12 Calculated number of respikes necessary to approach 0.05M $MgSO_4$ target concentration at 25°C.

Hydrate	Numbers of respikes
C-S-H 0.85	4
C-S-H 1.1	5
C-S-H 1.4	6
C-S-H 1.8	8
CH	9

4.1.1.5 Solubility Data, pH and Solid Phase Compositions for $MgSO_4$ Systems

The chemical system MgO- SiO_2- H_2O has been investigated previously; a 'M-S-H' gel in cements exposed to $MgSO_4$ was first noted by Cole [17] in a deteriorated part of a concrete sea wall. More recently, Bonen [18] has described the M-S-H product, as has Gollop and Taylor [19]. Attack is marked by the development of mineralogical zonation. The thickness of each zone is a complex function of $MgSO_4$ concentration, temperature and matrix permeability. The surface layers become depleted in Ca; $Ca(OH)_2$ dissolves, while high ratio C-S-H is altered by Ca leaching and Ca is replaced directly by Mg, forming a dense brucite-containing skin. Sulfate penetrates to greater depth than Mg and a transition zone between much altered and unaltered cement is marked by formation of a zone of brucite, M-S-H and gypsum. The Mg/Si ratio of the M-S-H was given as 4.0 by Cole [17] but Gollop and Taylor [19] found a lower value, 1.54 ± 0.35. The M-S-H product had a low degree of crystallinity, but the three main bands of its X-ray powder pattern were attributed to a serpentine-like phase. Studies on synthetic M-S-H preparations made at < 85°C indicate that an apparently identical product forms: its Mg/Si ratio varies between 0.75 and 1.5. The poorly crystalline product has been associated with sepiolite, the composition of which in nature has a Mg/Si

ratio, close to 0.67, i.e., outwith the limits claimed for the synthetic. The product obtained in the present study could be a mixture of phases.

At higher temperatures, >85°C, the M-S-H gel-like material crystallises: depending on its M:S ratio, either talc or chrysotile are reported as products.

Four crystalline Mg-Si hydrates occur naturally: talc ($3MgO{\cdot}4SiO_2{\cdot}H_2O$), sepiolite ($4MgO{\cdot}6SiO{\cdot}6H_2O$), chrysotile (serpentine family, $3MgO{\cdot}2SiO_2{\cdot}2H_2O$) and anthophyllite ($7MgO{\cdot}8SiO_2{\cdot}H_2O$). All four are variants of a layered structure, built from intercalated brucite-type and silicate sheets. Talc and chrysotile are the stable Mg hydroxysilicate phases at 25°C but their crystallisation from gels at this temperature is extremely slow. Sepiolite is believed to form metastably at ~5°C on deep ocean floors under conditions of sea water salinity and moderate pressure. Experimental studies show its formation is favoured by high pH and high Si activity, thus its occurrence is not unexpected.

25°C Isotherm

The number of actual respikes carried out at 25°C are shown in section 3.1, table 3.2. The total numbers of respikes are expected to be greatest at low Mg target concentrations. Up to 90 respikings might have been necessary for 0.005 M and 0.01 M Mg targets, so it was not practicable to run these experiments to their end. However, since the Mg threshold for reaction is so low relative to these targets, it is believed that equilibrium solids and final pH's are the same as those which would coexist with 0.05M $MgSO_4$. The higher concentrations were, however, fully reacted and the predicted products, which began to appear at early stages of reaction, simply increased in amount as the solid reactants were consumed. Tables 4.13 and 4.14 show the results of the analysis after the final respike. In 0.05 M $MgSO_4$, the pH decreases to ~ 9.3 (CH reactant) and in the range 8-9 (C-S-H reactant). It is expected that even though the lower Mg concentrations have not experienced a comparable decrease in pH at the end of the experiments, their pH would continue to decrease with respiking and the products formed and end point pH would eventually be the same as in 0.05 M $MgSO_4$. When the CH and C-S-H components of a backfill are exhausted, the pH will be controlled by dissolution of brucite and gypsum. Calculations in PHREEQE V2.0 shows that when gypsum and brucite are in equilibrium with each other and water at 25°C, the pH will be 10.6, [Ca] = 15.3 mM, [Mg] = 0.26 mM and [SO_4] = 15.3 mM. An experiment was set up to determine the phase relationships between gypsum and brucite. A summary table 4.15 shows the results of the three experiments/calculations: after $Ca(OH)_2$ has reacted the first results are high in Mg and SO_4 owing to the presence of unreacted but soluble $MgSO_4$. Thus PHREEQE gives lower solubilities than experiment because it was constrained to calculate a slightly different case, without excess $MgSO_4$.

Table 4.13 C-S-H and CH samples cured at 25°C in respiked $MgSO_4$ solutions.

Target Ca/Si ratio	Target [$MgSO_4$] mol/l	pH	Aqueous Characterisation, mmol/l				Charge imbalance OH, mmol/l
			Ca	Si	Mg	SO_4	
0.85	0.005	10.31	15.92	0.43	<0.01	14.58	4.4
	0.01	9.81	13.13	0.13	<0.01	12.29	2.2
	0.05	8.10	10.68	0.10	27.15	38.75	-1.4
1.1	0.005	11.67	14.62	0.05	0.05	12.11	5.3
	0.01	11.56	13.27	0.06	0.01	11.46	3.9
	0.05	8.28	10.08	0.22	28.79	35.42	7.8
1.40	0.005	12.08	16.27	0.04	<0.01	11.07	10.6
	0.01	11.82	13.87	0.04	0.02	10.63	6.7
	0.05	8.94	10.68	<0.01	15.43	21.67	8.9
1.80	0.005	12.62	25.25	<0.01	<0.01	10.81	28.9
	0.01	12.51	20.66	<0.01	<0.01	11.98	17.4
	0.05	9.01	9.28	<0.01	66.64	77.92	-4.0
CH	0.005	12.64	24.75	-	<0.01	10.68	28.1
	0.01	12.70	26.35	-	<0.01	11.04	30.6
	0.05	9.34	10.38	-	46.07	54.17	4.6

Table 4.14 Solid characterisation of C-S-H and CH cured in $MgSO_4$ solutions at 25°C. Note that the pattern of tobermorite is weak, but definite. This is one of the first recorded instances of tobermorite having formed at such a low temperature: see text for discussion .

Target Ca/Si ratio	Initial [$MgSO_4$] mol/l	CH	Gypsum	Brucite	Tobermorite
0.85	0.005		S		
	0.01		S		
	0.05		S		
1.1	0.005		S	W	
	0.01		S	W	
	0.05		S		
1.40	0.005		S		
	0.01		S	W	
	0.05		S		
1.80	0.005	S	S	M	W
	0.01		S	M	
	0.05		S	M	
CH	0.005	S	S	W	
	0.01	S	S	M	
	0.05		S	S	

Table 4.15 Summary table of experimental and calculated results at 25°C for the equilibria including gypsum, anhydrite and brucite.

System	pH	[Ca] mmol/l	[Mg] mmol/l	[SO_4] mmol/l	X-ray
CH in 0.05M $MgSO_4$	9.34	10.38	46.07	54.17	Gypsum, brucite
Gypsum + brucite in w/s ratio ~ 40	?	7.98	10.03	25.00	Gypsum, anhydrite, brucite
Gypsum + brucite calculated in PHREEQE V2.0	10.6	15.3	0.26	15.3	SI = 0 for both gypsum and brucite and -0.33 for anhydrite

The appearance of tobermorite at 25°C for C-S-H 1.8 in 0.005 M $MgSO_4$ is noteworthy. AEM examination discloses some plate-like tobermorite-like phase but the bulk of the C-S-H had the crumpled foil (amorphous) morphology. The average Ca/Si ratio of the flat plate-like crystals was ~1.2, whereas C-S-H with crumpled foil morphology had a mean Ca/Si ratio ~1.65. Some leaching had occurred in the course of the experiment which explains why the ratios are lower than the initial ratio, of 1.8.

AEM of C-S-H 1.4 at 25°C carried out before any respikes showed two morphologies, one consisting of a mixture of C-S-H and M-S-H and the other consisting of C-S-H. The mixed phase had an amorphous, crumpled foil C-S-H appearance with a Ca/Si ratio of 1.34 and a Mg/Si ratio of 1.61. There was no sign of either sepiolite or brucite, nor were they observed by XRD; the SO_4 content of the solids was very low: probably the Mg precipitate is amorphous. The aqueous analyses for Mg showed depletion, to below 0.01 mmol/l.

SUMMARY OF THE 25°C RESULTS:

- reaction of C-S-H and CH with $MgSO_4$ is reasonably rapid on laboratory time scales.
- both magnesium and sulfate components are reactive with CH. Two reactions occur:
  - base exchange, Mg for Ca, resulting in brucite formation.
  - calcium dissolution, partly balanced by gypsum precipitation
- the Mg-containing product(s) are brucite at higher Ca/Si ratio or brucite and M-S-H gel (or both) at lower ratios, together with gypsum
- pH decreases to ~ 9 for CH and high Ca/Si ratio and ~ 8 for lower Ca/Si ratios.
- solubility of both C-S-H and CH decrease with increasing [$MgSO_4$], because of phase changes.

55°C Isotherm

To complete the programme within time, the 55°C experiments were only analysed after initial $MgSO_4$ curing. The samples have been respiked but not yet analysed. The results will be presented in a thesis [20]. Tables 4.16 and 4.17 shows the results without respikes.

Table 4.16 C-S-H and CH samples cured at 55°C in $MgSO_4$ solutions. Note: these determinations were made without respiking. Curing time was 214 days.

Target Ca/Si ratio	Target [$MgSO_4$] mol/l	pH	Aqueous Characterisation, mmol/l				Charge imbalance
			Ca	Si	Mg	SO_4	OH, mmol/l
0.85	0.005	11.04	5.39	0.13	<0.01	4.87	1.56
	0.01	10.82	9.25	0.11	<0.01	8.78	1.38
	0.05	10.25	12.78	0.28	<0.01	12.73	1.22
1.1	0.005	11.62	6.09	0.06	<0.01	3.96	4.50
	0.01	11.69	11.08	0.05	<0.01	8.26	5.84
	0.05	11.59	14.60	0.04	<0.01	13.01	3.34
1.40	0.005	12.14	10.03	0.02	<0.01	2.17	15.80
	0.01	12.10	12.13	0.03	<0.01	4.81	14.76
	0.05	12.07	19.94	0.02	<0.01	13.14	13.68
1.80	0.005	12.28	13.85	0.01	<0.01	0.79	26.16
	0.01	12.29	15.77	0.01	<0.01	2.02	27.54
	0.05	12.20	21.14	0.02	<0.01	12.49	17.38
CH	0.005	12.31	19.94	-	<0.01	4.87	30.14
	0.01	12.24	22.46	-	<0.01	8.85	27.22
	0.05	12.31	26.45	-	<0.01	12.08	28.74

The Mg concentration is depleted to less than detection, so Ca replacement by Mg effectively ceases. The results do, however, indicate reaction direction. During reaction, the sulfate concentration of the aqueous phase decreases, but not by as much as the Mg concentration: the solid composition is also affected; the Ca/Si ratio of C-S-H decreases and gypsum precipitates. The net result is to increase the solubility of silica. CH solubility increases slightly. The 55°C solubility trends are incomplete but preliminary data show increasing solubility of Ca. This is opposite to the trends at both 25° and 85°C and requires to be confirmed. Partial crystallisation of C-S-H occurs of low Ca/Si ratios. Tobermorite crystallisation occurs at Ca/Si ratios 0.85 and 1.1, while jennite occurs at high ratio, 1.4, in both 0.005M and 0.01 M $MgSO_4$. Some samples show a tendency to crystallise more slowly in $MgSO_4$; see for example C-S-H 0.85, where tobermorite forms in water (table 4.4 section 4.1.1.2) and at low $MgSO_4$ concentration, but was not detected in 0.05M $MgSO_4$. C-S-H crystallises faster than it can react/dissolve in dilute $MgSO_4$. Tobermorite and jennite are observed and gypsum has been found in all samples cured in 0.05 M $MgSO_4$.

Table 4.17 Solid characterisation of C-S-H and CH cured in $MgSO_4$ solutions at 55°C without respiking. A + symbol denotes that the phase is present; letters give a semi-quantitative indication from XRD of the amount present. Curing time was 214 days.

Target C/S ratio	Initial mol/l	CH	C-S-H I/II	Brucite	Tob.	Jennite	Gypsum
0.85	0.005		+		S		
	0.01		+		M/S		
	0.05		+				M/S
1.1	0.005		+			W/M	
	0.01		+			W	
	0.05		+		W/M		M/S
1.40	0.005		+				
	0.01		+				
	0.05		+				M/S
1.80	0.005	M	+				
	0.01	W	+				
	0.05	W	+				M/S
CH	0.005	VS					
	0.01	VS					
	0.05	S		W			W/S

SUMMARY OF THE 55°C RESULTS:

Results for 55°C in $MgSO_4$ without respiking but cured for 214 days show that

- both magnesium and sulfate components are reactive with CH
  - base exchange occurs: Mg for Ca
  - Ca dissolution, partly balanced by gypsum precipitation, also occurs
- C-S-H crystallises faster than it can react/dissolve in dilute $MgSO_4$: tobermorite and jennite are observed.
- Crystallisation of C-S-H is inhibited by higher $MgSO_4$ concentrations, perhaps because replacement of Ca by Mg is so rapid.
- pH remains approximately unchanged in solutions without respikes.

85°C Isotherm

Results of the respiked experiments are shown in tables 4.18 and 4.19. The numbers of respikes for each sample are shown in table 3.2. Both calcium and silica solubilities are depressed by increasing $MgSO_4$ concentration, except at low C/S ratios where the solubility increases from 0.30 mmol/l in 0.005 M to 1.02 mmol/l in 0.05 M $MgSO_4$, while for Ca/Si 1.1 the increase is from 0.07 mmol/l to 0.31 mmol/l in 0.05 M $MgSO_4$. The aqueous pH decreases with increasing $MgSO_4$ concentration, e.g. from 12.18 to 8.93 (~ 3.3 pH units) for C-S-H 1.8 and ~ 3.2 pH units for Ca/Si ratio 0.85. Respiking ultimately exhausts the alkaline buffering reserves.

Table 4.18 C-S-H and CH samples cured in respiked $MgSO_4$ solutions at 85°C.

Target Ca/Si ratio	Target [$MgSO_4$] mol/l	pH (25°C)	Aqueous Characterisation, mmol/l				Charge imbalance
			Ca	Si	Mg	SO_4	OH, mmol/l
0.85	0.005	9.53	11.54	0.30	<0.01	12.08	0.1
	0.01	9.29	11.70	0.32	0.02	13.54	-2.4
	0.05	6.30	9.43	1.02	52.45	70.00	-12.2
1.1	0.005	11.41	12.06	0.07	0.12	12.08	0.5
	0.01	11.16	11.59	0.11	0.01	12.08	-0.5
	0.05	7.58	9.73	0.31	47.31	59.58	-4.5
1.40	0.005	11.47	12.48	0.07	0.03	11.88	1.5
	0.01	11.48	13.31	0.06	<0.01	13.33	0.2
	0.05	8.19	10.98	0.05	34.97	55.83	-19.6
1.80	0.005	12.18	17.15	0.04	<0.01	13.02	8.4
	0.01	12.11	12.99	<0.01	<0.01	12.40	1.2
	0.05	8.93	10.48	<0.01	70.96	90.00	-17.1
CH	0.005	12.38	19.54	-	<0.01	11.56	16.0
	0.01	12.38	18.09	-	<0.01	10.94	14.3
	0.05	8.14	9.83	-	68.28	73.75	8.7

Table 4.19 Solid characterisation of C-S-H and CH cured in respiked $MgSO_4$ solutions at 85°C.

Target C/S ratio	Target [$MgSO_4$] mol/l	CH	Brucite	Tober-morite	Jennite	Gypsum	Anhydrite	Calcite
0.85	0.005			S		S		
	0.01			S		S		
	0.05					S		
1.1	0.005			S		S		
	0.01					S	M	
	0.05					S		
1.40	0.005				S	S		t
	0.01				S	S		
	0.05		M			S	S	
1.80	0.005		M			S		
	0.01					S		
	0.05					S	S	
CH	0.005	S				S		
	0.01	S	S			S		
	0.05		S			S	S	

Partial crystallisation of C-S-H occurs, but its extent decreases with increasing Ca/Si ratio. Tobermorite crystallisation occurs at the lowest Ca/Si ratios, 0.85 and 1.1. Jennite crystallises of the C-S-H 1.4 in both 0.005 and 0.01 M $MgSO_4$. In table 4.4, section 4.1.1.2, afwillite

occurs at Ca/Si ratio 1.8 cured in water. However, even very low $MgSO_4$ concentrations inhibit afwillite formation. C-S-H I was not observed.

SUMMARY OF THE 85°C RESULTS:

Cement substances have been reacted with $MgSO_4$. Reactions are more rapid at 85 °C and 55 °C than at 25 °C.

- both magnesium and sulfate components are reactive with CH
  - base exchange occurs: Mg for Ca
  - Ca dissolution, partly balanced by gypsum and/or anhydrite precipitation occurs
- C-S-H crystallises faster than it can react/dissolve: tobermorite and jennite form.
- pH decreases to ~ 9 as CH reacts, and to 8-9 for C-S-H, depending on its initial C/S ratio.
- [Ca] decreases with increasing [$MgSO_4$].

4.1.1.6 The Combined Effect of Temperature and Salinity on pH in $MgSO_4$ Systems

The solubility of Ca in C-S-H and CH are found to decrease with increasing $MgSO_4$ concentration at 25°C and 85°C. Si solubilities are not much affected by $MgSO_4$ content, except at lower Ca/Si, where [Si] increases slightly.

The initial ability of both CH and C-S-H to buffer pH in $MgSO_4$ is not changed significantly relative to water. However a lower-pH regime develops as a consequence of reaction; CH reacts to form gypsum/anhydrite and brucite, while C-S-H undergoes both reaction and crystallisation. These reaction products condition a lower pH, ~ 8. As reported in previous studies [11] the pH is also affected by temperature; table 4.20 gives a summary.

Table 4.20 Short summary of results for C-S-H and CH cured in $MgSO_4$. Comparative results are relative to H_2O. Gyp = gypsum, MH = brucite.

	25°C, respiked	55°C, **not** respiked	85°C, respiked
CH	-Solubility decreases. *-pH decreases.* -Phase change to gypsum and MH.	-Solubility increases *-pH approx. unchanged.* -Phase change to gyp + MH at 0.05M.	-Solubility decreases. *-pH decreases.* -Phase change to gypsum and MH.
C-S-H	-Ca decreases. Si increases for C/S 1.1 and decreases for C/S 0.85 otherwise practically unchanged. *-pH decreases.* -Gyp found in all samples + MH in C/S≥1.1.	-Ca increases. Si increases for C/S 0.85 otherwise practically unchanged. *-pH approx. unchanged.* -Gyp found in all 0.05M samples.	-Ca decreases. Si increases slightly at lower C/S ratio. *-pH decreases.* - Gyp observed in all samples.

The following five figures illustrate the trends for the solubility data and solid phase compositions for C-S-H and CH cured in $MgSO_4$ at three temperature; dark solid boxes indicate that the reaction is complete and light boxes, that unconsumed reactants remain.

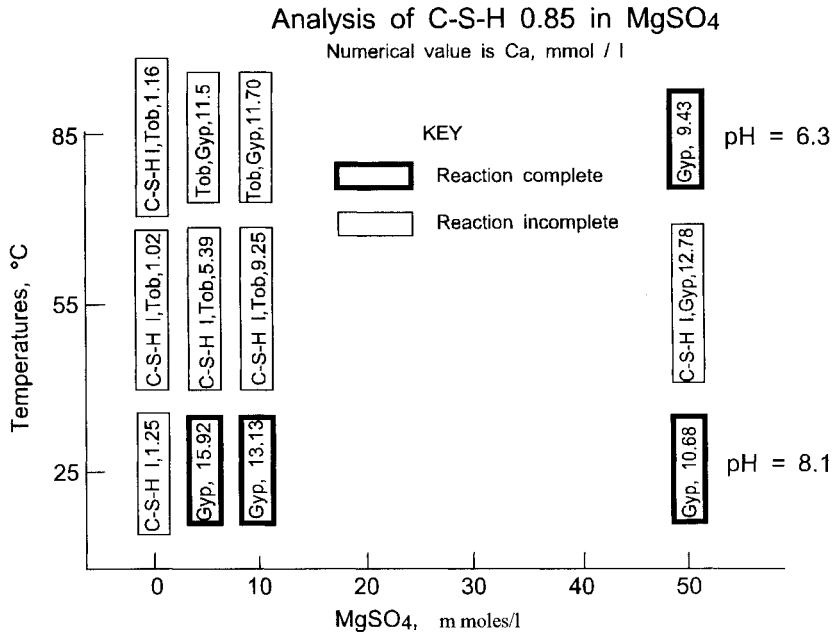

Figure 4.9.a Summary of solid and aqueous analyses of C-S-H 0.85 in $MgSO_4$ at 25°, 55° and 85°C.

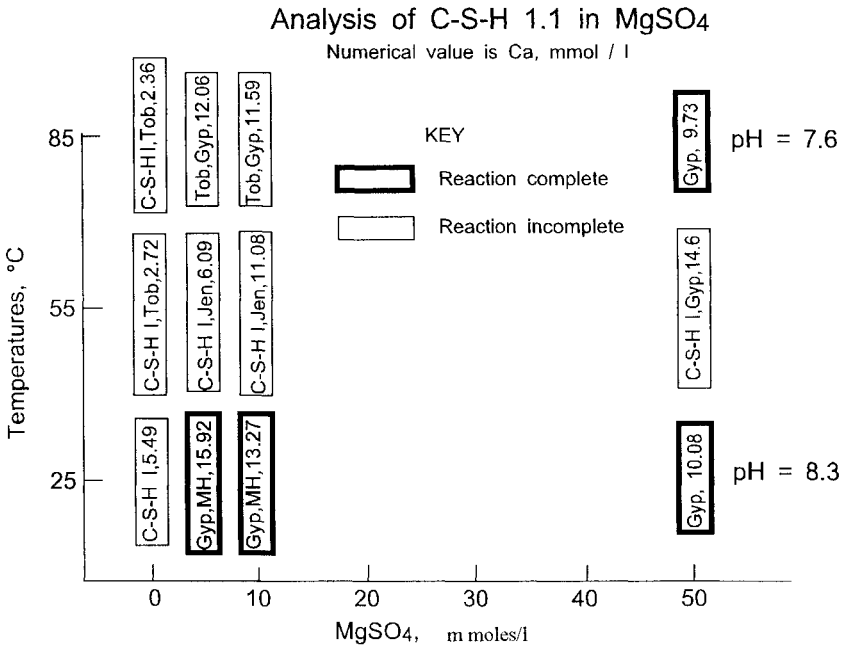

Figure 4.9.b Summary of solid and aqueous analyses of C-S-H 1.1 in $MgSO_4$ at 25°, 55° and 85°C.

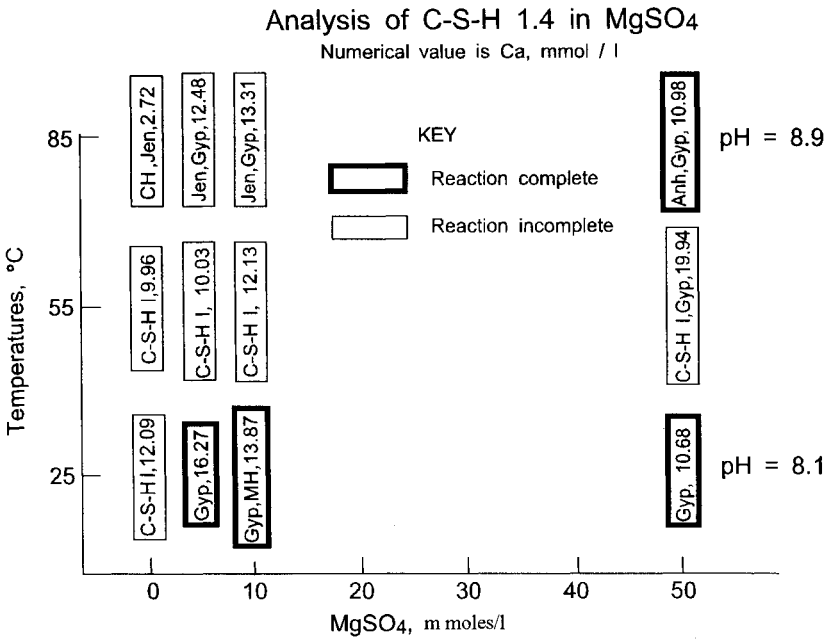

Figure 4.9.c Summary of solid and aqueous analyses of C-S-H 1.4 in $MgSO_4$ at 25°, 55° and 85°C

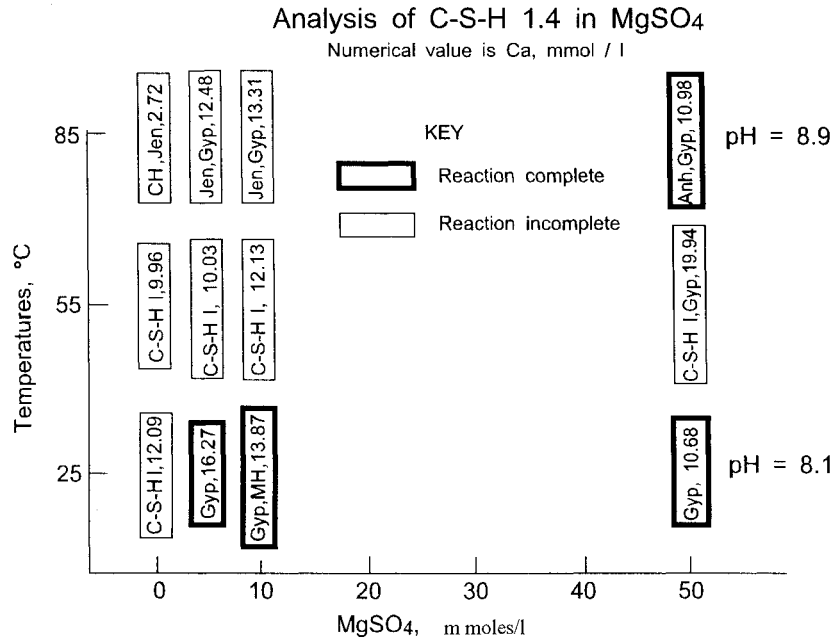

Figure 4.9.d Summary of solid and aqueous analyses of C-S-H 1.8 in $MgSO_4$ at 25°, 55° and 85°C.

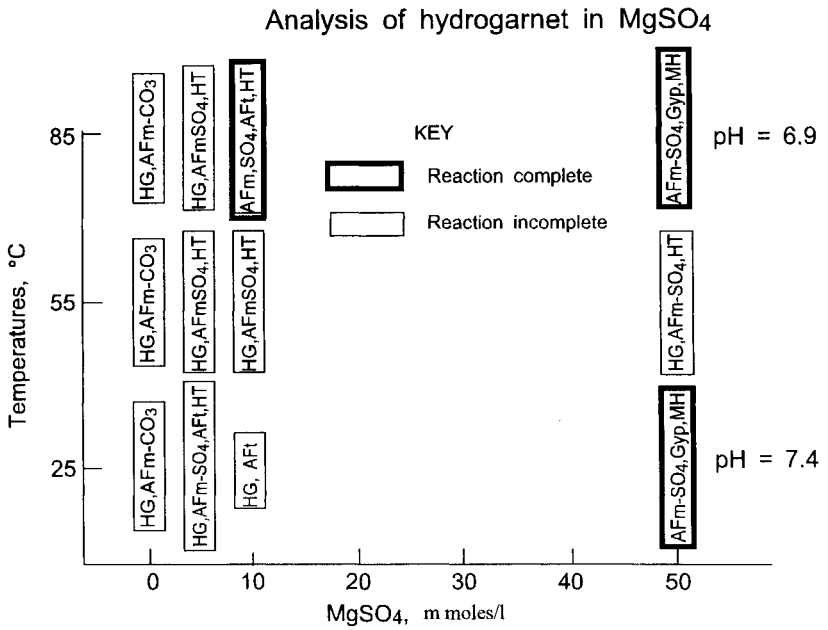

Figure 4.9.e Summary of solid and aqueous analyses of CH in $MgSO_4$ at 25°, 55° and 85°C.

References

1. A. Atkinson, M. Everitt and R.M.Gruppy. (1989) 'Time Dependence of pH in a Cementitious Repository'. Mat. Res. Soc. Symp. Proc., **127**, 439-446. (Mat. Res. Soc., Pittsburgh PA.)

2. U.R. Berner. (1988) 'Modelling the Incongruent Dissolution of Hydrated Cement Minerals'. Radiochimica Acta **44/45**, p.387-393.

3. F.P. Glasser and M. Atkins. (1994) 'Cements in Radioactive Waste Disposal'. MRS Bulletin/December, pp. 33-38.

4. F.B. Neall, PSI Report. (1995) 'Modelling the Long-Term Chemical Evolution of Cement-Groundwater Systems'. (Paul Scherrer Institute, Switzerland).

5. I. Klur (1996). 'Etude par RMN de la Structure des Silicates de Calcium Hydratés.' PhD thesis, Université Paris VI.

6. A. J. Majumdar, D. L. Rayment and K. Pettifer. (1988) 'Microstructure and Microanalysis of Some Ancient Building Materials'. DoE/RW/89.056.

7. J. D. C. McConnell. (1953) 'The Hydrated Silicates Riversideite, Tobermorite and Plombierite'. Mineralogical Magazine, **30**, p.293-305.

8. A.E Milodowski, J.M. Pearce, C.R. Hughes and H.N. Khoury. (1992) 'A Preliminary Mineralogical Investigation of a Natural Analogue of Cement-buffered Hyperalkaline Groundwater Interaction with Marl, Maqarin, Northern Jordan. Nagra Report Interner Bericht 92-50.

9. C.R. Wilding. (1992) 'The Performance of Cement based Systems', Proc. of the European Material Res. Soc. Symp. on "Chemistry of Cements for Nuclear Applications", Strasbourg, Nov. 1991, pp. 299-310.

10. Nirex Report 524. (Dec. 1993) 'The Geology and Hydrogeology of the Sellafield Area. Interim Assessment'. Investigation Results, Volume **4**.

11. M. Atkins et al. (1993) 'Thermodynamic Modelling of Blended Cements at Elevated Temperature (50-90°C)'. UK DoE Report no. DoE/HMIP/RR/94/011, Aberdeen University, Scotland

12. S. Stronach. (1996) 'Thermodynamic Modelling and Phase Relations of Cementitious Systems'. PhD. Thesis, Aberdeen University, Scotland.

13. M. Atkins et al. (1991) 'A Thermodynamic Model for Blended Cements'. UK DoE Report no. DoE/HMIP/RR/92/005, Aberdeen University, Scotland.

14. C.J. Newton and J.M. Sykes. (1987) 'The Effect of Salt Additions on the Alkalinity of $Ca(OH)_2$ Solutions'. Cem. and Con. Res., **17**, pp. 765-776.

15. W. Kurdowski and S. Duszak. (1995) 'Changes of C-S-H Gel in Strong Chloride Solution'. Advances in Cement Research. 7, Number 28. pp.143-149.

16. H.F.W. Taylor. (1964) 'The Chemistry of Cements'. Volume 2. Academic Press. (London and N.Y.).

17. W.F. Cole. (1953) 'A Crystalline Hydrated Magnesium Silicate Formed in the Breakdown of a Concrete Sea-wall.' Nature. **171**, No. 4347.

18. D. Bonen. (1992) 'Composition and Appearance of Magnesium Silicate Hydrate and Its Relation to Deterioration of Cement-Based Materials.' Journal of the American Ceramic Soc. **75**, No.10, pp.2904-2906.

19. R.S. Gollop and H.F.W. Taylor. (1992) 'Microstructural and Microanalytical Studies of Sulfate Attack. I. Ordinary Portland Cement Paste'. Cement and Concrete Research, **22**, pp.1027-1038.

20. K. Goldthorpe. (1998) 'Stability of Cementitious Materials in Saline Environments' PhD Thesis, University of Aberdeen, Scotland

4.1.2 Hydrogarnet, HG

4.1.2.1 Introduction and Background

Hydrogarnet, $3CaO{\cdot}Al_2O_3{\cdot}6H_2O$, is a thermodynamically stable phase in the $CaO\text{-}Al_2O_3\text{-}H_2O$ system. Its synthesis and solubility were defined by Wells, Clarke and McMurdie [1].

They used two approaches in their investigation, approaching equilibrium from both undersaturated and supersaturated solutions, and found that the only stable solid phases in the $CaO\text{-}Al_2O_3\text{-}H_2O$ system over the temperature range of 21° to 90°C at 1 bar were: gibbsite (AH_3); hydrogarnet (C_3AH_6); and calcium hydroxide (CH). The solubility curves of these phases were determined at 21°C and 90°C.

They found that gibbsite is the stable phase up to a concentration of 0.33 g/l CaO (5.9 mmol/l); at higher CaO concentrations, C_3AH_6 becomes stable, until CH appears as a solid phase. Figure 4.10 depicts the stable solubility curves; at 21°C these are H-F-Y-C and at 90°C, N-L-M-P. table 4.21 gives defining data. The diagram is cluttered, but usefully contrasts both stable and metastable phase relations.

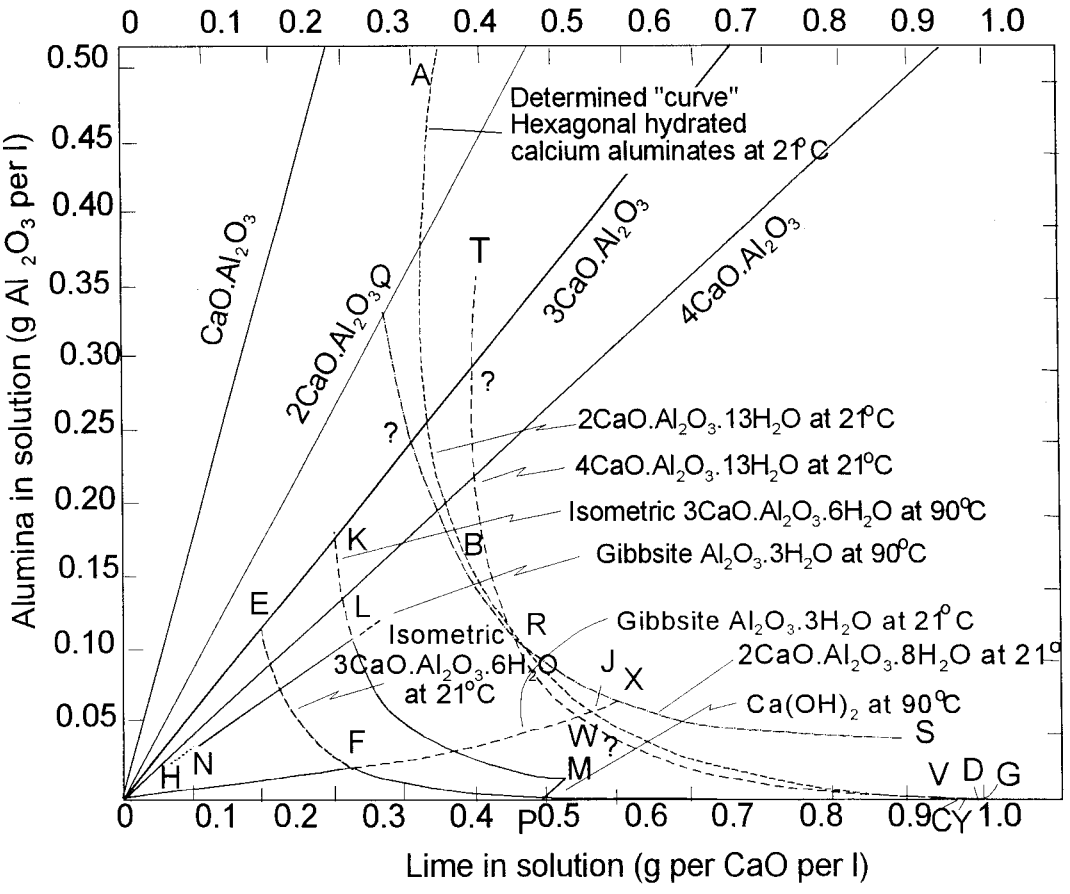

Figure 4.10 System $CaO\text{-}Al_2O_3\text{-}H_2O$ at 21°C and 90°C. Curves and points are described in table 4.21.

Table 4.21 Location of the solubility curves for hydrogarnet, gibbsite and calcium hydroxide in figure 4.10. The last two columns give solubilities.

Part of Solubility Curve	Explanation	$[Al_2O_3]$ (g/l)	[CaO] (g/l)
E-F-G	Solubility curve of hydrogarnet at 21°C		
E-F	Hydrogarnet, metastable with respect to gibbsite at 21°C		
F-G	Stable section for hydrogarnet at 21°C		
Y	Stable invariant point C_3AH_6-CH at 21°C	0.0005	1.15
Y-C	Solubility curve of CH at 21°C		
H-F-J	Solubility curve of gibbsite at 21°C		
H-F	Stable section for gibbsite at 21°C		
F-J	Gibbsite, metastable with respect to hydrogarnet at 21°C		
F	Stable invariant point C_3AH_6-AH_3 at 21°C	0.02	0.33
K-L-M	Hydrogarnet at 90°C		
K-L	Hydrogarnet, metastable with respect to gibbsite at 90°C		
L-M	Stable section for hydrogarnet at 90°C		
M	Stable invariant point C_3AH_6-CH at 90°C	0.015	0.63
N-L	Solubility curve of gibbsite at 90°C		
L	Stable invariant point C_3AH_6-AH_3 at 90°C	0.11	0.33
P-M	Solubility curve of CH at 90°C		

Wells, Clarke and McMurdie [1] determined curve A-B-D for the metastable solubility of mixtures of hexagonal hydrates, $2CaO{\cdot}Al_2O_3{\cdot}8H_2O$ and $4CaO{\cdot}Al_2O_3{\cdot}13H_2O$ at 21°C; T-R-V is the metastable solubility curve for hexagonal hydrate, C_4AH_{13}, at 21°C. More recent studies [3-8] will be described.

The relationships between hydrogarnet phases and hydroxy AFm types were also described by Lea [2]. Hydroxy AFm type phases, persistent at temperatures up to ~ 40°C, appear to be thermodynamically metastable at temperatures below 40°C. Experiments show that C_3AH_6 transforms into C_2AH_8 or to C_4AH_{19} at 5°C or lower: the phases produced also depend on the lime concentration in the solution [2]. Damidot and Glasser [8] refer to findings showing that the phases CAH_{10}, C_2AH_8, C_4AH_x are metastable with respect to C_3AH_6 at 25°C. Work done by Atkins et al. [4] shows that C_3AH_6 dissolves congruently (i.e. molar Ca and Al ratios in the solid and aqueous phases are approximately equal) at 25°C with Ca ~ 6.14 mmol/l and Al ~ 4.57 mmol/l. This is in accord with other findings: Lea [2]. Solubility changes little over the temperature range 25-85°C, with perhaps a slight calcium maximum near 55°C [5].

Table 4.22 Measured solubility properties of C_3AH_6 in the temperature range 25-85°C in water by Atkins et al [5] and Wells, Clarke and McMurdie [1].

Temperature	Atkins et al.		Wells, Clarke and McMurdie	
	Ca mmol/l	Al mmol/l	Ca mmol/l	Al mmol/l
21°C			5.9	0.4
25°C	6.14	4.57		
55°C	6.83	2.95		
85°C	6.07	4.50		
90°C			5.9	2.16

The data for aluminium do not agree well with those of Wells, Clarke, and McMurdie [1]: table 4.22. The chemistry of hydrogarnets is summarised in table 4.23.

Table 4.23 Substitutions of ions in hydrogarnet at 25°C, 1 atm

Substitution of ions in	**hydrogarnet**
Ion	**Comment**
Si^{4+} (or $Si(OH)_4$)	Complex substitution: see text
Na^+, K^+	Not significant
Mg^{2+}	Significant substitution only at very high pressure
Fe^{3+}	Extensive substitution for Al possible [2, 6, 10]
SO_4^{2-}, Cl^- or CO_3^{2-}	Not significant

Solid solutions occur between C_3AH_6 and grossularite, $Ca_3Al_2Si_3O_{12}$. Flint et al. [6] showed that these two compounds are the end members of a solid solution series, with the general formula, $3CaO{\cdot}Al_2O_3{\cdot}mSiO_2{\cdot}(6\text{-}2m)H_2O$, where m varies from 0 to 3. Effectively, $4OH^-$ are replaced by SiO_4^{4-}. Stability relationships at 95°C, 1 atm, were described by Jappy and Glasser [3]. They found that a miscibility gap appeared in the solid solution lying between the compositions $C_3AS_{0.42}H_{5.16}$ and $C_3AS_{0.76}H_{4.48}$. Although the location of the compositional gap will not necessarily remain the same in extent or position on other isotherms, Atkins et al. [4] found a miscibility gap in the series between $C_3AS_{0.43}$ $H_{5.16}$ and $C_3AS_{0.76}H_{4.48}$ at 25°C and 1 atm which is practically the same as that reported in [3].

Blended cements, i.e. those containing slag and fly ash, will almost certainly yield siliceous hydrogarnets and BRE have observed its formation in OPC. But there are as yet relatively little thermodynamic data on the siliceous hydrogarnet. In the absence of thermodynamic data for the complex solid solutions we have continued to use C_3AH_6 as the prototype for all hydrogarnets. However, the new version of the database includes additional data for solid solutions.

Hydrogarnet rapidly becomes unstable in saline solutions. For example, at [Cl^-] ≥ 9 mmol/kg [7], hydrogarnet decomposes with respect to other phases, the most important of which is monochloraluminate (AFm-Cl, also known as Friedel's salt).

4.1.2.2 Solubility Data, pH and Phase Compositions in NaCl systems

25°C Isotherm

Solubility data for C_3AH_6 in double distilled, degassed water (DDW), 1.0 and 1.5 M NaCl at 25°C are given in table 4.24; solid characterisation is presented in table 4.25.

Table 4.24 Solubility measurements for C_3AH_6 cured in water and NaCl at 25°C for 173 days.

Initial [NaCl] mol/l	pH	Aqueous Characterisation, mmol/l				charge imbalance	cal.
		Na	Cl	Ca	Al	OH,mmol/l	pH
0	12.3	3.0	3.0	5.44	3.03	19.97	12.3
0.91	12.8	972	863	0.11	23.2	116.2	13.1
0.92	12.7	952	863	0.16	21.0	152.3	13.2
1.44	12.7	1370	1338	0.08	22.2	98.76	13.0

Table 4.25 Solid characterisation of C_3AH_6 cured in water and NaCl solutions at 25°C for 173 days.

Initial [NaCl] mol/l	CH	HG	AFm-Cl	AFm-CO_3
0		S		M
0.91	S	S	S	
0.92	S	S	S	
1.44	S	S	S	

The dataset indicates that C_3AH_6 dissolves congruently in dilute NaCl solutions (DDW with [Na] = [Cl] = 3.0 mmol/l), but ≥ 0.5 M NaCl, X-ray data (table 4.25) indicate that a major phase change occurs; C_3AH_6 decomposes to calcium monochloroaluminate (AFm-Cl) and CH.

Table 4.24 shows that the pH of the aqueous phase remains approximately unchanged with increasing NaCl concentration up to 1.5 M. However, the literature on phase stability is inconsistent [7,14-17].

Kuzel [14] found two polymorphs of calcium monochloroaluminate ($3CaO{\cdot}Al_2O_3{\cdot}CaCl_2{\cdot}10H_2O$): α-AFm-Cl and β-AFm-Cl. The α-AFm-Cl is supposedly stable below 28±2°C and transforms to the trigonal β-AFm-Cl phase above this temperature. However, other studies cast doubt about this polymorphic scheme. Birnin Yauri [16] was unable to reproduce the 28°±2°C inversion; instead mixtures of α and β persisted unchanged across a wide range of temperatures, 20-40°C.

Friedel's salt forms only a limited range of reciprocal solid solution with hydroxy AFm and does not incorporate significant amounts of SO_4 [17]. Kuzel [14] studied synthetic systems of calcium monochloroaluminate and hydrocalumite ($3CaO{\cdot}Al_2O_3{\cdot}Ca(OH)_2{\cdot}12H_2O$) and found no solid solution between either α- or β-$3CaO{\cdot}Al_2O_3{\cdot}CaCl_2{\cdot}10H_2O$ and $3CaO{\cdot}Al_2O_3{\cdot}Ca(OH)_2{\cdot}12H_2O$. However, Fisher et.al [15] and U.A. Birnin-Yauri [16] noted that natural hydrocalumites form extensive solid solutions in the system $3CaO{\cdot}Al_2O_3{\cdot}CaCl_2{\cdot}10H_2O$ - $3CaO{\cdot}Al_2O_3{\cdot}Ca(OH)_2{\cdot}12H_2O$. In this study, made at relatively high Cl^- concentrations, AEM shows no significant solid solution of OH^-, ≥ 10 mol %, in Friedel's salt (AF_m-Cl).

The existence of two polymorphs is, however, not of great importance for thermodynamic modelling as their differences in their crystal structure are slight and both polymorphs will have essentially the same solubilities, close to the supposed phase transition.

Damidot et al. [7] investigated the CaO-Al_2O_3-$CaCl_2$-Na_2O-H_2O system at 25°C and found that calcium monochloroaluminate is stable in contact with NaCl up to ~ 8.4 mole/l. The minimum chloride concentration required to stabilise AFm-Cl was found to be ~ 0.105 mole/l at 0.25 mole/l Na_2O (= 0.5 mole/l Na). These calculations verify the experimental observations, where AFm-Cl was observed at 0.5, 1.0 and 1.5 M NaCl but not in dilute NaCl (<0.003 mole/l).

Figure 4.11 shows a three dimensional representation of the CaO-Al_2O_3-$CaCl_2$-H_2O system at 25°C [7] made using PHREEQ-A [9]. This figure gives an indication of which phases will be present at variable chloride concentrations. The chloride concentrations in the present experiments are between 0 and 1500 mmol/l, where AH_3, C_3AH_6 and CH are expected to be stable up to [Cl] ~ 105 mmol/l (when 0.5 mole/l NaCl is added) while above this concentration, AH_3, AFm-Cl and CH are expected to be stable until [Cl] ~ 3285 mmol/l; the threshold for other phases, such as $3CaO$-$CaCl_2$-$15H_2O$ (3-1-15), CaO-$CaCl_2$-H_2O (1-1-1), $CaCl_2$-H_2O and chlorine-ettringite will not be achieved under conditions likely to be encountered in most natural occurences. This figure is representative of zero sodium levels, the increasing range of Cl being achieved by adding $CaCl_2$, Damidot and Glasser calculated that the main differences arising from the presence of sodium will occur at lower chloride concentration, where the impact of sodium will increase chloride concentrations and decrease calcium concentrations.

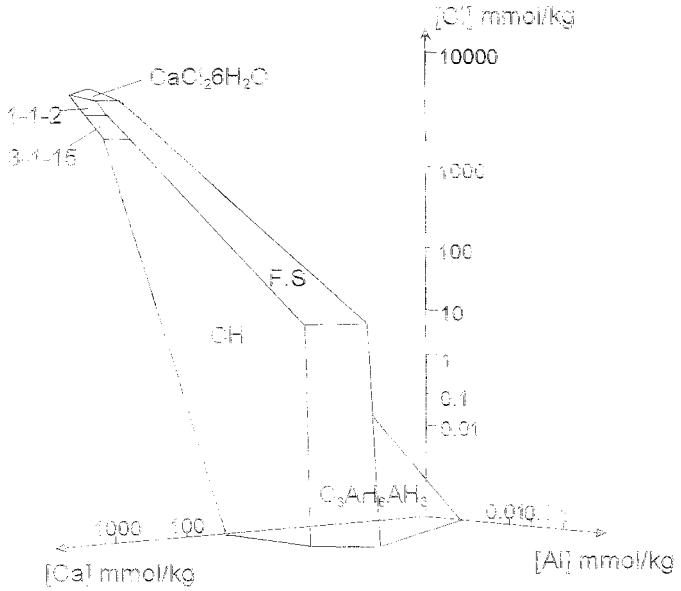

Figure 4.11 Three dimensional representation of the CaO-Al_2O_3-$CaCl_2$-H_2O system at 25°C (Na_2O= 0 mole/l). A non-linear concentration scale, ninth root of the concentration, is used.

SUMMARY OF THE 25°C RESULTS:

- C_3AH_6 dissolves congruently in water.
- At [NaCl] ≥ 0.5M a phase change is observed: $C_3AH_6 \rightarrow$ AFm-Cl + CH.
- The pH of the aqueous phase remains approximately unchanged with increasing NaCl concentrations to 1.5 M.

55°C Isotherm

Solubility data for C_3AH_6 in double distilled, degassed water (DDW), and normally 0.5 and 1.5 M NaCl at 55°C, are given in table 4.26; solid characterisation is presented in table 4.27.

Table 4.26 **Solubility measurements for C_3AH_6 cured in water and NaCl at 55°C for 186 days.**

Initial [NaCl] mol/l	pH	Aqueous Characterisation, mmol/l				charge imbalance	cal.
		Na	Cl	Ca	Al	OH, mmol/l	pH
0	12.18	0.16	0.11	6.55	2.01	19.18	12.3
0.41	12.66	468	386	0.34	4.29	95.55	13.0
1.50	12.59	1448	1342	0.19	2.92	115.14	13.1

Table 4.27 Solid characterisation of C_3AH_6 (abbreviated HG) cured in water and NaCl solutions at 55°C for 186 days.

Initial [NaCl] mol/l	CH	HG	AFm-Cl	AFm-CO_3	NaCl
0		VS		M	
0.41	W		S		t
1.50	W		S		W

The dataset indicates that C_3AH_6 dissolves congruently in dilute NaCl solutions, but at ≥ 0.5 M NaCl, a major phase change has occurred; C_3AH_6 decomposes to give mainly calcium monochloroaluminate (AFm-Cl) and CH. The pH of the aqueous phase remains approximately unchanged with increasing NaCl concentrations to 1.5 M (table 4.26). This trend is also observed for 25°C.

SUMMARY OF THE 55°C RESULTS:

- C_3AH_6 dissolves congruently in water.
- At [NaCl] ≥ 0.5M a phase change occurs: $C_3AH_6 \rightarrow$ AFm-Cl + CH.

The pH of the aqueous phase remains approximately unchanged with increasing NaCl concentrations to 1.5 M.

85°C Isotherm

Solubility data for C_3AH_6 in double distilled, degassed water (DDW), 1.0 and 1.5 M NaCl at 85°C are given in table 4.28; solid characterisation data are presented in table 4.29.

Table 4.28 Solubility measurements for C_3AH_6 cured in water or NaCl at 85°C for 173 days.

Initial [NaCl] mol/l	pH	Aqueous Characterisation, mmol/l				charge imbalance	calc.
		Na	Cl	Ca	Al	OH, mmol/l	pH
0	12.2	<1.0	<1.0	6.18	3.70	23.46	12.4
0.91	12.7	985	858	0.24	23.7	198.6	13.3
1.44	12.6	1370	1408	0.13	24.2	34.86	12.5

Table 4.29 Solid characterisation of C_3AH_6 (abbreviated HG) cured in water or NaCl solutions at 85°C for 173 days.

Initial [NaCl] mol/l	CH	HG	AFm-Cl	AFm-CO_3	NaCl
0		VS		M	
0.91	M		VS		M
1.44	M		VS		S

The dataset indicates that C_3AH_6 dissolves congruently in dilute NaCl solutions, but at ≥ 0.5 M NaCl a phase change occurs; C_3AH_6 decomposes to give calcium monochloroaluminate (AFm-Cl) and CH. The pH of the aqueous phase remains approximately unchanged with increasing NaCl concentrations up to 1.5 M. Aluminium solubility increases markedly as a consequence of alkaline hydrolysis, chloro-complexation and temperature.

SUMMARY OF THE 85°C RESULTS:

- C_3AH_6 dissolves congruently in water.
- At [NaCl] ≤ 0.9M a phase change is observed: $C_3AH_6 \rightarrow$ AFm-Cl + CH.
- The pH of the aqueous phase remains approximately unchanged with increasing NaCl concentrations up to 1.5 M.

4.1.2.3 The Combined Effect of Temperature and Salinity on Solubility, Stability and pH in NaCl Systems

Table 4.30 summaries the solid characterisation at the three temperatures and NaCl concentrations, 0 to 1.5M.

Table 4.30 X-ray analyses of hydrogarnet cured at various temperatures and brine conditions.

	NaCl Concentration in mol/l			
Temperature	0	0.5	1.0	1.5
25°C	C_3AH_6, AFm-CO_3	-	α&βAFm-Cl, CH	α&βAFm-Cl, CH
55°C	C_3AH_6, AFm-CO_3	α&βAFm-Cl, CH?	-	α&βAFm-Cl, CH
85°C	C_3AH_6, AFm-CO_3	-	α&βAFm-Cl, CH	α&βAFm-Cl, CH

It has been found that C_3AH_6 dissolves congruently at 25°C, 55°C and 85°C in DDW but when cured in [NaCl] ≥ 0.5 M, C_3AH_6 decomposes forming Friedel's salt and calcium hydroxide. Equilibrium, as reflected by phase transformations and steady-state solution concentrations, is attained relatively rapidly.

Atkins et al. [5] also showed that the solubility of hydrogarnet in water changes little over the temperature range 25-85°C: see table 4.22. The present studies indicate that its solubility in dilute NaCl also only changes little. However, when hydrogarnet is cured in NaCl between 0.5 -1.5 mole/l, Al solubility increases by a factor of ca. 10, at 25°C and 85°C. At 55°C, the Al solubility stays at approximately same level for NaCl concentrations up to 1.5 mole/l. However, Ca solubility decreases with increasing [NaCl].

Figure 4.12 illustrates the trends of solubility and the solid phase compositions for hydrogarnet cured in NaCl at three temperatures. The solid curve divides regions in which C_3AH_6 is stable, at least in part, from those where it decomposes. The boundary does not have the same

significance as an equilibrium diagram because in these experiments is position its influenced by the mass of reactant and solution volume.

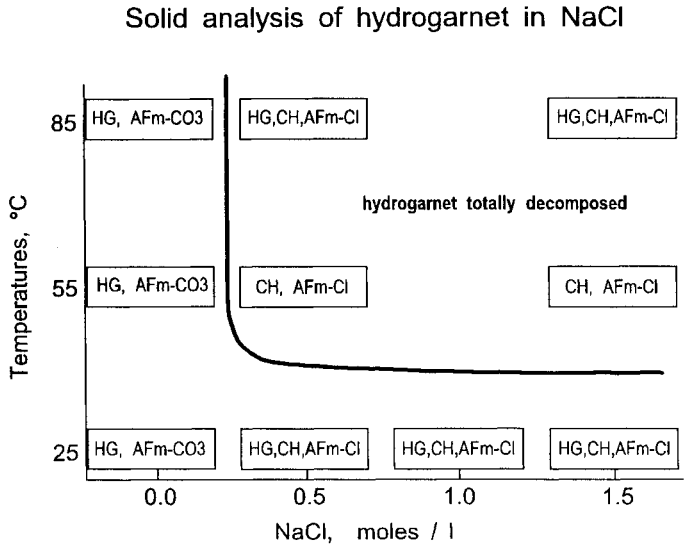

Figure 4.12 Summary for solid and aqueous analysis of hydrogarnet in NaCl at 25°, 55° and 85°C.

4.1.2.4 Kinetics and Respikes for $MgSO_4$ Systems

Initial calculations using PHRQPITZ V3.0/std at 25°C indicated a very low threshold of magnesium concentration which, when exceeded, results in formation of hydrotalcite in appropriate mixes. Hydrotalcite is calculated to precipitate at [Mg] between 3.78×10^{-9} M and 6.77×10^{-9} M, depending on aqueous [Ca] and [Al]: see table 4.31 and figure 4.13.

Table 4.31 Solution compositions for selected isothermally invariant points in the CaO-Al_2O_3-MgO-H_2O system at 25°C. Calculation performed using PHRQPITZ V3.0/std. Concentrations are in mol/kg. AU = Aberdeen data.

Solids in equilibrium	[Mg] in mol/kg	[Al] in mol/kg	[Ca] in mol/kg	pH
CH	0	0	2.19×10^{-2}	12.5
MH	1.60×10^{-4}	0	0	10.5
AH_3	0	5.15×10^{-9}	0	7.0
HT (AH_3 SI = 0.996)	3.00×10^{-5}	1.50×10^{-5}	0	9.7
CH + MH	1.15×10^{-7}	0	2.19×10^{-2}	12.5
AH_3 + HT	3.73×10^{-5}	2.42×10^{-6}	0	9.9
MH + HT	1.60×10^{-4}	1.97×10^{-9}	0	10.5
C_3AH_6 (AU)+ AH_3	0	5.70×10^{-4}	9.72×10^{-3}	12.2
C_3AH_6 (AU)+ CH	0	6.67×10^{-5}	2.19×10^{-2}	12.5
MH + CH + HT	1.15×10^{-7}	2.33×10^{-7}	2.19×10^{-2}	12.5
HT + CH + C_3AH_6(AU)	6.77×10^{-9}	6.69×10^{-5}	2.19×10^{-2}	12.5
C_3AH_6 (AU) + HT + AH_3	3.78×10^{-9}	5.70×10^{-4}	9.72×10^{-3}	12.2

A kinetic experiment was only carried out for ettringite, but it is assumed that both phases will follow the same general pattern of reaction; see section 4.1.4.4 for ettringite data. The calculated maximum numbers of respikes for 0.05 M $MgSO_4$ was 9: see Appendix 3.

Respikes

The aqueous phase at 85°C was analysed initially after one respike and again after 7 respikes; all systems were analysed again after 8 respikes. After 8 respikes the systems had reached the target concentration and the reaction had slowed so much that it was likely either approaching completion and not to need respiking, or else to require many months before the magnesium concentration would decrease sufficiently to be respiked again.

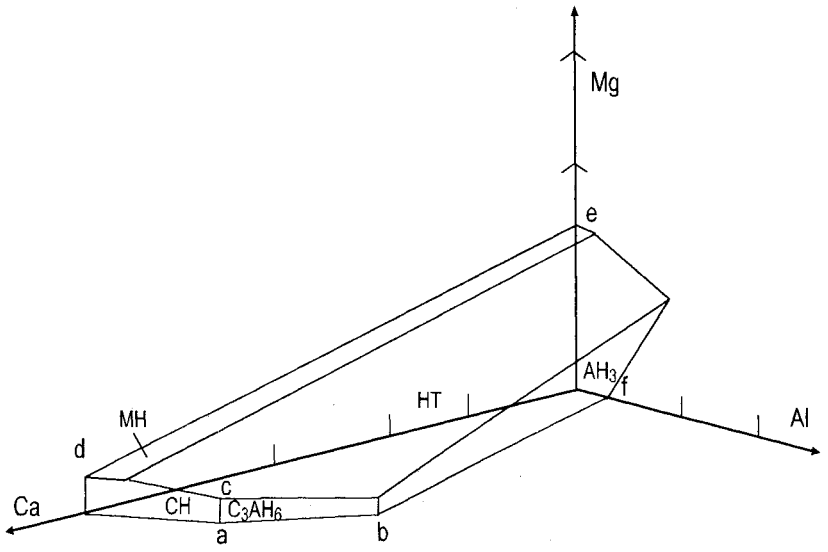

Figure 4.13 Threshold for magnesium in the system $CaO-Al_2O_3-MgO-H_2O$ system at 25°C. Calculations performed using PHRQPITZ V3.0V/std. The species concentrations calculated at selected invariant points are as follows (in mmol/kg H_2O).

Point	Ca	Mg	Al
a	22	O	0.07
b	9.7	O	0.6
c	~22	$6.7x10^{-6}$	~0.07
d	22	$1.2x10^{-4}$	0
e	0	16	0
f	0	O	$5x10^{-6}$

The calculations show the stable pattern of coexistence of solids with aqueous solutions is:

(a) CH + MH + HT
(b) CH + C_3AH_6 + HT
(c) C_3AH_6 + AH_3 + HT

4.1.2.5 Solubility Data, pH and Solid Phase Compositions for $MgSO_4$ Systems

The $CaO-Al_2O_3-CaSO_4-H_2O$ system shown in figure 4.14, was studied by Damidot and Glasser [8] who calculated seven coexistence regions of solids in equilibrium with solution at 25°C:

$0 < [SO_4^{2-}] < 0.015$ mmol/l	: AH_3, C_3AH_6 and CH
$0.015 \leq [SO_4^{2-}] \leq 0.030$ mmol/l	: AH_3, C_3AH_6 , ettringite and CH
$0.030 < [SO_4^{2-}] < 11.4$ mmol/l	: AH_3,ettringite and CH
$[SO_4^{2-}] = 11.4$ mmol/l	: AH_3,ettringite, CH and gypsum
$11.4 < [SO_4^{2-}] \leq 15$ mmol/l	: AH_3,ettringite and gypsum
$15.12 < [SO_4^{2-}] \leq 15.2$ mmol/l	: gypsum

Thus hydrogarnet is in equilibrium with solution at a sulfate concentration below 0.030 mmol/l above which it becomes unstable. This threshold value changes with temperature and in the presence of other ions: Glasser et.al.(11) calculated that at 50°C, depending on Ca/Al ratio (see Fig. 4.15), the following assemblages exist:

$0 < [SO_4^{2-}] \leq 0.040$ mmol/l	:AH_3, C_3AH_6 and CH
$0.040 \leq [SO_4^{2-}] < 0.042$ mmol/l	:AH_3, C_3AH_6 , monosulfoaluminate and CH
$0.042 \leq [SO_4^{2-}] \leq 0.060$ mmol/l	:AH_3, C_3AH_6, monosulfoaluminate, ettringite and CH
$0.060 < [SO_4^{2-}] \leq 0.064$ mmol/l	:AH_3,monosulfoaluminate, ettringite and CH
$0.064 < [SO_4^{2-}] < 11.67$ mmol/l	:AH_3, ettringite and CH

At 50°C hydrogarnet is in equilibrium with solution at a sulfate concentration below 0.060 mmol/l and ettringite is metastable for $[SO_4^{2-}] < 0.042$ mmol/l, although monosulfoaluminate is stable at sulphate concentrations between 0.040 and 0.064 mmol/l [11].

At 85°C both ettringite and monosulfoaluminate are calculated to become unstable at lower sulfate concentrations than at 55°C. Thus:

$0 < [SO_4^{2-}] < 0.060$ mmol/l	:AH_3, C_3AH_6 and CH
$0.060 \leq [SO_4^{2-}] < 0.078$ mmol/l	:AH_3, C_3AH_6, monosulfoaluminate, ettringite and CH
$0.078 \leq [SO_4^{2-}] \leq 0.410$ mmol/l	:AH_3, monosulfoaluminate and CH
$0.410 < [SO_4^{2-}] \leq 0.550$ mmol/l	:AH_3, monosulfoaluminate, ettringite and CH
$0.550 \leq [SO_4^{2-}] \leq 10.57$ mmol/l	:AH_3, ettringite and CH
$[SO_4^{2-}] = 10.57$ mmol/l	:AH_3,ettringite and gypsum
$10.57 < [SO_4^{2-}] \leq 12.57$ mmol/l	:AH_3 and gypsum

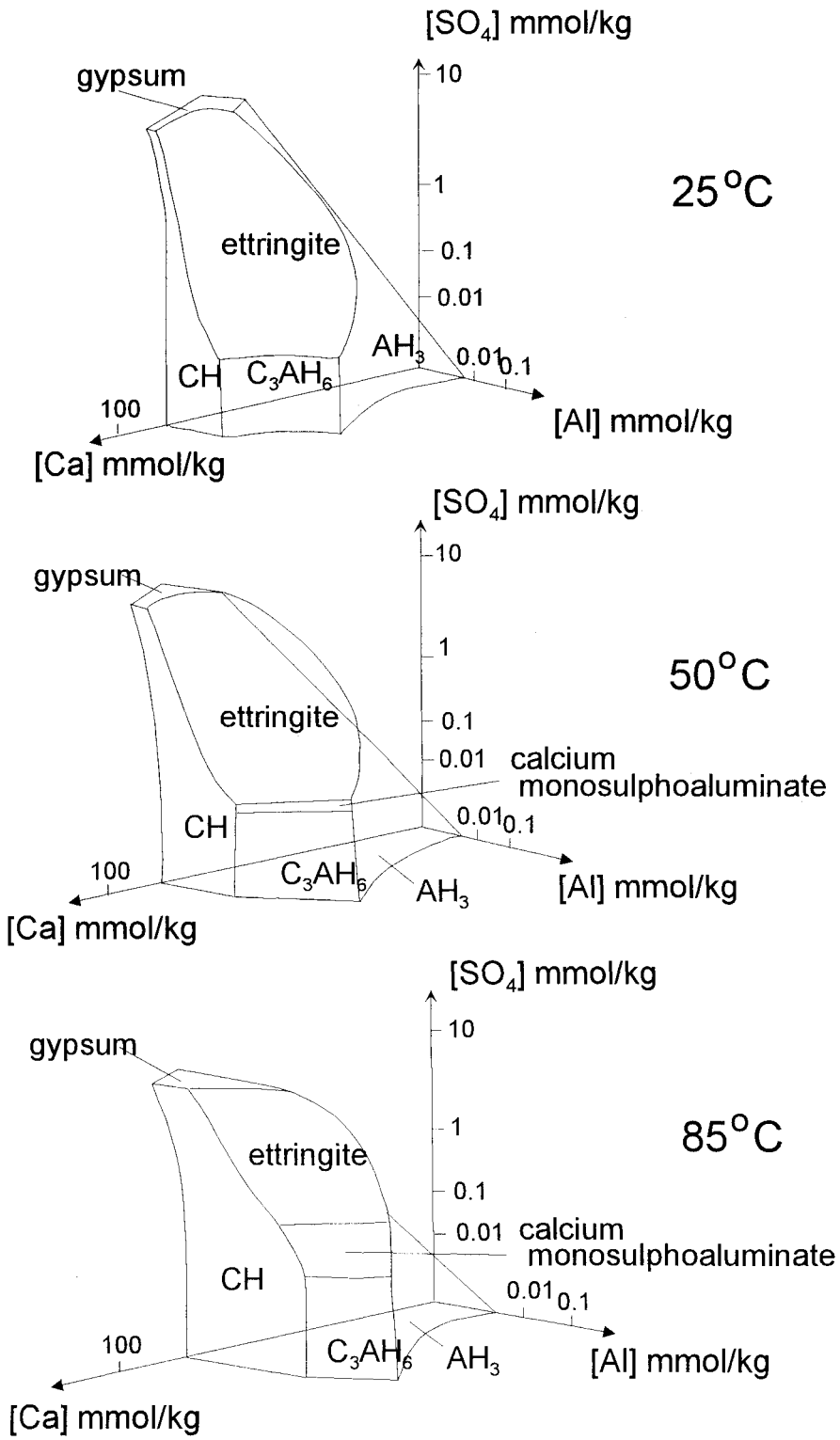

Figure 4.14 Phase relations in the C-A-s-H system at 25°, 50° and 85°C; the scale on each axis is proportional to the fifth root of concentration.

25°C isotherm

The results from the aqueous analysis without respiking cured for 146 days, and after one respike are shown in table 4.32

Table 4.32 Aqueous characterisation of hydrogarnet cured in $MgSO_4$ at 25°C. The results without parentheses are after 146 days curing and no respikes and the results in parentheses are after one respike and an additional 257 curing days (total, 403 days).

Target [$MgSO_4$] mol/l	pH	Aqueous Characterisation, mmol/l				Charge imbalance OH, mmol/l
		Ca	Al	Mg	SO_4	
0.005	12.10	6.84	3.94	<0.01	0.04	25.4 (20.8)
	(11.97)	(5.99)	(2.96)	(<0.01)	(0.02)	
0.010	12.05	6.14	3.50	<0.01	<0.01	22.8 (12.45)
	(11.96)	(4.99)	(4.15)	(<0.01)	(<0.01)	
0.050	12.00	5.04	2.76	<0.01	0.08	18.2 (15.32)
	(11.23)	(3.99)	(2.50)	(<0.01)	(0.02)	

The results of the solid analysis are shown in table 4.33

Table 4.33 Solid characterisation of hydrogarnet cured in $MgSO_4$ at 25°C. The results without parentheses are after 146 days curing and no respikes and the results in parentheses are after one respike and an additional 257 curing days (total, 403 days).

Target [$MgSO_4$], mol/l	C_3AH_6		AFm-SO_4		AFt		HT
0.005	S	(S)	S	(S)			(M)
0.010	S	(S)	S	(S)			(M)
0.050	S	(M)	S	(W)	S	(S)	(S)

AEM of hydrogarnet reacted in 0.05M $MgSO_4$, but without respike, showed semicrystalline hydrotalcite. With respiking, hydrotalcite could also be identified by XRD. Tables 4.32 and 4.33 show that the [Mg] had been almost totally depleted. Further respikes were needed. At 85°C (see later), reaction occurred rapidly and 8 respikes were carried out before further analysis. Results for the 25°C are shown in tables 4.34 and 4.35

Table 4.34 Aqueous characterisation of C_3AH_6 cured in $MgSO_4$ at 25°C; results after 8 respikes.

Target [$MgSO_4$] mol/l	pH	Aqueous Characterisation, mmol/l				Charge imbalance OH, mmol/l
		Ca	Al	Mg	SO_4	
0.005	11.74	4.62	4.78	<0.01	0.24	23.1
0.010	11.74	4.22	2.27	<0.01	0.02	15.2
0.050	7.39	10.28	<0.01	104.9	112.5	5.36

As seen in table 4.34 the [Mg] for nominally 0.05 M $MgSO_4$ is approximately double the target value, 50mmol. This is because of the respiking procedure and unexpected slow reaction of the system. It is expected that this concentration would diminish with time because some AFm-SO_4 still remains. [Mg] for the lower target values has depleted to near-zero. However, since the Mg threshold for product formation is low, it can be assumed that equilibrium solid phase distribution and pH will ultimately be similar to the phase distribution in 0.05M $MgSO_4$.

Table 4.35 shows that with increasing [$MgSO_4$], HT reacts leaving AFm-SO_4 as the Al-containing phase. This remaining AFm-SO_4 should be capable of conditioning a high pH,. ca 11, but does not, perhaps owing to its physical isolation from the aqueous phase.

Table 4.35 Solid characterisation of hydrogarnet cured in $MgSO_4$ at 25°C. The results were obtained after 8 respikes. ✓ denotes the phase is present.

Target [$MgSO_4$], mol/l	C_3AH_6	AFm-SO_4	AFt	HT	Gypsum	MH
0.005	✓	✓	✓	✓		
0.010	✓		✓			
0.050		✓			✓	✓

SUMMARY OF THE 25°C RESULTS:

- the reaction of hydrogarnet with $MgSO_4$ is slower than the analagous reaction with C-S-H.
- low sulfate phases convert to high sulfate phases.
- as the $MgSO_4$ concentration increases, gypsum and brucite dominate the remaining solids.
- pH decreases to ~ 7.4.

55°C Isotherm

To finish the programme, the 55°C experiments were given lower priority; samples have been respiked, but not analysed. Analysed results will be presented in a thesis: Goldthorpe (1998).

Table 4.36 and 4.37 shows the results without respiking.

Table 4.36 Aqueous characterisation of hydrogarnet cured in $MgSO_4$ at 55°C. The results are after 214 days curing and no respiking.

Target [$MgSO_4$] mol/l	pH	Aqueous Characterisation, mmol/l				Charge imbalance OH, mmol/l
		Ca	Al	Mg	SO_4	
0.005	12.01	6.42	3.31	<0.01	0.03	22.7
0.010	12.05	6.53	3.05	<0.01	0.01	22.2
0.050	11.94	4.81	2.82	<0.01	0.07	18.0

Although the target concentrations are not maintained, the results indicate reaction directions: [Ca] and [Al] decrease with increasing [$MgSO_4$]: [SO_4] is removed forming AFm-SO_4 (table 4.37). In these experiments no significant decrease in pH is observed. However from experiments at 25° and 85°C it is expected that pH would decrease with increasing numbers of respikes as the initial solid reactant becomes consumed.

Table 4.37 Solid characterisation of hydrogarnet cured in $MgSO_4$ at 55°C. These results were obtained after 214 days curing and no respiking.

Target [$MgSO_4$], mol/l	C_3AH_6	AFm-SO_4	HT
0.005	S	M	W
0.010	S	M	M
0.050	S	M	S

SUMMARY OF THE 55°C RESULTS:

- Hydrogarnet reacts to form AFm-SO_4 and a hydrotalcite-like phase.
- pH is still conditioned by AFm-SO_4.

85°C Isotherm

The results from the aqueous analysis without respiking and after one respike are shown in table 4.38.

Table 4.38 Aqueous characterisation of C_3AH_6 cured in $MgSO_4$ at 85°C. The results are after 187 days curing and no respikes; results in ( ) are after one respike and an additional 256 curing days (total, 443 days).

Target [$MgSO_4$] mol/l	pH	Aqueous Characterisation, mmol/l				Charge imbalance OH, mmol/l
		Ca	Al	Mg	SO_4	
0.005	11.94 (11.97)	5.29 (5.99)	4.00 (4.15)	<0.01 (<0.01)	0.07 (0.20)	22.4 (24.0)
0.010	12.01(12.02)	5.89 (5.99)	3.85 (3.89)	<0.01 (<0.01)	0.02 (0.03)	23.3 (23.6)
0.050	11.95 (11.62)	4.84 (4.99)	2.89 (1.40)	<0.01 (<0.01)	0.08 (1.65)	18.2 (10.9)

The results of the solid analysis are shown in table 4.39

Table 4.39 Solid characterisation of C_3AH_6 cured in $MgSO_4$ at 85°C. The results are after 187 days curing and no respikes; results in ( ) are after one respike and an additional 256 curing days (total, 443 days).

Target [$MgSO_4$], mol/l	C_3AH_6	AFm-SO_4	AFt	HT
0.005	S (S)	W/M (S)		W (M)
0.010	S (S)	W (S)		W (S)
0.050		W	(S)	W (M)

From tables 4.38 and 4.39 it seen that the [Mg] was depleted to near zero; HT is detected by XRD, weak at first but increasing after one respike.

Further respikes were needed and after 7 respikes the systems were analysed again. The results from these analyses are shown without parentheses in tables 4.40 and 4.41. Since reaction was fast, one further respike was carried out; these results are shown in the tables in parentheses. The results after 7 respikes have no significance except to help indicate to the reader how one can use the analytical results as an indicator of the completeness of reaction.

Table 4.40 Aqueous characterisation of hydrogarnet cured in $MgSO_4$ at 85°C. The results without parenthesis are after 7 respikes and the results in parentheses are after 8 respikes.

Target [$MgSO_4$] mol/l	pH	Aqueous Characterisation, mmol/l				Charge imbalance
		Ca	Al	Mg	SO_4	OH, mmol/l
0.005	11.94 (11.85)	5.09 (5.29)	5.74 (3.43)	1.34 (<0.01)	0.01 (0.02)	30.1 (20.8)
0.010	11.62 (11.55)	4.02 (4.82)	2.41 (2.04)	2.67 (<0.01)	1.33 (2.19)	18.0 (11.4)
0.050	10.86 (6.89)	14.12 (10.98)	0.46 (<0.01)	14.40 (1.17)	14.06 (10.42)	30.3 (3.46)

Table 4.41 Solid characterisation of hydrogarnet cured in $MgSO_4$ at 85°C. The results without parenthesis are for 7 respikes and the results in parentheses are after 8 respikes. + denotes that the phase is observed, but the relative amounts were not quantified.

Target [$MgSO_4$], mol/l	C_3AH_6	AFm-SO_4	AFt	HT	Gypsum	MH
0.005	S (+)	S (+)		W (+)		W
0.010		S (+)	W (+)	M (+)		M
0.050		S (+)	M		S (+)	M (+)

Tables 4.40 and 4.41 disclose that aqueous magnesium is almost totally depleted. Even though the calculations showed that the system needed to be respiked 9 times before all Al and Ca reacted with Mg, the pH of the solution had decreased to 6.9. The results from XRD also show no reflections for HG which indicate that it was absent or nearly so. For [$MgSO_4$] = 0.01 M the pH remained high, probably conditioned by AFm-SO_4. Because the lower concentration shows the same reaction trends it was not respiked.

SUMMARY OF THE 85°C RESULTS:

- hydrogarnet reacts with both Mg and SO_4 to form hydrotalcite, AFm-SO_4, AFt, gypsum and MH.
- pH decreases to ~ 6.9 as a consequence of reaction.

4.1.2.6 The Combined Effect of Temperature and Salinity on Solubility, Stability and pH in $MgSO_4$ Systems

Figure 4.15 illustrates the trends for the solubility data and the solid phase compositions for hydrogarnet cured in $MgSO_4$ at three temperatures.

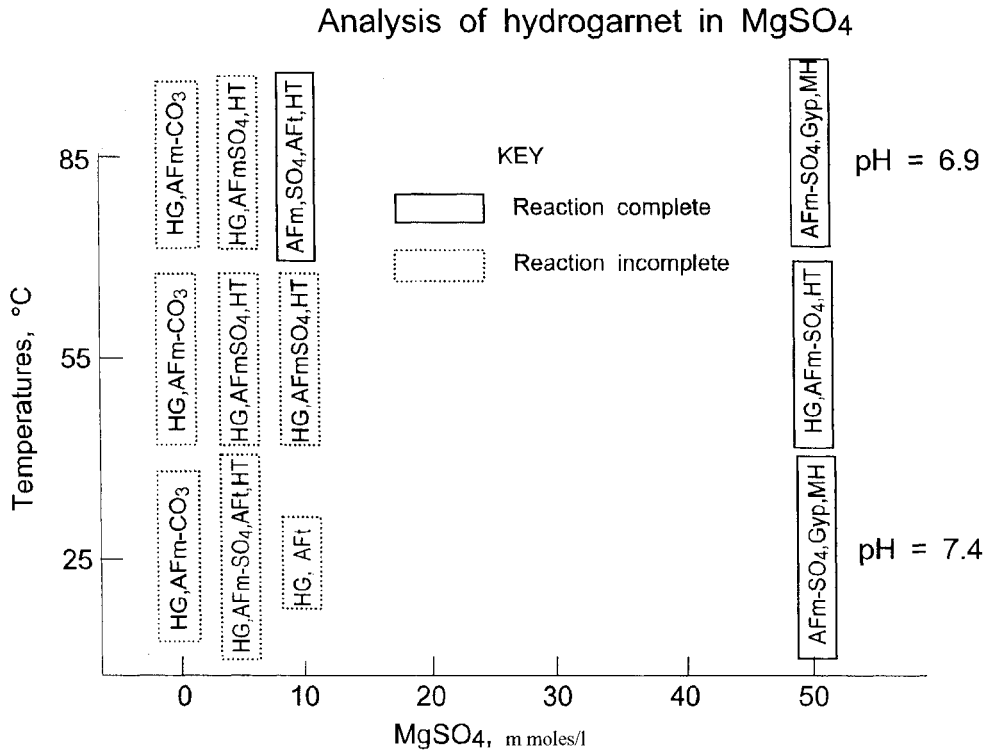

Figure 4.15 Summary for solid and aqueous analysis of hydrogarnet in $MgSO_4$ at 25°, 55° and 85°C.

Hydrogarnet becomes unstable with increasing $MgSO_4$ concentration and, as a consequence, the pH decreases. AFm-SO_4 , gypsum and brucite are the stable assemblage for 0.05 mol/l $MgSO_4$ both at 25°C and 85°C.

References

1. L.S. Wells, F. Clarke and H.F. McMurdie. (1943) 'Study of the System CaO-Al_2O_3-H_2O at Temperatures of 21° and 90°C'. Journal of Research of the National Bureau of Standards, **30**, R. P. 1539

2. F. M. Lea. (1970) 'The Chemistry of Cement and Concrete', Edward Arnold Ltd., London (Third Edition).

3 T. G. Jappy and F. P. Glasser. (1991/92) 'Synthesis and Stability of Silica substituted hydrogarnet $Ca_3Al_2Si_3$-$xO_{12-4x(0H)4x}$'. Advances in Cement Research **4**, No. 1, pp. 1 - 8

4. M. Atkins et.al. (1991) 'A Thermodynamic Model for Blended Cements'. UK DoE Report no. DoE/HMIP/RR/92/005, Aberdeen University.

5. M. Atkins et.al. (1993) 'Thermodynamic Modelling of Blended Cements at Elevated Temperature (50-90°C)'. UK DoE Report no. DoE/HMIP/RR/94/011, Aberdeen University, Scotland

6. E. P. Flint, H. F. McMurdie and L. S. Wells. (1941) 'Hydrothermal and X-ray Studies of the Garnet-hydrogarnet Series and the Relationship of the Series to Hydration Products of Portland Cement'. Journal of Research of the National Bureau of Standards **26**, R. P. 1355

7. D. Damidot, U.A. Birnin-Yauri and F.P. Glasser. (1994) 'Thermodynamic Investigation of the CaO-Al_2O_3-$CaCl_2$-H_2O System at 25°C and the Influence of Na_2O. Il Cemento **4**, pp.243-254.

8. D. Damidot and F. P. Glasser. (1993) 'Thermodynamic Investigation of the CaO-Al_2O_3-$CaSO_4$-H_2O System at 25°C and the Influence of Na_2O'. Cement and Concrete Research, **23**, pp.221-238.

9. D.L. Parkhurst, D.C. Thorstenson and L.N. Plummer. (1990) 'PHREEQE-A Computer Program for Geochemical Calculations'. US Geological Survey, Water Resources Investigations Report 80-96 Washington, D.C.

10. H.F.W Taylor. (1992) 'Cement Chemistry'. Academic Press, London and New York.

11. F.P. Glasser, D. Damidot and M. Atkins. (1992) 'Thermodynamic Investigation of the CaO-Al_2O_3-$CaSO_4$-H_2O System at 50°C and 85°C.' Cem. Concr. Res.**22**, pp.1179-1191.

12. F.P. Glasser, D. Damidot and M. Atkins. (1995) 'Phase Development in Cement in Relation to the Secondary Ettringite Problem'. Advances in Cement Research 7, No.26, pp.57-68.

13. H.M. May, P.A. Helmke and M.L. Jackson. (1979) 'Gibbsite Solubility and Thermodynamic Properties of Hydroxy-Aluminium Ions in Aqueous solution at 25°C'. Geochim. Cosmochim. Acta **43**, pp.861-868.

14. H.J. Kuzel. (1966) 'Röntgenuntersuchung in System $3CaO{\cdot}Al_2O_3{\cdot}CaSO_4{\cdot}nH_2O$ - $3CaO{\cdot}Al_2O_3{\cdot}CaCl_2{\cdot}nH_2O$'. N. Jahrbuch. Miner. Monatshefte, pp.193-200.

15. R. Fisher, H.J. Kuzel and H. Schellhorn. (1980) 'Hydrocalumit:Mischkristalle von "Friedelschem Salz", $3CaO{\cdot}Al_2O_3{\cdot}CaCl_2{\cdot}10H_2O$ und Tetracalciumaluminatehydrate $3CaO{\cdot}Al_2O_3{\cdot}Ca(OH)_2{\cdot}12H_2O$'. N. Jahrbuch. Miner. Monatshefte, pp.322-334.

16. U.A. Birnin-Yauri. (1993) 'Chloride in Cement: Study of the System $CaO{\cdot}Al_2O_3{\cdot}CaCl_2{\cdot}H_2O$'. Ph.D Thesis, Aberdeen University.

17. S. Stronach. (1996) 'Thermodynamic Modelling and Phase Relations of Cementitious Systems'. PhD. Thesis. Aberdeen University.

4.1.3 Calcium-monosulfoaluminate, AFm-SO_4

4.1.3.1 Introduction and Background

Taylor [1] gives the general formula of AFm as $[Ca_2(Al,Fe)(OH)_6]\cdot X\cdot xH_2O$, where X denotes one formula unit of a single charged ion, such as OH^- and Cl^-, or half a formula unit of a double charged anion, typically SO_4^{2-} or CO_3^{2-}.

Differences in layer stacking, water content and in the mean atomic number of anion substituents limit the value of X-ray powder diffraction as a characterisation tool, so AEM as also been used. AFm phases with mono- and divalent anions, e.g., Cl^- and SO_4^{2-}, exhibit little miscibility. Moreover, discrete compounds which exhibit anion ordering, e.g. Kuzel's salt containing essential Cl^- as well as SO_4^{2-}, have definite stability regions.

Extensive work on the behaviour of the calcium monosulfoaluminate hydrates in pure water systems and at various temperatures has been reported [2,3,4]. Ettringite, $3CaO\cdot Al_2O_3\cdot 3CaSO_4\cdot 32H_2O$, and hydrogarnet are the stable phases at normal temperature and pressure with respect to AF_m-SO_4, although AFm-SO_4, ($3CaO\cdot Al_2O_3\cdot CaSO_4\cdot 12H_2O$) does become stable at temperatures above ~ 40°C. However, AFm-SO_4 is normally observed in cement pastes cured at ambient temperatures despite its slight degree of metastability.

4.1.3.2 Solubility Data, pH and Solid Phase Compositions for NaCl Systems

25° Isotherm

Solubility data for AFm-SO_4 in double distilled, degassed water (DDW) and in 0.5, 1.0 and 1.5 M NaCl at 25°C are given in tables 4.42 and 4.43. From this table it is seen that the solid phase contains some soluble Na and Cl and that in general, sulfate concentration increases significantly with increasing [NaCl]. AFm-SO_4 cured in NaCl is transformed to mixtures of AFm-Cl + AFm-Cl-SO_4 + AFt and solid-phase solubility increases with increasing [NaCl], see table 4.44.

Table 4.42 Solubility of AFm-SO_4 cured in water and NaCl at 25°C for 134 days.

Initial [NaCl] mol/l	pH	Aqueous Characterisation, mmol/l					charge imbalance OH, mmol/l	cal. pH
		Na	Cl	Ca	Al	SO_4		
0	12.1	5.0	5.0	4.72	2.19	0.03	16.0	12.2
0.44	12.2	476	458	1.94	4.68	0.89	34.1	12.5
0.91	12.0	897	898	1.95	4.27	2.60	10.5	12.0
1.36	11.8	1305	1338	2.20	3.38	4.75	-28.0	-

Figure 4.16 shows the solubility equilibria for the AFm-SO_4 aged in NaCl solutions. Because phase transformations occur in the solid(s), it may not be strictly accurate to draw continuous trend lines linking data points.

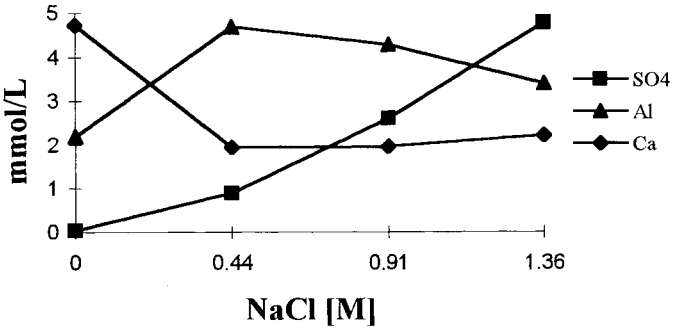

Figure 4.16 AFm-phase solubility in response to NaCl concentration at 25°C.

When AFm-SO_4 is dissolved into initially pure water, ratios of Ca, Al and OH concentrations are close to those required for congruency but SO_4 contents are much too low: see table 4.43.

Table 4.43 Species ratios verification of the dissolution of AFm-SO_4 in DDW at 25°C.

Component Ratio	Ratio in AF_m-SO_4	measured ratio
Ca:Al	2:1(2.00)	4.7:2.2 (2.14)
Ca:SO_4	4:1 (4.00)	4.7:0.3 (15.7)
Al:SO_4	2:1 (2.00)	2.2:0.3 (7.33)
OH:SO_4	12:1(12.0)	12.6:0.3(42.0)

The X-ray data (table 4.44) shows that AFm-SO_4 decomposes slowly in water as a consequence of its thermodynamic metastability relative to AFt + C_3AH_6. This well-known phenomenon is reported in previous studies [2,3,4,5].

Because of its incongruent dissolution behaviour, calculation of a simple K_{sp} value is not justified.

Table 4.44 Solid characterisation of AFm-SO_4 cured in water and NaCl solutions at 25°C for 134 days.

Initial [NaCl] mol/l	AFm-SO_4	AFm-Cl	AFm-Cl-SO_4	HG	AFt	NaCl
0	S			W	M	
0.44		S	W		S	W
0.91		M	W		S	W
1.36		M	W		S	M

At 25°C, AFm-SO_4 also undergoes complex reactions in NaCl to form AFt, AFm-Cl and AFm-Cl-SO_4. AEM of AFm-Cl thus formed showed classic plate-like morphology ~ 10 microns. It had nearly ideal Friedel's salt composition with only minor SO_4 substitution. The AFt phase had classic needle-like rod morphology, 10-30 microns in length. and its chemical composition was close to theoretical.

Despite some uptake of chloride ions by monosulfoaluminate type phases, the weight ratios of solid and aqueous phases were such that Na/Cl ratios did not depart significantly from 1.0, hence no respiking was necessary. As shown in table 4.42 and figure 4.17 the pH is approximately unchanged by curing in NaCl: the solid therefore continues to condition a high pH.

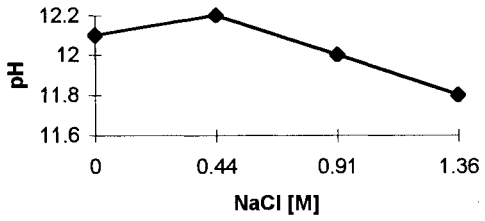

Figure 4.17 pH of AFm-phase in response to NaCl concentration at 25°C.

SUMMARY OF THE 25°C RESULTS:

- AFm-SO_4 dissolves incongruently both in water and in NaCl, 0.5 to 1.5M.
- AFm-SO_4 is thermodynamically metastable but persistent relative to hydrogarnet and ettringite in DDW at 25°C but it becomes stable at > 40°C.
- At [NaCl] ≥ 0.5M a phase change is observed: AFm-SO_4 → AFm-Cl-SO_4 + AFm-Cl.
- The solubility of sulfate increases is enhanced by NaCl: AFm-SO_4 alters to AFm-Cl-SO_4 + AFm-Cl .
- The pH of the aqueous phase remains approximately unchanged with increasing NaCl concentrations up to 1.5 M.

55° Isotherm

Solubility data for AFm-SO_4 cured in DDW, 0.5 M and 1.5 M NaCl are shown in table 4.45 and figure 4.18.

Table 4.45 Solubility measurements for AFm-phase cured in water and in NaCl at 55°C for 186 days.

Initial [NaCl] mol/l	pH	Aqueous Characterisation, mmol/l					charge imbalance OH, mmol/l	calc. pH
		Na	Cl	Ca	Al	SO_4		
0	11.77	0.05	0.04	3.99	3.22	0.62	16.4	12.22
0.41	11.93	483	439	3.91	21.3	4.99	105.7	13.02
1.50	11.60	1462	1357	6.71	24.2	15.09	160.8	13.21

The solid contributes traces of soluble sodium and chloride to the solution. AFm-SO_4 dissolves incongruently at 55°C but the aqueous Ca/SO_4 ratio is now ~ 6.4 (ideal = 4.0) compared with ~ 15.7 at 25°C. The observed ratio in NaCl is conditioned by a mixture of solids: AFm-SO_4, AFm-Cl and AFt. At 25°C Kuzel's salt (AFm-Cl-SO_4) was observed, but this phase has not been observed at 55°C. In 1.5 M NaCl, XRD analysis shows the reaction product is AFm-Cl: AFt is absent.

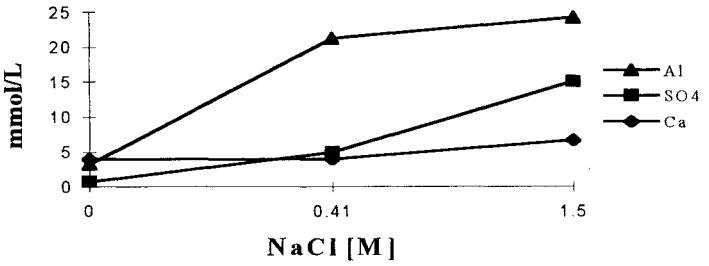

Figure 4.18 AFm-phase solubilities in NaCl solutions at 55°C: see text for the identity of the solids.

The aqueous concentration of Ca remains approximately constant for AFm-SO_4 cured in DDW and 0.5 M NaCl, but increases by a factor of ~1.5 in 1.5 M NaCl. Aluminium is solubilised when AFm-SO_4 is cured in 0.5 M NaCl (~7 fold), but there is only a slight further increase from 21.3 to 24.2 mmol/l in 1.5 M NaCl. The sulfate solubility increases with increasing [NaCl]; from 0.6 mmol/l in DDW to 5.0 mmol/l in 0.5 M NaCl and to 15.1 mmol/l in 1.5 M NaCl. These solubility changes are accompanied by solid phase changes. The pH measured at room temperature is shown in table 4.45 and figure 4.19.

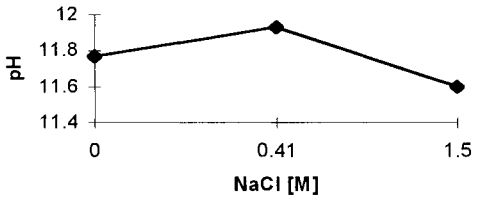

Figure 4.19 pH generated by AFm-SO_4 cured in NaCl solutions at 55°C.

Analysis of solids at 55°C (table 4.46) shows that a phase change, to Friedel's salt, occurs when AFm-SO_4 is cured in NaCl solutions.

Table 4.46 Solid characterisation of AFm-phase cured in water and NaCl solutions at 55°C for 186 days. AFm-SO_4.

Initial [NaCl] mol/l	AFm-SO_4	AFm-Cl	AFt	NaCl
0	M		W	
0.44		W	MS	
1.36		S	t	W

SUMMARY OF THE 55°C RESULTS:

- AFm-SO_4 dissolves incongruently both in water and in NaCl, but its dissolution is not as strongly incongruent as at 25°C.
- Solubility increases are accompanied by a phase change from AFm-SO_4 to AFm-Cl with increasing NaCl concentration.
- AFm-SO_4 is thermodynamically metastable relative to ettringite in DDW.
- At [NaCl] > 0.5M, AFm-SO_4 transforms to AFm-Cl.
- the pH conditioned by AFm-SO_4 remains approximately unchanged with increasing NaCl concentrations up to 1.5 M.

85°C Isotherm

AFm-SO_4 is stable in DDW and dissolves congruently, or nearly so; see table 4.47.

Table 4.47 Species ratios showing congruent dissolution of AFm-SO_4 at 85°C.

	Ratios in solid	**aqueous ratios**
Ca:Al	2:1(2.00)	4.7:2.2 (2.14)
Ca:SO_4	4:1 (4.00)	4.4:1.1 (4.0)
Al:SO_4	2:1 (2.00)	2.1:1.1 (1.9)
OH:SO_4	12:1(12.0)	17.2:1.1(15.6)

This is also confirmed by the solid analysis (table 4.48) where only AFm-SO_4 and a small amount of calcite were observed. However, when AFm-SO_4 is cured in NaCl it undergoes a phase change, giving AFm-Cl-SO_4 at 0.5 M NaCl and AFm-Cl at [NaCl] = 1.5 M.

Table 4.48 Solid characterisation of AFm-SO_4 cured in water and NaCl solutions at 85°C for 165 days: x indicates that AFt precipitated from the supersaturated solution upon standing at 25°C: see text.

Initial [NaCl] mol/l	AFm-SO_4	AFm-Cl	AFm-Cl-SO_4	AFt	Cc	NaCl
0	VS				W	
0.44			W	x		M
1.36		VS		x		S

Solubility data for AFm-SO_4 cured in DDW, 0.5 M and 1.5 M NaCl are shown in table 4.49.

Table 4.49 Solubility measurements for AFm-SO_4 cured in water and in NaCl at 85°C for 165 days.

Initial [NaCl] mol/l	pH	Aqueous Characterisation, mmol/l					charge imbalance OH, mmol/l	calc. pH
		Na	Cl	Ca	Al	SO_4		
0	11.9	<1	<1	4.38	2.10	1.09	17.2	12.2
0.44	11.9	469	480	8.31	3.59	7.19	2.0	11.3
1.36	11.5	1327	1394	7.20	3.17	16.14	-75.4	-

Table 4.49 and figure 4.20 show that SO_4 solubility increases with increasing [NaCl]. The enhancement is particularly marked at high chloride content, above ~0.5M.

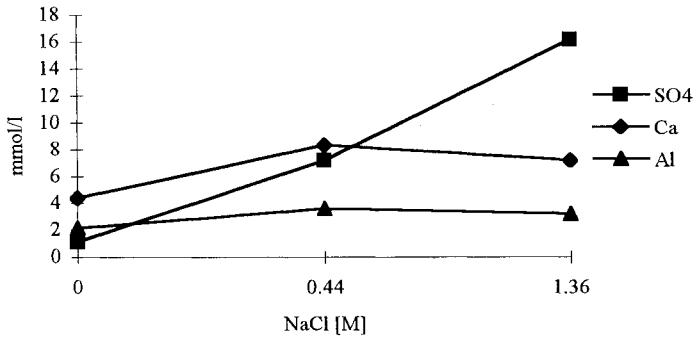

Figure 4.20 AFm-SO_4 solubility in NaCl solutions at 85°C.

AEM analysis of AFm-SO_4 cured in 0.5 M NaCl gave Kuzel's salt: $3CaO{\cdot}Al_2O_3{\cdot}0.5CaCl_2{\cdot}0.5Ca(SO_4){\cdot}12H_2O$ as relatively large hexagonal plates, 10-20 microns. The pH of the aqueous phase, shown in table 4.49, remains approximately constant with increasing [NaCl].

SUMMARY OF THE 85°C RESULTS:

- AFm-SO_4 is stable and dissolves congruently, or nearly so, in water.
- AFm-SO_4 is unstable in NaCl, giving Kuzel's salt at 0.5 M NaCl and Friedel's salt at higher NaCl concentrations.
- Solubility increases are accompanied by phase transformations from AFm-SO_4 to AFm-Cl-SO_4 and to AFm-Cl with increasing NaCl concentration. AFm-Cl-SO_4 is still stable at 85°C.
- pH remains approximately unchanged with increasing NaCl concentration up to 1.5 M.

4.1.3.3 The Combined Effect of Temperature and Salinity on Solubility, Stability and pH in NaCl Systems

It has been found that AFm-SO_4 dissolves incongruently at 25°C and 55°C, but congruently, or nearly so, at 85°C. AFm-SO_4 is unstable in water at 25°, forming AFt, but is stable at both 55°C and 85°C. When cured in 0.5 M NaCl at 25° and 85°C, AFm-SO_4 forms Kuzel's and Friedel's salts. At 55°C, only Friedel's salt was observed. AFm-SO_4 is decomposed in 1.5.M NaCl to give AFm-Cl (Friedel's salt) at all temperatures except 25°C where Kuzel's salt is stable. The pH appears to be slightly higher at 25°C (by only ~ 0.3 pH units) than at 55° and 85°C, but pH is not significantly affected by NaC1 concentrations up to 1.5M.

Equilibrium, as reflected by phase transformations and steady-state solution concentrations, is attained relatively rapidly. Thus, when permeable cement materials are contacted with brine, the AFm-SO_4 phase can be expected to change its phase composition relatively rapidly to reflect the anion content of a percolating fluid phase.

The findings somewhat simplify the number of phases needed to be included in calculations of repository performance in brine. Friedel's salt, or possibly mixtures of Friedel's and Kuzel's salt, are the only AFm solids which need be considered. Moreover, they become congruently soluble, or nearly so, in warm conditions.

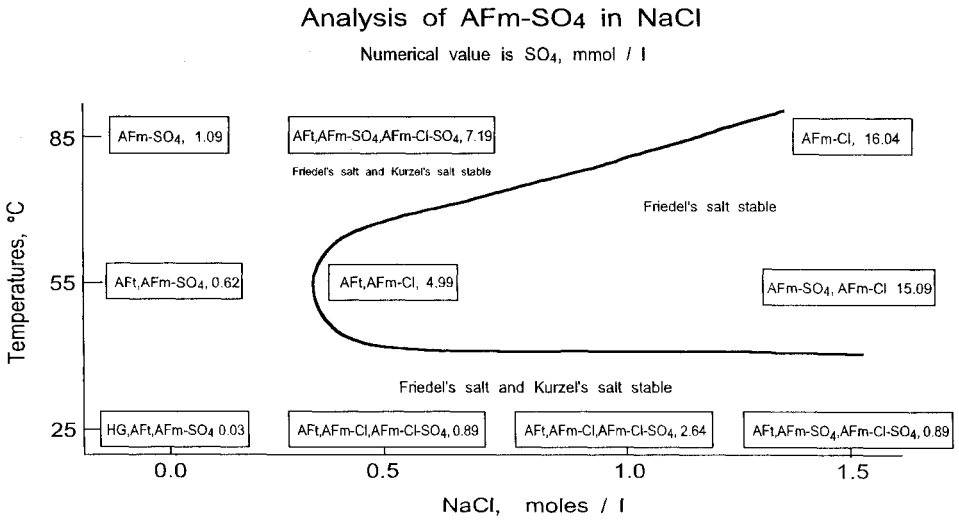

Figure 4.21 Summary for analysis of AFm-SO_4 in NaCl at 25°, 55° and 85°C.

4.1.3.4 Kinetics and Respikes in $MgSO_4$ Systems

Kinetic experiments were only made with ettringite as it is assumed that other phases will follow the same general pattern of reaction; see section 4.1.4.4 for ettringite data.

Respikes

The calculated maximum numbers of respikes in 0.05 M $MgSO_4$ was 6: see Appendix 3. However, after just one spike, the pH of the aqueous phase had decreased to 7.76: table 4.50, so the system was not respiked. The lower concentrations (0.01 M and 0.005M $MgSO_4$) did

not experience a comparable decrease in pH (table 4.50) although in this case the 0.01 M $MgSO_4$ system was not respiked because AFm-SO_4 could no longer be detected by XRD.

4.1.3.5 Solubility Data, pH and Solid Phase Compositions for $MgSO_4$ Systems

25°C isotherm

The results from the aqueous and solid analysis without respikes, cured for 146 days, and one respike (cured for an additional 257 days) are shown in tables 4.50 and 4.51.

Table 4.50 Aqueous characterisation of AFm-SO_4 reactant cured in $MgSO_4$ at 25°C. The results without parenthesis are after 146 days curing and no respikes. Results in parentheses are after one spike and an additional 257 curing days (total, 403 days).

Target [$MgSO_4$] mol/l	pH	Aqueous Characterisation, mmol/l				Charge imbalance
		Ca	Al	Mg	SO_4	OH, mmol/l
0.005	12.05 (11.91)	4.67 (3.99)	2.74 (2.22)	<0.01 (<0.01)	0.08 (0.02)	17.40 (14.60)
0.010	12.00 (11.46)	4.60 (1.75)	2.82 (0.95)	<0.01 (0.02)	0.01 (0.16)	17.64 (6.07)
0.050	9.90 (7.76)	14.22 (10.48)	0.11 (0.25)	0.03 (26.74)	16.6 (29.17)	-3.47 (16.85)

Table 4.51 Solid characterisation of AFm-SO_4 cured in $MgSO_4$ at 25°C. The results without parenthesis are after 146 days curing and no respikes. Results in parentheses are after one spike and an additional 257 curing days (total, 403 days).

Target [$MgSO_4$], mol/l	AFm-SO_4	AFt	HT	Gypsum	Gibbsite
0.005	S (M)	S (S)	(M)		
0.010	S	S (S)	(S)		
0.050	M (S)	S		S (S)	(W)

From the mass balances calculated for 0.05M $MgSO_4$ (Appendix 3), it was predicted that AFm-SO_4 would require 6 respikes, but this seems not to be the case as after one spike the pH decreased to near neutral and [Mg] is 26.74 mmol/l. Brucite was calculated to form, but was not identified by XRD or AEM. AEM discloses (i) a sulfate-containing, hydrotalcite-like phase in well-formed crystals with Mg:Al:SO_4 = 3.5:2.0:0.8. and (ii) gypsum, observed both by XRD and AEM. The reaction path is therefore likely to be:

$$\underset{(a)}{\text{AFm-SO}_4 + \text{MgSO}_4} \rightarrow \underset{(b)}{\text{HT + AFt}} \rightarrow \underset{(c)}{\text{HT + CaSO}_4\cdot 2\,\text{H}_2\text{O + AH}_3}$$

At lower $MgSO_4$ concentrations (0.005M and 0.01M) reaction has only proceeded as far as step (b). However, in the 0.01M $MgSO_4$, AFm-SO_4 is no longer observed by XRD and therefore further reaction is not expected. In a repository scenario the concentration of $MgSO_4$ is expected to remain essentially constant, so reaction will progress from (b) to (c) with corresponding decrease in pH. From consideration of the reaction direction, it is expected that AFm-SO_4 in 0.005 M $MgSO_4$ will experience the same changes as in 0.01M $MgSO_4$.

Soluble [Al] decreases with increasing [$MgSO_4$] but [Ca] at first increases with increasing [$MgSO_4$] but subsequently decreases, as respiking lowers the pH.

The persistence of hydrotalcite, rather than the expected brucite, requires comment. The order of anion stability in hydrotalcite is: OH^- > Cl^- for monovalent anions but divalent anions have higher ion selectivity than monovalent anions, with CO_3^{2-} > SO_4^{2+}. Thus, in the absence of carbonate, sulfate-hydrotalcite is formed more readily than hydroxy-hydrotalcite. Numerous field investigations also find the simultaneous presence of gypsum and hydrotalcite-like compounds as products of reaction of $MgSO_4$-containing solutions with mortars made with Portland cement. It appears probable, therefore, that hydrotalcite forms in preference to the predicted brucite because in computations we use data for hydroxy-hydrotalcite; when data become available for the sulfate-hydrotalcite, these calculations should be repeated.

SUMMARY OF THE 25°C RESULTS:

- pH decreases to ~ 7.7 when reaction is finished.
- low sulfate phases convert to high sulfate phases.
- as the $MgSO_4$ concentration increases, gypsum, gibbsite and minor hydrotalcite-like phases dominate the remaining solids.

55°C Isotherm

Data on this isotherm are incomplete: they were analysed only once, after initial $MgSO_4$ curing. The samples have been respiked, but not analysed. The respiked results will be presented in a thesis (Goldthorpe, 1998). Tables 4.52 and 4.53 show the results of an initial spike.

Table 4.52 Aqueous characterisation of AFm-SO_4 cured in $MgSO_4$ at 55°C without respiking. The cure duration is 214 days.

Target [$MgSO_4$] mol/l	pH	Aqueous Characterisation, mmol/l				Charge imbalance OH, mmol/l
		Ca	Al	Mg	SO_4	
0.005	11.79	4.08	2.33	<0.01	0.34	14.47
0.010	11.82	3.93	2.05	<0.01	0.28	13.45
0.050	10.49	9.48	0.28	<0.01	13.4	-7.0

As the Mg concentration is depleted to under its detection limit, the target concentrations shown in table 4.52 cannot be achieved. The results do, however, indicate the direction of reaction. [Ca] increases with increasing [$MgSO_4$] while [Al] decreases. The [SO_4] is very low for target $MgSO_4$ concentrations of 0.005 and 0.01 M; some is consumed in forming AFt. At the 0.05 M target concentration, AFm-SO_4 and AFt are mainly converted to gypsum. No significant decrease in pH is observed, but from experiments at 25° and 85°C it is expected that pH would decrease.

Table 4.53 Solid characterisation of AFm-SO_4 cured in $MgSO_4$ at 55°C. The results are after 214 days curing without respiking.

Target [$MgSO_4$], mol/l	AFm-SO_4	AFt	Gypsum
0.005	M	S	W
0.010	M	S	W
0.050	W	t	S

SUMMARY OF THE 55°C RESULTS:

These results are incomplete but after a single spike:

- pH remains approximately unchanged and is conditioned by remaining AFm-SO_4.
- as higher $MgSO_4$ concentrations, gypsum increasingly forms.
- Ca solubility increases as gypsum forms.
- even at low $MgSO_4$ concentrations, AFm-SO_4 is unstable, converting to the higher sulfate AFt phase .

85°C Isotherm

The results from the aqueous and solid analysis without respiking and after one respike are shown in tables 4.54 and 4.55.

Table 4.54 Aqueous characterisation of AFm-SO_4 cured in $MgSO_4$ at 85°C. The results without parenthesis are after 187 days curing without respiking. Results in parentheses are after one respike and an additional 256 days curing (total, 443 days).

Target [$MgSO_4$] mol/l	pH	Aqueous Characterisation, mmol/l				Charge imbalance
		Ca	Al	Mg	SO_4	OH, mmol/l
0.005	11.73	4.97	1.50	<0.01	2.15	10.14 (13.97)
	(11.65)	(5.24)	(2.33)	(<0.01)	(1.75)	
0.010	11.63	4.37	1.56	<0.01	2.13	9.16 (-4.40)
	(12.37)	(5.24)	(1.62)	(0.03)	(9.90)	
0.050	11.18	13.4	0.54	0.01	11.46	5.5 (18.21)
	(6.92)	(10.48)	(0.03)	(28.79)	(30.21)	

Table 4.55 Solid characterisation of AFm-SO_4 cured in $MgSO_4$ at 85°C. The results without parenthesis are after 187 days curing and no respikes and the results in parentheses are after one respike and an additional 256 curing days (total, 443 days): * main AFm-SO_4 reflection shows line broadening.

Target [$MgSO_4$], mol/l	AFm-SO_4	AFt	Gypsum	HT	Unidentified reflections
0.005	S (M)	MS (S)		(S)	(t)
0.010	MS	MS (S)	t	(S)	(t)
0.050	WM* (M)	S	M (S)	(S)	(t)

During solid characterisation, unidentified X-ray reflections were observed (6.44, 6.18, 5.34, 4.69, 3.28 and 2.63Å): AEM was carried out for AFm-SO_4 in 0.05M $MgSO_4$ both before and after the respike to identify where the Mg had gone and, in respiked experiments, to determine the phase responsible for the unidentified reflections. After the first spike the AFt phase apparently had small amounts of Mg present. Even though HT was not identified by XRD there was abundant microscopic evidence of platy HT-type phases. Thus a two-phase mixture of HT and AFt forms. In the respiked sample, no specific phase was identified that could explain the cause of the extra reflections. However, they are tentatively attributed to 'forbidden' reflections from the hydrotalcite-like phase.

The pH of AFm-SO_4 in 0.05M respiked $MgSO_4$ had decreased to ~ 7 at which point respiking was stopped before the target 0.05M $MgSO_4$ concentration was reached. The explanation for this decrease is that none of the remaining solids are able to elevate the pH. From calculations carried out in PHREEQE/V3.0, the pH of gypsum in equilibrium with 0.05 M $MgSO_4$ is calculated to be ~ 6.4; the calculated [Ca], 12.9 mmol/kg, fits well with the experimental data in table 4.54.

SUMMARY OF THE 85°C RESULTS:

- pH decreases to ~ 7 with increasing $MgSO_4$.
- AFm-SO_4 persists at lower $MgSO_4$ concentrations.
- AFm-SO_4 converts to gypsum and hydrotalcite.

Overall Summary of Solubility Data, pH and Solid Phase Compositions for $MgSO_4$ Systems.

From this study the interaction of $MgSO_4$ with AFm-SO_4 has been determined. It was found that pH decreases with increasing $MgSO_4$ concentration at 25°C and 85°C.

The ability of AFm-SO_4 to buffer pH in $MgSO_4$ is not changed significantly relative to water. As AFm-SO_4 is reacted with formation of other products, they condition a lower [OH] and hence lower pH: pH values are reduced by ~ 3 pH units. As reported in previous studies [11] the pH is also affected by temperature: see the short summary, table 4.56.

Table 4.56 Short summary of results for AFm-SO_4 cured in $MgSO_4$ at 25°, 55° and 85°C.

25°C, spiked	**55°C, one** spike	**85°C**, spiked
pH decreases. In DDW: C_3AH_6+ AFm-SO_4 + AFt In 0.005M: AFm-SO_4 + AFt + HT. In 0.01M: AFt + HT In 0.05M: AFm-SO_4 + Gyp + AH_3. Al decreases, Ca + SO_4 increase.	*pH decreases.* In DDW: AFm-SO_4 + AFt. In $MgSO_4$: AFt + AFm-SO_4 + Gyp. Ca and SO_4 increase. Al decrease	*pH decreases.* In DDW: No AFt In 0.005M: AFm-SO_4+Aft + HT. In 0.01M: AFt + HT. In 0.05M: AFm-SO_4 +Gyp + HT. Ca and SO_4 increase, Al decreases.

4.1.3.6 Combined Effect of Temperature and $MgSO_4$ Concentration

Figure 4.22 shows the combined effects of temperature and $MgSO_4$ concentration. It is not possible to completely evaluate the combined effect of both temperature and concentration of $MgSO_4$, as the lower concentrations were not sufficiently respiked to achieve the target.

Figure 4.22 Summary diagram of AFm-SO_4 cured in $MgSO_4$, showing the solid phases in the boxes. The heavy outline boxes indicate that one or more of the three criteria in section 3.4.2 have been achieved.

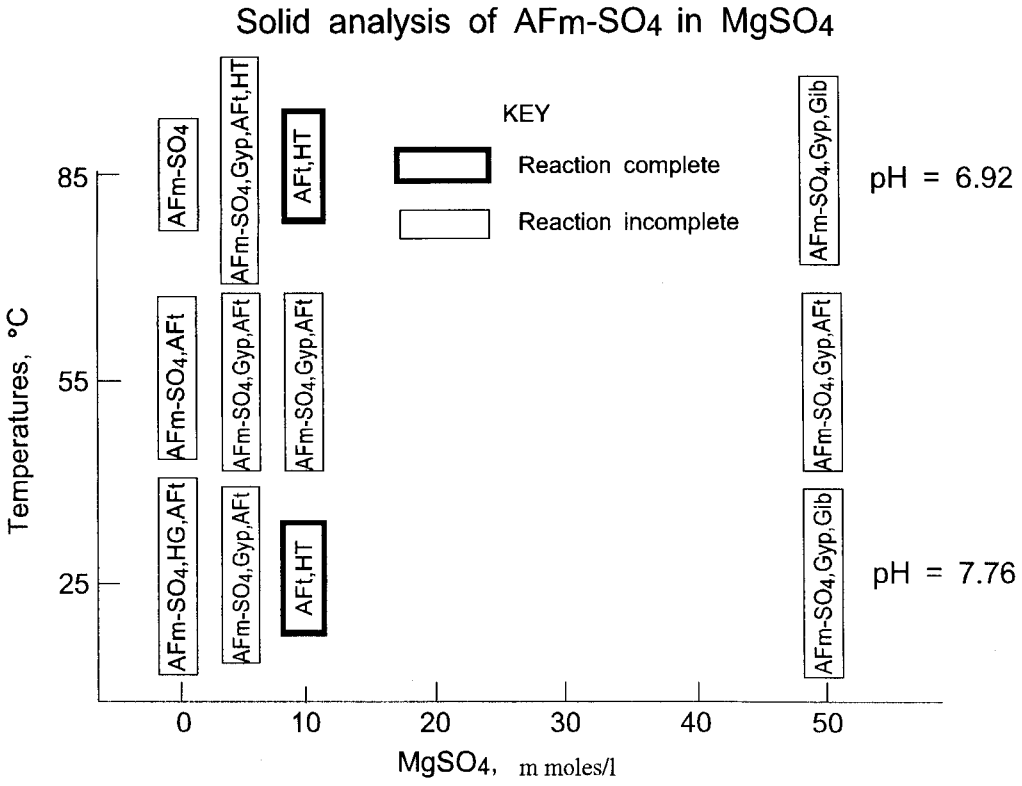

References

1. H.F.W Taylor. (1992) 'Cement Chemistry'. Academic Press, London and New York.

2. M. Atkins et al. (1993) 'Thermodynamic Modelling of Blended Cements at Elevated Temperature (50-90°C)'. UK DoE Report no. DoE/HMIP/RR/94/011, Aberdeen University, Scotland.

3. H. Y. Ghorab and E.A. Kishar. (1985) 'Studies on the Stability of the Calcium Sulfoaluminate Hydrates. Part 1: Effect of Temperature on The Stability of Ettringite in Pure Water. Cement and Concrete Research, **15**, No. 1, pp.93-99.

4. F.E. Jones. (1944) 'The Quaternary System $CaO-Al_2O_3-CaSO_4-H_2O$ at 25°C. Equilibria with Crystalline $Al_2O_3 \cdot 3H_2O$, Alumina Gel and Solid Solution'. Journal Phys. Chem. **48**(6), pp.311-356.

5. J. D'Ans und H. Eick. (1953) 'Das System $CaO-Al_2O_3-H_2O$ bei 20°C'. Zement Kalk-Gips. **6**, pp.302-311.

4.1.4 Calcium-trisulfoaluminate, AFt

4.1.4.1 Introduction and Background

The AFt-phases have the general formula $[Ca_3(Al,Fe)(OH)_6 \cdot 12 \cdot H_2O]X_3 \cdot xH_2O$, where X denotes one formula unit of a monovalent anion, such as OH^- and Cl^-, or half a formula unit of a divalent anion, such as SO_4^{2-} and CO_3^{2-} [1]. However, singly charged anions can be accommodated only to a limited extent. Silicate, with carbonate, can also substitute for Al, as occurs in thaumasite, $Ca_3[Si(OH)_6 \cdot 12H_2O](CO_3)(SO)_4$.

Lea [2] reports the solubility of ettringite to increase with temperature. It remains stable in contact with solution at 90°C but at higher temperatures decomposes with formation of AFm-SO_4 and gypsum. Lea also reports that in aqueous NaCl the solubility is slightly increased, compared with that in water, but apart from the slight decomposition arising from its incongruent dissolution, it remains stable [2].

There are several papers in the literature which deal with the thermal stability of ettringite. Ghorab and Kishar [3] studied the stability of ettringite at 30°, 60° and 100°C and found that ettringite is increasing soluble but stable at 60°C but decomposes at 100°C, agreeing with the previous literature and with this work.

The literature on AFt dissolution conflicts. Atkins et al. [4, p.24] found that ettringite dissolves congruently in water at 25°C, whereas Lea [2] and Turriziani [5] maintain that AFt dissolves incongruently, only becoming congruent in the presence of certain levels of aqueous calcium hydroxide. Turriziani [5] gives molar ratios of 0.15 for Ca/Al and 1.16 for Ca/SO_4 for AFt in water. The disagreement could be due to the numbers of dispersions that have been carried out. In Turriziani's and in our determinations, only one or two dispersions were carried out before solubility measurements: see Chapter 3 for discussion on redispersions.

Warren et al. [6] also determined solubility data for ettringite at 25°C from both undersaturated and supersaturated solutions and none of their results show congruent solubility of ettringite. Solubility data reported by Warren et al. are shown in table 4.57

Table 4.57 **Concentrations (mmol/kg) of Ca, Al, SO_4, and Na, and pH values for solution extracts after equilibration of ettringite approached from supersaturation and undersaturation. Data from Warren et al. [6]. For congruency, Ca/Al = 3.0 and Ca/SO_4 = 2.0.**

Supersaturation, concentration in mmol/kg							Undersaturation, concentration in mmol/kg						
[Ca]	[Al]	Ca/Al	$[SO_4]$	Ca/SO_4	[Na]	pH	[Ca]	[Al]	Ca/Al	$[SO_4]$	Ca/SO_4	[Na]	pH
6.31	0.052	121	7.85	0.80	4.47	10.36	4.14	0.317	13.06	4.06	1.02	1.02	10.65
4.79	0.187	26.6	6.85	0.70	3.55	10.45	3.43	0.395	8.68	3.71	0.92	1.70	10.74
1.51	0.485	3.11	5.13	0.29	7.50	11.15	1.88	0.537	3.50	3.71	0.51	4.34	11.15
0.486	1.38	0.35	5.58	0.09	14.6	11.66	0.929	0.879	1.06	2.99	0.31	5.90	11.51
0.222	2.00	0.11	5.94	0.04	28.1	12.07	0.459	1.02	0.45	2.81	0.16	11.4	12.03
0.132	2.50	0.05	6.21	0.02	65.9	12.53	0.280	1.16	0.24	3.03	0.09	30.8	12.48
0.138	2.25	0.06	6.76	0.02	139	13.05	0.266	1.08	0.25	3.42	0.08	70.7	12.68
0.185	2.49	0.07	7.49	0.02	273	13.22	0.285	1.13	0.25	3.40	0.08	110	12.88
0.127	0.84	0.15	13.1	0.01	737	13.47	0.307	0.859	0.36	4.71	0.07	329	13.01
0.075	1.06	0.07	42.5	0	1240	13.59	0.197	0.367	0.54	20.5	0.01	572	13.24
0.818	0.004	204	0.954	0.86	2.27	10.45	5.35	0.237	22.57	5.29	0.01	1.12	10.65
5.01	0.222	22.6	6.54	0.77	3.67	10.61	3.58	0.402	8.91	3.80	0.94	1.78	10.83
1.81	0.392	4.62	4.94	0.37	8.24	11.16	2.02	0.492	4.11	3.15	0.64	3.98	11.18
0.419	1.46	0.29	7.85	0.05	18.6	11.81	0.968	0.944	1.03	4.03	0.24	9.11	11.69
0.226	2.10	0.11	6.07	0.04	28.5	12.21	0.455	1.06	0.43	3.00	0.15	13.0	12.10
0.169	1.70	0.10	5.31	0.03	66.8	12.69	0.327	0.851	0.38	2.60	0.13	29.4	12.53
0.136	2.42	0.06	6.99	0.02	132	12.95	0.258	1.19	0.22	3.40	0.08	58.6	12.73
0.253	2.27	0.11	7.74	0.03	272	13.18	0.291	1.12	0.26	3.72	0.08	129.7	12.97
0.112	0.798	0.14	13.7	0.01	672	13.42	0.343	0.767	0.45	4.67	0.07	325	13.20
0.025	1.23	0.02	45.3	0	1200	13.56	0.190	0.365	0.52	21.4	0.01	603	13.33

One of the main features of ettringite is its association with physical expansion in fully hardened matrices [7]. Two mechanisms give rise to expansion: one involves sulfate uptake from external sources while the other is isochemical, involving a redistribution of sulfate internally. This latter can occur as a consequence of thermal cycling.

Glasser et.al. [7] have made a comprehensive study of the $CaO-Al_2O_3-SO_3-H_2O$ system for a range of temperatures, using thermodynamic modelling techniques. Figure 4.14, Section 4.1.2.4 summarises their results. With increasing temperature, especially above 50°C, the stability surface of AFm-SO_4 progressively enlarges while that of AFt contracts. The critical sulfate concentration at which gypsum becomes stable is nearly the same at both 25° and 55°C (~12.2 mM) decreasing at 85°C (~ 10.7 mM). Upon cooling, these changes are reversible.

4.1.4.2 Solubility Data, pH and Solid Phase Compositions for NaCl Systems

25° Isotherm

Solubility data for AFt in double distilled degassed water (DDW) and 0.5, 1.0 and 1.5 M NaCl at 25°C are given in table 4.58.

Table 4.58 Solubility data for AFt in water and NaCl at 25°C.

Initial [NaCl] Mol/l	pH	Aqueous Characterisation, mmol/l					charge imbalance mmol/l	cal. pH
		Na	Cl	Ca	Al	SO_4		
0	11.3	0	0	2.11	0.62	1.12	3.8	11.6
0.53	11.5	449	467	4.89	1.31	2.85	-10.0	-
1.04	11.5	952	960	5.89	1.48	3.18	1.9	11.3
1.55	11.4	1370	1437	6.35	1.63	3.23	-55.9	-

Figure 4.23 and table 4.58 show the solubility increases approximately three-fold when AFt is cured in 1.5 M NaCl, compared to DDW.

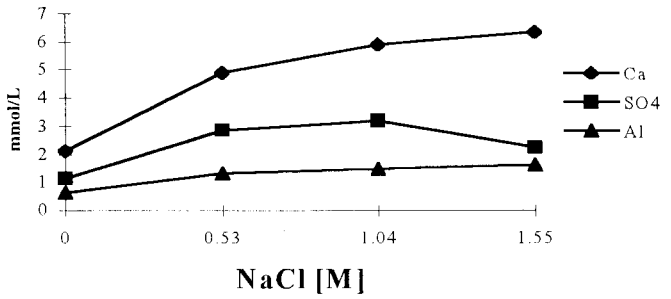

Figure 4.23 Solubility of AFt and its reactants as a function of NaCl concentration at 25°C.

The solubility data shows that AFt dissolves nearly congruently in DDW, with Ca/Al = 3.4 (for congruency, Ca/Al = 3.0); Ca/SO_4 = 1.9 (for congruency, Ca/SO_4 = 2.0). But when AFt is cured in NaCl, marked departures from congruency occur: see table 4.59.

Table 4.59 Molar ratios in the aqueous phase for AFt cured in DDW and in NaCl at 25°C.

	Molar ratio of Ca/Al (ideal 3.0)	Molar ratio of Ca/SO_4 (ideal = 2.0)
AFt in DDW	3.4	1.9
AFt in 0.53 M NaCl*	3.7	1.7
AFt in 1.04 M NaCl*	4.0	1.9
AFt in 1.55 M NaCl*	3.9	2.0

* Molarity of NaCl, by analysis

The solid analysis (table 4.60) shows that AFt is stable at all NaCl levels studied.

Table 4.60 Solid characterisation of AFt cured in water and NaCl solutions at 25°C.

Initial [NaCl] mol/l	AFt	NaCl
0	S	
0.53	S	
1.04	S	M
1.55	S	S

AEM of AFt cured in 0.5 M NaCl also confirm that only AFt is present. The classic AFt rod-like morphology with well formed crystals of 1- 10 microns in length is observed. Mean atom ratios of the solids are Ca/Al = 2.91 ±0.10, Ca/SO_4= 2.02 ±0.05 (10 analysis); chloride is absent. These ratios correspond to ideal AFt.

NaCl contents of the solids varied from 1 to 10 atom % but XRD gave a NaCl X-ray pattern. Na/Cl ratios are close to equimolar and it is therefore assumed that NaCl is precipitated as the aqueous phase is evaporated. Under these conditions, there is negligible interaction of Na and Cl with AFt; the latter remains essentially chloride-free, despite the precursor aqueous solution having a Cl/SO_4 mole ratio ~ 250.

pH measurements are shown in table 4.58 and figure 4.24 and show no major pH changes

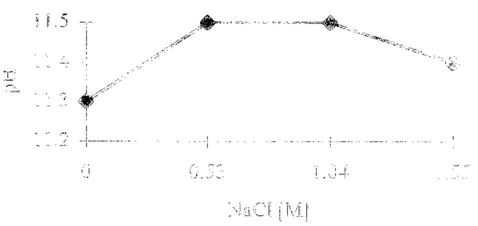

Figure 4.24 pH of AFt solution at different NaCl concentrations at 25°C

SUMMARY OF THE 25°C RESULTS:

- Ettringite is stable at all NaCl levels studied, up to ~1.5M.
- Solubility of AFt increases approximately three fold when cured in 1.5 M NaCl compared to DDW.
- AFt dissolves nearly congruently in DDW but incongruently in NaCl solutions.
- pH of the aqueous solution is approximately unchanged up to ~ 1.5 M NaCl.
- There is negligible solid solution of either Na or Cl in AFt.

55° Isotherm

Solubility data for AFt in DDW and nominally 0.5 (actually~0.41M) NaCl and 1.5 M NaCl at 55°C are presented in table 4.61

Table 4.61 Solubility data for AFt in DDW and NaCl at 55°C.

Initial [NaCl] mol/l	pH	Aqueous Characterisation, mmol/l					charge imbalance OH, mmol/l	calc. pH
		Na	Cl	Ca	Al	SO_4		
0	11.37	0.05	0.06	3.10	1.29	2.77	4.52	11.7
0.41	11.48	505	493	6.21	1.45	4.42	19.9	12.3
1.50	11.11	1252	1340	12.05	1.61	16.31	-91.7	-

Figure 4.25 shows how the solubility increases with increasing [NaCl].

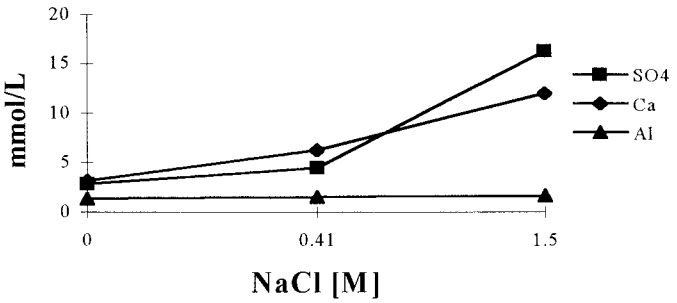

Figure 4.25 Solubility of AFt and its decomposition products in NaCl at 55°C.

The solubility data indicate that AFt dissolves incongruently at 55°C: see table 4.62. This confirms previous studies. [8]

Table 4.62 Molar ratio in the aqueous phase for AFt cured in DDW and in NaCl at 55°C.

	Molar ratio of Ca/Al (ideal 3.0)	Molar ratio of Ca/SO_4 (ideal = 2.0)
AFt in DDW	2.4	1.1
AFt in 0.41 M NaCl	4.3	1.4
AFt in 1.5 M NaCl	phase change	phase change

Solid analysis (table 4.63) shows that AFt is stable both in DDW and 0.5 M NaCl but AFt becomes unstable with respect to AFm-Cl in 1.5 M NaCl.

Table 4.63 Solid characterisation of AFt cured in DDW and NaCl solutions at 55°C.

Initial [NaCl] mol/l	AFt	AFm-Cl	NaCl
0	S		
0.41	S		
1.50	S	W	W

pH measurements are shown in table 4.61 and figure 4.26; no major pH changes occur.

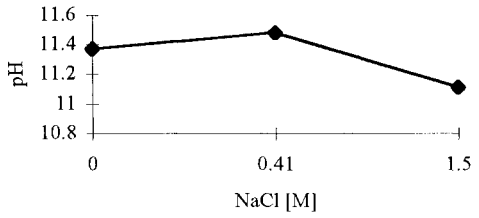

Figure 4.26 pH of solutions equilibrated with AFt at 55°C.

SUMMARY OF THE 55°C RESULTS:

- Solubility of AFt increases when cured in NaCl compared to DDW.
- AFt dissolves incongruently both in DDW and in NaCl solutions.
- AFt is stable at [NaCl] ≤ 0.4 M, but forms AFm-Cl at [NaCl] = 1.5 M.
- the pH remains approximately constant at NaCl concentrations up to 1.5 M.

85° Isotherm

Solubility data for AFt at 85°C in DDW, in 0.5 and 1.5 M NaCl at 85°C are presented in table 4.64.

Table 4.64 Solubility data for AFt in water and NaCl at 85°C.

Initial [NaCl] mol/l	pH	Aqueous Characterisation, mmol/l					charge imbalance OH, mmol/l	calc. pH
		Na	Cl	Ca	Al	SO_4		
0	11.7	5.0	5.6	4.75	1.41	2.67	7.8	11.9
0.53	11.6	442	467	14.05	1.70	10.88	-13.6	-
1.55	11.4	1414	1479	18.86	2.07	2.31	-31.9	-

Figure 4.27 shows solubility changes with increasing [NaCl]. AFt dissolves incongruently at 85°C in DDW (ideal Ca/Al = 3.0, experimental Ca/Al = 3.4 and ideal Ca/SO_4 = 2.0, experimental Ca/SO_4 = 1.8). The decrease in SO_4 solubility from [NaCl] = 0.5 M to [NaCl] = 1.5M, is perhaps associated with conversion of AFt to AFm-SO_4. The Al content in [NaCl] = 1.55 M was only slightly enhanced to 2.07 mM.

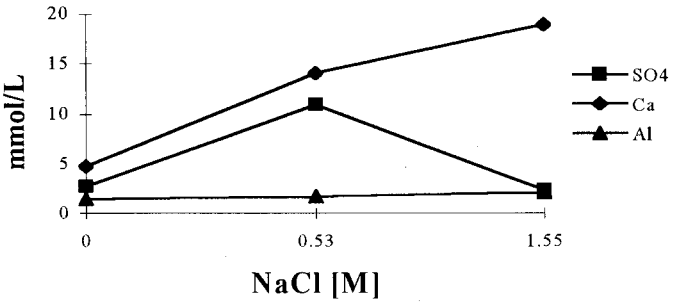

Figure 4.27 Solubility of AFt and its decomposition products at 85°C as a function of NaCl concentration.

Analysis of solids (table 4.65) indicates that AFt is stable in water at 85°C, but unstable in NaCl. XRD showed AFt, AFm-SO_4 and NaCl at [NaCl] = 0.5 M. At higher NaCl concentration, 1.5M, AFt decomposes to calcium hydroxide and Friedel's salt.

Table 4.65 Solid characterisation of AFt cured in water and NaCl solutions at 85°C.

Initial [NaCl] mol/l	AFt	AFm-SO_4	AFm-Cl	CH	NaCl
0	S				
0.53	S	M			M
1.55			VS	M	M

AEM of AFt in 0.5 M NaCl show abundant AFt with typical AFt rod-like morphology. The rods were well formed and about 2-10 microns in length. Mean atom ratios were Ca/Al = 3.09 ±0.12, Ca/SO_4= 1.99 ±0.05 (8 analyses), corresponding to ideal AFt. AFt coexists with a small amount of AFm-SO_4, occurring as irregular small platelets (~1.0 micron), and Friedel's salt; the latter has mean atom ratios of Ca/Al = 1.92 ±0.11, Ca/Cl = 2.20 ±0.36 (7 analyses).

It thus contained significant amounts of Cl and SO_4: SO_4/Cl ranged between 0.02 and 0.18. This indicates that Friedel's salt forms some solid solution with Kuzel's salt (ideal Ca/Al = 2, Ca/Cl = 4 and SO_4/Cl = 0.5). Little or no substitution occurs of Na and Cl into AFt. At 85°C, small amounts of AFm-Cl develop, with up to 18% mol substitution of SO_4 for Cl. This latter substitution was also noted by Kuzel [9].

Significant amounts of NaCl, occurring as 0.5 - 1.0 micron cubes, were observed. Apparent NaCl contents varied up to a maximum of 1.5 atom %, with NaCl ratios close to 1.0. This NaCl probably precipitates onto solid surfaces during drying. In the AFm-Cl phase Na (mean = 3.61 ±1.14 atom %) is also associated with equimolar amounts of Cl, again probably precipitated on solid surfaces.

pH measurements are shown in table 4.64 and figure 4.28; the pH declines only slightly with increasing NaCl concentration.

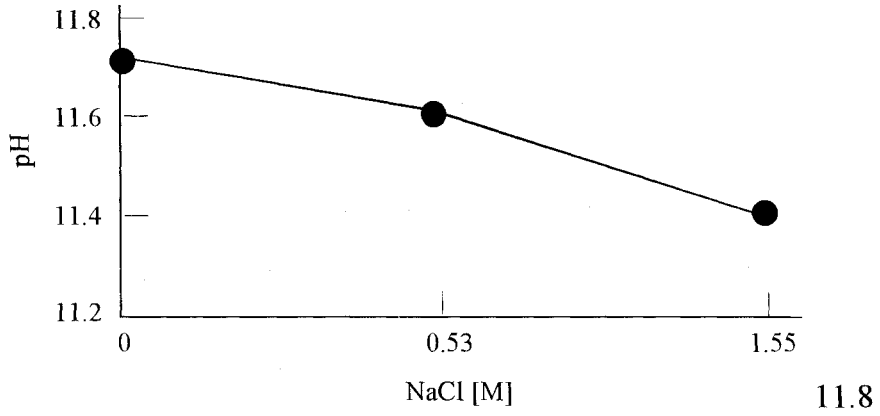

Figure 4.28 pH of AFt in NaCl at 85°C.

SUMMARY OF THE 85°C RESULTS:

- Ettringite is only stable in DDW. In 0.5 M NaCl, AFt persists together with its decomposition products, AFm-SO_4 and AFm-Cl; in 1.5 M NaCl, AFt is completely decomposed, yielding AFm-Cl and CH.
- AFt dissolves incongruently in DDW.
- There is little or no substitution of Na in AFt.
- pH is approximately unchanged with increasing NaCl concentrations up to 1.5 M.
- Friedel's salt may contain substantial sulfate at 85°C.

4.1.4.3 The Combined Effect of Temperature and Salinity on Solubility, Stability and pH in NaCl Systems

Ettringite dissolves nearly congruently in DDW at 55° and 85°C, but incongruently at 25°C. Its solubility in DDW increases with temperature. In DDW, AFt is stable in the range 25° - 85°C. This is in agreement with the previous literature (see section 4.1.4.1).

When cured in 0.5M NaCl solution, AFt remained stable at 25° and 55°C, but decomposed at 85°C yielding AFm-Cl. When AFt was cured in 1.5M NaCl, decomposition to AFm-Cl occurred at 55°C. At 85°C AFt is completely consumed, giving mixtures of AFm-Cl and CH. The pH of AFt is not significantly affected by saline environment or temperature; it remains nearly constant, between ~11.1-11.7. Figure 4.29 shows the combined effect of temperature and NaCl concentration on ettringite.

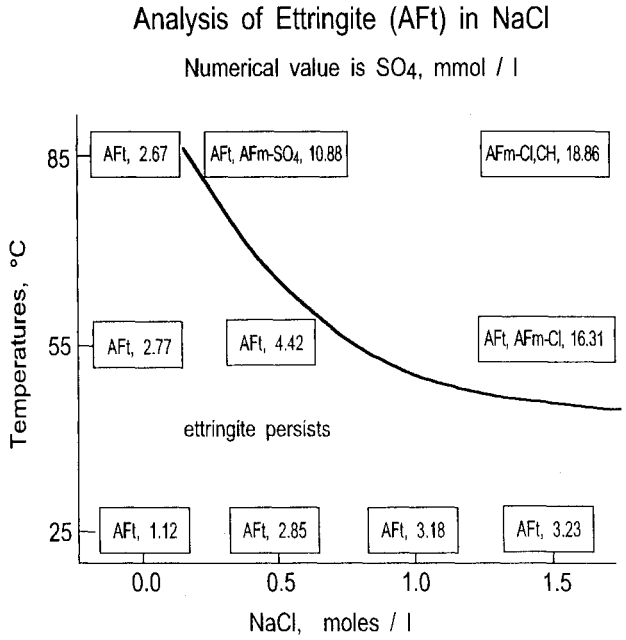

Figure 4.29 Summary of results: AFt cured in NaCl at 25°, 55° and 85°C. The curve marks the onset of AFt decomposition.

4.1.4.4 Kinetics and Respikes in $MgSO_4$ Systems

Due to slow reaction, the AFt-system still had the target $MgSO_4$ concentration (0.05M) after one addition of $MgSO_4$; it took about three months for the solution to decrease in Mg from 49.36 mmol to 43.19 mmol. The calculated number of respikes was 4, see Appendix 3, but experimentally only one respike was practical.

Respikes

As expected from the kinetic experiments, reaction of AFt with $MgSO_4$ was slow but even though the [Mg] had not much decreased, pH had decreased to less than 9. The results for the respiked AFt systems at 25° and 85°C are in the following section; the 55°C respiked experiments will be presented in a thesis (Goldthorpe, 1998).

4.1.4.5 Solubility Data, pH and Solid Phase Compositions for $MgSO_4$ Systems

Ettringite solubility has been studied by many authors [3,4,6,7] who find it increases between 25°C and 50°C, and even more between 50°C and 85°C. In other words, the minimum sulphate content in solution necessary to preserve AFt increases rapidly with temperature, especially above 50°C. The range of aqueous Ca concentrations is not large, but mirrors the solubility of $Ca(OH)_2$ itself; rising temperatures decrease calcium solubilities. Al, on the other hand, exhibits the reverse trend; its solubility increases with increasing temperature. AFm-SO_4 is thermodynamically metastable at 25°C, but becomes stable at ~50°C and above [8].

25°C isotherm

The results from the aqueous analysis without respikes, cured for 146 days, and one spike (cured for an additional 257 days) are shown in table 4.66

Table 4.66 Aqueous characterisation of ettringite cured in $MgSO_4$ at 25°C. The first set of results are without respike after 146 days curing. Results in ( ) are after one spike and an additional 257 curing days (total, 403 days).

Target [$MgSO_4$] mol/l	pH	Aqueous Characterisation, mmol/l				Charge imbalance OH, mmol/l
		Ca	Al	Mg	SO_4	
0.005	10.10 (8.42)	8.13 (13.97)	0.18 (0.10)	0.01 (0.07)	8.00 (11.67)	0.82 (4.76)
0.010	9.55 (8.63)	14.92 (13.97)	0.09 (0.13)	0.05 (0.08)	13.93 (12.19)	2.35 (4.11)
0.050	8.40 (7.67)	12.43 (10.98)	0.01 (<0.01)	14.28 (61.70)	28.75 (60.42)	-4.05 (24.52)

The results of the solid analysis are shown in table 4.67 where parenthesis have the same definition as in the preceding table.

Table 4.67 Solid characterisation of ettringite cured in $MgSO_4$ at 25°C. The first set of results are without respike after 146 days curing. Results in parentheses are after one spike and an additional 257 curing days (total, 403 days).

Target [$MgSO_4$], mol/l	AFt	AFm-SO_4	Gypsum	Gibbsite
0.005	S (S)		(S)	
0.010	S (S)		(S)	(M)
0.050		M (t)	S (S)	(M)

AEM of ettringite cured in 0.05M $MgSO_4$ without respiking showed two solid phases: one is an AFt with Ca/Al ratio = 2.9 (ideal = 3.0) and Ca/SO_4 ratio = 2.0 (ideal = 2.0). The other Mg-containing phase has atomic ratios: Mg:Al = 1.9, SO_4:Al = 0.5 and Ca:Al = 0.03. This analysis is associated with is a hydrotalcite-like phase, incorporating some sulfate (see section 4.1.3.5). From table 4.66 [Mg] has depleted to near 0 mmol/l for the lower $MgSO_4$ concentrations but, although some ettringite remained, the pH had decreased to ~ 8.5 and

spiking was therefore discontinued. For 0.05M $MgSO_4$ the [Mg] concentration is in fact above the required level. The pH has also decreased to 7.7 after the first spike. This decrease in pH could be due to formation of impermeable layers of reaction products around AFt, as AFt in contact with the aqueous phase should condition a high pH.

Fewer than calculated respikes were necessary because MH does not form; the mechanism for reaction between AFt and $MgSO_4$ is:

$C_6A\bar{S}_3H_{32} + MgSO_4 \rightarrow$ HT-like phase $+ CaSO_4 \cdot 2\,H_2O + AH_3$

It follows that Ca should be taken out of the equation: $X > (2Z + Y)$; see Appendix 3 for equation definitions. We are then left with $X > 2Z$ (=6.36). Some of the Al is converted to gibbsite (AH_3). The change in the basis for calculation makes the number of spikes required to complete reaction approximately one, in agreement with experiment.

SUMMARY OF THE 25°C RESULTS:

- the only Mg containing phase found was a hydrotalcite-like phase.
- as the $MgSO_4$ concentration increases, gypsum and gibbsite dominate the remaining solids.
- with increasing [$MgSO_4$] the aqueous pH decreases to ~ 7.7.
- reaction products forming around AFt isolate it from the aqueous phase giving an anomalously low pH
- the reaction of ettringite with $MgSO_4$ is relatively slow on a laboratory time scale.

55°C Isotherm

To be able to finish the programme, the 55°C experiments were only analysed after initial $MgSO_4$ curing. The samples have been respiked, but not analysed: results will be presented in a theses (Goldthorpe, 1998). Tables 4.68 and 4.69 shows the results without respiking:

Table 4.68 Aqueous characterisation of ettringite cured in $MgSO_4$ at 55°C. The results are after 214 days curing and without respiking.

Target [$MgSO_4$] mol/l	pH	Aqueous Characterisation, mmol/l				Charge imbalance
		Ca	Al	Mg	SO_4	OH, mmol/l
0.005	10.57	10.4	0.37	<0.01	9.76	2.39
0.010	10.29	15.52	0.37	<0.01	14.83	2.49
0.050	8.22	12.55	<0.01	19.75	21.86	-

As the Mg concentration is depleted to below detection limits (table 4.68) reaction is incomplete except at 0.05 M $MgSO_4$: see table 4.69. The solid phases observed are AFm-SO_4 and gypsum; as no AEM was done, it has not been possible to identify the Mg-containing phase(s), but it is expected that a hydrotalcite-like phase, present at both 25° and 85°C, will also occur at 55°C. Formation of AFm-SO_4 indicates that AFt is not stable at 0.05M $MgSO_4$

and 55°C. However, at 25°C gibbsite and gypsum are the end products and it would be most likely that if the system was respiked again the pH would decrease further and gibbsite would develop.

Table 4.69 Solid characterisation of ettringite cured in $MgSO_4$ at 55°C. The results are after 214 days curing and without respiking.

Target [$MgSO_4$], mol/l	AFt	AFm-SO_4	Gypsum
0.005	S		
0.010	S		M
0.050		M	S

SUMMARY OF THE 55°C RESULTS:

- With increasing [$MgSO_4$] AFt is metastable relative to gypsum and AFm-SO_4
- the pH conditioned by the stable phases decreases to ~ 8.2.

85°C Isotherm

The results from the aqueous analysis no respikes (cured for 187 days) and one spike cured an additional 256 days (total, 443 days) are shown in table 4.70

Table 4.70 Aqueous characterisation of ettringite cured in $MgSO_4$ at 85°C. The results without parenthesis are after 187 days curing and no respikes: results in parentheses are after one spike and additional of 256 curing days (total, 443 days).

Target [$MgSO_4$] mol/l	pH	Aqueous Characterisation, mmol/l				Charge imbalance OH, mmol/l
		Ca	Al	Mg	SO_4	
0.005	11.10	10.16	0.59	<0.01	9.13	3.83 (2.14)
	(10.71)	(12.48)	(0.41)	(0.05)	(11.46)	
0.010	11.07	12.40	0.53	0.03	10.94	5.57 (3.53)
	(10.81)	(13.97)	(0.43)	(0.07)	(12.92)	
0.050	8.84	11.65	0.01	20.16	23.33	- (39.45)
	(6.40)	(10.98)	(<0.01)	(80.21)	(72.08)	

The results of the solid analysis are shown in table 4.71 without respiking and with one respike.

Table 4.71 Solid characterisation of ettringite cured in $MgSO_4$ at 85°C. The results without parenthesis are after 187 days curing and no respikes: results in parentheses are after one spike and an additional 483 curing days (total, 670 days).

Target [$MgSO_4$], mol/l	AFt	AFm-SO_4	Gypsum	HT
0.005	S (S)		(S)	
0.010	S (S)	(S)	(S)	(M)
0.050		S (S)	M (S)	

AEM of AFt in a target concentration of 0.05M $MgSO_4$, but with no respike, shows a nearly amorphous, hydrotalcite-like phase containing sulfate; it had an average atomic ratio of 4Mg:2Al:SO_4. The pH has decreased to ~ 6.4 after the respike: AFm-SO_4 should control a higher pH but it is likely that formation of layers of reaction products have isolated the unconsumed AFm-SO_4 from contact with the aqueous phase.

Samples in 0.005M and 0.01M $MgSO_4$ did not satisfy criteria for discontinuing reaction but it is probable the end products of reaction will be the same as in 0.05 M $MgSO_4$. However sluggish kinetics prevented us from proving this.

SUMMARY OF THE 85°C RESULTS:

- pH decreases to ~ 6.4 with increasing $MgSO_4$ concentrations.
- AFm-SO_4 persists in preference to AFt
- AFt is converted to gypsum and AFm-SO_4, but with continuing reaction it is expected that AFm-SO_4 will convert to gypsum and hydrotalcite.

Overall Summary of Solubility Data, pH and Solid Phase Compositions for $MgSO_4$ Systems.

From this study the interaction of $MgSO_4$ with AFt has been determined. It was found that the pH decreases with increasing $MgSO_4$ concentration at all three temperatures.

The ability of AFt to buffer pH in the presence of $MgSO_4$ is reduced significantly, relative to water. It reacts, with formation of products which condition a lower [OH] and hence lower pH. The pH values are reduced by ~ 3 pH units. As reported in previous studies [4,8] the pH is also affected by temperature: table 4.72 gives a short summary of the results.

Table 4.72 Short summary of results for AFt cured in $MgSO_4$ at 25°, 55° and 85°C.

25°C, spiked once	55°C, spiked once	85°C, respiked
pH decreases. 0.005M and 0.01M : AFt + Gyp. 0.05M: AFm-SO_4 + Gyp. Al + Ca decreases, SO_4 increase.	*pH approx. unchanged* 0.005M: AFt. 0.01M : AFt + Gyp 0.05M : AFm-SO_4 + Gyp Ca and SO_4 increases, Al decreases.	*pH decreases.* 0.005M + 0.01M: AFt + Gyp. 0.05M:AFm-SO_4 + Gyp +AH_3 Ca and SO_4 decreases while Al increases.

4.1.4.6 Combined Effect of Temperature and $MgSO_4$ Concentration

Figure 4.30 shows the combined effect of temperature and $MgSO_4$ concentration on AFt stability. It is not possible completely to evaluate the combined effect of both temperature and concentration of $MgSO_4$, as the lower concentrations were not respiked to the target values; however reaction directions can be inferred.

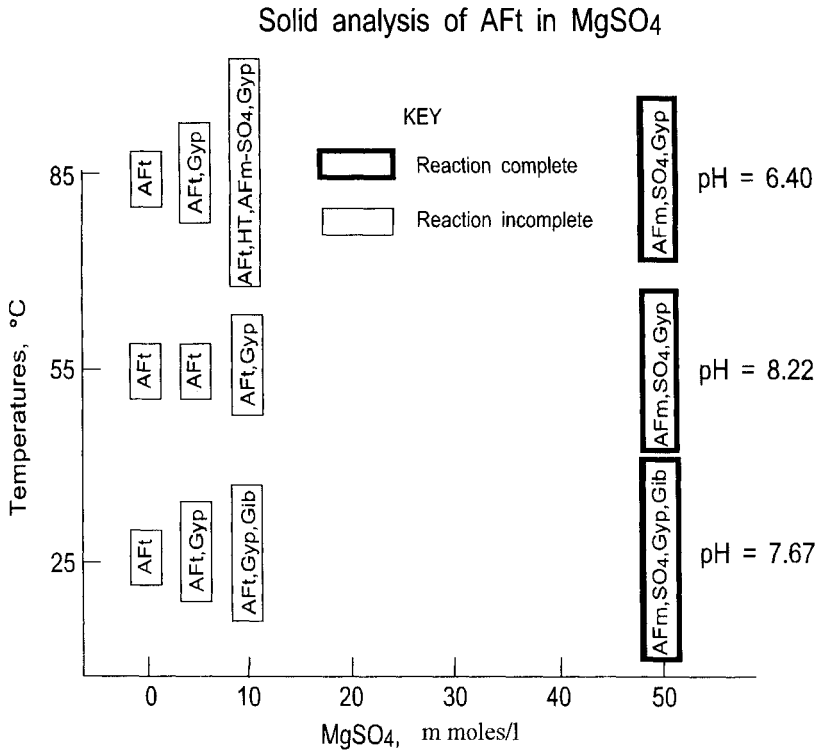

Figure 4.30 Summary diagram of AFt cured in $MgSO_4$, showing the solid phases in the boxes. The boxes in heavy outline indicate that one or more of the three criteria in section 3.4.2 have been achieved.

References

1. H.F.W Taylor. (1992) 'Cement Chemistry'. Academic Press, London and New York.

2. F.M. Lea. (1956) 'The Chemistry of Cement and Concrete'.3rd Edition. Edward Arnold Ltd., London.

3. H. Y. Ghorab and E.A. Kishar. (1985) 'Studies on the Stability of the Calcium Sulfoaluminate Hydrates. Part 1: Effect of Temperature on The Stability of Ettringite in Pure Water'. Cement and Concrete Research, **15**, No. 1, pp. 93-99.

4. M. Atkins et al. (1991) 'A Thermodynamic Model for Blended Cements'. UK DoE Report no. DoE/HMIP/RR/92/005, Aberdeen University, Scotland

5. R. Turriziani. (1964) 'The Calcium Aluminate Hydrates and Related Compounds', in 'The Chemistry of Cement', vol.1, ed. H.F.W. Taylor. Academic Press, London.

6. C. J. Warren and E. J. Reardon. (1994) 'The Solubility of Ettringite at 25°C'. Cement and Concrete Research, **24**, No. 8, pp.1515-1524.

7. F.P. Glasser, D. Damidot and M. Atkins. (1995) 'Phase Development in Cement in Relation to the Secondary Ettringite Problem'. Advances in Cement Research 7, No.26, pp. 57-68.

8. M. Atkins et al. (1993) 'Thermodynamic Modelling of Blended Cements at Elevated Temperature (50-90°C)'. UK DoE Report no. DoE/HMIP/RR/94/011, Aberdeen University, Scotland

9. H.J. Kuzel. (1966) 'Röntgenuntersuchung in System $3CaO{\cdot}Al_2O_3{\cdot}CaSO_4{\cdot}nH_2O$-$3CaO{\cdot}Al_2O_3{\cdot}CaCl_2{\cdot}nH_2O$'. N. Jahrbuch. Miner. Monatshefte **1966**, pp.193-200.

4.2 Phase Relations in Synthetic Sub-systems

4.2.1 $CaO-Al_2O_3-SiO_2-H_2O$

4.2.1.1.Introduction and background

This system includes most (~90%) of the total chemistry of backfills (excluding $CaCO_3$) and of BFS and FA blended cements. This system is complex and difficult to study; previous work over the past 50 years shows that it becomes increasingly difficult to determine the equilibrium state with decreasing Ca contents because of -

- Low crystallisation rates for some phases
- The tendency to form metastable but persistent gels
- Slow reaction kinetics between coexisting phases and
- Lack of reversibility and formation of persistent but metastable solids.

These difficulties are evident both at 25°C and at elevated temperatures [1,2]. The most difficult region of the phase diagram lies at < 40% CH, where zeolite and clay mineral formation may become important. Reactions in this range are applicable to high FA blends, for example, 60 PFA:40 OPC. In these studies we have investigated three blends related to BFS compositions (CASH 1,3 and 6) and three related to PFA (CASH 2, 4 and 5).

The introduction of groundwater components, Mg, SO_4, Na and Cl, into the CASH system raises the number of components to eight. Owing to the difficulties in verifying phase relations in complex multi-component systems, we have made no attempt to describe the full system but concentrate on the products obtained after the longest cure durations.

4.2.1.2 Kinetics and Respikes in $MgSO_4$ and NaCl Systems

The kinetic experiments were carried out at 25°C with an initial aqueous phase of 0.5 M NaCl + 0.02M $MgSO_4$. Experimental details are given in section 3.4.1: table 4.73 shows the results.

Table 4.73 Number of respikes necessary to reach 0.02M $MgSO_4$ target concentration at 25°C.

Phase Formation System	Number of respikes into 160 mls	Numbers of respikes in actual systems	[Mg] in mmol/l after last respike
CASH 1	8.5	17	10.3
CASH 2	1	2	15.6
CASH 3	5	10	14.0
CASH 4	2	4	18.1
CASH 5	2	4	16.0
CASH 6	4	8	19.3

To accelerate reaction, 160 mls, double the normal solution volume, was used so that the second column in table 4.73 is the number of respikes in the kinetic experiments and the third column is the number of respikes required for all other experiments.

The sulfate component reacts slower than magnesium and its concentration is therefore somewhat higher than the target 0.02M.

4.2.1.3 Solubility Data, pH and Solid Phase Compositions

Experimental details for the phase compatibility experiments on the CASH systems were given in section 3.1. Table 3.4 and figure 3.1 shows the compositional relationships of the mixtures. The results of the first analysis showed that uptake of magnesium into the solid is essentially complete, although no magnesium-containing solids were detected by XRD. The systems were therefore respiked according to the calculated numbers in table 3.3: results are summarised in tables 4.74 - 4.97. It was also found that most preparations still contained unreacted boehmite (γ-AlO(OH)) and therefore may have been deficient in reactive alumina. The uptake of both Na and Cl from solution appears to be significant in some instances but mass balance calculations indicate that apparent uptakes considerably exceed the amount incorporated into solid phases. The discrepancy is believed to arise through a combination of experimental error and occasional removal of wet solid samples for analysis.

Most of the experiments did not reach the target Mg concentration before the pH decreased to < 9, in which case respiking was not necessary.

25°C Isotherm
The aqueous and solid characterisation for CASH 1 are shown in tables 4.74 and 4.75.

Table 4.74 CASH 1* samples cured at 25°C in DDW, in 0.5 M NaCl + 0.02 M $MgSO_4$ and in 3.0 M NaCl + 0.02 M $MgSO_4$. Curing times are shown in table 3.3, section 3.1. The charge balance has been calculated as follows: 2[Ca] + 4[Si] + 3[Al] + [Na] - [Cl] + 2[Mg] - 2[SO_4]. Additional data are given in table 3.4 and figure 3.1.

Curing Media	No. of spikes	pH	Aqueous Characterisation, mmol/l							Charge balance
			Ca	Si	Al	Mg	SO_4	Na	Cl	OH, mmol/l
DD Water	-	12.91	17.7	0.01	0.03	<0.01	<0.01	0.04	<0.01	35.6
0.5 M NaCl + 0.02 M $MgSO_4$	0	12.81	26.2	0.01	<0.01	<0.01	4.31	394	414	23.7
0.5 M NaCl + 0.02 M $MgSO_4$	17	8.70	22.08	<0.01	<0.01	30.44	54.17	435	460	-28
3.0 M NaCl + 0.02 M $MgSO_4$	0	12.51	27.7	0.01	<0.01	<0.01	10.63	2370	2360	43.2
3.0 M NaCl + 0.02 M $MgSO_4$	17	8.14	29.82	0.01	<0.01	30.85	67.75	2501	2471	14

* CASH I: 75.7 CaO, 5.5 AlO(OH), 18.8 SiO_2 (wt%)

Table 4.75 Solid characterisation of CASH 1 cured in DDW, in 0.5 M NaCl + 0.02 M $MgSO_4$ and in 3.0 M NaCl + 0.02 M $MgSO_4$ solutions at 25°C. Total time taken for the respikes varied from 8 to 12 months in addition to the curing times shown in table 3.3 section 3.1. See CASH 1 composition in tables 3.4, 4.74 and figure 3.1.

Curing Media for CASH 1	Number of spikes	CH	AFt	Gypsum	Brucite	NaCl
DD Water	-	S				
0.5 M NaCl + 0.02 M $MgSO_4$	1	S	S			S
0.5 M NaCl + 0.02 M $MgSO_4$	17			S	M	S
3.0 M NaCl + 0.02 M $MgSO_4$	1	S	M			S
3.0 M NaCl + 0.02 M $MgSO_4$	17			S	S	S

From the XRD-results (table 4.75) it can be seen that the boehmite has reacted to form AFt in experiments without respiking. However, when reaction is allowed to continue in 0.02 M $MgSO_4$, crystalline Al-phases are no longer detected. After 17 respikes, all the calcium hydroxide has reacted to form brucite and gypsum and the pH had decreased to ~ 8. From the results in table 4.75 it can also be concluded that $MgSO_4$, not NaCl, is principally responsible for the phase changes and decreasing pH.

Results for CASH 2 are shown in tables 4.76 and 4.77.

Table 4.76 CASH 2* samples cured at 25°C in DDW, in 0.5 M NaCl + 0.02 M $MgSO_4$ and in 3.0 M NaCl+ 0.02 M $MgSO_4$. Curing times are shown in table 3.3 section 3.1. The charge balance has been calculated as follows: 2[Ca] + 4[Si] + 3[Al] + [Na] - [Cl] + 2[Mg] - 2[SO_4].

Curing Media*	No. of spikes	pH	Aqueous Characterisation, mmol/l							Charge balance OH, mmol/l
			Ca	Si	Al	Mg	SO_4	Na	Cl	
DD Water	-	10.18	2.59	2.18	<0.01	<0.01	<0.01	0.03	0.03	13.9
0.5 M NaCl + 0.02 M $MgSO_4$	1	10.27	21.81	1.40	<0.01	<0.01	12.71	394	414	3.70
0.5 M NaCl + 0.02 M $MgSO_4$	2	8.90	24.70	1.49	<0.01	0.21	26.04	419	425	-2
3.0 M NaCl + 0.02 M $MgSO_4$	1	9.41	32.04	1.51	<0.01	0.01	19.58	2420	2640	-192
3.0 M NaCl + 0.02 M $MgSO_4$	2	8.75	52.40	1.17	<0.01	0.04	27.50	2555	3017	-407

* CASH 2: 19.6 CaO, 39.2 AlO(OH), 41.1 SiO_2 (wt%)

Table 4.77 Solid characterisation of CASH 2 cured in DDW, in 0.5 M NaCl + 0.02 M $MgSO_4$ and in 3.0 M NaCl + 0.02 M $MgSO_4$ solutions at 25°C. Total time taken for the respikes varied from 8 to 12 months in addition to the curing times shown in table 3.3, section 3.1. See CASH 2 composition in tables 3.4, 4.76 and figure 3.1.

Curing Media for CASH 2	Number of spikes	C-S-H I	AFt	Gypsum	Boehmite	NaCl
DD Water	-	M			M	
0.5 M NaCl + 0.02 M $MgSO_4$	1		M		M	S
0.5 M NaCl +0.02 M $MgSO_4$	2			S	S	S
3.0 M NaCl + 0.02 M $MgSO_4$	1				M	S
3.0 M NaCl + 0.02 M $MgSO_4$	2			S	S	S

CASH 2 has the most Al-rich assemblage of those examined. Even though the mixes were left to react for long periods, equilibrium may not have been reached. The only conclusions are that (i) formation of C-S-H I is inhibited by the salinity of the curing media and (ii) some, perhaps much, of the boehmite reacted, as AFt is observed in 0.5 M NaCl + 0.02 M $MgSO_4$ system without respiking. (iii) pH in this system decreases with increasing total $MgSO_4$ and (iv) Ca solubility increases up to 20 times in the saline environment relative to initially pure water.

Results for CASH 3 are shown in tables 4.78 and 4.79.

Table 4.78 CASH 3* samples cured at 25°C in DDW, in 0.5 M NaCl + 0.02 M $MgSO_4$ and in 3.0 M NaCl + 0.02 M $MgSO_4$. Curing times are showed in table 3.3, section 3.1. The charge imbalance has been calculated as follows: 2[Ca] + 4[Si] + 3[Al] + [Na] - [Cl] + 2[Mg] - 2[SO_4].

Curing Media	No. of spikes	pH	Aqueous Characterisation, mmol/l							Charge balance
			Ca	Si	Al	Mg	SO_4	Na	Cl	OH, mmol/l
DD Water	-	12.01	2.74	0.07	<0.01	<0.01	<0.01	0.03	0.02	11.8
0.5 M NaCl + 0.02 M $MgSO_4$	1	11.42	13.62	0.12	0.07	<0.01	4.65	381	402	-3.02
0.5 M NaCl + 0.02 M $MgSO_4$	9	7.01	31.94	0.08	<0.01	6.17	48.96	418	419	-22
3.0 M NaCl + 0.02 M $MgSO_4$	1	11.33	26.55	0.08	0.03	<0.01	9.38	2390	2560	-130
3.0 M NaCl + 0.02 M $MgSO_4$	9	6.85	38.17	0.08	<0.01	16.45	34.58	2365	2385	20

*CASH 3: 47.4 CaO, 11.9 AlO(OH), 40.7 SiO_2 (wt%)

Table 4.79 Solid characterisation of CASH 3 cured in DDW, in 0.5 M NaCl + 0.02 M $MgSO_4$ and in 3.0 M NaCl + 0.02 M $MgSO_4$ solutions at 25°C. Total time taken for the respikes varied from 8 to 12 months in addition to the curing times shown in table 3.3, section 3.1; see CASH 3 data in tables 3.4, 4.78 or figure 3.1.

Curing Media for CASH 3	Number of spikes	Tob	AFt	Gypsum	Brucite	NaCl
DD Water	-	S				
0.5 M NaCl + 0.02 M $MgSO_4$	1		S			S
0.5 M NaCl +0.02 M $MgSO_4$	9			S		S
3.0 M NaCl + 0.02 M $MgSO_4$	1		M			S
3.0 M NaCl + 0.02 M $MgSO_4$	9			S	S	S

CASH 3 has a relatively low content of aluminium. From the XRD-results (table 4.79) it can be seen that the boehmite has reacted to form AFt in both saline environments without respiking. However, when reaction is allowed to continue in respiked 0.02 M $MgSO_4$, no crystalline Al- containing phases were detected. After 9 respikes, gypsum is observed in both samples: brucite is only observed in the more saline media, although probably present at the lower salinities. As a consequence of the phase changes the pH decreases to ~ 7. Formation of tobermorite from C-S-H is observed in DDW at 25°C. This has been observed to occur in C-S-H, C/S ratio 1.8, in 0.005M $MgSO_4$ (table 4.14) and in some of the CScH systems (section 4.2.2.3). If crystallisation is not achieved rapidly, it is effectively inhibited by progressive calcium replacement by Mg and by calcium leaching from C-S-H. The Ca solubility increases up to 14 times in saline environments, because of formation of relatively soluble gypsum.

Results for CASH 4 are shown in tables 4.80 and 4.81.

Table 4.80 CASH 4* samples cured at 25°C in DDW, in 0.5 M NaCl + 0.02 M $MgSO_4$ and in 3.0 M NaCl + 0.02 M $MgSO_4$. Curing times are showed in table 3.3 section 3.1. The charge balance has been calculated as follows: 2[Ca] + 4[Si] + 3[Al] + [Na] - [Cl] + 2[Mg] -2[SO_4]; see additional CASH 4 data in table 3.4 and figure 3.1.

Curing Media*	No. of spikes	pH	Aqueous Characterisation, mmol/l							Charge balance OH, mmol/l
			Ca	Si	Al	Mg	SO_4	Na	Cl	
DD Water	-	10.24	1.97	2.97	<0.01	<0.01	<0.01	0.03	0.02	15.8
0.5 M NaCl + 0.02 M $MgSO_4$	1	9.61	26.60	2.34	<0.01	<0.01	17.08	394	322	100
0.5 M NaCl + 0.02 M $MgSO_4$	4	8.23	34.93	1.60	<0.01	<0.01	26.67	402	435	-10
3.0 M NaCl + 0.02 M $MgSO_4$	1	11.06	13.29	2.22	0.22	<0.01	3.35	2200	2300	-67.6
3.0 M NaCl + 0.02 M $MgSO_4$	4	7.72	48.15	0.82	<0.01	1.03	41.46	2392	2471	-60

* CASH 4: 27.6 CaO, 23.1 AlO(OH), 49.3 SiO_2 (wt%)

Table 4.81 Solid characterisation of CASH 4 cured in DDW, in 0.5 M NaCl + 0.02 M $MgSO_4$ and in 3.0 M NaCl + 0.02 M $MgSO_4$ solutions at 25°C. Total time taken for the respikes varied from 8 to 12 months in addition to the curing times shown in table 3.3, section 3.1; see additional CASH 4 data in tables 3.4. 4.80 and figure 3.1.

Curing Media for CASH 4	Number of spikes	C-S-H I	Gypsum	Boehmite	NaCl
DD Water	-	M		M	
0.5 M NaCl + 0.02 M $MgSO_4$	1			M	S
0.5 M NaCl +0.02 M $MgSO_4$	9		S	S	S
3.0 M NaCl + 0.02 M $MgSO_4$	1				S
3.0 M NaCl + 0.02 M $MgSO_4$	9		S	S	S

CASH 4 is Si-rich, chosen to reflect slag-rich or fly ash-rich blends. Even though only 23 wt% boehmite has been added, it is too much fully to react with the other components. Sulfate reacts with Ca to give gypsum, thereby reducing the aqueous pH. The solubility of Ca in CASH 4 is increased ~24 times when cured in 3.0 M NaCl + 0.02 M $MgSO_4$, relative to DDW.

Results for CASH 5 are shown in tables 4.82 and 4.83

Table 4.82 CASH 5* samples cured at 25°C in DDW, in 0.5 M NaCl + 0.02 M $MgSO_4$ and in 3.0 M NaCl + 0.02 M $MgSO_4$. Curing times are showed in table 3.3, section 3.1. The charge balance has been calculated as follows: 2[Ca] + 4[Si] + 3[Al] + [Na] - [Cl] + 2[Mg] -2[SO_4]; see additional CASH 5 data in table 3.4 and figure 3.1.

Curing Media*	No. of spikes	pH	Aqueous Characterisation, mmol/l							Charge balance OH, mmol/l
			Ca	Si	Al	Mg	SO_4	Na	Cl	
DD Water	-	10.26	2.24	1.69	0.44	<0.01	<0.01	0.03	0.03	12.6
0.5 M NaCl + 0.02 M $MgSO_4$	1	9.64	26.05	1.58	<0.01	<0.01	17.08	381	465	-60.6
0.5 M NaCl + 0.02 M $MgSO_4$	4	8.83	33.68	0.71	<0.01	0.08	26.25	402	442	-22
3.0 M NaCl + 0.02 M $MgSO_4$	1	9.32	31.00	2.10	<0.01	0.01	17.08	2340	2500	-126
3.0 M NaCl + 0.02 M $MgSO_4$	4	8.20	49.90	0.64	<0.01	0.16	37.71	2447	2270	204

*CASH 5: 27.1 CaO, 34.1 AlO(OH), 38.8 SiO_2 (wt%)

Table 4.83 Solid characterisation of CASH 5 cured in DDW, in 0.5 M NaCl + 0.02 M $MgSO_4$ and in 3.0 M NaCl + 0.02 M $MgSO_4$ solutions at 25°C. Total time taken for the respikes varied from 8 to 12 months in addition to the curing times shown in table 3.3 section 3.1: see additional CASH 5 data in tables 3.4, 4.82 and figure 3.1.

Curing Media for CASH 5	Number of spikes	C-S-H I	Gypsum	Boehmite	NaCl
DD Water	-	S		S	
0.5 M NaCl + 0.02 M $MgSO_4$	1			S	S
0.5 M NaCl +0.02 M $MgSO_4$	4		S	M	S
3.0 M NaCl + 0.02 M $MgSO_4$	1			M	S
3.0 M NaCl + 0.02 M $MgSO_4$	4		S	S	S

CASH 5 simulates the FA blends and has an Al-rich assemblage, which is reflected in the XRD results. Unreacted boehmite is observed in all curing conditions indicating that, even though long curing times were used, equilibrium may not have been achieved. Gypsum is formed in the respiked experiments and the pH drops to near-neutral. C-S-H I, observed in DDW, is not observed in any of the saline environments. Ca solubility increases 22 times when cured in 3.0 M NaCl + 0.02M $MgSO_4$ compared with DDW.

Table 4.84 CASH 6* samples cured at 25°C in DDW, in 0.5 M NaCl + 0.02 M $MgSO_4$ and in 3.0 M NaCl + 0.02 M $MgSO_4$. Curing times are showed in table 3.3 section 3.1. The charge balance has been calculated as follows: 2[Ca] + 4[Si] + 3[Al] + [Na] - [Cl] + 2[Mg] -2[SO_4]; see additional CASH 6 data in table 3.4 and figure 3.1.

Curing Media*	No. of spikes	pH	Aqueous Characterisation, mmol/l							Charge balance OH, mmol/l
			Ca	Si	Al	Mg	SO_4	Na	Cl	
DD Water	-	12.10	4.01	0.04	0.01	<0.01	<0.01	0.03	0.01	8.23
0.5 M NaCl + 0.02 M $MgSO_4$	1	11.90	9.06	0.06	0.67	<0.01	0.33	394	414	-0.39
0.5 M NaCl + 0.02 M $MgSO_4$	8	7.00	29.44	0.06	0.02	1.65	30.00	413	408	7
3.0 M NaCl + 0.02 M $MgSO_4$	1	9.26	31.29	0.13	0.13	<0.01	19.58	2370	3130	-743
3.0 M NaCl + 0.02 M $MgSO_4$	8	8.22	31.06	<0.01	0.10	0.62	45.21	2501	2528	-54

* CASH 6: 41.3 CaO, 31.1 AlO(OH), 27.5 SiO_2 (wt%)

Table 4.85 Solid characterisation of CASH 6 cured in DDW, in 0.5 M NaCl + 0.02 M $MgSO_4$ and in 3.0 M NaCl + 0.02 M $MgSO_4$ solutions at 25°C. Total time taken for the respikes varied from 8 to 12 months in addition to the curing times shown in table 3.3, section 3.1; see CASH 6 composition in tables 3.4, 4.84 and figure 3.1.

Curing Media CASH 6	No. of spikes	C-S-H I	CH	C_3ASH_4 (Si-HG)	HG	Gyp	GH	Boe.	AFt	AFm-Cl	MH	NaCl
DD Water	-	M			M		S					
0.5 M NaCl + 0.02 M $MgSO_4$	1		M	S				M	S			S
0.5 M NaCl + 0.02 M $MgSO_4$	8					S						M
3.0 M NaCl + 0.02 M $MgSO_4$	1								S			S
3.0 M NaCl + 0.02 M $MgSO_4$	8					S		M		M	W	S

Results for CASH 6 are shown in tables 4.84 and 4.85. This composition is intended to simulate PFA-rich blends. From the XRD results (table 4.85) the high salinity inhibits formation of crystalline products from C-S-H.

Gehlenite hydrate (C_2ASH_8), hydrogarnet and C-S-H I develop in DDW but in more saline environments (0.5 M NaCl + 0.02 M $MgSO_4$), C_2ASH_8 becomes unstable forming instead siliceous hydrogarnet (C_3ASH_4). This has been observed by Locher (3), who reacted various C-A-S glasses in water with CH or OPC at ambient temperature. The phases observed were: AFt, C_4AH_{13}, C_2ASH_8, C_3ASH_4 and CH. He also noted that C_2ASH_8 was unstable in saturated CH solutions, forming Si-HG, and that a stoichiometric reaction could be written: C_2ASH_8 + CH $\Leftrightarrow$ C_3ASH_4. Furthermore he observed that with gypsum and CH present, C_2ASH_8 was also unstable, reacting to form AFt. The present study showed that AFt also formed in the presence of Si-HG and CH at low $MgSO_4$ (e.g. no respikes) but with increasing $MgSO_4$, AFt reacts further until only gypsum remained. At the highest salinity (3.0M NaCl + 0.02 M $MgSO_4$) the solid assemblage is brucite, gypsum and Friedel's salt (AFm-Cl).

Summary of the CASH system cured at 25°C in 0.5 M or 3.0 M NaCl and 0.02 $MgSO_4$

The Al-rich phase assemblages showed persistent unreacted boehmite, which is a possible indication of non-equilibrium. As gypsum forms, the pH decreases to near neutral. Figure 4.31 shows the relationship between the solids formed and the aqueous pH in 0.5 M NaCl and 0.02 M $MgSO_4$. For 3.0M NaCl and 0.02 M $MgSO_4$ the picture is not much different except that in CASH 6, unreacted boehmite persists: see figure 4.32. Gehlenite hydrate, a constituent of slag and fly ash-cement blends, is unstable in saline solutions. The solubility of the Ca component is much enhanced by the presence of both NaCl and $MgSO_4$; relative to distilled water, Ca solubilities are increased by factors of approximately 20-24. Mechanisms which limit the performance lifetimes of cementitious barriers tend to cumulate: Mg replaces calcium, while sulfate converts Ca phases typical of cement to gypsum, or anhydrite, or mixtures of the two. The $CaSO_4$ phases have increased solubility relative to C-S-H, etc. but do not condition a high aqueous pH. Moreover, NaCl enhances $CaSO_4$ solubility.

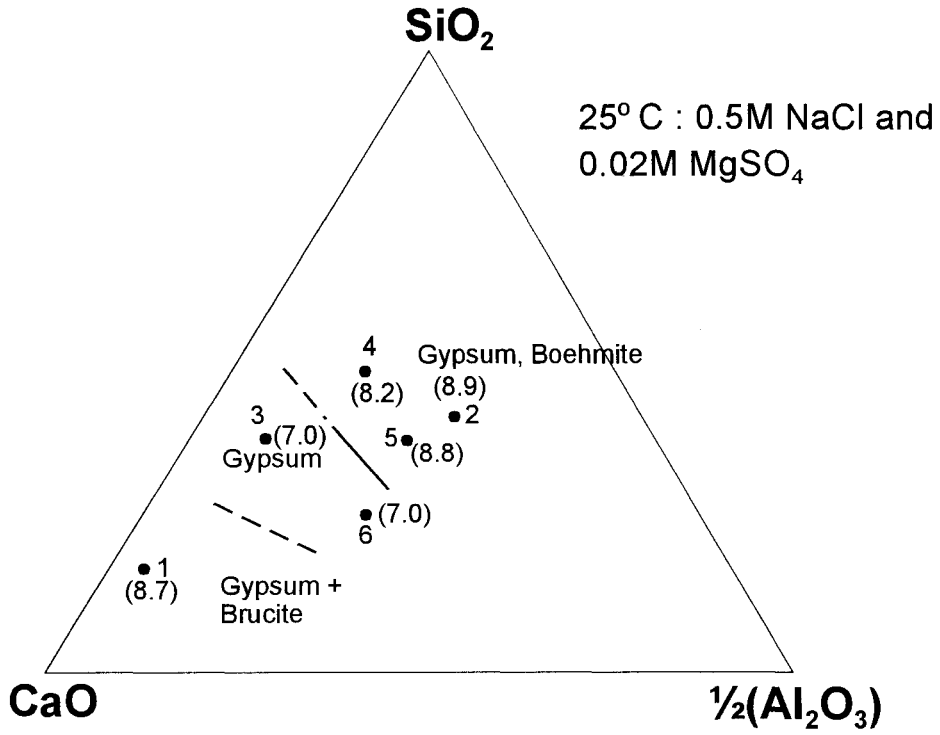

Figure 4.31 Ternary diagram of the CASH system cured in brine. Numbered points are the compositions studied; numbers in ( ) are aqueous pH. The results are for 25°C cured in 0.5 M NaCl and 0.02 M $MgSO_4$ after the number of respikes shown in table 4.73. Total curing time varied from 8 to 12 months, in addition to the curing times shown in table 3.3, section 3.1.

An estimate of the amount of unreacted boehmite was carried out on some of the samples and the results are shown in Appendix 4. The results confirm that the systems CASH 2, 4, 5 and 6 are difficult to homogenise.

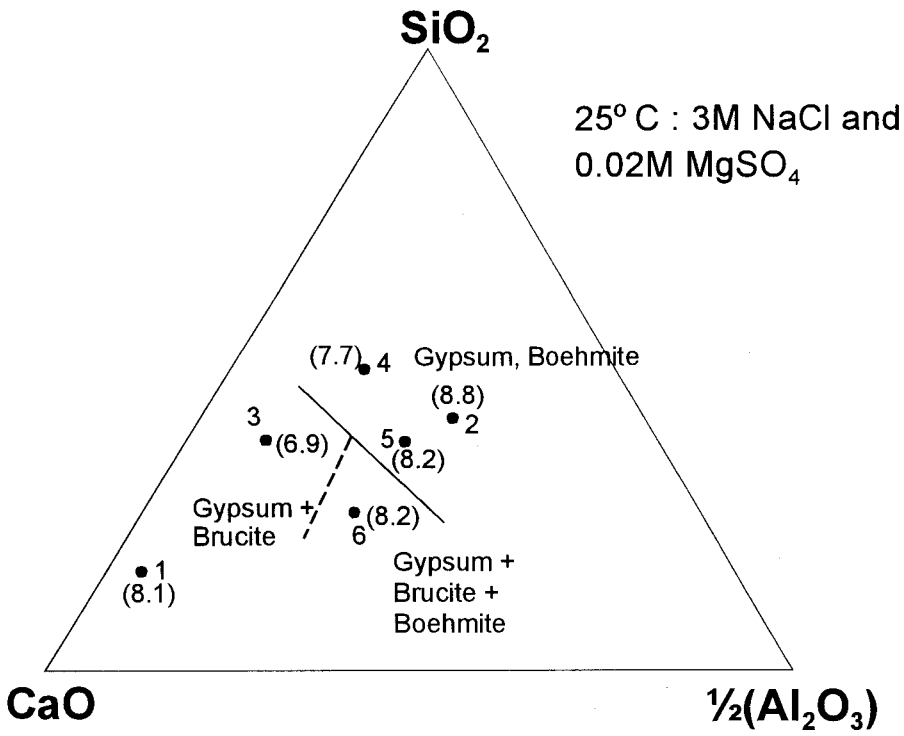

Figure 4.32 **Ternary diagram of the CASH system cured in brine. Numbered points are the composition points studied. numbers in ( ) are the aqueous pH. The results are for 25°C cured in 3.0 M NaCl and 0.02 M $MgSO_4$ after the number of respikes showed in table 4.73. Total curing time varied from 8 to 12 months, in addition to the curing times shown in table 3.3, section 3.1.**

SUMMARY OF THE 25°C RESULTS:

- Unreacted boehmite was observed in CASH compositions 2,4,5 and 6.
- pH decreases to near neutral in all CASH systems in saline environments.
- Gypsum is formed in all systems except from DDW environment.
- In CASH 6, AFm-Cl is observed at 3.0 M NaCl + 0.02M $MgSO_4$.
- The only Mg-containing phase observed was brucite.
- Mixed brines greatly enhance Ca solubility relative to initially pure water.

85°C Isotherm

Aqueous and solid characterisation for CASH 1 are shown in tables 4.86 and 4.87.

Table 4.86 **CASH 1 samples cured at 85°C in DDW, in 0.5 M NaCl + 0.02 M $MgSO_4$ and in 3.0 M NaCl + 0.02 M $MgSO_4$. Curing times are shown in table 3.3, section 3.1. The charge balance has been calculated as follows: 2[Ca]+4[Si]+3[Al]+[Na]-[Cl]+2[Mg]-2[SO_4]; see CASH 1 data in table 3.4 and figure 3.1. * indicates addition of DDW without respiking with NaCl.**

Curing Media for CASH 1	No. of spikes	pH	Aqueous Characterisation, mmol/l							Charge balance OH, mmol/l
			Ca	Si	Al	Mg	SO_4	Na	Cl	
DD Water	-	12.48	9.93	0.02	0.06	<0.01	<0.01	0.16	0.04	20.2
0.5 M NaCl + 0.02 M $MgSO_4$	1	12.49	23.15	0.02	0.07	<0.01	10.00	435	473	-43.5
0.5 M NaCl + 0.02 M $MgSO_4$	19	10.83	24.58	0.01	<0.01	0.16	29.79	335	325	-0.06
3.0 M NaCl + 0.02 M $MgSO_4$	1	12.29	19.41	0.03	0.04	<0.01	17.92	2540	2760	-221
3.0 M NaCl + 0.02 M $MgSO_4$	19	8.95	22.58	<0.01	<0.01	7.24	33.33	*1683	*1379	297

Table 4.87 **Solid characterisation of CASH 1 cured DDW, in 0.5 M NaCl + 0.02 M $MgSO_4$ and in 3.0 M NaCl + 0.02 M $MgSO_4$ solutions at 85°C. Total time taken for the respikes varied from 8 to 12 months, in addition to the curing times shown in table 3.3, section 3.1: see additional CASH 1 data in table 3.4 and figure 3.1.**

Curing Media for CASH 1	No. of spikes	CH	C-S-H I	HG	AFt	AFm-SO_4	AFm-Cl	Gyp	Anh	MH	NaCl
DD Water	-	S	t	S							
0.5 M NaCl + 0.02 M $MgSO_4$	1	S	W		S	W					S
0.5 M NaCl + 0.02 M $MgSO_4$	19							S	S	S	S
3.0 M NaCl + 0.02 M $MgSO_4$	1	S					S				S
3.0 M NaCl + 0.02 M $MgSO_4$	19								S	S	S

From the XRD-results on CASH I (table 4.87) boehmite has reacted forming AFt and AFm-SO_4 in 0.5 M NaCl. However when reaction is allowed to continue in respiked 0.02 M $MgSO_4$, crystalline Al-containing phases are no longer detected. After 19 spikes calcium hydroxide has reacted; brucite, anhydrite and gypsum are present. As a consequence the pH decreases to 10.8. Even though the pH has not decreased below 9, respiking was discontinued because the reactants appeared to have been consumed. For the CASH 1 samples cured in 3.0 M NaCl + 0.02M $MgSO_4$, AFm-Cl is observed in the experiments without respiking, but after

19 spikes it is no longer observed. No other Al- or Cl- phases are observed by XRD; only anhydrite and brucite remain and as a consequence the pH decreases to ~ 9.

Results for CASH 2 are shown in tables 4.88 and 4.89.

Table 4.88 CASH 2 samples cured at 85°C in DDW, in 0.5 M NaCl + 0.02 M $MgSO_4$ and in 3.0 M NaCl + 0.02 M $MgSO_4$. Curing times are shown in table 3.3, section 3.1. The charge balance has been calculated as follows: 2[Ca] + 4[Si] + 3[Al] + [Na] - [Cl] + 2[Mg] - 2[SO_4]; see CASH 2 data in table 3.4 and figure 3.1.

Curing Media for CASH 2	No. of spikes	pH	Aqueous Characterisation, mmol/l							Charge balance OH, mmol/l
			Ca	Si	Al	Mg	SO_4	Na	Cl	
DD Water	-	9.55	2.27	0.16	0.01	0.01	0.10	15.44	17.75	2.88
0.5 M NaCl + 0.02 M $MgSO_4$	1	9.21	30.24	0.61	0.02	<0.01	17.29	401	473	-43.5
0.5 M NaCl + 0.02 M $MgSO_4$	2	8.71	40.29	1.99	<0.01	0.02	25.83	500	494	43
3.0 M NaCl + 0.02 M $MgSO_4$	1	8.83	41.37	1.13	0.02	<0.01	19.79	2600	2760	-115
3.0 M NaCl + 0.02 M $MgSO_4$	2	7.96	47.16	1.01	<0.01	0.04	23.33	3072	3304	-180

Table 4.89 Solid characterisation of CASH 2 cured in DDW, in 0.5 M NaCl + 0.02 M $MgSO_4$ and in 3.0 M NaCl + 0.02 M $MgSO_4$ solutions at 85°C. Total time taken for the respikes varied from 8 to 12 months in addition to the curing times shown in table 3.3, section 3.1; see CASH 2 data in table 3.4 and figure 3.1.

Curing Media for CASH 2	No. of spikes	C-S-H I	HG	AFm-Cl-SO_4	Gyp.	Anh.	Boe.	NaCl
DD Water	-	M	S				M	
0.5 M NaCl + 0.02 M $MgSO_4$	1				M		M	S
0.5 M NaCl +0.02 M $MgSO_4$	2				M	S	S	S
3.0 M NaCl + 0.02 M $MgSO_4$	1	t		M			M	S
3.0 M NaCl + 0.02 M $MgSO_4$	2					S	S	S

CASH 2 was intended to simulate PFA blends and has the most Al-rich of the CASH compositions. In DDW, HG and C-S-H I are observed, but unreacted boehmite is also present, which may indicate that the system has not reached equilibrium. AEM and TG (see Appendix 4 for TG results) was carried out to examine the extent of reaction of boehmite. The TG showed that approximately 11.5wt% of the boehmite had reacted. In the study with AEM, boehmite was not observed. However, since AEM is selective and, as boehmite was observed both by XRD and by TG, it must be present. Nevertheless AEM analysis revealed that two

areas of compositions in the CASH sample exists: one type having high Al contents and the other, low Al contents. Furthermore, unreacted SiO_2 was identified occluded in C-S-H gel. All these data lead to the same conclusion, namely that the CASH 2 system may not have reached equilibrium and that the CASH 2 composition is difficult to homogenise even at 85°C.

Results for CASH 3 are shown in tables 4.90 and 4.91.

Table 4.90 CASH 3 samples cured at 85°C in DDW, in 0.5 M NaCl + 0.02 M $MgSO_4$ and in 3.0 M NaCl + 0.02 M $MgSO_4$. Curing times are shown in table 3.3 section 3.1. The charge balance has been calculated as follows: 2[Ca] + 4[Si] + 3[Al] + [Na] - [Cl] + 2[Mg] -2[SO_4]; see additional CASH 3 data in table 3.4 and figure 3.1. * See text for explanation.

Curing Media for CASH 3	No. of spikes	pH	Aqueous Characterisation, mmol/l							Charge balance OH, mmol/l
			Ca	Si	Al	Mg	SO_4	Na	Cl	
DD Water	-	12.1	3.14	0.03	0.04	<0.01	0.02	2.96	2.85	7.0
0.5 M NaCl + 0.02 M $MgSO_4$	1	12.1	21.41	0.02	0.03	<0.01	11.46	413	462	-28.8
0.5 M NaCl + 0.02 M $MgSO_4$	11	7.8	14.35	0.20	<0.01	8.89	23.75	83	261	-178
3.0 M NaCl + 0.02 M $MgSO_4$	1	11.8	23.98	0.04	0.08	<0.01	18.75	2480	2850	-357
3.0 M NaCl + 0.02 M $MgSO_4$	11	8.3	32.44	0.09	<0.01	0.10	27.71	1740*	1379*	371

Table 4.91 Solid characterisation of CASH 3 cured DDW, in 0.5 M NaCl + 0.02 M $MgSO_4$ and in 3.0 M NaCl + 0.02 M $MgSO_4$ solutions at 85°C. Total time taken for the respikes varied from 8 to 12 months in addition to the curing times shown in table 3.3, section 3.1: see additional CASH 3 data in table 3.4 and figure 3.1.

Curing Media for CASH 3	Number of spikes	C-S-H I	Tob	HG	AFt	Gyp	Anh	AFm-Cl	NaCl
DD Water	-	M	S	S					
0.5 M NaCl + 0.02 M $MgSO_4$	1	M	M		S				S
0.5 M NaCl +0.02 M $MgSO_4$	11					S			S
3.0 M NaCl + 0.02 M $MgSO_4$	1		M					M	S
3.0 M NaCl + 0.02 M $MgSO_4$	11						S		S

From the XRD-results for CASH 3 (table 4.91) it can be seen that the boehmite has reacted to form AFt in 0.5 M NaCl + 0.02M $MgSO_4$. When reaction is continued in respiked 0.02 M $MgSO_4$, crystalline Al-containing phases disappear until after 11 spikes only gypsum remains. As a consequence the pH decreases to ~ 7.8. Table 4.90 shows that the [Na] and [Cl] are lower than anticipated in respiked 0.5M NaCl + 0.02M $MgSO_4$. This is believed to be a result of a poor seal on the bottle; white crystals, forming around the neck of the bottle were identified as NaCl. AEM was consequently carried out to see whether this was the only cause of the decrease in [NaCl] or whether there had been an uptake from the aqueous phase into the solid. Unfortunately the AEM analysis did not clarify this matter; both low sodium C-S-H gel and tobermorite was observed, even though the latter was not detected by XRD.

When CASH 3 is cured in 3.0M NaCl + 0.02 M $MgSO_4$, tobermorite and Friedel's salt (AFm-Cl) are observed initially, but after 11 spikes both these phases react leaving anhydrite as the only phase detected by XRD. As a consequence the pH decreases to ~ 8.3. The Ca solubility increases by ~10 times relative to DDW in the saline environment because of the formation of relatively soluble anhydrite. In respiked 3.0M NaCl + 0.02M $MgSO_4$ the solution was diluted with DDW and no NaCl was added, hence the low [NaCl]; see data in table 4.90 marked (*).

Table 4.92 CASH 4 samples cured at 85°C in DDW, in 0.5 M NaCl + 0.02 M MgSO4 and in 3.0 M NaCl + 0.02 M $MgSO_4$. Curing times are shown in table 3.3, section 3.1. The charge balance has been calculated as follows: 2[Ca] + 4[Si] + 3[Al] + [Na] - [Cl] + 2[Mg] - 2[SO_4]; see additional CASH 4 data in table 3.4 and figure 3.1.

Curing Media for CASH 4	No. of spikes	pH	Aqueous Characterisation, mmol/l							Charge balance OH, mmol/l
			Ca	Si	Al	Mg	SO_4	Na	Cl	
DD Water	-	9.65	1.68	7.83	0.02	<0.01	0.02	0.85	0.97	34.5
0.5 M NaCl + 0.02 M $MgSO_4$	1	9.45	32.53	3.56	0.02	<0.01	17.92	397	428	12.4
0.5 M NaCl + 0.02 M $MgSO_4$	6	7.57	25.07	0.20	<0.01	19.09	31.25	313	284	55.6
3.0 M NaCl + 0.02 M $MgSO_4$	1	9.06	41.72	0.12	0.11	<0.01	18.13	2420	2510	-42
3.0 M NaCl + 0.02 M $MgSO_4$	4	7.32	41.79	0.66	<0.01	0.21	22.92	2664	2563	142

Table 4.93 Solid characterisation of CASH 4 cured in DDW, in 0.5 M NaCl + 0.02 M $MgSO_4$ and in 3.0M NaCl + 0.02 M $MgSO_4$ at 85°C. Total time taken for the respikes varied from 8 to 12 months, in addition to the curing times shown in table 3.3, section 3.1; see additional CASH 4 data in table 3.4 and figure 3.1.

Curing Media for CASH 4	Number of spikes	C-S-H I	HG	Anh	Boe	NaCl	unidentified
DD Water	-		S		M		
0.5 M NaCl + 0.02 M $MgSO_4$	1	M			M	S	
0.5 M NaCl +0.02 M $MgSO_4$	6						
3.0 M NaCl + 0.02 M $MgSO_4$	1	M			W	S	
3.0 M NaCl + 0.02 M $MgSO_4$	4			S		S	3.09 Å

Results for CASH 4 are shown in tables 4.92 and 4.93. CASH 4 is Si-rich, reflecting the composition of fly ash-rich blends. Even though only 23 wt% boehmite has been added, it is too much to react fully with the other components. When the systems have been respiked boehmite dissolves; gypsum remains and the pH of the solution decreases. The solubility of Ca from CASH 4 is 25 times greater when cured in 3.0 M NaCl + 0.02 M $MgSO_4$ than in DDW.

Table 4.94 CASH 5 samples cured at 85°C in DDW, in 0.5 M NaCl + 0.02 M $MgSO_4$ and in 3.0 M NaCl + 0.02 M $MgSO_4$. Curing times are shown in table 3.3, section 3.1. The charge imbalance has been calculated as follows: 2[Ca] + 4[Si] + 3[Al] + [Na] - [Cl] + 2[Mg] - 2[SO_4]; see additional CASH 5 data in table 3.4 and figure 3.1.

Curing Media for CASH 5	No. of spikes	pH	Aqueous Characterisation, mmol/l							Charge balance OH, mmol/l
			Ca	Si	Al	Mg	SO_4	Na	Cl	
DD Water	-	10.01	2.18	0.62	0.02	<0.01	0.02	3.52	4.05	6.3
0.5 M NaCl + 0.02 M $MgSO_4$	1	10.50	31.29	0.33	0.08	<0.01	17.08	397	473	-46
0.5 M NaCl + 0.02 M $MgSO_4$	4	7.12	38.55	0.17	<0.01	0.25	27.29	533	460	97
3.0 M NaCl + 0.02 M $MgSO_4$	1	9.95	41.72	0.12	0.11	<0.01	18.13	2420	2510	-42
3.0 M NaCl + 0.02 M $MgSO_4$	4	6.52	58.88	0.10	<0.01	2.84	17.71	2746	2817	17

Table 4.95 Solid characterisation of CASH 5 cured DDW, in 0.5 M NaCl + 0.02 M $MgSO_4$ and in 3.0 M NaCl + 0.02 M $MgSO_4$ solutions at 85°C. Total time taken for the respikes varied from 8 to 12 months in addition to the curing times shown in table 3.3, section 3.1; see additional CASH 5 data in table 3.4 and figure 3.1. Last column gives X-ray d spacings from an 'unknown' phase.

Curing Media for CASH 5	No. of spikes	CH	Cc	C-S-H I	HG	Boe	Gyp	Anh	Gis	NaCl	Un-identified
DD Water	-				S	M					
0.5 M NaCl + 0.02 M $MgSO_4$	1	W		M		M				S	
0.5 M NaCl +0.02 M $MgSO_4$	4						S		M	S	
3.0 M NaCl + 0.02 M $MgSO_4$	1			W		M				S	
3.0 M NaCl + 0.02 M $MgSO_4$	4		W			M	S	S		S	6.72, 4.37, 4.17, 2.79Å

Results for CASH 5 are shown in tables 4.94 and 4.95. CASH 5 is compositionally related to FA blends and its Al-rich assemblage is reflected in the XRD results. Unreacted boehmite is observed in almost all curing conditions, which indicates than even though long curing times were used, equilibrium may not have been achieved. Gypsum and/or anhydrite are formed in the respiked experiments and the pH drops to near-neutral. This is the only composition in which gismondine, a zeolite phase, has been observed at lower salinity.

Table 4.96 CASH 6 samples cured at 85°C in DDW, in 0.5 M NaCl + 0.02 M $MgSO_4$ and in 3.0 M NaCl + 0.02 M $MgSO_4$. Curing times are shown in table 3.3, section 3.1. The charge balance has been calculated as follows: 2[Ca] + 4[Si] + 3[Al] + [Na] - [Cl] + 2[Mg] - 2[SO_4]; see additional CASH 6 data in table 3.4 and figure 3.1. * DDW has been added without NaCl spiking.

Curing Media for CASH 6	No. of spikes	pH	Aqueous Characterisation, mmol/l							Charge balance OH mmol/L
			Ca	Si	Al	Mg	SO_4	Na	Cl	
DD Water	-	11.50	2.74	0.01	1.44	<0.01	0.03	4.22	4.39	9.5
0.5 M NaCl + 0.02 M $MgSO_4$	1	11.36	15.39	0.22	1.15	<0.01	11.04	413	485	[illegible]58
0.5 M NaCl + 0.02 M $MgSO_4$	10	7.36	23.58	0.12	<0.01	5.59	29.38	28[illegible]	261	[illegible]6
3.0 M NaCl + 0.02 M $MgSO_4$	1	11.31	10.88	0.04	2.14	<0.01	18.33	2430	2510	[illegible]58
3.0 M NaCl + 0.02 M $MgSO_4$	10	10.42	31.69	0.03	0.10	0.02	30.21	1740*	1638*	[illegible]05

Table 4.97 Solid characterisation of CASH 6 cured in DDW, in 0.5 M NaCl + 0.02 M $MgSO_4$ and in 3.0 M NaCl + 0.02 M $MgSO_4$ solutions at 85°C. Total time taken for the respikes varied from 8 to 12 months, in addition to the curing times shown in table 3.3, section 3.1; see additional CASH 6 data in table 3.4 and figure 3.1.

Curing Media for CASH 6	No. of spikes	C-S-H I	Tob	CH	C_3ASH_4 (Si-HG)	HG	Gyp	Anh	Boe	AFm	AFm-Cl	NaCl
DD Water	-	W	S			S			M			
0.5 M NaCl + 0.02 M $MgSO_4$	1	M		W					M	S		S
0.5 M NaCl + 0.02 M $MgSO_4$	10				M		S	S				M
3.0 M NaCl + 0.02 M $MgSO_4$	1	M									S	S
3.0 M NaCl + 0.02 M $MgSO_4$	10							S				S

The results for CASH 6 are shown in tables 4.96 and 4.97. CASH 6 composition also simulates PFA-rich blends. From the XRD results for cures in 0.5 M NaCl + 0.02 M $MgSO_4$ and 3.0 M NaCl + 0.02M $MgSO_4$, formation of C-S-H crystalline phases is inhibited by NaCl.

In DDW, hydrogarnet, tobermorite and C-S-H I coexist but in more saline environments (0.5 M NaCl + 0.02 M $MgSO_4$) hydrogarnet becomes unstable forming instead siliceous hydrogarnet (C_3ASH_4) and gypsum/anhydrite; pH drops to ~ 7. In 3.0M NaCl + 0.02 M $MgSO_4$ without respiking, Friedel's salt (AFm-Cl) and C-S-H I are stable but in the respiked experiments only anhydrite is observed, which accounts for the near-neutral pH.

SUMMARY OF THE 85°C RESULTS:

- Unreacted boehmite was observed in CASH 2,4,5 and 6.
- pH decreases to near neutral in all respiked CASH systems.
- Gypsum and/or anhydrite is formed in all respiked systems.
- In CASH 3 and 6, AFm-Cl is observed in 3.0 M NaCl + 0.02M $MgSO_4$.
- The only Mg-containing phase observed was brucite in CASH 1.
- Solubility of Ca increases up to 25 times in saline environments relative to DDW.

Summary of the CASH system cured at 85°C in 0.5 M or 3.0 M NaCl and 0.02 M $MgSO_4$

The Al-rich phase assemblages contain unreacted boehmite, a possible indication that the alumina component had not fully reacted: gibbsite, $Al(OH)_3$, is believed to be the stable alumina hydrate. As gypsum and/or anhydrite are formed by reaction with the simulate brine the pH decreases to near neutral. Figure 4.33 shows the relationship between the solids formed

and the aqueous pH in 0.5 M NaCl and 0.02 M $MgSO_4$. In the more saline simulant, 3.0M NaCl + 0.02 M $MgSO_4$, the picture is not much different except that gismondine is not observed.

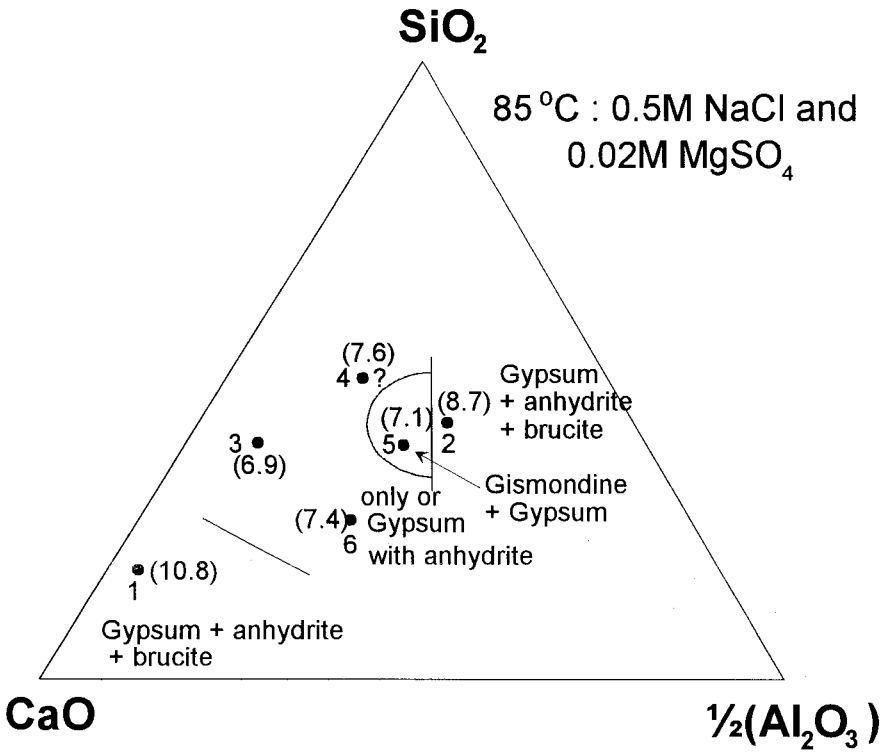

Figure 4.33 **Ternary diagram of the CASH system cured in brine. Numbered points are the composition points studied. The numbers in ( ) are aqueous pH. The results for 85°C, cured in 0.5 M NaCl and 0.02 M $MgSO_4$, after the number of respikes shown in table 4.73. Total curing time varied from 8 to 12 months, in addition to the curing times shown in table 3.3, section 3.1.**

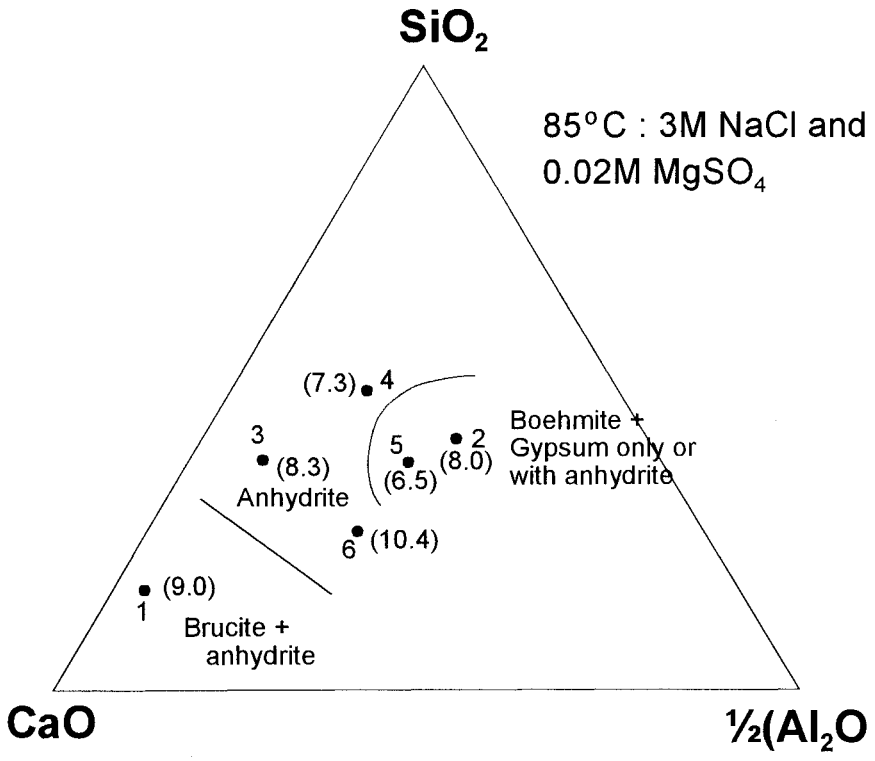

Figure 4.34 Ternary diagram of the CASH system cured in brine. Numbered points are the composition points studied. The numbers in ( ) are aqueous pH. The results are for 85°C cured in 3.0 M NaCl and 0.02 M $MgSO_4$ after the respikes shown in table 4.73. Curing time varied from 8 to 12 months, in addition to the curing times shown in table 3.3, section 3.1.

An estimate of unreacted boehmite was carried out on some of the samples; results are shown in Appendix 4. The results confirm that the systems CASH 2, 4, 5 and 6 are difficult to homogenise.

References

1. M. Atkins et al. (1991) 'A Thermodynamic Model for Blended Cements'. UK DoE Report no. DoE/HMIP/RR/92/005, Aberdeen University, Scotland.

2. M. Atkins et al. (1993) 'Thermodynamic Modelling of Blended Cements at Elevated Temperature (50-90°C)'. UK DoE Report no.DoE/HMIP/RR/94/011, Aberdeen University, Scotland

3. F. W. Locher. (1960) 'Hydraulic Properties and Hydration of Glasses in The System $CaO-Al_2O_3-SiO_2$'. Proceedings of the 4th. Int. Congress on Chemistry of Cement. National Bureau of Standards, Washington D.C.

4.2.2 $CaO-SiO_2-CaCO_3-H_2O$ System

4.2.2.1. Introduction and background

This system comprises 90-95 mol% of the components of reference backfill. The main concern of adding $CaCO_3$ is that it might react with other constituents in the backfill and form chemically inactive products such as scawtite. A wide range of compositions, shown in table 3.5 and figure 3.2, have been investigated to determine whether reactions occur between $CaCO_3$, CH, C-S-H, $MgSO_4$(aq) and NaCl (aq).

4.2.2.2 Kinetics and Respikes in $MgSO_4$+ NaCl Systems

The kinetic experiments were carried out at 25°C and for 0.5 M NaCl + 0.02M $MgSO_4$ for all the CScH systems. Experimental details for this part of the study are given in section 3.4.1: table 4.98 shows the results.

Table 4.98 Number of respikes necessary to reach 0.02M $MgSO_4$ target concentration at 25°C.

Phase Formation System	Number of spikes (160 mls)	Number of respikes in actual systems	[Mg] in mmol/l after last respike
CScH 1	4	8	17.28
CScH 2	5	10	14.40
CScH 3	5	10	16.04
CScH 4	1.5	3	18.10
CScH 6	1	1	15.63

To accelerate reaction, double the normal solution volume was used, so that the second column in table 4.98 is the number of respikes in the kinetic experiments and the third column is the number of respikes required for the actual systems.

Sulfate is much less strongly removed than magnesium and its concentration therefore increases above the target, 0.02M.

4.2.2.3 Solubility Data, pH and Solid Phase Compositions

Experimental details for the phase compatibility experiments on the CScH systems were given in section 3.1. Table 3.5 and figure 3.2 show the compositional relationships. The results of the first analysis showed that the uptake of magnesium into the solid was complete, although at this point magnesium-containing solids were not detected by XRD. The systems were therefore respiked: see table 3.3, section 3.1.

Accurate measurements of carbonate in solution were not practicable because solutions had a very low carbonate concentrations and the high levels of other dissolved components interfered with the determination.

25°C Isotherm

Results of slurry experiments in this system are presented in tables 4.99- 4.108. Starting compositions were given in table 3.5 and figure 3.2, which also shows hydrate phases which might form in this system, and their relationship to the reference backfill composition.

Table 4.99 CScH 1* samples cured at 25°C in DDW, in 0.5 M NaCl + 0.02 M $MgSO_4$ and in 3.0 M NaCl + 0.02 M $MgSO_4$. Curing times are shown in table 3.3, section 3.1; see CScH 1 data in table 3.5 and figure 3.2.

Curing Media for CScH 1	No. of spikes	pH	Aqueous Characterisation, mmol/l					
			Ca	Si	Mg	SO_4	Na	Cl
DD Water	-	11.59	1.30	0.16	<0.01	0.03	0.03	0.03
0.5 M NaCl + 0.02 M $MgSO_4$	1	10.59	27.30	0.23	<0.01	16.25	409	405
0.5 M NaCl + 0.02 M $MgSO_4$	8	6.43	30.81	0.17	9.46	30.21	435	362
3.0 M NaCl + 0.02 M $MgSO_4$	1	9.68	33.28	0.18	<0.01	17.71	2480	2510
3.0 M NaCl + 0.02 M $MgSO_4$	8	6.63	43.16	0.16	16.45	48.96	2610	2356

* wt%: 42.3 CaO, 45.3 SiO_2, 12.4 $CaCO_3$ (wt.%)

Table 4.100 Solid characterisation of CScH 1 cured DDW, in 0.5 M NaCl + 0.02 M $MgSO_4$ and in 3.0 M NaCl + 0.02 M $MgSO_4$ solutions at 25°C. Total time taken for the respikes varied from 8 to 12 months in addition to the curing times shown in table 3.3, section 3.1: see CScH 1 data in table 3.5 and figure 3.2.

Curing Media for CScH 1	Number of spikes	Cc	C-S-H I	Tob	Gypsum	NaCl
DD Water	-	S		W		
0.5 M NaCl + 0.02 M $MgSO_4$	1	S	M			S
0.5 M NaCl + 0.02 M $MgSO_4$	8	S			S	S
3.0 M NaCl + 0.02 M $MgSO_4$	1	S				S
3.0 M NaCl + 0.02 M $MgSO_4$	8	S			S	S

Results for CScH 1 are shown in tables 4.99 and 4.100. Composition CScH 1 was chosen because it has the same stoichiometry as scawtite, $6CaO{\cdot}CaCO_3{\cdot}6SiO_2{\cdot}2H_2O$, a candidate phase stable at elevated temperature. At 25°C no reaction with carbonate and C-S-H has been observed and $CaCO_3$ acts as an inert aggregate: see table 4.100. The occurrence of tobermorite at 25°C is noteworthy. Curing in NaCl and $MgSO_4$ results in formation of

gypsum, with a drop in pH to near-neutral. The changing solubility of Ca (see table 4.99) is believed to be due to two factors: (i) NaCl is known to increase the solubility of $CaCO_3$ and C-S-H (ii) the formation of gypsum, which has a higher solubility than either CH and C-S-H. No crystalline Mg-bearing phases were observed even though the Mg is removed from the solution.

Results from CScH 2 are shown in tables 4.101 and 4.102.

Table 4.101 CScH 2 samples* cured at 25°C in DDW, in 0.5 M NaCl + 0.02 M $MgSO_4$ and in 3.0 M NaCl + 0.02 M $MgSO_4$. Curing times are shown in table 3.3, section 3.1; see CScH 2 data in table 3.5 and figure 3.2.

Curing Media for CScH 2	Number of spikes	pH	Aqueous Characterisation, mmol/l					
			Ca	Si	Mg	SO_4	Na	Cl
DD Water	-	12.54	9.00	0.03	<0.01	0.01	0.03	0.04
0.5 M NaCl + 0.02 M $MgSO_4$	1	12.29	29.44	0.04	<0.01	16.67	422	391
0.5 M NaCl + 0.02 M $MgSO_4$	10	6.58	25.82	0.03	21.81	39.79	435	379
3.0 M NaCl + 0.02 M $MgSO_4$	1	12.17	33.53	0.01	<0.01	17.08	2500	2530
3.0 M NaCl + 0.02 M $MgSO_4$	10	6.14	33.68	<0.01	25.92	53.75	2338	1925

*wt.%: 19.6 CaO, 39.2 AlO(OH), 41.1 SiO_2

Table 4.102 Solid characterisation of CScH 2 cured DDW, in 0.5 M NaCl + 0.02 M $MgSO_4$ and in 3.0 M NaCl + 0.02 M $MgSO_4$ solutions at 25°C. Total time taken for the respikes varied from 8 to 12 months in addition to the curing times shown in table 3.3, section 3.1: see CScH 2 data in table 3.5 and figure 3.2.

Curing Media for CScH 2	Number of spikes	Cc	Tob.	Gypsum	Brucite	NaCl
DD Water	-	S	M			
0.5 M NaCl + 0.02 M $MgSO_4$	1	S				S
0.5 M NaCl + 0.02 M $MgSO_4$	10	S		S	W	S
3.0 M NaCl + 0.02 M $MgSO_4$	1	S				S
3.0 M NaCl + 0.02 M $MgSO_4$	10	S		S		S

The CScH 2 composition was designed to have the same stoichiometry as fukalite, $3CaO{\cdot}CaCO_3{\cdot}2SiO_2{\cdot}H_2O$, another mineral found in nature but not to the author's knowledge synthesised. Tobermorite formed at 25°C, but only in DDW. Brucite and gypsum are observed in respiked 0.5 M NaCl + 0.02M $MgSO_4$. The pH has declined to near neutral Brucite is believed to be present although not detected. Again, Ca solubility increases in saline environments. The increase is most significant between water and dilute brine; increasing the ionic strength further does not much enhance the solubility.

Results for CScH 3 are shown in tables 4.103 and 4.104

Table 4.103 CScH 3* samples cured at 25°C in DDW, in 0.5 M NaCl + 0.02 M $MgSO_4$ and in 3.0 M NaCl + 0.02 M $MgSO_4$. Curing times are shown in table 3.3 section 3.1; see CScH 3 data in table 3.5 and figure 3.2.

Curing Media	Number of spikes	pH	Aqueous Characterisation, mmol/l					
			Ca	Si	Mg	SO_4	Na	Cl
DD Water	-	12.80	17.27	0.01	<0.01	0.01	0.05	0.02
0.5 M NaCl + 0.02 M $MgSO_4$	1	12.68	35.88	0.01	<0.01	15.83	418	408
0.5 M NaCl + 0.02 M $MgSO_4$	12	7.01	20.71	<0.01	14.81	33.96	300	267
3.0 M NaCl + 0.02 M $MgSO_4$	1	12.57	34.88	0.01	<0.01	15.42	2460	2210
3.0 M NaCl + 0.02 M $MgSO_4$	10	8.67	39.80	0.03	18.92	57.50	2555	2528

* Solid composition, 41.1 CaO, 10.3 SiO_2, 48.7 $CaCO_3$ (wt%)

Table 4.104 Solid characterisation of CScH 3 cured in DDW, in 0.5 M NaCl + 0.02 M $MgSO_4$ and in 3.0 M NaCl + 0.02 M $MgSO_4$ solutions at 25°C. Total time taken for the respikes varied from 8 to 12 months in addition to the curing times shown in table 3.3, section 3.1: see CScH 3 data in table 3.5 and figure 3.2.

Curing Media for CScH 3	Number of spikes	Cc	CH	Gypsum	Brucite	NaCl
DD Water	-	S	S			
0.5 M NaCl + 0.02 M $MgSO_4$	1	S	S			M
0.5 M NaCl + 0.02 M $MgSO_4$	12	S		S	M	S
3.0 M NaCl + 0.02 M $MgSO_4$	1	S	S			S
3.0 M NaCl + 0.02 M $MgSO_4$	10	S		S	M	S

The CScH 3 composition is closest to the preferred composition for the reference backfill. Table 4.104 shows that no new carbonate phases have formed, but that calcium hydroxide reacts with $MgSO_4$ forming brucite and gypsum. These products cannot condition a high pH. If the results are compared with those for CH and C-S-H 1.8 in tables 4.1 and 4.2, for DDW, it can be seen that the Ca solubility in CScH 3 is very close to these values. This also supports the contention that $CaCO_3$ acts essentially as an inert aggregate. Furthermore, AEM of CScH 3 cured in DDW showed that Ca/Si ratio was high ~ 2.2 (10 analyses) but when cured in 0.5 M NaCl + 0.02M $MgSO_4$ (without respikes) both amorphous C-S-H gel and more crystalline material was found. An M-S-H phase with Mg:Si ~ 5.0 was also observed together with an amorphous gel containing variable amounts of Mg.

Table 4.105 CScH 4* samples cured at 25°C in DDW, in 0.5 M NaCl + 0.02 M $MgSO_4$ and in 3.0 M NaCl + 0.02 M $MgSO_4$. Curing times are shown in table 3.3, section 3.1; see CScH 4 data in table 3.5 and figure 3.2.

Curing Media in wt%: 16.1 CaO, 17.1 SiO_2, 66.7 $CaCO_3$ for CScH 4	Number of spikes	pH	Aqueous Characterisation, mmol/l					
			Ca	Si	Mg	SO_4	Na	Cl
DD Water	-	11.70	1.48	0.14	<0.01	0.01	0.01	0.01
0.5 M NaCl + 0.02 M $MgSO_4$	1	10.65	23.65	0.41	<0.01	16.67	431	422
0.5 M NaCl + 0.02 M $MgSO_4$	3.5	7.70	30.44	0.13	6.58	28.33	435	425
3.0 M NaCl + 0.02 M $MgSO_4$	1	10.08	27.00	0.32	<0.01	17.71	2500	2440
3.0 M NaCl + 0.02 M $MgSO_4$	3.5	6.55	46.53	0.18	5.76	45.42	2555	2414

*wt.%: 27.6 CaO, 23.1 AlO(OH), 49.3 SiO_2

Table 4.106 Solid characterisation of CScH 4 cured in DDW, in 0.5 M NaCl + 0.02 M $MgSO_4$ and in 3.0 M NaCl + 0.02 M $MgSO_4$ solutions at 25°C. Total time taken for the respikes varied from 8 to 12 months in addition to the curing times shown in table 3.3, section 3.1: see CScH 4 data in table 3.5 and figure 3.2.

Curing Media for CScH 4	Number of spikes	Cc	Tob	Gypsum	NaCl
DD Water	-	S	M		
0.5 M NaCl + 0.02 M $MgSO_4$	0	S			M
0.5 M NaCl + 0.02 M $MgSO_4$	3.5	S		S	M
3.0 M NaCl + 0.02 M $MgSO_4$	0	S			S
3.0 M NaCl + 0.02 M $MgSO_4$	3.5	S		S	S

Results for CScH 4 are shown in tables 4.105 and 4.106. CScH 4 was chosen is to verify that, even at high additions, $CaCO_3$ will not react with other constituents in the backfill. Table 4.106 shows no new carbonate phases to have formed; simulate groundwater reacts with the cementitious material to form mainly gypsum. Again, this leads to a reduction in pH and an increase in Ca solubility.

Table 4.107 CScH 5* samples cured at 25°C in DDW, in 0.5 M NaCl + 0.02 M $MgSO_4$ and in 3.0 M NaCl + 0.02 M $MgSO_4$. Curing times are shown in table 3.3, section 3.1; see CScH 5 data in table 3.5 and figure 3.2.

Curing Media for CScH 5	Number of spikes	pH	Aqueous Characterisation, mmol/l					
			Ca	Si	Mg	SO_4	Na	Cl
DD Water	-	10.07	1.11	3.20	<0.01	0.01	0.02	0.02
0.5 M NaCl + 0.02 M $MgSO_4$	0	9.62	22.75	2.14	<0.01	17.71	426	402
0.5 M NaCl + 0.02 M $MgSO_4$	1	8.28	36.80	0.98	0.31	25.42	457	437
3.0 M NaCl + 0.02 M $MgSO_4$	0	9.29	26.25	1.42	<0.01	18.54	2540	2530
3.0 M NaCl + 0.02 M $MgSO_4$	1	6.56	41.54	1.60	3.29	40.63	2501	2184

*wt.%: 27.1 CaO, 34.1 AlO(OH), 38.8 SiO_2

Table 4.108 Solid characterisation of CScH 5 cured in DDW, in 0.5 M NaCl + 0.02 M $MgSO_4$ and in 3.0 M NaCl + 0.02 M $MgSO_4$ solutions at 25°C. Total time taken for the respikes varied from 8 to 12 months in addition to the curing times shown in table 3.3, section 3.1: see CScH 5 data in table 3.5 and figure 3.2.

Curing Media for CScH 5	Number of spikes	Cc	Gypsum	NaCl
DD Water	-	S		
0.5 M NaCl + 0.02 M $MgSO_4$	0	S		S
0.5 M NaCl + 0.02 M $MgSO_4$	1	S	S	S
3.0 M NaCl + 0.02 M $MgSO_4$	0	S		S
3.0 M NaCl + 0.02 M $MgSO_4$	1	S		S

Results for CScH 5 are shown in tables 4.107 and 4.108. CScH 5 has a low Ca/Si ratio and, as a consequence, the Si solubility is higher than in the other samples.

SUMMARY OF THE 25°C RESULTS:

- $CaCO_3$ acts as an inert aggregate in all CScH compositions at ≤85°C.
- The CScH compositions act chemically like C-S-H gels.
- Tobermorite is found in CScH 1, 2 and 4, but only when cured in DDW.
- $MgSO_4$ react with CH and C-S-H to give brucite or M-S-H (observed in CScH 3) and gypsum.
- pH decreases to near neutral as a consequence of gypsum formation.
- Ca solubility is enhanced in brine, relative to water

85°C Isotherm

The results of slurry experiments are presented in tables 4.109 - 4.118; results for CScH 1 are shown in tables 4.109 and 4.110.

Table 4.109 CScH 1 samples cured at 85°C in DDW, in 0.5 M NaCl + 0.02 M $MgSO_4$ and in 3.0 M NaCl + 0.02 M $MgSO_4$. Curing times are shown in table 3.3, section 3.1; see CScH 1 data in table 3.5 and figure 3.2.

Curing Media for CScH 1	Number of spikes	pH	Aqueous Characterisation, mmol/l					
			Ca	Si	Mg	SO_4	Na	Cl
DD Water	-	11.31	1.15	0.10	<0.01	0.02	0.03	0.05
0.5 M NaCl + 0.02 M $MgSO_4$	1	10.62	21.73	0.15	<0.01	18.95	408.9	497.1
0.5 M NaCl + 0.02 M $MgSO_4$	8	7.08	27.69	1.02	10.28	34.58	462	454
3.0 M NaCl + 0.02 M $MgSO_4$	1	10.21	29.64	0.14	<0.01	18.87	2528	2999
3.0 M NaCl + 0.02 M $MgSO_4$	8	6.75	31.19	0.28	46.07	57.08	2664	2845

Table 4.110 Solid characterisation of CScH 1 cured in DDW, in 0.5 M NaCl + 0.02 M $MgSO_4$ and in 3.0 M NaCl + 0.02 M $MgSO_4$ solutions at 85°C. Total time taken for the respikes varied from 8 to 12 months in addition to the curing times shown in table 3.3, section 3.1: see CScH 1 data in table 3.5 and figure 3.2.

Curing Media for CScH 1	Number of spikes	Cc	sepiolite	Tob.	Gyp.	Anh.	NaCl
DD Water	-	S		S			
0.5 M NaCl + 0.02 M $MgSO_4$	1	M		W			S
0.5 M NaCl + 0.02 M $MgSO_4$	8	S			S		S
3.0 M NaCl + 0.02 M $MgSO_4$	1	W		W			S
3.0 M NaCl + 0.02 M $MgSO_4$	8	S	M		M	S	S

Composition CScH 1 has the same stoichiometry as scawtite, $6CaO{\cdot}CaCO_3{\cdot}6SiO_2{\cdot}2H_2O$. However, from table 4.110 it is seen that no new carbonate phases were formed. This is in accord with the reported thermal stability range of scawtite: 140-300°C [1]. In previous work at Aberdeen University [2] scawtite was also ruled out as a stable phase below 140°C. Tobermorite occurs in the samples without respikes but is not observed in the respiked experiments. The effect of curing in NaCl and $MgSO_4$ appears to be the formation of gypsum and/or anhydrite which is followed by a drop in pH to near neutral. The only Mg-bearing phase was observed was sepiolite (M-S-H) which occurred in 3.0 M NaCl + 0.02 M $MgSO_4$ after 8 respikes. The solubility of Ca (see table 4.109) changes with increasing salinity and it is

believed to be due to two factors: (i) NaCl increases the solubility of $CaCO_3$ and C-S-H (ii) formation of gypsum, which has a higher solubility than either CH and C-S-H.

Table 4.111 CScH 2 samples cured at 85°C in DDW, in 0.5 M NaCl + 0.02 M $MgSO_4$ and in 3.0 M NaCl + 0.02 M $MgSO_4$. Curing times are shown in table 3.3, section 3.1; see CScH 2 data in table 3.5 and figure 3.2.

Curing Media for CScH 2	Number of spikes	pH	Aqueous Characterisation, mmol/l					
			Ca	Si	Mg	SO_4	Na	Cl
DD Water	-	11.60	1.90	0.09	<0.01	0.02	0.03	0.03
0.5 M NaCl + 0.02 M $MgSO_4$	1	11.94	24.43	0.03	<0.01	17.70	435	503
0.5 M NaCl + 0.02 M $MgSO_4$	10	7.44	15.97	0.06	70.75	81.25	489	454
3.0 M NaCl + 0.02 M $MgSO_4$	1	11.63	20.53	0.03	<0.01	18.22	2474	2694
3.0 M NaCl + 0.02 M $MgSO_4$	10	6.86	17.47	0.06	312.6??	44.79	2882	2959

Table 4.112 Solid characterisation of CScH 2 cured in DDW, in 0.5 M NaCl + 0.02 M $MgSO_4$ and in 3.0 M NaCl + 0.02 M $MgSO_4$ solutions at 85°C. Total time taken for the respikes varied from 8 to 12 months in addition to the curing times shown in table 3.3, section 3.1: see CScH 2 data in table 3.5 and figure 3.2.

Curing Media for CScH 2	Number of spikes	Cc	Jen	Gypsum	Anh	NaCl
DD Water	-	S	S			
0.5 M NaCl + 0.02 M $MgSO_4$	1	W				W
0.5 M NaCl + 0.02 M $MgSO_4$	10	S		S		M
3.0 M NaCl + 0.02 M $MgSO_4$	1	W				S
3.0 M NaCl + 0.02 M $MgSO_4$	10	S			S	S

Results from CScH 2 are shown in tables 4.111 and 4.112. Jennite is formed in DDW, but is not observed in the saline environments. Anhydrite and gypsum are observed in respiked experiments and, in the absence of other phases, condition near-neutral pH; Ca solubilities increase in saline media.

Table 4.113 CScH 3 samples cured at 85°C in DDW, in 0.5 M NaCl + 0.02 M $MgSO_4$ and in 3.0 M NaCl + 0.02 M $MgSO_4$. Curing times are shown in table 3.3, section 3.1; see CScH 3 data in table 3.5 and figure 3.2.

Curing Media for CScH 3	Number of spikes	pH	Aqueous Characterisation, mmol/l					
			Ca	Si	Mg	SO_4	Na	Cl
DD Water	-	12.33	13.15	0.02	<0.01	0.01	0.06	0.05
0.5 M NaCl + 0.02 M $MgSO_4$	1	12.25	29.84	0.02	<0.01	16.24	426	511
0.5 M NaCl + 0.02 M $MgSO_4$	12	10.43	16.72	0.01	0.70	16.67	231	236
3.0 M NaCl + 0.02 M $MgSO_4$	1	11.99	24.78	0.02	<0.01	18.87	2528	2764
3.0 M NaCl + 0.02 M $MgSO_4$	12	11.80	32.81	<0.01	0.02	24.38	1847	172

Table 4.114 Solid characterisation of CScH 3 cured in DDW, in 0.5 M NaCl + 0.02 M $MgSO_4$ and in 3.0 M NaCl + 0.02 M $MgSO_4$ solutions at 85°C. Total time taken for the respikes varied from 8 to 12 months in addition to the curing times shown in table 3.3, section 3.1: see CScH 3 data in table 3.5 and figure 3.2.

Curing Media for CScH 3	Number of spikes	Cc	CH	Anh	Brucite	NaCl
DD Water	-	S	S			
0.5 M NaCl + 0.02 M $MgSO_4$	1	S	S			W
0.5 M NaCl + 0.02 M $MgSO_4$	12	S		S	S	
3.0 M NaCl + 0.02 M $MgSO_4$	1	S	S			S
3.0 M NaCl + 0.02 M $MgSO_4$	12	S		S	M	W

Results for CScH 3 are shown in tables 4.113 and 4.114. Table 4.114 shows that no new carbonate phases have formed, but that calcium hydroxide reacted with $MgSO_4$ to form brucite and anhydrite. Brucite maintains a somewhat alkaline pH. The samples were not respiked further because CH was no longer detected by XRD.

Table 4.115 CScH 4 samples cured at 85°C in DDW, in 0.5 M NaCl + 0.02 M $MgSO_4$ and in 3.0 M NaCl + 0.02 M $MgSO_4$. Curing times are shown in table 3.3, section 3.1; see CScH 4 data in table 3.5 and figure 3.2

Curing Media for CScH 4	Number of spikes	pH	Aqueous Characterisation, mmol/l					
			Ca	Si	Mg	SO_4	Na	Cl
DD Water	-	11.60	1.99	0.09	<0.01	0.01	0.07	0.02
0.5 M NaCl + 0.02 M $MgSO_4$	1	11.35	21.66	0.08	<0.01	18.32	422	457
0.5 M NaCl + 0.02 M $MgSO_4$	5.5	8.19	20.21	<0.01	19.09	38.13	313	313
3.0 M NaCl + 0.02 M $MgSO_4$	1	11.03	24.08	0.06	<0.01	17.96	2528	2837
3.0 M NaCl + 0.02 M $MgSO_4$	3.5	8.48	40.42	0.27	0.03	32.92	2583	2385

Table 4.116 Solid characterisation of CScH 4 cured in DDW, in 0.5 M NaCl + 0.02 M $MgSO_4$ and in 3.0 M NaCl + 0.02 M $MgSO_4$ solutions at 85°C. Total time taken for the respikes varied from 8 to 12 months in addition to the curing times shown in table 3.3, section 3.1: see CScH 4 data in table 3.5 and figure 3.2.

Curing Media for CScH 4	Number of spikes	Cc	Gyp.	Anh.	NaCl
DD Water	-	S			
0.5 M NaCl + 0.02 M $MgSO_4$	1	S			M
0.5 M NaCl + 0.02 M $MgSO_4$	5.5	S	M		
3.0 M NaCl + 0.02 M $MgSO_4$	1	S			S
3.0 M NaCl + 0.02 M $MgSO_4$	3.5	S		S	S

Results for CScH 4 are shown in tables 4.115 and 4.116. The CScH 4 composition was chosen to verify that large additions of $CaCO_3$ will not react with other constituents in the backfill. From table 4.116 it is shown that no new carbonate phases have formed. The simulate groundwater reacts with the cementitious material forming gypsum or anhydrite: this leads to a reduction in pH and an increase in Ca solubility.

Table 4.117 CScH 5 samples cured at 85°C in DDW, in 0.5 M NaCl + 0.02 M $MgSO_4$ and in 3.0 M NaCl + 0.02 M $MgSO_4$. Curing times are shown in table 3.3, section 3.1; see CScH 5 data in table 3.5 and figure 3.2.

Curing Media for CScH 5	Number of spikes	pH	Aqueous Characterisation, mmol/l					
			Ca	Si	Mg	SO_4	Na	Cl
DD Water	-	9.34	0.57	2.58	<0.01	0.01	0.05	0.03
0.5 M NaCl + 0.02 M $MgSO_4$	1	8.86	21.43	2.92	<0.01	18.53	405	451
0.5 M NaCl + 0.02 M $MgSO_4$	2	8.33	27.69	2.85	0.02	28.13	424	425
3.0 M NaCl + 0.02 M $MgSO_4$	1	8.54	23.18	1.87	<0.01	19.65	2420	2712
3.0 M NaCl + 0.02 M $MgSO_4$	2	7.98	37.05	1.78	0.03	31.88	2827	2543

Table 4.118 Solid characterisation of CScH 5 cured in DDW, in 0.5 M NaCl + 0.02 M $MgSO_4$ and in 3.0 M NaCl + 0.02 M $MgSO_4$ solutions at 85°C. Total time taken for the respikes varied from 8 to 12 months in addition to the curing times shown in table 3.3, section 3.1: see CScH 5 data in table 3.5 and figure 3.2.

Curing Media for CScH 5	Number of spikes	Cc	Anh.	NaCl
DD Water	-	S		
0.5 M NaCl + 0.02 M $MgSO_4$	1	W		M
0.5 M NaCl + 0.02 M $MgSO_4$	2	S		S
3.0 M NaCl + 0.02 M $MgSO_4$	1	S		S
3.0 M NaCl + 0.02 M $MgSO_4$	2	S	S	S

Results for CScH 5 are shown in tables 4.117 and 4.118. CScH 5 has a low Ca/Si ratio and as a consequence the Si solubility is higher than in the other samples.

SUMMARY OF THE 85°C RESULTS:

- $CaCO_3$ acts as an inert aggregate in all CScH compositions.
- Because $CaCO_3$ is inert, the CScH compositions react like the C-S-H gels diluted with an inert filler, in this instance $CaCO_3$.
- Jennite in CScH 2 and tobermorite in CScH 4 were the only crystalline C-S-H phases observed, but only when cured in DDW.
- $MgSO_4$ react with CH and C-S-H to give brucite (in CScH 3) or sepiolite (in CScH 1) and gypsum and/or anhydrite.
- pH decreases to near neutral as a consequence of gypsum formation, except in CScH 3 in which brucite conditions the pH to ~ 10.4-11.8.
- Saline media, relative to distilled water, enhance Ca solubility by a factor ranging between 2 and 20.

4.2.2.4 Combined Effect of Temperature and Salinity.

At both 25°C and 85°C no new carbonate phases were formed; $CaCO_3$ behaving almost as an 'inert aggregate'. On these grounds scawtite and fukalite can probably be ruled out as potential phases at temperatures ≤ 85°C and in brines with ≤ 3.0 M NaCl and 0.02 M $MgSO_4$. Thus $CaCO_3$ does behave as an almost inert filler.

References

1. G.M.M Bell. (1989) 'Cement Reactions in Hydrothermal Conditions', PhD Thesis, Aberdeen University, Scotland.

2. M. Atkins et al. (1993) 'Thermodynamic Modelling of Blended Cements at Elevated Temperature (50-90°C)'. UK DoE Report no.DoE/HMIP/RR/94/011, Aberdeen University, Scotland

5. ADDITIONAL CALCULATIONS ON THE PERFORMANCE OF BACKFILL.

5.1 Introduction

During the course of the project, a number of calculations were performed relevant to the performance of cement-conditioned backfills. While these calculations were simplistic, they nevertheless benchmark more sophisticated calculations.

Since the flow rate of groundwater is not known, solution volumes are expressed as a standard unit, 400l/m^3 backfill. This is equivalent to the volume required to saturate 1m^3 of a backfill which has 40% pore space. The calculations employ a "mixing tank" model in which each exchange is a standard unit Supplementary data used in the calculations are given in tables 5.2a to 5.2e, inclusive. Where backfill is used, it is taken from the "preferred composition" of the NIREX patent [1]: the cement composition is a generalised average of UK Portland cement to British Standard BS12, similar to an ASTM (American Society for Testing and Materials) Type 1.

At w/c = 0.25, ~6.5 wt % water will be used to hydrate the OPC, which leaves 29 wt % remaining water.

Table 5.1a The "preferred composition" for backfill.

Water	35.5 wt %
OPC	26.0 wt %
$Ca(OH)_2$	10.0 wt %
Limestone flour	28.5 wt %

Table 5.1b Average OPC composition.

CaO	67.50 wt %
Other MO (as MgO)	3.00 wt %
SiO_2	22.00 wt %
Al_2O_3	6.00 wt %
SO_3	1.59 wt %

Tables 5.1c CEMCHEM calculation of the hydrate assemblage (per kg OPC hydrated) at 25°C.

$Ca(OH)_2$	10.2 moles/kg OPC $\Rightarrow$ 5304 moles/1m^3 backfill
ettringite (AFt)	0.16 moles/kg OPC $\Rightarrow$ 83.2 moles/1m^3 backfill
hydrotalcite (HT)	0.47 moles/kg OPC $\Rightarrow$ 364 moles/1m^3 backfill
C-S-H, with Ca/Si ratio = 1.8	9.2 moles/kg OPC $\Rightarrow$ 4784 moles/1m^3 backfill
SiHG ($3CaO{\cdot}Al_2O_3{\cdot}0.5SiO_2{\cdot}5H_2O$)	0.85 moles/kg OPC $\Rightarrow$ 442 moles/1m^3 backfill

Table 5.1d Mean groundwater composition from [2].

Component	Mean Groundwater, mmol/l	Used in these calculations mmol/l
CO_2 as HCO_3^-	2.09	2.0
Ca^{2+}	23.7	24
Na^+	355	400
Mg^{2+}	17.7/3.84	12
Cl^-	398	400
pH >7.3		

Table 5.1e Densities, molar volume and formula weights.

Component	Density (g/cm^3)	Molar volume (cm^3/mol)	Formula weight (g/mol)
Ca	-	-	40.1
Mg	-	-	24.3
$CaCO_3$	2.71	36.9	100.1
$Ca(OH)_2$	2.24	33.1	74.1
$1.8\ CaO{\bullet}SiO_2{\bullet}3H_2O$	2.10	102	215
$Mg(OH)_2$	2.39	24.3	58.3
Al_2O_3	-	-	102
Backfill	2.00	-	-

5.2 Dissolution of the $Ca(OH)_2$ component

The density of a $Ca(OH)_2$ backfill, assuming 40% porosity, is ~1344 kg/m^3. The standard volume of leachant would dissolve 652 g $Ca(OH)_2$ at 25°C, assuming initially pure water, so ~2060 exchanges would be required to totally dissolve the $Ca(OH)_2$. However, the preferred backfill is only 27.55 wt % $Ca(OH)_2$, so the corresponding number of exchanges for $Ca(OH)_2$ dissolution would be reduced to ~568. Of course this ignores additional $Ca(OH)_2$ arising from hydrated cement which would prolong the lifetime for $Ca(OH)_2$ dissolution. A specimen calculation, including the calculated contribution of $Ca(OH)_2$ from the cement, gives 909 exchanges. *This last value is accepted as a benchmark for subsequent calculations.*

5.3 Impact of Groundwater Mg: Mg for Ca replacement

Magnesium in groundwater is effectively removed by reaction of $Ca(OH)_2$ and C-S-H components forming, respectively $Mg(OH)_2$ and hydrated magnesium silicates. Assuming the permeating groundwater to be 0.012M with respect to magnesium, 694 replacements would be required to replace 27.6% $Ca(OH)_2$ in backfill.

At the point of complete reaction, the main solid which remains to condition the pH is $Mg(OH)_2$ which will give pH ~10.1 at 18°C. If the calculation uses $Ca(OH)_2$ arising from cement as well as from backfill, the number of replacements is increased to 1109 replacements. *This last value is accepted as a benchmark for magnesium replacement.*

5.4. Combined Interactions

In practice neither of the above reactions occur independently. Indeed, four reactions occur simultaneously:

I. Replacement of Ca by Mg.
II. Replacement of OH in either $Ca(OH)_2$ or C-S-H by sulfate with precipitation of gypsum and/or anhydrite.
III. Reaction of dissolved carbonate species in groundwater resulting in $CaCO_3$ precipitation.
IV. Dissolution of Ca by groundwater depleted in both Mg and SO_4 but retaining most or all of its NaCl content.

In perfusive flow, reactions (II) and (III) are essentially cumulative: Mg and to a lesser extent, sulfate, are removed leaving the groundwater, now essentially $NaC\ell$ and Na_2SO_4, free to saturate itself in $Ca(OH)_2$. We have not attempted to calculate reaction (ii) but simple culmination of the above reactions, with allowance for slight enhancement of $Ca(OH)_2$ solubilities in $NaC\ell$, suggests that the backfill conditioning lifetime, including $Ca(OH)_2$ from all sources, will be on the order of 500 water replacement cycles at 25°C. Further and more sophisticated calculations would be required to quantify the impact of gypsum/anhydrite on barrier performance but the trend would be to reduce further barrier lifetimes because of the enhancement of gypsum/anhydrite solubility in $NaC\ell$.

A further factor leading to reduction in performance lifetime is the reaction between backfill and bicarbonate, a typical groundwater constituent. The reaction between $Ca(OH)_2$ and HCO_3, forming $CaCO_3$ and soluble "$CaCO_3$," goes substantially to completion. However, the HCO_3 concentration of perfusing groundwater is much lower than that of Mg; also, Mg ions replaces Ca more effectively, on a one-to-one basis. Nevertheless, carbonate formation and dissolution impacts combine to reduce the performance lifetime. Perhaps the principal concern is that because $CaCO_3$ solubility is so markedly affected by pH that pore blocking will occur selectively. We know that the solubility minimum of $CaCO_3$ occurs at pH close to 9 but, in the absence of more site-specific data, it is impossible to evaluate physically where the low solubility zone will occur with respect to backfill/rock interface.

5.5. Summary

Calculation discloses that each of the chemically abundant species reacts with backfill constituents. The impact is often cumulative: Ca is replaced by Mg; OH by sulfate

and carbonate. Moreover the solubility of phases present in the backfill, as well as of alteration products, is enhanced by salinity

Calculations have not been refined in this section,; section 6 reports more sophisticated calculations. But it is useful to note that the experimental observations of Section 4 are broadly supported by calculation and *vice versa*. An important aspect of the comparison of trends is that the decomposition of cements in groundwater occurs in response to the changes required to reach equilibrium. No processes have been observed which were in violation of this principle. However, the intermediate stages of reaction may not always be reflected by calculations: For example, a tendency occurs of solids, nominally capable of conditioning high pH, to become effectively isolated from contact with the aqueous phase by formation of an impermeable layer of reaction products. This can only be verified experimentally.

With exceptions, as noted in the text, we can perform experiments and calculations in chemically - complex systems which reproduce well the behaviour of cements and backfill in a range of naturally - occurring groundwater chemistries. Section 6 further reinforces these conclusions.

References

1. UK Patent Application no. 9316995.1 (1993)

6. MODELLING

6.1 Introduction

The post closure performance assessment of a cementitious repository will, to a large extent, rely on the predictions made by numerical models. The application of numerical and experimental methods allows such predictions to be made beyond the spatial and temporal limits imposed by physical observation alone and the work reported here illustrates the use of this combined approach.

Considerable recourse has been made to thermodynamic equilibrium methods, which simulate those equilibria attained between the cement hydrate phases and their developing pore solutions in a wide range of chemical environments. In applying these methods, extensions to conventional modelling techniques have been adopted or developed in order to examine the chemistry of the system in conditions of elevated temperature and at high ionic strength.

This Section addresses reports a number of specific tasks undertaken in support of the overall programme:

- Selection of an ionic strength correction method and development of supporting databases appropriate for cementitious systems (Section 6.2);
- Utilisation of the model to predict the solubilities of cement hydrate phases in saline waters (Section 6.3);
- Development of an enhanced solubility model for CSH gels in saline waters (Section 6.4);
- Simulation of the interaction of pure cement phases with simple solutions (NaCl and $MgSO_4$) and prediction of phase transformations (Section 6.5);
- Simulation of the interaction of blended cements with groundwaters (Section 6.6)
- Evaluation of groundwater reactions with cements using coupled chemical transport codes (Section 6.7); and
- Make recommendations for the enhancement of the near field model (Section 6.8).

6.2 Models, Data and Numerical methods

6.2.1 Equilibrium Modelling

Background

Throughout this project, the thermodynamic equilibrium model PHREEQE [1] has been used to examine the developing chemistry of the cement hydrate phases as they react with both pure water and brines representative of cement pore solutions and of saline groundwaters prevailing at depth. Geochemical codes such as PHREEQE have a number of important features relevant to the study of cement-groundwater interactions. For example, certain parameters such as pH, may be either specified as inputs, or may be predicted by the

code based on equilibrium calculations. This versatility is important as it allows the code to be used to predict pH - a key concern in relation to the effectiveness of a geochemical barrier. In addition, the code allows minerals to be specified as presumed present but subject to dissolution if conditions warrant, or definitely present at equilibrium and available in excess quantity. When used in conjunction with the pH capability above, this allows the code to be used to predict the likely geochemical evolution of the cementitious barrier.

PHREEQE is one of the most widely used geochemical codes, and as such, has undergone a number of modifications in recent years. In its original form, the code extends the conventional Debye-Hückle relationship in order to calculate the activity correction coefficient (γ) for a species in solution. In practice, this means that the maximum ionic strength at which reliable predictions may be made is around 0.3 $mol.dm^{-3}$ as imposed by the Davies equation below [2]:

$$Log\,\gamma = -Az_i^2\left(\frac{\sqrt{I}}{1+\sqrt{I}} - 0.3I\right) \qquad \{6.1\}$$

Where I is the ionic strength in $mol.dm^{-3}$, such that:

$$I = \tfrac{1}{2}\sum m_i z_i^2 \qquad \{6.2\}$$

where m_i is the molal concentration of the ion i, z_i is the charge carried by ion i and A is a variable which depends on the dielectric constant of the solution, ε, its density, ρ and temperature T according to:

$$A = 1.8 * 10^6 \rho^{\frac{1}{2}} (\varepsilon T)^{\frac{-3}{2}} \qquad \{6.3\}$$

In order to extend the use of the model into systems of high ionic strength, a number of alternative approaches have been proposed with which to calculate the activity correction coefficients. One of the better known is the Pitzer virial expansion [3] which builds on the Debye-Hückle relationship by the inclusion of terms describing the ionic repulsion and ternary effects. This approximation is based on an electrostatic term, to which is added a virial coefficient series, accounting for ionic strength. This model has been coded into a version of PHREEQE known as "PHRQPITZ" [4] which requires inclusion of the so-called Pitzer coefficients in the input files. Whilst the Pitzer approximation represents the most complete formalism with which to describe experimentally determined activity coefficients, there remains an acute lack of supporting data. This is particularly the case in mixed electrolyte systems such as those associated with cementitious and natural groundwater systems. Moreover, no virial coefficient data are available for radionuclides. As a consequence, an alternative method was sought with which to make predictions at high ionic strength.

Specific Interaction Theory

In order to investigate mixed electrolyte systems, a more general extension to the Debye-Hückle expression is required. The development of Specific Interaction Theory (SIT) largely pre-dates the work of Pitzer [5,6,7] and considers, in addition to the Debye-Hückle term, interactions between ions of opposite charge. The modified formula contains parameters termed interaction coefficients ε , for each cation - anion combination and it is assumed that multiple interactions are additive. The principal assumptions underlying SIT theory are as follows:

The activity coefficient γ_i of an ion i, carrying a charge z_i in a solution of ionic strength I, may be described by:

$$Log\,\gamma = -z_i^2\left(\frac{A\sqrt{I}}{1+Ba_i\sqrt{I}} + \sum_k \varepsilon\,(i,j,k)\,m_k\right) \qquad \{6.4\}$$

where the summation extends over all ions, k, present in the solution of molarity m_k .
The interaction coefficients e(i,j,k), are zero for ions of the same charge and for neutral species.

- The corresponding equations for the activity of water are:

$$Log\,a_{H_2O} = -\frac{\Phi\sum_k m_k}{\ln 10\,\Omega} \qquad \{6.5\}$$

$$(\Phi-1)\left(\sum_c m_c + \sum_a m_a\right) = \frac{\left(\Phi_{DH} + \ln 10\sum_c\sum_a \varepsilon_{(c,a)}\,m_c\,m_a\right)}{\sum_c m_c \sum_a m_a} \qquad \{6.6\}$$

and

$$\Phi_{DH} = 0.69685\left(1+1.5\sqrt{I} - 2\ln\left(1+1.5\sqrt{I}\right) - \left(\frac{1}{1+1.5\sqrt{I}}\right)\right) \qquad \{6.7\}$$

Where Φ is the osmotic coefficient of the mixture, Ω is a constant equal to the number of moles of water per kilogram (55.51) and the summations over a,c and k refer to anions, cations and all (cations + anions) ions respectively.

This approach has been adopted by the recent EC/HMIP CHEMVAL II Programme [8] resulting in a thermodynamic database (re-cast using the above principles) and a corresponding database of interaction coefficients. It is the latter which has been used in the present study, along with thermodynamic constants for cementitious minerals derived experimentally and supplemented by data taken from the literature.

6.2.2 Database development

In previous work commissioned by HMIP [9,14] a database specific to studies of cementitious systems was developed for use with PHREEQE. The original database, known as the CEMENTS database, had been enlarged and renamed CEMENTS 2 [10]. Under the current project, this has been further expanded and re-cast for use with the SIT version of PHREEQE, becoming CEMENTS 3. In addition to the phases found in cements, the database contains entries for solids which may form as a result of sample degradation such as drying artifacts or phases formed through carbonation etc. along with common rock-forming minerals. The database contains entries for approximately 150 solids and is shown in Appendix 5, together with ion interaction coefficients.

Limitations in the numerical treatment of reactions involving solid solutions require that they are reduced in the database to multiple discrete phases. Two solid solution series are included in the database. The hydrogarnet - siliceous hydrogarnet solid solution is treated explicitly as twenty eight discrete phases, ranging from true hydrogrossular (C_3AH_6) to true grossular garnet (C_3AS_3) with the discrete compositions spanning the low silica members up to hibschite (or plaziolite, $C_2AS_2H_2$) as more siliceous compositions are known to be unstable in the highly alkaline environments prevailing in cements. Thermodynamic data for phases of intermediate composition are sparse, hence the method of Tardy and Fritz [11] has been used to estimate the dissociation constants of the solids from those of the series end-members:

$$\log K_{sp} = X\log K_{GR} + (1-X)\log K_{HG} + X\log X + (1-X)\log(1-X) \qquad \{6.8\}$$

Where:

$\log K_{sp}$ = logK of solid solution series member

$\log K_{GR}$ = logK of grossular garnet

$\log K_{HG}$ = LogK hydrogrossular

X = mole fraction of grossular in solid solution

For a relatively broad compositional range, the relationship is close to a linear one and the deviation from a linear change of logK as a function of composition, is within the range of uncertainty introduced in these calculations from variations in the measured solubility of the end members. This ideal solid solution approach was applied by Atkins *et. al.* [9] for modelling hydrogarnet dissolution in an HMIP commissioned study and is adopted here principally for consistency. In the absence of published work which quantifies the change of dissolution enthalpy with composition, it has been assumed that this property varies as a linear function of composition.

By comparison, the calcium silicate hydrate (CSH) solid solution is treated implicitly, through the co-dissolution of pairs of salts. This approach has found favour with several authors [9,13,14] in recent years and accounts for the incongruous dissolution of CSH through the equilibration of congruously soluble solids with their pore solution. The

method is described and extended at length below (Section 6.3) but a note on the database entries is appropriate here. Work by Berner [12] invokes six solids; three of fixed logK and three of variable logK which in combination span the calcium to silicate ratios found in cementitious systems. Although the Berner model has not been used in this study, it is included in the database for completeness, should it be required for future calculations. This original model was developed on systems of low ionic strength (<0.1M) at around 25°C and considers the dissolution of relatively young CSH compounds of low crystalinity and correspondingly high solubility. Later work by Atkins *et al.* [14] extends these ideas to model the more crystalline solids likely to form following curing at the higher temperatures (85°C) expected in a repository. The four solids invoked in this low ionic strength model are also included in the database. The CEMENTS 3 database also may also contain variable solubility data for five solids used in a new model reported below, which attempts to predict the solubility of CSH at both elevated temperature and high ionic strength.

In addition to the CEMENTS 3 thermodynamic database, a collation of molar volume data is presented in Appendix 5 to enable estimates of the likely consequence of phase dissolution or precipitation on the bulk porosity of the system to be made. The formation reaction for each used in the PHREEQE calculations is considered to be definitive in terms of the work reported here. The dissociation constant (logK) is reported for use with SIT algorithms at high ionic strength. Bulk density measurements, averaged from a number of published sources [15,16,17] are compared with x-ray density data for each salt. The paucity of published molar volume data requires that for most solids, this property must be calculated from the density and relative molecular mass. This has been done for all database entries where density data are available and are compared with molar volume data where possible. It is encouraging to note that the differences between the published and calculated values are small.

6.2.3 Normative modelling : CEMCHEM

The CEMCHEM family of codes comprise normative models which estimate the phase composition following complete hydration of blended cements from the bulk oxide compositions of the unhydrated components. At integral blending ratios, a simple normative calculation is performed to estimate the relative molar oxide composition of the mixture at each blending ratio. CEMCHEM 1 considers the hydration of two blending components hydrated at 25°C and initially assigns all the magnesium in the system to hydrotalcite (M_4AH_{10}) and all the sulphur to ettringite (AFt-SO_4, $C_6AS_3H_{32}$), with stoichiometric quantities of aluminium and calcium. The remaining components are re-normalised to 100% and the calcium : silicon : aluminium ratio calculated, in order to assign the mixture to one of six mineral assemblages spanning the CSH -$Ca(OH)_2$ - hydrogarnet fields of the hydrous Ca-Si-Al system. The aluminium content of the remainder is used to determine the hydrogarnet portion of the hydrate mixture and the unassigned calcium and silicate are apportioned into the CSH.

A similar treatment is made of systems of high calcium content, assigning a portion of this element to free calcium hydroxide (portlandite) such as would be expected in a pure Portland cement. The calculations are repeated at the ninety eight integral compositions between the two end members. CEMCHEM 1 does not consider highly siliceous systems

such as blends containing a relatively high proportion of fly ash, the code containing error traps which prevent misleading predictions being made under such conditions.

CEMCHEM 2, similarly treats two blending components hydrated at elevated temperature (85°C) and assigns the integral compositions to a more complex set of mineral assemblages than CEMCHEM 1. This includes the zeolite phase Ca-P, similar to the gismondine-phillipsite type zeolites found in fly ash cements, which allows predictions to be made in siliceous systems. Additionally, gehlenite hydrate (strätlingite, C_2ASH_8) is estimated. The latter however, presents a potential problem in that the simplification of the system to relatively few components may violate the Gibbs phase rule, preventing subsequent calculations from running. As gehlenite hydrate is only sparingly soluble, it contributes little to the ions dissolved in the pore solution yet its formation will of course remove calcium, aluminium and silicate from solution. The consequence of excluding gehlenite hydrate on thermodynamic modelling is that for certain compositions an elevated pH is predicted, in comparison with that observed by experiment. Caution is therefore necessary in the use of the "no gehlenite hydrate" CEMCHEM 2 model, which, although it predicts a phase assemblage capable of producing a converged solution in subsequent thermodynamic modelling, may overestimate the alkalinity of the pore solution. As a consequence, two versions of CEMCHEM 2 have been developed, one considering gehlenite hydrate, the other ignoring it and assigning its components to the remaining phases.

A major part of this project focused on the behaviour of a cement-stabilised limestone backfill [18a]. This is a three component system and so an additional version of the code was developed, CEMCHEM 3. This uses the same chemical algorithms as CEMCHEM 2, but does not automatically calculate each integral blending ratio. This was done in order to minimise the size of the output file which would obviously grow as an exponential function of the number of components used to produce the blended cement.

6.3 Prediction of mineral hydrate compositions

6.3.1 Materials

The blended cements considered in this project comprise a pure Portland cement (OPC), a 40% Portland + 60% fly ash blend (PFA), a 25% Portland + 75% blast furnace slag blend (BFS) and the "preferred example" of the reference backfill [18a] which contains 40.3% OPC + 15.5% lime + 44.2% limestone. The raw materials used in both the experiments and simulations are as follows:

OPC:	BRE batch 995 (reference Portland cement)
BFS:	Appleby (formerly Frodingham) "CEMSAVE"
PFA:	Eggborough pulverised fuel ash
Lime:	Limbux (Buxton Lime) - strictly slaked lime, $Ca(OH)_2$
Limestone:	RMC Dove Hills Quarry, Carboniferous limestone

The relative oxide compositions of the materials are shown in table 6.1 below and are reported both as the analytical relative oxide compositions and also as normalised oxide compositions for the six components considered by the CEMCHEM models.

Table 6.1 Relative oxide compositions of unhydrated cement components (wt%).

	OPC		BFS		PFA		$Ca(OH)_2$		Limestone	
Oxide	Analyt.	Normal	Analyt.	Normal	Analyt.	Normal	Analyt.	Normal	Analyt.	Normal
CaO	64.1	68.46	39.39	40.38	1.45	1.80	72.6	98.17		
MgO	1.22	1.30	9.37	9.61	1.57	1.95	0.38	0.51	0.23	0.23
SiO_2	20.8	22.22	35.56	36.45	50.09	63.09	0.80	1.08	0.60	0.61
Al_2O_3	4.51	4.82	13.08	13.41	26.0	32.23	0.15	0.20	0.20	0.20
SO_3	3.00	3.20	0.15	0.15	0.76	0.94	0.02	0.03	0.02	0.02
$CaCO_3$	-	-	-	-	-	-	-	-	97.95	98.94
Total	93.63	100	97.55	100	80.68†	100.01	73.95‡	100.02	99	100

† PFA Contains 10.2% Fe_2O_3 and 5.1% (Na_2O + K_2O) by mass
‡ Limbux slaked lime contains considerable water: Loss on ignition = 23.7%

6.3.2 CEMCHEM predictions

Considering first the mineral hydrate assemblage likely to form after complete hydration at low temperature (25°C), the CEMCHEM1 code was used on all compositions except the relatively siliceous fly ash blend. These results (table 6.2) are included for comparison with high temperature predictions and have not been used in subsequent thermodynamic calculations.

Table 6.2 Mineral hydrate assemblages expected to form at 25°C. CEMCHEM1 predictions.

A Phase	Mole percent of phase formed on complete hydration of OPC at 25°C	
	Analytical composition	Normalised composition
Hydrotalcite M_4AH_{10}	0.95	0.95
Ettringite (AFt-SO_4)	1.56	1.55
CSH (Ca:Si = 1.7)	43.41	41.45
Portlandite $Ca(OH)_2$	51.05	53.07
Hydrogarnet C_3AH_6	3.02	2.98

B Phase	Mole percent of phase formed on complete hydration of $OPC_{25\%}$ $BFS_{75\%}$ blend at 25°C	
	Analytical composition	Normalised composition
Hydrotalcite M_4AH_{10}	7.78	7.86
Ettringite (AFt-SO_4)	0.63	0.62
CSH (Ca:Si = 1.3)	81.75	81.61
Hydrogarnet $C_3AS_{0.9}H_{4.2}$	9.84	9.92

Continued

C Phase	Mole percent of phase formed on complete hydration of reference backfill at 25°C	
	Analytical composition	Normalised composition
Hydrotalcite M_4AH_{10}	0.43	0.42
Ettringite (AFt-SO_4)	0.54	0.52
CSH (Ca:Si = 1.7)	15.61	15.31
Portlandite $Ca(OH)_2$	37.79	41.69
Hydrogarnet C_3AH_6	1.04	1.00
Calcite $CaCO_3$	44.58	41.04

These results predict that, as expected, the cement phase mineralogy of the Portland cement and reference backfill are similar, the limestone acting principally as a diluent in the latter, whilst the more siliceous OPC-BFS mixture is likely to form CSH of a lower calcium to silicate ratio than in pure OPC and to contain a silica-substituted hydrogarnet.

The higher temperatures expected in the potential repository (~85°C) require the use of versions 2 and 3 of the CEMCHEM code in order to satisfactorily predict the phase assemblages likely to form at complete hydration as shown in tables. The results demonstrate that for a blend of components whose relative oxide composition is close to that normalised to 100%, little difference is seen between the predictions made using the analytical and normalised compositions. This is not the case for the fly ash - rich blend, which shows a considerable change in the partitioning of aluminium between monosulphate and the zeolite phase, Ca-P.

It is important to note however, that even after extended periods of hydration, many of the crystalline components (such as quartz, mullite, hematite etc.) in the fly ash remain unhydrated, slightly enriching the hydrated fraction in calcium. Although the variation of predicted hydrate composition is not large between predictions based on the analytical and normalised results, it should be remembered that this normative assumes complete hydration of the blending components.

In considering the reference backfill composition, it must be noted that there is some latitude possible in the blending ratios of the constituents, [18]. In the tables reported here, the "Preferred Example" refers to the so-called preferred composition in the patent and is shown in table 6.4, above. Table 6.3 shows that the arithmetic differences between the two CEMCHEM 2 models (with and without gehlenite hydrate) are slight where this phase is not formed and can therefore be ignored. The assemblages predicted by each model for the various blended cements are similar, notably ettringite, stable at low temperature, is calculated to be metastable with respect to monosulphate at higher temperatures which is reflected in the CEMCHEM 2 and 3 predictions. Table 6.4 and figure 6.1 show the effect of compositional variation of the backfill composition. The original patent application [18] describing this material imposes compositional limits on its formulation. Varying the blending components between these limits has little effect on the mineral hydrate composition as shown above. Predictably, increasing the slaked lime content of the blend results in a portlandite-rich assemblage whilst maximising the OPC content correspondingly maximises the CSH. It is interesting to note however, that at high limestone contents (columns 2 & 3, table 6.4) the portlandite content may vary by over one third with little (~5%) change in the CSH component. This may have a modest but significant consequence for the persistence of alkaline conditions during service. In summary, thermodynamic

calculations reported below may be based on these predicted mineral assemblages. The absolute quantities predicted by CEMCHEM are a first approximation only and as a consequence, the absolute variations shown between the various calculation methods, once noted, need not be explicitly considered in subsequent calculations.

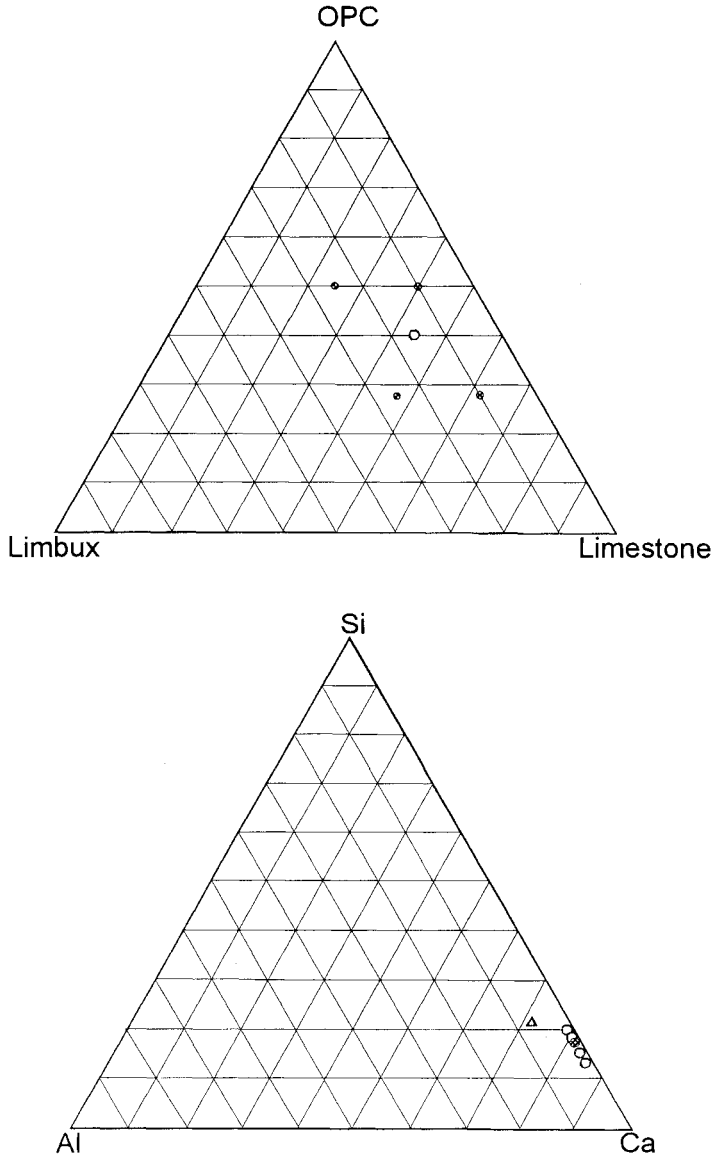

Figure 6.1 **Compositional variation of reference backfill as described in a Patent application [18].**

Above **Composition limits described by [18]. Open circle is preferred composition, closed circles are composition limits.**

Below **Chemical variation of backfill composition limits. Open circles are limits, closed circle is the preferred example and the triangle is OPC**

Table 6.3: Mineral hydrate assemblages expected to form at 85°C. CEMCHEM2 predictions.

A Phase	Mole percent of phase formed on complete hydration of OPC at 85°C	
	Analytical composition	Normalised composition
Hydrotalcite M_4AH_{10}	0.63	0.62
Monosulphate (AFm-SO_4)	2.68	2.68
Portlandite $Ca(OH)_2$	71.89	71.89
CSH (Ca:Si = 1.7, Al = 0.5%)	24.76	24.76
Hydrogarnet C_3AH_6	0.04	0.04

B Phase	Mole percent of phase formed on complete hydration of $OPC_{25\%}$ $BFS_{75\%}$ blend at 85°C			
	Analytical composition		Normalised composition	
Model ®	C_2ASH_8 absent	With C_2ASH_8	C_2ASH_8 absent	With C_2ASH_8
Hydrotalcite (M_4AH_{10})	7.53	7.36	7.46	7.55
Monosulphate (AFm-SO_4)	1.78	1.81	1.82	1.84
CSH (Ca:Si = 1.36, Al = 1.22%)	79.1	-	-	-
CSH (Ca:Si = 1.37, Al = 1.21%)	-	-	79.31	-
CSH (Ca:Si = 1.37, Al = 1.20%)	-	78.67	-	-
CSH (Ca:Si = 1.38, Al = 1.20%)	-	-	-	78.89
Hydrogarnet ($C_3AS_{0.71}H_{4.58}$)	11.58	-	11.41	-
Hydrogarnet ($C_3AS_{0.82}H_{4.36}$)	-	11.89	-	11.71

C	Mole percent of phase formed on complete hydration of $OPC_{40\%}$ $PFA_{60\%}$ at 85°C	
Phase	Analytical composition	Normalised composition
Hydrotalcite (M_4AH_{10})	2.86	2.56
Monosulphate (AFm-SO_4)	15.51	5.62
CSH (Ca:Si = 0.8, Al = 0.26%)	33.69	-
CSH (Ca:Si = 0.8, Al = 0.31%)	-	36.50
Ca-P (Zeolite)	47.93	55.13

Table 6.4 Mineral hydrate assemblages expected to form at 85°C from reference backfill. CEMCHEM3 predictions. Compositions normalised to 100%.

COMPONENT	Percent by mass of blending component				
OPC	40.3†	28	28	50	50
Lime	15.5	25	10	25	10
Limestone	44.2	47	62	25	40
PHASE	Mole percent of phase formed on complete hydration at 85°C				
Hydrotalcite (M_4AH_{10})	0.42†	0.33	0.33	0.48	0.49
Monosulphate (AFm-SO_4)	0.52	0.35	0.37	0.64	0.67
$Ca(OH)_2$	39.50	43.78	25.90	56.11	38.37
CSH (Ca:Si = 1.7, Al = 0.5%)	14.17	9.74	10.17	17.04	17.84
Hydrogarnet ($C_3AS_{0.82}H_{4.36}$)	0.82	0.53	0.58	0.98	1.05
$CaCO_3$	44.58	45.27	62.65	24.76	41.62

† Preferred example, as described in [18].

As far as it has been possible to quantitatively determine the solid phase composition of the hydrated systems (see previous sections) the CEMCHEM predictions are in agreement with the experimental findings. Much of the development of the CEMCHEM approach is reported by Atkins *et.al.* [14,19] and these documents suggest that the method satisfactorily predicts the phase assemblage expected on complete hydration of these cementitious systems.

6.4. Modelling CSH Solubility

The incongruous dissolution of CSH is treated implicitly, by modelling the co-dissolution of pairs of congruously soluble salts. The general behaviour of CSH is that the calcium-rich structural units are more soluble than their silicate-bearing counterparts, thus continuous replacement of the pore solution at equilibrium with a CSH results in a gradual fall of dissolved calcium and rise in silicate ions in solution, with an associated reduction in solution alkalinity. Current numerical models are not yet sophisticated enough to explicitly treat this phenomenon, hence alternative modelling solutions have been sought. Considering the co-dissolution of two congruously soluble salts both of which, in this case, influence solution pH through hydrolysis, it is possible to simulate a desired solution chemistry through careful choice of both the stoichiometry of the solids and their solubility behaviour. This has formed the basis for modelling CSH chemistry in recent years and of the model reported here.

6.4.1 Previous models

Berner model

Initial work by Berner [12] resulted in a model for the dissolution of relatively young (*i.e.* low crystallinity) CSH in solutions of low ionic strength. The model divides the calcium to silicon ratio of the CSH into discrete regions and simulates the dissolution behaviour of each solid by using one salt of fixed dissociation constant (logK) and one of variable logK. The solids comprise the solid solution series end-members; portlandite and silica, with a phase of intermediate composition CaH_2SiO_4, subsequently referred to as the 'Berner "fictive" solid'. The logK value for a solid with variable dissolution coefficients is calculated directly from the calcium to silicon ratio of the CSH. The result is a generally good approximation of the solution chemistry overlying a CSH of known composition. This model was from the outset, intended to be a wholly pragmatic solution to CSH modelling and it is recognised that it bears little relationship to the structural chemistry of CSH.

Aberdeen model

The development of a model with which to simulate the solubility behaviour of CSH phases cured at high temperature (or for very long periods) resulted in a pair of models known respectively as the Partial and Fully Crystalline Models (14). As in the Berner model, pairs of salts are chosen according to the calcium to silicon ratio of the CSH, with which to simulate phase dissolution. The solids in increasing calcium content are: tobermorite, the 'fictive solid', afwillite and portlandite, chosen in part, for their similarity to the structural domains within relatively crystalline CSH. The dissolution coefficients and enthalpies chosen for the model are those of the synthesised minerals, the only difference between the

two models being the inclusion of a Ca:Si = 1 phase in the Partial Crystallisation Model to represent the existence of CSH gel. Model testing shows that generally good agreement is obtained between observed and predicted calcium and pH values but with less satisfactory simulation of silicate concentrations for CSH of low Ca: Si ratio.

Model limitations

It has been shown that both the Berner and Aberdeen model predictions deviate progressively from experimentally determined results with increasing ionic strength. Two phenomena are thought to be responsible for this. First and foremost, the high ionic strength of the electrolyte alters the solubility behaviour of the CSH, such that it is no longer adequately represented by the model. This effect has been investigated experimentally in the sodium chloride system during this project and is discussed above. Secondly, uptake of ions from the electrolyte, presumably by adsorption onto the surface of the CSH, alters the solution chemistry in a way which neither model is intended to simulate. Finally it should be born in mind that standard approaches to ionic strength correction break down above an ionic strength of 0.3 molal. An enhanced model of CSH solubility for use in saline systems must address all these phenomena.

6.4.2. Low temperature models for CSH solubility at high ionic strength

Sorption of sodium and chloride by CSH

Three possible options exist which would satisfy the modelling criteria described above. A single model which invokes simulation of true adsorption of sodium and chloride in addition to predicting CSH solubility in saline systems is possible using the version of PHREEQE recently consolidated on behalf of the Environment Agency [20]. This code is the first to combine reversible sorption algorithms with those for SIT activity correction, but this option was rejected owing principally to the relatively small amount of data available with which to describe the reversible sorption of sodium and chloride onto CSH and also due to the resulting complexity of such an approach. Similarly, the uptake of sodium and chloride could be simulated through inclusion of 'fictive' sodium- and chloride-bearing salts in the thermodynamic simulations. This would require inclusion of solids of limited solubility, which, through simulated precipitation, would remove these ions from solution and partition them into the solid phase. Such an approach was thought to be too cumbersome for inclusion in an model for CSH solubility and was therefore rejected.

A third option exists, in which the uptake of sodium and chloride by the CSH is treated arithmetically from the experimental data derived in the project, allowing the sorption relationships of the sodium and chloride to be treated independently to those of CSH solubility. This pragmatic approach has been adopted as a first approximation with the following caveats:

- It is recognised that accounting for sodium and chloride arithmetically represents irreversible rather than reversible sorption. This is an unavoidable consequence of arithmetically adjusting the Na and Cl contents of the solution.

- As a consequence, this method is only suitable for systems where the salinity is fixed or likely to increase. It is not suitable for use in systems of falling salinity. In this study for example, the reserve of sodium chloride dissolved in the groundwater is considered to be so large as to remain constant, (a reasonable approximation, except perhaps in those regions occluded from the body of the groundwater and thus not replenished by ingress of saline solutions).

The experimental results reported above suggest that there is not a simple relationship between the initial and final sodium chloride solution concentrations. The general trend is that greatest sorption of both sodium and chloride occurs in CSH of low calcium to silicate ratio (figure 6.2). The effect of temperature however, is much more difficult to ascertain. At low temperature, 25°C, a maximum sorptive capacity occurs for CSH of low Ca:Si ratio at around 1 mol dm^{-3} which decreases with either increasing or decreasing salinity. As the temperature increases to 55°C, the effect is most pronounced for high Ca:Si ratio CSH in systems of high salinity (~1.5 mol dm^{-3}). By comparison the high temperature experiments show almost the opposite effect, with the degree of sodium and chloride uptake falling as a function of ionic strength.

It must be noted that some of the reported sodium and chloride analyses show a negative sorption, that is to say, the CSH seems to be contributing some of these ions to the equilibrium solution. As this is highly unlikely, we must consider the possibility of an error in the sodium and chloride measurements. Re-working of the results, considering both a fixed error of - 4.7% (the maximum "negative sorption" reported at 55°C for the Ca:Si = 0.85 CSH in 1.35 mol dm^{3} NaCl) and a systematic random error of the same magnitude, does not simplify these relationships. It is tentatively suggested, therefore, that the sorptive capacity of the CSH changes markedly as the solid changes from its amorphous state (as shown by the 25°C samples) to the more crystalline forms stable at elevated temperature. The effect of temperature on the sorption reactions should only be determined once the recrystallisation is complete and this is hence outside the scope of the work undertaken here. Clearly, this requires further investigation before it can be quantified and subsequently predicted. As a first approximation, a look-up table is proposed (table 6.5) with which to estimate the approximate degree of sodium and chloride uptake by CSH and is presented for use over the temperature interval 25 to 85°C.

Table 6.5 Uptake of Na^+ and Cl^- onto CSH as a function of ionic strength.

Ionic Strength mol dm^{-3} NaCℓ	Calcium to silicon ratio of CSH phases				
	0.85	1.1	1.4	1.8	$Ca(OH)_2$
	Percent uptake of sodium and chloride from solution				
0.42	0	0	0	0	0
0.52	2	2	2	2	1
1.05	11	9	6	4	3
1.35	4	1	2	2	4
1.46	2	5	2	2	1

It must be noted first, that these experiments were not originally intended to measure sorption phenomena, and that treatment of the results in this way assumes a constant solid to liquid ratio in each experiment and secondly that the effect is, in any case, relatively minor as noted in Section 4.

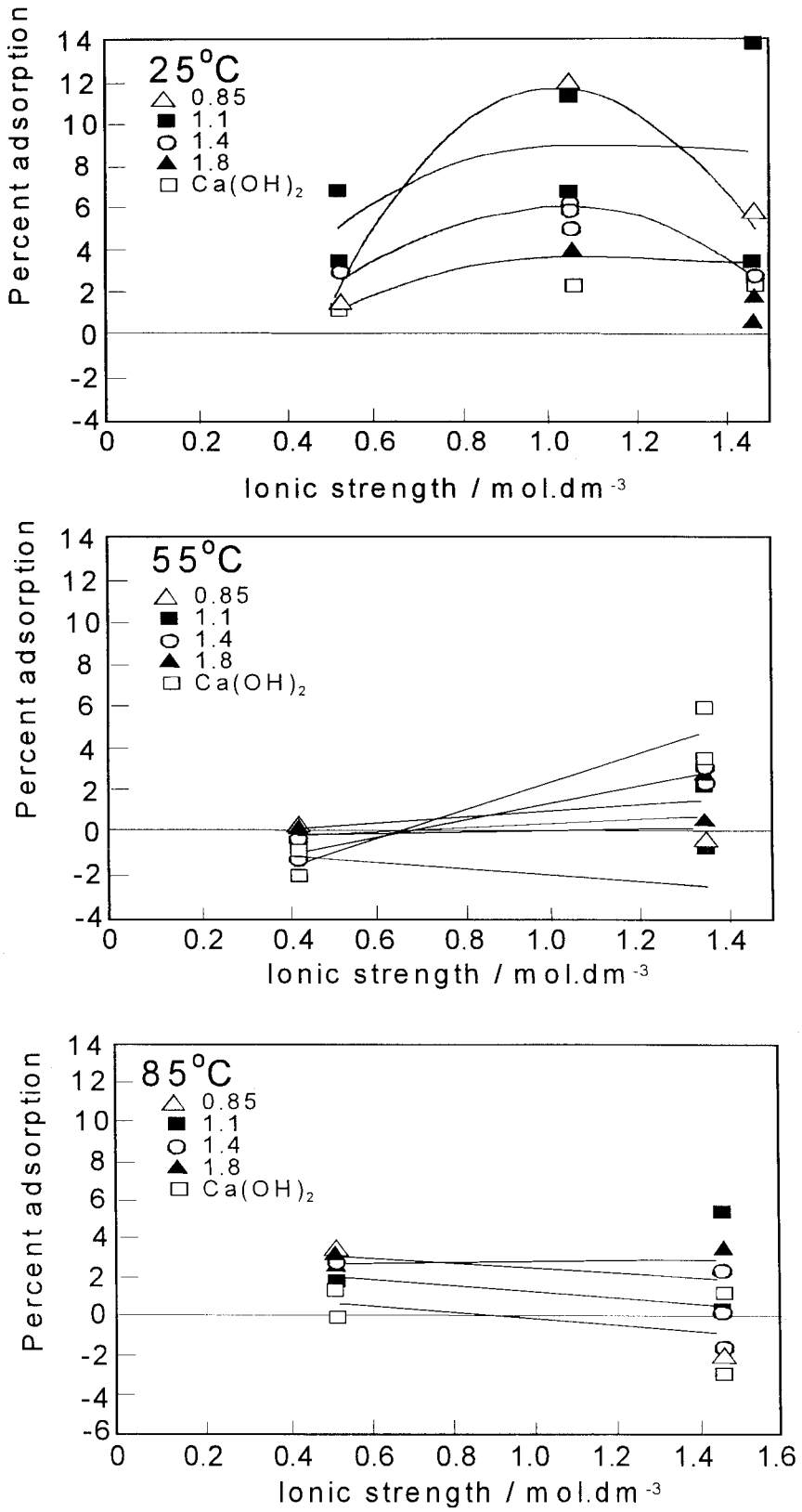

Figure 6.2 **Uptake of sodium and chloride ions onto CSH is a complex phenomenon. Single points are sodium and chloride in single experiments. Line are plotted through mean values.**

Solubility of CSH in sodium chloride brines

Experimental investigations of the dissolution of CSH into sodium chloride solutions are reported in a previous section of this report. In order to simulate the analytical results observed, the phases used in the partial and fully crystalline models of Atkins *et. al.* [14] were adopted in the first instance. Unfortunately, the dissociation coefficients determined in previous work could not be simply re-cast for use in these saline systems for, as already noted, the actual solubility of the CSH is different in the saline environment to that encountered at low ionic strength. For each pair of salts, this required repeated adjustment of the dissociation coefficients in order to match the predicted solution composition to that measured experimentally. In order to optimise these calculations, contour diagrams showing the variation of predicted calcium and silicate concentrations to the dissociation constant of the solids were plotted for each pair of salts. An example is shown in figure 6.3 (top). This approach allows the observed and predicted compositions to be matched to within 95% confidence limits, but requires approximately one hundred calculations.

The following tables show, for each calcium to silicon ratio interval, the analytical (observed) and modelled (predicted) compositions of the solutions at equilibrium with CSH. In the original models by Atkins *et. al.* [14] the low Ca:Si ratio calculations overestimate the concentration of silicate in solution. This is due to the adoption of tobermorite as the single phase governing solution composition. The Ca:Si ratio of tobermorite is 5:6, thus calculations representing its congruous dissolution will maintain this ratio in the equilibrium solution. For example, in the low ionic strength case shown below, the silicate concentration is predicted to be over five times greater than found by analysis. Whilst the model is a reasonable structural analogue of low calcium CSH, an alternative model is proposed with which to estimate its solubility.

Table 6.6 illustrates the limitations of the tobermorite model in representing siliceous CSH; the adoption of a congruously soluble salt to model incongruous dissolution must fail as the solution composition predicted will represent the stoichiometry of the dissolving solid. In order to make more realistic predictions both of dissolved silicate and solution pH, an alternative model is proposed in which the co-equilibrium of tobermorite and amorphous silica occurs. In this model, as tobermorite dissolves releasing both calcium and silicate into solution, the silica precipitates, thus reducing the dissolved silicate concentration and raising the pH (through hydrolysis) to a value closer to that seen in experiment. By careful selection of the dissociation constants for the two salts, the solubility behaviour of CSH at Ca:Si = 0.85 can be successfully reproduced by the model as shown in table 6.7.

Table 6.6 Observed and predicted solution compositions at equilibrium with CSH (Ca:Si = 0.85) using a tobermorite model for CSH dissolution. Concentrations are in mol dm^{-3}.

Observed solution composition					Predicted solution composition			
pH	Ca	Si	Ionic strength	Tobermorite log K	pH	Ca	Si	Ionic strength
11.65	1.25e-3	2.78e-4	0.0050	70.4	10.99	1.26e-3	1.51e -3	0.0038

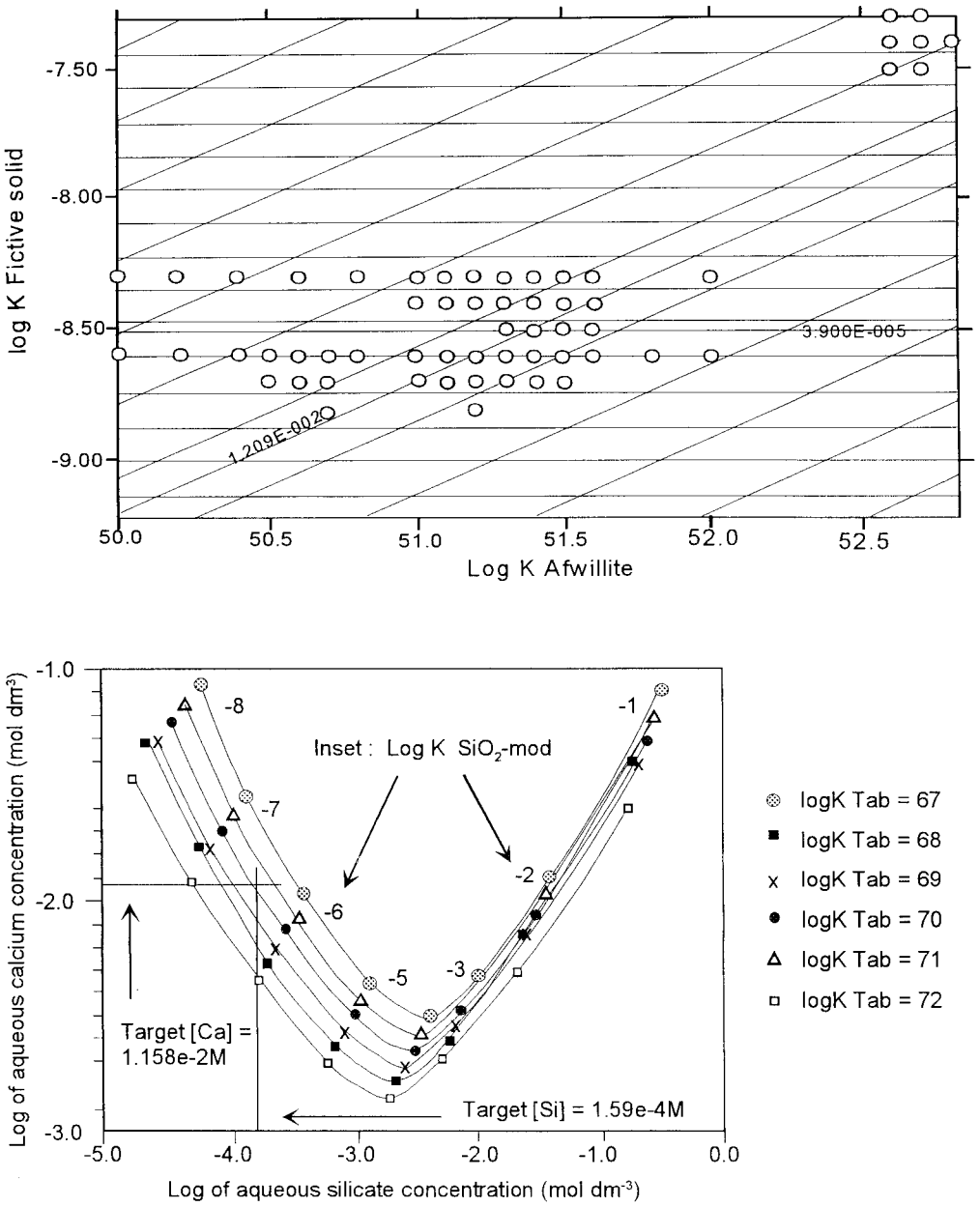

Figure 6.3

Above: **Example of contour plot for logK of the fictive solid $Ca_2H_2SiO_4$ and for afwillite. Target experimental concentrations are shown in bold for Ca (1.2E-2 M) and Si (3.9E-5 M).**

Below **An alternative method for estimating appropriate log K values when fitting model to experimental data.**

Table 6.7 Observed and predicted solution compositions at equilibrium with CSH Ca:Si = 0.85) using a tobermorite and silica model for CSH dissolution at 25°C. All concentrations are in mol dm^{-3}.

Initial NaCℓ		Observed solution composition					
		pH	Na	Cl	Ca	Si	Ionic strength
0		11.65	0	8.00e-3	1.25e-3	2.78e-4	0.0050
0.52		11.20	4.89e-1	4.53e-1	1.158e-3	1.59e-4	0.4952
1.05		11.14	7.99e-1	7.84e-1	1.262e-2	1.87e-4	0.8177
1.46		11.02	1.33e 0	1.359e0	1.609e-2	1.72e-4	1.3774
Log K of solids in model							
Tobermorite	SiO_2-mod	Predicted solution composition					
67.5	-5.1	11.32	0	8.00e-3	1.292e-3	2.855e-4	0.0039
70.0	-6.5	12.21	4.89e-1	4.53e-1	1.214e-2	1.560e-4	0.5056
70.1	-6.5	12.23	7.99e-1	7.84e-1	1.286e-2	1.857e-4	0.8280
70.2	-6.7	12.33	1.33e 0	1.359e0	1.596e-2	1.817e-4	1.3894

These calculations simulate the equilibrium of a solid of the same stoichiometry as silica ("SiO_2-mod") and tobermorite with a solution containing the sodium and chloride concentrations measured experimentally. Figure 6.3 (bottom) shows the changing chemistry of the system as the dissociation constants of both salts are altered. The effect of reducing the logK of the silica ($SiO_{2\text{-mod}}$) is marked by solubility minima in the model. To the right of the minima, the $SiO_{2\text{-mod}}$ simulates dissolution, whilst to the left, precipitation is predicted to occur. In this way, the overall system chemistry of the simulation can be controlled to provide a close approximation to the analytical observations. Figure 6.4 shows the variation of log K for this model with respect to ionic strength at 25°C.

This approach of adopting stoichiometrically appropriate phase pairs with which to represent the solid solution series, builds on previous models [9,11,12-14] and attempts to determine solubility constants which simulate the dissolution of the CSH. The fitting of empirically determined solubilities to these components cannot be justified in terms of structural chemistry but, in as far as they simulate the dissolution behaviour of the CSH phase in conditions of changing salinity, are of pragmatic value.

The partial and fully crystalline models [14] propose two alternative methods for simulating the dissolution of CSH at the higher Ca:Si ratio of 1.1. used originally to represent differing degrees of crystallinity. The co-dissolution of afwillite and tobermorite was compared to that of tobermorite and the fictive solid CaH_2SiO_4 and the results are reported in tables 6.8 and 6.9.

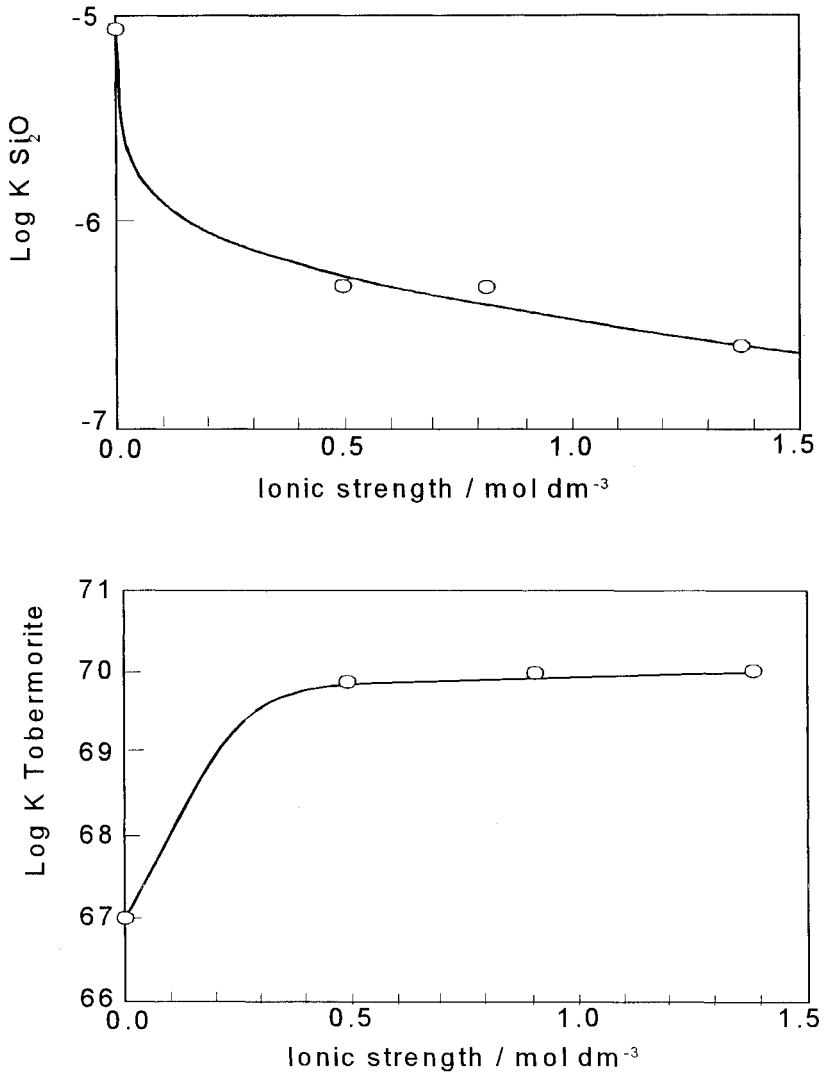

Figure 6.4 **Apparent log K for tobermorite (above) and silica (below) for CSH model at Ca:Si = 0.85.**

Table 6.8 **Observed and predicted solution compositions at equilibrium with CSH (Ca:Si = 1.1) using a tobermorite and afwillite model for CSH dissolution at 25°C. All concentrations in mol dm^{-3}.**

Initial NaCℓ		Observed solution composition					
		pH	Na	Cl	Ca	Si	Ionic strength
0		12.20	7.40e-4	7.50e-5	5.49e-3	3.1e-5	0.0195
0.52		12.11	4.35e-1	3.48e-1	1.48e-2	3.4e-5	0.4289
1.05		12.14	9.21e-1	8.80e-1	1.771e-2	3.3e-5	0.9443
1.46		12.12	1.283e0	1.373e0	1.979e-2	3.9e-5	1.3751
Log K of solids in model		Predicted solution composition					
Tobermorite	Afwillite						
66.7	50.7	11.94	7.40e-4	7.50e-5	5.29e-3	3.44e-5	0.0154
66.8	51.6	12.27	4.35e-1	3.48e-1	1.40e-2	3.62e-5	0.4310
66.3	52.2	12.56	9.21e-1	8.80e-1	1.79e-2	2.92e-5	0.9588
65.1	51.8	12.56	1.283e0	1.373e0	1.82e-2	2.08e-5	1.3862

Similarly, two alternative phase combinations are possible with which to model the equilibrium of a CSH where Ca:Si = 1.4; the fully crystalline model employs afwillite and tobermorite whilst the partially crystalline model uses afwillite and CaH_2SiO_4, shown in tables 6.10 & 6.11.

Table 6.9 Observed and predicted solution compositions at equilibrium with CSH (Ca:Si = 1.1) using a tobermorite and CaH_2SiO_4 model for CSH dissolution at 25°C. All concentrations in mol dm^{-3}.

Initial NaCℓ		Observed solution composition					
		pH	Na	Cl	Ca	Si	Ionic strength
0		12.20	7.40e-4	7.50e-5	5.49e-3	3.1e-5	0.0195
0.52		12.11	4.35e-1	3.48e-1	1.48e-2	3.4e-5	0.4289
1.05		12.14	9.21e-1	8.80e-1	1.771e-2	3.3e-5	0.9443
1.46		12.12	1.283e0	1.373e0	1.979e-2	3.9e-5	1.3751
Log K of solids in model		Predicted solution composition					
Tobermorite	CaH_2SiO_4						
65.6	-8.6	11.97	7.40e-4	7.50e-5	5.75e-3	2.81e-5	0.0169
67.0	-8.3	12.28	4.35e-1	3.48e-1	1.45e-2	3.76e-5	0.4323
66.2	-8.4	12.38	9.21e-1	8.80e-1	1.82e-2	2.98e-5	0.9514
65.7	-8.3	12.42	1.283e0	1.373e0	1.97e-2	3.74e-5	1.3826

Table 6.10 Observed and predicted solution compositions at equilibrium with CSH (Ca:Si = 1.4) using a tobermorite and afwillite model for CSH dissolution at 25°C. All concentrations in mol dm^{-3}.

Initial NaCℓ		Observed solution composition					
		pH	Na	Cl	Ca	Si	Ionic strength
0		12.52	6.10e-4	7.10e-4	1.209e-2	3.9e-5	0.0411
0.52		12.41	4.35e-1	4.64e-1	1.477e-2	3.8e-5	0.4945
1.05		12.41	8.70e-1	8.82e-1	1.948e-2	1.9e-5	0.9304
1.46		12.32	1.381e0	1.381e0	2.128e-2	2.3e-5	1.435
Log K of solids in model		Predicted solution composition					
Afwillite	Tobermorite						
51.8	67.2	12.19	6.10e-4	7.10e-4	1.005e-2	2.11e-5	0.0282
50.9	65.0	12.25	4.35e-1	4.64e-1	1.332e-2	1.983e-5	0.4872
51.5	65.3	12.40	8.70e-1	8.82e-1	1.911e-2	1.965e-5	0.9292
51.8	65.6	12.46	1.381e0	1.381e0	2.165e-2	2.314e-5	1.4405

Finally, in the relatively simple case of portlandite only, change in solubility of this phase with increasing ionic strength is simulated using the parameters shown in table 6.13.

Table 6.11. Observed and predicted solution compositions at equilibrium with CSH (Ca:Si = 1.4) using an afwillite and CaH_2SiO_4 model for CSH dissolution at 25°C. All concentrations in mol dm^{-3}.

Initial NaCℓ		Observed solution composition					
		pH	Na	Cl	Ca	Si	Ionic strength
0		12.52	6.10e-4	7.10e-4	1.209e-2	3.9e-5	0.0411
0.52		12.41	4.35e-1	4.64e-1	1.477e-2	3.8e-5	0.4945
1.05		12.41	8.70e-1	8.82e-1	1.948e-2	1.9e-5	0.9304
1.46		12.32	1.381e0	1.381e0	2.128e-2	2.3e-5	1.435
Log K of solids in model		Predicted solution composition					
Afwillite	CaH_2SiO_4						
51.3	-8.5	12.18	6.10e-4	7.10e-4	9.764e-3	1.281e-5	0.0274
51.7	-8.3	12.28	4.35e-1	4.64e-1	1.442e-2	3.934e-5	0.4901
51.6	-8.5	12.40	8.70e-1	8.82e-1	1.944e-2	2.101e-5	0.9300
52.0	-8.6	12.70	1.381e0	1.381e0	2.323e-2	1.304e-5	1.456

In the case of CSH where the Ca:Si ratio is 1.8, both the partial and fully crystalline models use a combination of afwillite and portlandite to simulate the pore solution chemistry. The results of this model are compared to the experimental results in table 6.12.

Table 6.12 Observed and predicted solution compositions over CSH (Ca:Si = 1.8) using an afwillite and portlandite model for CSH dissolution at 25°C. All concentrations in mol dm^{-3}.

Initial NaCℓ		Observed solution composition					
		pH	Na	Cl	Ca	Si	Ionic strength
0		12.54	9.48e-3	1.015e-2	1.633e-2	1.2e-5	0.0580
0.52		12.50	4.6e-1	4.67e-1	2.277e-2	1.5e-5	0.5273
1.05		12.50	8.9e-1	9.21e-1	2.527e-2	1.2e-5	0.9739
1.46		12.40	1.44e0	1.401e0	2.584e-2	2.0e-5	1.4856
Log K of solids in model		Predicted solution composition					
Afwillite	Portlandite						
52.3	22.5	12.40	9.48e-3	1.015e-2	1.586e-2	1.319e-5	0.0561
51.8	22.5	12.45	4.6e-1	4.67e-1	2.169e-2	1.558e-5	0.5231
51.6	22.5	12.46	8.9e-1	9.21e-1	2.265e-2	1.380e-5	0.9678
52.0	22.6	12.51	1.44e0	1.401e0	2.458e-2	2.092e-5	1.4874

Table 6.13 Observed and predicted solution compositions over portlandite at 25°C All concentrations in mol dm^{-3}.

Initial NaCℓ	Observed solution composition				
	pH	Na	Cl	Ca	Ionic strength
0	12.50	2.27e-3	2.0e-3	2.011e-2	0.0561
0.52	12.45	4.95e-1	4.89e-1	2.770e-2	0.5628
1.05	12.45	9.95e-1	9.24e-1	2.640e-2	1.0280
1.46	12.40	1.402e0	1.352e0	2.660e-2	1.4439
Log K of solid in model					
Portlandite	Predicted solution composition				
22.8	12.50	2.27e-3	2.0e-3	1.992e-2	0.0558
22.6	12.45	4.95e-1	4.89e-1	2.760e-2	0.5628
22.5	12.45	9.95e-1	9.24e-1	2.580e-2	1.0265
22.4	12.39	1.402e0	1.352e0	2.577e-2	1.4418

The methods and models described above are summarised in figures 6.5 to 6.7 and show that it is possible accurately to simulate the solution chemistry for the equilibrium of CSH with sodium chloride solutions of varying ionic strength at 25°C. In these calculations, the charge imbalance of the solutions, as analysed, is maintained for a number of reasons: First, the conventional method of adjusting a single analyte (for example pH) to impose electrical neutrality on a system cannot readily be adopted here as the range of ionic strengths varies markedly between samples. Adjustment of any constituent common to all the sample pore solutions would have markedly different and inconsistent effects on the samples according to their ionic strength and apparent charge imbalance. Secondly, the absolute confidence in the analysis of each pore solution depends on its concentration (see discussion on confidence limits in appendix), thus confidence in the charge balance similarly depends on the ionic strength of the solution. As a result, the simulations deliberately preserve the analytical charge imbalance, as a consistent means of imposing neutrality is not available.

The general behaviour of these models are compared to the experimental results in figure 6.7. This empirical fitting of the dissociation coefficients allows a more generalised model for CSH solubility to be developed for intermediate salinities, through simple numerical analysis of the variation of log K for each phase as a function of ionic strength. Before this is described, a degree of data reduction for the 25°C calculations must be undertaken in order to simplify the model.

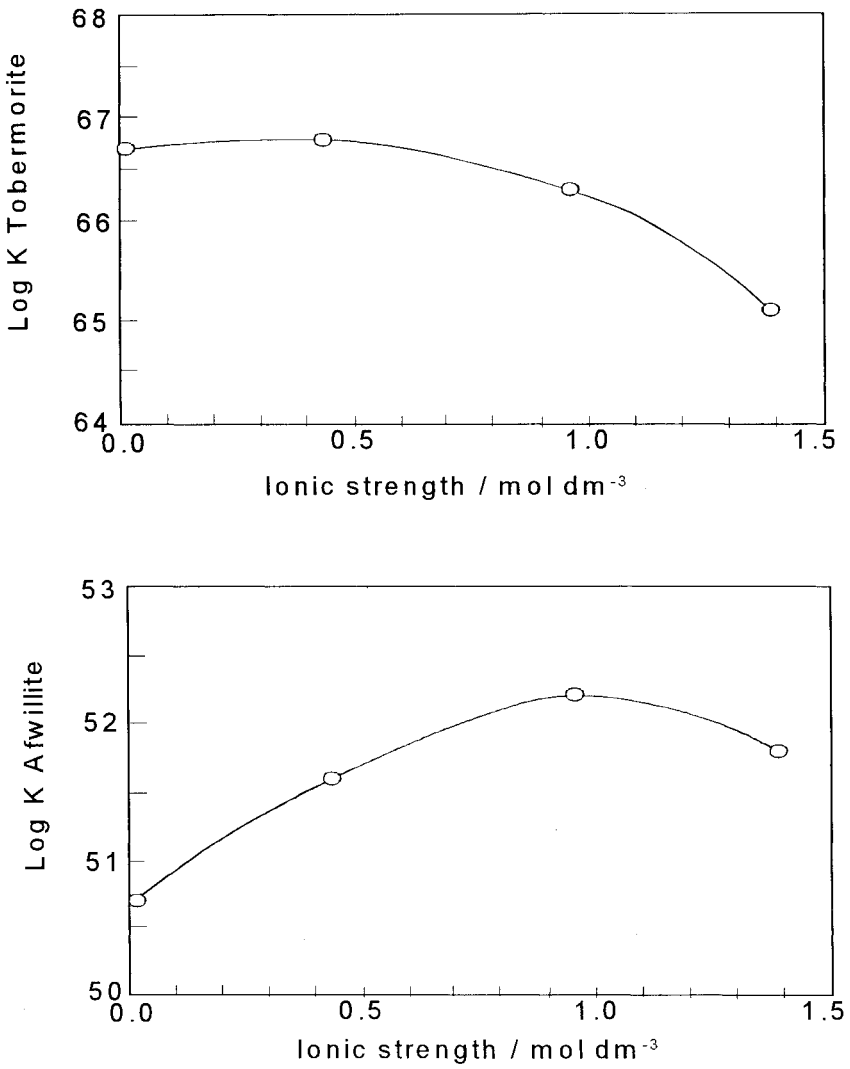

Figure 6.5 **Apparent log K of afwillite and tobermorite as a function of salinity when Ca:Si = 1.4.**

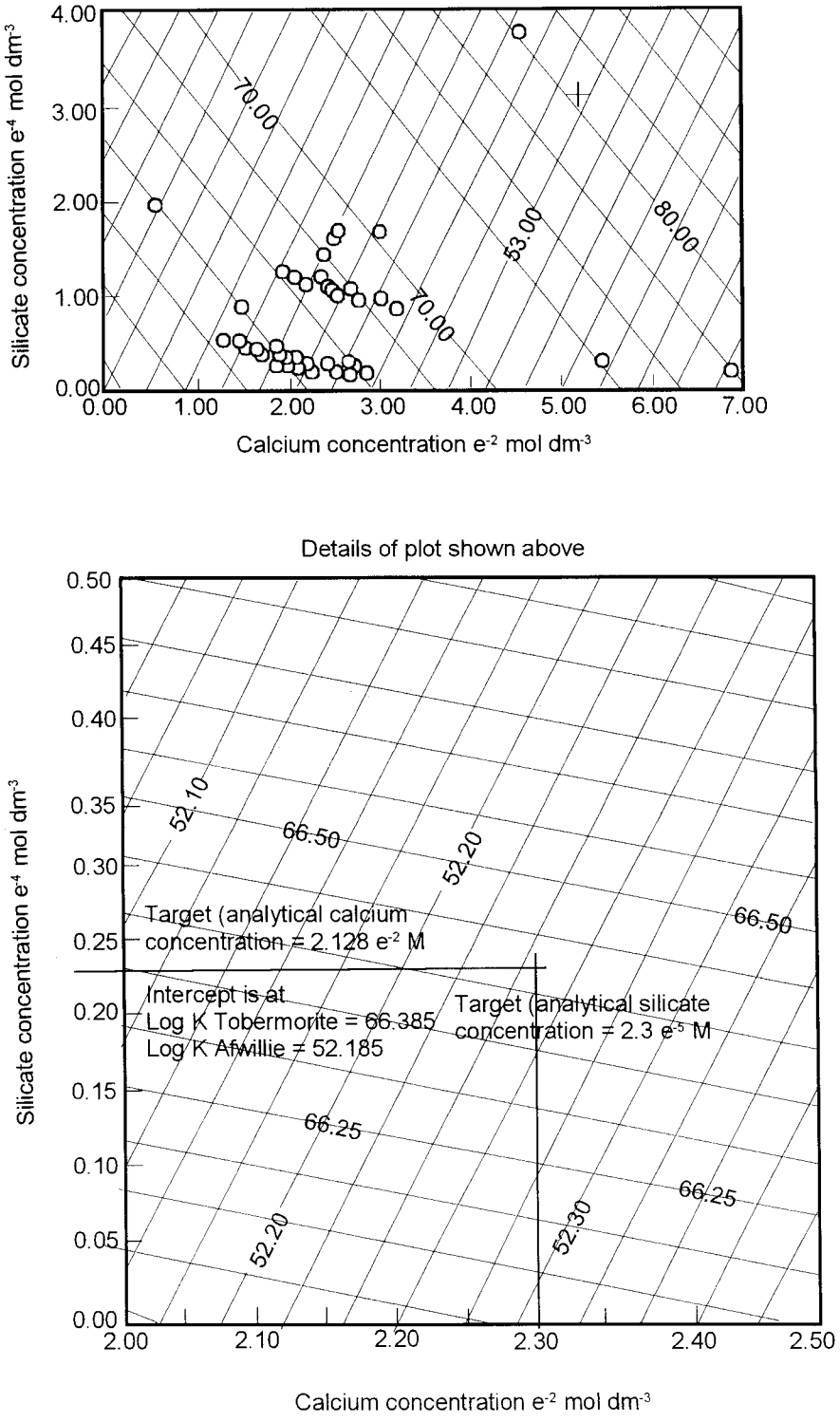

Figure 6.6 Graphical method of intersecting iso-concentration contours used to fit model log K values to experimental data.

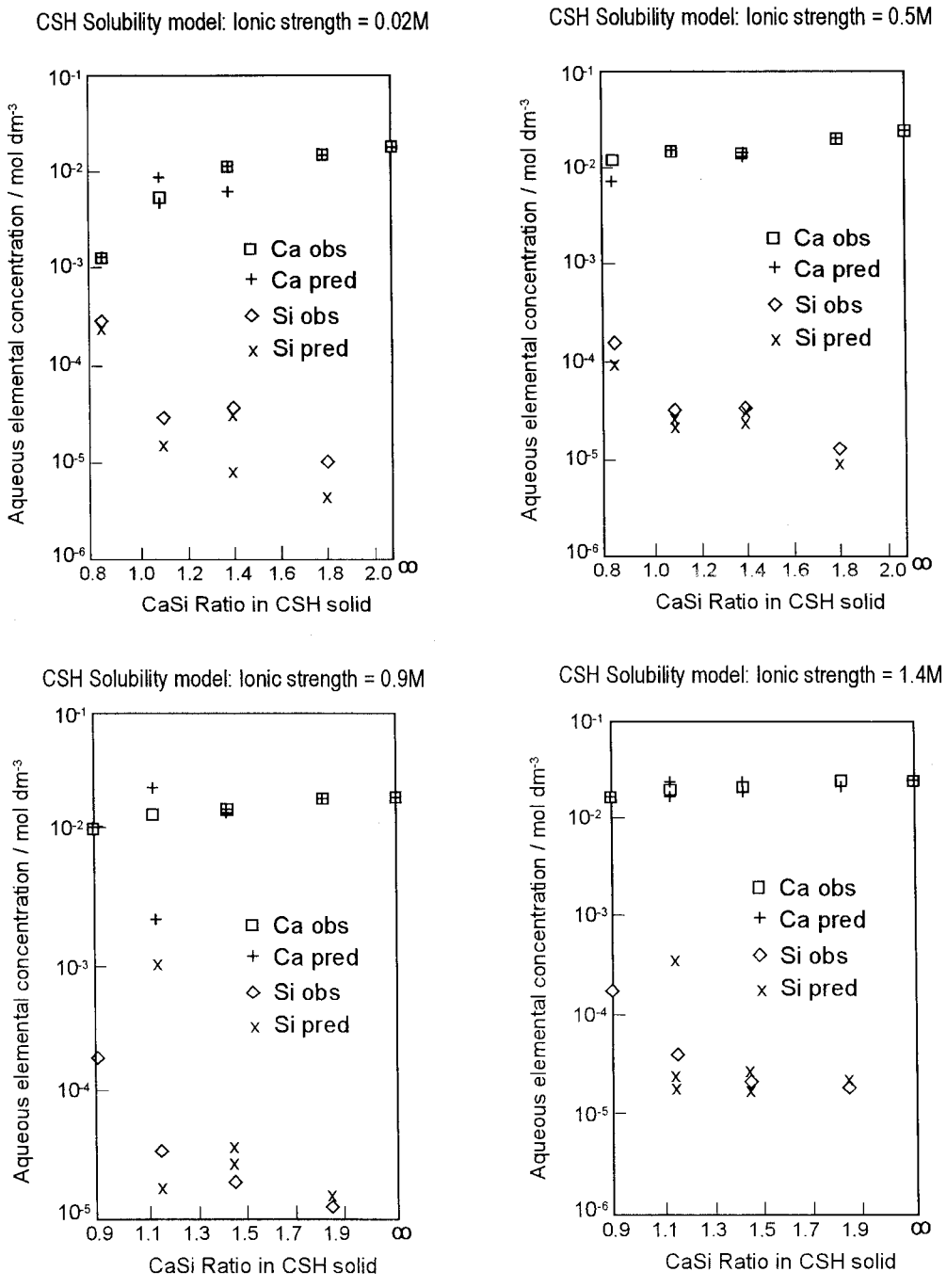

Figure 6.7 **Relative performance of CSH solubility model at 25°C. Where more than one equation is available with which to model solubility, the closest fit was adopted. Hence outlying points at low Ca:Si ratios were rejected.**

6.4.3 Unified model of the 25°C isotherm for CSH solubility at high ionic strength

Tables 6.6 to 6.13 show the variation in logK for a range of phases used to simulate the dissolution of CSH. A number of these phases are used in more than one model and examination of their logK values shows some obvious trends as a function of salinity. Tobermorite, or more strictly, compositional units in the model of the same stoichiometry as tobermorite, shows two distinct rates of change, depending on the solid in simulated co-equilibrium with it. In the Ca:Si = 0.85 case, the logK of tobermorite rises rapidly from a value of 67.5 at ionic strengths of around 40 mmol dm^{-3} to a near plateau value of 70 to 70.2 between 0.5 and 1.5 mol dm^{-3}. This is mirrored by a rapid fall in the corresponding logK of $SiO_{2\text{-mod}}$ over the same salinity interval. By comparison, where tobermorite is invoked in the other models, both the numerical value of its logK and its rate of change with ionic strength are markedly different.

This effect is illustrated in figure 6.8 (top). It is suggested therefore, that the line of best fit for the change of tobermorite logK as a function of salinity be drawn through the results of all models invoking tobermorite, where the Ca:Si ratio of the CSH is greater than unity. For the single case of Ca:Si = 0.85, a simple relationship is drawn allowing direct calculation of logK from ionic strength. This illustrates that although a model may be constructed to fit the available data, it need not necessarily be an accurate guide to the structural chemistry. Where other phases are invoked in more than one model, they have been subject to a similar data reduction, the example of afwillite is illustrated in figure 6.8 (bottom). Table 6.14 summarises these results.

It must be noted that the use of such conditional constants requires some care. For example, the logarithmic relationship invoked to describe the rate of change of the effective logK for tobermorite as a function of salinity breaks down at very low salinities. As a consequence, these (logarithmic) relationships should only be used with ionic strength values at or above those associated with the dissolution of tobermorite in water *i.e.* approximately $I > 0.05M$. This is a rather obvious statement, in that a solution of zero ionic strength will not exist at equilibrium with a sparingly soluble salt. It is therefore necessary to apply this lower limit to the numerical value of I in order to use this approach successfully.

The final choice of model, where more than one option is available for a particular Ca:Si ratio, was made simply by selecting the combination which, after averaging the results, predicts the closest solution chemistry to the experimental observation. The unified model for CSH solubility on the 25°C isotherm is summarised in table 6.15.

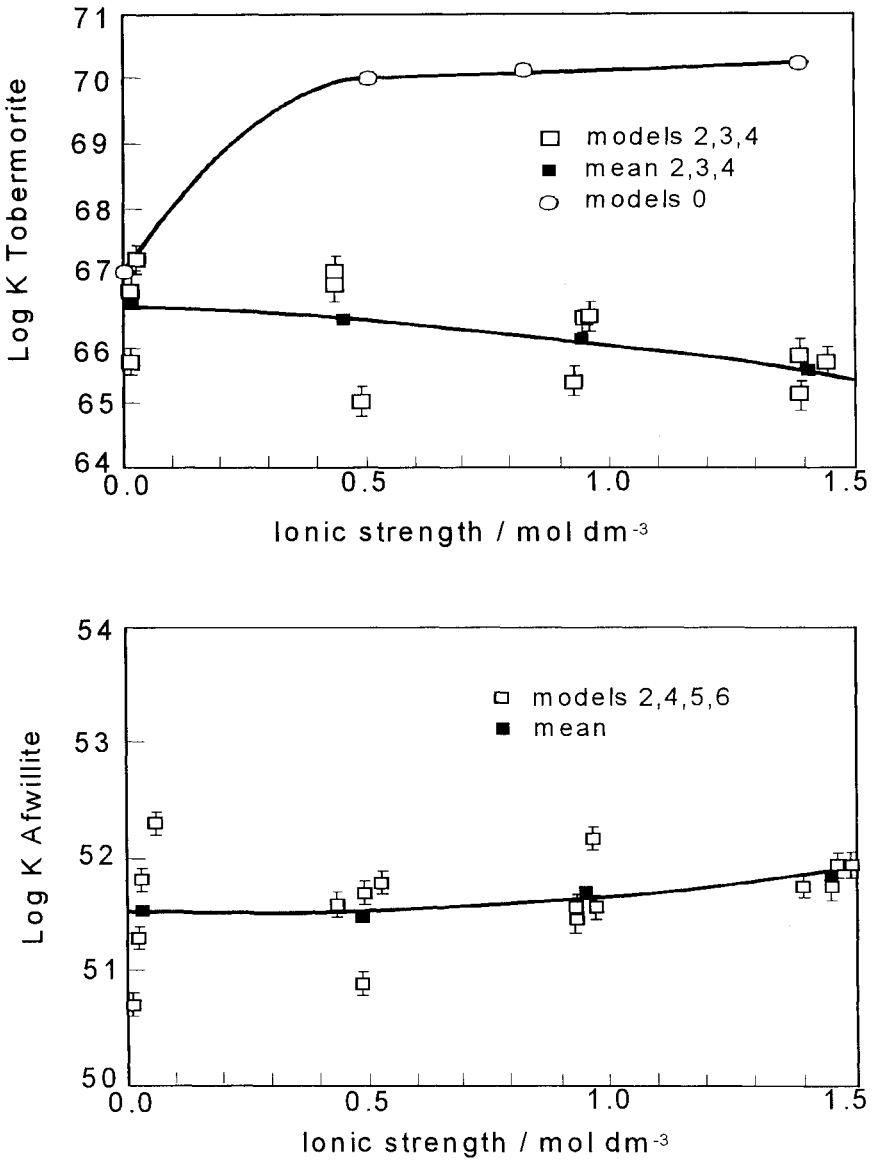

Figure 6.8 **Effective log K for tobermorite (above) □ tobermorite in co-equilibrium with afwillite, $Ca_2H_2SiO_4$ or in solution; mean log K for above estimates; tobermorite in equilibrium with SiO_2 only.**

Effective log K for afwillite (below): afwillite is in co-equilibrium with tobermorite and $Ca_2H_2SiO_4$; Mean log K for above estimates.

Apparent logK of tobermorite as a function of ionic strength representing the dissolution of CSH where Ca:Si = 0.85

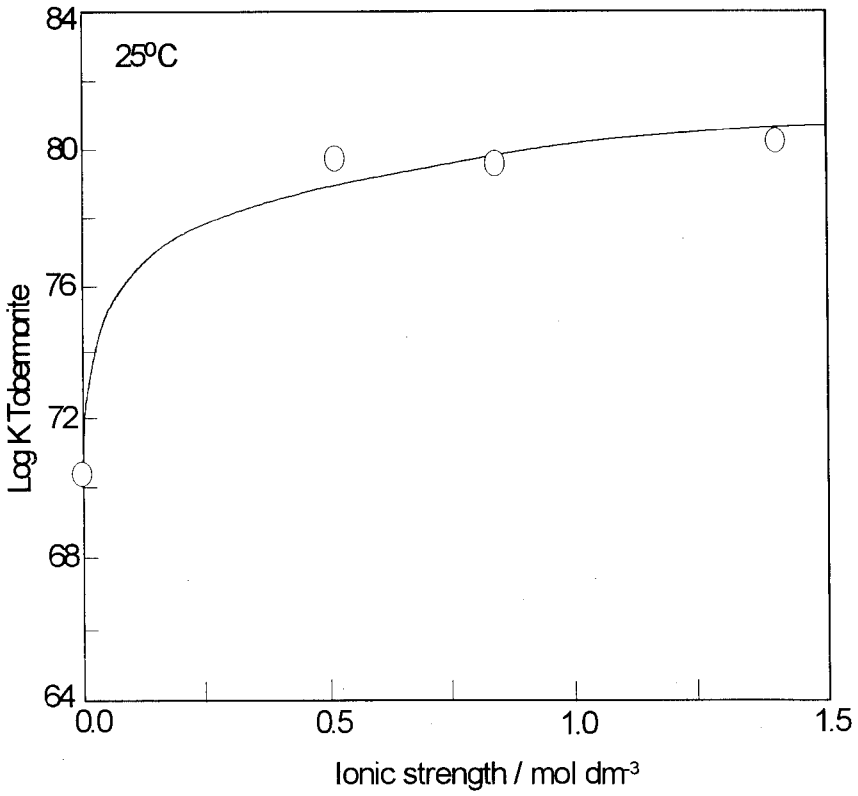

Figure 6.9 **Variation of logK for tobermorite only as a function of ionic strength at 25 °C. Tobermorite is used as a model for crystalline CSH where Ca:Si = 0.85.**

Table 6.14 Solubility relationships between compositional components in CSH and salinity. 25°C isotherm in the aqueous sodium chloride system.

Ca:Si ratio of CSH in experiments	Stoichiometric phases and dissociation reaction relating to log K_{diss}	SIT compatible $\log K_{diss}$ (dissociation constants) I = Ionic strength / mol dm^{-3}
0.85	Tobermorite Ca(5) H_4SiO_4 (6) H_2O (2) H(-10) Silica-mod H_4SiO_4 (1) H_2O(-2)	70.177+1.104 log (I) † -6.613 - 0.616 log (I) †
1.1	Tobermorite Ca(5) H_4SiO_4 (6) H_2O (2) H(-10) Afwillite Ca(3) H_4SiO_4 (2) H_2O (2) H(-6)	66.502 - 0.373 (I) - 0.258 $(I)^2$ 51.508 - 0.015 (I) + 0.206 $(I)^2$
1.1	Tobermorite Ca(5) H_4SiO_4 (6) H_2O (2) H(-10) Fictive solid Ca(1) H_4SiO_4 (6)	66.502 - 0.373 (I) - 0.258 $(I)^2$ -8.528 + 0.438 (I) - 0.283 $(I)^2$
1.4	Tobermorite Ca(5) H_4SiO_4 (6) H_2O (2) H(-10) Afwillite Ca(3) H_4SiO_4 (2) H_2O (2) H(-6)	66.502 - 0.373 (I) - 0.258 $(I)^2$ 51.508 - 0.015 (I) + 0.206 $(I)^2$
1.4	Afwillite Ca(3) H_4SiO_4 (2) H_2O (2) H(-6) Fictive solid Ca(1) H_4SiO_4 (6)	51.508 - 0.015 (I) + 0.206 $(I)^2$ -8.528 + 0.438 (I) - 0.283 $(I)^2$
1.8	Afwillite Ca(3) H_4SiO_4 (2) H_2O (2) H(-6) Portlandite Ca(1) H (-2) H_2O (2)	51.508 - 0.015 (I) + 0.206 $(I)^2$ 22.5 fixed value
Portlandite only	Portlandite Ca(1) H (-2) H_2O (2)	22.819 - 0.418 (I) + 0.091 $(I)^2$

† For I < $5x10^{-2}$ mol dm^{-3}, LogK tobermorite = 67.0 and logK $SiO_{2\text{-mod}}$ = -5.1

Table 6.15 Solids used to model CSH solubility on the 25°C isotherm.

Ca:Si ratio interval of CSH components	Solids used in model
< 1.0	Tobermorite and SiO_2mod
1.0 - 1.2	Tobermorite and afwillite
1.2 - 1.6	Afwillite and fictive solid (CaH_2SiO_4)
1.6 - 2.0	Afwillite and portlandite
> 2.0	Portlandite only

In these models, similar phase assemblages have been used as those proposed by Atkins *et. al.* [14] in the partial and fully crystalline models. In doing so, the adoption of a portlandite (only) model with which to represent calcium-rich (Ca:Si > 2) CSH compositions ignores any contribution to the solution chemistry made by co-existing CSH phases such as afwillite. This is not a major shortcoming in the simulation of pore solution compositions where, in comparison to portlandite, such phases contribute relatively little to the ions in solution. Subsequent calculations of the system buffering capacity however, should not ignore the afwillite contribution, as this phase is expected to condition the pore solution following exhaustion of the co-existing portlandite.

6.4.4 Extensions of the model to higher temperatures

In order to predict the solubility behaviour of a salt at non-standard (25°C) temperatures, PHREEQE applies the Van't Hoff equation:

$$\frac{\partial}{\partial T}(\ln K) = \frac{\Delta H_r^O}{RT^2} \qquad \{6.9\}$$

Where ΔH_r° is the enthalpy of reaction, R the gas constant and T the thermodynamic temperature. This of course is only appropriate for solids where the change in heat capacity is constant over the temperature interval of interest. This implies that the enthalpy of reaction is similarly constant over the same temperature interval. In addition to the simplified Van't Hoff expression, PHREEQE also contains an option to fit known heat capacity data to a polynomial expansion with which to describe the change of dissociation enthalpy with respect to temperature. For most of the mineral phases considered in this study, such changes in enthalpy are not well characterised and in many cases, not known at all. This is particularly the case here, where an empirical model is proposed using solids which represent structural domains in a solid solution series and therefore cannot be characterised independently.

In order to extend the CSH solubility model to conditions of higher temperature, little option exists other than to determine the enthalpy for each solid which reproduces the experimental findings at a particular temperature. This was done in a similar manner to the determination of logK in the previous section. By associating a variable enthalpy with the logK of each solid in the model its absolute value was adjusted until the closest agreement with the experimental result was found. This rather laborious process was undertaken on both the 55° and 85°C isotherms in order to estimate the enthalpy values necessary to extend the model to high temperatures. In this way, some indication of the dependence of the enthalpy of dissociation for each solid is obtained for the three temperatures of interest. The validity of this approach is discussed in the next section.

Considering first the simplest case of portlandite solubility at elevated temperature, it is a simple matter to calculate the 25°C logK at a given ionic strength for this phase from the expression shown in table 6.14. To simulate its behaviour at elevated temperatures, its enthalpy of dissolution was adjusted to reproduce the values recorded experimentally. The results are shown below in table 6.15.

Table 6.16 Model of portlandite solubility at elevated temperatures and salinities.

Dissolution of portlandite at 55°C			
Ionic strength / mol dm^{-3}	0.1771	0.5199	0.9470
log K @ 25°C	22.75	22.65	22.44
Enthalpy / $kJmol^{-1}$	-137.0	-125.7	-111.0
[Ca] / mol dm^{-3} (observed)	1.442 e-2	2.186 e-2	2.360 e-2
[Ca] / mol dm^{-3} (predicted)	1.425 e-2	2.187 e-2	2.360 e-2
pH (observed)	12.50	12.41	12.41
pH (predicted)	11.420	11.539	11.576
Predicted pH adjusted to 25°C	12.28	12.40	12.44
Dissolution of portlandite at 85°C			
Ionic strength / mol dm^{-3}	0.0327	0.9783	1.5428
log K @ 25°C	22.82	22.63	22.40
Enthalpy / $kJmol^{-1}$	-133.3	-125.1	-116.9
[Ca] / mol dm^{-3} (observed)	1.277 e-2	2.036 e-2	2.171 e-2
[Ca] / mol dm^{-3} (predicted)	1.276 e-2	2.038 e-2	2.168 e-2
pH (observed)	-	12.54	12.42
pH (predicted)	10.62	10.75	10.74
Predicted pH adjusted to 25°C	11.42	11.56	11.55

A similar treatment of the 1.8 Ca:Si ratio CSH yields the results for portlandite and afwillite in co-equilibrium shown above in table 6.16. Considering next the solubility relationships of the Ca:Si = 1.4 CSH and 1.1 the afwillite and fictive solid model can be extended to elevated temperatures using the data shown in tables 6.17 and 6.18.

In tables 6.16 to 6.18, three ionic strength intervals are shown for each composition and temperature combination. These correspond to the initial concentrations of sodium chloride used in the experiments and correspond to the zero, 0.5 and 1.5 molar solutions reported in a previous section. Due mainly to the uptake of both sodium and chloride ions by the solid phases, the solution ionic strengths were reduced to the values shown below. In each case, the total elemental composition of the solutions analysed in the experimental work was used to calculate the total ionic strength of the individual solutions reported here.

The thermodynamic model PHREEQE predicts the pH of the solutions at the simulation temperature. By comparison, the experimental measurement of pH was undertaken at laboratory temperature (~25°C) and as the ionic product of water rises with temperature, the values are not directly comparable. As a consequence, the tables contain a corrected pH value, showing the predicted pH adjusted to 25°C, which allows such comparisons to be made.

Table 6.17 Portlandite and afwillite model of CSH solubility at 55 °C in saline conditions.

Co-dissolution of portlandite and afwillite at 55°C			
Ionic strength / mol dm^{-3}	0.0003	0.4215	1.303
log K portlandite @ 25°C	25.5	25.5	25.5
log K afwillite @ 25°C	51.51	51.54	51.84
Enthalpy portlandite / $kJmol^{-1}$	-304	-318	-323
Enthalpy afwillite / $kJmol^{-1}$	-261	-316	-365
[Ca] / mol dm^{-3} (observed)	1.367 e-2	1.767 e-2	1.769 e-2
[Ca] / mol dm^{-3} (predicted)	1.355 e-2	1.777 e-2	1.770 e-2
[Si] / mol dm^{-3} (observed)	1 e-5	1 e-5	1 e-5
[Si] / mol dm^{-3} (predicted)	1.053 e-5	1.0025 e-5	1.008 e-5
pH (observed)	12.56	12.41	12.21
pH (predicted)	11.40	11.46	11.46
Predicted pH adjusted to 25°C	12.26	12.32	12.32
Ionic strength / mol dm^{-3}	0.0002	0.4815	1.3994
log K portlandite @ 25°C	25.5	25.5	25.5
log K afwillite @ 25°C	51.51	51.54	51.89
Enthalpy portlandite / $kJmol^{-1}$	-232	-242	-245
Enthalpy afwillite / $kJmol^{-1}$	-273	-304	-346
[Ca] / mol dm^{-3} (observed)	1.013 e-2	1.243 e-2	1.238 e-2
[Ca] / mol dm^{-3} (predicted)	1.03 e-2	1.232 e-2	1.242 e-2
[Si] / mol dm^{-3} (observed)	2 e-5	3 e-5	2 e-5
[Si] / mol dm^{-3} (predicted)	2.06 e-5	3.081 e-5	2.051 e-5
pH (observed)	12.42	12.42	12.26
pH (predicted)	10.54	10.55	10.55
Predicted pH adjusted to 25°C	12.034	12.044	12.044

Table 6.18 Model of CSH solubility at elevated temperatures and salinities where Ca:Si = 1.4 simulated by co-dissolution of afwillite and CaH_2SiO_4.

Co-dissolution of CaH_2SiO_4 and afwillite at 55°C			
Ionic strength / mol dm^{-3}	0.0016	0.4485	1.2760
log K CaH_2SiO_4 @ 25°C	-8.527	-8.388	-8.430
log K afwillite @ 25°C	51.54	51.54	51.82
Enthalpy CaH_2SiO_4 / $kJmol^{-1}$	+ 9	-20	-38
Enthalpy afwillite / $kJmol^{-1}$	-261	-306	-362
[Ca] / mol dm^{-3} (observed)	9.96 e-3	1.467 e-2	1.644 e-2
[Ca] / mol dm^{-3} (predicted)	1.024 e-2	1.477 e-2	1.624 e-2
[Si] / mol dm^{-3} (observed)	1 e-5	2 e-5	2 e-5
[Si] / mol dm^{-3} (predicted)	2.186 e-5	2.128 e-5	1.356 e-5
pH (observed)	12.30	12.25	12.02
pH (predicted)	11.28	11.38	11.43
Predicted pH adjusted to 25°C	12.14	12.24	12.29
Ionic strength / mol dm^{-3}	0.0012	0.4630	1.4495
log K CaH_2SiO_4 @ 25°C	-8.527	-8.391	-8.487
log K afwillite @ 25°C	51.51	51.55	51.92
Enthalpy CaH_2SiO_4 / $kJmol^{-1}$	+8	-13	-35
Enthalpy afwillite / $kJmol^{-1}$	-259	-307	-367
[Ca] / mol dm^{-3} (observed)	2.27 e-3	1.038 e-2	1.208 e-2
[Ca] / mol dm^{-3} (predicted)	3.06 e-3	1.063 e-2	1.236 e-5
[Si] / mol dm^{-3} (observed)	7 e-5	3 e-5	3 e-5
[Si] / mol dm^{-3} (predicted)	1.77 e-3	4.735 e-5	1.066 e-5
pH (observed)	12.08	12.30	12.21
pH (predicted)	9.94	10.48	10.55
Predicted pH adjusted to 25°C	11.434	11.974	12.044

Table 6.18 shows that for the low ionic strength case at 85°C the model overestimates the silicate concentration in solution by a factor of 25. The reason for this is shown in figure 6.9. When fixing the $logK_{25}$ for the solids according to table 6.14, no single CaH_2SiO_4 enthalpy exists with which to satisfactorily simulate the measured calcium and silicate concentrations. As a consequence, the model was adjusted to accurately predict the calcium concentration only. CSH with a Ca:Si ratio of 1.1 were subject to the same approach but also with an unsatisfactory prediction of the dissolved silicate concentration as shown in table 6.19.

The behaviour of the model is illustrated in figure 6.8 (bottom), where for a fixed $logK_{25}$ for both salts, increasing the enthalpy of dissolution of afwillite, results in a corresponding increase in silicate at the expense of a predicted fall in calcium concentration. Obviously this can never result in a model which simulates the desired values for both calcium and silicate and, in the examples shown in table 6.18, silicate is overestimated by two orders of magnitude. This suggests that the solubility relationship between the low and high temperature systems are markedly different in low Ca:Si ratio CSH, not only is their solubility changing as a function of temperature but the nature of the degree of incongruity changes also.

Table 6.19 Model of CSH solubility at elevated temperatures and salinities where Ca:Si = 1.1 simulated by co-dissolution of afwillite and tobermorite. All concentrations in mol dm^{-3}.

Co-dissolution of tobermorite and afwillite at 55°C			
Ionic strength / mol dm^{-3}	0.0057	0.4265	1.3360
log K tobermorite @ 25°C	66.5	66.3	65.5
log K afwillite @ 25°C	51.51	51.53	51.85
Enthalpy tobermorite / $kJmol^{-1}$	225	305	270
Enthalpy afwillite / $kJmol^{-1}$	-261	-316	-366
[Ca] / mol dm^{-3} (observed)	2.72 e-3	1.188 e-2	1.639 e-2
[Ca] / mol dm^{-3} (predicted)	3.58 e-3	1.184 e-2	1.639 e-2
[Si] / mol dm^{-3} (observed)	8 e-5	5 e-5	4 e-5
[Si] / mol dm^{-3} (predicted)	5.64 e-3	2.89 e-2	4.173 e-2
pH (observed)	12.02	11.96	11.73
pH (predicted)	10.26	9.83	9.67
Predicted pH adjusted to 25°C	11.12	10.69	10.53
Ionic strength / mol dm^{-3}	0.0011	0.4550	0.9710
log K tobermorite @ 25°C	66.5	66.3	65.9
log K afwillite @ 25°C	51.51	51.54	51.69
Enthalpy tobermorite / $kJmol^{-1}$	89	-39	-49
Enthalpy afwillite / $kJmol^{-1}$	-273	-307	-341
[Ca] / mol dm^{-3} (observed)	2.36 e-2	9.21 e-3	1.233 e-2
[Ca] / mol dm^{-3} (predicted)	2.384 e-2	9.186 e-3	1.225 e-2
[Si] / mol dm^{-3} (observed)	8 e-5	9 e-5	6 e-5
[Si] / mol dm^{-3} (predicted)	1.16 e-1	2.504 e-2	3.79 e-2
pH (observed)	11.91	11.92	11.85
pH (predicted)	8.71	9.19	9.947
Predicted pH adjusted to 25°C	10.20	10.68	11.44

A similar behaviour is seen in the lowest calcium to silicate ratio model where Ca:Si = 0.85. Although on the 25°C isotherm the tobermorite-SiO_{2mod} model adequately simulates the solution chemistry its extension to higher temperatures, through the fitting of appropriate enthalpies, grossly overestimates the dissolved silicate concentration. As a consequence, the adoption of tobermorite as a single phase model of CSH at Ca:Si = 0.85 is proposed as, although it overestimates dissolved silicate, this overestimation is fixed to that of the stoichiometric ratio of calcium to silicate in the solid, numerically 5:6. In order to use this model, the appropriate logK values on the 25°C isotherm were determined as shown in table 6.20 and figure 6.10.

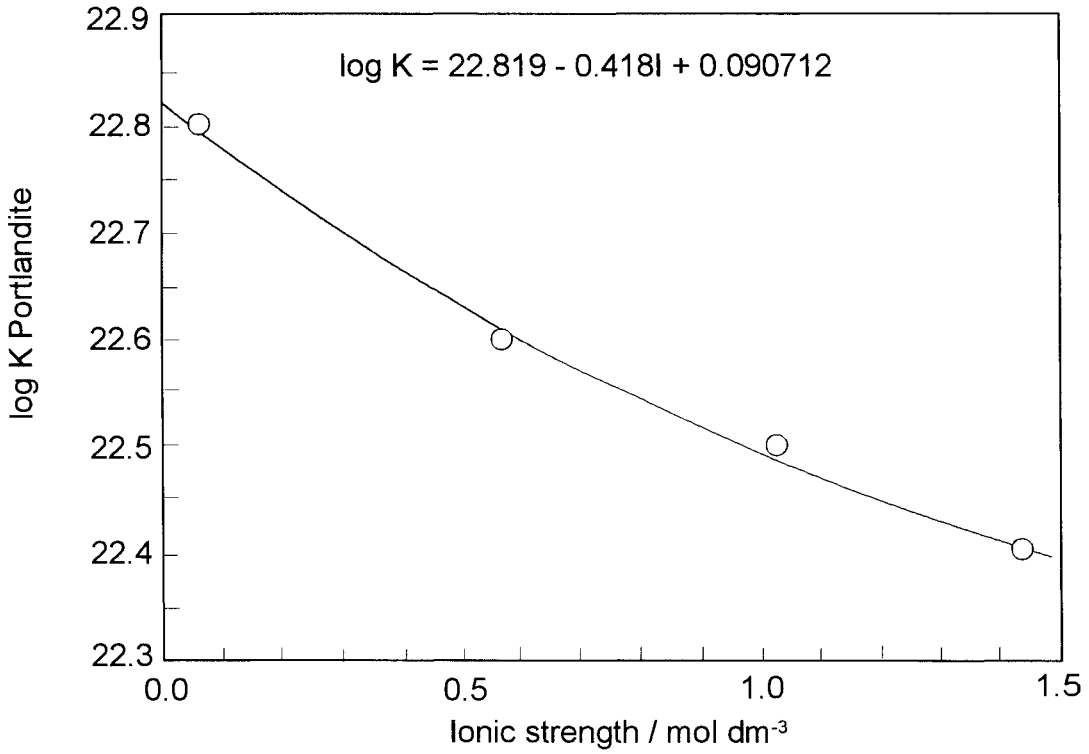

Figure 6.10 Variation of Log K for portlandite as a function of ionic strength.

Table 6.20 Observed and predicted solution compositions over CSH (Ca:Si = 0.85) using a tobermorite model for CSH dissolution at 25°C. All concentrations in mol dm^{-3}.

Initial NaCℓ	Observed solution composition					
	pH	Na	Cl	Ca	Si	Ionic strength
0	11.65	< 0.09	8 e-5	1.25 e-3	2.78 e-4	0.0050
0.52	11.20	4.89 e-1	4.53 e-1	1.158 e-2	1.59 e-4	0.4952
1.05	11.14	7.99 e-1	7.84 e-1	1.262 e-2	1.87 e-4	0.8177
1.46	11.02	1.330 e0	1.359 e0	1.609 e-2	1.72 e-4	1.3774
Log K of tobermorite	Predicted solution composition					
70.4	10.993	0	8 e-5	1.257 e-3	1.509 e-3	0.0038
79.8	11.753	4.89 e-1	4.53 e-1	1.167 e-2	1.401 e-2	0.5078
79.7	11.775	7.99 e-1	7.84 e-1	1.264 e-2	1.516 e-2	0.8318
80.5	11.862	1.330 e0	1.359 e0	1.596 e-2	1.915 e-2	1.3965

Agreement between the observed and predicted solution chemistry is tolerable, given that the silicate concentration will always be lower than the calcium in solution. Finally, this model may be extended for use at elevated temperatures by selection of appropriate enthalpy values with which to describe the change of tobermorite solubility with respect to temperature. This requires the $\log K_{25}$ of tobermorite to be calculated for the ionic strength of interest and a least squares fitted line to the data in table 6.20 suggests the following relationship:

$$\log K_{25} = 80.28 + 4.04 \log (I) \qquad \{6.10\}$$

Where I is the ionic strength in mol dm^{-3} and as before, for I < 50mmol dm^{-3} , $LogK_{25}$ is a constant, in this case 70.4. The results of this model are shown in table 6.21. It is interesting to notice that although the model can be made to simulate the experimental results, extension to the highest temperatures (85°C) can only be achieved at extremely high enthalpies (figure 6.11).

Calcium and silicon concentrations predicted during co-dissolution of afwillite and the fictive solid.

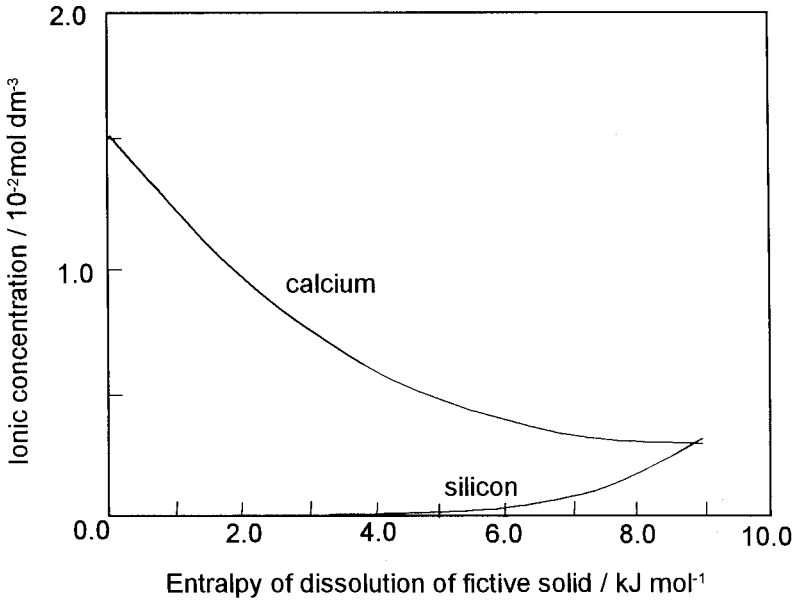

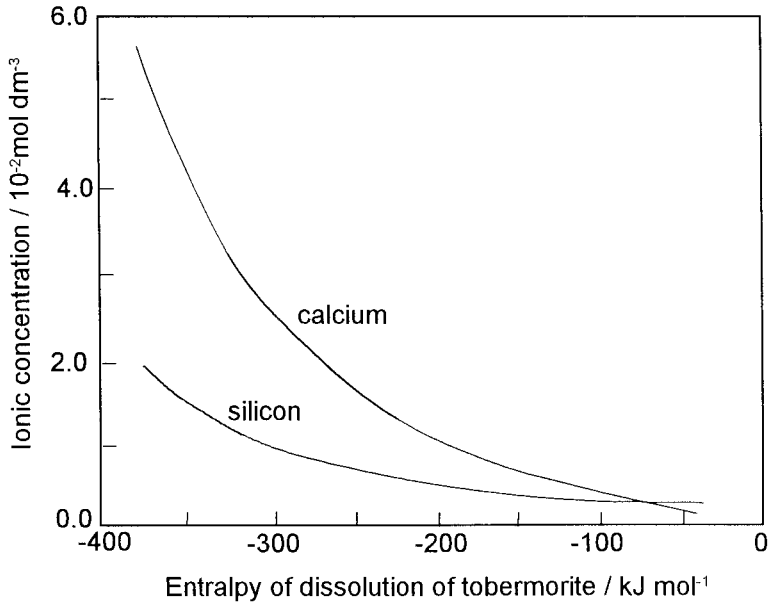

Figure 6.11 Model behaviour at 85°C illustrating over-prediction of aqueous phase [Ca] and [Si].

Table 6.21 Model of CSH solubility at elevated temperatures and salinities where Ca:Si = 0.85 simulated by the dissolution of tobermorite only. All concentrations in mol dm^{-3}.

Dissolution of tobermorite at 55°C			
Ionic strength / mol dm^{-3}	< 1e-4	0.4395	0.9414
log K tobermorite @ 25°C	70.4	78.8	80.2
Enthalpy tobermorite / $kJmol^{-1}$	-111	-90	-90
[Ca] / mol dm^{-3} (observed)	1.02 e-3	9.56 e-3	1.455 e-2
[Ca] / mol dm^{-3} (predicted)	1.015e-2	9.52 e-3	1.458 e-2
[Si] / mol dm^{-3} (observed)	2 e-4	2.9 e-4	2.3 e-4
[Si] / mol dm^{-3} (predicted)	1.22 e-3	1.14 e-2	1.75 e-2
pH (observed)	11.46	10.86	10.81
pH (predicted)	10.068	10.78	10.92
Predicted pH adjusted to 25°C	10.93	11.64	11.78
Dissolution of tobermorite at 85°C			
Ionic strength / mol dm^{-3}	0.0016	0.4640	1.4820
log K tobermorite @ 25°C	70.4	78.9	80.4
Enthalpy tobermorite / $kJmol^{-1}$	-9821	-10881	-10874
[Ca] / mol dm^{-3} (observed)	1.16 e-3	7.06 e-3	1.062 e-2
[Ca] / mol dm^{-3} (predicted)	1.16e-3	7.06 e-3	1.062 e-2
[Si] / mol dm^{-3} (observed)	8.5 e-5	1.3 e-4	1.9 e-4
[Si] / mol dm^{-3} (predicted)	1.392 e-3	8.47 e-3	1.27 e-2
pH (observed)	11.66	11.28	10.09
pH (predicted)	9.43	9.94	10.07
Predicted pH adjusted to 25°C	10.92	11.43	11.56

6.4.5. Discussion and recommendations for further development

The models described above illustrate a method by which the approaches adopted by Berner *et al.*, [12] and subsequently applied and developed by Atkinson *et al.*, [11] and by Atkins *et al.*, [14] may be extended to model CSH dissolution in environments of high salinity and at elevated temperature. The models described above generally predict the solution chemistry observed by experimental investigation with acceptable accuracy with the sole exception of overprediction of silicate at high temperature in CSH solids with a Ca:Si ratio less than 1.2. This implication of this shortcoming is that care must be exercised when using the models under conditions where portlandite is absent, for example with blended cements containing fly ash or very large proportions of blast furnace slag. Nonetheless, the model represents a considerable advance over previous work and accepting the caveats above, is suitable for use in saline systems.

Considering the function of the CSH model and comparing its behaviour to that of the CSH examined experimentally (see Section 4) a number of observations should be discussed. The analytical measurements show that the change in solubility and incongruity of the CSH components are gradual and change smoothly with the calcium to silicon ratio of the CSH, the solution salinity and solution temperature. It would be reasonable therefore, to expect the conditional constants used in the model to vary in a similarly smooth and predictable way. If we examine the values chosen for modelling the CSH system on the 25°C isotherm, this is the case, and the predicted solution chemistries are a reasonable representation of the experimental results.

Once the model is extended to higher temperatures however, the rate at which the solubility constants change as a function of temperature is not constant. For example, the experiments include three temperatures (25°, 55°C and 85°C), at which CSH solubilities are modelled by empirically fitting the enthalpy of dissolution for each phase in a phase pair, so that the predicted solution chemistry is as close as possible to that determined experimentally. It would be reasonable to expect that the enthalpy value required to do this would be of a similar magnitude in both the lower and upper temperature intervals but this is not so. This is a disappointing feature of the model which is thought to be a function of the numerical method, and certainly cannot be ascribed to any features of the system chemistry measured in this study. As a consequence of calibrating the model at three temperatures, the confidence with which predictions at intermediate temperatures may be made is not high. This is particularly so above 55°C, where required enthalpy values are considerably different to those used under standard conditions (25°C).

Extensive testing of these models confirms that a unique combination of solubilities is required of each pair of phases in order to predict a specified pH and calcium and silicon concentrations in solution. Should this approach be adopted in further studies, determination of these solubilities for each temperature may be necessary, rather than relying on the current implementation of the Van't Hoff equation to calculate these values.

The existence of solubility minima in the model which prevent the satisfactory prediction of the observed silicate concentrations are undoubtedly numerical artifacts and in no way should be interpreted as representing the behaviour of the solids. Indeed, the use of true mineral names to describe postulated compositional units in CSH may be misleading in as much as these units have the same stoichiometry as the natural minerals, yet exhibit somewhat different solubility behaviour.

The experiments suggest that at low Ca:Si ratios, conversion of the CSH to tobermorite occurs, whilst at high ratios, the recrystallisation favours afwillite. These salts have been chosen to represent the CSH in the model, yet the experimental work shows considerable recrystallisation to jennite at intermediate CSH compositions whereas the model invokes the fictive solid CaH_2SiO_4. The degree of crystallinity is one aspect of the CSH system not considered in this model but which undoubtedly influences the dissolution of this component. There was from the outset no intention to attempt to quantify this parameter for inclusion in the model. This is notoriously difficult to measure in practice yet with, hindsight, may have been a valuable addition to the study. For example, it is assumed that a small quantity of the poorly crystalline and relatively soluble CSH will readily condition the pore solution chemistry and hence dominate the experimental results. To make predictions about the long-term stability of cements under repository conditions, it would be valuable to have a better understanding of the kinetics of crystallisation. This may lead to a prediction of the partitioning of CSH into gel and crystalline components. The two solids may then be treated independently, reflecting their different solubilities and ability to condition the near field.

As it stands, the model represents the effect of temperature as simply a change in solubility, the thermodynamic data being fitted empirically to the solution phase results without any more thorough treatment of the degree of crystallinity in the solid. Should a small quantity of CSH gel remain in any of the high temperature samples, it will presumably condition the supernatant solution. In a closed system such as that investigated here, this may lead to an

overestimation of the solubility of these phases after high temperature curing. In the absence of better knowledge, it must be assumed that the influence of temperature on CSH solubility is as seen in the experiments and that as such, the experimental model is a true representation of this system.

The use of a numerical model which considers both CSH gel and its crystalline counterparts may be considerably simplified by adoption of finite mineral accounting in PHREEQE. This would allow absolute quantities to be assigned to the minerals in a simulated assemblage expressed in terms of moles of solid per litre of solution. In this way dissolution of the most soluble phases (in the case of CSH, the gel components) may go to completion. This approach allows repeated exchanges of pore solution to simulate sequential depletion of an assemblage of solids in order of their solubility.

6.5 The Interaction of Pure Cement Phases With Simple Solutions

6.5.1 Sodium chloride system

Introduction

The models described in the previous section have been used to investigate the interaction of pure cement phases with solutions of NaCl and $MgSO_4$. In doing so, estimates of the sodium and chloride concentrations according to table 6.5 were not necessary as the concentrations of both ions before and after equilibration with the solids are known from the analyses. The SIT implementation of PHREEQE was used for all calculations and the appropriate logK and enthalpy values for phases in the CSH model chosen according to the method described in Section 6.4.

Portlandite in NaCℓ

The dissolution of calcium hydroxide in sodium chloride solutions ranging in ionic strength from zero to around 1.5 has been examined experimentally and numerically (tables 6.13 and 6.16. The change in solubility as a function of salinity shows approximately a 30% increase in calcium concentration on the 25°C isotherm as ionic strength rises from close to zero to around 1.5 mol dm^{-3}. This effect rises to a value of approximately 70% at a temperature of 85°C. The modelled results are in excellent agreement with the experimental findings.

Calcium silicate hydrate in NaCℓ

The simulation of NaCl solutions at equilibrium with all CSH compositions in this study suggest that no other phases are oversaturated in these systems. Interestingly, the predicted excess of dissolved silica in the Ca:Si = 1.1 CSH calculations, raises the saturation index of quartz close to zero in the high temperature simulations. In the high salinity 55°C simulations, this phase is reported to be oversaturated but is not detected experimentally. In all other cases, the agreement between the observed and predicted solution chemistry is good, suggesting that the model satisfactorily represents the experimental conditions.

Calcium trisulfo-aluminate (ettringite: AFt-SO_4) in NaCℓ

The effect of high salinity and elevated temperature on the solubility of ettringite has been shown by experiment to increase its solubility and result in the formation of new phases. Simulation of this system suggests that on the 25°C isotherm, equilibration of ettringite with pure water leaves the solution slightly oversaturated with respect to gibbsite. Following re-equilibration with gibbsite the following solution chemistry is predicted (mol dm^{-3}):

Ca = 1.575 e-3	S = 7.877 e-4
Al = 9.096 e-5	pH = 11.122

By comparison, simulations at elevated temperatures suggest that the both gibbsite and portlandite may precipitate from solution. Re-equilibration of ettringite with either gibbsite or portlandite at 55°C leaves the system oversaturated with the other phase but no converged solution can be obtained for all three phases. This is true across the salinity range whilst at 85°C, the system is additionally predicted to be oversaturated with respect to anhydrite. Similarly, equilibration of each phase with ettringite leaves the remaining phases oversaturated but no converged solution was obtained for these phases in combination.

Table 6.22 Equilibrium of AFt-SO_4 in sodium chloride solutions.

Temp (°C)	Minerals predicted to be oversaturated and their saturation indices			
NaCl ($mol.dm^{-3}$)	**0**	**0.5**	**1.0**	**1.5**
25°C	Diaspore 1.66 Boehmite 1.04 Gibbsite 0.91	Diaspore 1.64 Boehmite 1.01 Gibbsite 0.88	Diaspore 1.62 Boehmite 0.99 Gibbsite 0.86	Diaspore 1.61 Boehmite 0.98 Gibbsite 0.83
55°C	Gibbsite 5.43 Portlandite 3.52	Gibbsite 5.40 Portlandite 3.92	Gibbsite 5.35 Portlandite 4.23	Gibbsite 5.37 Portlandite 4.09
85°C	Gibbsite 9.19 Portlandite 9.81 Anhydrite 0.72	Gibbsite 9.16 Portlandite 10.19 Anhydrite 0.42	Gibbsite 9.14 Portlandite 10.36 Anhydrite 0.35	Gibbsite 9.12 Portlandite 10.52 Anhydrite 0.32

Note:
Boehmite = γ-AlO(OH)
Diaspore = α- AlO(OH)
Gibbsite = $Al(OH)_3$
Portlandite = $Ca(OH)_2$
Anhydrite = $CaSO_4$

Table 6.22 shows the predicted saturation state of phases in the ettringite - sodium chloride system which contrasts somewhat with the experimental findings in that Friedel's salt (AFm-Cl) is not predicted to oversaturate under conditions of high salinity.

Calcium monosulphoaluminate (AFm-SO_4) in NaCℓ

The behaviour of calcium monosulpho aluminate in sodium chloride contrasts with that of its trisulphate analogue. Initial simulated equilibrium of the solid in water suggests that its solubility increases slightly between 25° and 85°C, shown by a rise in calcium concentration of approximately 75%. This increasing trend is also predicted at higher salinities.

Dissolution in water leaves the solution oversaturated with aluminium hydroxides at all temperatures but with different additional minerals oversaturated according to the system chemistry.

Table 6.23 Equilibrium of AFm-SO_4 in sodium chloride solutions (continued).

Temp (°C)	Minerals predicted to be oversaturated and their saturation indices			
NaCl ($mol.dm^{-3}$)	**0**	**0.5**	**1.0**	**1.5**
25 °C	Diaspore 1.67 Boehmite 1.04 Gibbsite 0.91	Diaspore 1.65 Boehmite 1.02 Gibbsite 0.89 AFm-Cl 2.07	Diaspore 1.63 Boehmite 1.00 Gibbsite 0.86 AFm-Cl 2.79 AFm-Cl-SO_4 0.23	Diaspore 1.61 Boehmite 0.98 Gibbsite 0.84 AFm-Cl 3.27 AFm-Cl-SO_4 0.46
55 °C	Gibbsite 5.44 Portlandite 4.62 Ettringite 3.70	Gibbsite 5.41 Portlandite 4.79 Ettringite 2.72	Gibbsite 5.38 Portlandite 4.87 Ettringite 2.29	Gibbsite 5.35 Portlandite 4.93 Ettringite 1.92
85 °C	Portlandite 10.54 Anhydrite 0.63	Portlandite 10.71 Anhydrite 0.23 Ettringite 0.99	Portlandite 10.79 Anhydrite 0.16 Ettringite 0.55 Hydrogarnet 0.07	Portlandite 10.86 Anhydrite 0.02 Ettringite 0.18 Hydrogarnet 0.22

Table 6.22 above shows the saturation state of the minerals which are predicted to be able to precipitate following the dissolution of AFm-SO_4 in sodium chloride solutions. The aluminium hydroxides are ubiquitous in these simulations and in subsequent calculations, gibbsite was chosen as the most likely phase to form. Considering first the 25°C isotherm, equilibrium of monosulphate with gibbsite suggests that ettringite should precipitate from the resulting solution. Indeed, some evidence is seen experimentally that both ettringite and hydrogrossular form following the dissolution of monosulphate. As salinity increases, initially Friedel's salt and ultimately Kuzel's salt are expected to precipitate, as the dissolution of ettringite releases sulphate into solution. Equilibration of monosulphate, gibbsite and ettringite with water does leave the resulting solution oversaturated with hydrogrossular although simulation of this four component assemblage does not result in convergence of the code. Monosulphate, ettringite and gibbsite in co-equilibrium with water result in the following predicted solution chemistry ($mol\ dm^{-3}$):

Ca = 8.921 e-3 S = 7.966 e-7
Al = 9.806 e-5 pH = 12.12

This leaves the solution oversaturated with respect to the hydrogarnet, C_3AH_6, which is in general agreement with the experimental findings. Similar equilibration of monosulphate with ettringite, gibbsite and Friedel's salt in saline systems is shown in table 6.24 below:

Table 6.24 Predicted solution chemistry at equilibrium with AFm-SO4 at 25°C.

Salinity / $mol\ dm^{-3}$	0	0.5	1.0	1.5
Ca	8.92 e-3	1.13 e-4	5.57e-5	3.78 e-5
Al	9.81 e-4	2.856 e-2	5.93 e-2	9.12 e-2
S	7.97 e-7	1.19 e-3	8.38 e-3	3.04 e-2
pH	12.12	13.487	13.77	13.94

Considering next the AFm-SO_4 chemistry at elevated temperatures, there is considerable divergence between the predicted behaviour and that seen experimentally. Whereas laboratory examination of this system reveals that Kuzel's salt, the chloride analogue of AFm-SO_4, readily forms and that ettringite is unstable at higher temperatures, the simulations show almost the reverse. Table 6.25 illustrates that Friedel's salt is only predicted to be oversaturated in the low temperature simulations and that at higher temperatures the solution is oversaturated with respect to ettringite. As was seen above, calculated equilibrium with all the oversaturated phases was not possible but at 55°C, equilibrium was simulated between monosulphate and any two minerals from the three which were predicted to be oversaturated; an example is shown below:

Table 6.25 Equilibrium chemistry of AFm-SO4 in sodium chloride at 55°C.

Salinity (mol dm^{-3})	0.5	1.0	1.5
Temperature (°C)	Minerals at equilibrium and solution chemistry		
	AFm-SO_4	AFm-SO_4	AFm-SO_4
	Gibbsite	Gibbsite	Gibbsite
	Ettringite	Ettringite	Ettringite
55 °C	Ca = 2.37 e-1	Ca = 2.35 e-1	Ca = 2.29 e-1
	Al = 6.67 e-7	Al = 7.03 e-7	Al = 7.25 e-7
	S = 2.21 e-5	S = 3.32 e-5	S = 5.14 e-5
	pH = 12. 44	pH = 12.44	pH = 12.45

At 85°C, the convergence problems are acute, in that no predictions could be made which simulate the co-equilibrium of monosulphate with either portlandite or gibbsite, both of which are greatly oversaturated. In any case, model predictions for oversaturated phases at 85°C depart from experimental evidence suggesting that further refinements to the model and / or high temperature data are required.

Hydrogarnet in NaCℓ

The simulated equilibrium of hydrogarnet (C_3AH_6) with sodium chloride solutions, shows a relatively simple suite of minerals oversaturated as shown in table 6.26. Considering first the 25°C isotherm, and again assuming that gibbsite is the most likely aluminium hydroxide phase to form, equilibrium between the hydrogarnet and water is simply achieved through co-equilibrium of C_3AH_6 and gibbsite. The predicted calcium concentration is 7.6 x10^{-3} mol dm^{-3} and aluminium 8.4 x10^{-3} mol dm^{-3}.

Table 6.26 Equilibrium of C_3AH_6 in sodium chloride solutions.

Temp /°C	Minerals predicted to be oversaturated and their saturation indices			
NaCl / M	0	0.5	1.0	1.5
	Diaspore 0.63	Diaspore 1.65	Diaspore 1.63	Diaspore 1.62
25 °C	Boehmite 1.67	Boehmite 1.02	Boehmite 1.00	Boehmite 0.99
	Gibbsite 1.04	Gibbsite 1.89	Gibbsite 0.86	Gibbsite 0.83
		AFm-Cl 4.10	AFm-Cl 4.26	AFm-Cl 4.94
55 °C	Gibbsite 5.31	Gibbsite 5.31	Gibbsite 5.30	Gibbsite 5.26
85 °C	Gibbsite 4.01	Gibbsite 4.33	Gibbsite 4.37	Gibbsite 4.37

As temperature increases gibbsite solubility decreases, such that the aluminium concentration is very low indeed at 85°C. This again contrasts with the experimental results, in which the dominant hydroxide formed is portlandite. The results of the hydrogarnet simulations are summarised in table 6.27.

Table 6.27 Dissolution of hydrogarnet into sodium chloride solutions.

NaCℓ/ mol dm^{-3}	0	0.5	1.0	1.5
Temp / °C	Minerals at equilibrium and solution chemistry			
	Gibbsite	Gibbsite	Gibbsite	Gibbsite
		AFm-Cl	AFm-Cl	AFm-Cl
25°	Ca = 7.62 e-3	Ca = 8.64 e-5	Ca = 4.23 e-5	Ca = 2.82e-5
	Al = 8.43 e-4	Al = 2.64 e-2	Al = 5.56 e-2	Al = 8.78 e-2
		Cl = 7.58 e-2	Cl = 1.58 e-1	Cl = 2.48 e-1
	pH = 12.43	pH = 13.44	pH = 13.74	pH = 13.93
	Gibbsite	Gibbsite	Gibbsite	Gibbsite
	Ca = 2.89 e-5	Ca = 6.11 e-5	Ca = 6.47 e-5	Ca = 6.43 e-5
	Al = 1.13 e-10	Al = 2.53 e-10	Al = 2.85 e-10	Al = 3.02 e-10
55°		Cl = 0.5	Cl = 1.0	Cl = 1.5
	pH = 8.86	pH = 9.03	pH = 9.05	pH = 9.06
	Gibbsite	Gibbsite	Gibbsite	Gibbsite
	Ca = 1.11 e-8	Ca = 5.89 e-8	Ca = 7.04 e-8	Ca = 7.38 e-8
85°	Al = 1.53 e-15	Al = 2.43 e-15	Al = 2.62 e-15	Al = 2.72 e-15
		Cl = 0.5	Cl = 1.0	Cl = 1.5
	pH = 7.00	pH = 7.00	pH = 7.01	pH = 7.01

The prediction of the stability of Friedel's salt at low temperatures is in keeping with the experimental findings yet it is interesting to note that the observed stability of hydrogarnet is low where both salinity and temperature are high. The evidence is that this solid completely denatures under these conditions to form a new assemblage comprised of portlandite and Friedel's salt. Unfortunately, under conditions of high salinity and temperature, the model does not reach a numerically stable solution so the phase relationships between these two salts remains un-modelled.

Discussion

For low temperature simulations, the predicted interaction of single cement hydrates and sodium chloride solutions show similarities to the experimental observations. Unfortunately however, as both temperature and salinity increase the divergence between observed and predicted results also increases to the point that code convergence problems occur. The probability of non-convergence is often increased by the complexity of the simulation and, as is to be expected of any iterative model, by large discrepancies in the charge balance. It has been shown in Section 3 that satisfactory (indeed, in many cases very good) results may be obtained by the SIT implementation in PHREEQE but only through careful selection of the thermodynamic data used in the model. At first consideration, this may be attributed to the use of inappropriate thermodynamic data. This hypothesis was rejected in that the dissolution phenomena reported in the literature can be satisfactorily reproduced by this code. For example, Atkins [14] reports the following change in calcium concentration in a solution above ettringite (AFt-SO_4) which are compared in table 6.28 to the predictions using the current model.

It seems more likely to be a function of the modelling approach itself and undoubtedly warrants further investigation.

Table 6.28 Comparison of SIT model results with published data for dissolution of ettringite.

Temperature / °C	Calcium concentration mmol dm^{-3}		
	Mineql prediction	Measured	Current model
25 °C	1.85	1.47	1.33
55 °C	3.62	3.41	2.53
85 °C	6.39	6.5	4.51

6.5.2 Magnesium sulphate system

Portlandite in $MgSO_4$

Experimental studies reported above show that the cement minerals considered in this study are extremely sensitive to both magnesium and sulphate ions. Initial equilibration of portlandite with magnesium sulphate solutions of increasing concentration show that the threshold of magnesium necessary for conversion of portlandite to brucite is very low in a 25°C solution dominated by portlandite buffered to a pH of 12.47, the predicted threshold is at 1.36 e-8 mol dm^{-3} Mg. With increasing temperature the falling solubility of brucite reduces this limit much further, suggesting that any magnesium in this system reacts almost quantitatively with portlandite. The results are shown in table 6.29.

Table 6.29 Solution chemistry for co-dissolution of portlandite and brucite. Mol dm^{-3}.

Temperature / °C	Ca	Mg	pH
25 °C	2.66 e-2	1.36 e-8	12.47
55 °C	1.52 e-2	3.37 e-14	11.44
85 °C	1.19e-2	7.33 e-19	10.59

As the magnesium sulphate concentration of the system increases, so too do the saturation indices of anhydrite and gypsum. Considering first the portlandite-brucite anhydrite system, a similarly small magnesium concentration is predicted to initiate conversion of portlandite to brucite. The predicted solution chemistry at equilibrium with this assemblage is shown in table 6.30.

Table 6.30 Solution chemistry for co-dissolution of portlandite anhydrite and brucite. Mol dm^{-3}.

Temperature / °C	Saturation index of Gypsum	Ca	Mg	S	pH	pH adjusted to 25°C
25 °C	0.238	4.89 e-2	3.97 e-8	2.99 e-2	12.37	12.37
55 °C	-0.889	1.75 e-2	4.30 e-14	2.51 e-3	11.43	12.29
85 °C	-1.827	1.21 e-2	7.74 e-19	3.07 e-4	10.59	12.08

It is interesting to note that at 25°C, gypsum is predicted to be oversaturated and is therefore the dominant sink for sulphate ions in the solid phase. As the temperature increases however, anhydrite is predicted to become increasingly oversaturated, such that at 55° and 85°C, it becomes the major sulphate sink. The continued capacity of the system to precipitate magnesium is shown in table 6.31 which illustrates the alternative equilibrium assemblage; that of anhydrite with portlandite and brucite. When magnesium is added $MgSO_4$, both magnesium and sulphate components can react with portlandite. Sulphate is as precipitated as either gypsum ($CaSO_4.2H_2O$) or anhydrite ($CaSO_4$). Neither conditions a high aqueous pH. Both phases may form but anhydrite occurs mainly at higher temperatures and salinities and, as both minerals tie up equal numbers of calcium per sulphate, differences in polymorphism do not affect mass balances in the system.

Table 6.31 Solution chemistry for co-dissolution of portlandite, anhydrite and brucite. Units are mol dm^{-3}.

Temperature / °C	Saturation index of anhydrite	Ca	Mg	S	pH	pH adjusted to 25°C
25 °C	-0.238	3.74 e-2	2.89 e-8	1.79 e-2	12.41	12.41
55 °C	0.889	3.21 e-2	1.04 e-14	1.80 e-2	11.36	12.22
85 C°	1.827	2.94 e-2	3.45 e-18	1.85 e-2	10.49	11.98

Comparison of tables 6.30 and 6.31, illustrates the conditions under which each assemblage predominate. The saturation index of either anhydrite or gypsum is shown in the second column and suggests that the stable assemblage comprises portlandite and brucite with gypsum at low temperatures or anhydrite at higher temperatures. Ultimately a state is reached in which the magnesium concentration in solution rises appreciably as the portlandite in the solid phase is finally exhausted. This leaves two possible assemblages which dominate the solution chemistry; either anhydrite and brucite or gypsum and brucite, depending on the prevailing conditions.

Tables 6.32 and 6.33 report similar solution chemistries at equilibrium with the two assemblages, the brucite-gypsum pair being slightly favoured in low temperature, low magnesium systems than the brucite-anhydrite pair. These trends are in general agreement with the experimental findings and suggest that the portlandite magnesium sulphate system is not simply dominated by base exchange of magnesium for calcium but in part sulphate replaces hydroxide. The dominance of sulphate-bearing salts is illustrated by the relative stability of anhydrite and gypsum in this system.

Table 6.32 Solution chemistry for co-dissolution of gypsum and brucite. Units are mol dm^{-3}.

Temperature / °C	Ca	Mg	S	pH	pH adjusted to 25°C
25 °C	2.12 e-2	2.11 e-4	2.12 e-2	10.48	10.48
55 °C	2.03 e-2	2.43 e-6	2.03 e-2	7.69	8.55
85 °C	2.01 e-2	6.73 e-11	2.01 e-2	6.87	8.36

Table 6.33 Solution chemistry for co-dissolution of portlandite, anhydrite and brucite. Concentrations are in mol dm^{-3}.

Temperature / °C	Ca	Mg	S	pH	pH adjusted to 25°C
25 °C	3.14 e-2	2.35 e-4	3.31 e-2	10.49	10.49
55 °C	4.34 e-3	1.68 e-6	4.34 e-3	7.63	8.22
85 °C	1.05 e-3	1.20 e-11	1.01 e-3	6.96	8.45

Calcium silicate hydrate in $MgSO_4$

Considering next the CSH system, at the highest Ca:Si ratio of 1.8, a similar behaviour is seen to that of calcium hydroxide. Initially insufficient silicate is dissolved in the equilibrium solution to oversaturate it in any silicate minerals and a similar sequence of stability domains is seen to that for calcium hydroxide, with $CSH_{1.8}$ instead of portlandite. The solution compositions overlying these solids at 25°C are shown in table 6.34.

Table 6.34 Equilibrium between $CSH_{1.8}$ and $MgSO_4$ solutions $CSH_{1.8}$ is represented in the model by co-equilibrium of afwillite and portlandite.

Solids in equilibrium	Solution composition /mol dm^{-3}				
	pH	Ca	Mg	Si	S
$CSH_{1.8}$ brucite	12.23	3.25 e-2	5.28 e-8	4.42 e-6	1.85 e-2
$CSH_{1.8}$ brucite anhydrite	12.24	4.42 e-2	7.48 e-8	4.16 e-6	3.06 e-2
$CSH_{1.8}$ brucite gypsum	12.35	1.54 e-2	4.42 e-6	5.07 e-6	-

This general relationship is seen throughout the high Ca:Si range but as dissolved silicate increases, ultimately the solution will oversaturate with respect to a silicate mineral. This becomes apparent at low Ca:Si ratios in the CSH, especially as the high temperature model overestimates the dissolved silicate concentration. To illustrate this effect, the dominant assemblages and their equilibrium solutions are shown in table 6.35.

Table 6.35 Controlling phase relationships during simulated equilibrium of $CSH_{0.85}$ with magnesium sulphate solutions. All concentrations in mol dm^{-3}.

A	Solution chemistry at equilibrium with $CSH_{0.85}$ and sepiolite				
Temperature / °C	Ca	Mg	Si	S	pH
25 °C	1.25 e-3	5.42 e-8	1.51 e-3	-	10.99
55 °C	3.49 e-3	1.07 e-7	4.19 e-3	-	10.51
85 °C	8.85 e-3	1.97 e-7	1.06 e-2	-	10.11

B	Solution chemistry at equilibrium with $CSH_{0.85}$ sepiolite and anhydrite				
Temperature / °C	Ca	Mg	Si	S	pH
25 °C	Gypsum oversaturated				
55 °C	6.46 e-3	2.38 e-7	3.64 e-3	3.42 e-3	10.43
85 °C	9.12 e-3	2.10 e-7	1.05 e-2	3.12 e-4	10.11
C	Solution chemistry at equilibrium with $CSH_{0.85}$ sepiolite and gypsum				
Temperature / °C	Ca	Mg	Si	S	pH
25 °C	2.14 e-2	1.06 e-6	6.82 e-4	2.09 e-2	10.58
55 °C	anhydrite oversaturated				
85 °C	anhydrite oversaturated				

The likelihood is that sepiolite will act as a sink for magnesium in the solutions associated with low Ca:Si ratio CSH systems (*i.e.* those which relatively contain the most silicate) in much the same way as brucite is predicted to do in the silica-poor systems typical of high Ca:Si CSH and portlandite. It seems probable, both from the calculations presented here and from the experimental evidence, that magnesium ions will readily react with cement mineral assemblages over a wide range of compositions. As a consequence, dissolved magnesium will undergo almost quantitative removal until the bulk of the cement minerals have reacted. The consequence of this is that in a service application where a continuous supply of magnesium ions is available, reactions to form brucite or sepiolite or both must be expected to occur.

Considering the molar volumes of the phases involved, a net porosity increase would be expected in both cases; around 40% for the conversion of tobermorite to sepiolite and 20% for the portlandite - brucite reaction. In addition to this physical effect, consideration must be given to the possibility of chemical passivation of the mineral surfaces of the cement phases in such a way that the ingress of magnesium causes an overgrowth of brucite on the portlandite, thus occluding it from the pore solution. If this effect should occur a reduction in pH from the 12-13 region of portlandite to 10 or below may be expected, typical of pore solutions whose pH is conditioned by brucite.

This argument is something of a simplification as, in reactions between cement minerals and magnesium sulphate, mineral zonation is seen to develop spontaneously. The experimental and predictive studies above show that although conversion of portlandite to brucite is shown to occur at very low aqueous magnesium concentrations, it is likely to be associated with formation of either gypsum or anhydrite. As a consequence, an expansive zone of gypsum/brucite or gypsum/anhydrite would be expected to form at the reaction sites. Whilst theoretical predictions of the *maximum* porosity changes possible in a given mineral assemblage are possible from a knowledge of the molar volumes involved, such estimates are only illustrative, as little is known of the spatial distribution of the nucleation sites.

6.6 Interaction of Groundwaters with Blended Cements

6.6.1 Introduction

A number of end-member groundwater chemistries are likely to be encountered. For the purposes of this study, two "representative" groundwaters have been selected. One is a

highly saline water mass of ionic strength in excess of 3 molal as shown by borehole 3, discrete extraction test 8 (BH3 det8, NIREX, [18]. Another is a brackish groundwater (approximately 0.5 molal, borehole 2, discrete extraction test 7 (BH2 det7)) which is also sodium chloride rich. These analyses have been selected for use in this study. In order to effectively simulate the interaction of these waters with the proposed repository materials, two studies have been undertaken. One, an experimental model of the system is discussed above and the second, a numerical simulation of the expected equilibrium chemistry, reported here.

The predictions of the probable cement hydrate mineral assemblages expected to form in the blended cements are shown in Section 6.3, above. Simulation of the equilibria between these phases and the groundwaters has been undertaken using the SIT implementation in PHREEQE along with the CSH solubility model described in Section 6.4.

First of all, corrections to the reported ground water chemistry were undertaken as follows. It is assumed that the groundwater at depth is saturated with respect to calcite and that upon extraction, a degree of degassing occurs which depletes the samples in carbon dioxide prior to analysis. To redress this each analytical groundwater composition was re-equilibrated with calcite which, in addition to returning the simulated solution to the carbon dioxide phase boundary, also increases the calcium content by a few percent.

As the subsequent simulations impose equilibria with calcium-bearing salts, this is thought not to be particularly crucial. Secondly, the uptake of sodium chloride by both CSH and portlandite has been shown in the experimental work to occur and consequently a simple correction according to both sodium and chloride was applied before the simulations were undertaken. Table 6.5 shows that at the ionic strengths of the two groundwaters considered, adjustment of NaCl by <2% is required for simulations involving CSH assemblages and 1% for the portlandite only system. In practice, as all the blended cements are expected to contain at least some CSH, this requires a universal reduction of NaCl by these small amounts. Using saline waters, the experimental depletions were not particularly significant for either Na or Cl and it is recognised that the corrections are close to the limits of measurement accuracy.

The analytical and adjusted solution chemistries are shown in table 6.36.

Table 6.36 Groundwater chemistry used in simulations.

	Water A = BH3 det8		Water B = BH2 det7	
	Analytical	Adjusted	Analytical	Adjusted
Ca (mol dm^{-3})	7.30 e-2	7.35 e-2	2.85 e-2	2.85 e-2
Mg (mol dm^{-3})	2.00 e-2	2.00 e-2	6.30 e-3	6.30 e-3
Na (mol dm^{-3})	2.83 e0	2.77 e0	3.71 e-1	3.71 e-1
K (mol dm^{-3})	1.40 e-2	1.40 e-2	3.90 e-3	3.90 e-3
Si (mol dm^{-3})	6.21 e-5	6.21 e-5	4.81 e-7	4.81 e-7
Cl (mol dm^{-3})	2.93 e0	2.87 e0	4.21 e-1	4.42 e-1
C (CO_3^{2-}) (mol dm^{-3})	-	7.60 e-4	-	1.55 e-3
S (SO_4^{2-}) (mol dm^{-3})	3.50 e-2	3.50 e-2	1.30 e-2	1.30 e-2
pH	6.47	7.31	<7.85	7.31
Eh(mV)	+72	-100	+90	-100

The last parameter which must be adjusted is the redox potential of the system which is reported to be positive but this is assumed to be due to aerial oxidation. The simulations were performed at Eh of -100mV, which represents a mildly reducing environment. As few species in the simulation are involved in strong redox couples, this is expected to make little practical difference to the system chemistry as calculated; no allowance has been made for waste components.

6.6.2 Ordinary Portland cement

Considering first, the ordinary Portland cement system, tables 6.2 and 6.3 show that the only difference in predicted mineral assemblage between the 25° and 85°C systems is the high temperature stability of AFm-SO_4 over that of ettringite. In order to examine the pore solution chemistry of OPC as a function of salinity, simulations were performed initially in pure water and subsequently in the two saline waters. The equations which describe the variation of dissociation constant and enthalpy shown in table 6.14 were used to calculate the logK and the enthalpies taken from table 6.17, extrapolated to 3 molal, to represent groundwater "A". The saturation state of the simulated solutions with respect to phases likely to precipitate is shown in table 6.37.

Table 6.37 Saturation state of OPC pore solutions at 25°C*.

Solution	Pure water	BH2 det7	BH3 det8
Approximate Ionic Strength (mol dm^{-3})	2 e-2	0.5	3.0
Oversaturated phases		AFm-Cl AFm-CO_3	AFm-Cl AFm-CO_3

* In this and subsequent tables, "det" = discrete extraction test

Convergence was not achieved for simulations at elevated temperatures, however, the low temperature calculations suggest that conversion of ettringite to chloro- and carbo- AFm phases is probable. This is seen in both the pure phase experiments and investigations of the blended cements. The simulated dissolution of OPC into pure water predicts the following solution chemistry:

Table 6.38 OPC pore solution chemistry predicted at 25 °C (all units are mol dm^{-3}).

Ca = 1.54 e-2	Al = 1.14 e-4	SO_4 = 1.01 e-6
Mg = 4.79 e-9	Si = 5.07 e-6	pH = 12.36

Table 6.38 predicts a pH which is slightly lower than might be expected for a Portland cement, which reflects the solubility of portlandite in the afwillite-portlandite model used to represent the $CSH_{1.8}$. The solubility of portlandite in this model is slightly lower than that of the true mineral and is associated with a predicted pH below that expected of this phase. Nonetheless the underestimate is slight (~0.1 pH units) and is subsequently ignored.

In the more saline solutions, equilibrium must be simulated between the OPC assemblage predicted in Section 6.3, with those phases shown during preliminary calculations to be oversaturated; the AFm-Cl and AFm-CO_3. The solution chemistry at equilibrium with these phases is shown in table 6.39.

Table 6.39 Solution chemistry predicted to be at equilibrium with both an OPC mineral hydrate assemblage and the AFm phases AFm-Cl and AFm-CO_3.

Element in solution / mol dm^{-3}	BH2 det7	BH3 det8
Ca	5.62 e-4	1.07 e-4
Mg	7.43 e-11	2.88 e-12
Na	3.63 e-1	2.77 e0
K	3.9 e-3	1.40 e-2
Al	1.54 e-3	1.15 e-2
Si	3.23 e-4	2.23 e-1
Cl	2.74 e-2	1.95 e-1
C (CO_3^{2-})	4.42 e-2	6.51 e-5
S (SO_4^{2-})	2.35 e-4	6.19 e-2
pH	13.40	14.01

It can be seen that rather large amounts of aluminium are predicted to be released into solution as hydrogarnet dissolves to maintain equilibrium with the two substituted AFm phases. There is a similar increase in dissolved silicate in these predictions although these effects are probably overestimated by this model; predictions should be treated with care. As a consequence, the silicate minerals shown to be oversaturated on establishing this new equilibrium (gehlenite hydrate and siliceous hydrogarnets) are not considered as likely to precipitate.

6.6.3 Portland - blast furnace slag blended cement

The Portland - blast furnace slag blends by comparison, contrast with the pure Portland cements in that they show lower predicted pH values and are expected to yield considerably less aluminium to solution. As with previous calculations, the relatively complex mineral assemblage representing the BFS-OPC blend limits the permutations which result in a converged calculation using this method and prevent simulation of the high temperature saline conditions. For the case of BFS-OPC at equilibrium with water, the assemblage predicted by CEMCHEM, when examined by PHREEQE-SIT, suggests that gehlenite hydrate would precipitate from the pore solution. Re-equilibration of the OPC-BFS assemblage with gehlenite hydrate has little influence on the predicted chemistry of the system and the two solutions (before and after equilibration with gehlenite hydrate) are compared in table 6.40. This suggests that the OPC-BFS assemblage at equilibrium with water lies close to the gehlenite hydrate phase boundary. That is to say, if this phase is stable, it is expected only to be marginally so.

Table 6.40 Comparison of pore solution chemistry of BFS_{75} : OPC_{25} blend in pure water with and without gehlenite hydrate in the assemblage.

Element in solution / mol dm^{-3}	BFS assemblage only	BFS assemblage and C_2ASH_8
Ca	1.28 e-2	9.08 e-3
Mg	1.42 e-8	1.71 e-8
Al	1.96 e-5	2.78 e-5
Si	8.40 e-6	1.96 e-5
S (SO_4^{2-})	4.89 e-6	7.75 e-6
pH	12.28	12.15

Similarly, examination of the results of this system in saline conditions suggests that both the AFm-CO_3 and AFm-Cl are oversaturated at equilibrium. Simulating the solution chemistry for the OPC-BFS assemblage with AFm-CO_3 and AFm-Cl for the lower ionic strength groundwater predicts the solution chemistry at equilibrium shown in table 6.41, although both the chloride and carbonate predictions are lower than might be expected from the experimental results.

Table 6.41 Pore solution chemistry of BFS_{75} : OPC_{25} blend at equilibrium with AFm-CO_3 and AFm-Cl in BH2 det7 groundwater (all units are mol dm^{-3}).

Ca = 8.53 e-4	Si = 2.73 e-4
Mg = 8.95 e-10	Cl = 2.47 e-4
Na = 3.63 e-1	C (CO_3^{2-}) = 3.76 e-5
K = 3.9 e-3	S (SO_4^{2-}) = 5.56 e-4
Al = 1.74 e-4	pH = 12.22

It is well known that the presence of sparingly soluble hydrotalcite (M_4AH_{10}) in slag and Portland cements governs the availability of magnesium in solution. Although attack by magnesium ions has been demonstrated both experimentally and numerically in previous sections it would appear that for systems in which abundant aluminium is present hydrotalcite plays a major role in partitioning magnesium into the solid phase.

6.6.4 Portland - pulverised fuel ash blended cement

The second blended system studied is that of 40% Portland - 60% pulverised fuel ash (PFA) cement. This is considerably richer in silica than those above as is shown in tables 6.1 to 6.3 and is characterised by the formation of zeolite phases. The experimental studies of this blended material shows strong evidence for phillipsite and possibly thompsonite, yet in the CEMCHEM model, the phases included in the PFA assemblages are the calcium and sodium zeolite-P. Preliminary examination of the blend by modelling reveals that when PFA-OPC equilibrates with water, the mineral assemblage is sufficiently siliceous and magnesium-rich to leave the pore solution oversaturated with sepiolite.

As has already been noted, the threshold concentration of magnesium for both sepiolite and brucite precipitation is very low (tens of nanomolar) and in this material the small quantities of magnesium dissolved from the hydrotalcite seem sufficient to cross the sepiolite phase boundary. It was noted in Section 6.3 that the model used to represent the $CSH_{0.85}$ (which is typical of fly ash blends) somewhat overestimates the dissolved silicate concentration. Nonetheless at both 25° and 55°C equilibration of the fly ash assemblage with sepiolite in water additionally leaves the system oversaturated with respect to brucite. Unfortunately, at these two temperatures (25° and 55°C), equilibrium can only be established between this assemblage and one of the two magnesium-bearing phases whilst the initial speciation calculations suggest both are oversaturated. As would be expected, the presence of brucite reduces the pH considerably, from over pH 12 to below pH 10. However, this effect is expected to be minor as the total available magnesium content of the blend is small (equivalent to ~2.5 mol% M_4AH_{10}, see table 6.3C). Geological evidence suggests that sepiolite, whilst abundant in sea-floor rock weathering, is itself metastable with respect to talc.

At higher salinities, the model only converged for simulations at 25°C. As might be expected from previous calculations, the presence of chloride and soluble carbonate from the groundwater carbonate, show that pore solutions from the fly ash blend are likely to precipitate both AFm-CO_3 and AFm-Cl. Re-equilibration of the Portland-fly ash cement hydrate assemblage with both AFm-Cl and AFm-CO_3 predicts the following solution chemistry; table 6.42.

Table 6.42 Solution chemistry predicted to be at equilibrium with a PFA-OPC assemblage with AFm-Cl and AFm-CO_3 in two groundwaters at 25°C.

Element in solution / mol dm^{-3}	BH2 det7	BH3 det8
Ca	4.79 e-4	9.71 e-5
Mg	5.20 e-11	2.58 e-12
Na	3.63 e-1	2.77 e0
K	3.9 e-3	1.40 e-2
Al	3.14 e-3	1.81 e-2
Si	3.53 e-4	3.05 e-4
Cl	1.84 e-2	1.49 e-1
C (CO_3^{2-})	2.01 e-3	3.85 e-5
S (SO_4^{2-})	2.02 e-4	5.28 e-2
pH	13.41	14.18

6.6.5 Reference backfill

Lastly, the same approach was applied to the backfill, which in terms of modelling, is an identical phase assemblage to OPC but with the addition of calcite with which to represent the limestone flour. As in the OPC calculations, the backfill shows oversaturation with gehlenite hydrate (unlikely) and with AFm-Cl and in the saline waters, AFm-CO_3 phases, but as the mineral assemblage contains calcite the AFm-CO_3 is ubiquitous, whereas AFm-Cl is only stable in the saline solutions.

Although predicted to be oversaturated, equilibrium cannot be reached by simply adding the AFm and/or the gehlenite hydrate to the backfill hydrate assemblage without violating the Gibbs phase rule or the code failing to converge on a unique solution. To circumvent this, the mineral hydrate assemblage must be simplified, reducing the number of components to include only those which will dominate the chemical conditioning of the backfill. Considering first the aluminium-bearing hydrates, hydrotalcite, hydrogarnet and (depending on the temperature) AFt-SO_4 and AFm-SO_4. These comprise a small fraction of the total backfill composition and whilst they are important sinks for magnesium and chloride ions in the solid phase, their capacity is limited due to the small amount of aluminium in the backfill. All the aluminates comprise a combined total of only 1.8 mole-percent and so, for the purposes of the next calculations, have been ignored. The remainder of the backfill (in increasing molar ratio) comprises CSH, $Ca(OH)_2$ and $CaCO_3$, together totalling over 98 mole percent.

For purposes of thermodynamic modelling, the CSH is considered to contain some portlandite, representing the calcium-rich structural units, along with afwillite, which represents the silicate-bearing domains. For these reasons, the bulk chemistry has been represented by calcite and portlandite which together will be responsible for most of the chemical conditioning effects of the barrier. To a first approximation this is acceptable as

portlandite is the most soluble phase in the backfill mineral assemblage.

Considering next the interaction of these two minerals with pure water and the two groundwaters, we might rightly expect to see dissolution of both phases in the pure water conditioning the pH to ~12.5, but precipitation of some calcite after equilibrium with the groundwaters, owing to the combination of the relatively high solubility of portlandite and the carbonate initially in solution. In addition, a simple speciation calculation shows that for each of the two groundwaters, brucite is considerably oversaturated with respect to the solution. Equilibration of portlandite, calcite and brucite with each of the solutions will simulate a first and presumably long-lived chemical environment to be established as groundwater permeates through the backfill.

Table 6.43 illustrates the conditions likely to prevail once this chemistry is established.

Table 6.43 The initial chemical environment established in the backfill following groundwater ingress.

	Mass transfer in or out of solution to establish equilibrium at 25°C Moles of solid per kg solution. Positive value = dissolution		
	Pure water	BH2 det7 water	BH3 det8 water
Mineral phases at equilibrium	Brucite = 1.26 e-8 Portlandite = 2.07 e-2 Calcite = 1.19 e-5	Brucite = -6.30 e-3 Portlandite = 2.90 e-2 Calcite = -1.54 e-3	Brucite = -1.99 e-2 Portlandite = 3.76 e-2 Calcite = -7.46 e-4
Ca (mol dm^{-3})	2.06 e-2	5.60 e-2	1.11 e-1
Mg (mol dm^{-3})	1.26 e-8	3.74 e-8	5.83 e-8
Na (mol dm^{-3})		3.63 e-1	2.77 e0
K (mol dm^{-3})		3.90 e-3	1.40 e-2
Si (mol dm^{-3})		4.81 e-7	6.21 e-5
Cl (mol dm^{-3})		4.33 e-1	2.87 e0
C (CO_3^{2-}) (mol dm^{-3})	1.19 e-5	1.29 e-5	1.30 e-5
S (SO_4^{2-}) (mol dm^{-3})		1.30 e-2	3.30 e-2
pH	12.47	12.39	12.26

The table (6.43) above clearly shows that portlandite is expected to dissolve, thus buffering the system to a pH between 12.2 and 12.5. As the backfill is expected to contain over 30 wt% $Ca(OH)_2$ (around 15% in the initial mix with a similar amount provided by the OPC component) this phase will contribute a large proportion of the system alkalinity.

Assuming that the bulk density of the backfill is around 2.0 kg dm^{-3}, then each cubic metre of backfill will contain 600 kg $Ca(OH)_2$, equivalent to 8097 mol m^{-3} of portlandite. If we consider the mass transfer of portlandite shown in table 6.43 and assume a 40% porosity, a similar type of scoping calculation as was illustrated in Section 5 may be undertaken. This suggests that for a cubic metre of backfill percolated by pure water, some 978 exchanges of pore solution are required to deplete the system of portlandite and reduce the pH below 12.4. Similarly, for the two groundwaters, somewhat smaller numbers of solution exchanges are required; 698 for BH2 det7 and 538 for BH3 det8 which compare favourably with the estimates calculated in Section 5.

If we assume homogeneous porosity distribution, uniform flow and no restriction on pore solution movement from precipitates, a knowledge of the groundwater flow rates allows a

simple estimate to be made of the longevity of the alkaline conditions due to portlandite buffering. In the case of pure water reacting with portlandite in the backfill, this is around 3.9 million years whereas the two groundwaters BH2 det7 and BH3 det8, are predicted to maintain pH > 12.2 for 2.8 and 2.1 million years for respectively.

These scoping calculations, although illustrative of relative potential performance do not consider either kinetic or geometric effects which may be crucial in determining the performance of repository materials in service. For example, whilst both thermodynamic calculations and experimental observation show that the base exchange conversion of portlandite to brucite and associated precipitation of gypsum is very likely for reactions involving these groundwaters, the persistence of an alkaline environment may be determined by other factors. The dissolution of portlandite and precipitation of brucite may result in the overgrowth of a protective brucite layer occluding the portlandite from the solution. If this occurred extensively, the solution may be buffered by brucite, despite there still being unreacted portlandite remaining in the system. This type of uncertainty cannot readily be addressed by existing modelling tools and illustrate the need to treat scoping calculations with care. Nevertheless, it would be a reasonable first approximation to say the backfill has the potential to maintain an alkaline environment (>12.2) in excess of two million years.

Eventually, when the portlandite reserve (and calcium-rich units in the CSH) have been depleted, the solution will be conditioned by brucite and calcite only. Under these conditions the brucite would be expected to re-dissolve, itself acting as the dominant buffer in saline conditions. Calcite is predicted to precipitate under these conditions, suggesting that its contribution to the buffering reserve will be most important following dissolution of the brucite. Table 6.44 illustrates the chemistry likely to prevail under these conditions and shows the quantities of brucite dissolution and calcite precipitation predicted necessary to maintain equilibrium with 1dm^{-3} of solution. This suggests that the mass transfer per unit volume of solution is somewhat smaller for the most saline solution, which intuitively seems reasonable.

Table 6.44 The second chemical environment established in the backfill following groundwater ingress.

	Mass transfer in or out of solution to establish equilibrium at 25°C Moles of solid per kg solution.		
	Pure water	BH2 det7 water	BH3 det8 water
Mineral phases at equilibrium	Positive value = dissolution, negative value = precipitation		
	Brucite = 1.04 e-4	Brucite = 9.03 e-4	Brucite = 4.47 e-4
	Calcite = 1.8 e-4	Calcite = -1.53 e-3	Calcite = -7.46 e-4
Ca (mol dm^{-3})	1.18 e-4	2.70 e-2	7.30 e-2
Mg (mol dm^{-3})	1.02 e-4	7.20 e-3	2.04 e-2
Na (mol dm^{-3})		3.63 e-1	2.77 e0
K (mol dm^{-3})		3.90 e-3	1.40 e-2
Si (mol dm^{-3})		4.81 e-7	6.21 e-5
Cl (mol dm^{-3})		4.33 e-1	2.87 e0
C (CO_3^{2-}) (mol dm^{-3})	1.18 e-5	2.07 e-5	1.99 e-5
S (SO_4^{2-}) (mol dm^{-3})		1.30 e-2	3.50 e-2
pH	10.3	9.75	9.49

This represents a considerable change in the buffered pH of the system, which will undoubtedly change the solubility and sorption characteristics of mobile species in the repository. The base exchange reaction, altering portlandite to brucite, is also associated with a change in molar volume, resulting in an increase in porosity of approximately 25%. Given that the portlandite comprises over 30 mole percent of the backfill, a bulk porosity increase of the order of 10% may be expected.

The increase in porosity and reduction in pH are likely to have long-ranging consequences on the performance of the backfill in service. Greater groundwater mobility through enhancements to the pore system are to be expected as is an increase in solubility of transuranic elements due to the reduction in pH.

6.7 Groundwater Reactions With Repository Host Materials

6.7.1 Introduction

The modelling discussed thus far has investigated the likely chemistry of porewaters in equilibrium with backfill materials, and also the interaction of simple solutions and groundwaters with backfill materials. By calibrating and testing the predictions against laboratory data it has been possible to establish, with a reasonable degree of confidence, the capabilities and limitations of the models.

Modelling in the previous section considered dominant mineral reactions caused by groundwater attack of the backfill demonstrated the replacement of portlandite by brucite to be a potentially important processes. However, although the solubility modelling can be used to investigate resultant chemistries following complete equilibration of backfill with groundwaters, it provides no information on the gradual progression of groundwater attack. This is investigated in the following section using two complementary approaches. First, end-member pore solutions have been mixed over a range of mixing ratios in simple "mixing models" in PHREEQE and supersaturated phases predicted. These simple models have then been used to identify the critical reactions for inclusion in coupled chemical transport models which can be used to evaluate the time and space frame of groundwater attack.

6.7.2 Mixing calculations

Introduction

Mixing calculations represent a useful first step in investigating the effects of groundwater attack on backfill. The approach involves the mixing of backfill-equilibrated porewater with groundwaters in varying proportions, in a geochemical model. Simple "mixing tank" calculations do not include space or time dimensions. However, the results provide a basis from which to select key chemical reactions for more detailed coupled chemical transport modelling.

Mixing calculations were carried out using PHREEQE 96 [19], which includes the SIT ionic strength correction module, in conjunction with the CEMENTS3 thermodynamic database (Section 6.2). Six different groundwater attack scenarios were selected for modelling: three

temperature conditions were specified, 25°C, 55°C and 85°C; at each of these temperatures, single backfill porewater was defined by equilibrating pure water with six principle cement minerals (M_4AH_{10}, AFt, C_3AH_6, $Ca(OH)_2$, CaH_2SiO_4, and $CaCO_3$). This was then mixed with one of two Sellafield groundwaters which equilibrated with calcite prior to mixing. The selected groundwaters were BH2 det8, having an ionic strength (after calcite equilibration) of 0.5 and the more saline BH3 det7, having a post calcite-equilibrated ionic strength of 3.1.

As one would expect, the chemistries of backfill porewaters contrast strongly with the groundwater analyses selected (table 6.45). Note that in reality the backfill porewater will contain Cl, Na and K as a result of reaction with cement minerals. However, the six idealised cement minerals selected here for equilibration do not contain these elements; they are consequently not present in the simulated backfill porewater.

Table 6.45 Groundwater and backfill porewater chemistries used in simulations.

	BH3 det8 (Adjusted)	BH2 det7 (Adjusted)	Backfill Porewater
Ca	7.35 e-2	2.85 e-2	1.83 e-2
Mg	2.00 e-2	6.30 e-3	6.19 e-10
Na	2.77 e0	3.71 e-1	
K	1.40 e-2	3.90 e-3	
Si	6.21 e-5	4.81 e-7	1.35 e-4
Cl	2.87 e0	4.42 e-1	
C (CO_3^{2-})	7.60 e-4	1.55 e-3	1.23 e-5
S (SO_4^{2-})	3.50 e-2	1.30 e-2	4.17 e-6
pH	7.31	7.31	12.42
Eh (mV)	-100	-100	-100

Results

Six different groundwater attack scenarios were simulated: for each of three temperature conditions, 25° C, 55° C and 85° C, backfill porewater was mixed separately with BH2 det8 and BH3 det7. figures 6.12 and 6.13 indicate that the two different groundwaters give rise to similar mixing products with the backfill porewaters, but that temperature exerts a strong control on speciation and solubility.

In more detail, the results indicate the following:

i) for all scenarios, brucite is undersaturated or close to saturation in the two end-member waters, but is prone to precipitation over the entire mixing zone;

ii) for all scenarios, supersaturation with respect to calcite and dolomite occurs, particularly at the groundwater-rich end of the mixing spectrum;

iii) at 25°C monochloroaluminate and monocarboaluminate are supersaturated at the backfill-rich end of the mixing spectrum;

iv) at 55°C supersaturation is dominated by brucite;

v) at 85°C a number of additional supersaturates are present including kaolinite, tobermorite, and calcium and sodium zeolite phases.

Implications

The results give an overview of likely precipitation reactions in the groundwater/backfill porewater mixing zone over a range of conditions. They also provide an indication of the profile of mineral supersaturation across the mixing zone. A number of the mineral phases are likely be relatively unimportant in volumetric terms. For example, aluminium-bearing phases are likely to be minor in mediating the physico-chemical evolution of the backfill because of the low concentrations of aluminium in both the backfill porewater and groundwaters. The potential for precipitation of zeolite phases is uncertain. If these zeolite phases form and persist they will modify the sorption characteristics of the backfill and also the microfabric and permeability of the evolving backfill and thus influence long term performance.

Compared with the reactions described above, the effect of replacement of portlandite by brucite is predicted to be more significant. There are two aspects to consider. First, as discussed in Section 6.5.5, this transformation is accompanied by a reduction in molar volume and consequent increase in bulk porosity. Secondly, since portlandite is responsible for the buffering of pH, to a value of approximately 12.4 in the backfill, its depletion and replacement by brucite, which buffers pH to a lower value of approximately 9.8, is potentially one of the most important aspects of the degradation and long term performance of the backfill. This was investigated further using coupled chemical transport models.

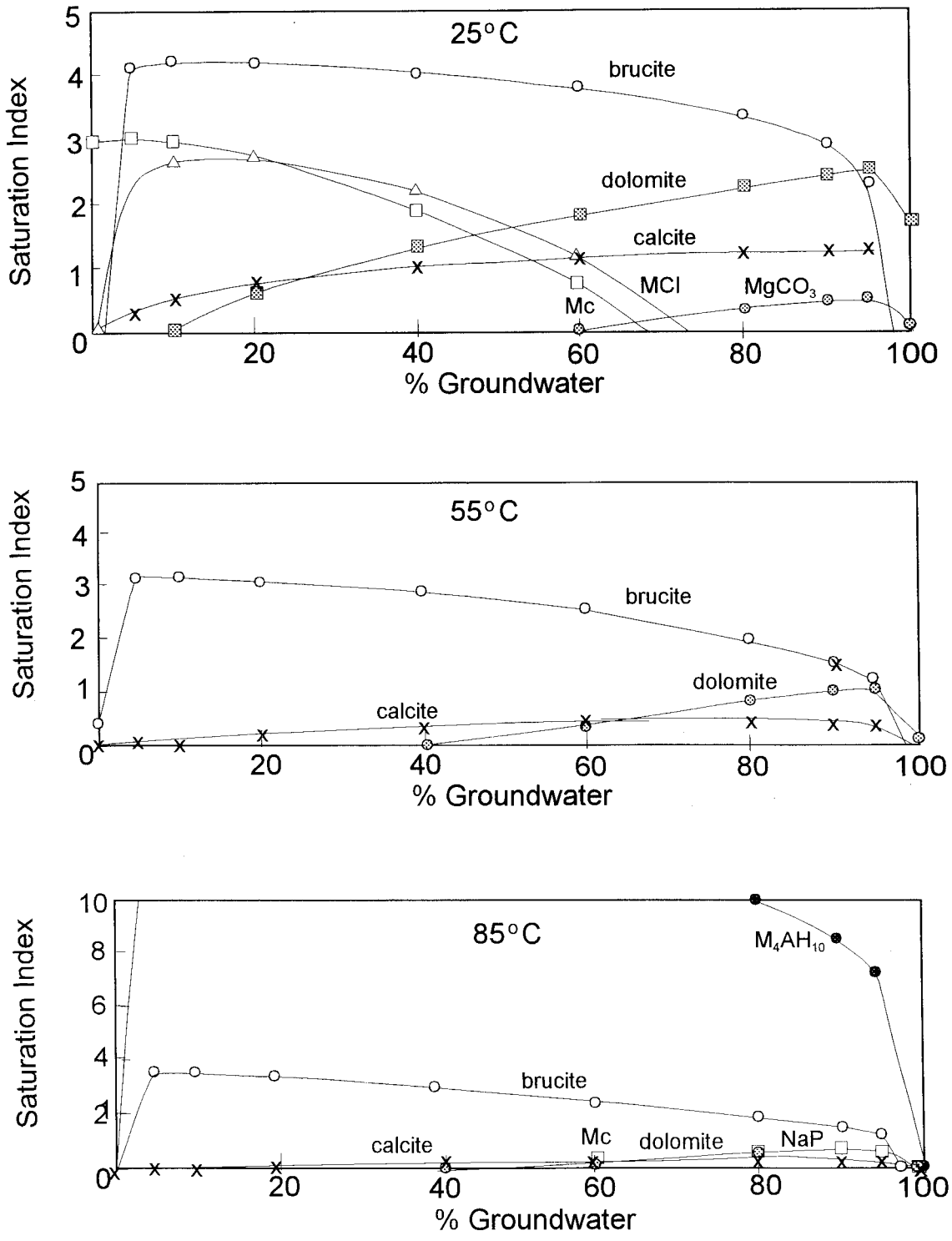

Figure 6.12 **Results of mixing calculations for backfill porewater with borehole 3 det. 8 groundwater. Symbols: brucite, O; dolomite,. ▨; calcite, X; Friedel's salt (MCℓ), Δ; calcium monocarboaluminate, □ and $MgCO_3$, ⊗.**

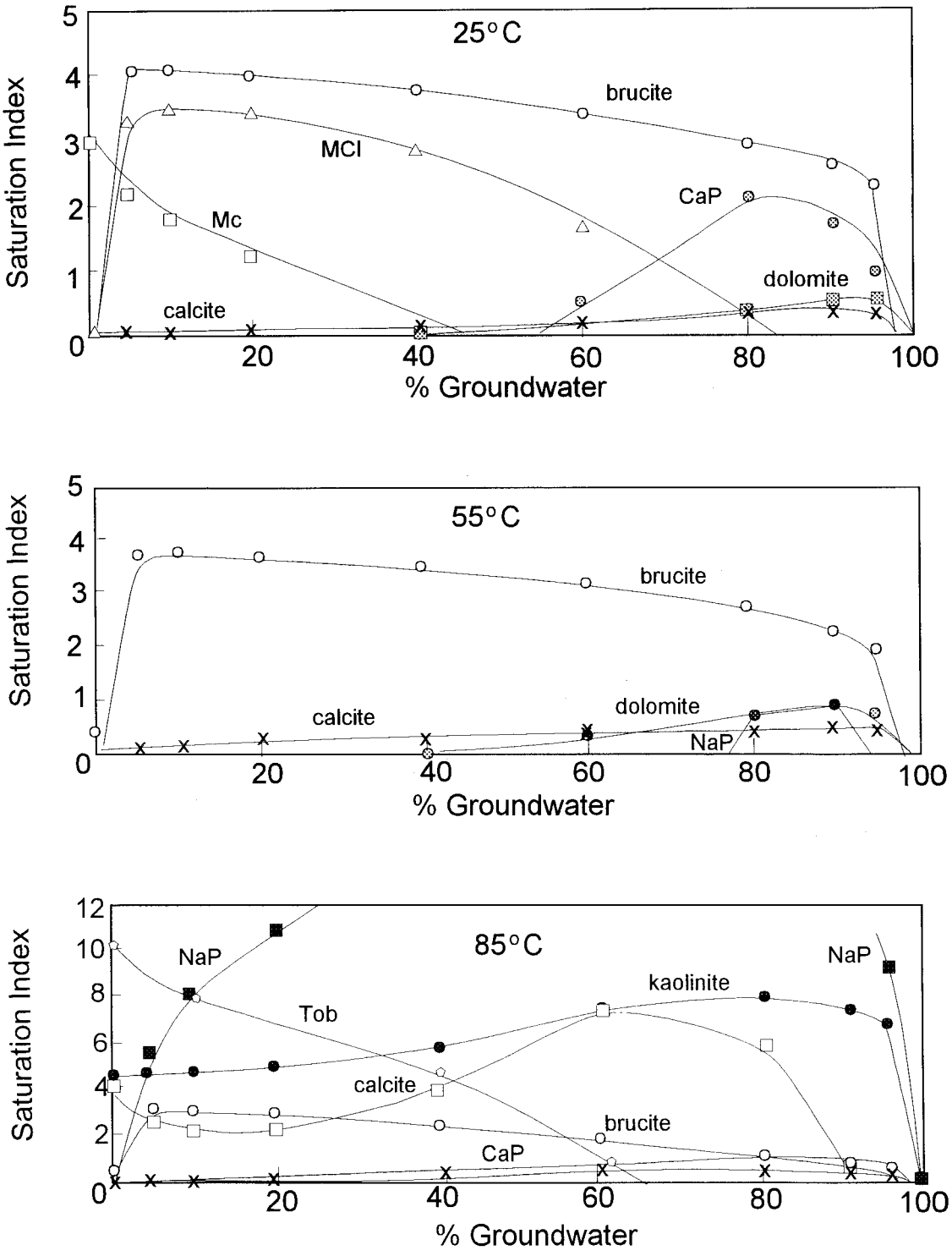

Figure 6.13 Results of mixing calculations for backfill porewater with borehole 2 det. 7 groundwater.

6.7.3 Coupled Chemical Transport Modelling

Introduction

In order to evaluate the long term performance of cementitious barriers it is necessary to investigate the likely time and space frames of degradation processes and ultimately of radionuclide egress. Since the time scales of concern are far greater than those of experimental studies, extrapolation using numerical models will inevitably form an important component of performance assessment studies.

The development of coupled chemical transport models for performance assessment has, in the past, focused on the representation of contaminant transport processes. HMIP's Quality Assured one-dimensional chemical transport code CHEMTARD [10] has been adopted as a benchmark code in international code intercomparison exercises [8] and has extensively tested against experimental data. However, although CHEMTARD code has been tested over a wide range of conditions relevant to radionuclide migration, its capability to represent barrier degradation has not been investigated.

Approach and model selection

In defining the approach to coupled chemical transport modelling of barrier performance, several factors were taken into consideration, in particular:

i) the need to represent mineral dissolution and precipitation along a flow path;

ii) the need to represent high ionic strength effects;

iii) the numerical robustness of the model.

Given the potential importance of high salinity groundwaters in potential repository zones, the inclusion of a high ionic strength capability in coupled transport calculations was considered a worthwhile objective. The groundwork for this development had been established through first, the development of the a PHREEQE-compatible SIT database under CHEMVAL II [20], and secondly, the development of the PHREEQE-compatible iterative transport code CHEMNET [21]. The development of an SIT capability within CHEMTARD remains a possibility but was beyond the scope of this project.

In determining the scope of coupled chemical transport modelling, the effect of magnesium ingress and the consequent dissolution of portlandite and precipitation of brucite were prioritised for study, for the reasons set out in Section 6.6. More specifically, it was intended to equilibrate the inflowing groundwater with calcite and portlandite along the modelled flow path and to model pH evolution. Because it was not specifically developed to represent barrier degradation processes, the CHEMTARD code only permits equilibration with one mineral phase, and only at the inflow point, not along the entire flow path.

Within the scope of this project, the relatively minor developments required of the CHEMNET code were considered to be represent the most efficient approach to achieve

both a high ionic strength capability and a flexible representation of leaching processes. Therefore, although the additional capabilities of CHEMTARD are important with regard to radionuclide migration calculations, the CHEMNET code was selected in preference to CHEMTARD to carry out degradation modelling. Capabilities of the CHEMTARD and CHEMNET codes are compared in table 6.46.

Table 6.46 Comparison of CHEMTARD and CHEMNET codes.

Aspect of Modelling	CHEMTARD	CHEMNET
Coupling Strategy	Direct	Sequential iterative
Source of Thermodynamic Data	User specified	Any PHREEQUE-compatible code
Leaching	1 mineral, first grid node only	Multiple minerals along grid
Precipitation	Along grid	Along grid
Ionic Strength	Low ionic strength	SIT compatible

Two end-member conceptual models regarding the availability of $Ca(OH)_2$, the critical active component of the backfill, were investigated. In the first, equilibrium with calcite and portlandite was imposed along the flow path, implying an inexhaustible source of these phases to mediate in chemical reactions. In the second, no equilibrium was maintained. Brucite precipitation was included in both models. The reality is likely to lie between these end members. Assuming brucite precipitation occurs on the active portlandite component, this component will gradually become isolated from porewaters by skin effects arising from the authigenic brucite. This intermediate case was not specifically addressed. However, by simulating of the two end members, capability of CHEMNET to simulate degradation processes was investigated and, moreover, the results indicate the wide potential for pH modification in the backfill porewater. Simulations were carried out using a porewater velocity of $1x10^{-4}$ m y^{-1} over a time scale of 100,000 years.

Results

Successful simulations were achieved for both conceptual models. For the model without calcite and portlandite leaching, the magnesium-rich groundwaters penetrate conservatively into the backfill. Magnesium concentrations close to those in the groundwater occur through the first six metres of the backfill, beyond which concentrations drop off (to 50 % of the inflow concentration by a distance of ten metres) (figure 6.14). This non-leaching case equates to conservative transport. By contrast, if OH- ions are available from portlandite dissolution, brucite precipitation in the first modelled grid cell prevents penetration of magnesium further into the backfill, even after 100,000 years.

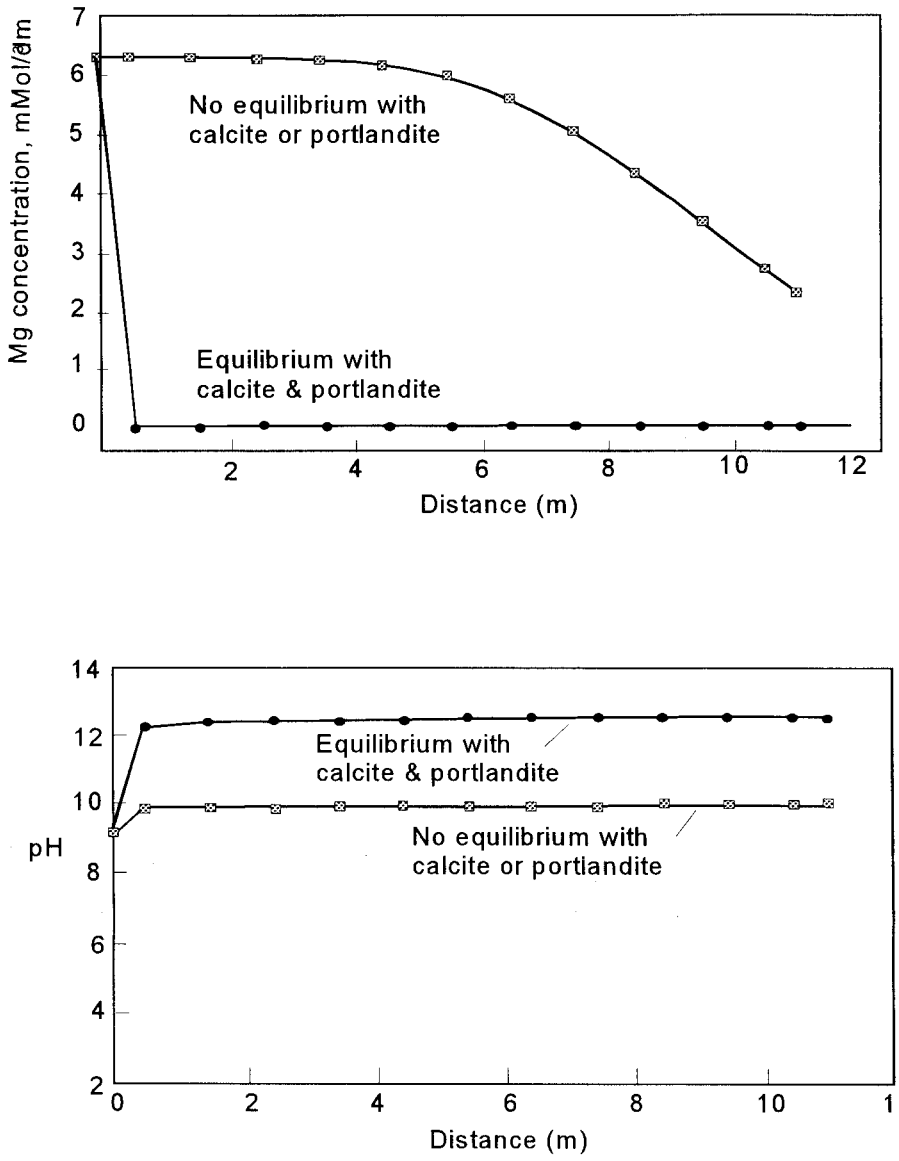

Figure 6.14 Distance profiles for magnesium concentration and pH after 100,000 years.

A similarly profound effect is noted for pH evolution. For the model without calcite or portlandite leaching, pH is buffered to equilibrium with brucite (pH 9.8) beyond the first grid cell. By contrast, where calcite and portlandite leaching are permitted, equilibrium with portlandite buffers the pH to 12.4 (figure 6.14)

Discussion and recommendations for model development

The inhibition of contaminant release by cementitious barriers relies upon chemical conditioning to high pH in conjunction with low hydraulic conductivity. In models that purport to represent long term contaminant transport through such barriers, the evolution of both of these factors must be adequately represented.

With regard to chemical evolution, the results above indicate that the availability of portlandite is critical in conditioning the pH evolution. The two end member conceptual models presented above are extreme. In the first case, portlandite is not available for reaction along the flow path. Clearly this is an inadequate representation of the behaviour of the barrier and inclusion of leaching along the flow path is considered essential if chemical transport models are to be used to simulate barrier degradation. The current EA Quality Assured code, CHEMTARD, does not include this facility and it is recommended that either CHEMTARD is developed to include this facility or that an alternative code, such as the CHEMNET code used above, is adopted for this purpose. Given the likely restriction in numerical flexibility arising from a simplified SIT correction procedure in CHEMTARD, the latter option is recommended.

In the second conceptual model, equilibrium with calcite and portlandite is imposed at all grid nodes. In standard thermodynamic codes, the imposition of equilibrium with a mineral phase is taken to imply an inexhaustible supply of the mineral. This explains why, in the "equilibrium case" model above, the chemical effects of groundwater attack are limited to the first grid cell of the simulation. In order to improve representation of the evolution of chemical buffering the availability of portlandite, the key active component, must be limited to the mass available within the grid cell. In this way, a more realistic simulation of degradation of the chemical performance of the barrier will become feasible. From this foundation, scoping calculations that include variable availability of portlandite due to skin effects may be developed.

In summary, adequate representation of mineral dissolution is essential if chemical transport models are to be used to assess the long term performance of cementitious barriers. The development code CHEMNET, or an alternative public domain iteratively coupled code, such as PHREEQ C, [18b] is recommended for this purpose as such codes are less susceptible to the numerical restrictions of directly coupled codes such as CHEMTARD. The two key aspects of dissolution that require representation are: mineral leaching along the flow path and restriction of mineral availability to the mass available within the grid cell.

6.8 Discussion of Modelling Near Field Processes

6.8.1 Existing Near Field Model.

Radionuclide releases from the near-field are currently represented in the VANDAL performance assessment code [22]. The near-field model *sensu stricto* in VANDAL comprises only the containerised waste form; the repository structure and buffer material being represented in the far-field model. Given the focus of this project on cement and backfill, however, representation of the buffer material is considered here. Representation of the near-field model in VANDAL is simple but flexible, with different nearfield environments being represented by varying the values of relatively few parameters (figure 6.15).

The approach to prediction of radionuclide releases currently includes the following components:

1) failure of the engineered barrier (loss of waterproof integrity), specified as a start time and a time required for saturation;

2) container failure, based on a corrosion concept, specified as a corrosion rate and wall thickness;

3) concentration of radionuclides in the waste form based on a decay-corrected inventory, modified by losses due to diffusion and mass flow and corrected for sorption onto the conditioning matrix.

Progress made in this project relates particularly to the third of these components, which is discussed in more detail below.

The average liquid phase concentration of a radionuclide within the condition and packaged wasteform is given as:

$$C_l^i = \frac{I^i(t)}{V_d \bullet \varepsilon_m \bullet \left[1 + f_v \bullet \rho_m \frac{(1-\varepsilon_m)}{\varepsilon_m} \bullet K_d^i(t)\right]} \qquad \{6.11\}$$

where:

$I^i(t)$ is the time varying inventory of nuclide I

V_d is the volume of containers in the repository

f_v is the fraction of the waste on which sorption occurs

ε_m is the total porosity of the waste matrix

ρ_m is the grain density of the waste matrix and

$K_d^i(t)$ is the equilibrium distribution coefficient for nuclide i at time t

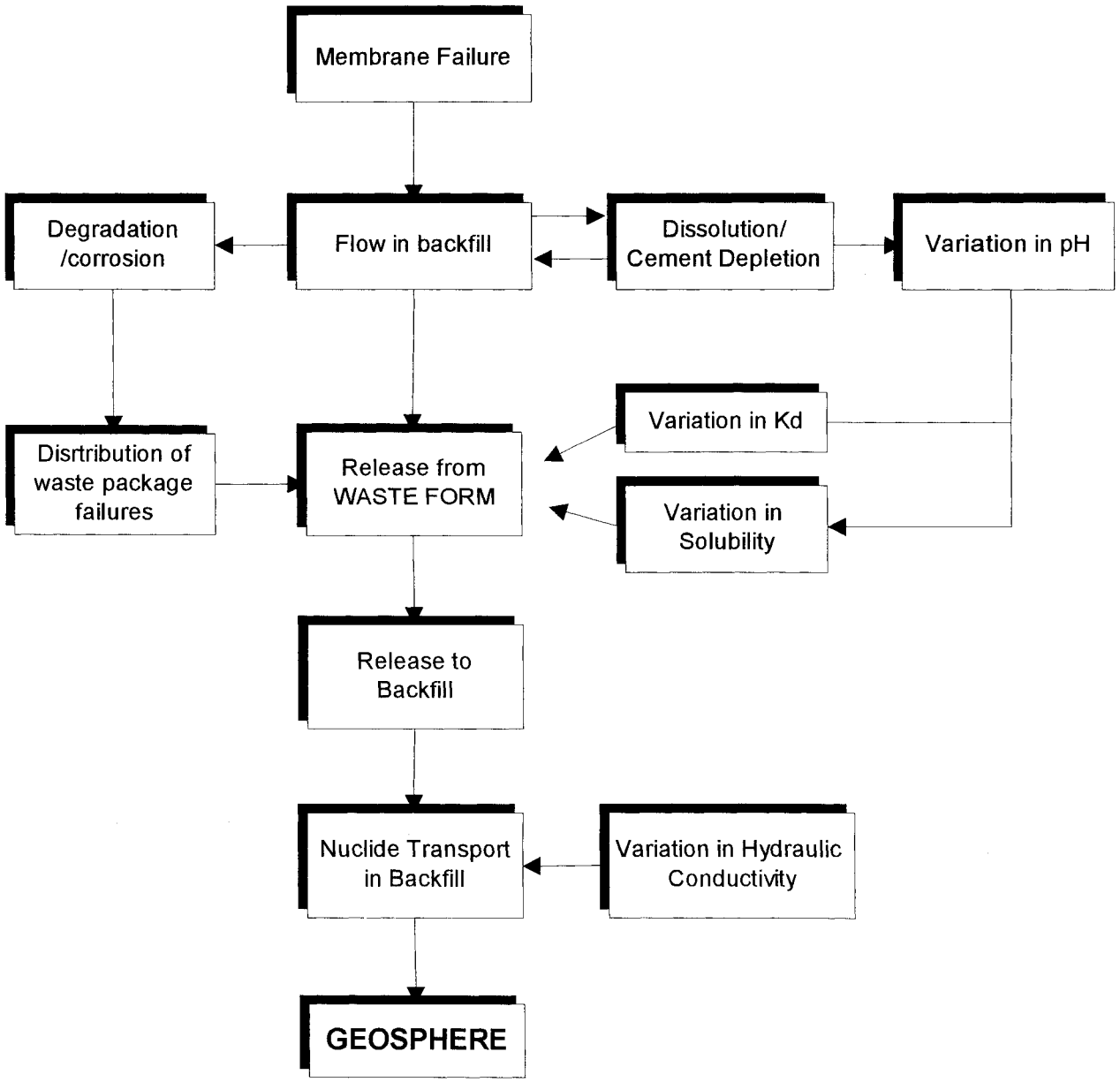

Figure 6.15 Schematic description of current near field model

The Kd dependence of this equation can, in effect, be varied by altering fv and Kd. This allows the physicochemical behaviour of different wasteforms to be represented. Important factors in defining the aqueous phase concentrations are as follows:

1) If the liquid phase concentration is higher than the solubility limit, then the latter is used to define liquid phase concentrations;

2) Both Kd and solubility may be represented as pH dependent properties;

3) Sorption is represented by two Kds, one for high pH and one for low pHs, with a changeover pH being specified

4) The time to depletion of pH-buffering is calculated by an equation including mass of concrete in the vault and the rate of loss of cement;

5) pH before, during and after pH-buffering is specified by the user.

Finally, in describing the current status of the near-field model, the representation of radionuclide transport should be considered. In VANDAL, radionuclide release is represented by two physical processes: diffusion and advection. Diffusive flux is calculated as the sum of the concentration differential, a wasteform-dependent leach rate and a time varying surface area for release. Advective flux is calculated as the sum of the liquid phase concentration, the Darcy velocity and time varying cross sectional area. The total activity flux is then calculated as the sum of the diffusive and advective fluxes.

6.8.2 Key areas of uncertainty

In view of the description of the current near-field model above, and based upon the developments made in this project, a number of important uncertainties regarding near-field interactions can be identified:

1) Prediction of radionuclide solubility and Kds in the near-field requires an adequate method for activity correction in high ionic strength solutions - the current SIT model represents an important step forward, but requires further calibration and testing.

2) Sensitivity studies disclose that different solids vary in their ability to buffer pH. Studies have also demonstrated the likelihood that portlandite (which buffers pH to 12.5) will be gradually replaced by brucite (which buffers pH to 9.8) as a consequence of groundwater attack. Further investigation into the pH evolution of the repository is considered a priority, particularly as the pH-dependence of radionuclide solubilities and Kds is likely to remain an explicit function in future versions of VANDAL or its successor.

3) Studies into volume changes arising from groundwater attack demonstrate the possibility of porosity creation as a result of mineral replacements (eg replacement of portlandite by brucite causes an increase in porosity of approximately 25%). Further

studies into this effect are warranted, and if found to be significant, it would be necessary to define time-dependent hydraulic conductivity relationships in order to adequately represent advective radionuclide fluxes.

4) Volume change studies also indicate that cracks may develop in backfill material as a result of groundwater attack. This may give rise to channelled flow, in which case large masses of backfill may become isolated. If further investigation suggests that this process is important, it may be appropriate to represent the backfill volume as an "effective" rather than a "total" volume.

5) The focus of this study has been the representation of groundwater attack rather than radionuclide escape. Future studies should aim to enhance the representation of radionuclide transport in the near-field. In particular, recent research into radionuclide sorption to cement phases should be consolidated and an appropriate database of quality assured Kds and, if possible, surface complexation data established. This would be of value not only for near-field calculations but also when considering the effect of an alkaline plume in the far-field.

6.8.3 Recommendations for an Enhanced Near Field Model.

The current use of pH to determine both the absolute solubility and sorption K_D for a released species is a pragmatic and practical choice. Whilst there undoubtedly are more elegant methods with which to make predictions of these quantities, the paucity of data is a serious limiting factor.

For some radionuclides, thermodynamic and kinetic data are plentiful, but this is more often not the case. The same is true for physical data with which to describe the flow regime in and around the proposed repository and more particularly, as a successful planning application has not yet been submitted to construct such a facility in the UK, no vault geometry can be assumed with certainty. As a consequence, whilst developmental work in more advanced modelling methods must continue, the proposal outlined here seeks to extend current methods rather than replace them, maintaining the flexibility of a simplistic treatment of the near field.

The present conceptual model of near field chemistry relies almost exclusively on pH as the sole factor controlling species concentration. Over the duration of this project, mounting evidence has been accumulated which shows two distinct chemical environments are likely to prevail in the repository as a direct consequence of reactions between the backfill and percolating groundwaters.

Figure 6.16 shows a schematic cross section through a backfilled vault. Stage 1 represents the immediate post closure service life of the repository, at which stage, a sharp chemical discontinuity exists between the backfill and host rocks. Any pore solution present in the backfill at this stage is likely to be buffered to around pH 12.5 by the dissolution of portlandite. As ingress of water proceeds, conversion of portlandite to a brucite-gypsum (or at elevated temperatures brucite-anhydrite) containing assemblage is predicted to occur as an advancing reaction front, but it is not until the portlandite is either exhausted or occluded from the solution by overgrowth of brucite that a change in pH may be expected. This condition marks the boundary of stage 2, where the conversion of portlandite to brucite and calcium sulphate is complete and alkalinity is buffered to ~ pH 9.5. This simplification of the system chemistry allows a more realistic distribution of pH to be simulated by the model than hitherto, but readily lends itself to incorporation into the current VANDAL system.

The two regions will be associated with distinct solubility and sorption regimes and will reflect the assumed increase in mobility of ions in the brucite-dominated second stage where porosity is predicted to increase. This can be effected through the advection - diffusion equations presently in use although at an assumed diffusion rate of 1×10^{-4} m yr^{-1} the effect is likely to be very slight. The current model in VANDAL uses a single "shrinking core" approach, where the cross-sectional area (strictly volume) is calculated from flow velocities and effective solubility data. It is proposed that this approach is maintained but applied to both of the cement conditioned regions. Radionuclides realised from the source term will initially be released to (and in many cases concentrated in) the immediate inner region of the cementitious vault. Each element will be assigned a solubility and distribution coefficient which is governed by the pH of the inner core, region (1). Accumulation of radionuclides will be accommodated here as in the present model. A similar transfer process is envisaged

Stage 1

Portlandite dominated

pH = ~ 12.5

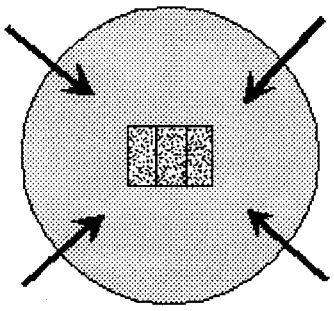

Initially, all the vault backfill is at a high pH, chemically conditioned By portlandite

Stage 2

pH inner = ~ 12.5
pH outer = ~ 9.5

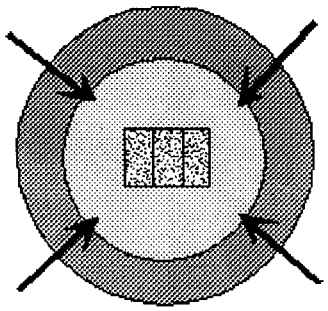

Transition phase : Waste package area buffered by portlandite but an outer region buffered by brucite and $CaSO_4$ grows inwards

Stage 3

Brucite dominated

pH outer = ~ 9.5

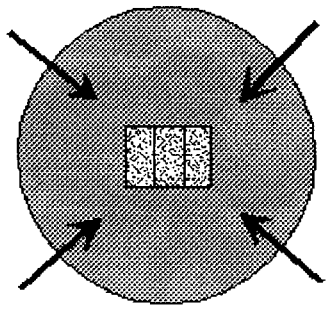

Ingress of Mg-bearing groundwaters converts all portlandite to $CaSO_4$ and brucite

Figure 6.16 Proposed enhancement to the current near field model.

for movement of radionuclides from this inner region (1) to the outer, brucite dominated region (2) where they will also be subject to further partitioning and solubility calculations. As in the inner core, storage of radionuclides will be possible in this outer region, reflecting the chemistry of the species released, thus providing a more realistic fractionation of nuclides according to two chemical environments and two rate determining steps. Shrinkage of the outer shell will be simulated according to the arithmetic methods currently employed in VANDAL.

Ultimately, the near field model will simulate the condition where no portlandite remains, and the vault is dominated by an assemblage of brucite-calcite-gypsum. In the most saline (3M) conditions, this buffers the local pH to around 9.5 and in the 0.5 molar groundwater, to between 9.7 and 9.8. As migration of pore fluids continues, dissolution of brucite and gypsum is expected in the outer region of the vault. Following depletion of brucite, the remaining calcite and gypsum will buffer the system to a predicted pH of around 7.2. This latter stage is chemically similar to the geosphere in that it is dominated by the groundwater at equilibrium with calcite. It is recognised that this is a simplification of a more complex chemical system, which contains a number of additional components. For example, because of the relatively small aluminium content of the backfill, aluminates are expected to have only a small influence on the chemical evolution of the vault and therefore contribute little to its chemical conditioning.

The expected value of this approach is that relative solubilities, sorption and hence release and storage are likely to vary for each element in the inventory in accordance with the prevailing pH of the local environment. A representation of the major chemical domains around the repository will allow more realistic simulation of the elemental fractionation likely to result from this sequential conditioning of the near field. In adapting the striker of the present model, this approach may be implemented simply, without any problems of interfacing a deterministic method such as coupled chemical transport modelling. Until such time as a detailed repository design is submitted and the associated site investigation complete, a more sophisticated approach is likely to be redundant due to lack of supporting data and operational uncertainties.

6.9 Summary remarks

In the preceding section, an attempt has been made to develop a thermodynamic model suitable for prediction of the chemical conditions prevailing in a cementitious repository. This has relied on the carefully controlled experiments reported in Section 4 to provide the data necessary for model development.

Considerable effort has been focused on the development of a model of CSH solubility in saline systems which has proved a useful approach for simulations on the 25°C isotherm but less so at elevated temperatures. In general, the SIT implementation in the geochemical code PHREEQE, has proved unreliable at high temperature and as a consequence, interpretation of the modelling results must be treated with some caution. Despite this however, a number of key results from the modelling tasks reinforce the experimental findings.

In the aqueous sodium chloride system, CSH dissolves incongruently, the calcium solubility

increasing whilst the silicate solubility decreases as a function of calcium to silicon ratio in the gel. This effect (most pronounced at low ionic strengths) is replicated by the model in the light of *a priori* knowledge of the system chemistry obtained from the experiments. Simulation of the reaction of cement hydrate phases with sodium chloride brines and magnesium sulphate solutions has provided thermodynamic data with which the database has been extended.

Using these models and data, the interaction of blended cements and the reference backfill have been studied. It has been shown that reaction between the groundwater and repository materials will result in a number of principal reactions. Dissolution of the aluminium-bearing cement hydrates is likely to be associated with precipitation of AFt-carbonate and AFt-chloride, whilst the dominant reaction conditioning the local chemical environment is dissolution of portlandite. This latter reaction is expected to be closely associated with the precipitation of brucite and gypsum from magnesium sulphate rich groundwaters.

The solubility modelling described above indicates the likely end point of groundwater interactions with backfill. These results formed the basis for three additional investigations of the spatial and temporal evolution of groundwater attack of backfill.

- Scoping calculations allowed estimates to be made of the potential longevity of the alkaline environment due to portlandite dissolution. This is of the order 2-4 million years for a cubic metre of reference backfill, exposed to percolating groundwaters.

- Mixing calculations were carried out to simulate the likely distributions of supersaturated minerals between end members of backfill porewaters and two saline groundwaters. These indicated that, with the exception of the pure end-members, minerals such as brucite, calcite, dolomite and AF_t-carbonate and AF_t-chloride were supersaturated over a broad range of mixing ratios.

  Two chemical transport simulations over 100.000 years were performed. The first which assumed equilibrium with portlandite and calcite indicated that very limited groundwater penetration would occur. The second which assumed conservative transport indicated groundwater penetration over 10 metres into backfill material. In reality, processes such as porosity increase due to molar volume reduction and the armouring of portlandite by new precipitates will add complexity. Further experimental and modelling work would be required to investigate these processes

References

1. D.L. Parkhurst, D.C. Thorstenson and L.N. Plummer. (1980) PHREEQE - A computer programme for geochemical calculations. Report U.S Geol. Surv. WRI-80-96.

2. C.W. Davies. (1962) "Ionic Solution Theory". Interscience Publishers: New York 256pp..

3. K.S. Pitzer. (1973) Thermodynamics of electrolytes: Theoretical basis and general equations. J. Phys. Chem. 77, 268.

4. L.N. Plummer, D.L. Parkhurst, D.L. Fleming, and G.W. Dunkle. (1988) A computer program incorporating Pitzer's equations for calculation of geochemical reactions in brines. U.S. Geol. Surv. Report WRI-88-4153.310pp.

5. J.N. Bronsted. (1922) Studies on solubility; IV. The principle of the specific interaction of ions. J. Am. Chem. Soc. **44**, 877-898.

6. G. Scatchard. (1936) Concentrated solutions of strong electrolytes. Chem Review. **19**, 309-327.

7. E.A. Guggenheim. (1966) "Applications of Statistical Mechanics". Oxford, Clarendon Press.

8. D. Read and W.E. Falck. (1996) Editors. CHEMVAL-2 A co-ordinated research initiative for evaluating and enhancing chemical models in radiological risk assessment. Report EUR 16648, Commission of the European Communities DGXII.

9. M. Atkins, D. Bennett, A. Dawes, F.P. Glasser, A. Kindness, and D. Read. (1991) A thermodynamic model for blended cements. Report UK DoE No. DoE/HMIP/RR/92/005.

10. D. Bennett, D. Read, M. Atkins and F.P. Glasser. (1992) A thermodynamic model for blended cements II: Cement hydrate phases: Thermodynamic values and modelling studies. J. Nucl. Mater **190**, 315-328.

11. Y. Tardy and B. Fritz. (1981) An ideal solid solution model for calculating solubility of clay minerals. Clay Minerals **16**, 361 -373.

12. U.R. Berner. (1988) Modelling the incongruent dissolution of hydrated cement minerals Radiochimica Acta **44/45,** 387 - 393.

13. A. Atkinson, J.A. Hearne, and C.F. Knights. (1990) Thermodynamic modelling and Aqueous Chemistry in the CaO-Al_2O_3-SiO_2-H_20 system. UKAEA Report No. AERE-R13732, AEA Harwell, UK.

14. Atkins, F.P. Glasser, L.P. Moroni, and J.J. Jack. (1993) Thermodynamic modelling of blended cements at elevated temperatures (50-90°C). UK DoE Report No. DoE/HMIP/RR/94.011.

15. F.M. Lea. (1971) "The Chemistry of Cement and Concrete". Chemical Publishing Co. Inc. New York.

16. R. Weast. (Editor) (1987). "CRC Handbook of Chemistry and Physics". 67th Edition. CRC Press, Boca Raton, Florida.

17. H.F.W. Taylor. (1990) "Cement Chemistry". Academic Press, London and New York.

18a. U K Nirex (1993) UK Patent Application for a Cementitious Backfill, August 1993.

18b D.L. Parkhurst. (1995) User guide to PHREEQ C - A computer program for speciation, reaction path, advective transport and inverse geochemical calculations. U.S. Geol. Surv. Report WRI-95-4227.

19. D.J.W. Arthur and D. Read. (1996) PHREEQE-96 Theoretical Overview. UK DoE Report No. DoE/RR/DRAFT/96.

20. W.E. Falck, D. Read and J.B Thomas. (1996) CHEMVAL-2 Thermodynamic database. Report EUR 16897, Commission of the European Communities, DGXII.

21. D.J.W. Arthur. (1996) The development of a coupled chemical transport network code, CHEMNET. UK DoE Report No. DoE/RR/DRAFT/96.

22. Z.A. Gralewski. (1993) VANDAL Version 2.0: Technical overview. UK DoE Report No DoE/RR/93.068.

7. TESTING AND HYDRATION CHEMISTRY OF CEMENT MATERIALS.

7.1 Introduction

Blended Portland cements of different compositions are likely to be used extensively in a repository; for construction, encapsulation of the waste, sealing, grouting and backfilling

Cementitious materials may play an important role in the containment of radionuclides. They can act as a physical barrier to radionuclide containment, but in the long term they are expected to act as a chemical barrier to radionuclide migration, mainly by establishing a high pH in the groundwater saturating the repository. A high pH, above about 10, will inhibit the corrosion of metal canisters used to contain the waste, limit radionuclide solubility and suppress microbiological activity[1]. Cements can also contribute to radionuclide immobilisation through surface adsorption, lattice incorporation and direct reaction to form low solubility precipitates[2-5].

The pH of the aqueous phase in contact with a cement in the repository will be controlled by several factors described subsequently.

7.1.1 The formation and dissolution of the compounds formed on cement hydration.

Under static conditions and in the absence of reactive species from the groundwater the composition of the aqueous phase, and therefore the pH, will be governed by the formation and dissolution of hydrates in the cement. On hydrating OPC the water in contact with it will initially have a pH of over 13 due to the presence of small amounts of alkali metal hydroxides [6]. These are removed from the aqueous phase at a comparatively early stage either through leaching or by reaction with other cement constituents. The pH will then be controlled, mainly by the dissolution of calcium hydroxide, at about 12.5 at room temperature.

In the early stages of hydration cements in which OPC is blended with latently hydraulic materials (such as ground granulated blastfurnace slag, ggbs) or pozzolanic materials (such as pulverised fuel ash, pfa) will, from a chemical viewpoint, primarily behave like neat OPC. However, over the lifetime of a repository the hydraulic components of ggbs and pfa will slowly react leading to the formation of other hydrates. $Ca(OH)_2$, which is formed through the hydration of the OPC component, can eventually be consumed by these later reactions. If all the $Ca(OH)_2$ present is consumed the pH of the aqueous phase will fall[3] to a level controlled by the dissolution of calcium silicate hydrate gel (C-S-H). Further reaction of the ggbs or pfa components will reduce Ca/Si ratio of the gel and lead to the formation of Al-bearing phases and further reductions in pH[2]. Over long periods of time crystallisation of the C-S-H gel may occur, reducing its solubility and leading to a further drop in the pH, particularly at elevated temperatures as discussed below.

7.1.2 Reactions between cement components and species present in the ground water.

Species present in the ground water, such as chloride, sulphate and carbonate ions, may have significant effects on the cement hydrates that are present and could lead to further reductions

in the pH buffering capacity of the cement. Such reactions can also lead to the formation of deleterious materials such as ettringite ($C_6A\bar{S}H_{32}$) and thaumasite ($C_3S\bar{S}CH_{15}$). The formation of ettringite is an expansive process and its formation may therefore lead to cracking in the cementitious components of a repository. The solubility of ettringite increases with temperature and it may be absent in cement pastes and concretes at elevated temperatures. However, its formation on cooling (delayed ettringite formation) can also lead to expansion and cracking[7-9]. The formation of thaumasite can occur at low temperatures in OPC when there is a ready supply of carbonate and sulphate[10].

7.1.3 The leaching effects of groundwater flow.

The soluble hydrates that are responsible for establishing the high pH can be removed from the repository through the effects of dissolution and groundwater flow leading to a fall in the pH. The rate at which these hydrates are removed will significantly determine the length of time during which the cementitious materials used will maintain a high pH in the repository.

7.1.4 Temperature

The temperature in a repository may rise to 80°C or more, due to the presence of any heat generating wastes and the exothermic reactions involved in cement hydration, followed by gradual cooling. Such temperatures will strongly influence the hydration process. Cement hydrates formed at ambient temperatures may not be stable at elevated temperatures. The crystallisation of gelatinous or semi-crystalline materials such as C-S-H may also be accelerated at higher temperatures. Such processes will reduce the solubility of these phases and potentially reduce the pH in the groundwater.

Cements used in a repository may be exposed to high temperatures and high salinity groundwaters for long periods. The likely effects of such conditions on blended OPC cements over long periods are not known. The aim of the work reported here was to study the chemistry of blended Portland cements on exposure to high salinity groundwaters over a range of temperatures. Two approaches were used:

1. Accelerated reaction techniques, using powdered cements, high water: solid ratios and constant mixing, were used to determine the compositions of the solid and aqueous phases as equilibrium conditions were approached.

2. The effects of the groundwater on high porosity cement blocks were studied by exposing precured cement paste blocks to groundwaters under static conditions.

   A range of test periods was used in both cases to monitor changes in the solid and solution phase compositions.

The techniques used in the current work have also been used to study the interactions of blended OPC cements with high sulphate-containing and high carbonate-containing groundwaters [11]. The solid phases present in these experiments after extended reaction times were ettringite, calcite, portlandite, hydrotalcite, gehlenite hydrate, thomsonite, a zeolite phase similar to phillipsite, AFm, afwillite, C-S-H(1) and a tobermorite-like phase. A further zeolite phase similar to rhodesite, erionite or gmelinite may also have been formed. Aragonite and thaumasite were formed in experiments in which the groundwater was periodically

replaced. The actual phases present in any mix depended on the cement composition, the temperature and the reaction time used.

7.2. Experimental

7.2.1 Materials

7.2.1.1 Composition of cement blends

Four cement compositions were used in the study:

75 ggbs:25 OPC
60 pfa:40 OPC
OPC
Reference backfill

where OPC is Ordinary Portland cement (Castle cement Co., BRE sample number 955), ggbs is ground granulated blastfurnace slag (Cemsave, supplied by the Frodingham Cement Company) and pfa is pulverised fuel ash (Eggborough). The composition of the backfill is that of the `preferred example' given in a vault backfill patent application[12]. The composition of the backfill used in the current study was:

OPC	40.35%	
$Ca(OH)_2$	15.25%	(Limbux, supplied by Buxton Lime Industries Ltd).
$CaCO_3$	44.40%	(supplied by RMC Roadstone, Dove Hills Quarry).

The chemical compositions of the materials used in the study are given in table 7.1.

7.2.1.2 Groundwater composition

Two synthetic groundwaters were used throughout the programme. These have been described as groundwater A and groundwater B in this report. It was originally intended to use only one groundwater in the current study (groundwater A). However, due to the wide range of groundwater compositions prevalent at depth in the UK, a second groundwater (groundwater B) was added. Boiled deionised water was used as a control.

The composition of groundwater A was based on that of the highest salinity groundwater reported from the Sellafield site; borehole 3 determination 7. Groundwater B was based [13] on borehole 2 determination 8 and had a significantly lower salinity than Groundwater A. Groundwaters were prepared using `AnalaR' grade reagents (weighed to 4 significant figures on an analytical balance). Dilution was carried out using boiled deionised water. The composition of the groundwater was determined using the same analytical procedures as were used for the determination of aqueous phase compositions as discussed below. The target compositions for both groundwaters are given in table 7.2. The compositions were also measured using the techniques described in Section 7.2.5 and these are given in table 7.3.

The main analyses were carried out using X-ray fluorescence spectroscopy. The total sulphate content was determined using a LECO CS-244 Induction Furnace. Na and K were determined by flame emission. Free lime was determined in accordance with BS4550 pt 2.

Table 7.1 Raw materials analysis.

	OPC 955	ggbs	pfa (Eggborough)	Limbux	limestone
Al_2O_3	4.51	13.08	26.0	0.15	0.20
SiO_2	20.8	35.56	50.9	0.80	0.60
CaO	64.1	39.39	1.45	72.6	55.1
Fe_2O_3	2.86	0.64	10.2	0.08	0.10
MgO	1.22	9.37	1.57	0.38	0.23
TiO_2	0.49	0.71	0.96	<0.0	0.01
K_2O	0.56	0.46	3.79	0.02	0.04
Na_2O	0.15	0.27	1.35	0.20	0.18
SO_3	3.00	0.15	0.76	0.02	0.02
Mn_2O_3	0.09	0.48	0.06	0.02	0.02
P_2O_5	0.07		0.23	nd	nd
SrO	0.06	0.04	0.04	0.03	
BaO	0.01		0.10	nd	nd
Cr_2O_3			0.03	nd	nd
LOI	1.10	0.89	2.72	23.7	42.9
Free lime	3.26				

The composition of borehole 2 determination 8 is based on that given in Nirex report 524[13] all species were set to its estimated values in table 4.6 except Na (set to its highest value in the given range to accommodate extra Cl) and Cl (which fell below the estimated level despite the increased Na level).

Table 7.2 Target compositions of synthetic groundwaters.

Target Compositions	Borehole 2 Determination 8 g/l	Borehole 3 Determination 7 g/l
NaCl	21.021	161.3
KCl	0.288	1.028
$Na_2SO_4.10H_2O$	4.031	11.201
$CaCl_2.6H_2O$	5.904	15.91
$MgCl_2.6H_2O$	1.255	2.641
$NaHCO_3$	0.198	0.0402
NaBr	0.0334	0.139
$SrCl_2$	0.0465	0.0935
$FeSO_4.7H_2O$	0.0433	

Table 7.3 Measured compositions of synthetic groundwaters.

Separate aliquots were prepared for each test age for groundwater A.
The same sample was used for all test ages for groundwater B.

Groundwater A	pH	Ca^{2+}	Mg^{2+}	Na^{+}	K^{+}	Fe	SiO_2	Cl^{-}	SO_4^{2-}	CO_3^{2-}	Al
7 days	6.60	2910	310	76490	490	0	0	120840	3390	nd	0
3 months	7.08	2890	293	60200	481	0	0	104300	3150	nd	0
9 months	6.98	2890	311	63450	535	0	0	104300	3070	nd	0
12 months	7.02	2790	310	63300	549	0	0	104900	2920	nd	0
20 months	6.80	2860	313	61740	500	0	0	104900	3590	nd	0
Groundwater B	7.80	1050	149	7980	142	0	0	15200	1300	nd	0

7.2.2 Powder experiments

7.2.2.1 Precure

Mixes were prepared by adding 10 cm^3 boiled deionised water to 5 g cement in 100 cm^3 polypropylene bottles. 10 cm^3 water was found to be the minimum required to prevent setting over a period of 28 days. The bottles were sealed with PTFE tape and the mixes were shaken continuously by end-over-end tumbling using Heidolph REAX 2 rotators. The precure times were 24 weeks for 75 ggbs:25 OPC, 60 pfa:40 OPC and OPC mixes and 20 weeks for backfill mixes (the shorter precure time for the backfill arose as a result of a delay in confirming its composition). It was intended to remove any excess water after the precure by filtration under nitrogen. However, preliminary tests showed that very little water could be removed from OPC and 75 ggbs:25 OPC blends by filtration. The maximum amount of water that could be removed from backfill and 60 pfa:40 OPC blends by filtration was about 2 - 3 cm^3. A significant amount of solid would have been lost in the filtration process and the likelihood of carbonation would have been greater, therefore the samples were not filtered at this stage.

7.2.2.2 Cement/groundwater mixes

Precured cements were mixed with 100 cm^3 groundwater or boiled deionised water. The mixes were shaken vigorously to remove any solid adhering to the bottle sides and to break up any lumps. 25°C and 55°C mixes were resealed in polypropylene bottles. PTFE tape was wrapped around the bottle necks before the lids were fitted to ensure a waterproof seal. 85°C mixes were transferred to PTFE bottles. Again the lids were sealed by using PTFE tape. Mixes were shaken continuously by end-over-end tumbling for periods of 7 days, 3 months, 9 months, 12 months and 20 months when deionised water or groundwater A were used and for 7 days, 3 months and 12 months when groundwater B was used. Temperature control was

achieved by means of a constant temperature room at 25°C and specially adapted ovens at 55°C and 85°C. The mixes were filtered under nitrogen at the end of each test period (see Section 7.2.4). The solids were dried to constant weight over saturated LiCl prior to analysis.

7.2.3 Cement blocks

Cement paste blocks were prepared for all cement compositions. For 75 ggbs:25 OPC, 60 pfa:40 OPC and OPC samples a w/c ratio of about 0.8 was used. Backfill blocks were prepared using a w/c ratio of 0.67 which is the maximum of the range given in a patent[12]. Truncated pyramidal rather than cubic moulds were used as they produced more consistent results and reduced the preparation time: 150 g of each cement were shaken for 30 minutes using an end-over-end tumbler to ensure thorough mixing. 120 cm^3 of boiled deionised water were added to the OPC, OPC/ggbs and OPC/pfa blends and 100 cm^3 added to the backfill. The mixes were shaken vigorously for several minutes then poured into truncated pyramidal moulds (about 4 cm^3 of mix per mould). The blocks were left to set for 48 hours prior to demoulding and then cured in boiled deionised water at 20°C for 2 months.

The cured blocks were transferred to 250 cm^3 polypropylene jars (for treatment at 25°C and 55°C) and 100 cm^3 PTFE bottles (for treatment at 85°C). Five blocks of the same cement composition were placed in each jar (one block per test age). The containers were filled with groundwater or boiled deionised water and the lids sealed using PTFE tape. Samples were left to stand for periods of 7 days, 3 months, 9 months, 12 months and 20 months when deionised water or groundwater A were used and for 7 days, 3 months and 12 months when groundwater B was used. Temperature control was achieved by the same means as those described in Section 7.2.2.2. At the end of each test period one block was removed from each bottle, dried on filter paper to remove any excess water then dried and stored in a desiccator over 'Carbsorb'. The dried blocks were inspected visually for signs of degradation and photographed. Selected samples were analysed using X-ray diffractometry and scanning electron microscopy as discussed below.

7.2.4 Analysis of solids

7.2.4.1 X-ray diffractometry

Solid phases were identified by X-ray diffractometry (XRD) by means of a Siemens D500 diffractometer using Cu Kα radiation operating at 40 KV and 30 mA. Data were accumulated over one scan of 2θ between 5° and 50°. Assignments of lines were made by comparisons with JCPDS files using Siemens software.

Selected cement paste blocks were analysed using X-ray diffraction and scanning electron microscopy. Samples for XRD analysis were prepared by breaking up the blocks, grinding pieces using a mortar and pestle and analysing as described above.

7.2.4.2 Quantitative determination of ettringite

Ettringite was determined quantitatively by X-ray diffractometry (XRD) using a technique based on that of Crammond[14]. Calibration standards were prepared using up to 30% ettringite (supplied by Aberdeen University) in OPC (hydrated for 1 month at 90°C, shown to be ettringite-free by XRD) with 10% boehmite added as a standard. The standards were

micronised for 5 minutes in cyclohexane using a McCrone micronising mill. Calibration curves have been produced by plotting the ratio of the peak heights for ettringite (15.7° 2θ peak) and boehmite (14.5° 2θ peak) against the ettringite content. Background counts were removed using Siemens software. The plots were linear. A set of calibration curves were also prepared using the 9.1° 2θ peak. However, the spread of points about the best straight line was greater here than for the 15.7° peak. The 9.1° peak also overlapped with AFm phase peaks in the traces for some samples. For these reasons the amount of ettringite was estimated using the 15.7° peak only. Three sets of calibration curves were produced and averaged. The equation used for calculating the weight percentage ettringite content was:

$$E = (36.72 \pm 0.59) \bullet \frac{I_E}{I_B} - (0.28 \pm 0.24)$$

Where E is the percentage weight of ettringite, I_E is the intensity of the 15.7° ettringite peak and I_B the intensity of the 14.5° 2θ boehmite peak. The error in measuring the ratio of peak heights was estimated to be 5%.

7.2.4.3 Thermogravimetric analysis

Calcite and calcium hydroxide were determined by thermogravimetric analysis using a Du Pont 2000 instrument. About 20 mg of cement was heated from ambient temperature to 1000°C at a rate of 15°C/min. The amounts of calcite and calcium hydroxide present were calculated from the respective weight losses between 650°C and 750°C (due to the loss of CO_2 from calcite) and at about 450°C (due to the loss of water from calcium hydroxide).

7.2.4.4 Weight increase on hydration

The weights of powder samples were recorded after drying to constant weight to allow the weight increase on hydration to be determined.

7.2.4.5. TEM analysis

Selected powder samples were analysed by transmission electron microscopy by Emily Hodgkinson at the University of Manchester. Full details of the experimental technique used and the results are included in Annex A. The results are also discussed in the context of the XRD analyses in Section 7.3.1. The powder samples analysed using TEM were:
75 ggbs:25 OPC reacted with deionised water at 85°C for 20 months.
60 pfa:40 OPC reacted with deionised water at 85°C for 20 months.
60 pfa:40 OPC reacted with groundwater A at 85°C for 20 months.
Backfill reacted with groundwater A at 85°C for 20 months.

7.2.4.6 SEM analysis

Selected cement blocks were analysed using scanning electron microscopy. Full details of the experimental technique used and the results are included in Annex B. The results are also discussed in the context of the XRD analyses in Section 7.3.1.6.

7.2.5 Solution analysis

The aqueous solutions were analysed, where possible, for Ca, Mg, Al, Fe, Na, K, Si, Cl^-, SO_4^{2-}, NO_3^-, CO_3^{2-} and pH. Ca, Fe, Mg and Al were determined using atomic absorption spectrophotometry and Na and K using flame emission spectrophotometry (both techniques have been carried out using a Pye Unicam SP9 spectrophotometer). Silica was determined using a molybdenum blue photometric method[15] and anions using a Dionex ion chromatograph. Cl was determined using a potentiometric Volhard titration technique[16]. Analysis for Al using atomic absorption spectroscopy did not prove to be sufficiently sensitive, particularly in the high saline solutions and a photometric technique[17] was used instead. It was not always possible to measure the concentrations of minor ions for mixes prepared using high saline groundwater due to the swamping effects of Na and Cl ion concentrations. Analyses are shown in table 7.3.

7.3. Results and Discussion

7.3.1. Solid phase composition in cement powder experiments

The results of the solid phase analyses for the powder experiments are shown in tables 7.4 to 7.15 and are summarised below. In the case of mixes prepared using deionised water direct comparisons with earlier tests (carried out at 20°C, 50°C and 90°C but over longer test periods) have been made. The ettringite, calcite and portlandite contents are given as percentage weights in the tables. The hydrated weight is included as a fraction of the initial, unhydrated weight. NaCl was present in all dried solids from mixes that had been prepared using groundwater A and in some prepared using groundwater B (see tables 7.4 to 7.7). This is likely to have been formed on drying. Details concerning phase identification and further discussions concerning the formation of individual phases are given in Section 7.3.1.7.

7.3.1.1. 75 ggbs:25 OPC blends

a) 25°C results

75 ggbs:25 OPC blends reacted with deionised water at 25°C contained C-S-H (gel), a hydrotalcite-like phase and AFm phases at all test ages. The XRD patterns for the C-S-H gel were similar at all test ages suggesting that little, if any, crystallisation of this phase occurred at this temperature. The actual compositions of the AFm phases present varied with the test age. Monosulphate was present in large quantities at 7 days, 3 months and 12 months but was absent (or present only in trace quantities) after 9 months and 20 months. $C_4AC_{0.5}H_{12}$ or an AFm phase with a similar XRD pattern (possibly $C_4A\bar{S}_{½}ClH_{12}$ although this is unlikely to form in deionised water mixes) was present after 7 days, 9 months and 20 months, but was absent at other test ages. Ettringite was absent or was present only in trace quantities throughout. The sulphate ion concentration in these mixes remained low throughout (see Section 7.3.2). In the absence of any crystalline sulphate-containing phases it is possible that any sulphate was taken up by the C-S-H gel although it is also possible that the phase identified as AFm-½CO_2 in table 7.4 contained some sulphate as discussed in Section 7.3.1.7. A comparison of these results with those obtained for 75 ggbs:25 OPC blends reacted with deionised water for up to

1160 days at 20°C shows that similar phases are present in both sets of results although calcite was also present in the 20°C sample[11]. There was no evidence of crystallisation of C-S-H phases at 20°C.

The phases present in 75 ggbs:25 OPC blends reacted with groundwaters at 25°C differed from those reacted with deionised water. Ettringite was present in large quantities, particularly groundwater A mixes (36% ettringite by weight was present after 3 months although the amount fell at later ages to about 22% after 20 months as shown in figure 7.1) due to the high sulphate level (see table 7.3). Smaller amounts (up to about 10% by weight) were formed in groundwater B mixes. The AFm and hydrotalcite-like phases present in the deionised water mixes were replaced by a Cl-containing AFm phase (AFm-Cl). Other AFm phases were probably present after 7 days in groundwater A as there were broad bands on the XRD trace between about 10.4 Å and 7.1 Å and between 4.3 Å and 3.8 Å but individual phases could not be identified by XRD. Of these AFm phases only AFm-Cl was present at test ages later than 7 days. Again there was no evidence of any crystallisation of the C-S-H gel in any mix.

Table 7.4. Solid phase development in 75 ggbs:25 OPC blends at 25°C*.

Deionised water	Age	W_h/W_u	AFt/%	CH	CSH	Afw	HT	Si-HG	GH	AFm-½CO_2	AFm-SO_4	AFm-Cl	AFm	NaCl	Anh
	7d	1.3	nd		*		*			*	*				
	3m	1.23	nd		*		*				*				
	9m	1.17	tr		*		*			*	?				
	12m	1.2	tr		*		*				*				
	20m	1.14	nd		*		*			*	?				
Groundwater A	**Age**	**W_h/W_u**	**AFt/%**	**CH**	**CSH**	**Afw**	**HT**	**Si-HG**	**GH**	**AFm-½CO_2**	**AFm-SO_4**	**AFm-Cl**	**AFm**	**NaCl**	**Anh**
	7d	1.71	6.5±0.7		*							*		*	
	3m	1.8	36±3		*					?		*	?	*	
	9m	1.8	31±3		*							*		*	
	12m	1.9	25±2		*							*		*	
	20m	1.84	21.8±0.7		*							*		*	
Groundwater B	**Age**	**W_h/W_u**	**AFt/%**	**CH**	**CSH**	**Afw**	**HT**	**Si-HG**	**GH**	**AFm-½CO_2**	**AFm-SO_4**	**AFm-Cl**	**AFm**	**NaCl**	**Anh**
	7d	1.39	9.2±0.9		*			?		?		*		*	
	3m	1.39	10±1		*						?	*		*	
	12m	1.42	8.3±0.8		*			?				*		*	

*Abbreviations in table 7.4 - 7.15. * = present; ? = possibly present; tr = present in trace amounts

Table 7.5. Solid phase development in 75 ggbs:25 OPC blends at 55°C.

Deionised water	Age	W_h/W_u	AFt/%	CH	CSH	Afw	HT	Si-HG	GH	AFm-½CO_2	AFm-SO_4	AFm-Cl	AFm	NaCl	Anh
	7d	1.23	nd		*		*				*				
	3m	1.19	nd		*		*	*			*				
	9m	1.12	5.0±0.5		*		*	*							
	12m	1.2	7.5±0.8		*		*	*							
	20m	1.14	nd		*		*	*	?						
Groundwater A	**Age**	**W_h/W_u**	**AFt/%**	**CH**	**CSH**	**Afw**	**HT**	**Si-HG**	**GH**	**AFm-½CO_2**	**AFm-SO_4**	**AFm-Cl**	**AFm**	**NaCl**	**Anh**
	7d	1.7	nd		*							*		*	
	3m	1.71	32.5±2.5		*							*		*	
	9m	1.86	23±2		*							*		*	
	12m	1.82	22.5±2		*							*		*	
	20m	1.91	27.3±2		*			?				*		*	
Groundwater B	**Age**	**W_h/W_u**	**AFt/%**	**CH**	**CSH**	**Afw**	**HT**	**Si-HG**	**GH**	**AFm-½CO_2**	**AFm-SO_4**	**AFm-Cl**	**AFm**	**NaCl**	**Anh**
	7d	1.37	17.5±1.4		*			?				*		tr	
	3m	1.4	20.4±1.5		*			*				*			
	12m	1.33	10.9±1		*			*				*		?	

Table 7.6. Solid phase development in 75 ggbs:25 OPC blends at 85°C.

Deionised water	Age	W_h/W_u	AFt/%	CH	CSH	Afw	HT	Si-HG	GH	AFm-½CO_2	AFm-SO_4	AFm-Cl	AFm	NaCl	Anh
	7d	1.19	nd	?	*		*	*			tr				
	3m	1.17	nd		*		tr	*							
	9m	1.18	nd		tob		*	*							
	12m	1.16	nd		tob	*	tr	*							
	20m	1.18	nd		tob		tr	*							
Groundwater A	**Age**	**W_h/W_u**	**AFt/%**	**CH**	**CSH**	**Afw**	**HT**	**Si-HG**	**GH**	**AFm-½CO_2**	**AFm-SO_4**	**AFm-Cl**	**AFm**	**NaCl**	**Anh**
	7d	1.83	nd		*							*		*	
	3m	2.47	nd		*							*		*	
	9m	2.61	nd		*							*		*	
	12m	3.48	nd		tob?			?				*		*	*
	20m	3.32	nd		*			*				*		*	*
Groundwater B	**Age**	**W_h/W_u**	**AFt/%**	**CH**	**CSH**	**Afw**	**HT**	**Si-HG**	**GH**	**AFm-½CO_2**	**AFm-SO_4**	**AFm-Cl**	**AFm**	**NaCl**	**Anh**
	7d	1.31	3.9±0.6		*			*		*		*		*	
	3m	1.37	4.9±0.5		*			*				*		*	
	12m	1.46	nd		?			*		?		?		*	

Table 7.7. Solid phase development in 60 pfa:40 OPC blends at 25°C.

Deionised water	Age	W_h/W_u	AFt/%	Cc	CSH	Th	GH	Si-HG	Phi	AFm-½CO_2	AFm-SO_4	AFm-CO_3	AFm-Cl	AFm	NaCl	Anh
	7d	1.1	1.0±0.3		*		*				*					
	3m	1.1	1.1±0.3		*		*			*	*					
	9m	1.09	1.0±0.3		*		*			*	*					
	12m	1.13	1.8±0.4		*		*				*					
	20m	1.11	nd		*		*			*	*					
Groundwater A	**Age**	**W_h/W_u**	**AFt/%**	**Cc**	**CSH**	**Th**	**GH**	**Si-HG**	**Phi**	**AFm-½CO_2**	**AFm-SO_4**	**AFm-CO_3**	**AFm-Cl**	**AFm**	**NaCl**	**Anh**
	7d	1.54	7.5±0.8		*		*				*		*		*	
	3m	1.57	35.6±2.6		*		*								*	
	9m	1.52	39±3		*		*								*	
	12m	1.57	31.2±2.2		*		*								*	
	20m	1.51	48.6±3.4		*		*								*	
Groundwater B	**Age**	**W_h/W_u**	**AFt/%**	**Cc**	**CSH**	**Th**	**GH**	**Si-HG**	**Phi**	**AFm-½CO_2**	**AFm-SO_4**	**AFm-CO_3**	**AFm-Cl**	**AFm**	**NaCl**	**Anh**
	7d	1.31	11.6± 1		*		*									
	3m	1.27	22.6±1.3		*		*	?								
	12m	1.26	18.9		*		*									

Table 7.8. Solid phase development in 60 pfa:40 OPC blends at 55°C.

Deionised water	Age	W_h/W_u	AFt/%	Cc	CSH	Th	GH	Si-HG	Phi	AFm-½CO_2	AFm-SO_4	AFm-CO_3	AFm-Cl	AFm	NaCl	Anh
	7d	1.09	7.5		*		*	?		*	*					
	3m	1.1	tr		*		*	tr			*	tr				
	9m	1.12	tr		*		*					*				
	12m	1.13	0.7±0.3		*		*					tr				
	20m	1.11	nd		*	?	*									
Groundwater A	**Age**	**W_h/W_u**	**AFt/%**	**Cc**	**CSH**	**Th**	**GH**	**Si-HG**	**Phi**	**AFm-½CO_2**	**AFm-SO_4**	**AFm-CO_3**	**AFm-Cl**	**AFm**	**NaCl**	**Anh**
	7d	1.46	tr		*		*			?	?	?	*	?	*	
	3m	1.38	tr		*		*						*		*	
	9m	1.42	?		*	?	*					*	?		*	
	12m	1.47	tr		*	*	*					*	*		*	
	20m	1.46	nd		*	*	*						?		*	
Groundwater B	**Age**	**W_h/W_u**	**AFt/%**	**Cc**	**CSH**	**Th**	**GH**	**Si-HG**	**Phi**	**AFm-½CO_2**	**AFm-SO_4**	**AFm-CO_3**	**AFm-Cl**	**AFm**	**NaCl**	**Anh**
	7d	1.2	13.6		*		*									
	3m	1.23	10.2±1.0		*		*	*							?	
	12m	1.19	tr		*	tr	*	tr?								

Table 7.9. Solid phase development in 60 pfa:40 OPC blends at 85°C.

Deionised water	Age	W_h/W_u	AFt/%	Cc	CSH	Th	GH	Si-HG	Phi	AFm-½CO_2	AFm-SO_4	AFm-CO_3	AFm-Cl	AFm	NaCl	Anh
	7d	1.1	nd		*		*	?								
	3m	1.08	nd		*		*	tr								
	9m	1.13	nd		*	*	*		*							
	12m	1	nd		*	*	*	?								
	20m	1.1	nd		*	*	*		*							
Groundwater A	**Age**	**W_h/W_u**	**AFt/%**	**Cc**	**CSH**	**Th**	**GH**	**Si-HG**	**Phi**	**AFm-½CO_2**	**AFm-SO_4**	**AFm-CO_3**	**AFm-Cl**	**AFm**	**NaCl**	**Anh**
	7d	1.6	nd		*		*	?					*		*	*
	3m	1.54	nd		*		?	tr	*			*			*	*
	9m	2.09	nd		*	*						*			*	*
	12m	1.6	nd		*	*		?	*			*			*	*
	20m	2.14	nd		*	*									*	*
Groundwater B	**Age**	**W_h/W_u**	**AFt/%**	**Cc**	**CSH**	**Th**	**GH**	**Si-HG**	**Phi**	**AFm-½CO_2**	**AFm-SO_4**	**AFm-CO_3**	**AFm-Cl**	**AFm**	**NaCl**	**Anh**
	7d	1.15	tr	?	*		*	*								
	3m	1.18	nd		*	*	*	*								
	12m	1.22	nd		*	*		?								

Table 7.10. Solid phase formation in OPC mixes at 25°C.

Deionised water	Age	W_h/W_u	AFt/%	CH	CSH	Cc	CSH	AFm	HG	AFm-½CO_2	AFm-SO_4	AFm-CO_3	AFm-Cl	NaCl	Anh
	7d	1.23	2.3±0.4	19.5	*				*		*	?			
	3m	1.2	6.0±0.7	17.1	?				*			tr			
	9m	1.2	2.8±0.4	19.6	*				*	*		*			
	12m	1.22	6.9±0.7	18.3	?				?			?			
	20m	1.07	9.2±0.8	17.4	?				*			?			
Groundwater A	**Age**	**W_h/W_u**	**AFt/%**	**CH**	**CSH**	**Cc**	**Afw**	**AFm**	**HG**	**AFm-½CO_2**	**AFm-SO_4**	**AFm-CO_3**	**AFm-Cl**	**NaCl**	**Anh**
	7d	1.67	3.4±0.5	15.9	*			?	*	?			*	*	
	3m	1.64	7.2±0.7	13	?				*				tr	*	
	9m	1.53	8.5±0.8	16.4	?				*			?	?	*	
	12m	1.68	12.0±1.0	16	?			?	?				?	*	
	20m	1.57	13.8±1.2	11.4	?				*					*	
Groundwater B	**Age**	**W_h/W_u**	**AFt/%**	**CH**	**CSH**	**Cc**	**Afw**	**AFm**	**HG**	**AFm-½CO_2**	**AFm-SO_4**	**AFm-CO_3**	**AFm-Cl**	**NaCl**	**Anh**
	7d	1.36	5.4±0.6	17	?				*						
	3m	1.32	5.9±0.6	16.5	?				*				*	?	
	12m	1.28	7.6	17	?				*				*		

Table 7.11. Solid phase formation in OPC mixes at 55°C.

Deionised water	Age	W_h/W_u	AFt/%	CH	CSH	Cc	Afw	AFm	HG	AFm-½CO_2	AFm-SO_4	AFm-CO_3	AFm-Cl	NaCl	Anh
	7d	1.21	2.4±0.4	22	?				*			?			
	3m	1.2	7.1±0.8	17.1	?				*			tr			
	9m	1.15	5.0±0.6	15.9	?				*			*			
	12m	1.12	6.3±0.7	18.2	?		*	?	*			?			
	20m	1.05	12.3±1.1	21.2	?		*		*			?			
Groundwater A	**Age**	**W_h/W_u**	**AFt/%**	**CH**	**CSH**	**Cc**	**Afw**	**AFm**	**HG**	**AFm-½CO_2**	**AFm-SO_4**	**AFm-CO_3**	**AFm-Cl**	**NaCl**	**Anh**
	7d	1.59	2.2±0.4	16.8	?				*				*	*	
	3m	1.65	8.9±0.9	14.8	?				*				*	*	
	9m	1.69	9.9±0.9	15.1				?	*				*	*	
	12m	1.6	12.1±1.1	17	?				*				*	*	
	20m	1.72	12.1±1.1	17.8	?				*				*	*	
Groundwater B	**Age**	**W_h/W_u**	**AFt/%**	**CH**	**CSH**	**Cc**	**Afw**	**AFm**	**HG**	**AFm-½CO_2**	**AFm-SO_4**	**AFm-CO_3**	**AFm-Cl**	**NaCl**	**Anh**
	7d	1.34	6.6±0.7	17.8	?				*						
	3m	1.31	11.6±1.0	14.2	?	?			*				*	*	
	12m	1.28	11.2	19	?				*				*	*	

Table 7.12. Solid phase formation in OPC mixes at 85°C.

Deionised water	Age	W_h/W_u	AFt/%	CH	CSH	Cc	Afw	AFm	HG	AFm-½CO_2	AFm-SO_4	AFm-CO_3	AFm-Cl	NaCl	Anh
	7d	1.21	1.7±0.4	23.1	?				*						
	3m	1.18	nd	19.3	?				*			tr			
	9m	1.15	nd	22.4	?			?	*						
	12m	1.16	tr	22	?				*						
	20m	1.17	nd	23.6	?				*			?			
Groundwater A	**Age**	**W_h/W_u**	**AFt/%**	**CH**	**CSH**	**Cc**	**Afw**	**AFm**	**HG**	**AFm-½CO_2**	**AFm-SO_4**	**AFm-CO_3**	**AFm-Cl**	**NaCl**	**Anh**
	7d	1.83	nd	12.6	?				*				*	*	
	3m	1.79	nd	14.4	?				*				*	*	
	9m	2.07	nd	10.3	?				*			*	*	*	*
	12m	2.01	nd	14.6	?				?				*	*	*
	20m	2.22	nd	13.7	?				?				*	*	*
Groundwater B	**Age**	**W_h/W_u**	**AFt/%**	**CH**	**CSH**	**Cc**	**Afw**	**AFm**	**HG**	**AFm-½CO_2**	**AFm-SO_4**	**AFm-CO_3**	**AFm-Cl**	**NaCl**	**Anh**
	7d	1.27	3.7±0.5	17.9	?				*						
	3m	1.32	7.5±0.8	17.3	?	?			*				?	*	
	12m	1.33	tr	23	?				*				?	*	

Table 7.13. Solid phases in reference backfill mixes at 25°C.

Deionised water	Age	W_h/W_u	AFt/%	CH	Cc	CSH	Afw	AFm	HG	AFm-½CO_2	AFm-SO_4	AFm-CO_3	AFm-Cl	NaCl	Anh
	7d	1.07	1.9±0.4	19.9	38.9			*				*			
	3m	1.06	2.2±0.4	19.2	39			*				*			
	9m	1.06	1.7±0.4	18.3	37.7	?			*	*		*			
	12m	1.06	3.4±0.5	20.1	37.6			*	*			*			
	20m	1.05	2.4±0.4	20.5	36.6	?		?	*	?		*			
Groundwater A	**Age**	**W_h/W_u**	**AFt/%**	**CH**	**Cc**	**CSH**	**Afw**	**AFm**	**HG**	**AFm-½CO_2**	**AFm-SO_4**	**AFm-CO_3**	**AFm-Cl**	**NaCl**	**Anh**
	7d	1.31	2.4±0.4	15.9	36	?							*	*	
	3m	1.33	6.9±0.7	13.9	30.3								tr	*	
	9m	1.35	7.5±0.7	12.1	34.3	?			?					*	
	12m	1.4	8.6±0.9	13.5	30.3				?				tr	*	
	20m	1.1	7.5±0.8	14.3	28.2	?			?				tr	*	
Groundwater B	**Age**	**W_h/W_u**	**AFt/%**	**CH**	**Cc**	**CSH**	**Afw**	**AFm**	**HG**	**AFm-½CO_2**	**AFm-SO_4**	**AFm-CO_3**	**AFm-Cl**	**NaCl**	**Anh**
	7d	1.09	3.4±0.5	20.4	37.6	?			?				*		
	3m	1.16	6.2±0.6	13.2	33	?			*				*	?	
	12m	1.1	5.4	18	34.3	?			*				*	*	

Table 7.14. Solid phases in reference backfill mixes at 55°C.

Deionised water	Age	W_h/W_u	AFt/%	CH	Cc	CSH	Afw	AFm	HG	AFm-½CO_2	AFm-SO_4	AFm-CO_3	AFm-Cl	NaCl	Anh
	7d	1.06	1.5±0.5	22.3	34.6	?		*				*			
	3m	1.02	1.9±0.4	18.9	42.4				*			tr			
	9m	1.02	2.1±0.4	17.1	36.4		*		*			?			
	12m	0.97	3.0±0.4	23.1	39.3		*		?			tr			
	20m	0.95	3.1±0.5	22.8	36.6	?	*		?			?			
Groundwater A	**Age**	**W_h/W_u**	**AFt/%**	**CH**	**Cc**	**CSH**	**Afw**	**AFm**	**HG**	**AFm-½CO_2**	**AFm-SO_4**	**AFm-CO_3**	**AFm-Cl**	**NaCl**	**Anh**
	7d	1.23	1.7±0.4	17.9	32	?							*	*	
	3m	1.33	5.0±0.6	12.6	32.8								*	*	
	9m	1.34	5.9±0.6	13.7	30.3				?				*	*	
	12m	1.25	5.7±0.6	16.4	29.2				?				*	*	
	20m	1.25	8.2±0.8	14	28.9										
Groundwater B	**Age**	**W_h/W_u**	**AFt/%**	**CH**	**Cc**	**CSH**	**Afw**	**AFm**	**HG**	**AFm-½CO_2**	**AFm-SO_4**	**AFm-CO_3**	**AFm-Cl**	**NaCl**	**Anh**
	7d	1.16	5.3±0.6	17.1	35.6				*						
	3m	6	7.4±0.8	17.3	37.1	?			*				*	*	
	12m	1.06	10.1	15	34.9				*				?	?	

Table 7.15. Solid phases in reference backfill mixes at 85°C.

Deionised water	Age	W_h/W_u	AFt/%	CH	Cc	CSH	Afw	AFm	HG	AFm-½CO_2	AFm-SO_4	AFm-CO_3	AFm-Cl	NaCl	Anh
	7d	0.99	tr	21.2	36.6	?			*			?			
	3m	1.02	nd	17.7	42				*						
	9m	1.04	nd	15.6	42.6		*		*						
	12m	1.02	nd	20.5	40.8		*		?						
	20m	0.96	nd	20.2	40.2	?			*						
Groundwater A	**Age**	**W_h/W_u**	**AFt/%**	**CH**	**Cc**	**CSH**	**Afw**	**AFm**	**HG**	**AFm-½CO_2**	**AFm-SO_4**	**AFm-CO_3**	**AFm-Cl**	**NaCl**	**Anh**
	7d	1.42	tr	21.2	36.6	?			?				*	*	
	3m	1.51	nd	13.7	23.2				?				*	*	
	9m	1.62	nd	10.1	23.2								*	*	*
	12m	1.64	nd	11.7	27.8				?				*	*	
	20m	1.61	nd	13	25.6				?				*	*	
Groundwater B	**Age**	**W_h/W_u**	**AFt/%**	**CH**	**Cc**	**CSH**	**Afw**	**AFm**	**HG**	**AFm-½CO_2**	**AFm-SO_4**	**AFm-CO_3**	**AFm-Cl**	**NaCl**	**Anh**
	7d	1.11	1.2±0.4	17.9	36.3	?			?						
	3m	1.09	1.0±0.3	16.3	37.7	?			*				*	*	
	12m	1.09	tr?	19	38.5	?			*				?	*	

b) 55°C results

Monosulphate was present in 75 ggbs:25 OPC blends reacted with deionised water after 7 days and 3 months at 55°C but was replaced by ettringite at 9 months and 12 months. Both of these phases were absent after 20 months. Siliceous hydrogarnet, C-S-H gel and a hydrotalcite-like phase were also present. There was no evidence of any crystallisation of C-S-H gel at this temperature. XRD analysis suggested that the 20 month sample may have contained trace quantities of gehlenite hydrate although the assignment of XRD lines to this phase was not conclusive. Similar lines were also present in a 75 ggbs:25 OPC blend hydrated using deionised water at 50°C for 1380 days in a previous series of experiments[11]. These lines were assigned to the semi-crystalline material C-S-H(I). The sample from the earlier test series also contained significant quantities of a crystalline, tobermorite-like calcium silicate hydrate phase. This phase probably formed as a consequence of the extended reaction times used and its absence from 75 ggbs:25 OPC samples cured at 55°C in the current work suggests that equilibrium was not reached.

75 ggbs:25 OPC mixes prepared using groundwater A at 55°C contained large quantities (up to 32%) of ettringite at test ages of 3 months and greater. The amount of ettringite present fell slightly with time after 3 months as shown in figure 7.1. A Cl-containing AFm phase (AFm-Cl) was also formed. These phases largely replaced the siliceous hydrogarnet and AFm phases which were present in equivalent deionised water mixes. C-S-H (gel) was present in all mixes with no evidence of any crystallisation. There was little or no change in the XRD traces for mixes prepared using the groundwater A mixes after 3 months. Mixes prepared using groundwater B contained similar crystalline phases to those prepared using groundwater A. However, less ettringite was present (up to 20.4% after 3 months), probably due to the lower sulphate content of groundwater B compared to that of groundwater A. The amount of siliceous hydrogarnet present was larger than in the equivalent samples prepared using groundwater A.

c) 85°C results

XRD analyses of 75 ggbs:25 OPC blends reacted with deionised water at 85°C showed that a tobermorite-like phase was present at test ages of 9 months and over (see Section 7.3.1.7d). C-S-H gel was present at test ages up to 3 months but could not be detected by XRD at later ages. Siliceous hydrogarnet (with a composition of approximately C_3ASH_4) was present at all test ages. Traces of AFm or hydrotalcite-like phases were also present. Afwillite was detected after 12 months. The XRD peaks for this phase were substantial and the match to the JCPDS pattern was good. However, it was not detected in the equivalent 20 month test. This point is discussed further in Section 7.3.1.7d. Annex C shows the reactivity of the slag, which reached ~ 60% at 20 months.

TEM analysis of the sample reacted with deionised water for 20 months at 85°C largely confirmed the results of the XRD analysis (see Annex A). It confirmed the formation of a crystalline C-S-H. The composition of this phase was most consistent with those of foshagite, afwillite, jennite and xonolite rather than that of tobermorite.

In the earlier programme 75 ggbs:25 OPC blends hydrated in deionised water at 90°C for periods of up to 1090 days contained similar phases to those detected here, although afwillite was not formed [11]

Mixes prepared using groundwater A contained C-S-H gel at all test ages although a tobermorite-like phase was also present in small quantities after 12 months. The d-spacings for this phase differed from those of the tobermorite-like phase detected in deionised water mixes with the main peak at 11.88 Å rather than 10.64 Å. AFm-Cl phase was present at all test ages. Anhydrous calcium sulphate was present after 12 months and 20 months.

Figure 7.1. Ettringite in 75 ggbs:25 OPC blends.

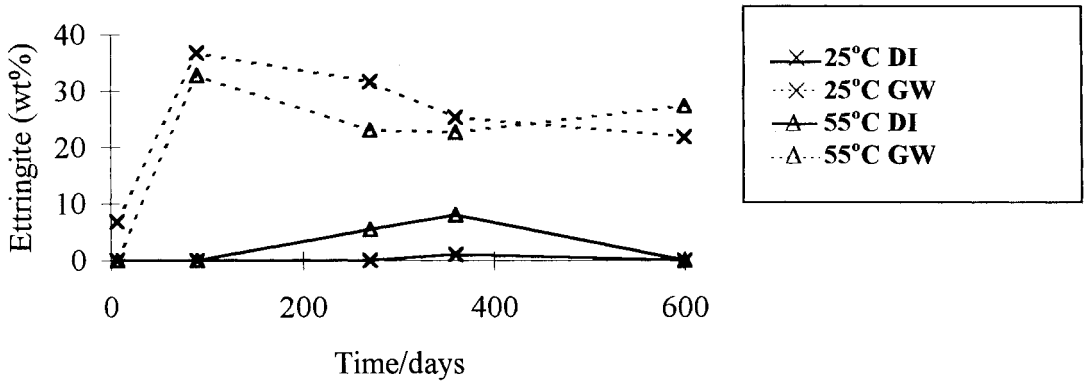

In this and subsequent figures, Di = Deionised water and GW is groundwater.

Mixes prepared with groundwater B contained C-S-H gel and siliceous hydrogarnet. The chloride-containing Afm phase (AFm-Cl) was present after 7 days and may have been present in trace amounts after 12 months. The amount of siliceous hydrogarnet present was again higher than in equivalent mixes prepared using groundwater A (based on a comparison of XRD peak heights), due to the lower chloride ion concentration in the groundwater and the consequent formation of only small amounts of AFm-Cl. Trace quantities of another Afm phase (AFm-½CO_3 may also have been present. Ettringite, which is likely to have formed during the initial precure, persisted for up to 3 months but was not detected by XRD after 12 months.

7.3.1.2 60 pfa:40 OPC blends

a) 25°C results

60 pfa:40 OPC blends reacted with deionised water at 25°C contained small quantities of ettringite (around 1-1.8%), C-S-H gel, monosulphate and gehlenite hydrate (C_2ASH_8) at all test ages. An AFm phase with an XRD pattern similar to $C_4A\overline{C}_{0.5}H_{12}$ was present at some test ages and may have occurred due to carbonation of the monosulphate phase. There was no evidence of any crystallisation of the C-S-H gel. In the earlier series of tests (11) 60 pfa:40 OPC blends reacted with deionised water at 20°C for test periods of up to 1160 days contained similar phases although AFm-CO_2, which was not detected in the current work after 20 months, was present after 1160 days at 20°C.

Mixes reacted with groundwaters A and B at 25°C contained C-S-H gel and gehlenite hydrate at all test ages. Monosulphate, which may have been formed during the precure, was present after 7 days exposure to groundwater A but was replaced by ettringite at later test ages. Ettringite was present in quantities of up to 49% by weight in mixes prepared using

groundwater A (see figure 7.2) and up to 23% in mixes prepared using groundwater B. A chloride-containing AFm phase may have been present after 7 days in the mix prepared using groundwater A but was not detected at later ages. It was absent at all ages from the mixes prepared using groundwater B.

b) 55°C results

60 pfa:40 OPC blends reacted with deionised water at 55°C contained mainly C-S-H gel and gehlenite hydrate at all test ages. There was no evidence of any crystallisation of the C-S-H gel. Monosulphate was present at 7 days and 3 months but was absent thereafter. Ettringite was present only in trace quantities at test ages up to 12 months and was absent at 20 months. Thomsonite may have been present in trace quantities after 20 months. Similar phases were also present in 60 pfa:40 OPC blends reacted with deionised water at 50°C for test periods of up to 1380 days [11] although small amounts of ettringite (up to 5%) persisted throughout and larger amounts of thomsonite were present at the end of the test (based on a comparison of XRD peak heights).

Figure 7.2 Ettringite in 60 pfa:40 OPC blends.

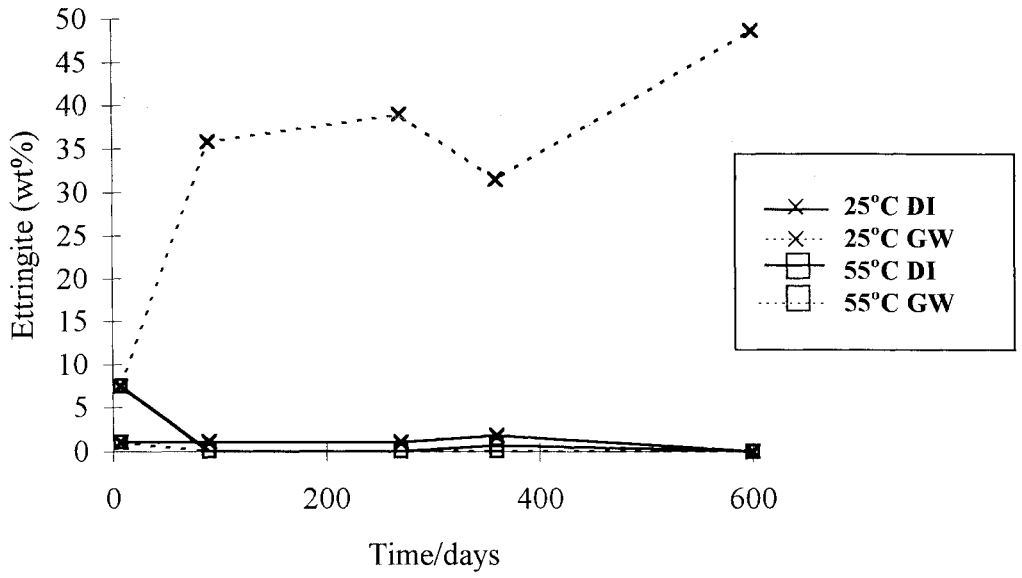

C-S-H gel and gehlenite hydrate were also present in 60 pfa:40 OPC blends reacted with groundwater A at 55°C although the XRD peak heights were small in comparison to equivalent deionised water mixes. Again there was no evidence of any crystallisation of the C-S-H gel. AFm-Cl was present in substantial amounts after 7 days and 3 months, but was present only in trace quantities thereafter. Trace quantities of other AFm phases were also present in some mixes (see table 7.5). Thomsonite was present in mixes at test ages of 9 months and later and may also have been present in trace quantities after 3 months. There was little change in the XRD patterns of samples prepared using groundwater A after 9 months. The disappearance of the Cl-containing AFm phase may have been linked with the formation of thomsonite and the consequent reduction in the availability of aluminium.

Mixes prepared using groundwater B contained C-S-H gel and gehlenite hydrate. Significant quantities of ettringite were present after 7 days and 3 months but not after 12 months. The absence of ettringite after 12 months suggests that it formed during the initial precure at 25°C and gradually redissolved at the higher temperature. Hydrogarnet was also present after 3 months and may have been present in trace quantities after 12 months. Trace quantities of thomsonite were present after 12 months.

c) 85°C results

60 pfa:40 OPC blends reacted with deionised water at 85°C contained C-S-H gel and gehlenite hydrate at all test ages. There was no evidence of any crystallisation of the C-S-H gel with time. Thomsonite and a zeolite mineral similar to phillipsite were also present at test ages of 9 months and over although phillipsite was not detected in the 12 month sample. The intensities of the phillipsite XRD peaks relative to those of thomsonite increased with time.

TEM analysis on the 60 pfa:40 OPC sample reacted with deionised water for 20 months at 85°C confirmed the presence of a crystalline zeolite but was unable to distinguish different types as identified by XRD. However, the zeolite detected by TEM was found to be alkali-free and is therefore not consistent with the 'ideal' compositions of thomsonite and phillipsite stated in Section 7.3.1.7c. A poorly-ordered, Al-rich C-S-H 'gel' material was also identified by TEM. This had a greater degree of ordering than a typical gel.

The phases detected in the current work differed in some respects to those present in earlier tests in which 60 pfa:40 OPC blends were reacted with deionised water at 90°C for test periods of up to 1090 days [11]. Phillipsite was absent at 90°C, but thomsonite was present in larger quantities than in the current programme (this point is discussed further in Section 7.3.1.7). The 90°C samples also gave a broad XRD band at between 14.5Å and 11Å. This was assigned to a C-S-H gel. Tests to determine the extent of pfa reaction, Annex C, were inconclusive.

Blends reacted with groundwater A at 85°C contained C-S-H gel in all cases. There was evidence of a change in the composition of the C-S-H gel as a broad band formed at about 11.9 Å after 9 months. Thomsonite was present at test periods of at least 9 months. Phillipsite was present after 3 months and 12 months, but was not detected in the 9 months and 20 months samples. Gehlenite hydrate, which was probably formed during the initial precure, persisted for up to 3 months under these conditions, but was absent thereafter. AFm-Cl was present after 7 days but was absent thereafter. Its disappearance was probably due to the consumption of available aluminium in the formation of the zeolite phases phillipsite and thomsonite. $C_4A\overline{C}H_{11}$ was present in trace quantities at test ages between 3 months and 12 months. Anhydrous calcium sulphate was present in all cases.

TEM analysis on the 60 pfa:40 OPC sample reacted with groundwater for 20 months at 85°C showed that the sample contained an Al-substituted crystalline C-S-H (containing trace quantities of chlorine although this could arise from the presence of NaCl) with a C/S ratio of 0.6, an unidentified zeolite (largely alkali free although some analyses indicated the presence of trace quantities of sodium) and a gel with an inferred composition of about 50% Si, 25% Ca and 25% Al with small amounts of magnesium. Sulphate was not detected in any phase although the sulphate ion concentration in the aqueous phase clearly fell with time as shown in table 7.21 and figure 7.2.

Mixes prepared using groundwater B contained C-S-H gel, siliceous hydrogarnet and gehlenite hydrate after 7 days. Thomsonite was also present at test ages of 3 months and 12 months. Gehlenite hydrate was not detected after 12 months.

7.3.1.3. OPC

a) 25°C results

Mixes in which OPC was reacted with deionised water at 25°C contained ettringite, hydrogarnet, portlandite and trace quantities of an AFm phase ($C_4A\bar{C}H_{11}$) at all test ages. C-S-H gel was also likely to have been present but it could not readily be identified by XRD. Monosulphate was present after 7 days but was absent at later ages. An AFm phase with an XRD pattern similar to $C_4A\bar{C}_{0.5}H_{12}$ or $C_4A\bar{S}H_{12}$ was present at 9 months. The latter is more likely as the ettringite content of this mix was lower than the equivalent mixes at other test ages. Similar phases to those formed in the current work were also present in an earlier series of experiments in which OPC mixes were reacted with deionised water at 20°C for test periods of up to 1160 days[11] although hydrogarnets were not detected at any stage.

OPC mixes prepared using the groundwaters contained similar phases to those prepared using deionised water although different AFm phases were formed (only in trace quantities) as given in table 7.6. The compositions of these phases could not be determined by XRD. Ettringite formed in slightly larger quantities in samples prepared using groundwater A than in equivalent samples prepared using deionised water and groundwater B due to the increased availability of sulphate.

b) 55°C results

Mixes in which OPC was reacted with deionised water at 55°C contained ettringite, portlandite, an AFm phase ($C_4A\bar{C}H_{11}$) in trace quantities and siliceous hydrogarnet (composition approximately C_3ASH_4) at all test ages. Afwillite was present in small quantities after 12 months and in larger quantities after 20 months. C-S-H gel was likely to have been present at earlier ages but it could not readily be identified by XRD. The amount of ettringite present generally increased with time with about 12% present after 20 months (as shown in table 7.11). Similar phases were also detected in earlier work in which OPC mixes were reacted with deionised water at 50°C for test periods of up to 1380 days although an unidentified phase, 'phase 4', was also detected [11].

OPC mixes prepared using groundwater A at 55°C contained large quantities of a Cl-containing AFm phase (AFm-Cl) at all test ages. The amount of ettringite present increased with time (as shown in figure 7.3) but was comparable to that formed in equivalent deionised water mixes despite the increased availability of sulphate from the groundwater (see table 7.11). The XRD traces suggest that less hydrogarnet was present than in equivalent deionised water mixes. There was no evidence of the crystallisation of C-S-H gel. Similar results were obtained for mixes prepared using groundwater B although the chloride containing AFm phase (AFm-Cl) was not detected at 7 days.

Figure 7.3 Ettringite in OPC.

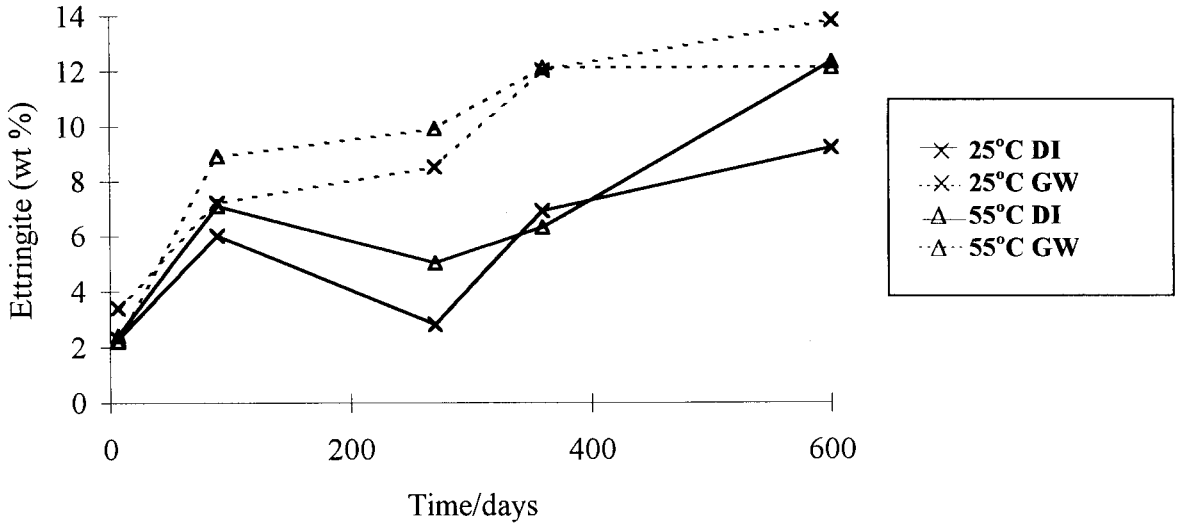

c) 85°C results

Mixes in which OPC was reacted with deionised water at 85°C contained portlandite and siliceous hydrogarnet in large quantities at all test ages. C-S-H was also likely to have been present but it could not readily be identified by XRD. Ettringite was present in small quantities after 7 days and was absent thereafter. Small quantities of AFm phases were detected at some test ages. Earlier work in which OPC mixes were reacted with deionised water at 90°C for test periods of up to 1090 days [11] contained similar phases although calcite and small quantities of afwillite were also present. An unidentified phase, 'phase 4,' was also detected.

OPC mixes prepared using groundwater A at 85°C contained portlandite and hydrogarnet (although the latter phase was present in smaller amounts than in deionised water mixes, based on a comparison of the XRD peak heights). A Cl-containing AFm phase (AFm-Cl) was also present in large quantities at all ages. Anhydrous calcium sulphate was present at test ages of 9 months and over. Ettringite was not detected at any age.

OPC mixes prepared using groundwater B contained ettringite, portlandite and siliceous hydrogarnet at 7 days and 3 months. The chloride-containing AFm phase (AFm-Cl) may have been present in trace quantities after 3 months and 12 months.

7.3.1.4. Reference backfill mixes

a) 25°C results

Backfill mixes prepared using deionised water at 25°C contained portlandite and calcite in large quantities at all test ages. C_4AH_{13} (or an AFm phase with a similar XRD pattern), $C_4A\bar{C}H_{11}$ and small amounts of ettringite were also present throughout. Siliceous hydrogarnet (C_3ASH_4) was present at 9 months and after. C-S-H could not be detected by XRD.

Backfill mixes reacted with groundwater A contained ettringite, calcite and portlandite. Trace quantities of hydrogarnet and a Cl-containing AFm phase may also have been present. Mixes

reacted with groundwater B contained ettringite, calcite, portlandite, siliceous hydrogarnet and a Cl-containing AFm phase at all test ages. The amounts of ettringite present in mixes prepared using groundwaters were higher than in the equivalent deionised water mixes, probably due to the increased availability of sulphate from the groundwaters.

b) 55°C results

Backfill mixes prepared using deionised water at 55°C contained portlandite and calcite in large quantities at all ages. Small amounts of ettringite were also present throughout, with trace quantities of hydrogarnet and/or various AFm phases in some mixes as shown in table 7.14. Afwillite was present at test ages of 9 months and longer. C-S-H gel may have been present but could not be detected by XRD in any mix.

Reference backfill mixes reacted with groundwater A at 55°C contained ettringite, calcite, portlandite and a Cl-containing AFm phase, although this latter phase was absent after 20 months. Mixes reacted with groundwater B after 3 months and 12 months contained substantial amounts of siliceous hydrogarnet in addition to those phases formed in the groundwater A mixes. AFm-Cl was present after 3 months, but was only present in trace amounts (if at all) after 12 months. Afwillite was not formed in the presence of either groundwater.

c) 85°C results

Reference backfill mixes prepared using deionised water at 85°C contained portlandite and calcite in large quantities at all test ages. Hydrogarnet was also present at all ages. Ettringite, which probably formed during the precure, was present in trace quantities after 7 days but was absent thereafter. Afwillite was present at test ages of 9 months and 12 months but could not be detected in the 20 month sample. C-S-H gel could not be detected by XRD.

Reference backfill mixes reacted with groundwater A at 85°C contained calcite, portlandite and a Cl-containing AFm phase at all ages. Hydrogarnet may have been present in small quantities in all mixes. These phases were also present in mixes reacted with groundwater B after 3 months. Ettringite was also present in groundwater B mixes after 7 days and 3 months, probably as a result of forming during the initial precure. It was not detected after 12 months. Afwillite was not formed in the presence of either groundwater.

7.3.1.5. Weight increase on hydration

The weight increases on hydration for all samples are shown in tables 7.4 to 7.15. The weight increase on hydration for 75 ggbs:25 OPC blends prepared using deionised water was generally between 9% and 23%. For 60 pfa:40 OPC mixes it was between 8% and 13%. For OPC mixes prepared using deionised water the weight increase on hydration was between 5% and 23 % although it appeared to fall with time, particularly at 25°C and 55°C (see tables 7.10 to 7.12). There may also have been a fall with time for backfill mixes, although the weight increases on hydration here were small. The largest increase was 7%. In some cases there was an apparent loss in weight, due to losses of material during the filtering stage.

The weights of samples prepared using groundwater were consistently higher than equivalent samples prepared using deionised water. This result is due mainly to the presence of NaCl formed during the drying process.

7.3.1.6. Analysis of cement paste blocks

It was initially intended that the cement paste blocks would only be inspected visually. However, visual inspection of cement blocks showed no signs of deterioration in any case and selected samples have also been analysed using X-ray diffractometry and scanning electron microscopy. The main results of this study are discussed here. Full details of the SEM analysis are included in Annex B. The phases present in cement blocks after 20 months exposure to high saline groundwater (groundwater A) and to deionised water have been determined by XRD. The phases present in equivalent deionised water mixes have also been determined. The results are summarised in tables 7.16 - 7.19.

75 ggbs:25 OPC blends at 25°C

75 ggbs:25 OPC cement blocks stored in deionised water at 25°C showed some differences from the equivalent powder samples. Calcium hydroxide was still present, illustrating the fact that the hydration of the ggbs component had not proceeded as quickly as in the powder sample. Monosulphate (C_4ASH_{12}) was present in large amounts in the block but was absent in the equivalent powder sample after 20 months. It was, however, present in 75 ggbs:25 OPC powder samples reacted with deionised water at earlier test ages.

The 75 ggbs:25 OPC block stored in groundwater for 20 months contained only trace quantities of ettringite, unlike the equivalent powder sample which contained over 20% crystalline ettringite. This was due to the limited migration of SO_4^{2-} into the sample. AFm-Cl was probably present in the cement block, but only in small amounts. Small quantities of NaCl were present in the block.

75 ggbs:25 OPC blends at 85°C

75 ggbs:25 OPC cement blocks stored in deionised water at 85°C showed that the hydration and crystallisation processes had proceeded less quickly in the block samples than in the equivalent powder samples. The tobermorite-like phase, which was detected in the equivalent powder sample reacted with deionised water was not present. Significant amounts of siliceous hydrogarnet were detected in both block and powder samples after 20 months. Calcite was present in the block sample after 20 months but not in the equivalent powder sample.

75 ggbs:25 OPC blocks stored in groundwater at 85°C contained AFm-Cl (as in the 20 month powder sample). Significantly less siliceous hydrogarnet was present in the 75 ggbs:25 OPC block stored in groundwater after 20 months than in equivalent block stored in deionised water (based on a comparison of the relative peak heights). Only a small quantity of NaCl was present compared to the equivalent powder sample.

60 pfa:40 OPC blends at 25°C

60 pfa:40 OPC cement blocks stored in deionised water and groundwater A at 25°C for 20 months differed from the equivalent powder samples. C_2ASH_8, which was present in the

powder samples, was either absent (in the groundwater mix) or present only in trace quantities (in the deionised water mix) in 60 pfa:40 OPC block samples. In this respect the samples differed substantially in their hydrate composition from the equivalent powder samples which contained significant amounts of C_2ASH_8. Its absence was probably due to the slow hydration of the pfa component in these mixes. Calcite was again present in the blocks. Ettringite was present in larger amounts in the block stored in groundwater than in the equivalent one stored in deionised water, based on a comparison of the XRD peak heights.

Table 7.16 Solid phase formation in 75 ggbs:25 OPC blocks after 20 months*.

T/°C		AFt/%	CH	Cc	CSH	Afw	HT	Si-HG	GH	AFm-½CO_2	AFm-CO_3	AFm-SO_4	AFm-Cl	AFm	NaCl	Tho	Phi	Anh
25	DI		*	*	*		*					*						
25	GWA	tr		*	*		*						*	?	*			
85	DI			*	*	*	*	*						?				
85	GWA			*	*			*					*		*			

Table 7.17 Solid phase formation in 60 pfa:40 OPC blocks after 20 months*.

T/°C		AFt/%	CH	Cc	CSH	Afw	HT	Si-HG	GH	AFm-½CO_2	AFm-CO_3	AFm-SO_4	AFm-Cl	AFm	NaCl	Tho	Phi	Anh
25	DI	*		*	*				tr		tr	*						
25	GWA	*		*	*								*		*			
85	DI			*	*			*	tr								?	
85	GWA			*	?			*							*		?	

Table 7.18 Solid phase formation in OPC blocks after 20 months*.

T/°C		AFt/%	CH	Cc	CSH	Afw	HT	Si-HG	GH	AFm-½CO_2	AFm-CO_3	AFm-SO_4	AFm-Cl	AFm	NaCl	Tho	Phi	Anh
25	DI	tr	*	tr	?			?			*	*						
25	GWA	*	*	?	?			?					*		*			
85	DI		*	*	?			*										
85	GWA		*	*	?			*					*	?	*			

Table 7.19 Solid phase formation in reference backfill blocks after 20 months*.

T/°C		AFt/%	CH	Cc	CSH	Afw	HT	Si-HG	GH	AFm-½CO_2	AFm-CO_3	AFm-SO_4	AFm-Cl	AFm	NaCl	Tho	Phi	Anh
25	**DI**	*	*	*	?			tr			*							
25	**GWA**	*	*	*	?			tr					tr					
85	**DI**		*	*	?			*										
85	**GWA**		*	*	?			tr					*		*			

*Tables 7.16-7.19. Abbreviations: DI = deionised water; GWA = Groundwater A. Other mineral abbreviations: Tho = Thomsonite, Phi = phillipsite and Anh = anhydrite

60 pfa:40 OPC blends at 85°C

60 pfa:40 OPC blocks stored in deionised water and groundwater A for 20 months at 85°C both contained thomsonite in trace quantities although phillipsite, which was found in powder samples, was absent in both cases. Traces of C_2ASH_8 were present in the block stored in deionised water. Calcite was again present in the blocks.

OPC at 25°C and 85°C

The OPC blocks stored in groundwater and deionised water at 25°C for 20 months contained similar phases to those in powder samples although calcite was also present in the blocks.

The phases present in the OPC block stored in deionised water at 85°C for 20 months were similar to those in the equivalent powder sample although again calcite was also present. AFm-Cl and anhydrite, $CaSO_4$, were detected in the sample stored in groundwater.

Reference backfill blocks at 25°C and 85°C

Blocks prepared using the reference backfill and stored in deionised and groundwater for 20 months at 25°C and 85°C contained similar hydrates to the equivalent powder samples although there were some minor differences in the AFm phases present in block and powder samples prepared using deionised water at 25°C. Afwillite may have been present in the deionised water block at 85°C although the XRD peaks were small.

7.3.1.7. Details of phase identification and discussion

Hydrated phases were identified using XRD by comparison with JCPDS cards as described in Section 7.2. The identification of hydrates was fairly straightforward in some cases. However, there were problems with the identification of some of the other phases present due to the similarity between the JCPDS patterns of possible phases, and poor matches between the standard and measured patterns. NaCl was present in samples prepared using saline groundwaters as a consequence of the experimental procedures used.

a. Sulphate-containing phases

Ettringite, $C_6A\bar{S}_3H_{32}$, was identified by comparison with JCPDS card 41-1451. Ettringite formed in all compositions at 25°C and 55°C (although only in trace amounts in 60 pfa:40 OPC blends at 55°C) and was present in significantly larger quantities in mixes prepared using groundwater than in the equivalent deionised water samples, particularly in 75 ggbs:25 OPC and 60 pfa:40 OPC blends. This was probably due to the increased availability of alumina in these mixes. The largest amount detected was 46% in the 60 pfa:40 OPC mix at 25°C after 20 months. Ettringite was absent from mixes at 85°C at extended ages. It is thought [18] to remain a stable phase at elevated temperatures, although it does not appear to be present at equilibrium at the compositions studied. It was present at early ages (up to 3 months) in OPC and reference backfill blends at 85°C but this is likely to be due to its persistence after formation during the precure.

The formation of ettringite with time in mixes prepared using groundwater A is shown, together with the aqueous sulphate ion concentrations, in figures 7.1 to 7.7. Ettringite formed

in large amounts in 75 ggbs:25 OPC blends reacted with groundwaters at 25°C and 55°C. The amount present appeared to reach a maximum after 3 months before falling with time (see figure 7.1). The sulphate ion concentration in the aqueous phases of these mixes fell up to 3 months and was then approximately constant. The amount of ettringite present in 60 pfa:40 OPC blends reacted with groundwaters at 25°C generally increased with time, possibly as a result of the slow hydration of the pfa component increasing the availability of aluminium. Ettringite was absent, or present only in small amounts in equivalent mixes prepared using deionised water and at higher temperatures. Its absence at 55°C may have been due to the low pH (see table 20) or the preferential formation of AFm-Cl (at 7 days and 3 months) and thomsonite (after 3 months) as aluminium-containing phases (see table 7.8). Work carried out under the current programme at Aberdeen University on pure ettringite in NaCl solutions has shown that the its solubility increases with increasing NaCl concentration. This may contribute to the fact that ettringite was not detected in significant amounts in 60 pfa:40 OPC prepared using groundwaters at 55°C.

The amount of ettringite formed in OPC and backfill mixes reacted with groundwaters at 25°C and 55°C was similar to the amounts formed in equivalent deionised water mixes and was generally less than that formed in other blends reacted with groundwater. Figures 7.3 and 7.4 show that the amount of crystalline ettringite detected in OPC and backfill mixes prepared using groundwater A generally increased with time throughout the test. The sulphate ion concentration, however, generally fell up to 3 months and was then approximately constant. The apparent increase in ettringite content may have arisen as a consequence of crystallisation from an ettringite 'gel'.

Figure 7.4 Ettringite in reference backfill mixes

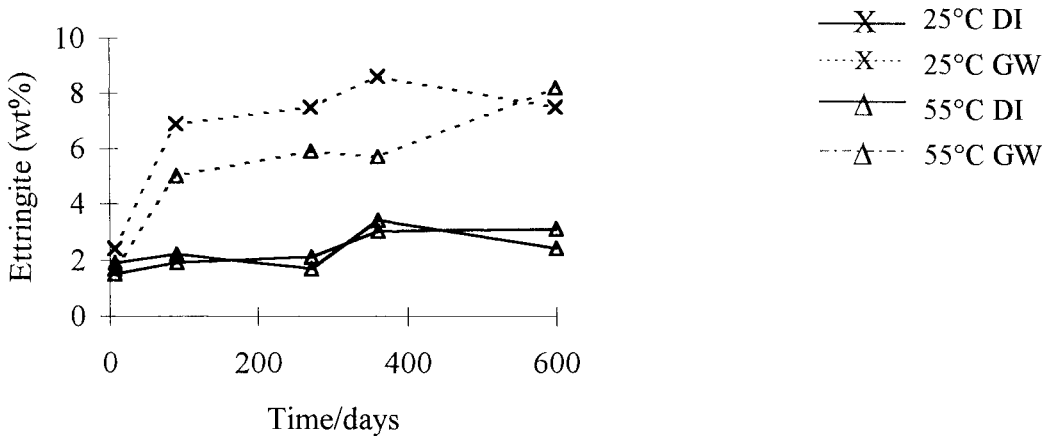

Figure 7.5 Ettringite and sulphate in 75 ggbs:25 OPC blends prepared using groundwater A

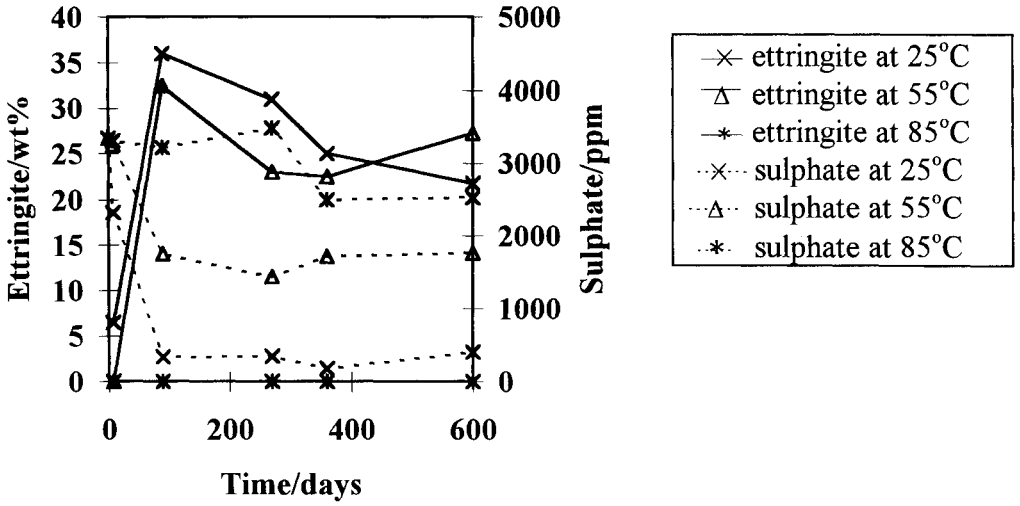

Figure 7. 6 Ettringite and sulphate in 60 pfa: 40 OPC blends prepared using groundwater A

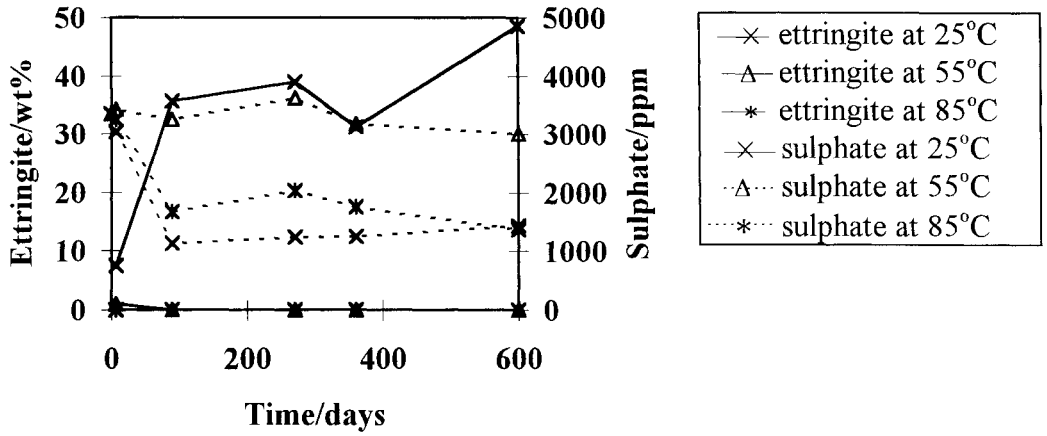

Figure 7.7 Ettringite and sulphate in OPC mixes prepared using groundwater A.

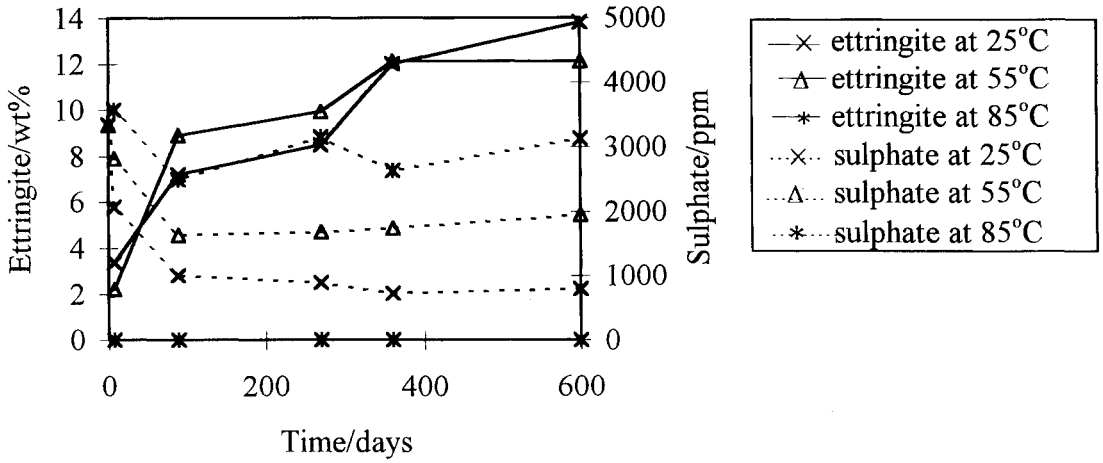

The formation of ettringite is an expansive process and can lead to cracking where it occurs in previously set concretes. The current work suggests that it is likely to form in large quantities under repository conditions, particularly in 75 ggbs:25 OPC and 60 pfa:40 OPC blends but also in the backfill, through interactions with the groundwater and on cooling and could therefore lead to expansion and cracking.

Anhydrous calcium sulphate, $CaSO_4$, was identified by comparison with JCPDS card 37-0184. It formed in mixes prepared using groundwaters at 85°C. It may be a stable phase and has also been detected in the pure phase dissolution experiments carried out under the current programme at Aberdeen University in which C-S-H was aged in $MgSO_4$ solutions at 85°C.

The AFm phase monosulphate ($C_4A\bar{S}H_x$) forms as a series of hydrated states. The actual hydrate that is present in a dried solid depends on the humidity. $C_4A\bar{S}H_{12}$ (JCPDS card 18-0275) was the most commonly detected form of monosulphate in the current work, although $C_4A\bar{S}H_{14}$ (JCPDS 42-0062) and possibly $C_4A\bar{S}H_{11}$ (JCPDS 41-0477) were also found. $C_4A\bar{S}H_{10}$ can also form although this phase cannot be readily distinguished from $C_4A\bar{C}_{0.5}H_{12}$ and Kuzel's salt, $C_4A\bar{S}_{0.5}ClH_{12}$. As with other AFm phases, 'solid solutions' can be formed through the replacement of SO_4^{2-} by other anions[6]. Monosulphate was present in 75 ggbs:25 OPC and 60 pfa:40 OPC mixes prepared using deionised water at 25°C and 55°C at early test ages (although it was also present in the 60 pfa:40 OPC mix at 25°C after 20 months). It was absent in all groundwater mixes, probably as a result of the formation of ettringite and AFm-Cl.

Sulphate-containing phases may also have formed in small quantities (below the detection limits of the XRD technique used). The sulphate ion concentration fell with time in some cases (for example 60 pfa:40 OPC blends reacted with groundwater A at 55°C) in which no

sulphate-containing phases were identified and it is possible that trace amounts of ettringite or monosulphate were present.

b. Hydrogarnet

The XRD lines for hydrogarnet phases were generally close to those of C_3ASH_4 (JCPDS card 38-0368). This composition has been abbreviated as Si-Hg (for siliceous hydrogarnet) in tables 7.4 to 7.15. However, the XRD peaks were often small and it is possible that hydrogarnets with lower silica contents were present in some OPC and reference backfill mixes. Solid solutions are known to form in the range C_3AH_6 to C_3AS_3 and the composition can be determined from the XRD line shifts[25] although an accurate analysis has not been carried out here. Fe substitution for Al will also occur but the extent to which this occurs cannot readily be determined by XRD and so has not been studied here. TEM analysis of a 75 ggbs:25 OPC blend cured at 85°C for 20 months in deionised water is consistent with a hydrogarnet composition close to C_3ASH_4. It has also shown that iron and sulphur are present in the hydrogarnet structure (see Annex A).

Work carried out under the current programme at Aberdeen University on pure C_3AH_6 in NaCl solutions has shown that C_3AH_6 is replaced by AFm-Cl and CH at all temperatures studied. The cement - groundwater interaction experiments carried out at BRE are consistent with these results. Siliceous hydrogarnet was absent from 75 ggbs:25 OPC mixes at 55°C and 85°C prepared using groundwater, but was present in significant quantities in deionised water mixes. In OPC and backfill mixes hydrogarnet was present in many groundwater mixes, but in smaller quantities (based on a comparison of XRD peak heights) than in equivalent deionised water mixes.

c. Zeolites

A zeolite phase with an XRD trace similar to thomsonite, ideal composition $NaCa_2(Al,Si)_5O_{20}.6H_2O$, was identified by comparison with JCPDS card 35.0498. The match with the standard pattern was good in cases where the sample peaks were substantial. However, as discussed in Section 7.3.1.2, TEM showed that the zeolite phase present in a 60 pfa:40 OPC mix reacted with deionised water for 20 months at 85°C was alkali free. The composition of the phase formed in deionised water was consistent with that of scolecite ($CA_2S_3H_3$) although a definite composition could not be determined. TEM did not distinguish between the two zeolites expected from the XRD results for the deionised water sample. The composition of the zeolite phase in the groundwater sample did not match that of any specific zeolite.

The assignment of XRD peaks in 60 pfa:40 OPC blends at 55°C and 85°C to the zeolite mineral phillipsite ($KCa(Si_5Al_3)O_{16}.6H_2O$, JCPDS card 39.1375) was not conclusive. Other zeolites that are consistent with the XRD trace are garronite ($NaCa_{2.5}(Si_{10}Al_6)O_{32}.14H_2O$, JCPDS card 39.1374), gismondine ($CaAl_2Si_2O_8.4H_2O$, JCPDS card 20.0452) and an unnamed mineral ($K_{0.8}Na_{0.7}Ca_{0.7}Al_{2.8}Si_{5.1}O_{16.6}.6.4H_2O$, JCPDS card 34.0542). Phillipsite is chemically similar to synthetic sodium zeolites (described as Na-P) and has a similar XRD pattern. Thomsonite peaks were stronger in the mixes reacted with groundwater than in equivalent deionised water mixes. This was matched by the absence of phillipsite in groundwater mixes after 3 months. This observation may be associated with the increased availability of alkali metals in the groundwater.

The amounts of thomsonite formed in the current work were substantially smaller (based on a comparison of the XRD peak heights) than in previous experiments in which 60 pfa:40 OPC blends were reacted with high sulphate-bearing and high carbonate-bearing groundwaters and deionised water at 90°C for up to 3 years and 9 months [11]. Phillipsite, however, was formed in larger quantities in the current work than in the earlier work. These differences may have been due to the use of different experimental conditions (including the temperatures), the longer reaction times used in the earlier series, or to small variations in the compositions of the materials used in the two sets of experiments. One other important difference between the two sets of results is the presence of gehlenite hydrate, C_2ASH_8, in deionised water samples at 85°C. C_2ASH_8 is likely to have formed during the initial 20°C precure and then persisted for the duration of the test at 85°C. However, its stability at 85°C has not been confirmed. It was not present in the earlier series of tests (which were not precured) at 90°C. It is possible that C_2ASH_8 is not stable at 85°C and would eventually have been replaced by more thomsonite.

d. Calcium silicate hydrates

A number of calcium silicate hydrates were detected in the experimental programme. Gel phases were persistent at lower temperatures but were replaced after prolonged ageing at temperatures of 50°C and above by crystalline phases as discussed below.

C-S-H gel was identified by the presence of a broad band on the XRD trace at about 3 Å. It has not been possible to establish its presence using XRD in all cases because of background noise and overlaps with peaks arising from other phases. It may therefore have persisted at extended ages even in mixes where crystalline calcium silicate hydrates had formed. An additional broad peak at about 15 Å occurred in the XRD traces for 75 ggbs:25 OPC blends, but this line disappeared with time as the tobermorite-like phase discussed below formed.

The tobermorite-like phase was characterised by XRD peaks at between 10.1 and 10.8 Å and at about 3.1 Å. The peaks were sharper than those of the C-S-H gel discussed above. The XRD pattern was similar to, but not an exact match for, those of 11 Å tobermorite, $C_5S_6H_5$ (JCPDS card 19.1364) and jennite, $C_9S_6H_{11}$ (JCPDS card 18.1206). TEM analysis of 75 ggbs:25 OPC blends reacted with groundwater at 85°C for 20 months showed that the composition of this phase was consistent with that of jennite rather than tobermorite. Foshagite (C_4S_3H), afwillite ($C_3S_2H_3$) and xonotlite (C_6S_6H) were also consistent with the TEM results, although these phases were not consistent with the XRD trace.

Some 75 ggbs:25 OPC blends also contained a peak at about 12.3 Å. This is likely to be due to the presence of a calcium silicate hydrate and were assigned to the synthetic semicrystalline material C-S-H(I) [6]. Again the match was not exact. The crystalline calcium silicate hydrate, afwillite, $C_3S_2H_3$, (JCPDS card 29.0030), has been detected in OPC mixes at 55°C and in one 75 ggbs:25 OPC blend at 85°C. The agreement with the reference pattern was good. Pure C-S-H gels dissolved in NaCl solutions have shown that the presence of NaCl inhibits the formation of crystalline calcium silicate hydrates. This observation is consistent with the results of the current experiments in which the tobermorite-like phase and afwillite were not respectively formed in 75 ggbs:25 OPC blends and in OPC mixes prepared using groundwater.

Amorphous calcium silicate hydrate gels, described as C-S-H to indicate that no particular composition is implied, are formed in large quantities when blended cements are hydrated and have important effects on the properties of the cement. The C/S ratio of the gel is in the range

0.8 to 1.7 depending on the composition of the starting materials [6]. The degree of crystallinity may depend on the conditions and the duration of the hydration process. Tobermorite, jennite and afwillite have not been detected in Portland-based cements under normal conditions but they can be synthesised below 100°C. Afwillite has been reported [6] to be the stable calcium silicate hydrate phase in contact with $Ca(OH)_2$ and solution at temperatures under 100°C. Crystalline calcium silicate hydrates are thermodynamically more stable and therefore less soluble than gels and their formation from C-S-H gel would lead to a reduction in the pH of the aqueous phase.

X-ray examinations of ancient lime mortars of up to 2000 years old have shown that crystalline calcium silicate hydrates can form from C-S-H gels over long periods [19]. The crystalline calcium silicate hydrates tobermorite, hillebrandite, afwillite, gyrolite and riversidite have all been detected. Some of these hydrates can be formed in OPC under hydrothermal conditions and their presence in these ancient lime mortars suggests that they may form in OPC and blended OPC cements under ordinary conditions after prolonged ageing. However, a separate study of ancient building materials [20] showed that C-S-H gel, with a composition that was very similar to that found in modern concretes, was still present in 1700 year old concrete from Hadrian's wall. Naturally occurring calcium silicate hydrate gels have also been found in Scawt Hill [21] and in Israel [22]. These latter materials are millions of years old and suggest that amorphous calcium silicate hydrates can exist for very long periods in the absence of aggressive agents.

e. Calcite

Calcite, $CaCO_3$, was identified by comparison with JCPDS card 5.0586. Calcite was only detected in backfill mixes which were prepared using limestone filler. It was, however, also detected in cement paste blocks, presumably as a result of carbonation due to atmospheric CO_2 arising as a consequence of the experimental procedure used.

f. Calcium hydroxide (portlandite)

Calcium hydroxide (portlandite), $Ca(OH)_2$, was identified by comparison with JCPDS card 4.0733. $Ca(OH)_2$ formed in all OPC and reference backfill mixes. The amount of $Ca(OH)_2$ present in OPC and reference backfill mixes was determined using TGA. The amounts detected are included in tables 7.10 to 7.15.

g. Gehlenite hydrate (strätlingite)

Gehlenite hydrate, $C_2A\bar{S}H_8$, was identified by comparison with JCPDS card 29.0285. It was present in all 60 pfa:40 OPC mixes except those prepared using groundwater A at 85°C after at least 9 months. Based on the heights of XRD peaks C_2ASH_8 was present in smaller quantities in mixes prepared using groundwater than deionised water. At 25°C this may have been due to the formation of large quantities of ettringite due to the high sulphate content of the groundwater. The high NaCl concentration may also have inhibited the formation of C_2ASH_8.

The stability of gehlenite hydrate at 85°C is uncertain. It persisted in mixes prepared using deionised water at this temperature for the duration of the test having formed during the initial precure at 20°C. However, it is possible that it would eventually have disappeared. It did not form in the earlier series of tests carried out at 90°C[11]. A separate experiment [23] in which

CaO, AH_3 and silicic acid, in the proportions needed to form C_2ASH_8, were mixed with excess water at 90°C using similar accelerated reaction techniques to those used here did not lead to the formation of C_2ASH_8. A siliceous hydrogarnet with a composition of approximately $C_3AS_{0.3}H_{5.4}$ together with a zeolite phase with an XRD pattern similar to those of thomsonite ($NaCa_2Al_5SiO_{20}.6H_2O$) and scolecite ($CaAl_2Si_3O_{10}.3H_2O$) were identified by XRD. A calcium silicate hydrate phase with an XRD pattern similar to that of hillebrandite (C_2SH) may also have been present. However, this experiment was not repeated and the result has not therefore been confirmed.

h. Hydrotalcite and calcium carboaluminate hydrate (AFm-CO_3)

XRD peaks at 7.58 Å and 3.78 Å were frequently found in all mix compositions. They matched those of the hydrotalcite phase M_4AH_{10} (JCPDS card 35.0964). The d-spacings are also consistent with the tetracalcium carboaluminate hydrate (AFm-CO_3), $C_4A\bar{C}H_{11}$ (JCPDS card 41.0219). Hydrotalcite is most likely to form in 75 ggbs:25 OPC mixes due to the enhanced Mg level. $C_4A\bar{C}H_{11}$ was probably present in the other compositions.

i. Calcium hemicarboaluminate hydrate (AFm-½CO_2)

XRD peaks were often detected at 8.08 - 8.48 Å and 4.04 - 4.22 Å. These peaks were consistent with a number of AFm phases. The range was such that it is likely that the composition of this phase varied from one mix to the next or that two different compounds with slightly different XRD patterns were present This phase was probably either calcium hemicarboaluminate hydrate, $C_4A\bar{C}_{0.5}H_{12}$ (JCPDS card 41.0221), or the monosulphate $C_4A\bar{S}H_{10}$, both of which are known to form in cement systems. Both these phases form solid solutions with C_4AH_{13} which may account for variations in the XRD pattern. Kuzel's salt, $C_4A\bar{S}_{0.5}ClH_{12}$ (JCPDS card 19.0203) is also consistent with these peaks.

j. Calcium hydroxyaluminate hydrate (AFm)

XRD peaks were detected at 7.80 Å, 3.90 Å and 2.60 Å in some OPC and reference backfill mixes prepared using deionised water. The d-spacings correspond to those of calcium hydroxyaluminate, C_4AH_{13} (JCPDS card 16.0339), but also match those of Friedel's salt $C_4ACl_2H_{10}$ (JCPDS card 42.0558: see AFm-Cl below). C_4AH_{13} is more likely to have been formed in mixes prepared using deionised water: $C_4ACl_2H_{10}$ is likely to have been present in mixes prepared using groundwater due to the high chloride content.

These d-spacings are also consistent with the hydrotalcite-type phase $M_6AH_{13.5}$ (JCPDS card 35.0965) although this phase is unlikely to have formed in OPC and backfill mixes on compositional grounds.

k. AFm-Cl

This phase was present in mixes prepared using groundwater. It formed in larger quantities in mixes prepared using groundwater A than in those prepared using the lower salinity groundwater B and was absent in equivalent deionised water mixes suggesting that it was a chloride-containing phase. It was characterised by strong XRD lines at 7.80 Å and 3.90 Å. The peaks present did not match exactly any of the JCPDS standards, but they were very similar to calcium monochloroaluminate (Friedel's salt), $C_4ACl_2H_{10}$ (JCPDS card 42.0558).

7.3.2. Aqueous phase composition.

The results of the aqueous solution analyses are given in figs 7.8-7.16 and tables 7.20 -7.31. Some species present in low concentrations were difficult to determine due to the high sodium and chloride ion concentrations in groundwater A. The high sodium concentrations increased the noise levels in atomic absorption spectroscopy, making it difficult to determine aluminium and iron using this technique. Aluminium has been determined using an absorptiometric technique. The high saline concentrations have also caused problems through overloading the Dionex ion chromatogram columns. As a result bromide, ammonium, nitrate and carbonate could not be determined.

i) pH values, shown in figs 7.13-7.16, are consistently lower in mixes prepared using groundwater than in those prepared using deionised water. The pH was also lower in samples prepared using groundwater A than for equivalent mixes prepared using groundwater B. The lowest levels were detected in water reacted with 60 pfa:40 OPC blends at elevated temperatures. The pH fell to 8.81 in the 60 pfa:40 OPC blend prepared using groundwater A after 20 months at 85°C and to 9.3 in the equivalent blend at 55°C. pH values in equivalent deionised water mixes were 11.15 and 11.45 respectively.

   In the previous series of tests [11] similar pH values to those observed in the current deionised water samples were recorded at comparable test ages for 75 ggbs:25 OPC and OPC mixes although the values fell slightly with further ageing. The pH in a 60 pfa:40 OPC mix prepared using deionised water fell to 8.45 after 1090 days.

   Similar results have been observed in pure hydrate dissolution experiments carried out at Aberdeen University as part of this programme. The pH of solutions formed by dissolving CH in NaCl solutions have been found to be lower than equivalent ones formed by dissolving CH in deionised water. However, it has been reported [24] that NaCl solutions do not alter the pH of calcium hydroxide solutions and that misleading results can arise due to the sodium selectivity of glass electrodes.

ii) Magnesium ion concentrations were significantly lower than in the initial (unreacted) groundwaters at all ages. In some cases this was caused by the formation of hydrotalcite-like phases. However, this phase was not present in all mixes.

iii) Silicate ion concentrations were highest in 60 pfa:40 OPC blends reacted with deionised water. These are significantly higher than the equivalent mixes prepared using either groundwater. The silicate ion concentrations generally increased with time in 60 pfa:40 OPC blends prepared using deionised water at all temperatures. Maximum values of 34 ppm were measured at 55°C and 85°C. The maximum value measured at 25°C was 16.8 ppm.

iv) Sodium and chloride ion concentrations in mixes prepared using groundwater were comparable with those in the unreacted groundwater. The Na and Cl concentrations for the 12 month 75 ggbs:25 OPC and the 20 month reference backfill blends reacted with groundwater A at 85°C were both significantly higher than the groundwater. This is likely to have been due to slow evaporation of water during the tests.

v) Sulphate levels in the aqueous phases were generally lower than those in the unreacted groundwaters, especially at 25°C and 55°C. The aqueous sulphate levels generally correlate well with the ettringite content of the paste (see figures 7.5 to 7.8) at 25°C and 55°C. At 85°C the sulphate content in mixes is generally lower than in the unreacted groundwater, especially for 60 pfa:40 OPC blends, possibly due to uptake of sulphate by the C-S-H gel although TEM analyses of selected mixes (see Annex A) were unable to confirm this point.

Table 7.20 Solution analyses for 75 ggbs:25 OPC at 25°C. Concentrations in ppm.

Deionised water	Age	pH	Ca^{2+}	Mg^{2+}	Na^{+}	K^{+}	Fe	SiO_2	Cl^{-}	SO_4^{2-}	CO_3^{2-}	Al
	7d	13.1	427	0.09	105	193	nd	1.06	10.2	0.6	6	
	3m	12.7	481	nd	91	183	0.6	0.14	8.3	0.6	7.7	
	9m	12.51	330	nd	83	195	nd	0.38	3.6	1.4	6.2	2.1
	12m	12.02	389	nd	99	239	0.13	0.31	3.32	3.6	12.8	2.06
	20m	12.64	399	0.02	85	181	1.08	0.2	6	3.7	6.3	1.26
Groundwater A	**Age**	**pH**	Ca^{2+}	Mg^{2+}	Na^{+}	K^{+}	**Fe**	SiO_2	Cl^{-}	SO_4^{2-}	CO_3^{2-}	**Al**
	7d	12.28	2510	0.18	71100	608	4	0.94	113400	2320		
	3m	11.94	1910	0.08	55000	630	3.5	0.39	95100	330		
	9m	11.85	1520	0.1	54200	690	2	0.8	94800	340		0.21
	12m	11.81	1440	0.08	55700	743	4.6	0.51	109300	180		0.24
	20m	11.98	1440	0.08	54800	687	0	0.34	97175	400		0.19
Groundwater B	**Age**	**pH**	Ca^{2+}	Mg^{2+}	Na^{+}	K^{+}	**Fe**	SiO_2	Cl^{-}	SO_4^{2-}	CO_3^{2-}	**Al**
	7d	12.14	680	0.02	7510	309	0.3	0.44	13030	36	9	1.01
	3m	12.05	711	0.02	7670	315	0.27	0.44	13630	44	<5	1.21
	12m	12.16	668	0.03	6974	236	0.8	0.51	13570	20		0.74

Table 7.21 Solution analyses for 75 ggbs:25 OPC at 55°C. Concentrations in ppm.

Deionised water	Age	pH	Ca^{2+}	Mg^{2+}	Na^{+}	K^{+}	Fe	SiO_2	Cl^{-}	SO_4^{2-}	CO_3^{2-}	Al
	7d	13.13	413	0.09	100	188	nd	1.17	8.1	10.1	7.1	
	3m	12.57	424	nd	87	189	0.6	0.22	7	70.7	10	
	9m	12.29	105	nd	84	200	nd	0.9	7.5	165	12.2	0.11
	12m	11.91	227	0.02	102	243	0.14	0.46	10.3	102	4.9	0.24
	20m	12.42	199	0.02	97	191	1.19	0.48	7.9	248	5.9	0.46
Groundwater A	**Age**	**pH**	Ca^{2+}	Mg^{2+}	Na^{+}	K^{+}	**Fe**	SiO_2	Cl^{-}	SO_4^{2-}	CO_3^{2-}	**Al**
	7d	12.2	2560	0.18	72300	596	4	1.08	114500	3240		
	3m	11.83	2200	0.09	56300	612	3.5	0.33	95500	1750		
	9m	11.54	1590	0.05	55900	740	2.1	0.72	98300	1430		0.17
	12m	11.54	1690	0.09	58000	768	4.6	0.51	112700	1710		0.21
	20m	11.61	1620	0.09	56800	729	0	0.44	101400	1770		0.3
Groundwater B	**Age**	**pH**	Ca^{2+}	Mg^{2+}	Na^{+}	K^{+}	**Fe**	SiO_2	Cl^{-}	SO_4^{2-}	CO_3^{2-}	**Al**
	7d	12.14	711	0.02	7710	321	0.28	0.39	13350	158	9.5	1.82
	3m	11.98	632	0.02	7835	326	0.24	0.33	13770	74	16.5	0.89
	12m	11.78	668	0.015	7271	254	0.8	0.71	15290	656		0.48

Table 7.22 Solution analyses for 75 ggbs:25 OPC at 85°C. Concentrations in ppm.

Deionised water	Age	pH	Ca^{2+}	Mg^{2+}	Na^{+}	K^{+}	Fe	SiO_2	Cl^{-}	SO_4^{2-}	CO_3^{2-}	Al
	7d	13.1	356	0.09	102	181	nd	1.11	22.7	49.3	8.1	
	3m	12.37	120	nd	91	193	0.7	0.84	11	170	8.6	
	9m	12.16	160	nd	94	220	nd	2.04	11	213	10.4	0.85
	12m	11.72	132	0.03	111	261	0.16	0.83	15.7	316	14.8	0.33
	20m	12.19	152	0.02	109	235	1.4	0.84	7.9	248	5.9	0.3
Groundwater A	**Age**	**pH**	**Ca^{2+}**	**Mg^{2+}**	**Na^{+}**	**K^{+}**	**Fe**	**SiO_2**	**Cl^{-}**	**SO_4^{2-}**	**CO_3^{2-}**	**Al**
	7d	12.2	2590	0.18	69900	612	4	0.92	113400	3300		
	3m	11.57	2410	0.08	57400	626	3.8	0.31	96300	3210		
	9m	11.38	2190	0.1	59000	780	2.3	0.66	105400	3480		0.25
	12m	10.94	2110	0.03	89200	1070	7	0.42	162000	2500		0.33
	20m	11.22	1960	0.09	68420	899	0	0.4	120900	2530		0.21
Groundwater B	**Age**	**pH**	**Ca^{2+}**	**Mg^{2+}**	**Na^{+}**	**K^{+}**	**Fe**	**SiO_2**	**Cl^{-}**	**SO_4^{2-}**	**CO_3^{2-}**	**Al**
	7d	12.06	1090	0.06	7700	308	0.37	0.21	13740	1240	<5	0.21
	3m	11.9	1070	0.03	7790	314	0.34	0.15	13970	1464	<5	0.15
	12m	11.71	764	0.015	7197	253	0.8	0.89	14270	1130		0.26

Table 7.23. Solution analyses for 60pfa:40 OPC at 25°C. Concentrations in ppm.

Deionised water	Age	pH	Ca^{2+}	Mg^{2+}	Na^{+}	K^{+}	Fe	SiO_2	Cl^{-}	SO_4^{2-}	CO_3^{2-}	Al
	7d	12.84	16	0.06	185	479	nd	7.9	18.4	172	45.8	
	3m	12.33	2	0.02	143	398	0.2	8.8	5	337	110	
	9m	12.22	110	nd	140	420	0.05	11.4	4	316	6.3	13.34
	12m	11.91	6	0.02	185	452	0	16.8	40.5	329	17.9	10.39
	20m	12.18	25	0.02	155	1150	1.18	13.4	1.6	454	8.3	18.8
Groundwater A	**Age**	**pH**	**Ca^{2+}**	**Mg^{2+}**	**Na^{+}**	**K^{+}**	**Fe**	**SiO_2**	**Cl^{-}**	**SO_4^{2-}**	**CO_3^{2-}**	**Al**
	7d	10.9	2390	0.3	71200	865	4	1.6	114000	3040		
	3m	10.18	2350	nd	54700	911	4.9	2	96800	1130		
	9m	10.35	2030	0.4	54600	1030	2.3	4.2	95500	1240		0.48
	12m	10.47	1910	0.35	53100	1110	4.6	3.4	96400	1250		0.4
	20m	10.39	2021	0.38	52400	1010	0	2.9	96700	1430		1.99
Groundwater B	**Age**	**pH**	**Ca^{2+}**	**Mg^{2+}**	**Na^{+}**	**K^{+}**	**Fe**	**SiO_2**	**Cl^{-}**	**SO_4^{2-}**	**CO_3^{2-}**	**Al**
	7d	11.51	564	nd	7330	534	0.31	2.6	14053	175		5.04
	3m	11.28	521	0.08	7750	648	0.28	4.72	13920	186	43	1.12
	12m	10.91	514	0.15	7123	534	0.8	6.2	14165	286		3.1

Table 7.24. Solution analyses for 60pfa:40 OPC at 55°C. Concentrations in ppm.

Deionised water	Age	pH	Ca^{2+}	Mg^{2+}	Na^{+}	K^{+}	Fe	SiO_2	Cl^{-}	SO_4^{2-}	CO_3^{2-}	Al
	7d	12.78	21	0.06	217	573	nd	8.8	23.3	410	48.3	
	3m	12.16	31	0.02	167	438	0.3	16.8	5	630	47.3	
	9m	11.82	34	nd	170	480	nd	22.5	3.7	709	23.2	0.8
	12m	11.48	14	0.06	171	575	0.09	34.2	9.6	653	29.7	2.15
	20m	11.45	56	0.04	184	496	1.4	25.6	25.1	960	19.4	2.22
Groundwater A	**Age**	**pH**	**Ca^{2+}**	**Mg^{2+}**	**Na^{+}**	**K^{+}**	**Fe**	**SiO_2**	**Cl^{-}**	**SO_4^{2-}**	**CO_3^{2-}**	**Al**
	7d	11.04	3060	0.36	70100	911	4	1.6	114000	3240		
	3m	10.76	2970	0.02	54700	977	3.6	2.3	95700	3240		
	9m	9.91	2940	0.4	55400	1200	2.4	4.8	98030	3620		0.48
	12m	10.14	2890	0.15	54300	1380	4.7	5.5	99800	3180		0.37
	20m	9.3	3357	0.2	58900	1770	0	5.8	109900	3000		0.79
Groundwater B	**Age**	**pH**	**Ca^{2+}**	**Mg^{2+}**	**Na^{+}**	**K^{+}**	**Fe**	**SiO_2**	**Cl^{-}**	**SO_4^{2-}**	**CO_3^{2-}**	**Al**
	7d	11.43	739	nd	7553	527	0.31	3.05	13965	796		7.47
	3m	8.19	718	0.15	7740	734	0.3	0.82	13970	1108	48.5	0.17
	12m	10.39	979	0.075	7011	773	1	15.1	14975	1620		0.92

Table 7.25. Solution analyses for 60pfa:40 OPC (ppm) at 85°C. Concentrations in ppm.

Deionised water	Age	pH	Ca^{2+}	Mg^{2+}	Na^{+}	K^{+}	Fe	SiO_2	Cl^{-}	SO_4^{2-}	CO_3^{2-}	Al
	7d	12.53	35	0.09	205	606	nd	8.1	5.2	742	19.6	
	3m	11.66	24	0.02	156	506	0.4	30.7	11	840	120	
	9m	11.29	60	nd	170	420	0.05	33.8	4.2	916	11.4	0.48
	12m	10.96	27	0.06	86	617	0.06	19.8	8.2	712	32.1	0.34
	20m	11.15	159	0.04	240	911	1.49	14.8	14	1930	24.4	1.59
Groundwater A	**Age**	**pH**	**Ca^{2+}**	**Mg^{2+}**	**Na^{+}**	**K^{+}**	**Fe**	**SiO_2**	**Cl^{-}**	**SO_4^{2-}**	**CO_3^{2-}**	**Al**
	7d	10.77	2960	0.24	70900	1000	4	1.2	117000	3240		
	3m	10.44	3020	0.08	55300	1290	3.6	3.7	100800	1670		
	9m	8.05	3210	0.1	57000	1530	2.4	2.6	104300	2030		0.42
	12m	9.27	3060	0.17	57600	1580	4.9	1.3	105500	1750		0.37
	20m	8.81	3400	0.24	65800	1860	nd	2	124200	1370		0.69
Groundwater B	**Age**	**pH**	**Ca^{2+}**	**Mg^{2+}**	**Na^{+}**	**K^{+}**	**Fe**	**SiO_2**	**Cl^{-}**	**SO_4^{2-}**	**CO_3^{2-}**	**Al**
	7d	11.33	982	nd	7479	568	0.36	3.91	14048	1588		1.07
	3m	10.3	1025	0.06	7649	927	0.31	12.6	14030	2210	20.5	0.08
	12m	10.67	1236	0.045	7605	843	1	6.3	15120	1880		1.09

Table 7.26. Solution analyses for OPC mixes at 25°C. Concentrations in ppm.

Deionised water	Age	pH	Ca^{2+}	Mg^{2+}	Na^{+}	K^{+}	Fe	SiO_2	Cl^{-}	SO_4^{2-}	CO_3^{2-}	Al
	7d	13.29	771	0.03	57	251	nd	0.08	7.2	1.2	7.3	
	3m	12.6	700	0.05	165	319	0.3	0.07	5	1.8	16.8	
	9m	12.66	740	nd	50	270	nd	0.16	1	1.2	3.8	0.14
	12m	12.32	674	0	60	318	0.02	0.12	0.8	1.56	6.4	0.39
	20m	12.86	688	0.02	53	243	1.22	0.08	1.1	1.5	7.8	0.43
Groundwater A	**Age**	**pH**	Ca^{2+}	Mg^{2+}	Na^{+}	K^{+}	Fe	SiO_2	Cl^{-}	SO_4^{2-}	CO_3^{2-}	Al
	7d	12.65	2870	0.12	70600	675	4	0.1	113000	2070		
	3m	12.3	2320	0.08	56800	683	3.3	0.02	105000	1000		
	9m	12.23	1990	0.2	54900	780	1.9	0.14	95900	890		0.17
	12m	12.22	1860	0.06	54500	820	4.7	0.1	96700	730		0.19
	20m	12.29	1730	0.08	53600	782		0.06	97800	800		0.19
Groundwater B	**Age**	**pH**	Ca^{2+}	Mg^{2+}	Na^{+}	K^{+}	Fe	SiO_2	Cl^{-}	SO_4^{2-}	CO_3^{2-}	Al
	7d	12.47	1321	nd	7553	343	0.26	0.04	14030	72		0.21
	3m	12.39	1132	0.02	7783	381	0.35	0.15	13665	49	8.5	0.22
	12m	12.47	1121	0.015	7270	334	0.6	0.13	13935	25		0.17

Table 7.27. Solution analyses for OPC mixes at 55°C. Concentrations in ppm.

Deionised water	Age	pH	Ca^{2+}	Mg^{2+}	Na^{+}	K^{+}	Fe	SiO_2	Cl^{-}	SO_4^{2-}	CO_3^{2-}	Al
	7d	13.29	577	0.06	185	264	nd	0.06	1.8	11.9	7.9	
	3m	12.67	630	0.02	57	272	0.4	0.11	2	4	12.5	
	9m	12.58	630	nd	44	290	nd	0.16	1.8	56	11.1	0.1
	12m	12.29	604	0.02	59	318	0.06	0.11	2.2	55.5	12.2	0.12
	20m	12.79	686	0.02	56	272	1.33	0.08	4.3	72.5	7.6	0.35
Groundwater A	**Age**	**pH**	Ca^{2+}	Mg^{2+}	Na^{+}	K^{+}	Fe	SiO_2	Cl^{-}	SO_4^{2-}	CO_3^{2-}	Al
	7d	12.56	3260	0.18	75400	519	4	0.08	123000	2820		
	3m	12.32	2580	nd	60100	720	3.6	0.01	100300	1630		
	9m	12.2	2140	0.2	56600	810	1.9	0.14	98800	1680		0.16
	12m	12.14	2110	0.06	55800	840	4.9	0.06	101700	1740		0.18
	20m	12.24	2210	0.08	62400	907	0	0.04	111600	1950		0.15
Groundwater B	**Age**	**pH**	Ca^{2+}	Mg^{2+}	Na^{+}	K^{+}	Fe	SiO_2	Cl^{-}	SO_4^{2-}	CO_3^{2-}	Al
	7d	12.42	1271	nd	7790	343	0.22	0.07	14395	202		0.22
	3m	12.38	1064	0.02	8005	390	0.31	0.11	13935	125	10	0.17
	12m	12.44	1175	0.015	7864	331	0.7	0.12	15040	146		0.3

Table 7.28. Solution analyses for OPC mixes at 85°C. Concentrations in ppm.

Deionised water	Age	pH	Ca^{2+}	Mg^{2+}	Na^{+}	K^{+}	Fe	SiO_2	Cl^{-}	SO_4^{2-}	CO_3^{2-}	Al
	7d	13.22	601	0.06	70	274	nd	0.12	19	392	10.8	
	3m	12.67	300	0.04	56	276	0.4	0.04	5	375	13.3	
	9m	12.52	570	nd	60	330	nd	0.08	1.3	195	6.4	0.06
	12m	12.29	699	0.02	73	369	0.16	0.07	2.74	280	5.3	0.12
	20m	12.69	678	0.02	63	220	1.29	0.1	10.2	394	7.6	0.07
Groundwater A	**Age**	**pH**	Ca^{2+}	Mg^{2+}	Na^{+}	K^{+}	**Fe**	SiO_2	Cl^{-}	SO_4^{2-}	CO_3^{2-}	**Al**
	7d	12.54	3210	0.12	70200	662	4	0.1	113000	3570		
	3m	12.22	2550	0.08	56300	712	3.6	0.01	95300	2500		
	9m	12.15	2540	0.2	56700	810	2.3	0.08	98100	3150		0.16
	12m	12.09	2290	0.08	61600	921	5.2	0.04	109700	2630		0.18
	20m	12.17	2290	0.08	60700	874	0	0.06	109900	3130		0.16
Groundwater B	**Age**	**pH**	Ca^{2+}	Mg^{2+}	Na^{+}	K^{+}	**Fe**	SiO_2	Cl^{-}	SO_4^{2-}	CO_3^{2-}	**Al**
	7d	12.33	1350	nd	7612	327	0.22	0.04	14048	734		0.21
	3m	12.34	1318	0.02	7842	391	0.35	0.17	13710	1119	16	0.16
	12m	12.3	1389	0.03	7531	344	0.7	0.11	15070	1330		0.12

Table 7.29. Solution analyses in reference backfill mixes at 25°C. Concentrations in ppm.

Deionised water	Age	pH	Ca^{2+}	Mg^{2+}	Na^{+}	K^{+}	Fe	SiO_2	Cl^{-}	SO_4^{2-}	CO_3^{2-}	Al
	7d	13.23	784	nd	28	104	nd	0.09	4	1.8	7.8	
	3m	12.82	730	nd	22	108	0.1	0.05	5	2.1	12	
	9m	12.11	543	nd	25	130	nd	0.14	1.1	1.3	5.6	0.26
	12m	12.35	779	nd	38	141	nd	0.1	9.8	1.9	10.7	0.28
	20m	12.49	664	0.02	22	108	1.1	0.08	0.3	1.4	14.3	0.6
Groundwater A	**Age**	**pH**	Ca^{2+}	Mg^{2+}	Na^{+}	K^{+}	**Fe**	SiO_2	Cl^{-}	SO_4^{2-}	CO_3^{2-}	**Al**
	7d	12.56	3360	nd	73100	525	3	0.07	113400	2860		
	3m	12.26	2830	0.05	53800	500	3.2	0.04	94100	1600		
	9m	12.13	2400	nd	54900	620	2	0.12	97400	1380		0.21
	12m	12.13	2230	0.06	51700	641	4.4	0.11	96000	1240		0.28
	20m	12.26	2390	0.08	52600	583	0	0.06	96700	1430		0.25
Groundwater B	**Age**	**pH**	Ca^{2+}	Mg^{2+}	Na^{+}	K^{+}	**Fe**	SiO_2	Cl^{-}	SO_4^{2-}	CO_3^{2-}	**Al**
	7d	12.33	1732	nd	7545	207	0.34	0.01	14400	484		0.46
	3m	12.29	1336	0.02	7865	253	0.31	0.15	14055	192	<5	0.19
	12m	12.43	1343	0.015	7494	195	0.8	0.13	14035	35		0.64

Table 7.30. Solution analyses in reference backfill mixes at 55°C. Concentrations in ppm.

Deionised water	Age	pH	Ca^{2+}	Mg^{2+}	Na^{+}	K^{+}	Fe	SiO_2	Cl^{-}	SO_4^{2-}	CO_3^{2-}	Al
	7d	13.26	787	0.03	19	40	nd	0.13	6	5.2	5	
	3m	12.74	720	nd	24	110	0.2	0.05	2	43.4	15.2	
	9m	12.54	605	nd	24	130	nd	0.08	2.2	53.5	12.5	0.15
	12m	12.35	724	nd	36	162	0.16	0.09	8.6	68.9	9.9	0.14
	20m	12.4	529	0.04	38	102	101	0.36	27.1	63	5.9	0.3
Groundwater A	**Age**	**pH**	**Ca^{2+}**	**Mg^{2+}**	**Na^{+}**	**K^{+}**	**Fe**	**SiO_2**	**Cl^{-}**	**SO_4^{2-}**	**CO_3^{2-}**	**Al**
	7d	12.58	2860	nd	70700	689	3	0.16	114000	2410		
	3m	12.24	2760	nd	54900	546	3.6	0.04	95600	1910		
	9m	12.13	2550	nd	55300	640	2.1	0.08	99100	1900		0.28
	12m	12.12	2540	0.06	53800	680	4.5	0.05	99700	2030		0.32
	20m	12.19	2610	0.08	55100	622	0	0.04	103000	2260		0.23
Groundwater B	**Age**	**pH**	**Ca^{2+}**	**Mg^{2+}**	**Na^{+}**	**K^{+}**	**Fe**	**SiO_2**	**Cl^{-}**	**SO_4^{2-}**	**CO_3^{2-}**	**Al**
	7d	12.3	1493	nd	7568	215	0.28	0.04	14485	194		0.31
	3m	12.29	1336	0.02	7865	253	0.31	0.15	14055	192	<5	0.19
	12m	12.4	1382	0.015	7716	202	0.8	0.12	14995	237		0.31

Table 7.31. Solution analyses in reference backfill mixes at 85°C. Concentrations in ppm.

Deionised water	Age	pH	Ca^{2+}	Mg^{2+}	Na^{+}	K^{+}	Fe	SiO_2	Cl^{-}	SO_4^{2-}	CO_3^{2-}	Al
	7d	13.16	644	0.06	20	49	nd	0.18	8	200	8.8	
	3m	12.71	720	nd	28	116	0.4	0.13	2	127	11.9	
	9m	12.54	295	nd	38	145	nd	0.42	3.3	180	4.1	0.42
	12m	12.37	582	nd	29	168	0.03	0.07	3.95	163	7.3	0.15
	20m	12.45	599	0.04	35	177	1.45	0.12	2.3	192	6.5	3.97
Groundwater A	**Age**	**pH**	**Ca^{2+}**	**Mg^{2+}**	**Na^{+}**	**K^{+}**	**Fe**	**SiO_2**	**Cl^{-}**	**SO_4^{2-}**	**CO_3^{2-}**	**Al**
	7d	12.49	2990	nd	68900	546	4	0.1	113000	3300		
	3m	12.18	2940	nd	56700	579	3.5	0.05	98900	2660		
	9m	12.12	2580	nd	57500	660	2.2	0.08	101400	2100		0.21
	12m	12.09	2290	0.08	61600	921	5.2	0.04	109700	2630		0.24
	20m	12.01	2700	0.08	79900	863	0	0.06	141000	2030		0.32
Groundwater B	**Age**	**pH**	**Ca^{2+}**	**Mg^{2+}**	**Na^{+}**	**K^{+}**	**Fe**	**SiO_2**	**Cl^{-}**	**SO_4^{2-}**	**CO_3^{2-}**	**Al**
	7d	12.23	1504	nd	7568	215	0.26	0.07	14490	794		0.35
	3m	12.22	1464	0.03	7716	253	0.28	0.11	13755	1251	21	0.08
	12m	12.3	1567	0.03	7939	202	0.8	0.14	15020	1100		0.4

Figure 7.8 Ettringite and sulphate in reference backfill mixes prepared using groundwater A.

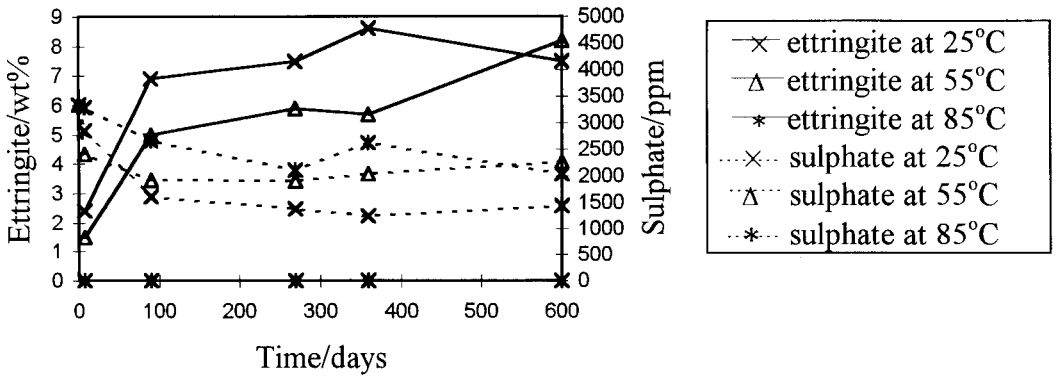

Figure 7.9 Calcium ion concentration in 75 ggbs: 25 OPC mixes.

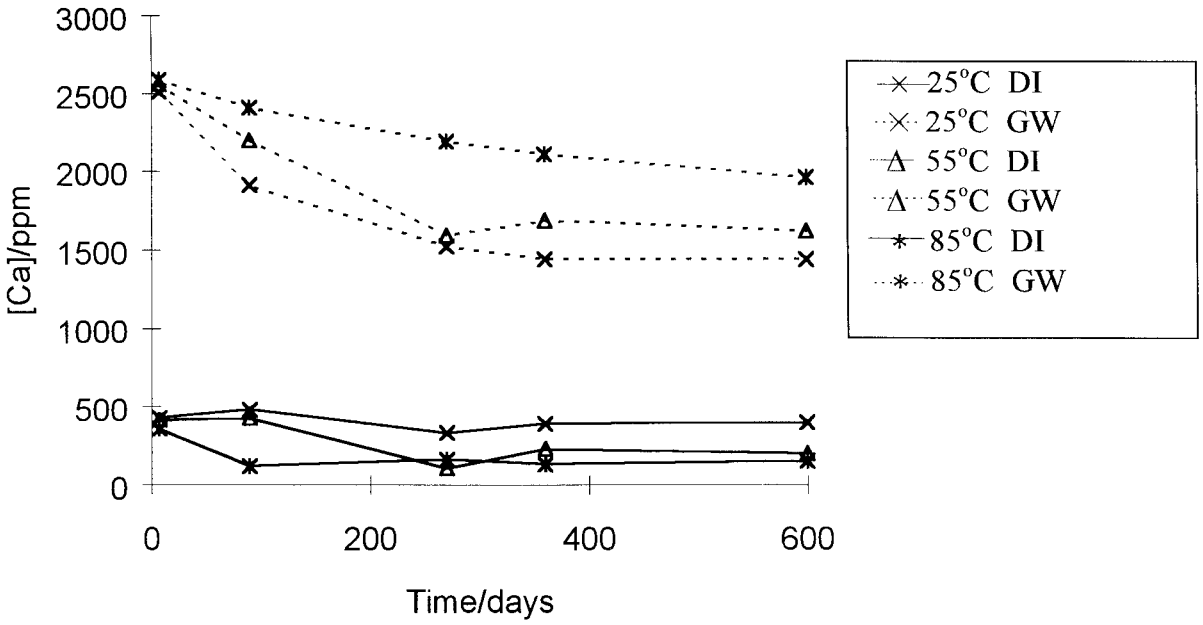

Figure 7.10 Calcium ion concentration in 60 Pfa: 40 OPC mixes.

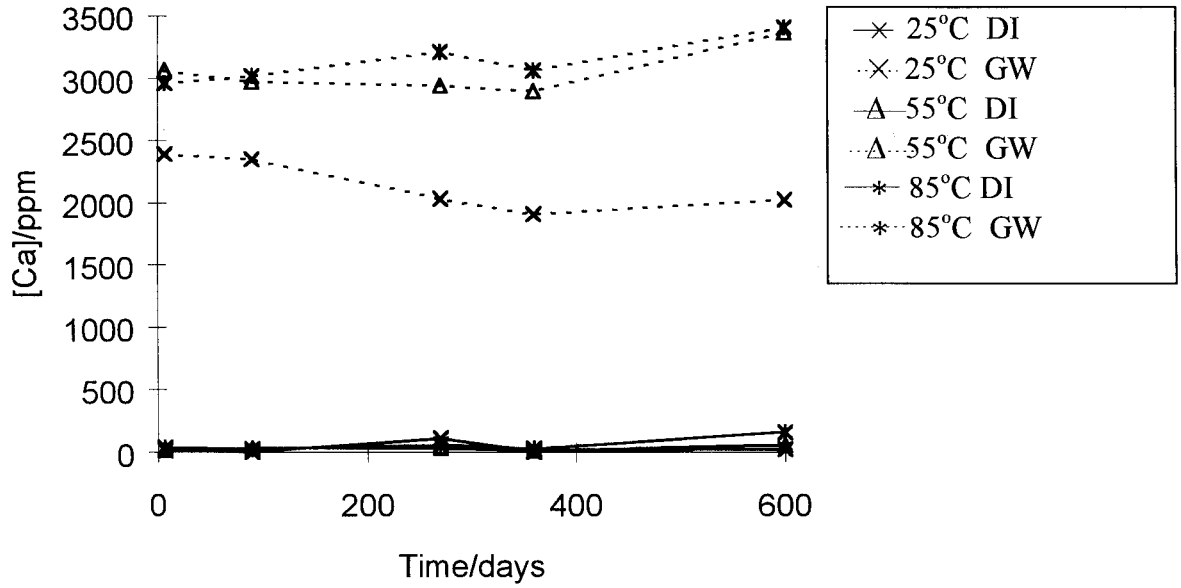

Figure 7.11 Calcium ion concentration in OPC mixes.

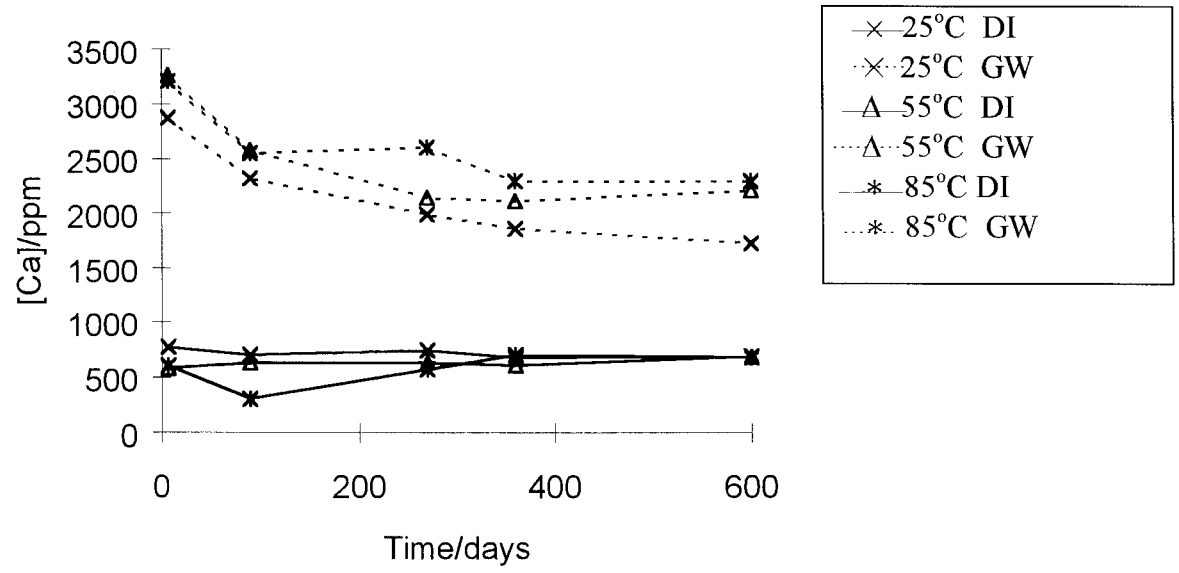

Figure 7.12 Calcium ion concentration in reference backfill mixes.

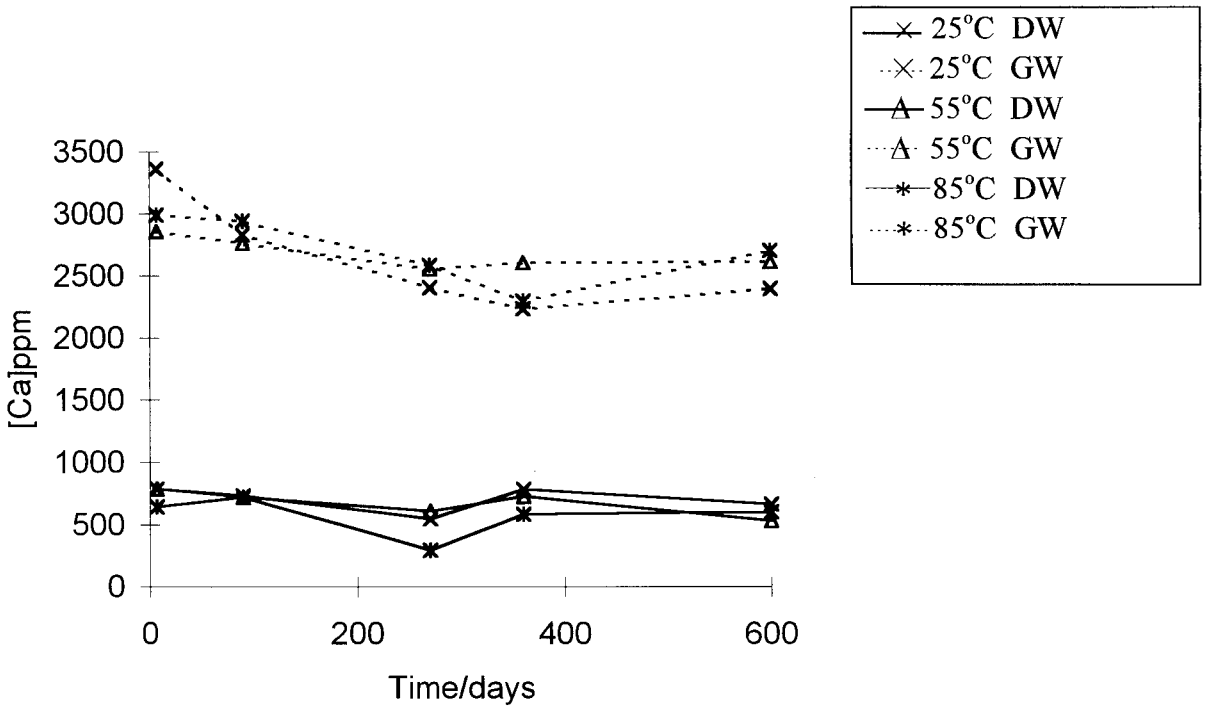

Figure 7.13 pH in 60 Pfa: 40 OPC mixes.

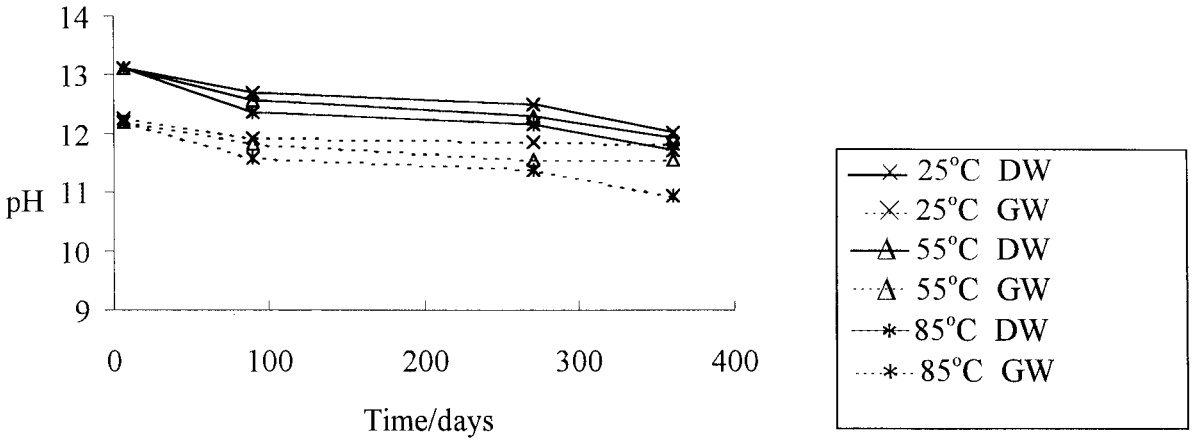

Figure 7.14 pH in 60 pfa : 40 OPC mixes

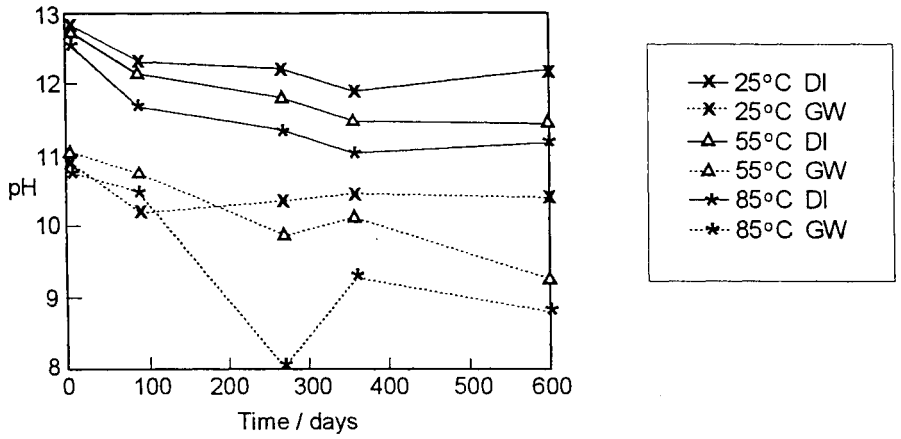

Figure 7.15 pH in OPC mixes

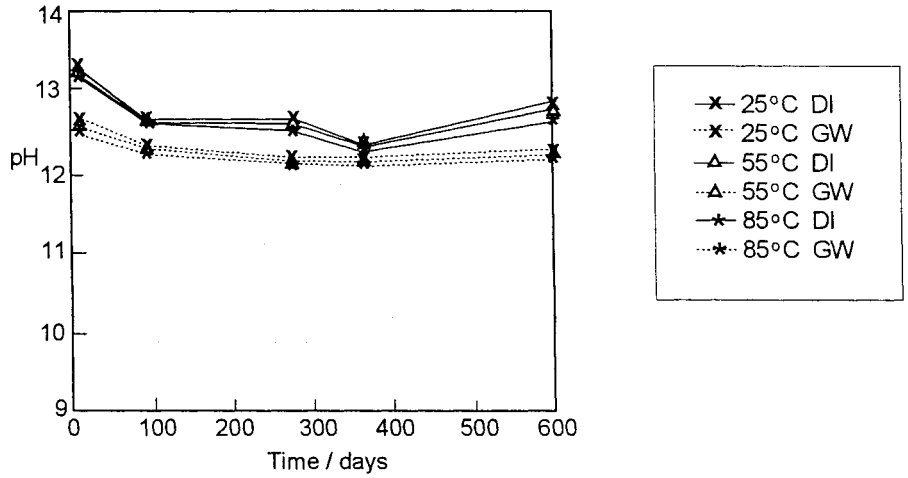

Figure 7.16 pH in Reference backfill mixes

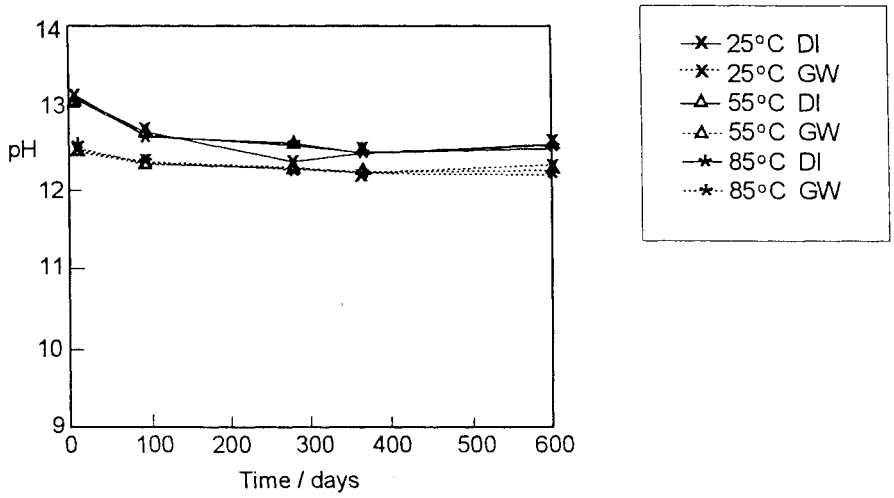

CONCLUSIONS

The hydration of blended Portland cements has been studied under accelerated reaction conditions using a high water: solid ratio and by constantly tumbling the mixes. The interaction between these cements and saline groundwaters have also been studied. The groundwaters were not replaced or spiked in these experiments. Test ages of 7 days, 3 months, 9 months, 12 months and 20 months were used in the study. The results of this work have helped to establish the solid phases that may form in cementitious materials after long ages under conditions that may prevail in a repository used for the disposal of radioactive waste and the compositions of the groundwaters in contact with them. All these phases need to be considered in thermodynamic modelling studies of cement systems. It has also provided solid and solution compositional data for the validation of computer models of cementitious systems.

i) The results of the completed tests show that, in addition to the expected cement hydrates, chloride ions are included in an AFm phase in the hydrated cement. The zeolite mineral thomsonite has been detected in 60 pfa:40 OPC blends at 85°C. Afwillite has been detected in OPC and 75 ggbs:25 OPC blends at 85°C. A tobermorite-like phase has been detected in 75 ggbs:25 OPC blends at 85°C. Anhydrous calcium sulphate has been detected in all mixes prepared using high saline groundwater. All these phases need to be considered in thermodynamic modelling studies of cement systems.

ii) All these phases need to be considered in thermodynamic modelling studies of cement systems. The presence of high saline groundwater led to the formation of a Cl-containing AFm phase in all 75 ggbs:25 OPC blends and in OPC and reference backfill blends at elevated temperatures. The amounts of ettringite present in mixes prepared using groundwater were substantially higher than the equivalent deionised water mixes. This phase generally replaced any AFm phases that were present in the equivalent mixes prepared using deionised water. The formation of ettringite is an expansive process and could cause cracking in the cement paste if formed in large amounts. Other solid phases present in mixes prepared using high saline groundwater were similar to those prepared using deionised water.

iii) The results of experiments carried out on cement paste blocks are generally consistent with those using powders. However, the extent of reaction with the groundwater is considerably less than that in equivalent cement powders, demonstrating the benefit of the accelerated reaction techniques used. The results of the SEM analysis of the cement paste blocks show that the samples have a zonal structure with the equilibrium products, formed in the powder samples, only present in the outer layer. There is also evidence of cracks running parallel to the sample faces in many cases.

iv) A comparison with earlier tests carried out at temperatures of 20°C, 50°C and 90°C over test periods of up to 1380 days has been carried out. This has shown that the results from the two sets of experiments are generally consistent. However, crystalline calcium silicate hydrate phases, which were formed at 50°C in the earlier tests were absent from some mixes hydrated at 55°C in the current work. The pH values for 60 pfa:40 OPC mixes after 20 months were also higher in the current work than in similar mixes in the earlier tests. These result suggests that the longer reaction times used in the earlier series had allowed the mixes to approach equilibrium to a greater extent than in the current work.

7.5 ACKNOWLEDGEMENTS

The Author thanks Roger Bollinghaus for carrying out the thermogravimetric and x-ray diffraction analyses, Mike Bowley and Freda Halliwell for the solution analyses, David Rayment for the Scanning Electron Microscopy analysis, Emily Hodgkinson of Manchester University for the TEM analyses and Adrian Brough of Imperial College for the selective dissolution of blended cements.

REFERENCES

1. A. Atkinson, N.M. Everitt & R. Guppy. (1989) Evolution of pH in a Radwaste Repository. DOE Report No. DOE/RW/89/025.

2. M. Atkins, F.P. Glasser, L.P. Moroni and J.J. Jack. (1994) 'Thermodynamic Modelling of Blended Cements at Elevated Temperatures' (50°C to 90°C), DOE/HMIP/RR/94.011.

3. F.P. Glasser. (1992) Progress in the immobilisation of radioactive wastes in cement. Cem. Conc. Res., **22**, 201.

4. F.P. Glasser & M. Atkins. (1994) 'Cements in Radioactive Waste Disposal', Materials Research Society Bulletin, XIX (No. 12), p 33.

5. F.P. Glasser. (1993) `Chemistry of Cement Solidified Waste Forms', in Chemistry and Microstructure of Solidified Waste Forms, Ed. R.D. Spence, Lewis.

6. H.F.W. Taylor. (1990) Cement Chemistry, (Academic Press, London).

7. H.F.W. Taylor. (1994) 'Delayed Ettringite Formation', Proc. Engineering Foundation Conference `Advances in Cement and Concrete', Durham, New Hampshire.

8. CD Lawrence. (1995) `Mortar expansions due to delayed ettringite formation. Effects of curing period and temperature', Cem. Conc. Res., **25**, 903.

9. FP. Glasser, D. Damidot & M. Atkins. (1995) `Phase development in cement in relation to the secondary ettringite problem.' Adv. Cem. Res, **7**, 57.

10. N Crammond & M Halliwell, In press. `Assessment of the conditions required for the thaumasite form of sulphate attack', Mat. Res. Soc. Symp. Proc.

11a. K.C. Quillin, S.L. Duerden & A.J. Majumdar. (1993) `Accelerated ageing of blended Portland cement for use in radioactive waste disposal'. UK DoE report No. DoE/HMIP/RR/93.023.

11b. K.C. Quillin, S.L. Duerden & A.J. Majumdar. (1993) `Formation of zeolites in OPC - pfa mixtures', Cem. Conc. Res., **23**, 991.

11c. K. Quillin, S.L. Duerden and A.J. Majumdar. (1994) 'Accelerated ageing of blended OPC cements'. Mat. Res. Soc. Symp. Proc., Vol. 333, pp 341 - 348.

12. UK Patent Application (1993) no. 9316995.1.

13. UK Nirex report 524, Volume 4.

14. N.J. Crammond. (1985) 'Quantitative x-ray diffraction analysis of ettringite, thaumasite and gypsum in concretes and mortars', Cem. Conc. Res., **15**, 431.

15. BS 4550 Part 2: 1970. (1970) 'Methods for testing cement. Part 2. Chemical tests'. British Standards Institution, London.

16. Internal BRE documented procedure.

17. Dougan and Wilson. (1974) 'The absorptiometric determination of aluminium in water. The Analyst, **99**, 413. This method has been amended for use with high saline solutions in the current programme by J. Pedersen, Aberdeen University.

18. D. Damidot & F.P. Glasser. (1992) 'Thermodynamic investigation of the $CaO-Al_2O_3-CaSO_4-H_2O$ system at 50°C and 80°C'. Cem, Conc. Res., **22**, 1179.

19. O.P. Mchedlov-Petrosyan, I.P. Vyrodov I.P & L.P. Papkova. (1968) Unpublished proceedings of the 5th I.C.C.C., part II, Vol II, p32.

20. A.J. Majumdar, D.R. Rayment & K. Pettifer. 'Microstructure and microanalysis of some ancient and modern building materials', BRE note CR32/87.

21. J.D.C. McConnell. (1954) 'The hydrated calcium silicates riversideite, tobermorite and plombierite'. Miner. Mag **30**, 293-305.

22. S. Gross. (1977) 'The mineralogy of the hatrurim formation'. Geol. Surv. Israel Bull., **70**, pp 1-80.

23. K Quillin. (1996) 'Phase equilibria in the $CaO-Al_2O_3-SiO_2-H_2O$ system in relation to blended high alumina cements', Proc. Int. Conf. 'Concrete in the Service of Mankind', Appropriate Concrete Technology 289.

24. CJ Newton and JM Sykes. (1987) 'The effect of salt additions on the alkalinity of $Ca(OH)_2$ solutions', Cem. Conc. Res., **17**, 765.

25. F.P. Glasser & T.G. Jappy, (1992) 'Synthesis and stability of silica-substituted hydrogarnet'. Advances in Cement Research, **4**, 1.

SECTION 7, ANNEX A. ATEM ANALYSIS OF CEMENT POWDERS

by E S Hodgkinson, University of Manchester.

A1 SAMPLE DESCRIPTION

Four samples were analysed in the current study. Two samples had been reacted with deionised water for 20 months at 85°C. These were:

- 75 % GGBS, 25 % OPC
- 60 % PFA, 40 % OPC.

The remaining 2 samples had been reacted with groundwater A at 85°C for 20 months. These were:

- 60 % PFA, 40 % OPC
- Reference backfill.

A2 PREPARATION AND ANALYSIS

A small amount (less than 0.01 g) of each sample powder was suspended in about 10 ml of acetone and given 5 minutes of ultrasonic agitation to encourage dispersion of particles. The suspensions were then stored in glass bottles and sealed in polythene bags in a vacuum desiccator over soda lime and silica gel. Immediately before TEM analysis, a single drop of each suspension was placed on a 3 mm diameter carbon-coated copper grid, and left to evaporate.

A Philips em400T transmission electron microscope was used, operated at 120 kV with an emission current between 10 and 25 mA and equipped with an EDAX energy-dispersive X-ray spectrometer.

Where possible the conditions of analysis (beam size, emission current, detected count rate) were the same as those under which the machine is calibrated, but it was often impossible to obtain analyses in such ideal conditions. In particular, the material was frequently too thick to fulfill the 'thin film criterion' for analytical TEM, which requires that the material under the beam is thin enough for absorption and fluorescence effects to be neglected from the calculation of chemical composition.

A3 RESULTS AND DISCUSSION

A3.1 75 ggbs: 25 OPC deionised water, 85°C, 20 months

Most of the material observed has a clearly crystalline, prismatic to fibrous or needle-like morphology, varying from less than 0.5 μm to 10 μm in length (see figures A1 and A5). All

of this material has calc-silicate composition (see ternary plot), with a small Al component which may be due to contamination from other phases present. The closest crystalline CSH phase to these compositions is foshagite, but the material could also be afwillite, jennite or xonotlite, or a mixture of some of these four phases.

Also ubiquitous, but less abundant, are grains of an equant (sub-spherical), electron dense C-A-S phase, up to 1 mm in diameter. Their appearance is typical of hydrogarnet imaged by TEM and their compositions lie close to the hydrogarnet solid solution. These grains were always seen embedded amongst the prisms and needles of the CSH (see figures A1 and A2) and so some contamination is expected in the chemical data, which lie between the hydrogarnet solid solution and the composition of the crystalline CSH seen. Moreover, they were often too thick to comply with the 'thin film' criterion for analytical TEM. The analysis with the lowest count rate is therefore given as the 'best hydrogarnet' data point on the ternary plot. Note that Fe^{3+} has been included as equivalent to Al on the plot in order to take account of the minor Fe (2-3 mol%) present in the hydrogarnet.

Lastly, there is a small amount of Mg-rich C-A-S material, usually extremely fine grained but where coarser grains are present they appear to be platy (see figures A1 and A4). It was not possible to obtain analyses of any single grain of this material, and so the chemical data may represent mixtures of phases.

The XRD analysis of this sample showed it to consist of crystalline CSH, hydrogarnet and either trace monosulphate of trace hydrotalcite. The presence of crystalline CSH (probably foshagite) and hydrogarnet is confirmed by ATEM observations, but neither hydrotalcite nor monosulphate were seen. The presence of sclphur sulphur was only detected in some of the hydrogarnet analyses, and then only in trace amounts, so it is unlikely that any monosulphate is present in this sample. The magnesian material seen could be a mixture of hydrotalcite and other phases though. Analyses of the Mg-rich material were manipulated accordingly: all Mg was assumed to be in hydrotalcite and on this basis hydrotalcite (M_4AH_{10}) was subtracted from the compositions. The resulting compositions of the remaining material were plotted as 'Mg - hydrotalcite' on the ternary plot and may correspond to residual iron blast-furnace slag.

By assuming that the data for the hydrogarnet include some contamination from crystalline CSH, the (very) approximate composition of the former can be inferred. By projecting the hydrogarnet compositions back from the 'average CSH' composition, the hydrogarnet is inferred to be close to C_3ASH_4. If the 'best hydrogarnet' composition is projected back from foshagite, it is inferred to lie close to $C_3AS_{1.5}H_3$. While these compositions are only rough estimates, it is certain that the hydrogarnet is Si-substituted to a partial extent. It also clearly contains minor Fe and sulphur.

7. A3.2 60 pfa: 40 OPC deionised water, 85°C, 20 months

Most of this sample consists of prismatic to needle-like material forming from a poorly ordered, ultra-fine grained mass, with individual grains varying from less than 0.05 μm to 2 μm in length (see figures A6, A7, A10 and A11). They have zeolitic compositions, close to scolecite although not clearly enough to be reliably identified as such. The poorly ordered material has a slightly lower Al content and lies on the edge of the zeolite compositional field. It is called 'gel' for simplicity on the ternary plots. As it was rarely possible to isolate the 'gel'

from the prismatic to needle-like material, the ternary plots also show data collected from a 'mixture' of the two. Some of the analyses from both the 'gel' and the 'mixtures' include minor Na and K (up to 8 mol%) but the zeolite is alkali-free. Mg is sometimes present in all this material but reaches much higher levels in the 'gels' and mixtures' (up to 12 mol%) than in the zeolite.

The ultra-fine grained prismatic to needle-like material is sometimes present in association with ultra-fine (0.05 μm) equant grains, probably hexagonal to sub-hexagonal plates, although they are so small that the morphology was not clear (see figure A14). This material could also be a phase with tabular morphology.

A single, large (greater than 2 μm), sub-prismatic grain was seen, surrounded by very poorly ordered, ultra-fine grained material (see figure A13). The poorly ordered material is similar in composition to the other 'gel', but the large grain is relatively Al-poor (called 'sub-prismatic' on the ternary plots).

Hexagonal plates are present in association with an electron-dense prismatic phase of pure Fe (see figures A8 and A9). The Fe material is presumably iron oxide from the fuel ash, while the hexagonal plates could be portlandite, although no chemical data were obtained from them. Note that Fe is present in minor amounts (mostly less than 5 mol%) in all the material analysed in this sample.

Some coarse grained (2-5 μm) alumino-silicate material is present, with or without minor K and Mg (see figure A15). Lastly, one cluster was seen of sub-cubic or octahedral grains, about 0.2 mm in diameter, with no diffraction contrast features (see figure A12). The grains were unfortunately too thin to yield any compositional information.

The XRD analysis of this sample showed it to consist of CSH gel and two zeolites, possibly similar to thomsonite and phillipsite. Some poorly ordered CSH material (with a considerable Al content) was seen by TEM, which could correspond to the 'CSH gel' identified by XRD. Note that this material is not generally as poorly ordered as a typical gel would be. Identification of the zeolitic needles and prisms remains uncertain, but the most likely candidate is scolecite ($CaAl_2Si_3O_{10}.3H_2O$), a fibrous zeolite. The main problem was that this material is usually finely intermixed with the 'CSH gel' (and could in fact be forming from it) so it was difficult to obtain uncontaminated chemical analyses. Furthermore, the material observed was often too thick to fulfil the 'thin film criterion' for analytical TEM. Overall, the data do not clearly identify any zeolite and do not distinguish between the two zeolites expected.

The aluminosilicate and the prismatic Fe phase seen could both be unreacted residues from the fuel ash; mullite, haematite and magnetite from fuel ash would normally be expected to remain inactive in cementitious formulations.

The relatively coarse hexagonal plates could be portlandite, which would have been present in the original OPC before reaction.

The electron-thin sub-cubic/octahedral grains seen remain problematic; they are unlikely to be hydrogarnets, which always appear far more electron dense at this size. A cubic phase such magnetite (as might be expected in the fuel ash) would, like hydrogarnet, be expected to appear far more electron-dense.

7. A3.3 60 pfa: 40 OPC Groundwater A, 85°C, 20 months

A platy to sheet-like material, with a grain size of less than 1 μm, was commonly seen. Figure A16 shows typical plates while the sheets (which tend to be curled up at the edges) can be seen in figures A17, A21 and A22. The compositional data for all of this material plots in a cluster around an Al-substituted CSH, with more Al than tacharanite (about 10 mol%) and a C/S ratio of approximately 0.6. The analyses are alkali-free but include minor amounts of Fe and Cl. A couple of analyses included a significant Mg content (up to 16 mol%) and these were also relatively depleted in Ca to a similar extent. Some clearly rectangular shaped plates were also seen (figure A18) but unfortunately they were too thin to provide compositional data, so they may or may not be the same phase as the other platy material.

The other major phase seen in this sample is a prismatic zeolite, shown in figures A20 to A22. The prisms can be up to 3 μm long and have compositions clearly clustering around a single point in the zeolite compositional field. This 'average' point does not, however, match the composition of any specific zeolite. The material is largely alkali-free, with just three analyses including a minor Na component. Unlike the CSH, Cl and Mg are absent from most analyses, but minor Fe is present.

A gel was often seen in close association with both zeolite and CSH, but usually in very small amounts (see figures A21 and *A22*). It is ultra-fine grained with the typical irregular morphology of a gel. Figure A19 shows an unusual cluster largely composed of this gel, along with a little of the prismatic phase. It was unfortunately not possible to obtain a chemical analysis of the gel but it sometimes contaminated analyses of both the zeolite and the crystalline CSH. These data plot mainly between the pure zeolite and pure CSH data. Lastly, some equant grains of pure Fe (see figure A17) and some relatively coarse (i.e. 2 μm) Al-rich plates were seen, both probably residual fuel ash.

The XRD analysis of this sample showed it to consist of C-S-H gel, a thomsonite-like phase, $CaSO_4$ and NaCl. The zeolite observed by ATEM, although its exact phase cannot be identified, could correspond to the 'thomsonite-like phase'. The 'C-S-H gel' of the XRD analysis could correspond to either the crystalline Al-CSH or gel. The ternary plots (especially the C-A-S-H plot) of the data show there is not a direct mixing line between the zeolite and the crystalline CSH. The analyses which plot between the two extremes were contaminated by small amounts of the gel, and so the geometry of these plots show possible mixing with a gel of approximate composition $C_2AS_4H_n$. (This deduction is of course very tentative.)

Of the minor elemental components, Cl is notably present in the CSH but not the zeolite, while the only alkali (Na) goes into the zeolite and Mg is mainly present in those analyses which are contaminated by gel. The presence of minor Fe in all the material implies a generally widespread contamination by the residual fuel ash rather than Fe-substitution in any phases. There is no S in any of the material analysed here (including the gel which contaminated some analyses), which suggests that any S present in the sample has gone into a phase *not* seen by TEM. The $CaSO_4$ detected by XRD could therefore be part of the (meta)stable assemblage of this sample, despite not being observed by TEM. Halite, also, was not seen but this does not mean that it is not present.

The equant iron oxide grains (cubic magnetite?) and the Al-rich plates seen may be residual fuel ash and the Al-rich plates seen may be residual fuel ash material.

7. A3.4 Reference Backfill, Groundwater A, 85°C, 20 months

Two principal Ca-Al-Si phases were seen. The first is a fibrous CSH with fibres less than 2 μm long, shown in figures A29 and A30. Chemical analyses of this material contain little or no Al, plot around a C/S ratio of 1.8 and are alkali-free but include minor Cl and Fe.

The other Ca-Al-Si material forms hexagonal plates which vary quite widely in composition but all the data plot roughly between AFm and thaumasite, as can be seen in the ternary plots. Their S and Cl levels are fairly consistent with identification as AFm and/or AFt.

A lot of Fe-rich material was seen: figure A23 shows relatively coarse (0.5 μm) hexagonal plates of pure Fe covered in much smaller (less than 0.1 μm), very thin hexagonal plates of unknown composition. Figure A27 shows a large (greater than 2 μm), electron-dense, hexagonal plate of pure Fe and in figure A28 an electron-dense phase of pure Fe appears as elongated grains, but these could actually be plates edge-on to the plane of the image.

Some aluminosilicate material was seen, including the large hexagonal platy grain shown in figure A24. The smaller equant grains also shown here are of unknown composition.

Halite was commonly seen and is shown in figure A26. Lastly some relatively coarse-grained (i.e. 2 μm) calcite was seen (see figure A23).

The XRD analysis of this sample showed it to consist of $Ca(OH)_2$, $CaCO_3$, a Cl-bearing AFm, NaCl and possibly hydrogarnet. CSH was assumed to be present although it was not identified by XRD.

The $CaCO_3$ and the NaCl were clearly identified by ATEM. Hydrogarnet was not seen, but this does not mean it is not present in the sample.

The electron-dense Fe-rich grains (hexagonal plates) are probably Fe oxides and the minor Fe component of most of the chemical data collected from this sample could be widespread contamination from such Fe oxide phases. If the initial backfill contains no Fe oxides then the presence of this material is hard to explain and could be a contaminating phase. The presence of the platy aluminosilicate is likewise hard to explain.

The hexagonal platy material whose compositional data plot between AFm and thaumasite could correspond to the Cl-bearing AFm phase identified by XRD. All AFm phases occur as hexagonal plates so the morphology suggests that this might be AFm, but the compositional data are ambiguous: they do not match the stoicheiometry of one particular AFm or AF_t phase and do not show a clear mixing line between two phases; the data are far too variable. Most of the analyses include minor S and Cl, with Cl usually higher. One analysis has a high level of S and another has very high Mg. Note also that this is not the only Cl-bearing phase seen: the fibrous CSH also contains minor Cl, although at lower levels. It is, however, the only S-bearing phase. The identification of the other fine grained hexagonal plates seen is also ambiguous. These plates were all too thin for any chemical data to be collected and could be portlandite and/or AFm or any other material of similar morphology.

A fibrous CSH phase, with a significant degree of ordering, was clearly present, although not seen by XRD. The relative amount of CSH in the sample cannot be estimated by ATEM.

7. A4 CONCLUSIONS

7. A4.1 75 GGBS: 25 OPC - Deionised water, 85°C, 20 months

ATEM shows this sample to contain at least one clearly crystalline (fibrous) CSH phase, possibly foshagite, and a Si-substituted hydrogarnet. Monosulphate is probably not present and there may be trace amounts of hydrotalcite. Some residual iron blast-furnace slag may also be present.

7. A4.2 60 pfa: 40 OPC - Deionised water, 85°C, 20 months

ATEM shows this sample to contain an Al-rich CSH 'gel' (with a greater degree of ordering than a typical gel) and some prismatic to needle-like zeolitic material of unknown phase, mostly forming from, or at least in association with, the gel. The closest zeolitic composition to this material is scolecite. Portlandite plates may also be present, with both the zeolitic material and some fuel ash residue.

7. A4.3 60 pfa: 40 OPC - Groundwater water A, 85°C, 20 months

ATEM shows this sample to contain an Al-substituted crystalline CSH, an unidentified zeolite and some typical gel with a composition which is unknown but is inferred to be roughly 50 mol% Si, 25 mol% Ca, 25 mol% Al. There is no S in any of these phases but minor Cl is present in the crystalline CSH, while the only alkali (minor Na) appears to go into the zeolite and Mg into the gel.

7. A4.2 Reference Backfill - Groundwater water A, 85°C, 20 months

ATEM shows this sample to contain $CaCO_3$, halite, a fibrous CSH with a high C/S ratio, Fe oxides and aluminosilicates, which may both be due to contamination, and one or more fine grained hexagonal platy phases. These latter could include a Cl-bearing AFm phase and portlandite but the chemical data are either non-existent (owing to the extreme thinness of the plates) or too ambiguous for a reliable identification. No hydrogarnet was seen, but this does not mean it is not present in the sample. The material tentatively identified as AFm is the only S-bearing material seen, while minor Cl is present in both this and the fibrous CSH.

Table 7. A1. ATEM analysis of 75 ggbbs: 25 OPC blend reacted with deionised water at 85 °C after 20 months.

	CSH	CSH	CSH	CSH	CSH	CSH	CSH	average CSH	hydro garnet	hydro garnet	hydro garnet	hydro garnet	hydro garnet	magne sian	magn esian	magne sian
mol % element									0	0	0	0	0	0	2.376	0
Na	0	0	0	0	0	0	0	0	0	0	0	0	0	28.266	45.072	23.833
Mg	0	0	3.59	0	0	0	0	0.598	24.244	19.014	23.343	8.488	24.09	21.165	19.621	20.005
Al	5.71	0	2.9	2.7	0	2.36	4.24	2.985	24.639	28.681	21.781	33.058	21.71	26.846	25.993	25.295
Si	41.5	42.5	43	44.4	41.4	43.2	41.1	42.604	2.137	0	2.205	0	2.219	0	0	0
S	0	0	0	0	0	0	0	0	0	0	0	0	0	0	0	0
Cl	0	0	0	0	0	0	0	0	0	0	0	0	0	0	0	0
K	0	0	0	0	0	0	0	0	45.951	50.172	49.889	57.256	48.518	22.706	6.938	28.301
Ca	52.8	57.5	50.5	52.9	58.6	49.8	54.6	53.029	0	0	0	0	0	0	0	2.566
Ti	0	0	0	0	0	0	0	0	0	0	0	0	0.66	0	0	0
Mn	0	0	0	0	0	0	0	0	0	0	0	0	0	0	0	0
Fe_2	0	0	0	0	0	0	0	0	3.029	2.132	2.782	1.198	2.803	1.017	0	0
Fe_3	0	0	0	0	0	4.7	0	0.784								
									100	100	100	100	100	100	100	100
total	100	100	100	100	100	100	100	100								
wt % oxide																
Na_2O	0	0	0	0	0	0	0	0	0	0	0	0	0	0	1.52	0
MgO	0	0	2.53	0	0	0	0	0.361	0	0	0	0	0	21.98	37.53	18.16
Al_2O_3	5.06	0	2.59	2.38	0	2.05	3.76	2.263	21.66	17.07	20.89	7.56	21.54	20.8	20.65	19.26
SiO_2	43.4	44.2	45.2	46.2	43.1	44.1	43	44.169	25.95	30.36	22.98	34.69	22.88	31.1	32.26	28.72
SO3	0	0	0	0	0	0	0	0	3	0	3.1	0	3.12	0	0	0
Cl	0	0	0	0	0	0	0	0	0	0	0	0	0	0	0	0
K_2O	0	0	0	0	0	0	0	0	0	0	0	0	0	0	0	0
CaO	51.6	55.8	49.6	51.4	56.9	47.5	53.3	52.293	45.16	49.57	49.13	56.08	47.72	24.55	8.03	29.99
TiO_2	0	0	0	0	0	0	0	0	0	0	0	0	0	0	0	3.87
MnO	0	0	0	0	0	0	0	0	0	0	0	0	0.82	0	0	0
FeO	0	0	0	0	0	0	0	0	0	0	0	0	0	0	0	0
Fe_2O_3	0	0	0	0	0	6.39	0	0.913	4.24	3	3.9	1.67	3.93	1.57	0	0
	100	100	100	100	100	100	100	99.999	100	100	100	100	100	100	100	100

Table 7. A2. ATEM analysis of 60 pfa: 40 OPC blend reacted with deionised water at 85 °C for 20 months.

mol % element	zeolite	zeolite	zeolite	zeolite	gel'	gel'	gel'	mixture	mixture	mixture
Na	0	0	0	0	0	5.4	0	4.84	0	0
Mg	0	0	2.85	0	3.2	9.5	0	11.389	0	0
Al	32.156	32.255	24.121	30.839	18	15	22	15.256	15.564	11.812
Si	46.412	49.199	48.99	49.635	48	40	52	42.305	49.823	53.381
P	0	0	0	0	0	0	0	0	0	0
S	0	0	0	0	0	0	0	0	0	0
Cl	0	0	0	0	0	0	0	0	0	0
K	0	0	0	0	1.8	2.4	0	2.892	0	0
Ca	19.454	15.677	20.375	17.833	23	23	22	15.72	28.606	30.676
Ti	0	0	0	0	0	0	0	0	0	0
Fe_2	0	0	0	0	0	0	0	0	0	0
Fe_3	1.978	2.869	3.664	1.692	5.4	5.4	3.6	7.598	6.007	4.131
total	100	100	100	100	100	100	100	100	100	100
wt % oxide										
Na_2O	0	0	0	0	0	3.1	0	2.7	0	0
MgO	0	0	2.01	0	2.2	6.9	0	8.27	0	0
Al_2O_3	28.88	28.8	21.49	27.63	16	14	20	14	13.51	10.28
SiO_2	49.13	51.78	51.44	52.42	50	44	54	45.78	50.99	54.74
P_2O_5	0	0	0	0	0	0	0	0	0	0
SO_3	0	0	0	0	0	0	0	0	0	0
Cl	0	0	0	0	0	0	0	0	0	0
K_2O	0	0	0	0	1.4	2	0	2.45	0	0
CaO	19.22	15.41	19.96	17.58	22	23	21	15.88	27.32	29.35
TiO_2	0	0	0	0	0	0	0	0	0	0
FeO	0	0	0	0	0	0	0	0	0	0
Fe_2O_3	2.77	4.01	5.1	2.37	7.5	7.8	5	10.92	8.18	5.63
total	100	100	100	100	100	100	100	100	100	100

Table 7. A2. Continued.

mol % element	mixture	mixture	mixture	mixture	mixture	sub-prismatic	sub-prismatic	A-S material	A-S material	A-S material	Fe phase
Na	0	0	0	0	0	0	0	0	0	0	0
Mg	0	0	0	2.615	2.849	0	0	0	2.358	2.333	0
Al	21.182	23.837	18.998	25.375	17.309	14.104	13.606	35.89	41.746	42.683	0
Si	53.301	50.945	54.035	47.748	54.15	49.564	49.204	50.346	46.168	46.967	0
P	0	0	0	0	0	0	0	0	0	0	0
S	0	0	0	0	0	0	0	0	0	0	0
Cl	0	0	0	0	0	0	0	0	0	0	0
K	0	0	1.315	1.049	0	0	0	0	8.156	5.633	0
Ca	22.323	22.127	22.728	20.178	21.92	32.239	33.88	4.12	0	0	0
Ti	0	0	0	0	0	0	0	0	0	0	0
Fe_2	0	0	0	0	0	0	0	0	0	0	0
Fe_3	3.194	3.091	2.925	3.035	3.771	4.093	3.311	9.643	1.572	2.383	100
total	100	100	100	100	100	100	100	100	100	100	100
wt % oxide											
Na_2O	0	0	0	0	0	0	0	0	0	0	0
MgO	0	0	0	1.85	1.99	0	0	0	1.73	1.7	0
Al_2O_3	18.64	21.08	16.74	22.73	15.27	12.32	11.93	31.23	38.63	39.22	0
SiO_2	55.33	53.11	56.12	50.41	56.29	51.08	50.85	51.65	50.37	50.88	0
P_2O_5	0	0	0	0	0	0	0	0	0	0	0
SO_3	0	0	0	0	0	0	0	0	0	0	0
Cl	0	0	0	0	0	0	0	0	0	0	0
K_2O	0	0	1.07	0.87	0	0	0	0	6.98	4.78	0
CaO	21.63	21.53	22.03	19.88	21.26	31	32.68	3.95	0	0	0
TiO_2	0	0	0	0	0	0	0	0	0	0	0
FeO	0	0	0	0	0	0	0	0	0	0	0
Fe_2O_3	4.4	4.28	4.03	4.26	5.2	5.6	4.54	13.16	2.29	3.43	100
total	100	100	99.99	100	100.01	100	100	99.99	100	100.01	100

Table 7. A3. ATEM analysis of 60 pfa: 40 OPC blend reacted with ground water A at 85 °C for 20 months.

mol% element	CSH	CSH	CSH	CSH	CSH	CSH	CSH	CSH	CSH	average CSH	CSH + gel	CSH + gel	CSH + gel	CSH + gel	CSH + gel
Na	0	0	0	0	0	0	0	0	0	0	0	0	0	0	0
Mg	4.45	0	0	0	0	0	0	0	0	0.49	15.6	0	2.26	12.42	4.04
Al	10.6	10.5	10.7	9.37	9.5	11.3	10.2	14.5	16.8	11.5	11.81	9.28	39.7	12.18	17.42
Si	49.8	53.1	51.9	55.8	52.5	52.8	51.7	53.4	50.1	52.34	45.61	54.07	48.51	47.86	46.55
P	0	0	0	0	0	0	0	0	0	0	0	0	0	0	0
S	0	0	0	0	0	0	0	0	0	0	0	0	0	0	0
Cl	2.92	0	3.04	0	2.72	2.71	3.17	2.2	2.52	2.14	1.72	2.69	0	1.34	1.53
K	0	0	0	0	0	0	0	0	0	0	0	0	0	1.18	0
Ca	29.9	32.8	31.7	34.9	33.1	30.9	33.1	27.4	28.2	31.3	18.86	32.58	8.68	20.77	26.25
Fe_2	0	0	0	0	0	0	0	0	0	0	0	0	0	0	0
Fe_3	2.34	3.64	2.7	0	2.15	2.31	1.8	2.59	2.46	2.22	6.41	1.37	0.86	4.25	4.22
total	100	100	100	100	100	100	100	100	100	100	100	100	100	100	100
wt% oxide															
Na_2O	0	0	0	0	0	0	0	0	0	0	0	0	0	0	0
MgO	3.17	0	0	0	0	0	0	0	0	0.35	11.23	0	1.63	8.93	2.85
Al_2O_3	9.55	9.12	9.48	8.26	8.4	10	9.07	12.8	14.9	10.18	10.74	8.22	36.23	11.07	15.55
SiO_2	52.7	54.6	54.1	58	54.8	55.1	54.1	55.6	52.5	54.59	48.94	56.46	52.2	51.32	48.97
P_2O_5	0	0	0	0	0	0	0	0	0	0	0	0	0	0	0
SO_3	0	0	0	0	0	0	0	0	0	0	0	0	0	0	0
Cl	1.83	0	1.87	0	1.67	1.67	1.95	1.35	1.56	1.32	1.09	1.66	0	0.85	0.95
K_2O	0	0	0	0	0	0	0	0	0	0	0	0	0	0.99	0
CaO	29.5	31.4	30.8	33.8	32.2	30	32.4	26.6	27.6	30.47	18.88	31.75	8.71	20.79	25.77
FeO	0	0	0	0	0	0	0	0	0	0	0	0	0	0	0
Fe_2O_3	3.29	4.96	3.73	0	2.99	3.21	2.5	3.58	3.43	3.08	9.13	1.91	1.23	6.05	5.9
total	100	100	100	100	100	100	100	100	100	100	100.01	100	100	100	99.99

Table 7. A3. Continued.

mol% element	zeolite	zeolite	zeolite	zeolite	zeolite	zeolite	ave zeolite	zeolite + gel	zeolite + gel	zeolite + gel	zeolite + gel
Na	0	0	0	3.41	0	2.99	1.07	3.46	0	5.63	5.08
Mg	0	0	0	0	0	3.49	0.58	0	5.16	2.39	2.55
Al	34.49	39.52	40.87	37.83	39.28	34.3	37.72	36.22	11.04	29.68	23.45
Si	55.38	52.06	50.89	48.51	49.83	45.56	50.37	48.6	48.4	44.9	45.72
P	0	0	0	0	0	0	0	0	0	0	0
S	0	0	0	0	0	0	0	0	0	0	0
Cl	0	0	0	0	0	0	0	0	1.78	0	1.07
K	0	0	0	0	0	0	0	0	1.25	0	0
Ca	10.13	7.7	8.24	9.05	9.56	11.51	9.37	11.08	29.28	12.91	21.02
Fe_2	0	0	0	0	0	0	0	0	0	0	0
Fe3	0	0.72	0	1.2	1.33	2.16	0.9	0.64	3.1	4.49	1.1
total	100	100	100	100	100	100	100	100	100	100	100
wt% oxide											
Na_2O	0	0	0	1.9	0	1.67	0.6	1.93	0	3.14	2.86
MgO	0	0	0	0	0	2.54	0.42	0	3.65	1.73	1.87
Al_2O_3	31.09	35.76	37.17	34.74	35.52	31.57	34.31	33.28	9.89	27.19	21.7
SiO_2	58.86	55.54	54.57	52.51	53.1	49.44	54	52.65	51.12	48.48	49.88
P_2O_5	0	0	0	0	0	0	0	0	0	0	0
SO_3	0	0	0	0	0	0	0	0	0	0	0
Cl	0	0	0	0	0	0	0	0	1.11	0	0.69
K_2O	0	0	0	0	0	0	0	0	1.03	0	0
CaO	10.05	7.67	8.26	9.13	9.51	11.66	9.38	11.2	28.85	13.01	21.39
FeO	0	0	0	0	0	0	0	0	0	0	0
Fe_2O_3	0	1.03	0	1.71	1.87	3.12	1.29	0.93	4.34	6.44	1.61
total	100	100	100	99.99	100	100	100	99.99	99.99	99.99	100

Table 7. A4. ATEM analysis of backfill mix reacted with groundwater A at 85 °C for 20 months.

mol% element	fibrous CSH	fibrous CSH	fibrous CSH	fibrous CSH	fibrous CSH	fibrous CSH	fibrous CSH	average CSH
Na	0	0	0	0	0	0	0	0
Mg	0	0	2.7	0	0	0	0	0.39
Al	0	0	2.54	0	2.65	0	0	0.74
Si	35.97	34.5	32.28	36.22	33.55	33.63	32.05	34.03
P	0	0	0	0	0	0	0	0
S	0	0	0	0	0	0	0	0
Cl	2.72	3.32	3.19	3.3	2.8	3.34	4.93	3.37
K	0	0	0	0	0	0	0	0
Ca	61.31	60.91	58.06	60.49	59.35	61.68	63.03	60.69
Fe_2	0	0	0	0	0	0	0	0
Fe_3	0	1.27	1.23	0	1.66	1.34	0	0.79
total	100	100	100	100	100	100	100	100
wt% oxide								
Na_2O	0	0	0	0	0	0	0	0
MgO	0	0	1.92	0	0	0	0	0.27
Al_2O_3	0	0	2.29	0	2.37	0	0	0.67
SiO_2	37.95	36.32	34.36	38.28	35.3	35.42	34.18	35.97
P_2O_5	0	0	0	0	0	0	0	0
SO_3	0	0	0	0	0	0	0	0
Cl	1.69	2.07	2.01	2.06	1.74	2.08	3.1	2.11
K_2O	0	0	0	0	0	0	0	0
CaO	60.36	59.84	57.67	59.67	58.27	60.62	62.73	59.88
FeO	0	0	0	0	0	0	0	0
Fe_2O_3	0	1.77	1.75	0	2.32	1.88	0	1.1
total	100	100	100	100.01	100	100	100.01	100

Table 7. A4. Continued.

mol% element	CSH + plates	CSH + plates	hex plates	hex plates	hex plates	hex plates	hex plates
Na	0	0	0	0	0	0	0
Mg	0	0	0	9.24	4.82	37.87	64.33
Al	0	0	0	6.51	4.11	13.28	18.54
Si	21.12	26.39	4.67	11.58	12.8	2.04	0
P	0	0	0	0	2.74	0	0
S	1.72	1.85	2.28	2.01	14.49	0	0
Cl	5.47	9.1	0	8.51	5.31	8.08	0
K	0	0	0	0	0	0	0
Ca	71.69	61.79	16.7	60.61	55.03	37.43	9.23
Fe_2	0	0	0	0	0	0	0
Fe_3	0	0.87	76.34	1.54	0.71	1.29	7.9
total	100	100	100	100	100	100	100
wt% oxide							
Na_2O	0	0	0	0	0	0	0
MgO	0	0	0	6.92	3.32	31.71	55.34
Al_2O_3	0	0	0	6.16	3.57	14.06	20.16
SiO_2	22.58	28.36	3.74	12.92	13.13	2.55	0
P_2O_5	0	0	0	0	3.32	0	0
SO_3	2.45	2.65	2.44	2.99	19.8	0	0
Cl	3.45	5.77	0	5.6	3.21	5.95	0
K_2O	0	0	0	0	0	0	0
CaO	71.53	61.97	12.49	63.11	52.68	43.6	11.04
FeO	0	0	0	0	0	0	0
Fe_2O_3	0	1.24	81.32	2.3	0.97	2.13	13.46
total	100.01	99.99	99.99	100	100	100	100

Figure A1. 75 GGBS: 25 OPC Deionised water, 85°C, 20 months:
Typical needles/prisms of CSH with sub-spherical hydrogarnets and, in the bottom right of the plate, some small plates of the magnesian material. Magnification x 17,000.

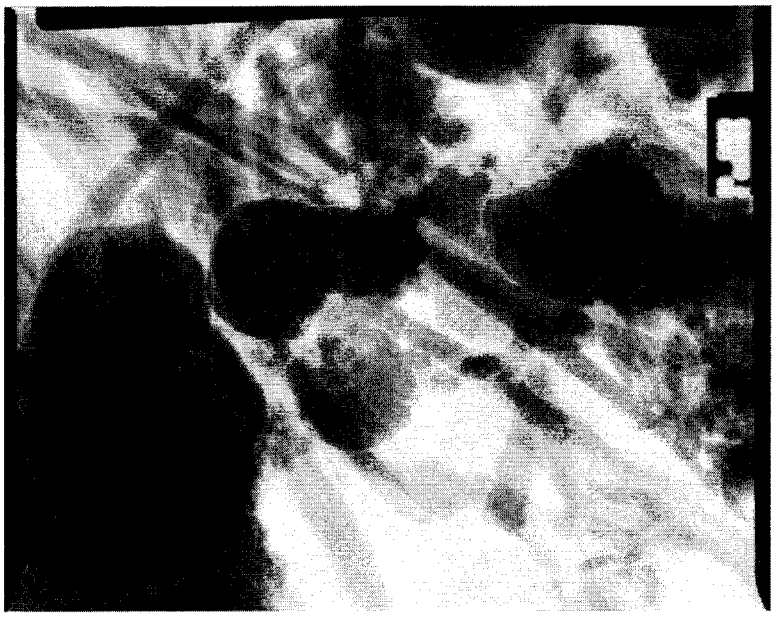

Figure A2. 75 GGBS: 25 OPC Deionised water, 85°C, 20 months:
Hydrogarnets amongst CSH needles. Magnification x 60,000.

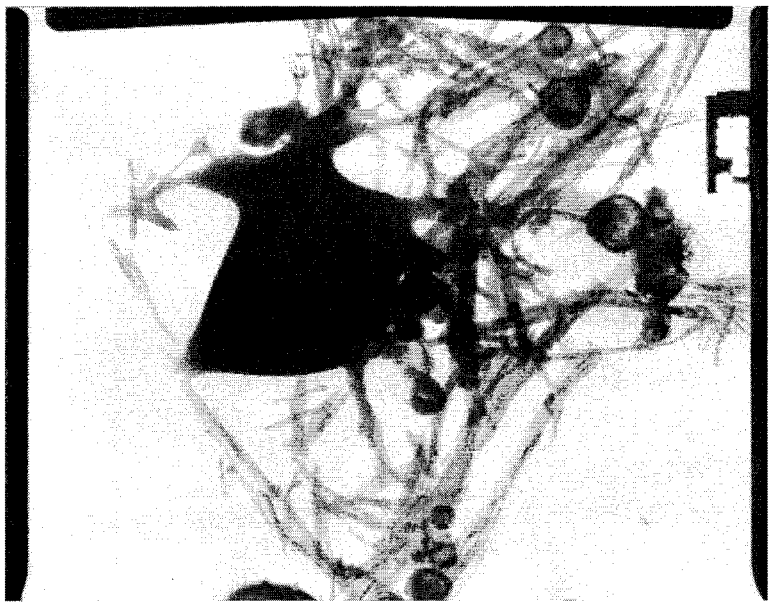

Figure A3. 75 GGBS: 25 OPC Deionised water, 85°C, 20 months:
CSH and hydrogarnet forming on a grain which may be a remnant of reactant material. Magnification x 17,000.

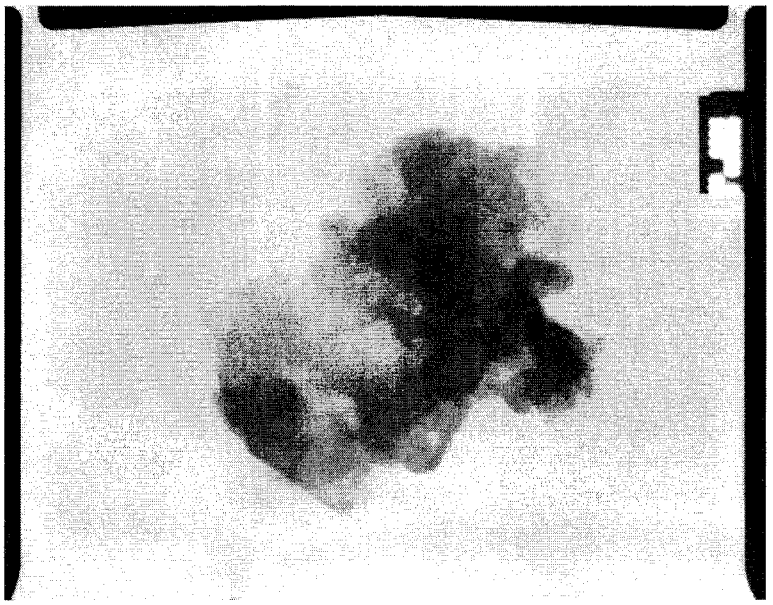

Figure A4. 75 GGBS: 25 OPC Deionised water, 85°C, 20 months:
A cluster of magnesian platy material. Magnification x 80,000.

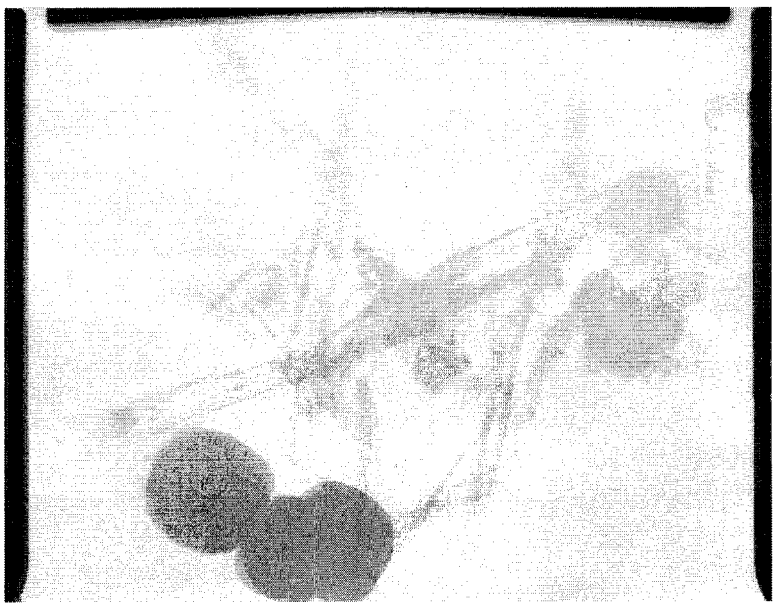

Figure A5. 75 GGBS: 25 OPC Deionised water, 85°C, 20 months:
Typical hydrogarnets and CSH needles and prisms. Magnification x 22,000.

Figure A6. 60 pfa: 40 OPC Deionised water, 85°C, 20 months:
Prismatic zeolite amongst fine grained C-A-S-H. Magnification x 100,000.

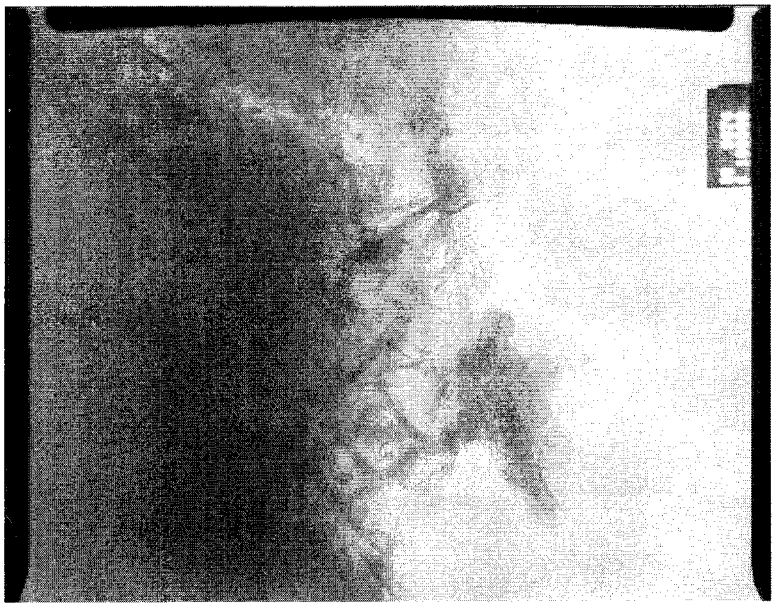

Figure A7. 60 pfa: 40 OPC Deionised water, 85°C, 20 months:
Prisms/needles amongst poorly ordered C-A-S-H. Magnification x 100,000.

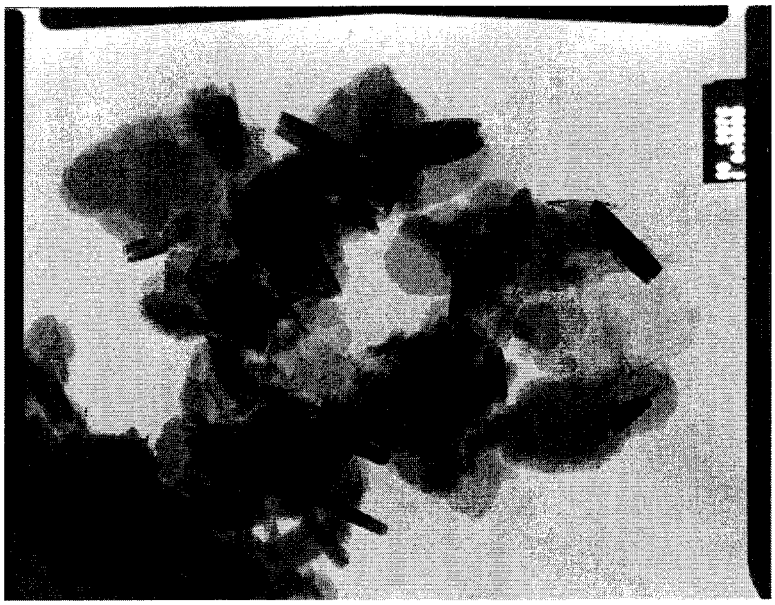

Figure A8. 60 pfa: 40 OPC Deionised water, 85°C, 20 months:
Stubby prisms of an Fe phase with hexagonal plates (possibly of portlandite).
Magnification x 46,000.

Figure A9. 60 pfa: 40 OPC Deionised water, 85°C, 20 months:
Enlargement of Figure A8 showing a stubby prismatic Fe-bearing grain and some hexagonal plates. Magnification x 220,000.

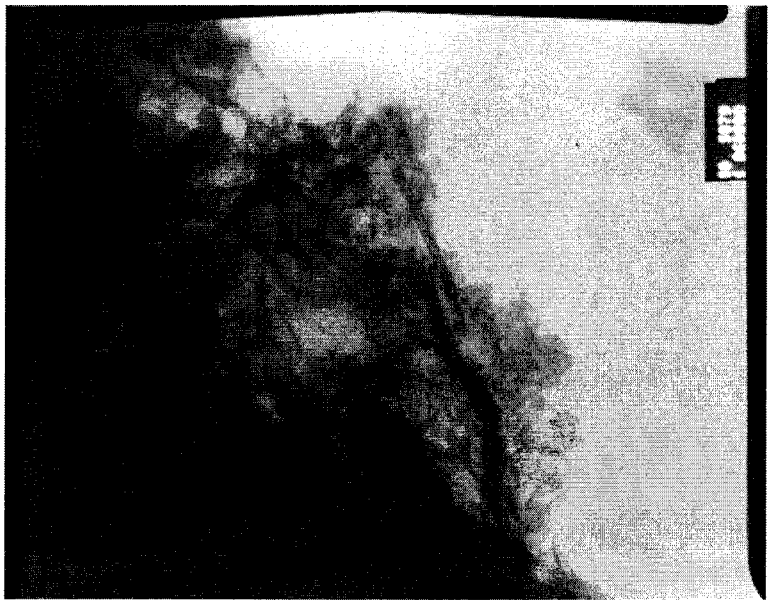

Figure A10. 60 pfa: 40 OPC Deionised water, 85°C, 20 months:
Needle-like zeolites amongst poorly ordered C-A-S-H. Magnification x 60,000.

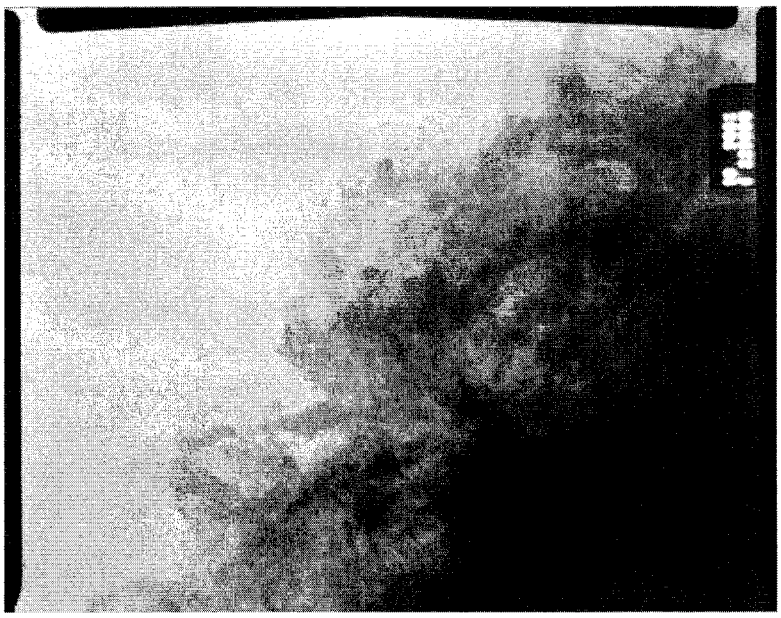

Figure A11. 60 pfa: 40 OPC Deionised water, 85°C, 20 months: C-A-S-H material with variable degrees of ordering. Magnification x 220,000.

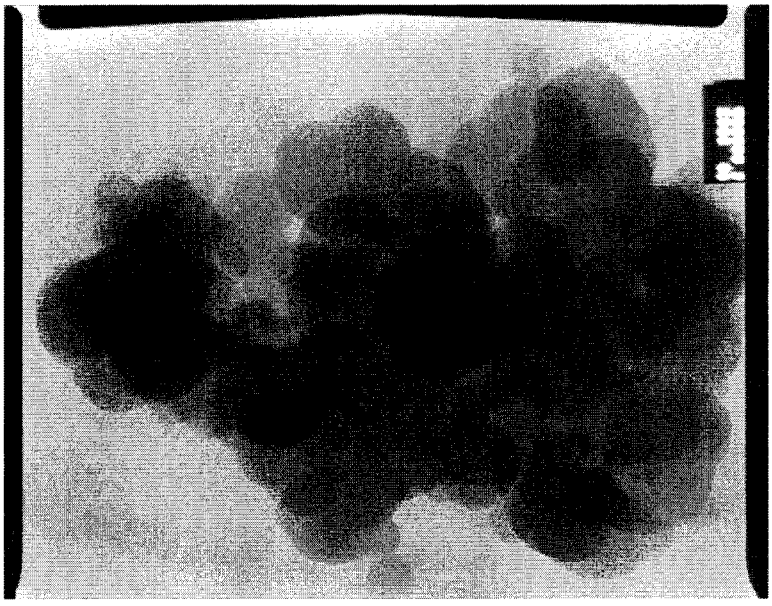

Figure A12. 60 pfa: 40 OPC Deionised water, 85°C, 20 months: Relatively electron-transparent grains with sub-cubic/octahedral morphology. Magnification x 80,000.

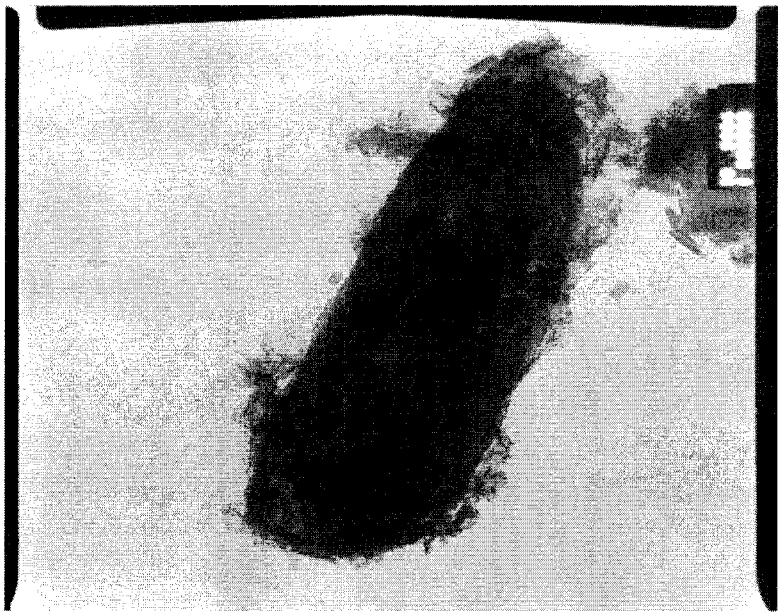

Figure A13. 60 pfa: 40 OPC Deionised water, 85°C, 20 months:
Coarse, sub-prismatic C-A-S-H grain with gel-like surrounding material.
Magnification x 28,000.

Figure A14. 60 pfa: 40 OPC Deionised water, 85°C, 20 months:
Typical mixture of needles and hexagonal plates. Magnification x 100,000.

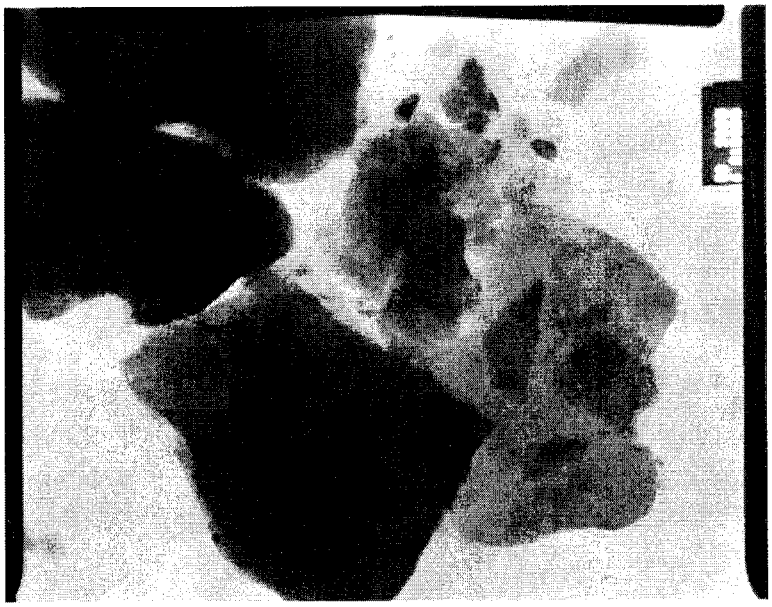

Figure A15. 60 pfa: 40 OPC Deionised water, 85°C, 20 months:
Aluminosilicate grains. Magnification x 10,000.

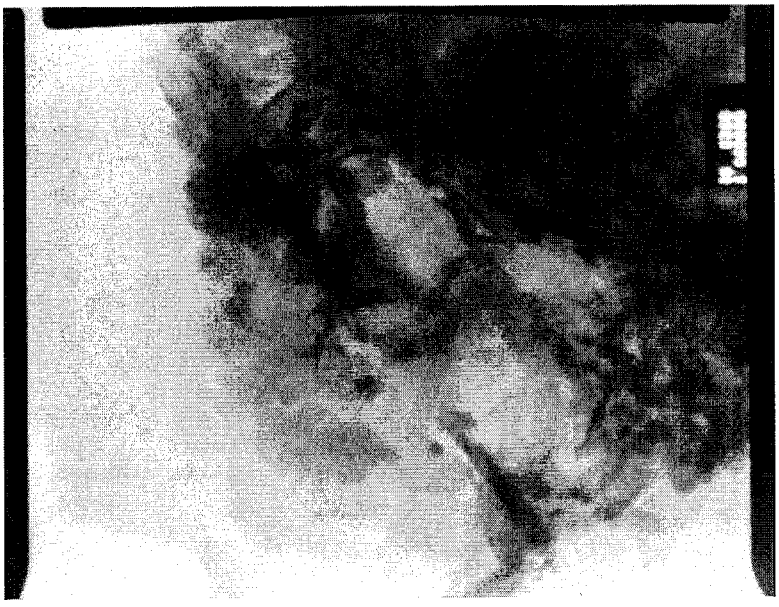

Figure A16. 60 pfa: 40 OPC Groundwater water A, 85°C, 20 months:
CSH plates and curled up sheets with some prismatic zeolite. Magnification x 60,000.

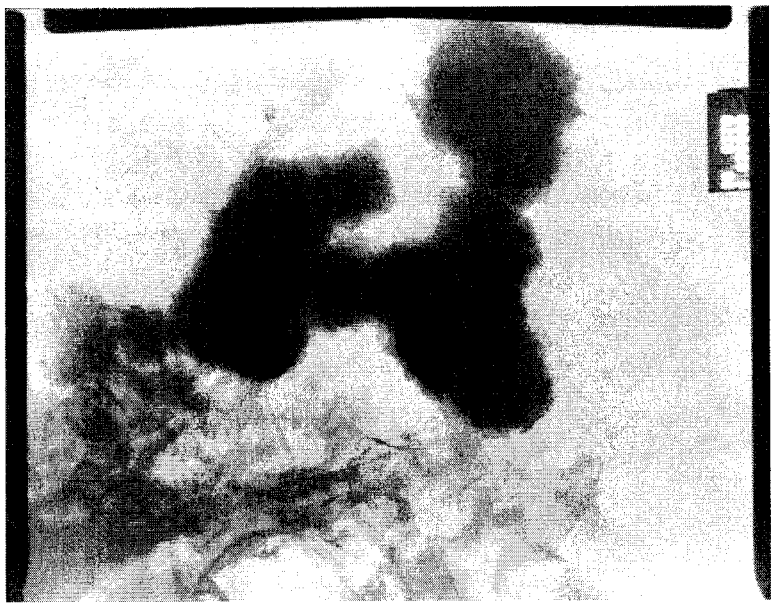

Figure A17. 60 pfa: 40 OPC Groundwater water A, 85°C, 20 months: Electron-dense equant iron oxide grains possibly coated with gel, along with CSH plates and curled up sheets and a single prismatic zeolite. Magnification x 36,000.

Figure A18. 60 pfa: 40 OPC Groundwater water A, 85°C, 20 months: Coarse rectangular plates of unknown composition. Magnification x 22,000.

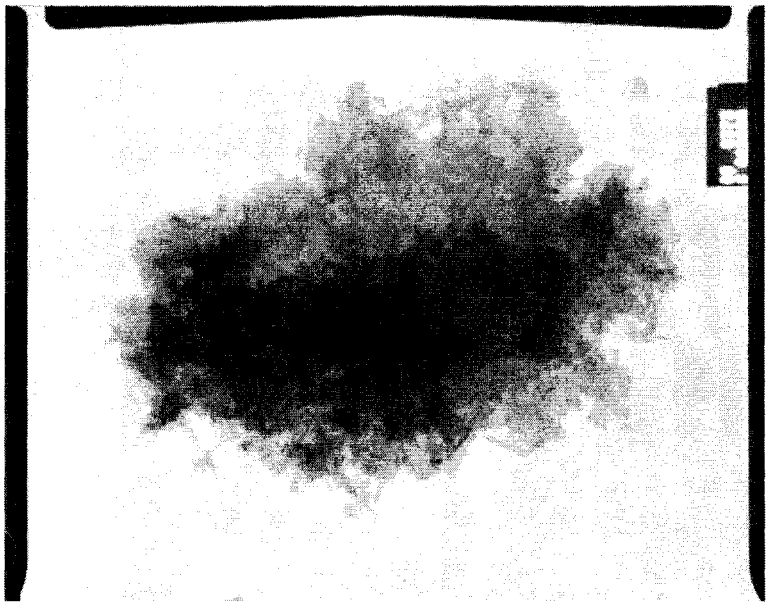

Figure A19. 60 pfa: 40 OPC Groundwater water A, 85°C, 20 months: Unusual cluster of gel with a fine grained acicular phase (possibly a zeolite). Note the dark specks on the gel (this may be finely disseminated halite). Magnification x 22,000.

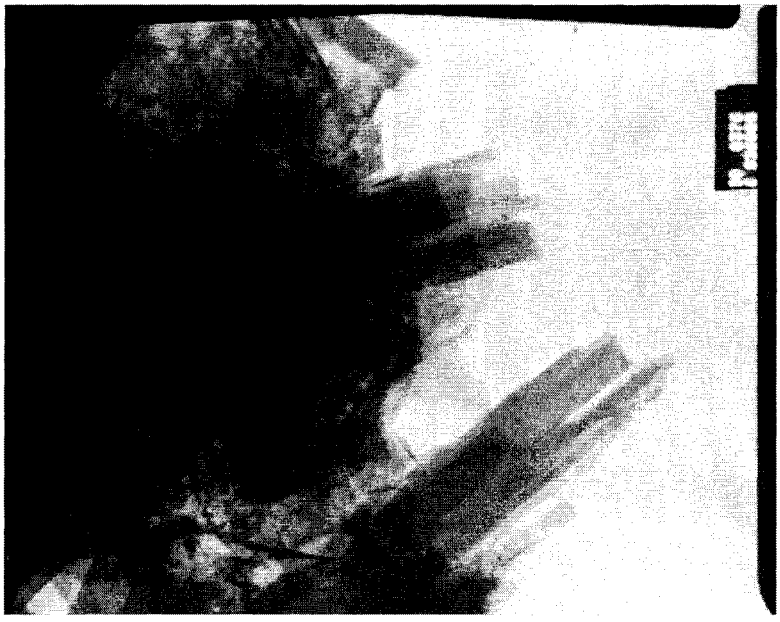

Figure A20. 60 pfa: 40 OPC Groundwater water A, 85°C, 20 months: Relatively coarse zeolite prisms amongst CSH sheets (whose curled up edges appear as electron-dense spikes). Magnification x 36,000.

Figure A21. 60 pfa: 40 OPC Groundwater water A, 85°C, 20 months:
A few coarse zeolite prisms amongst CSH sheets (whose curled up edges appear as electron-dense spikes), some finer grained prismatic zeolites and a few tiny patches of gel. Magnification x 28,000.

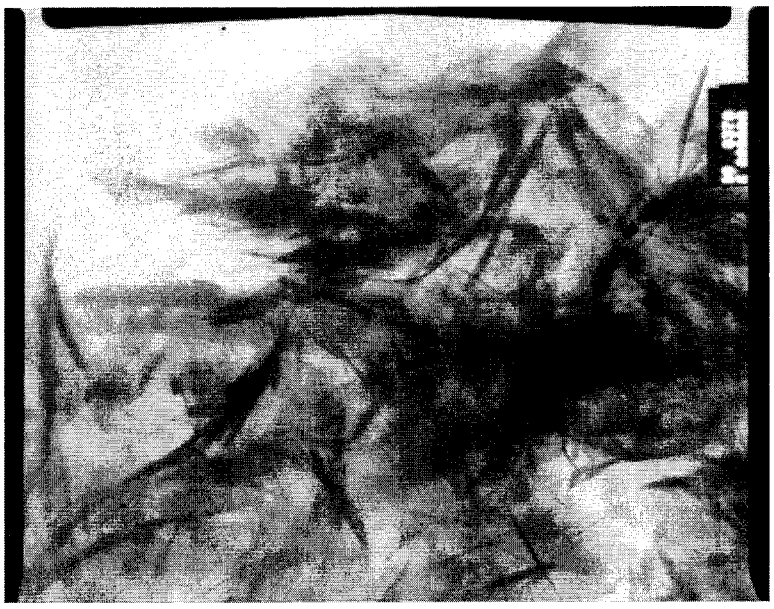

Figure A22. 60 pfa: 40 OPC Groundwater water A, 85°C, 20 months:
Enlargement of plate *0377* showing prismatic zeolites amongst CSH sheets (whose curled up edges appear as electron-dense spikes) and a few tiny patches of gel. Magnification x 80,000.

Figure A23. Reference Backfill Groundwater water A, 85°C, 20 months: The large electron-dense region to the lower right is a calcite grain. The large hexagonal plate (and the dark elongated shapes, which may be plates edge-on) are of pure Fe. The smaller hexagonal plates forming on these plates are unknown composition but may be portlandite or an AFm phase. Magnification x 60,000.

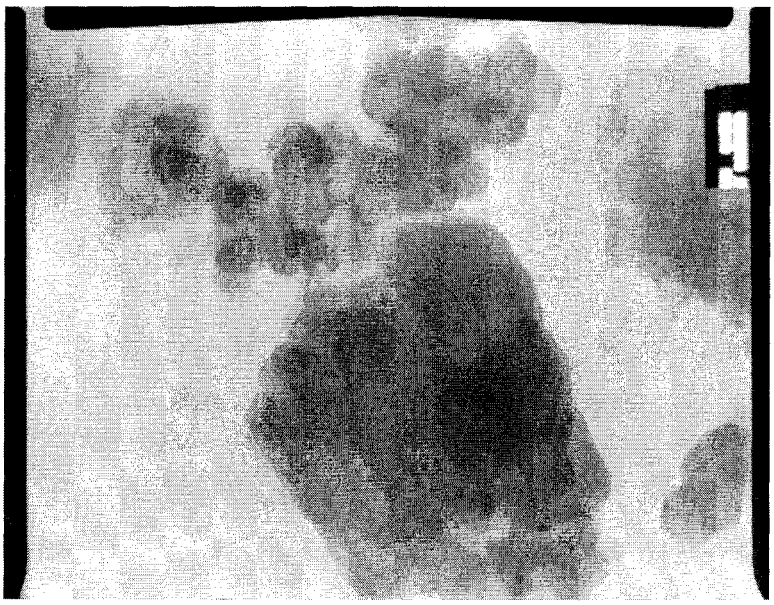

Figure A24. Reference Backfill Groundwater water A, 85°C, 20 months: Large hexagonal platy aluminosilicate with smaller equant grains of unknown composition. Magnification x 80,000.

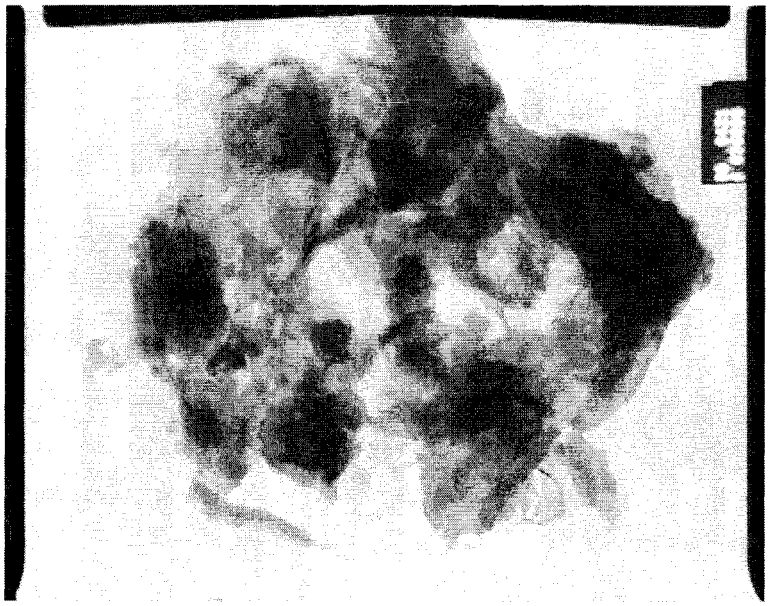

Figure A25. Reference Backfill Groundwater water A, 85°C, 20 months: Cluster of platy (hexagonal) material which may be AFm, with a little fibrous CSH. Magnification x 36,000.

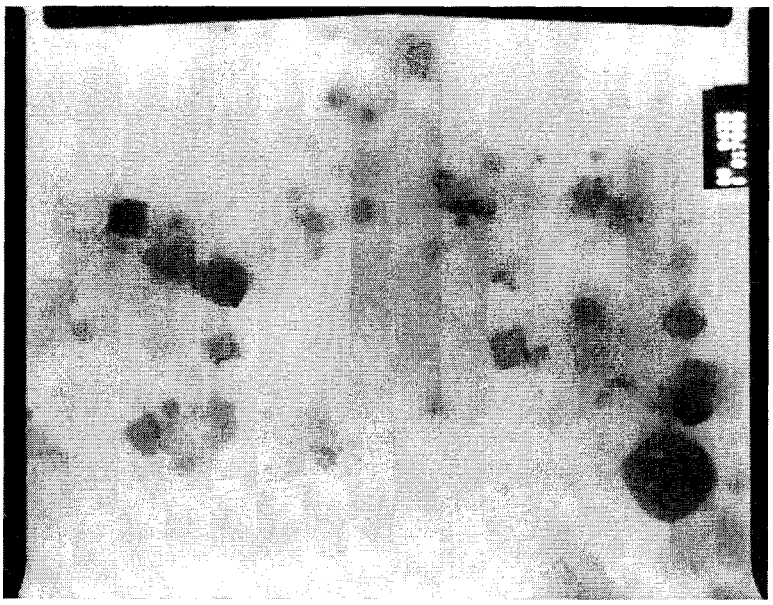

Figure A26. Reference Backfill Groundwater water A, 85°C, 20 months: Typical image of halite grains. Magnification x 17,000.

Figure A27. Reference Backfill Groundwater water A, 85°C, 20 months: Coarse hexagonal plates of pure Fe. Magnification x 17,000.

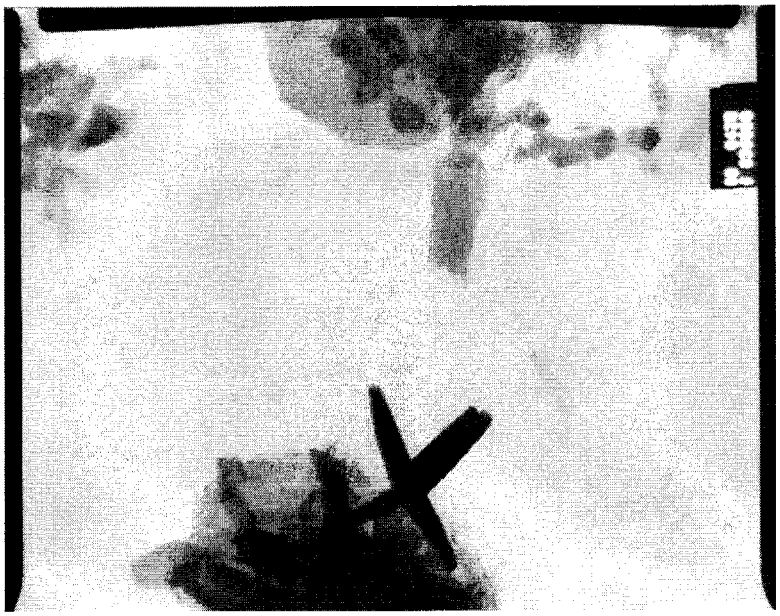

Figure A28. Reference Backfill Groundwater water A, 85°C, 20 months: Some coarse electron-dense prismatic grains (or possibly edge-on plates) of pure Fe with some fibrous CSH, possibly some gel, and some Fe-rich hexagonal plates. Magnification x 36,000.

Figure A29. Reference Backfill Groundwater water A, 85°C, 20 months: Fibrous CSH. Magnification x 28,000.

Figure A30. Reference Backfill Groundwater water A, 85°C, 20 months: Enlargement of Figure A29 showing fibrous CSH. Magnification: x 60,000.

A5 Note on the limitations of analytical TEM

X-ray dispersive chemical analysis by TEM, as carried out at Manchester, usually gives a precision of better than 5 % for major elements and about 11 % for minors. For elements comprising less than 5 wt% of the sample, the data is qualitative only and should be considered ambiguous for elements comprising less than 0.5 wt%. Thermolabile elements (e.g. Na and K) are especially hard to quantify as they can migrate under the electron beam.

The method of data manipulation used requires that the material being analysed is thin enough to satisfy the 'thin film criterion' which allows the effects of X-ray absorption and fluorescence to be neglected from the calculation. When the material has been prepared by the 'dispersed mounts' method (as is the case with this work) then it is frequently too thick to satisfy this 'thin film criterion' and so a further limitation is imposed on the reliability of the data.

Lastly, it should be stressed that TEM allows examination of only a tiny fraction of the sample, which cannot therefore be said to be representative of the whole sample. If a phase is not observed by TEM, it does not follow that the phase is not present.

SECTION 7, ANNEX B. SEM ANALYSIS OF SELECTED CEMENT PASTE CUBES.

7. B1. Introduction

Selected cement cubes that had been aged in groundwater A or deionised water for 20 months were analysed by scanning electron microscopy to help identify the phases formed and to investigate the effects of leaching and chloride ingress arising from exposure to the high saline groundwater. The samples that have been analysed to date are:

60 pfa:40 OPC	Groundwater A, 25°C
60 pfa:40 OPC	Deionised water, 25°C
60 pfa:40 OPC	Groundwater A, 85°C
60 pfa:40 OPC	Deionised water, 85°C
75 ggbs:25 OPC	Groundwater A, 25°C
75 ggbs:25 OPC	Deionised water, 25°C
75 ggbs:25 OPC	Deionised water, 85°C
OPC	Groundwater A, 85°C
Reference backfill	Groundwater A, 25°C
Reference backfill	Deionised water, 85°C

7. B2. Experimental

Samples were potted in epoxy resin and polished to 1/4 micron using diamond abrasive and paraffin oil lubricant. Samples were then coated with a vacuum coated layer of carbon. Analysis was carried out using a `CamScan' S4-80DV scanning electron microscope and energy dispersive X-ray analysis (EDXA, using a Link Systems `Exl' system). All the analyses were carried out using an accelerating voltage of 15 kV and a probe current of 0.5 nA. Quantitative `spot' analyses have been carried out for Na, Mg, Al, Si, S, Cl, K, Ca and Fe. The outer 3mm of each sample was analysed to allow the effects of groundwater on the sample to be determined. Analyses were made using a 10 x 10 or a 10 x 5 grid of analysis points.

All of the data collected during the analysis has been electronically archived and are available for further analysis.

7. B3. Results

Only limited analysis of the collected data has been possible due to the limited resources available for this part of the work. X-ray maps for each sample showing the distributions of Ca, Si, S and Cl are given in figures B1 to B 10. Backscattered electron micrographs are also shown. C/S ratios for the gel phases have not been calculated due to the limited resources available for this part of the programme.

60 pfa:40 OPC reacted with groundwater A at 25°C for 20 months

An electron micrograph and X-ray dispersion maps for this sample are shown in figure B1. Calcium and chlorine levels are depleted in the outer 500 μm of the sample although there is evidence of the formation of calcium and chlorine-rich layers on the surface of the sample. These may be calcite and NaCl although XRD also showed that the sample contained the Cl-containing AFm phase AFm-Cl (see table 29). There is no evidence of zonation from the electron micrograph.

60 pfa:40 OPC reacted with deionised water at 25°C for 20 months

Figure B2 shows that the calcium and silica levels in the outer 200 μm of this sample appear to be slightly higher here than in the bulk of the sample. The sulphate distribution appears to be fairly even throughout. There is no evidence of zonation from the backscattered electron image.

60 pfa:40 OPC reacted with deionised water at 85°C for 20 months

The backscattered electron image in figure B3 shows that some zonation has occurred in the outer layer of the sample. There is also cracking in the sample around this zone. The calcium level appears to be higher in the outer 1 mm than in the bulk of the sample, possibly due to the formation of calcite through atmospheric CO_2. NaCl probably formed on the surface of the sample and possibly in a layer at a depth of about 1 mm (indicated by a Cl-rich layer). AFm-Cl was not detected by XRD. There are also silicon-rich and magnesium-rich layers near the sample surface.

60 pfa:40 OPC reacted with deionised water at 85°C for 20 months

Figure B4 shows that some zonation has occurred in the outer 1 μm of the sample with some cracking around this area. This area appears to be depleted in silicon but rich in calcium (possibly due to the formation of calcite) when compared to the bulk of the sample. There is evidence of the formation of calcite and of a silicon rich layer on the sample surface.

75 ggbs:25 OPC reacted with groundwater A at 25°C for 20 months

Figure B5 shows that the outer layer (approximately 700 μm) has become depleted in calcium and silicon with cracking approximately parallel to the sample face around this zone. This area also contains less chlorine than the bulk of the sample. The figure also suggests that calcium is present in higher levels in the outer 100 μm, possibly due to the formation of calcite. XRD also showed that the sample contained the Cl-containing AFm phase, AFm-Cl, and monosulphate (see table 28). The sulphur and chlorine dispersions suggest that these may have formed in the outer 100 μm of the sample.

75 ggbs:25 OPC reacted with deionised water at 25°C for 20 months

Figure B6 shows zonation in the outer layer of the sample. There is evidence of cracking parallel to the outer surface at a depth of about 100-200 μm. Calcium has been leached from the outer 200 mm of the sample. There is also evidence of sulphur and chlorine having been leached from this area.

75 ggbs:25 OPC reacted with deionised water at 85°C for 20 months

Figure B7 shows zonation in the outer layer of the sample. The amount of calcium levels has been reduced, probably through leaching, in the outer 300 μm of the sample. The silicon level is also lower here than in the bulk of the sample. There is evidence of cracking parallel to the outer surface at a depth of about 1 μm. Calcite has probably formed on the surface of the sample, due to atmospheric carbonation.

OPC reacted with groundwater A at 85°C for 20 months.

Figure B8 suggests that NaCl (or AFm-Cl) has formed on the face of the sample although the next 500 μm appears to be depleted in chlorine. This may have been due to the drying stage of sample preparation. Chlorine in the bulk of the sample may be due to ingress from the groundwater, possibly leading to the formation of AFm-Cl. The silicon level in the outer 100 μm of the sample has also been depleted.

Reference backfill reacted with groundwater A at 25°C for 20 months.

Figure B9 shows that the outer 1 μm of this sample appears to be richer in calcium and chlorine than the bulk of the sample, possibly due to the formation of NaCl, AFm-Cl (detected in small amounts by XRD) and additional calcite.

Reference backfill reacted with deionised water at 85°C for 20 months.

The outer 500 μm of the sample are richer in calcium (and possibly sulphur) than the bulk of the sample. Silicon may have become depleted in this area. The outer 500 μm may be more dense than the bulk of the sample.

7. B4. Conclusions

The results of the SEM analysis of the cement paste blocks show that the samples have a zonal structure with the equilibrium products, formed in the powder samples, only present in the outer layer. There is also evidence of cracks running parallel to the sample faces in many cases.

The analysis included in this report are preliminary due to the limited resources available for this part of the programme. More data than that included here has been collected and may be analysed at a later date.

Figure B1. Backscattered electron micrograph amd X-ray maps for 60 pfa:40 OPC. Groundwater A, 25°C

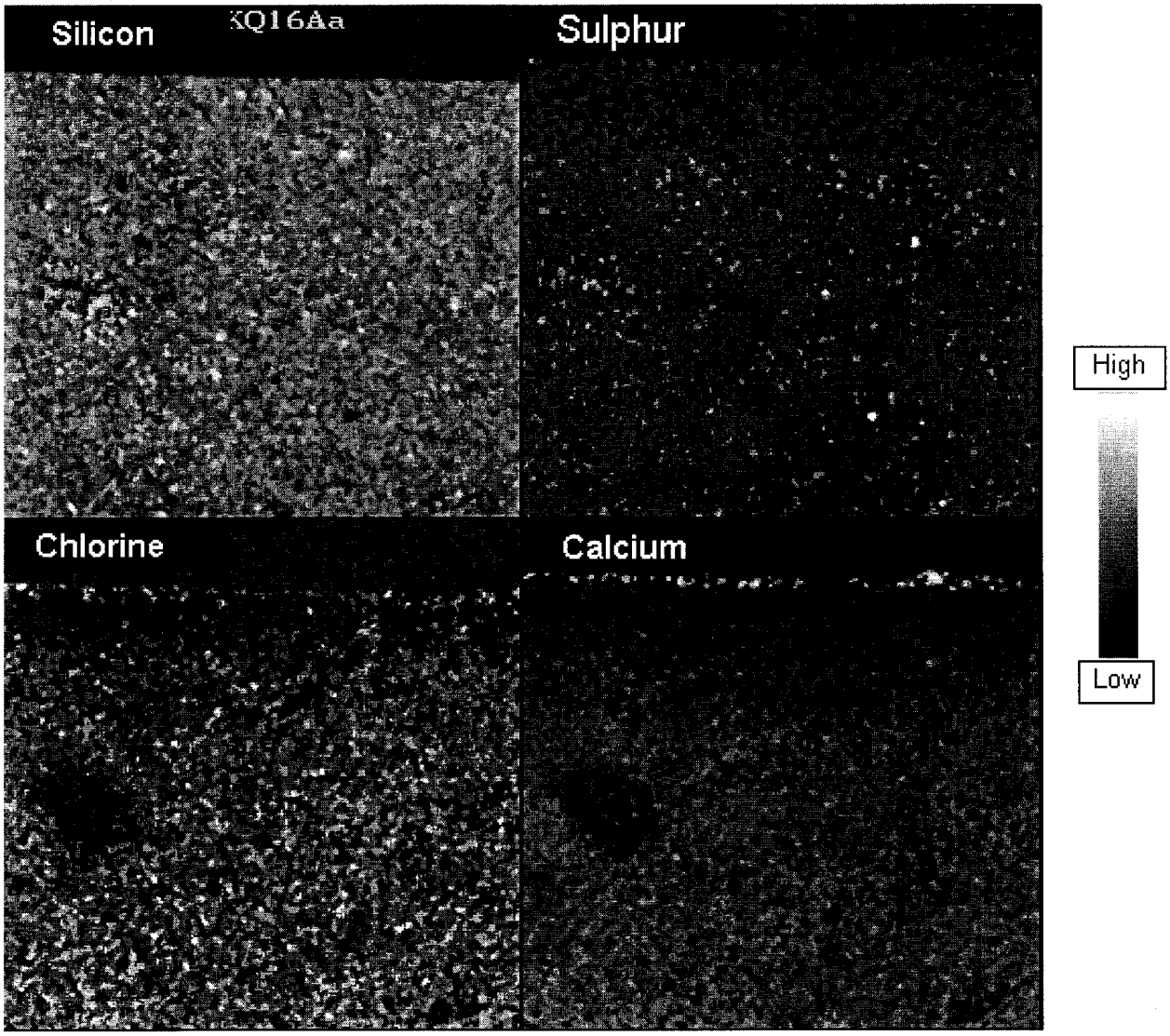

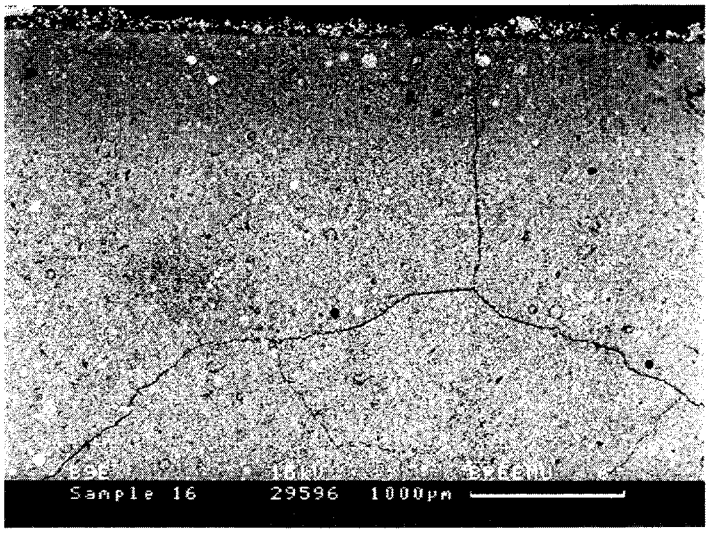

Figure B2. Backscattered electron micrograph amd X-ray maps for for 60 pfa:40 OPC
Deionised water, 25°C

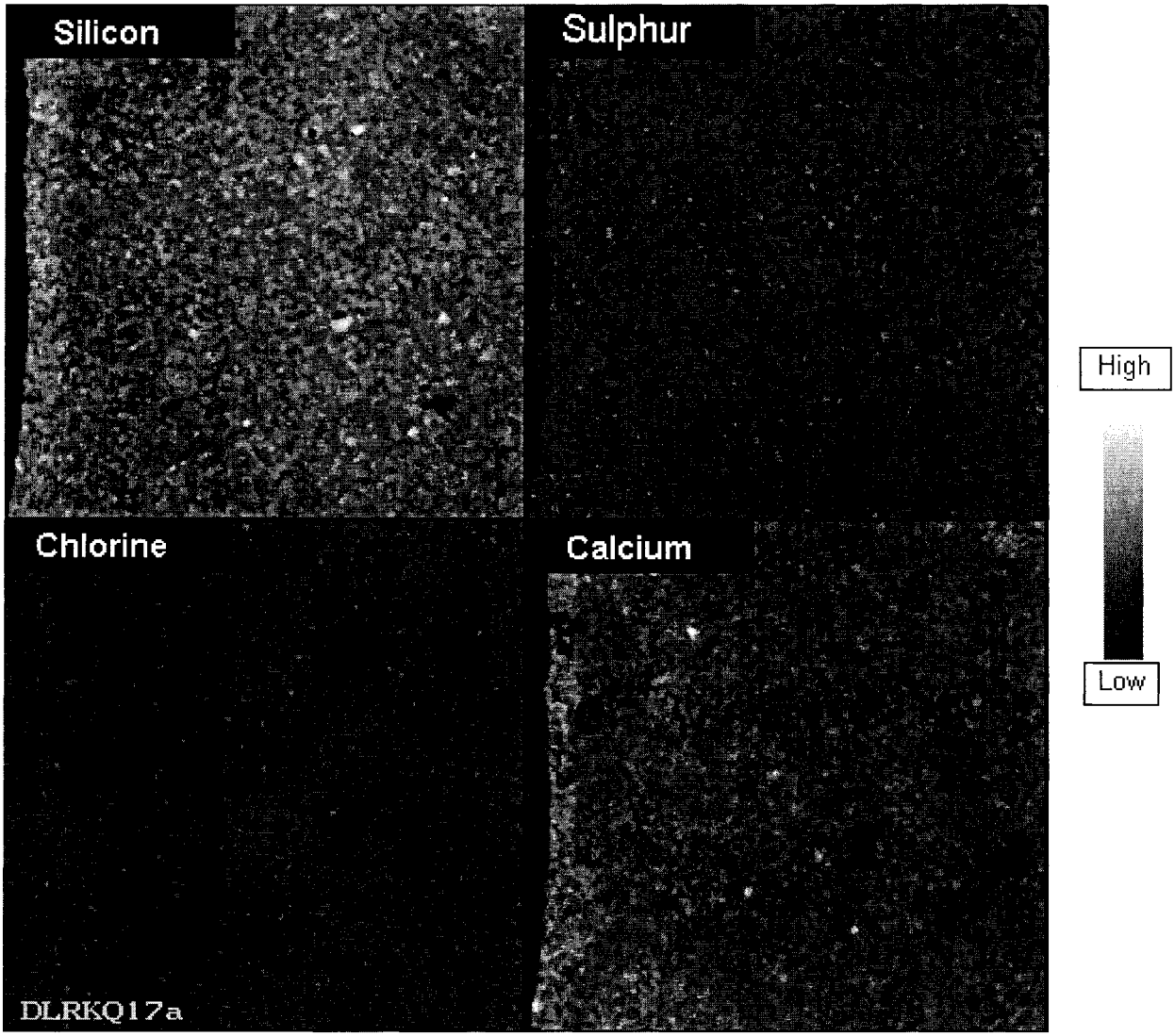

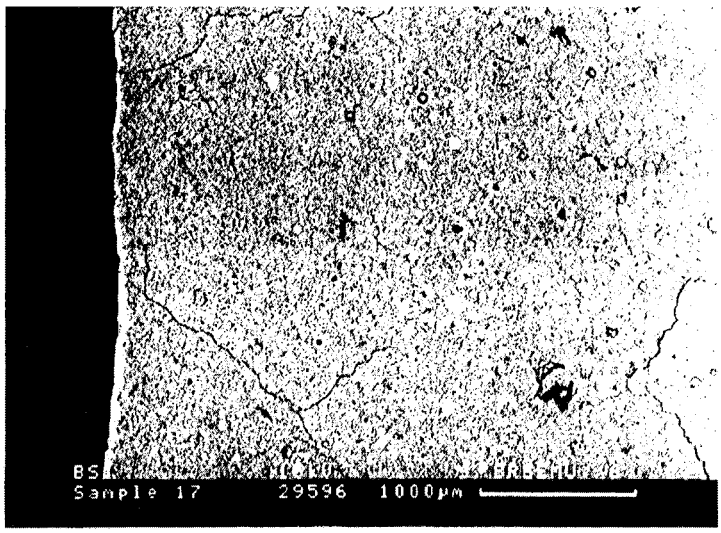

Figure B3. Backscattered electron micrograph amd X-ray maps for 60 pfa:40 OPC Groundwater A, 85°C

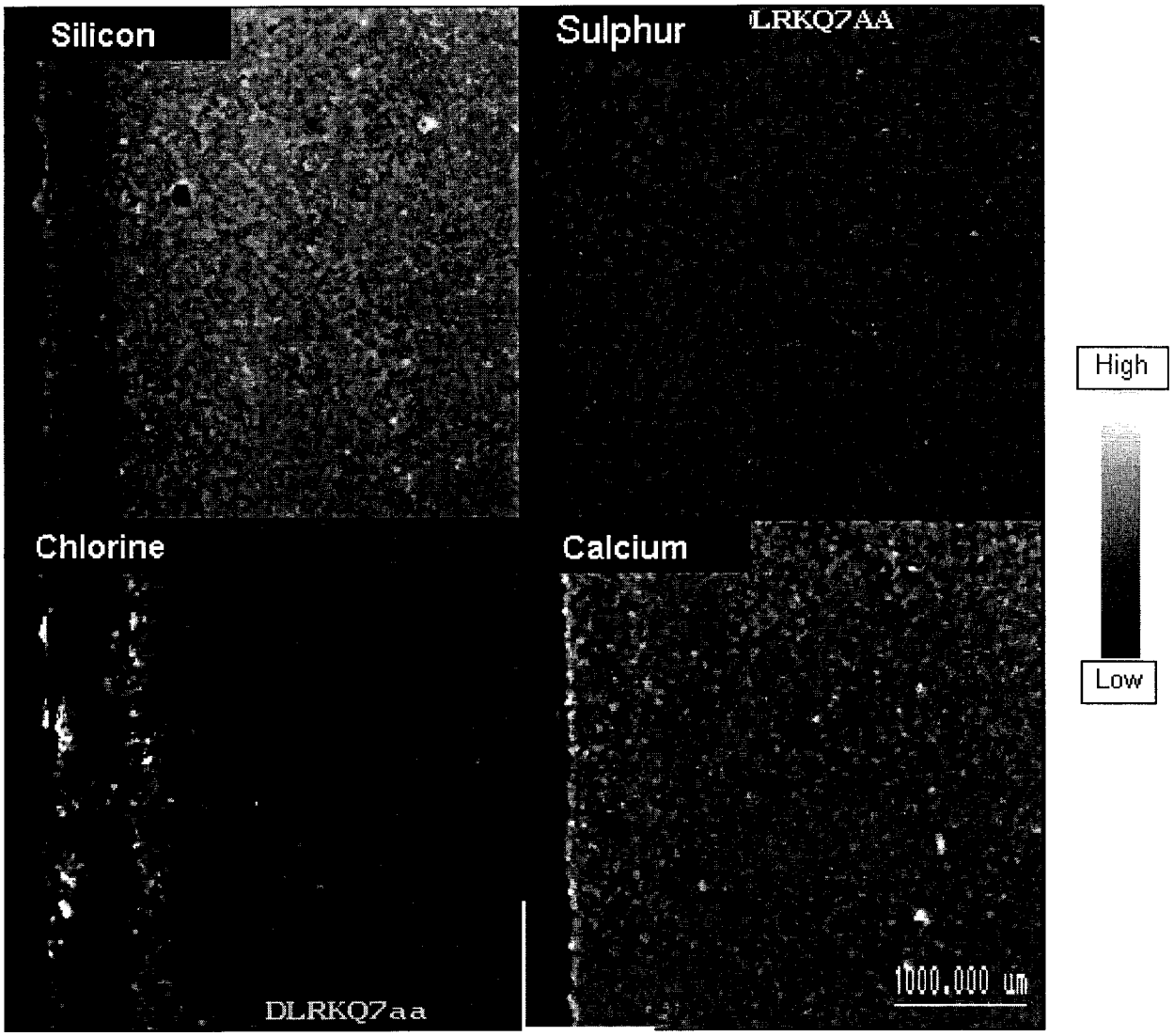

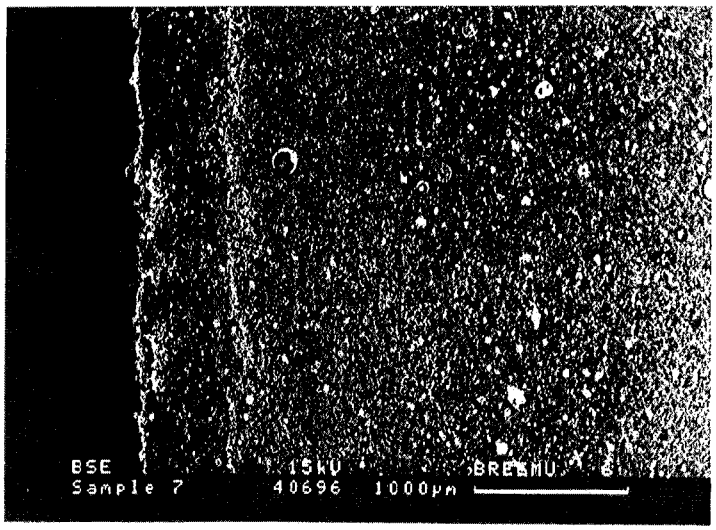

Figure B4. Backscattered electron micrograph amd X-ray maps for 60 pfa:40 OPC Deionised water, 85°C

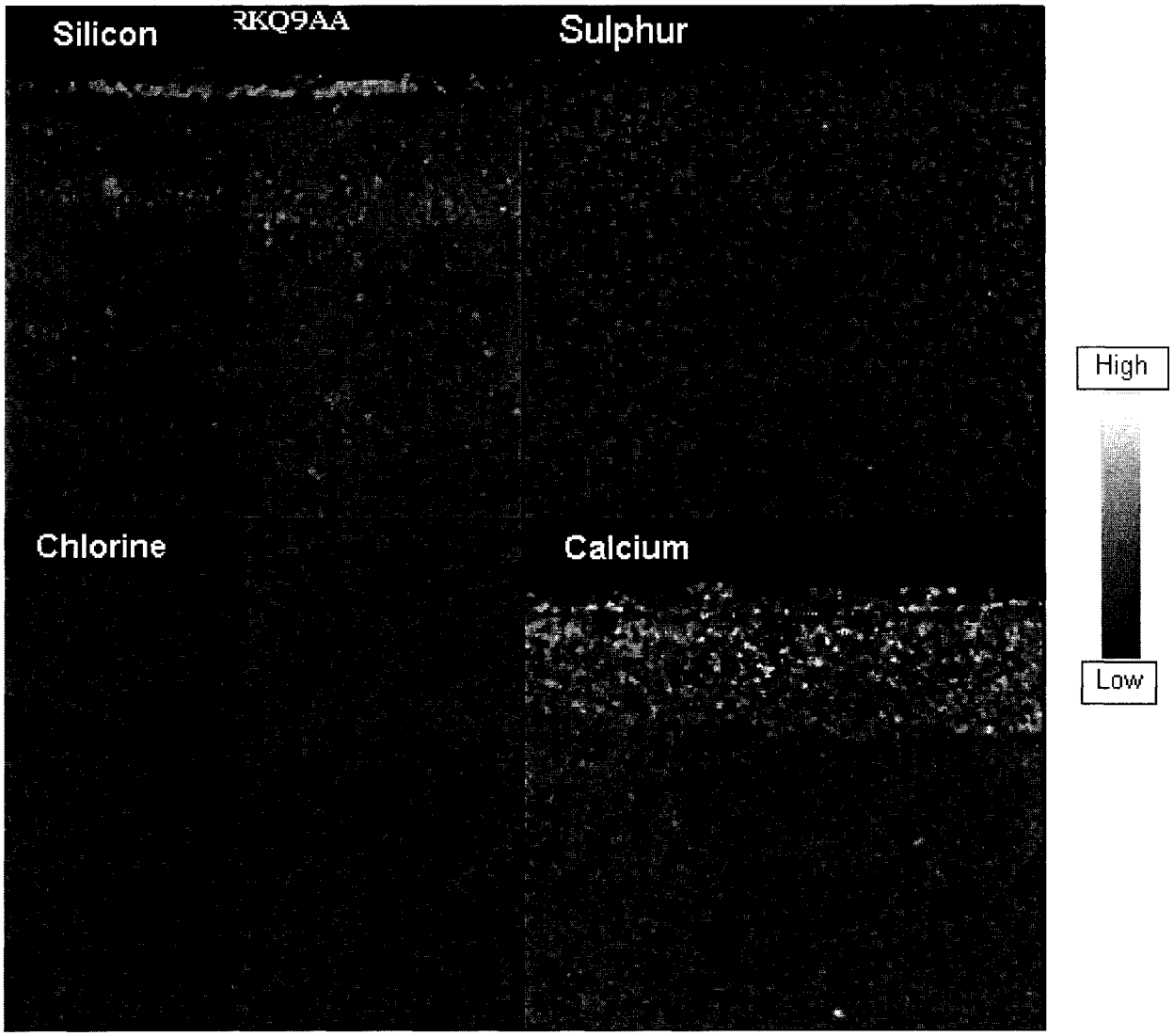

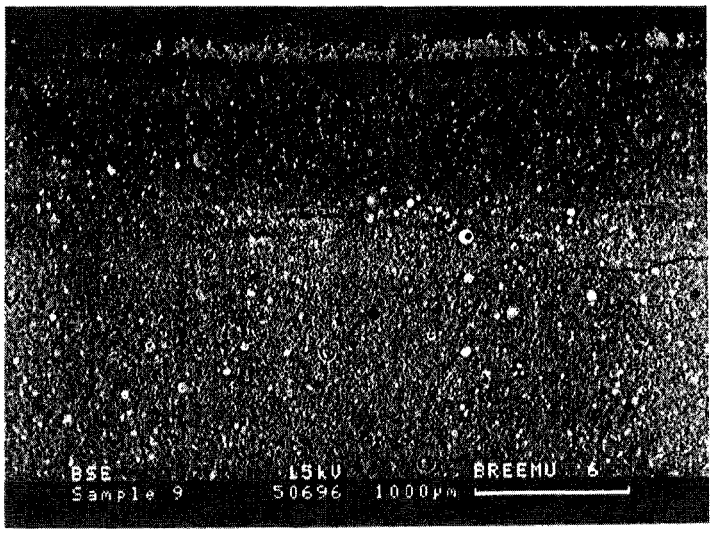

Figure B5. Backscattered electron micrograph amd X-ray maps for 75 bbbs:25 OPC Groundwater A, 25°C

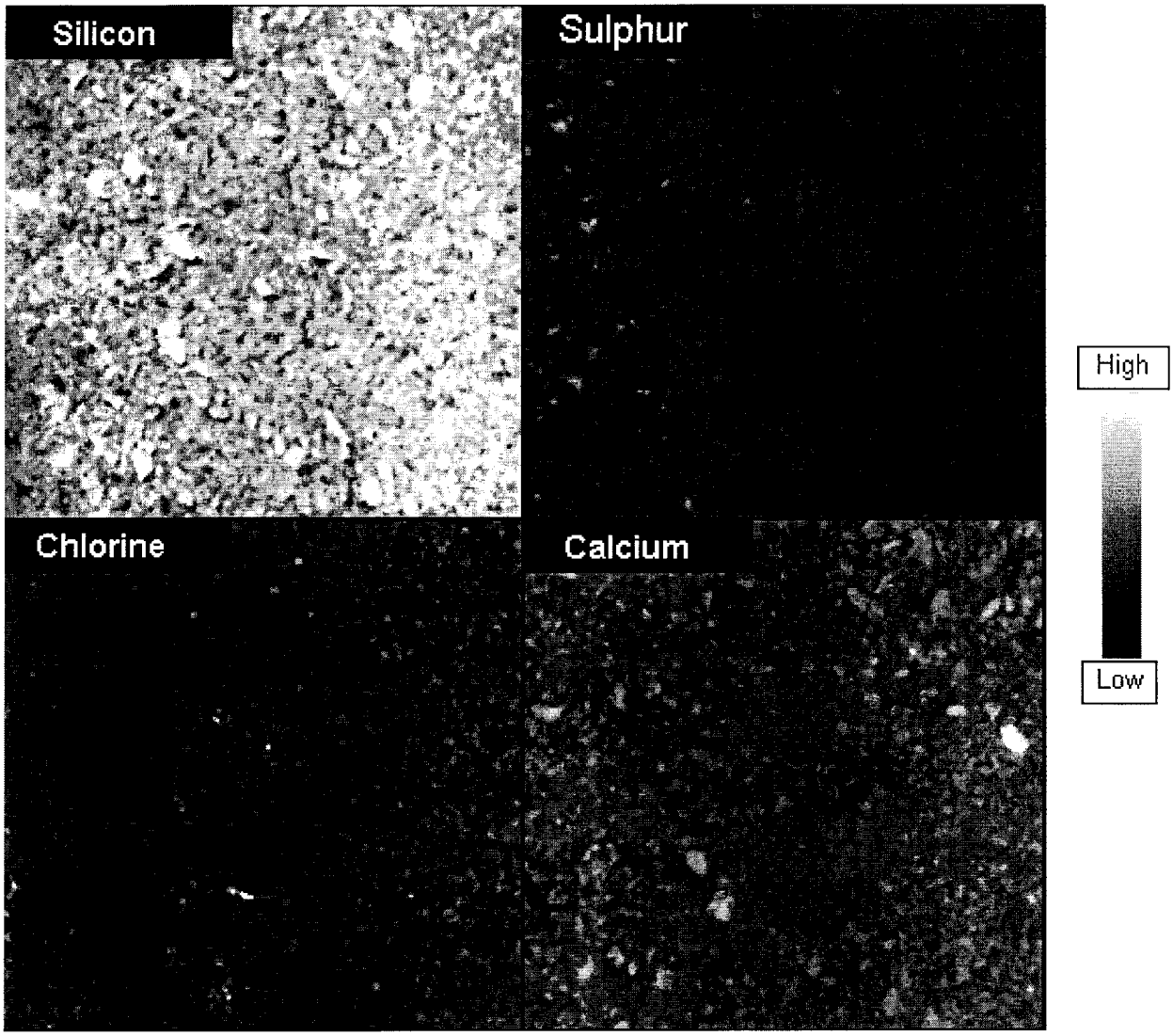

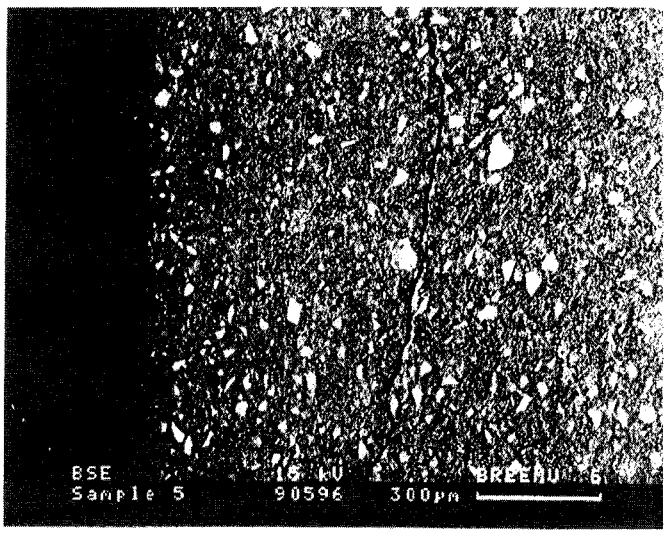

Figure B6. Backscattered electron micrograph amd X-ray maps for 75 bbbs:25 OPC
Deionised water, 25°C

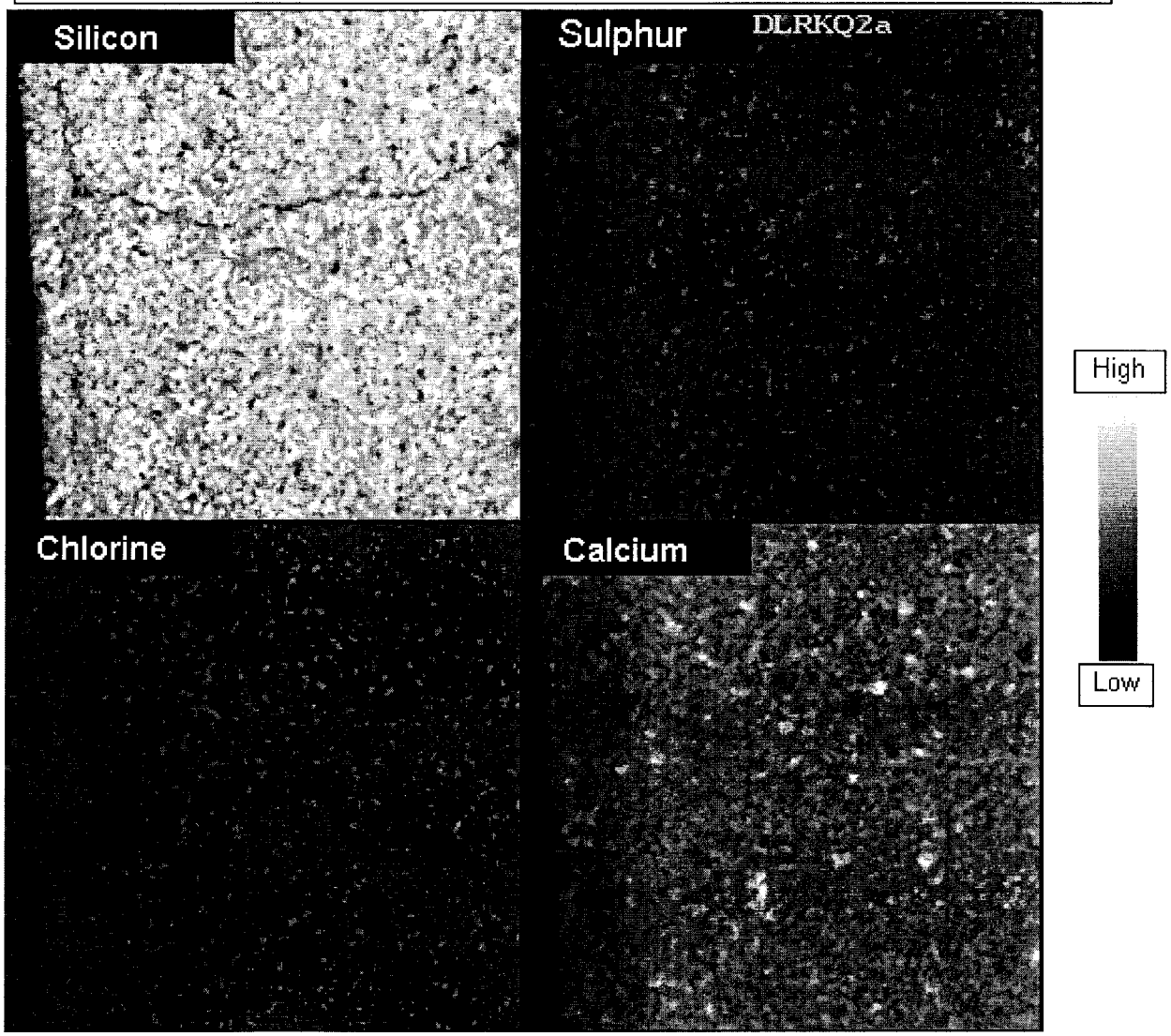

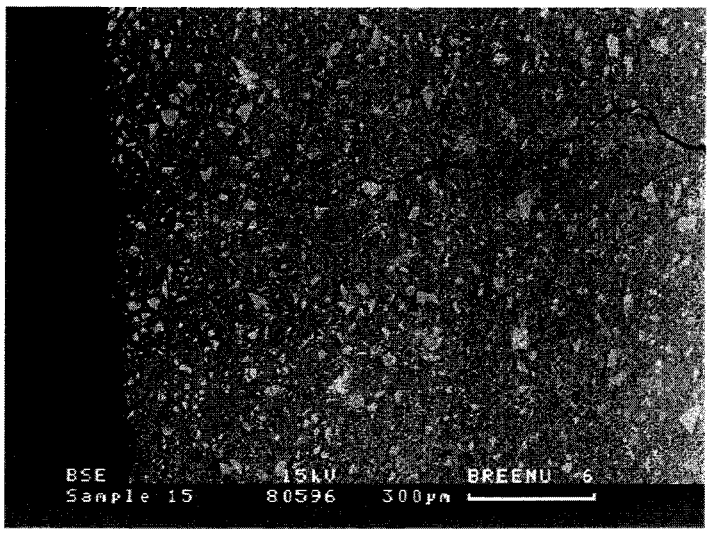

Figure B7. Backscattered electron micrograph amd X-ray maps for 75 bbbs:25 OPC Deionised water, 85°C

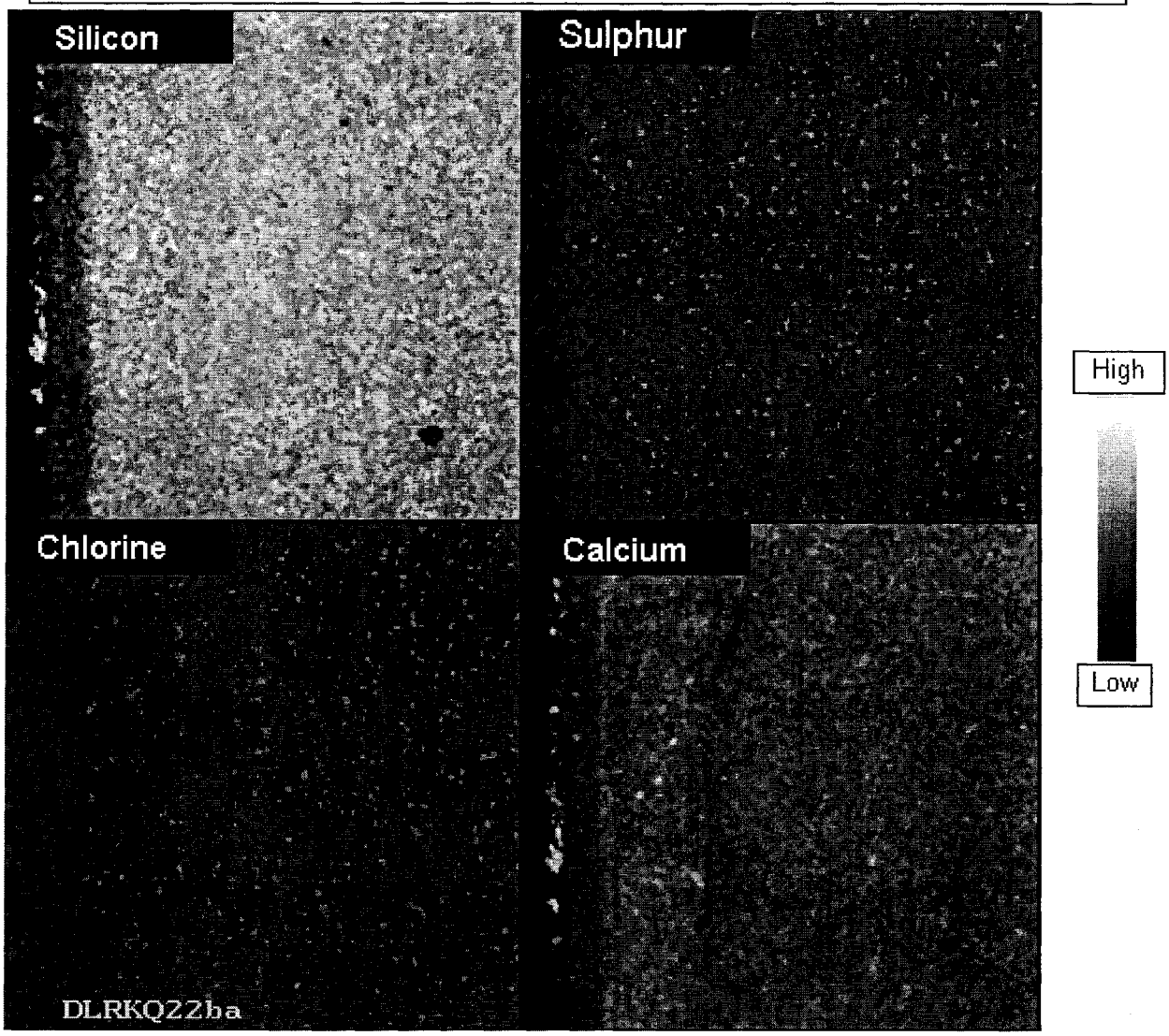

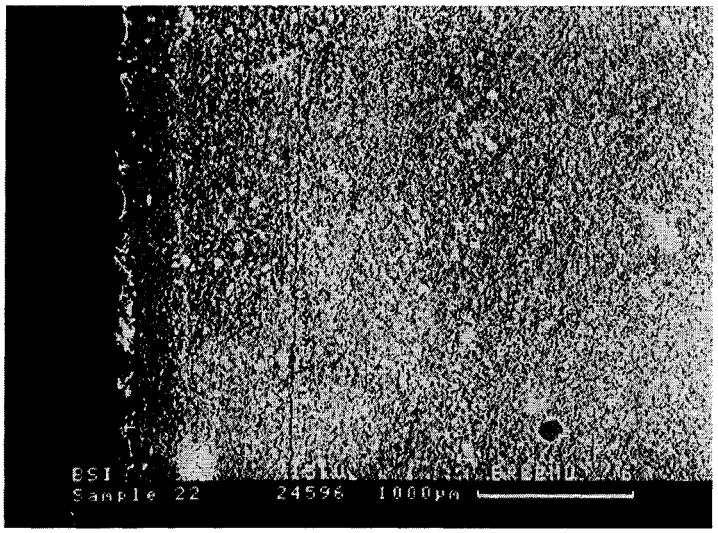

Figure B8. Backscattered electron micrograph amd X-ray maps for OPC, Groundwater A, 85°C

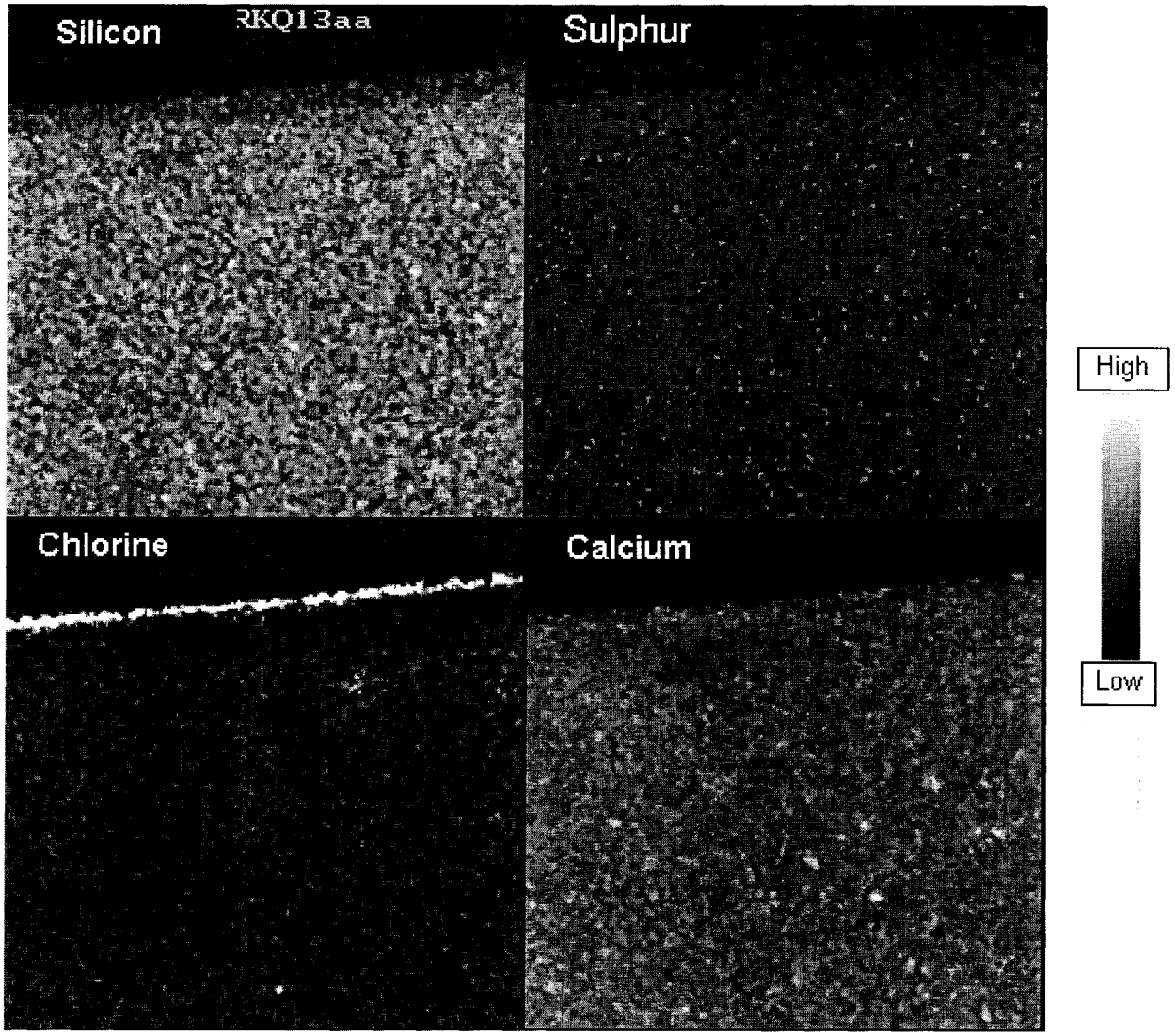

25°C

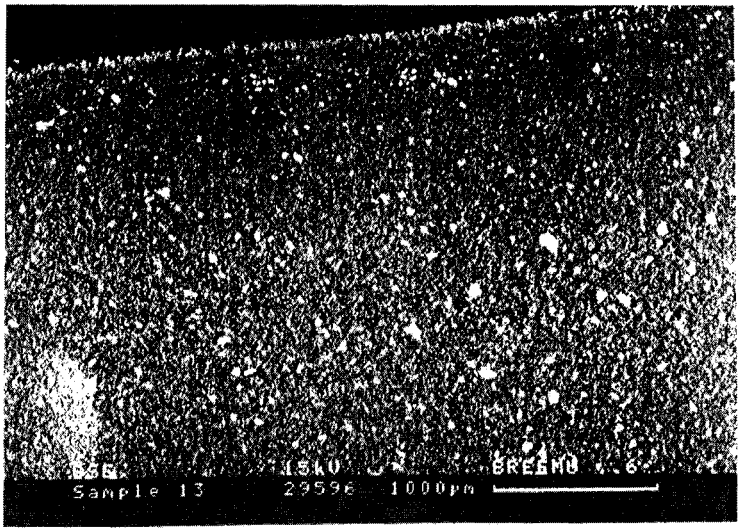

Figure B9. Backscattered electron micrograph amd X-ray maps for Reference backfill. Grounwater A, 25°C

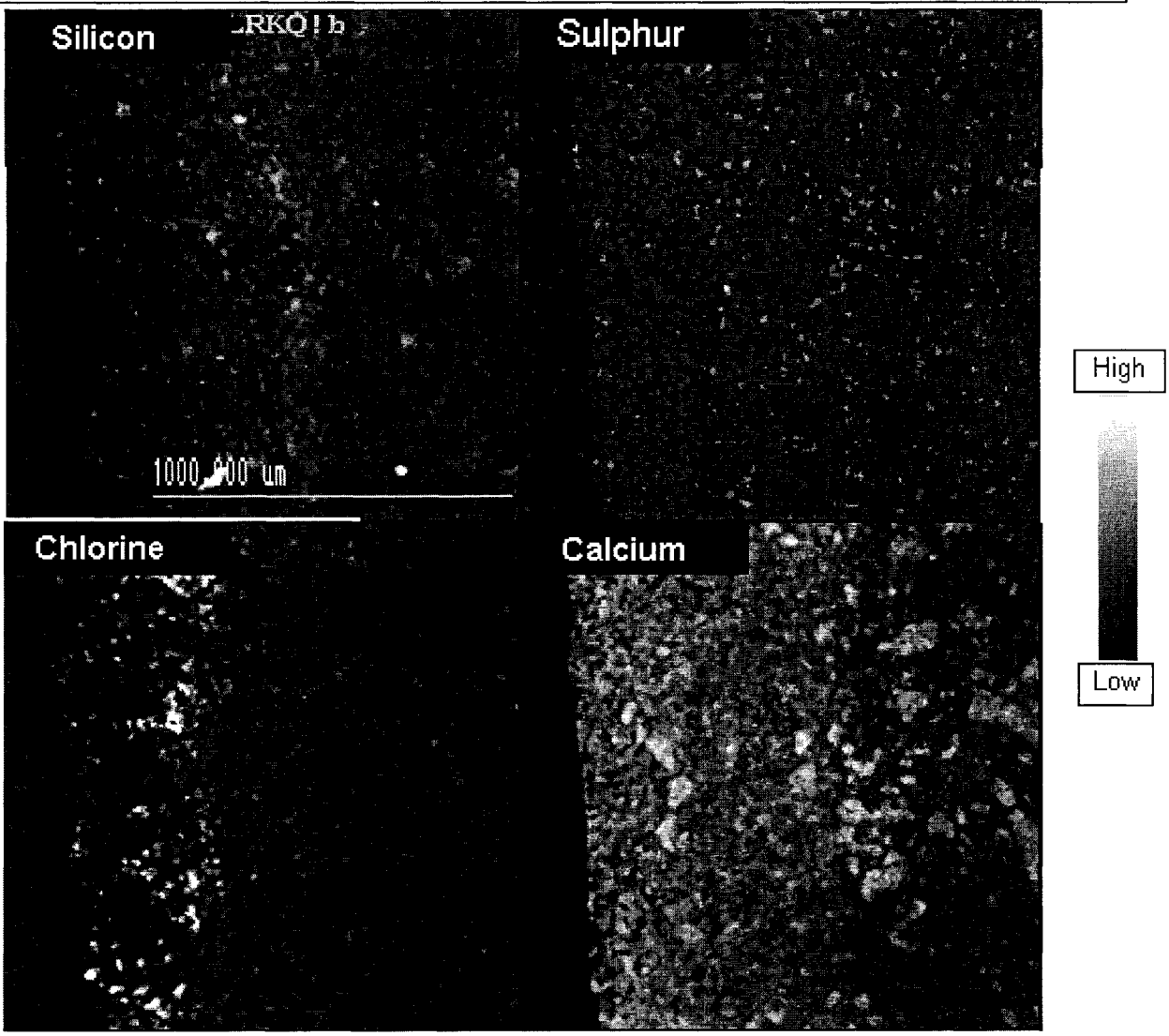

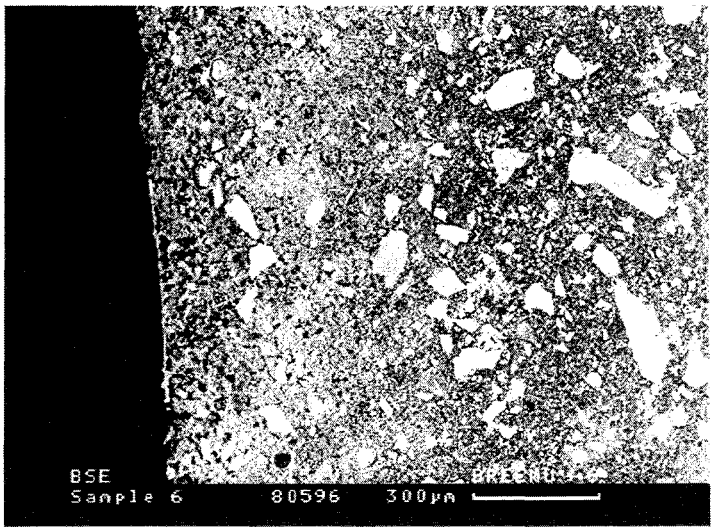

Figure B10. Backscattered electron micrograph amd X-ray maps for Reference backfill. Deionised water, 85°C

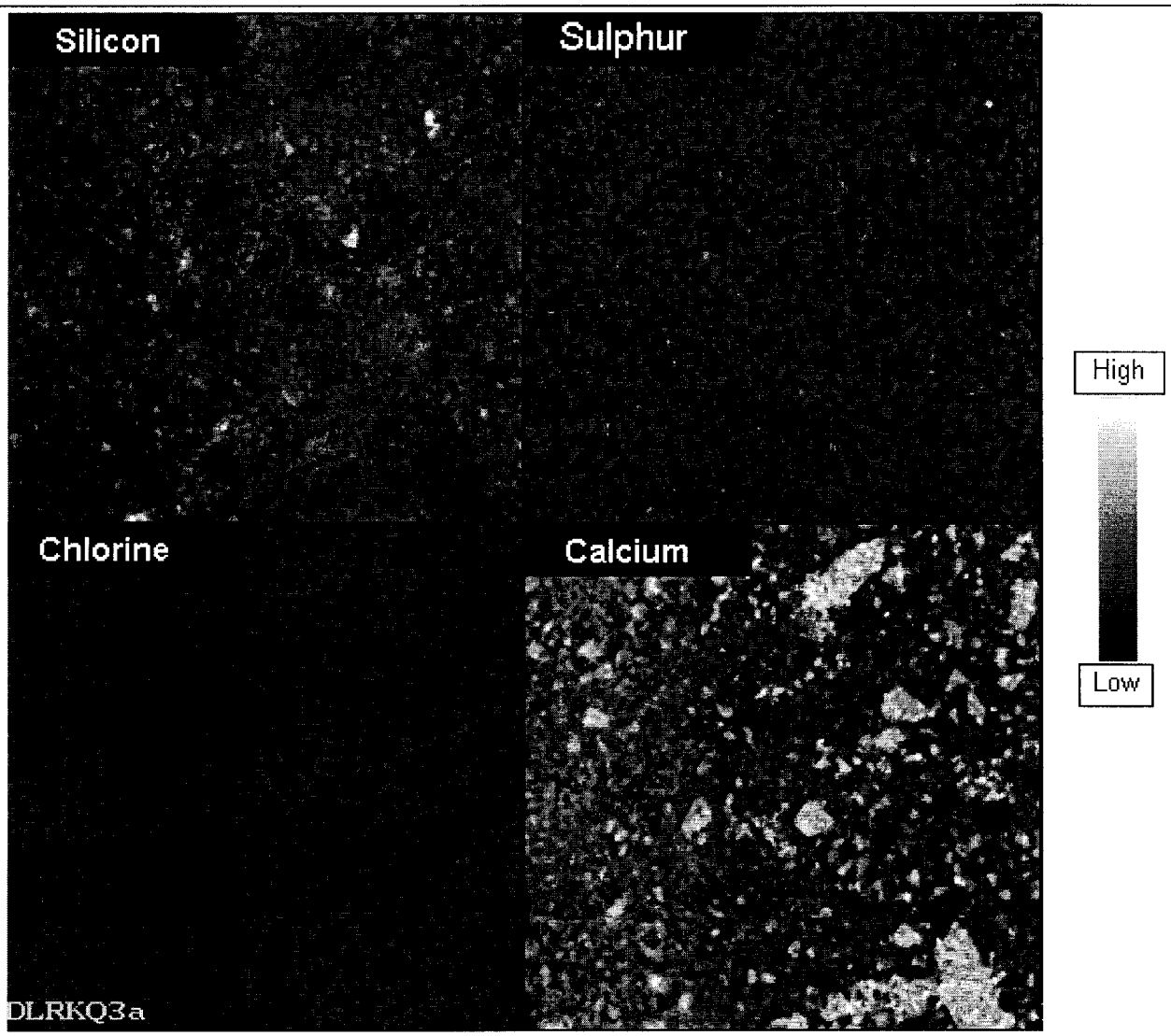

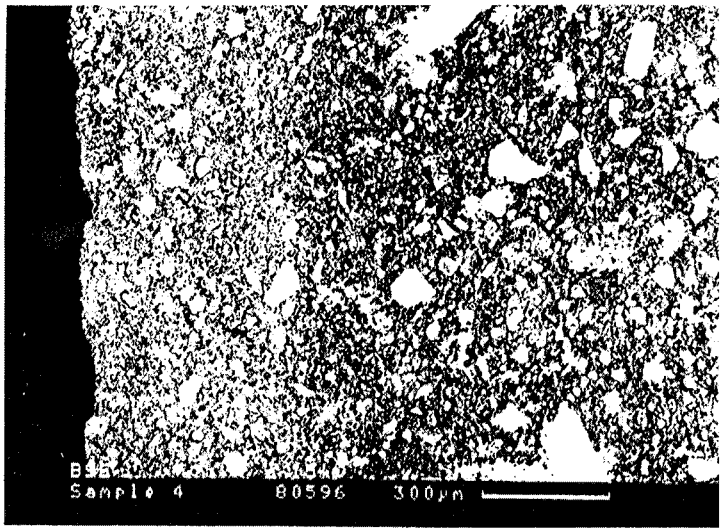

SECTION 7, ANNEX C. EXTENT OF REACTION OF OPC/ggbs AND OPC/pfa BLENDS.

The extent of reaction of selected 75 ggbs:25 OPC and 60 pfa:40 OPC blends was estimated by Dr Adrian Brough of Imperial College of Science, Technology and Medicine. The technique used in this study was based on that used by Luke and Glasser [1]. It was developed to determine the content of ggbs in blended OPC/ggbs cements and may not be suitable for OPC/pfa blends. In this technique the hydration products and unhydrated OPC are preferentially dissolved in an EDTA/triethanolamine/NaOH mixture. The remaining residue, consisting of unreacted ggbs, can then be weighed to determine the proportion of the ggbs that had not reacted. The samples studied were:

75 ggbs:25 OPC reacted with deionised water at 85°C for 20 months

60 pfa:40 OPC reacted with deionised water at 85°C for 20 months

The samples were dried at 105°C and ground prior to testing to allow adequate dispersal in the EDTA/triethanolamine/NaOH mixture. The samples were stirred for 1 hour using a magnetic stirrer and filtered through Whatman 540 paper. Small losses due to magnetic phases occurred. These should be similar in the dissolutions of hydrated and anhydrous materials. Some minor loss of fine material through the paper may also have occurred. The measured and calculated residues are given in table C1.

Table C1. Selective dissolution analysis

	Residue (wt%)		
		Calculated	
Material	measured	assuming no reaction of ggbs or pfa	assuming complete reaction of ggbs or pfa
OPC	< 1	-	-
pfa	88	100	0
ggbs	56	100	0
Insoluble control	98	100	0
75 ggbs:25 OPC	18	42	<1 (from OPC residue
60 pfa: 40 OPC	61	53	<1 (from OPC residue)

Note: The measured value of 1% for the OPC residue seems low and cannot be confirmed from the available results. The values given in the reference are between 3.5 and 5.6%.

The results suggest that about 60% of the ggbs had reacted after 20 months at 85°C. Less dissolution than expected occurred for the 60 pfa:40 OPC blend and it appears that the method is inappropriate for this system, possibly due to the precipitation of silica.

Reference

(1). K. Luke and F.P. Glasser. (1987) Cem. Conc. Res., **17**, 273.

APPENDIX 1. CONFIDENCE LIMITS AND ANALYTICAL ERRORS

Solid Phase

X-ray diffraction (XRD)

The Hägg Guinier camera is best for the detection of crystalline material. However detection limits vary with phase crystallinity, so highly crystalline materials can be detected at the ~ 2% level but poorly-crystalline materials have to be present at ≥ 10% before any diffractions are observed. For example, to estimate the amount of hydrogarnet in some samples, a film with pure hydrogarnet (C_3AH_6 cured in double distilled water at 55°C) was compared with the sample film. A semi-quantitative evaluation of the amount present was based on the following scale of visual comparisons:

Reflection intensity

very weak-	(VW)	< 5%
weak-	(W)	< 10%
medium:	(M)	< 20%
strong:	(S)	> 25%
very strong	(VS)	> 80%

Analytical Electron Microscopy (AEM)

The detection limit of the analytical electron microscope is controlled by the small volume that is analysed, the quantum efficiency of characteristic X-ray production and by the detector efficiency, which varies with atomic number, decreasing rapidly in efficiency below atomic number 12 magnesium. Suitable in-house calibrants were used.

Thermal analysis

Thermal analysis is reliable for determination of calcium hydroxide and calcite (± 5%), but less reliable for pseudo-boehmite as the sample immediately began to release loosely bound water, which overlaps water loss from C-S-H, in the temperature range up to 400°C. Mackenzie and Berggren [1] describe the decomposition of pseudo-boehmite as giving rise to a fairly broad endotherm at about 500-550°C (approximately the same temperature as for $Ca(OH)_2$, ~ 400-580°C) in addition to a fairly large sorbed moisture peak at 100-150°C. The reaction represented by the peak for pseudo-boehmite is:

$$2AlO(OH) \xrightarrow{\text{endothermic}} Al_2O_3 + H_2O$$

thus analysis for boehmite is complicated by (i) a broad range of temperatures of water loss and (ii) overlapping ranges of water loss temperatures, arising from other phases known to be present in mixtures with pseudo-boehmite. Figure A.1 illustrates characteristic ranges of thermal analysis activity. For these reasons, it was only practicable to determine accurately the content of unreacted pseudo-boehmite by thermal analysis in selected cases, where interfering phases were shown to be absent by XRD.

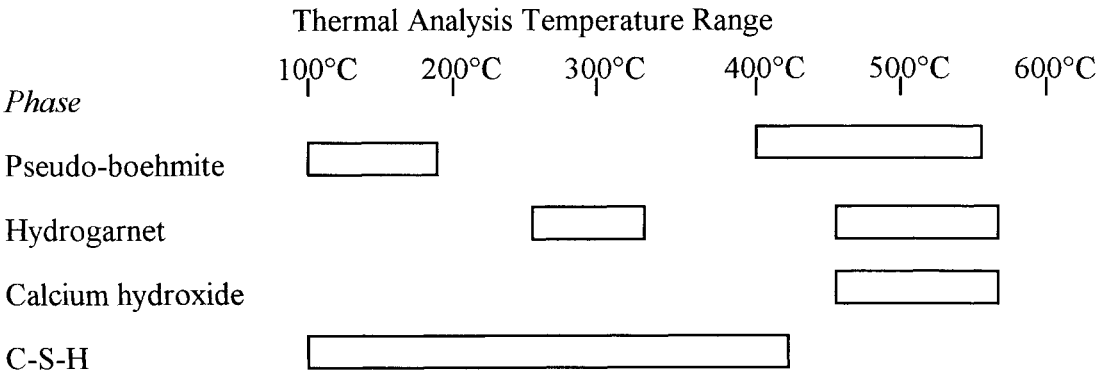

Figure A.1 **Bars showing weight loss temperatures in thermal analysis of individual hydrates [1]. It illustrates the difficulties of resolving mixtures of C-S-H and pseudo-boehmite.**

Nuclear Magnetic Resonance (NMR with MAS) for ^{29}Si

The confident limits for NMR have been given in connection with individual results, see section 4.1.1.

Aqueous Phase

Calcium:

Main sources of errors: Dilutions
Lowest detection limit: 0.5 ppm (~ 0.01mmol/l)
Analytical and instrumental confidence limit: **±5%**

Magnesium:

Main sources of errors: Dilutions
Lowest detection limit: 0.01 ppm (~ 0.0004 mmol/l)
Analytical and instrumental confidence limit: **±5%**

Sodium:

Main sources of errors: Standard range 0-10 ppm (3.0 M NaCl ~ 69000 ppm Na)
Dilutions above 2000 times, which is achieved by double dilutions.
Calibration standards.
Lowest detection limit: 1 ppm (~0.04 mmol/l)
Analytical and instrumental confidence limit: **±10%**

Aluminium:

Main sources of errors: Weighing chemicals
Adjusting reagent solutions to volume.
Dispensing the required volume of reagent solution.
Calibration standards.
Lowest detection limit: Reference claim ~ 0.01 ppm (~ 0.0004 mmol/l)
AU found 0.2 ppm (~0.007 mmol/l) lowest acceptable working limit.

Analytical and instrumental confidence limit: **±4% in DDW**
±5% in all the $MgSO_4$ solutions and 0.5M NaCl solutions.
±6% in > 1.0 M NaCl and in mixed NaCl and $MgSO_4$ solutions.

Silicate:
Main sources of errors: Same as for aluminium determination.
Lowest detection limit: Reference claim ~ 0.05 ppm (~ 0.002 mmol/l).
AU found 0.3 ppm (~0.01 mmol/l) more reasonable.
Analytical and instrumental confidence limit: **±5% in DDW**
±6% in all the $MgSO_4$ solutions and 0.5M NaCl solutions.
±7% in > 1.0 M NaCl and in mixed NaCl and $MgSO_4$ solutions.
This is for Si ~ 0.5 ppm, when Si concentration is lower the error margin in percent will probably be higher.

Chloride:
Main sources of errors: Standard range 2-10 ppm (3.0 M NaCl ~ 106500 ppm Cl)
Dilutions above 4000 times, which is achieved by double dilutions.
Accuracy of sample injections, instrumental response.
Lowest detection limit: 2 ppm (~0.06 mmol/l)
Analytical and instrumental confidence limit: ± **10%**

Sulfate:
Main sources of errors: Standard range 5-25 ppm
Accuracy of sample injections, instrumental response.
Lowest detection limit: 2 ppm (~ 0.02 mmol/l)
Analytical and instrumental confidence limit: ± **5%**

References

[1] R.C. Mackenzie and Berggren. (1970) 'Differential Thermal Analysis', Edited by R.C. Mackenzie. Volume 1. Academic Press, London.

APPENDIX 2. CALCULATION OF APPARENT UPTAKE OF SODIUM

The apparent uptake of sodium by calcium silicate hydrogel was measured and calculated as an uptake, using the following procedure:

Example

C-S-H 0.85 at 25°C
Initial NaCl = 520 mmol/l, 80 mls solution = 41.6 mmol
Finial NaCl = 489 mmol/l, 80 mls solution = 39.12 mmol
41.6-39.12 = 2.48 mmol NaCl has been removed from solution into solid.
Initial mass solid = 1.793 g , so the uptake per gram solid is 1.39 mmol Na^+
The mole weight of Na^+ is: 0.02299 g Na^+/mmol, thus 1.39 mmol/g x 0.002299 g/mmol x100% = 3.18% (apparent uptake).

APPENDIX 3. RESPIKING CALCULATIONS

Hydrogarnet

To calculate the maximum numbers of respikes required to convert hydrogarnet to the anticipated products, hydrotalcite and brucite, a mass balance calculation (using mmoles in solid) was carried out:

Assuming the following reaction:

$C_3AH_6 + MgSO_4 \rightarrow HT + CH \rightarrow HT + MH + CaSO_4 \cdot 2\ H_2O$

X = moles of magnesium required for reaction to go to completion

Y = moles of calcium present in the system

Z = moles of aluminium present in the system

In order for the reaction to go to completion, $X > (2Z + Y)$

The original mass of the Ca in solid = 15.87 mmol and Al in solid = 10.29 mmol, so the mmoles of magnesium must be $X > 2\ (10.29) + 15.87 \Rightarrow X > 36.45$. Thus the minimum number of mmoles $MgSO_4$ required for reaction to go to completion is 36.45.

Using a standard volume of 80 mls and with Mg = 0.05 M, the number of respikes must be 36.45/ 4 = 9 respikes.

Monosulfoaluminate

Assuming that AFm-SO_4 will convert to hydrotalcite and brucite, the maximum numbers of respikes was calculated. A mass balance (mmoles in solid) was carried out for monosulfo-aluminate.

Assuming the following reaction:

$AFm\text{-}SO_4 + MgSO_4 \rightarrow HT + CH \rightarrow HT + MH + CaSO_4 \cdot 2\ H_2O$

X = moles of magnesium required for reaction to go to completion

Y = moles of calcium present in the system

Z = moles of aluminium present in the system

In order for the reaction to go to completion: $X > (2Z + Y)$ assuming that HT corresponds to the atomic ratio M_4AH_{10}.

The original mass of the Ca in solid = 11.64 mmol and Al in solid = 5.82 mmol, so the number of moles of magnesium must be $X > 2\ (5.82) + 11.64 \Rightarrow X > 23.28$. Thus, the minimum numbers of mmoles $MgSO_4$ required for reaction to go to completion is 23.28.

Using a standard volume of 80 mls and Mg = 0.05 M number of respikes must be 23.28/ 4 = 6 respikes.

Ettringite

To calculate the maximum numbers of respikes, it was initially assumed that ettringite would form hydrotalcite, gypsum and brucite, a mass balance (using mmoles in solid) was carried out for ettringite:

Assuming the following reaction:
$C_6As_3H_{32} + MgSO_4 \rightarrow M_4AH_{10}$ (HT) + CH $\rightarrow$ HT + MH + $CaSO_4 \cdot 2\ H_2O$
X = moles of magnesium required for reaction to go to completion
Y = moles of calcium present in the system
Z = moles of aluminium present in the system

In order for the reaction to go to completion the following must be true: $X > 2Z + Y$
The original mass of the Ca in solid = 9.54 mmol and Al in solid = 3.18 mmol, so the mmoles of magnesium must be $X > 2\ (3.18) + 9.54 \Rightarrow X > 15.90$. Thus the minimum number of mmoles $MgSO_4$ required for reaction to go to completion is 15.90.

Using a standard volume of 80 mls and Mg = 0.05 M, the number of respikes must be 15.90/ 4 = 4 respikes.

Comment
The mass balance calculations worked remarkably well. Where divergences occurred, it was because:

- the reaction assumed for calculation was not strictly observed in practice
- no allowance was made for dissolution and mass wastage of solid between respikes
- in some instances, the kinetics were so sluggish that the leachant was renewed before its potential for reacting with solid had been exhausted.

APPENDIX 4. SEMIQUANTITAVE ESTIMATE OF BOEHMITE

To estimate the amount of boehmite in the samples, a film with unhydrated pseudo-boehmite was compared with the sample film. The evaluation of the quantitative amount was divided into following categories:

very weak:	VW	(less than approximately 5%)
weak:	W	(less than approximately 10%)
medium:	M	(less than approximately 20%)
strong:	S	(more than approximately 25%)
very strong	VS	(more than approximately 80%)

Furthermore thermal analysis was carried out on selected samples, see Appendix 1.

The sample was dried at 105°C until constant weight, then heated at a constant rate 15°C min^{-1}, and with N_2 flow rate of 15 ml min^{-1}.

Semiquantitative results are given in table 4.A.1 below.

Table 4.A.1 CASH samples with unreacted boehmite: semi-quantitative XRD results. The bold samples were also analysed by TA. Abbreviations: boe = boehmite

Sample	Curing environment	Temp. (°C)	Solid characterisation (XRD)
CASH 2	**H_2O**	**25**	**CSH I (M) / boe (M)**
CASH 2	**H_2O**	**85**	**CSH I (M) / boe(S) / C_3AH_6(VW)**
CASH 2	0.5 M NaCl + 0.02 M $MgSO_4$	25	AFt (S) / boe (M)
CASH 2	0.5 M NaCl + 0.02 M $MgSO_4$	85	boe(M) / gypsum (M)
CASH 2	**3.0 M NaCl + 0.02 M $MgSO_4$**	**25**	**boe (M)**
CASH 2	3.0 M NaCl + 0.02 M $MgSO_4$	85	CSH I(VW) / boe(M) / AFm-Cl-SO_4(M)
CASH 4	**H_2O**	**25**	**CSH I (M) / boe (M)**
CASH 4	H_2O	85	boe(M) / C_3AH_6(M)
CASH 4	0.5 M NaCl + 0.02 M $MgSO_4$	25	CSH I(M) / boe (M)
CASH 4	0.5 M NaCl + 0.02 M $MgSO_4$	85	CSH I (M) / boe (M)
CASH 4	3.0 M NaCl + 0.02 M $MgSO_4$	85	CSH I (M) / boe (M)
CASH 5	**H_2O**	**25**	**CSH I (M) / boe (M)**
CASH 5	H_2O	85	boe(M)/ C_3AH_6(M)
CASH 5	**0.5 M NaCl + 0.02 M $MgSO_4$**	**25**	**boe (S)**
CASH 5	3.0 M NaCl + 0.02 M $MgSO_4$	25	boe (M)
CASH 5	3.0 M NaCl + 0.02 M $MgSO_4$	85	CSH I (W) / boe (M)
CASH 6	H_2O	25	CSH I(M) / C_3AH_6(VW) / C_2ASH_8(S)
CASH 6	H_2O	85	boe(M) / C_3AH_6(M)
CASH 6	0.5 M NaCl + 0.02 M $MgSO_4$	25	CH (M) / C_3ASH_4(S) / boe (M) / AFt(S)

The original amounts of pure boehmite in samples are shown in table A.2:

Table 4.A.2 Original amounts of boehmite in the CASH samples.

Sample	Original amount of AlO(OH) in wt%
CASH 1	5.5
CASH 2	39.2
CASH 3	11.9
CASH 4	23.1
CASH 5	34.1
CASH 6	31.1

In CASH 1 and 3 samples, boehmite is never observed, which can be due to (i) the amount of boehmite has to be above ~10 wt% to be detected by XRD or (ii) boehmite has reacted, forming another alumina-phase (AFt/AFm-SO_4/C_3AH_6).

The bold samples in table A.1 were chosen to be analysed by TA and the results are shown in the following table.

Table 4.A.3 Results of thermal analysis of the samples which are marked bold in table 4.A.1. The samples which are marked bold in this table have been analysed by AEM.

Sample	Curing environment	Temperature	Original wt% boehmite	wt% boehmite in cured sample (± 3%)	% boehmite reacted
CASH 2	H_2O	25°C	33.5	34	none
CASH 2	**H_2O**	**85°C**	**33.5**	**22**	**11.5**
CASH 2	3.0 M NaCl + 0.02 M $MgSO_4$	25°C	33.5	25	8.5
CASH 4	H_2O	25°C	19.7	25	none
CASH 5	H_2O	25°C	29	33	4
CASH 5	**0.5 M NaCl + 0.02 M $MgSO_4$**	**25°C**	**29**	**21**	**8**

The samples marked in bold have been analysed with AEM. Results of these analysis is as follows: in CASH 2 areas with C-S-H containing Al, some with low Al-content and some with high content. In CASH 5 only C-S-H with low Al-content was seen. Pure AlO(OH) phases were not observed in any of the samples, but this does not imply that these phases were absent.

APPENDIX 5. DATA RECORDS

Introduction

Section A records the cements 3 Database. It comprises SIT - compatible data in PHREEQE format taken from the existing Aberdeen database and from The Commission of the European Communities CHEMVAL (Version 6) database.

Section B records the molar volume data collected in this project - Bulk density measurements were taken from the serial publications of The Joint Committee on Powder Diffraction Standards (Swathmore PA, USA) and compared with data from :

R.C. Weast (1987). "A Handbook of Physics and Chemistry" 67th edition. CRC Press, Boca Raton, Florida.
R.S. Carmichael (1989). "A Practical Handbook of the Physical Properties of Rocks and Minerals" CRC Press, Boca Raton, Florida.

Section C records the Ion Interaction Coefficients Database, used in SIT calculation.

Appendix 5a. Cement 3 Database

5 47	NUMBER	SPECIES	1	2	3	4	5
	14 15	Cl-	H+	e-	H2O	Ca+2	Mg+2
	16 17	CO3-2	0.120	0.000	0.000	0.140	0.190
	19 20	SO4-2	0.000	0.000	0.000	0.000 -	0.000 -
		NO3-	0.000	0.000	0.000	0.610	0.390
		PO4-3	0.070	0.000	0.000	0.020	0.170
		F-	0.000	0.000	0.000	0.000	0.000
			0.000	0.000	0.000	0.000	0.000

6	7	8	9	10	11	12	13
Na+	K+	Fe+2	Mn+2	Al+3	Ba+2	Sr+2	H4SiO4
0.030 -	0.000	0.140	0.130	0.330	0.070	0.130	0.000
0.050 -	0.020 -	0.000	0.000 -	0.000 -	0.000	0.000	0.000
0.120 -	0.060 -	0.000	0.480	0.540	0.000 -	0.000 -	0.000
0.040 -	0.110 -	0.000	0.000	0.000	0.280	0.060	0.000
0.250	0.090	0.000	0.000	0.000	0.000	0.000	0.000
0.020	0.030	0.000	0.000	0.000	0.000	0.000	0.000

18	21	23	24	25	26	27	30
H3BO3	Li+	U+4	Np+4	Pu+4	Am+3	Cm+3	Cs+ -0.050
0.000	0.100	0.000	0.000	0.000	0.280	0.000	0.000 -
0.000	0.000 -	0.000	0.000	0.000	0.000	0.000	0.130 -
0.000	0.030	0.000	0.000	0.000	0.000	0.000	0.160
0.000	0.080	0.000	0.000	0.000	0.200	0.000	0.000
0.000	0.000	0.000	0.000	0.000	0.000	0.000	0.060
0.000	0.000	0.000	0.000	0.000	0.000	0.000	

31	32	34	35	49	203	208	212
Pb+2	Ra+2	Th+4	Pa+4	Ni+2	Fe+3	FeOH+2	Fe2OH2+4
0.080	0.000	0.250	0.000	0.170	0.000	0.000	0.000
0.000	0.000	0.000	0.000	0.000 -	0.000	0.000	0.000
0.000 -	0.000	0.000	0.000	0.510	0.000	0.000	0.000
0.200	0.000	0.110	0.000	0.000	0.420	0.000	0.000
0.000	0.000	0.000	0.000	0.000	0.000	0.000	0.000
0.000	0.000	0.000	0.000	0.000	0.000	0.000	0.000

294	299	366	393	394	414	416	427
AlOH+2	Al3OH4+	NH4+ -	UO2+	UO2+2	UCl+3	UO2Cl+	USO4+2
0.090	5 0.660	0.010	0.000	0.210	0.000	0.000	0.000
0.000	0.000	0.000 -	0.000	0.000 -	0.000	0.000	0.000
0.000	0.000	0.230 -	0.000	0.610	0.000	0.000	0.000
0.000	0.000	0.060	0.000	0.240	0.000	0.000	0.000
0.000	0.000	0.000	0.000	0.000	0.000	0.000	0.000
0.000	0.000	0.000	0.000	0.000	0.000	0.000	0.000

432	433	436	450	451	452	454	462
UNO3+3	UNO32+2	UO2NO3	UF+3	UF2+2	UF3+	UO2F+	UO2Br+
0.000	0.000	+ 0.000	0.000	0.000	0.310	0.040	0.000
0.000	0.000	0.000	0.000	0.000	0.000	0.000	0.000
0.000	0.000	0.000	0.000	0.000	0.000	0.000	0.000
0.000	0.000	0.000	0.000	0.000	0.000	0.000	0.000
0.000	0.000	0.000	0.000	0.000	0.000	0.000	0.000
0.000	0.000	0.000	0.000	0.000	0.000	0.000	0.000

493	575
NpO2+	PuO2+
0.000	0.000
0.000	0.000
0.000	0.000
0.000	0.000
0.000	0.000
0.000	0.000

NUMBER	SPECIES	1	2	3			
22 28	Br-	H+	e- 0.000	H2O			
29 45	TcO4-	0.150	0.000	0.000			
46 48	I-	0.000	0.000	0.000			
	OAC-	0.000	0.000	0.000			
	CIT-3	0.000	0.000	0.000			
	EDTA-4	0.000	0.000	0.000			
		0.000		0.000			

4	5	6	7	8	9	10	11
Ca+2	Mg+2	Na+	K+	Fe+2	Mn+2	Al+3	Ba+2
0.180	0.260	0.050	0.010	0.000	0.000	0.000	0.130
0.000	0.000	0.010	0.000	0.000	0.000	0.000	0.000
0.270	0.320	0.080	0.020	0.000	0.000	0.000	0.230
0.000	0.000	0.080	0.090	0.000	0.000	0.000	0.000
0.000	0.000	0.000	0.000	0.000	0.000	0.000	0.000
0.000	0.000	0.000	0.000	0.000	0.000	0.000	0.000

12	13	18	21	23	24	25	26
Sr+2	H4SiO4	H3BO3	Li+	U+4	Np+4	Pu+4	Am+3
0.180	0.000	0.000	0.130	0.000	0.000	0.000	0.000
0.000	0.000	0.000	0.000	0.000	0.000	0.000	0.000
0.250	0.000	0.000	0.160	0.000	0.000	0.000	0.000
0.000	0.000	0.000	0.050	0.000	0.000	0.000	0.000
0.000	0.000	0.000	0.000	0.000	0.000	0.000	0.000
0.000	0.000	0.000	0.000	0.000	0.000	0.000	0.000

27	30	31	32	34	35	49	203
Cm+3	Cs+ -	Pb+2	Ra+2	Th+4	Pa+4	Ni+2	Fe+3
0.000	0.040	0.000	0.000	0.000	0.000	0.000	0.000
0.000	0.000 -	0.000	0.000	0.000	0.000	0.000	0.000
0.000	0.060	0.000	0.000	0.000	0.000	0.000	0.000
0.000	0.110	0.000	0.000	0.000	0.000	0.000	0.000
0.000	0.000	0.000	0.000	0.000	0.000	0.000	0.000
0.000	0.000	0.000	0.000	0.000	0.000	0.000	0.000

208	212	294	299	366	393	394	414
FeOH+2	Fe2OH2+	AlOH+2	Al3OH4+5	NH4+	UO2+	UO2+2	UCl+3
0.000	4 0.000	0.000	0.000	0.000	0.000	0.000	0.000
0.000	0.000	0.000	0.000	0.000	0.000	0.000	0.000
0.000	0.000	0.000	0.000	0.000	0.000	0.000	0.000
0.000	0.000	0.000	0.000	0.000	0.000	0.000	0.000
0.000	0.000	0.000	0.000	0.000	0.000	0.000	0.000
0.000	0.000	0.000	0.000	0.000	0.000	0.000	0.000

416	427	432	433	436	450	451	452
UO2Cl+	USO4+2	UNO3+3	UNO32+2	UO2NO3	UF+3	UF2+2	UF3+
0.000	0.000	0.000	0.000	+ 0.000	0.000	0.000	0.000
0.000	0.000	0.000	0.000	0.000	0.000	0.000	0.000
0.000	0.000	0.000	0.000	0.000	0.000	0.000	0.000
0.000	0.000	0.000	0.000	0.000	0.000	0.000	0.000
0.000	0.000	0.000	0.000	0.000	0.000	0.000	0.000
0.000	0.000	0.000	0.000	0.000	0.000	0.000	0.000

454	462	493	575				
UO2F+	UO2Br+	NpO2+	PuO2+				
0.000	0.000	0.000	0.000				
0.000	0.000	0.000	0.000				
0.000	0.000	0.000	0.000				
0.000	0.000	0.000	0.000				
0.000	0.000	0.000	0.000				
0.000	0.000	0.000	0.000				

NUMBER		1					
102 347	SPECIES	H+					
348 350	OH-	0.000					
351 363	H3SiO4-	0.000					
	H2SiO4-2	0.000					
	ClO4-	0.000					
	HCO3-	0.000					
	NO2-	0.000					
2	3	4	5	6	7	8	9
e- 0.000	H2O	Ca+2	Mg+2	Na+	K+	Fe+2	Mn+2
0.000	0.000	0.000	0.000	0.400 -	0.900	0.000	0.000
0.000	0.000	0.000	0.000	0.080 -	0.000	0.000	0.000
0.000	0.000	0.000	0.000	0.010	0.000 -	0.000	0.000
0.000	0.000	0.270	0.330	0.010 -	0.060	0.000	0.000
0.000	0.000	0.000	0.000	0.030	0.000 -	0.000	0.000
	0.000	0.000	0.000	0.000	0.040	0.000	0.000
10	11	12	13	18	21	23	24
Al+3	Ba+2	Sr+2	H4SiO4	H3BO3	Li+ -	U+4	Np+4
0.000	0.000	0.000	0.000	0.000	0.020	0.000	0.000
0.000	0.000	0.000	0.000	0.000	0.000	0.000	0.000
0.000	0.000	0.000	0.000	0.000	0.000	0.000	0.000
0.000	0.150	0.230	0.000	0.000	0.150	0.800	0.820
0.000	0.000	0.000	0.000	0.000	0.000	0.000	0.000
0.000	0.000	0.000	0.000	0.000	0.000	0.000	0.000
25	26	27	30	31	32	34	35
Pu+4	Am+3	Cm+3	Cs+	Pb+2	Ra+2	Th+4	Pa+4
0.000	0.000	0.000	0.000	0.000	0.000	0.000	0.000
0.000	0.000	0.000	0.000	0.000	0.000	0.000	0.000
0.000	0.000	0.000	0.000	0.000	0.000	0.000	0.000
1.030	0.000	0.000	0.000	0.150	0.000	0.000	0.000
0.000	0.000	0.000	0.000 -	0.000	0.000	0.000	0.000
0.000	0.000	0.000	0.040	0.000	0.000	0.000	0.000
49	203	208	212	294	299	366	393
Ni+2	Fe+3	FeOH+2	Fe2OH2+4	AlOH+2	Al3OH4+5	NH4+	UO2+
0.000	0.000	0.000	0.000	0.000	0.000	0.000	0.000
0.000	0.000	0.000	0.000	0.000	0.000	0.000	0.000
0.000	0.000	0.000	0.000	0.000	0.000	0.000 -	0.000
0.000	0.560	0.380	0.820	0.310	1.300	0.080	0.260
0.000	0.000	0.000	0.000	0.000	0.000	0.000	0.000
0.000	0.000	0.000	0.000	0.000	0.000	0.000	0.000
394	414	416	427	432	433	436	450
UO2+2	UCl+3	UO2Cl+	USO4+2	UNO3+3	UNO32+2	UO2NO3+	UF+3
0.000	0.000	0.000	0.000	0.000	0.000	0.000	0.000
0.000	0.000	0.000	0.000	0.000	0.000	0.000	0.000
0.000	0.000	0.000	0.000	0.000	0.000	0.000	0.000
0.460	0.630	0.310	0.000	0.660	0.530	0.310	0.540
0.000	0.000	0.000	0.000	0.000	0.000	0.000	0.000
0.000	0.000	0.000	0.000	0.000	0.000	0.000	0.000
451	452	454	462	493	575		
UF2+2	UF3+	UO2F+	UO2Br+	NpO2+	PuO2+		
0.000	0.000	0.000	0.000	0.000	0.000		
0.000	0.000	0.000	0.000	0.000	0.000		
0.000	0.000	0.000	0.000	0.000	0.000		
0.300	0.310	0.290	0.240	0.250	0.170		
0.000	0.000	0.000	0.000	0.000	0.000		
0.000	0.000	0.000	0.000	0.000	0.000		

NUMBER 377 378 389 422 423 425							
 SPECIES HPO4-2 H2PO4- HF2- UO2CO32-2 UO2CO33-4 UO23CO36	1 H+ 0.000 0.000 0.000 0.000 0.000 0.000	2 e- 0.000 0.000 0.000 0.000 0.000 0.000	3 H2O 0.000 0.000 0.000 0.000 0.000 0.000	4 Ca+2 0.000 0.000 0.000 0.000 0.000 0.000	5 Mg+2 0.000 0.000 0.000 0.000 0.000 0.000	6 Na+ - 0.150 - 0.080 - 0.110 0.060 0.090 0.550	7 K+ -0.100 -0.140 0.000 0.000 0.000 0.000
8 Fe+2 0.000 0.000 0.000 0.000 0.000 0.000	9 Mn+2 0.000 0.000 0.000 0.000 0.000 0.000	10 Al+3 0.000 0.000 0.000 0.000 0.000 0.000	11 Ba+2 0.000 0.000 0.000 0.000 0.000 0.000	12 Sr+2 0.000 0.000 0.000 0.000 0.000 0.000	13 H4SiO4 0.000 0.000 0.000 0.000 0.000 0.000	18 H3BO3 0.000 0.000 0.000 0.000 0.000 0.000	21 Li+ 0.000 0.000 0.000 0.000 0.000 0.000
23 U+4 0.000 0.000 0.000 0.000 0.000 0.000	24 Np+4 0.000 0.000 0.000 0.000 0.000 0.000	25 Pu+4 0.000 0.000 0.000 0.000 0.000 0.000	26 Am+3 0.000 0.000 0.000 0.000 0.000 0.000	27 Cm+3 0.000 0.000 0.000 0.000 0.000 0.000	30 Cs+ 0.000 0.000 0.000 0.000 0.000 0.000	31 Pb+2 0.000 0.000 0.000 0.000 0.000 0.000	32 Ra+2 0.000 0.000 0.000 0.000 0.000 0.000
34 Th+4 0.000 0.000 0.000 0.000 0.000 0.000	35 Pa+4 0.000 0.000 0.000 0.000 0.000 0.000	49 Ni+2 0.000 0.000 0.000 0.000 0.000 0.000	203 Fe+3 0.000 0.000 0.000 0.000 0.000 0.000	208 FeOH+2 0.000 0.000 0.000 0.000 0.000 0.000	212 Fe2OH2+4 0.000 0.000 0.000 0.000 0.000 0.000	294 AlOH+2 0.000 0.000 0.000 0.000 0.000 0.000	299 Al3OH4+5 0.000 0.000 0.000 0.000 0.000 0.000
366 NH4+ 0.000 0.000 0.000 0.000 0.000 0.000	393 UO2+ 0.000 0.000 0.000 0.000 0.000 0.000	394 UO2+2 0.000 0.000 0.000 0.000 0.000 0.000	414 UCl+3 0.000 0.000 0.000 0.000 0.000 0.000	416 UO2Cl+ 0.000 0.000 0.000 0.000 0.000 0.000	427 USO4+2 0.000 0.000 0.000 0.000 0.000 0.000	432 UNO3+3 0.000 0.000 0.000 0.000 0.000 0.000	433 UNO32+2 0.000 0.000 0.000 0.000 0.000 0.000
436 UO2NO3+ 0.000 0.000 0.000 0.000 0.000 0.000	450 UF+3 0.000 0.000 0.000 0.000 0.000 0.000	451 UF2+2 0.000 0.000 0.000 0.000 0.000 0.000	452 UF3+ 0.000 0.000 0.000 0.000 0.000 0.000	454 UO2F+ 0.000 0.000 0.000 0.000 0.000 0.000	462 UO2Br+ 0.000 0.000 0.000 0.000 0.000 0.000	493 NpO2+ 0.000 0.000 0.000 0.000 0.000 0.000	575 PuO2+ 0.000 0.000 0.000 0.000 0.000 0.000

	NUMBER	SPECIES	1	2	3	4	5
	430	UO2SO42-	H+	e-	H2O	Ca+2	Mg+2
	460	2	0.000	0.000	0.000	0.000	0.000
	461	UO2F3-	0.000	0.000	0.000	0.000	0.000
	772	UO2F4-2	0.000	0.000	0.000	0.000	0.000
	969	IO3-	0.000	0.000	0.000	0.000	0.000
	970	HAsO4-2	0.000	0.000	0.000	0.000	0.000
		H2AsO4-	0.000	0.000	0.000	0.000	0.000
6	7	8	9	10	11	12	13
Na+	K+	Fe+2	Mn+2	Al+3	Ba+2	Sr+2	H4SiO4
0.550	0.000	0.000	0.000	0.000	0.000	0.000	0.000
0.000 -	0.000	0.000	0.000	0.000	0.000	0.000	0.000
0.012 -	0.000	0.000	0.000	0.000	0.000	0.000	0.000
0.060 -	0.000 -	0.000	0.000	0.000	0.000	0.000	0.000
0.210 -	0.020 -	0.000	0.000	0.000	0.000	0.000	0.000
0.080	0.120	0.000	0.000	0.000	0.000	0.000	0.000
18	21	23	24	25	26	27	30
H3BO3	Li+	U+4	Np+4	Pu+4	Am+3	Cm+3	Cs+
0.000	0.000	0.000	0.000	0.000	0.000	0.000	0.000
0.000	0.000	0.000	0.000	0.000	0.000	0.000	0.000
0.000	0.000	0.000	0.000	0.000	0.000	0.000	0.000
0.000	0.000	0.000	0.000	0.000	0.000	0.000	0.000
0.000	0.000	0.000	0.000	0.000	0.000	0.000	0.000
0.000	0.000	0.000	0.000	0.000	0.000	0.000	0.000
31	32	34	35	49	203	208	212
Pb+2	Ra+2	Th+4	Pa+4	Ni+2	Fe+3	FeOH+2	Fe2OH2+4
0.000	0.000	0.000	0.000	0.000	0.000	0.000	0.000
0.000	0.000	0.000	0.000	0.000	0.000	0.000	0.000
0.000	0.000	0.000	0.000	0.000	0.000	0.000	0.000
0.000	0.000	0.000	0.000	0.000	0.000	0.000	0.000
0.000	0.000	0.000	0.000	0.000	0.000	0.000	0.000
0.000	0.000	0.000	0.000	0.000	0.000	0.000	0.000
294	299	366	393	394	414	416	427
AlOH+2	Al3OH4+5	NH4+	UO2+	UO2+2	UCl+3	UO2Cl+	USO4+2
0.000	0.000	0.000	0.000	0.000	0.000	0.000	0.000
0.000	0.000	0.000	0.000	0.000	0.000	0.000	0.000
0.000	0.000	0.000	0.000	0.000	0.000	0.000	0.000
0.000	0.000	0.000	0.000	0.000	0.000	0.000	0.000
0.000	0.000	0.000	0.000	0.000	0.000	0.000	0.000
0.000	0.000	0.000	0.000	0.000	0.000	0.000	0.000
432	433	436	450	451	452	454	462
UNO3+3	UNO32+2	UO2NO3+	UF+3	UF2+2	UF3+	UO2F+	UO2Br+
0.000	0.000	0.000	0.000	0.000	0.000	0.000	0.000
0.000	0.000	0.000	0.000	0.000	0.000	0.000	0.000
0.000	0.000	0.000	0.000	0.000	0.000	0.000	0.000
0.000	0.000	0.000	0.000	0.000	0.000	0.000	0.000
0.000	0.000	0.000	0.000	0.000	0.000	0.000	0.000
0.000	0.000	0.000	0.000	0.000	0.000	0.000	0.000
493	575						
NpO2+	PuO2+						
0.000	0.000						
0.000	0.000						
0.000	0.000						
0.000	0.000						
0.000	0.000						
0.000	0.000						

Appendix 5b. Density and Molar Volume Data

Mineral Name	Description	Formula 1	Bulk Density	Formula	Molar volume cm^3/mol	
			$kg\ dm^{-3}$	mass	RBB *	Calculated
Tobermorite	$C_5S_6H_{5-9}$	$Ca_5(Si_6O_{18}H_2).4 - 8H_2O$				
Tobermorite 14A	$C_5S_6H_9$	$Ca_5(Si_6O_{18}H_2).9H_2O$	2.224	821		369
Tobermorite 11A	$C_5S_6H_7$	$Ca_5(Si_6O_{18}H_2).7H_2O$	2.44	785		322
Tobermorite 9A	$C_5S_6H_5$	$Ca_5(Si_6O_{18}H_2).5H_2O$	2.656	749		282
Jennite	$C_9S_6H_{11}$	$Ca_9(Si_6O_{18}H_2)(OH)_8.6H_2O$	2.332	984		422
Xonotlite	C_6S_6H	$Ca_6(Si_6O_{17})(OH)_2$	2.7	715		265
Afwillite	$C_3S_2H_3$	$Ca_3(SiO_4)_2.2H_2O$	2.63	341		130
Halloysite	ASH_2	$Al_2Si_2O_6(OH)_2.3H_2O$		258		
Hydrogrossular	C_3AH_6	HG000, $Ca_3[Al(OH)_6]_2$	2.52	378		150
		HG010	2.53			
		HG033	2.556			
		HG063	2.588			
		HG067	2.592			
		HG072	2.597			
		HG100	2.628			
		HG110	2.638			
		HG133	2.663			
		HG137	2.667			
		HG143	2.674			
	$C_3AS_{0.5}H_5$	HG167 }	2.699	390		144
		HG183 } Miscibility gap	2.717			
		HG200 } 25 °C - 95 °C	2.735			
		HG227 }	2.764			
		HG233	2.771			
		HG253	2.785			
		HG287	2.828			
		HG292	2.834			
		HG300	2.842			
		HG317	2.86			
Katoite	C_3ASH_4	HG367,$Ca_3Al_2SiO_8.4H_2O$	2.878	402		140
		HG417	2.968			

Hydrogarnet solid solution series nomenclature:

HG 167 = 16.7% grossular

RBB* - R.A. Robie, P.M. Becka, K.M. Beardsley. (1986) 'X-ray Crystallographic Data, Molar Volumes and Densities of Minerals, and Related Substances', from Weast, 'Handbook of Chemistry, and Physics 67th Edition'. CRC Press, Boca Raton, Florida

Hibschite, Plaziolite	$C_3AS_2H_2$	HG667	3.237			
Grossular	C_3AS_3	$Ca_3Al_2Si_3O_5$	3.595	338	125.3	94
Gehlenite hydrate, Stratlingite	C_2ASH_8	$2CaO.Al_2O_3.SiO_2.8H_2O$	1.936	418		216
	C_4AH_7	$4CaO.Al_2O_3.CaCl_2.4H_2O$	2.28	509		223
	C_4AH_{11}	$4CaO.Al_2O_3.CaCl_2.8H_2O$	2.117	581		274
AFm -OH, hydroxy AFm	C_4AH_{13}	$4CaO.Al_2O_3.CaCl_2.10H_2O$	2.033	617		303
	C_4AH_{19}	$4CaO.Al_2O_3.CaCl_2.16H_2O$	1.8015	726		403
	C_2AH_8	$2CaO.Al_2O_3.CaCl_2.5H_2O$	2.12	415		196
	CAH_{10}	$CaO.Al_2O_3.CaCl_2.9H_2O$	1.83	431		236
Quartz		SiO_2	2.65	60.1	22.688	22.7
SiO2-amorph.		SiO_2	2.2	60.1		27.3
Chalcedony		SiO_2	2.6	60.1		23.1
NaOH		NaOH	2.13	40		18.7
KOH		KOH	2.044	56.1		27.4
Diaspore		alpha - AlO(OH)	3.03	43	17.6	14.19
Boehmite		gamma - AlO(OH)	3.4	43	19.535	12.64
Gibbsite		$Al(OH)_3$	2.3	78	31.956	33.9
Portlandite		$Ca(OH)_2$	2.25	74.1	33.056	32.9
Brucite		$Mg(OH)_2$	2.38	58.3	24.63	24.5
Hydrotalcite	M_4AH_{10}	$Mg_4Al_2O_7.10H_2O$	1.95	443		
Sepiolite	Meerschaum	$Mg_4(Si_6O_{15})(OH)_2.6H_2O$	2	648		
Talc		$Mg_3(Si_4O_{10})(OH)_2$	2.73	379	136.25	139
Epsomite		$MgSO_4.7H_2O$	1.68	246	146.83	146.4
		$MgSO_4.6H_2O$		228	132.58	
Leonhardite		$MgSO_4.4H_2O$	2.695	192		71.2
Kieserite		$MgSO_4.H_2O$	2.53	138		54.5
		$MgSO_4$	2.66	120		45.1
Polyhalite		$MgCa_2K_2(SO_4)_4.2H_2O$	2.778	603		217.1
Ettringite - AFt SO_4	$C_6A\underline{S}_3H_{32}$	$[Ca_3Al(OH)_6.12H_2O]_2.(SO_4)_3.2H_2O$	1.775	1255		707
Monosulphate AFm -SO_4	$C_4A\underline{S}H_{18}$	$Ca_2[Al(OH)_6]_2.(OH)_2].12H_2O$	1.75	310		177
Gypsum	$C\underline{S}H_2$	$CaSO_4.2H_2O$	2.32	172	74.69	74.1

Hemihydrite		$(CaSO_4)_2.H_2O$		290		
Anhydrite	Cs	$CaSO_4$	2.95	136	45.94	46.1
Syngenite	Kaluszite	$CaK_2(SO_4)2.H_2O$	2.6	328	127.76	126.1
Arcanite		K_2SO_4	2.662	174	65.5	65.4
Thenardite		Na_2SO_4	2.67	142	53.33	53.2
Mirabilite	Glauber's salt	$Na_2SO_4.10H_2O$	1.474	322	219.8	218
Glauberite		$Na_2Ca(SO_4)_2$	2.81	278		102
Kalinite		$KAl(SO_4)_2.12H_2O$	1.75	474		271
Alunite		$KAl_3(SO_4)_2(OH)_6$	2.7	414	146.8	153
Natroalunite		$NaAl_3(SO_4)_2(OH)_6$		398		
		$AlOHSO_4$		140		
		$Al_2(SO_4)_3$	2.17	342		158
		$Al_2(SO_4)_3.6H_2O$		450		
Alunogene		$Al_2(SO_4)_3.16H_2O$		630		
		$Al_4SO_4(OH)_{10}$		374		
		$Na_2SO_4.10H_2O$		322		
Pentasalt		$Ca_5K_2(SO_4)_6.H_2O$		873		
Kuzel's salt AFm-Cl-SO_4	$C_6A_2C\underline{s}CaCl_2.24.H_2O$	$[4(Ca_2Al(OH)_6)SO_4.Cl_2].12H_2O$		592		
Trichloroaluminate AFt -Cl	Chloroettringite	$3CaO.Al_2O_3.3CaCl_2.xH_2O$		1221		
Monochloroaluminate AFm -Cl	Friedel's salt	$3CaO.Al_2O_3.CaCl_2.10H_2O$	1.892	561		297
Hemichloroaluminate AFm -0.5Cl		$3CaO.Al_2O_3.CaOHCl.12H_2O$		579		
Calcium oxychloride $(3,1,15_{Cl})$		$3CaO.CaCl_2.12H_2O$		495		
		$CaCl_2.6H_2O$		219		
		$CaCl_2.4H_2O$		183		
		$CaCl_2.2H_2O$		147		
Hydrophyllite		$CaCl_2$		111		
Bischofite		$MgCl_2.6H_2O$	1.86	203		109
		$MgCl_2.4H_2O$		167		
		$MgCl_2.2H_2O$		131		
Chloromagnesite		$MgCl_2$	2.327	95.2	40.81	40.9
Halite		NaCl	2.17	58.4	27.15	26.9
Sylvite		KCl	1.99	74.6	37.524	37.5

Tricarboaluminate, AFt-CO_3		$3CaO.Al_2O_3.3CaCO_3.27H_2O$		1057		
Monocarboaluminate, AFm-CO_3	$C_4A\underline{c}H_{11}$	$3CaO.Al_2O_3.CaCO_3.10H_2O$	2.14	550		257
Hemicarboaluminate, AFm-0.5CO_3	$C_4A\underline{c}_{(0.5)}H_{12}$	$3CaO.Al_2O_3.(CaCO_3)_{0.5}.10H_2O$		546		
Calcite		$CaCO_3$	2.175	100.1	36.934	46
Aragonite		$CaCO_3$	2.94	100.1	34.15	34
Dolomite		$Ca.Mg(CO_3)_2$	2.869	184	64.341	64
Lansfordite		$MgCO_3.5H_2O$	1.73	174		100.6
Nesquehonite		$MgCO_3.3H_2O$	1.85	138		74.6
Magnesite		$MgCO_3$	3.081	84.3	28.018	27.3
Artinite		$MgCO_3.Mg(OH)_2.3H_2O$	2.02	197		97.5
Hydramagnesite		$Mg_4(CO_3)_3.5H_2O$	2.198	367		167
Hydromagnesite		$Mg_5(CO_3)_4.6H_2O$	2.165	470		217
Huntite		$CaMg_3(CO_3)_4$	2.696	353	122.58	131
Natronite		$Na_2CO_3.10H_2O$	1.45	286		197
Nahcotite		$NaHCO_3$	2.159	84		38.9
Thermonatron		$Na_2CO_3.H_2O$	2.253	124		55
Gaylussite		$Na_2Ca(CO_3)_2.5H_2O$	1.99	296		148.7
Pirsonite		$Na_2Ca(CO_3)_2.2H_2O$		242		
Thaumasite	AFt-CO_3-SO_4	$Ca_3[Si(OH)_6).12H_2O](CO_3)(SO_4)$		607		
Ca zeolite P		$CaAl_2Si_{2.6}O_{9.4}.6H_2O$		426		
Na zeolite P		$Na_2Al_2Si_{2.6}O_{9.4}.6H_2O$	2.2	431		196
Ca Phillipsite		$CaAl_2Si_5O_{14}.5H_2O$		549		
Na Phillipsite		$Na_2Al_2Si_{15}O_{14}.5H_2O$		835		
K Phillipsite		$K_2Al_2Si_{15}O_{14}.5H_2O$		868		
Natrolite		$Na_2Al_2Si_3O_{10}.2H_2O$	2.231	380	169.39	170
Chabazite		$CaAl_2Si_4O_{12}.6H_2O$	2.05	506		247
Wairakite		$CaAl_2Si_4O_{12}.2H_2O$		434		
Kaolinite		$Al_4Si_4OH_{10}(OH)_8$	2.629	382	99.52	145
Muscovite		$KAl_3Si_3O_{18}$	2.828	492	140.71	152

Appendix 5C. Ion Interaction Coefficients Database

5	47						
NUMBER	SPECIES	14	15	16	17	19	20
		Cl-	CO3-2	SO4-2	NO3-	PO4-3	F-
1	H+	0.12	0	0	0.07	0	0
2	e-	0	0	0	0	0	0
3	H2O	0	0	0	0	0	0
4	Ca+2	0.14	0	-0.61	0.02	0	0
5	Mg+2	0.19	0	-0.39	0.17	0	0
6	Na+	0.03	-0.05	-0.12	-0.04	-0.25	0.02
7	K+	0	0.02	-0.06	-0.11	-0.09	0.03
8	Fe+2	0.14	0	0	0	0	0
9	Mn+2	0.13	0	-0.48	0	0	0
10	Al+3	0.33	0	-0.54	0	0	0
11	Ba+2	0.07	0	0	-0.28	0	0
12	Sr+2	0.13	0	0	-0.06	0	0
13	H4SiO4	0	0	0	0	0	0
18	H3BO3	0	0	0	0	0	0
21	Li+	0.1	0	-0.03	0.08	0	0
23	U+4	0	0	0	0	0	0
24	Np+4	0	0	0	0	0	0
25	Pu+4	0	0	0	0	0	0
26	Am+3	0.28	0	0	0.2	0	0
27	Cm+3	0	0	0	0	0	0
30	Cs+	-0.05	0	-0.13	-0.16	0	0.06
31	Pb+2	0.08	0	0	-0.2	0	0
32	Ra+2	0	0	0	0	0	0
34	Th+4	0.25	0	0	0.11	0	0
35	Pa+4	0	0	0	0	0	0
49	Ni+2	0.17	0	-0.51	0	0	0
203	Fe+3	0	0	0	0.42	0	0
208	FeOH+2	0	0	0	0	0	0
212	Fe2OH2+4	0	0	0	0	0	0
294	AlOH+2	0.09	0	0	0	0	0
299	Al3OH4+5	0.66	0	0	0	0	0
366	NH4+	-0.01	0	-0.23	-0.06	0	0

393	UO2+	0	0	0	0	0	0
394	UO2+2	0.21	0	-0.61	0.24	0	0
414	UCl+3	0	0	0	0	0	0
416	UO2Cl+	0	0	0	0	0	0
427	USO4+2	0	0	0	0	0	0
432	UNO3+3	0	0	0	0	0	0
433	UNO32+2	0	0	0	0	0	0
436	UO2NO3+	0	0	0	0	0	0
450	UF+3	0	0	0	0	0	0
451	UF2+2	0	0	0	0	0	0
452	UF3+	0.31	0	0	0	0	0
454	UO2F+	0.04	0	0	0	0	0
462	UO2Br+	0	0	0	0	0	0
493	NpO2+	0	0	0	0	0	0
575	PuO2+	0	0	0	0	0	0
END BLOCK	1						
NUMBER		22	28	29	45	46	48
	SPECIES	Br-	TcO4-	I-	OAC-	CIT-3	EDTA-4
1	H+	0.15	0	0	0	0	0
2	e-	0	0	0	0	0	0
3	H2O	0	0	0	0	0	0
4	Ca+2	0.18	0	0.27	0	0	0
5	Mg+2	0.26	0	0.32	0	0	0
6	Na+	0.05	0.01	0.08	0.08	0	0
7	K+	0.01	0	0.02	0.09	0	0
8	Fe+2	0	0	0	0	0	0
9	Mn+2	0	0	0	0	0	0
10	Al+3	0	0	0	0	0	0
11	Ba+2	0.13	0	0.23	0	0	0
12	Sr+2	0.18	0	0.25	0	0	0
13	H4SiO4	0	0	0	0	0	0
18	H3BO3	0	0	0	0	0	0
21	Li+	0.13	0	0.16	0.05	0	0
23	U+4	0	0	0	0	0	0
24	Np+4	0	0	0	0	0	0

25	Pu+4	0	0	0	0	0	0
26	Am+3	0	0	0	0	0	0
27	Cm+3	0	0	0	0	0	0
30	Cs+	-0.04	0	-0.06	0.11	0	0
31	Pb+2	0	0	0	0	0	0
32	Ra+2	0	0	0	0	0	0
34	Th+4	0	0	0	0	0	0
35	Pa+4	0	0	0	0	0	0
49	Ni+2	0	0	0	0	0	0
203	Fe+3	0	0	0	0	0	0
208	FeOH+2	0	0	0	0	0	0
212	Fe2OH2+4	0	0	0	0	0	0
294	AlOH+2	0	0	0	0	0	0
299	Al3OH4+5	0	0	0	0	0	0
366	NH4+	0	0	0	0	0	0
393	UO2+	0	0	0	0	0	0
394	UO2+2	0	0	0	0	0	0
414	UCl+3	0	0	0	0	0	0
416	UO2Cl+	0	0	0	0	0	0
427	USO4+2	0	0	0	0	0	0
432	UNO3+3	0	0	0	0	0	0
433	UNO32+2	0	0	0	0	0	0
436	UO2NO3+	0	0	0	0	0	0
450	UF+3	0	0	0	0	0	0
451	UF2+2	0	0	0	0	0	0
452	UF3+	0	0	0	0	0	0
454	UO2F+	0	0	0	0	0	0
462	UO2Br+	0	0	0	0	0	0
493	NpO2+	0	0	0	0	0	0
575	PuO2+	0	0	0	0	0	0
END BLOCK	2						
NUMBER		102	347	348	350	351	363

	SPECIES	OH-	H3SiO4-	H2SiO4-2	ClO4-	HCO3-	NO2-
1	H+	0	0	0	0	0	0
2	e-	0	0	0	0	0	0
3	H2O	0	0	0	0	0	0
4	Ca+2	0	0	0	0.27	0	0
5	Mg+2	0	0	0	0.33	0	0
6	Na+	0.4	-0.08	-0.01	0.01	-0.03	0
7	K+	0.9	0	0	-0.06	0	-0.04
8	Fe+2	0	0	0	0	0	0
9	Mn+2	0	0	0	0	0	0
10	Al+3	0	0	0	0	0	0
11	Ba+2	0	0	0	0.15	0	0
12	Sr+2	0	0	0	0.23	0	0
13	H4SiO4	0	0	0	0	0	0
18	H3BO3	0	0	0	0	0	0
21	Li+	-0.02	0	0	0.15	0	0
23	U+4	0	0	0	0.8	0	0
24	Np+4	0	0	0	0.82	0	0
25	Pu+4	0	0	0	1.03	0	0
26	Am+3	0	0	0	0	0	0
27	Cm+3	0	0	0	0	0	0
30	Cs+	0	0	0	0	0	-0.04
31	Pb+2	0	0	0	0.15	0	0
32	Ra+2	0	0	0	0	0	0
34	Th+4	0	0	0	0	0	0
35	Pa+4	0	0	0	0	0	0
49	Ni+2	0	0	0	0	0	0
203	Fe+3	0	0	0	0.56	0	0
208	FeOH+2	0	0	0	0.38	0	0
212	Fe2OH2+4	0	0	0	0.82	0	0
294	AlOH+2	0	0	0	0.31	0	0
299	Al3OH4+5	0	0	0	1.3	0	0
366	NH4+	0	0	0	-0.08	0	0
393	UO2+	0	0	0	0.26	0	0
394	UO2+2	0	0	0	0.46	0	0
414	UCl+3	0	0	0	0.63	0	0
416	UO2Cl+	0	0	0	0.31	0	0
427	USO4+2	0	0	0	0	0	0
432	UNO3+3	0	0	0	0.66	0	0
433	UNO32+2	0	0	0	0.53	0	0
436	UO2NO3+	0	0	0	0.31	0	0
450	UF+3	0	0	0	0.54	0	0

451	UF2+2	0	0	0	0.3	0	0
452	UF3+	0	0	0	0.31	0	0
454	UO2F+	0	0	0	0.29	0	0
462	UO2Br+	0	0	0	0.24	0	0
493	NpO2+	0	0	0	0.25	0	0
575	PuO2+	0	0	0	0.17	0	0
END BLOCK	3						
NUMBER		377	378	389	422	423	425
	SPECIES	HPO4-2	H2PO4-	HF2-	UO2CO 32-2	UO2CO 33-4 U	O23CO 36-
1	H+	0	0	0	0	0	0
2	e-	0	0	0	0	0	0
3	H2O	0	0	0	0	0	0
4	Ca+2	0	0	0	0	0	0
5	Mg+2	0	0	0	0	0	0
6	Na+	-0.15	-0.08	-0.11	0.06	0.09	0.55
7	K+	-0.1	-0.14	0	0	0	0
8	Fe+2	0	0	0	0	0	0
9	Mn+2	0	0	0	0	0	0
10	Al+3	0	0	0	0	0	0
11	Ba+2	0	0	0	0	0	0
12	Sr+2	0	0	0	0	0	0
13	H4SiO4	0	0	0	0	0	0
18	H3BO3	0	0	0	0	0	0
21	Li+	0	0	0	0	0	0
23	U+4	0	0	0	0	0	0
24	Np+4	0	0	0	0	0	0
25	Pu+4	0	0	0	0	0	0
26	Am+3	0	0	0	0	0	0
27	Cm+3	0	0	0	0	0	0
30	Cs+	0	0	0	0	0	0
31	Pb+2	0	0	0	0	0	0
32	Ra+2	0	0	0	0	0	0
34	Th+4	0	0	0	0	0	0
35	Pa+4	0	0	0	0	0	0
49	Ni+2	0	0	0	0	0	0
203	Fe+3	0	0	0	0	0	0
208	FeOH+2	0	0	0	0	0	0
212	Fe2OH2+4	0	0	0	0	0	0
294	AlOH+2	0	0	0	0	0	0
299	Al3OH4+5	0	0	0	0	0	0
366	NH4+	0	0	0	0	0	0
393	UO2+	0	0	0	0	0	0
394	UO2+2	0	0	0	0	0	0

212	Fe2OH2+4	0	0	0	0	0	0
294	AlOH+2	0	0	0	0	0	0
299	Al3OH4+5	0	0	0	0	0	0
366	NH4+	0	0	0	0	0	0
393	UO2+	0	0	0	0	0	0
394	UO2+2	0	0	0	0	0	0
414	UCl+3	0	0	0	0	0	0
416	UO2Cl+	0	0	0	0	0	0
427	USO4+2	0	0	0	0	0	0
432	UNO3+3	0	0	0	0	0	0
433	UNO32+2	0	0	0	0	0	0
436	UO2NO3+	0	0	0	0	0	0
450	UF+3	0	0	0	0	0	0
451	UF2+2	0	0	0	0	0	0
452	UF3+	0	0	0	0	0	0
454	UO2F+	0	0	0	0	0	0
462	UO2Br+	0	0	0	0	0	0
493	NpO2+	0	0	0	0	0	0
575	PuO2+	0	0	0	0	0	0
END BLOCK	5						

414	UCl+3	0	0	0	0	0	0
416	UO2Cl+	0	0	0	0	0	0
427	USO4+2	0	0	0	0	0	0
432	UNO3+3	0	0	0	0	0	0
433	UNO32+2	0	0	0	0	0	0
436	UO2NO3+	0	0	0	0	0	0
450	UF+3	0	0	0	0	0	0
451	UF2+2	0	0	0	0	0	0
452	UF3+	0	0	0	0	0	0
454	UO2F+	0	0	0	0	0	0
462	UO2Br+	0	0	0	0	0	0
493	NpO2+	0	0	0	0	0	0
575	PuO2+	0	0	0	0	0	0
END BLOCK	4						
NUMBER		430	460	461	772	969	970
	SPECIES	UO2SO42-2	UO2F3-	UO2F4-2	IO3-	HAsO4-2	H2AsO4-
1	H+	0	0	0	0	0	0
2	e-	0	0	0	0	0	0
3	H2O	0	0	0	0	0	0
4	Ca+2	0	0	0	0	0	0
5	Mg+2	0	0	0	0	0	0
6	Na+	0.55	0	-0.012	-0.06	-0.21	-0.08
7	K+	0	0	0	0	-0.02	-0.12
8	Fe+2	0	0	0	0	0	0
9	Mn+2	0	0	0	0	0	0
10	Al+3	0	0	0	0	0	0
11	Ba+2	0	0	0	0	0	0
12	Sr+2	0	0	0	0	0	0
13	H4SiO4	0	0	0	0	0	0
18	H3BO3	0	0	0	0	0	0
21	Li+	0	0	0	0	0	0
23	U+4	0	0	0	0	0	0
24	Np+4	0	0	0	0	0	0
25	Pu+4	0	0	0	0	0	0
26	Am+3	0	0	0	0	0	0
27	Cm+3	0	0	0	0	0	0
30	Cs+	0	0	0	0	0	0
31	Pb+2	0	0	0	0	0	0
32	Ra+2	0	0	0	0	0	0
34	Th+4	0	0	0	0	0	0
35	Pa+4	0	0	0	0	0	0
49	Ni+2	0	0	0	0	0	0
203	Fe+3	0	0	0	0	0	0
208	FeOH+2	0	0	0	0	0	0